A HIGH RESOLUTION SPECTROSCOPIC STUDY OF THE GROUND STATE AND THE LOWEST TRIPLET STATE OF BENZOIC ACID

By

WILLIAM LOUIS CLEVELAND

A thesis submitted to
The Graduate School
of
Rutgers University
in partial fulfillment of the requirements
for the degree of
Doctor of Philosophy

Written under the direction of
Professor Lionel Goodman
of the Department of Chemistry
and approved by

Harvey Schugar
Lionel Goodman
Donald S. McClure
Sidney Toby

New Brunswick, New Jersey

May, 1975

ABSTRACT OF THE THESIS

A High Resolution Spectroscopic Study of the Ground State and the Lowest Triplet State of Benzoic Acid

By WILLIAM LOUIS CLEVELAND

Thesis director: Professor Lionel Goodman

In this study we have caried out a detailed analysis of the phosphorescence emission of benzoic acid. The use of low temperatures (4.2°K) and carefully chosen hosts has yielded highly resolved phosphorescence spectra for fourteen guest-host systems. In addition to the expected totally symmetric ring modes, in-plane carboxyl group modes and out-of-plane ring modes are observed with strong intensity in the spectra of some guest-host systems. The latter two groups of modes have been found to be highly sensitive to environmental perturbations. In order to explain the environmental dependence of in-plane carboxyl group modes we postulate that the carboxyl group deviates from the plane of the benzene ring and that the magnitude of the deviation differs in the various guest-host systems. X-ray data shows that the carboxyl group is non-planar in the crystal. The degree of non-planarity of the carboxyl group is expected to influence the mixing of the lowest carboxyl group triplet state with ^3L_a , the benzenoid component of the total benzoic acid triplet state. This should, in turn, influence the activity of carboxyl group modes in the phosphorescence

spectrum.

In line with previous work on benzene and substituted benzenes, we have attempted to account for the non-totally symmetric, out-of-plane modes in terms of spin-orbit vibronic coupling. In order to gain physical insight into the spin-orbit vibronic interactions we have expanded the various $n\pi^*$ and $\pi\pi^*$ states in terms of locally excited (LE) and charge transfer (CT) components. Qualitative arguments based on overlap and orthogonality considerations indicate that the $\pi\pi^*$ states must possess ring to carboxyl group charge transfer character and that the $n\pi^*$ states must be delocalized over the benzene ring in order for spin-orbit virbonic coupling to account for the activity of the out-of-plane ring modes. The environmental sensitivity of out-of-plane activity has been rationalized in terms of H-bonding effects on the LE, CT compositions of the $n\pi^*$ and $\pi\pi^*$ states. H-bonding effects on $\pi\pi^*$ states have been calculated by Baum, 1974, Intuitive considerations have been used to predict H-bonding effects on $n\pi^*$ states.

An essential part of the foundation upon which our model of the lowest triplet state has been constructed is a detailed understanding of the ground state normal modes. In order to achieve this understanding we have obtained high resolution infrared and Raman spectra at 4.2° K. Rigorous assignments have been facilitated by the use of

four isotopes of benzoic acid (d_o , $4d_1$, d_5, $1d_1$). The data obtained in this study, together with polarized infrared spectra in the literature, has allowed a nearly complete assignment of the normal modes of the benzoic acid unit cell.

ACKNOWLEDGMENTS

In the course of the work leading to this thesis I have received important and often invaluable assistance from a number of individuals. Most notable is Professor Lionel Goodman, my thesis director. His imaginative suggestions and critical judgment have played an essential role in the development of the ideas contained in this thesis. I am also grateful to him for giving me the freedom and independence that was so important for the development of my own initiative and imagination.

Valuable contributions to this thesis have been made by the members of my committee through their many helpful suggestions. I am also indebted to them for their cooperation in reading this thesis in time for me to meet an important deadline.

The substance of this thesis as well as my personal scientific development has greatly benefited from a collaboration with Clayton Baum and Professor Donald S. McClure of Princeton University. This collaboration has been characterized by a spirit of cooperation in which there has been a free exchange of ideas and data, some of which are contained in this thesis.

The members of Professor Goodman's research group have all contributed in some way to the completion of this thesis. Special thanks go to Dr. R. Shimada for initiating our interest in benzoic acid. I am indebted to Dr. R.

Zwarich for providing a polarized infrared spectrum and for many helpful discussions. I have also benefited from valuable discussions with Dr. M. Koyanagi. In the latter stages of this research I was aided in the interpretation of the data by Dr. Omar S. Khalil, Dr. San Yan Chu and Mr. Ilker Ozkan.

Spectra of benzoic acid 4d_1 have played an important role in the development of our understanding of benzoic acid. The synthesis of this important compound with high isotopic purity was made possible by an ingenious procedure suggested by Dr. J. SanFilippo.

I am especially indebted to Mr. Charles Brown, departmental Instrument Maker, and his assistant, Mr. E. Csordas for their cooperation and skilled construction of some of the apparatus used to obtain the data presented in this thesis.

My wife Fay deserves much appreciation for carrying out the onerous and time consuming task of reducing the phosphorescence data and checking and rechecking the results.

Miss Helen Sedlowski is to be thanked for her cooperation and care in the typing of this thesis.

Finally, I would like to express my deep appreciation to Professor B. F. Erlanger of the College of Physicians and Surgeons, Columbia University, for his generosity in giving me a leave of absence and for his patience and realistic advice, all of which were essential to the completion of this thesis.

To

My Wife and My Parents, whose love and
support made this thesis possible.

"The Moving Finger writes; and, having writ,
Moves on: nor all your Piety nor Wit,
Shall lure it back to cancel half a Line,
Nor all your Tears wash out a Word of it"

(From "The Rubaiyat" of Omar Khayyam)

TABLE OF CONTENTS

CHAPTER I

INTRODUCTION

Recently, aromatic aldehydes and ketones have been found to exhibit phenomena which challenge some of the basic principles used to interpret the electronic spectra of molecules, such as the Born-Oppenheimer and Franck-Condon principles (Goodman and Koyanagi, 1972). These unusual properties are attributed to the presence of low-lying $n\pi^*$ states which are close to the lower $\pi\pi^*$ states of aromatic origin (Duben, et al. 1974). This proximity of states of different orbital type gives one a unique opportunity to study interstate interactions. In this context, it seemed possible that interesting phenomena might be observed in benzoic acid, the simplest aromatic carboxylic acid.

Unlike aldehydes and ketones, benzoic acid forms hydrogen-bonded dimers. Since the non-bonding electrons of the carbonyl oxygen atom are intimately involved in hydrogen bonding, it was our expectation that hydrogen bonding effects could be used to probe the interactions between $n\pi^*$ and $\pi\pi^*$ states.

A previous study by Kanda and coworkers (1963) provided additional evidence that benzoic acid was a favorable molecule in which to study interstate interactions. These authors obtained the phosphorescence spectrum of benzoic acid in benzene at 90° K. This spectrum, which was moderately resolved, revealed the presence of intense ring out-of-plane modes. For a planar molecule, out-of-plane modes are non-totally symmetric and should have vanishing Franck-Condon factors. The presence of intense "forbidden" activity in the phosphorescence spectrum suggested that the nature of the interstate interactions in benzoic acid might be revealed through a study of the lowest triplet state. Accordingly, we decided to undertake a detailed investigation of the phosphorescence emission of benzoic acid.

In our study we have obtained highly resolved phosphorescence spectra of benzoic acid in five different polycrystalline hosts at 4.2° K. We have also studied parafluorobenzoic acid and methyl benzoate. The use of a wide range of matrices has revealed a striking environmental dependence of the out-of-plane modes.

In Chapter III we present the data obtained in this study and suggest a model of the lowest triplet state that is cast in terms of localized molecular orbitals. A review of previous work is also contained in this chapter.

Since phosphorescence emission at 4.2° K occurs from the lowest vibrational level of the triplet state to the vibrational levels of the ground state, an understanding of the phosphorescence spectrum requires a detailed knowledge of the ground state normal modes. Accordingly, we have undertaken a comprehensive study of the infrared and Raman spectra of benzoic acid. These spectra have been obtained at the same temperature and, where possible, in the same environment used for the phosphorescence spectra in order that a more precise comparison could be made between the phosphorescence frequencies and those obtained from the Raman and infrared data. A nearly complete assignment of the normal modes has been given.

In addition to its value as a tool for interpreting phosphorescence spectra, a normal coordinate analysis has considerable value in its own right. First of all benzoic acid is the simplest carboxylic acid that exists as a dimer in the solid state. Consequently, an understanding of the H-bond and carboxyl group modes in benzoic acid would facilitate an understanding of these modes in a large class of similar molecules. Benzoic acid is also an important example of a monosubstituted benzene. An understanding of its normal modes would contribute to the growing body of knowledge of the normal modes of substituted benzenes. The data obtained in this study, along with detailed arguments in support of assignments are presented in Chapter II. Previous Raman and infrared studies are also discussed in this chapter.

CHAPTER II

AN ANALYSIS OF THE GROUND STATE NORMAL MODES OF BENZOIC ACID

A. A Summary of Previous Studies of Benzoic Acid

There have been many studies of the infrared and Raman spectra of benzoic acid. Most of these studies have been concerned with the carboxyl group modes and the low frequency H-bond modes. The most complete analyses of the spectra have been given for the region below 200 cm^{-1}. No analysis of the Raman spectrum above 200 cm^{-1} has been given despite the importance of benzoic acid as the simplest aromatic carboxylic acid. Partial assignments of ring modes in the IR spectrum have been attempted in three studies. However, no comprehensive analysis of the IR spectrum above 200 cm^{-1} has been given.

In 1920 Latimer and Rodebush predicted that carboxylic acids should form hydrogen-bonded dimers. This prediction was verified for formic acid vapor by Pauling and Brockway in 1934. Subsequently, a number of infrared studies of carboxylic acids were undertaken in order to determine the nature of hydrogen bonding in these compounds. Most of these studies focused on the O-H and C=0 stretching modes, probably because these modes occur in a region of the spectrum that was easily accessible with instrumentation available at that time.

In 1938 Bushwell _et_ _al_. obtained the IR spectra of benzoic acid d_o and $1d_1$ and other carboxylic acids dissolved in carbon tetrachloride. The spectra included the region between 2100 and 3800 cm^{-1}. Two bands split into pairs were observed. On the basis of the large shift caused by $d_o \rightarrow 1d_1$ substitution, the bands were attributed to the O-H stretching mode. The splitting of the bands was observed to disappear in the $1d_1$ spectrum. This suggested to the authors that tunneling of the H-bonding protons was the cause of the splitting.

Also in 1938, Davies and Sutherland studied the O-H stretching mode in the IR spectra of carboxylic acids in solution. These authors assigned the weak band at 3520 cm^{-1} to the O-H stretching mode of the monomer. This assignment was based on the temperature dependence of the intensity of this mode. Having made the assignment, they were able to measure the monomer-dimer equilibrium constant. They also noted that the monomer O-H stretching band was much sharper than the dimer band. This fact led them to propose the interesting hypothesis that the broadness of the dimer band was due to the presence of combination bands involving the O-H stretching mode and H-bond modes. The intensity of the combination bands was assumed to be enhanced by Fermi resonance with the O-H stretching fundamental. These authors also noted that the coupling of the carboxyl groups in the dimer by the H-bonds should lead to appreciable splitting between the Raman and infrared active carboxyl group modes of the dimer.

In 1939, Wall and Claussen reconsidered the suggestion of Bushwell et al. that the structure of the O-H stretching bands was due to proton tunneling. However, these authors were unable to come to definite conclusions.

Bratoz, Hadzi, and Sheppard in 1956 obtained the IR spectra of benzoic acid and four other carboxylic acids in the region between 1500 and 3700 cm^{-1}. Deuterium analogues were also studied. These authors concluded that the complex structure of the O-H stretching band of benzoic acid was most likely due to the presence of combination bands enhanced by Fermi resonance. This paper, together with a companion paper by Hadzi and Sheppard dealing with the region between 500 and 1500 cm^{-1} established ranges and assignments for those carboxyl group modes that undergo a shift in frequency for $d_o \rightarrow 1d_1$ substitution. In 1958 Hadzi and Pintar obtained the IR spectra of benzoic acid d_o and $1d_1$ vapor in order to further clarify the assignments of the carboxyl group modes.

Similar solution studies of the carboxyl group modes of benzoic acid and related compounds were carried out by Murray and Sundaram (1961) and by Brooks et al. (1961). Odinokov et al. (1969) studied the effect of basic solvents on the IR spectra of benzoic and salicyclic acid.

Pinchas and coworkers (1961, 1965) studied the IR spectra of 0^{18}- and C^{13}-labelled benzoic acids. These authors were interested in the intensity changes that occur for these isotopic substitutions.

The only IR studies of benzoic acid in which low temperature spectra in the region above 200 cm^{-1} were obtained, were carried out by Hayashi and Kimura (1966) and very recently by Hayashi and Umemura (1974). These authors obtained polarized spectra of benzoic acid crystals grown between salt discs. In the earlier study, spectra of benzoic acid d_o and $1d_1$ were obtained at -150^oC. In the latter study, the temperature was lowered to 7^oK. These authors focused their attention on the carboxyl group modes, which were found to be split into pairs. Their interpretation of this splitting will be discussed later in detail. No attempt was made to assign ring modes in this study.

In 1958 Gonzales-Sanchez published the IR spectra of 12 benzene carboxylic acids. Although specific assignments of ring modes were not given, an attempt was made to sort these modes into types, i.e., C-C stretching modes, skeletal deformation modes, etc. This author's assignments of carboxyl group modes are basically in agreement with those of Hadzi and coworkers.

Kakiuti in 1961 attempted to assign the out-of-plane ring modes of benzoic acid d_o, ld_1 and six esters. In Kakiuti's opinion, only four of the six predicted fundamentals were observed.

McWhinnie and Poller (1966) obtained the infrared spectra of benzoic acid and twenty eight other monosubstituted benzenes in the region between 222 and 667 cm^{-1}. Nujol mulls and carbon tetracholide solutions were employed. Assignments for ν_{6a} , ν_{6b} , ν_{16b} and two carboxyl group modes in the region were given.

Relatively few Raman studies of the region above 200 cm^{-1} have appeared in the literature, presumably because of the considerable experimental difficulty of obtaining Raman spectra before the advent of laser sources. Murty and Seshadri in 1942 obtained the Raman spectrum of benzoic acid in benzene and were able to distinguish between monomer and dimer bands. Kohlraush reported the spectra of molten and crystalline benzoic acid in 1943. The spectrum of the crystalline material revealed sixteen bands between 181 and 3070 cm^{-1}. A later spectrum by Cojan and Renaux (1958) revealed only eight bands. However, a powdered sample was used in this case. In 1963, Kanda _et_ _al_. published the Raman spectra of benzoic acid in benzene and ethanol. About 20 bands were revealed by these spectra. The quality of previous Raman spectra can be evaluated by comparing the number of modes observed with the number predicted by group theory, namely, 84 for the free dimer and 177 for the unit cell. In none of these studies were detailed assignments given.

Early far infrared spectra of benzoic acid were obtained by Genzel and coworkers (1956, 1959) and analyzed by Maier *et al*. (1962). A comparison of these spectra with more recent ones shows that they are of poor quality, revealing little of the structure observed in later studies. A high quality spectrum was obtained by Stanevich in 1964. Spectra were obtained at 20 and -175° C. An attempt was made to assign the three IR active H-bond modes and the ring-carboxyl group out-of-plane bend. Lattice modes and the monomer torsion were not assigned. Another study in 1964 by Delorme yielded spectra of poor quality, showing only two bands as opposed to the six bands observed by Stanevich at room temperature. Room temperature solution spectra by Statz and Lippert (1967) and Meshitsuka *et al*. (1972) reveal very little structure.

Polarized far IR spectra of oriented crystals have been obtained by Wyncke *et al*. (1968) and Meshitsuka *et al*. (1972). Detailed assignments of H-bond modes and lattice modes were given in both studies. Since our own analysis depends heavily on the results of these studies we will discuss them in detail in the section dealing with assignments of low frequency modes.

Maier and coworkers (1954, 1962) were the first to study the low frequency Raman spectrum. Polarized spectra of oriented crystals were obtained. Using the IR data of Genzel and coworkers, detailed assignments were given, even though all of the modes predicted by group theory were not observed. Colombo and Furic in 1971 obtained the polarized Raman spectra of an oriented cystal at temperatures ranging from 210 to 350° C. In this study, a laser source was used. Only the region below 200 cm^{-1} was considered. Temperature variations in the spectra were used to identify the lattice modes. Detailed assignments were given. This study will be discussed in more detail in the section dealing with the assignments of low frequency modes.

A survey of previous attempts to assign the normal modes of benzoic acid reveals that most have been based on a comparison of the spectra of a series of closely related compounds that differ only by judiciously chosen substitutent groups. The prime advantage of this procedure is that the various compounds are usually available commercially, or else can easily be synthesized and purified. A disadvantage is that changing substituent groups tends to change force constants and even geometry. Further, introducing substituent groups can change the number of atoms and therefore the number of normal modes.

All of these changes tend to complicate matters. Nonetheless, in favorable cases this approach can be a useful adjunct to other procedures.

If, in addition to chemical substitutions, isotopic substitutions are also considered, assignments of normal modes can be placed on a much firmer basis. For isotopic substitutions, the number of atoms is unchanged, and the force constants and geometry are unchanged to a high degree of approximation (Herzberg, 1945, p. 227). Consequently, the effects of isotopic substitutions are more easily understood than those of chemical substitutions. The only major disadvantage of this procedure is the expense of purchasing or synthesizing compounds of high isotopic and chemical purity. No doubt, this is the reason that most studies of benzoic acid have not employed isotopes. In our opinion, the failure to study a series of isotopic substitutions has been a serious obstacle in the majority of previous studies.

Another important obstacle in interpreting Raman and infrared data has been a lack of resolution in the spectra. This lack of resolution has prevented the observation of all the modes active in the spectra, and may have led to erroneous polarization ratios, particularly in the low frequency Raman spectra that were obtained at room temperature. Fortunately, the problem of poor resolution is readily solved by cooling the sample to low temperatures, preferably liquid helium temperature. Furthermore, important information can sometimes be gained by studying the temperature dependence of the spectra.

Each band in an infrared or Raman spectrum is characterized by at least four parameters: frequency, intensity, width and polarization. A knowledge of the last parameter can be of great value in assigning the normal modes, particularly if the structure of the unit cell of the crystal is known and the symmetry of the molecule and unit cell are favorable. Even without knowledge of the unit cell, polarization data can be of great value in tracking isotope shifts. Still another inadequacy of most studies of benzoic acid has been the failure to obtain the spectra of oriented single crystals, particularly at low temperatures where the increased resolution allows valid polarization measurements.

In summary, most previous infrared and Raman studies of benzoic acid have been severely hindered by the failure to study a sufficient variety of isotopes and the failure to obtain polarized spectra of oriented crystals at low temperatures. In this study, we have attempted to remove these inadequacies and have succeeded in obtaining the Raman and infrared spectra at 4.2° K of benzoic acid and three of its isotopes. Unfortunately polarized spectra were not obtained. However, this lack is partially compensated by the low temperature polarized infrared and far infrared spectra very recently reported in the literature. We have also benefited from a polarized infrared spectrum taken at room temperature that was kindly supplied by Dr. R. Zwarich. This data, in conjunction with our data has allowed a nearly complete assignment of all the modes of benzoic acid dimers in crystals.

B. Construction of Benzoic Acid Normal Modes from the Normal Modes of Benzene and Formic Acid

The analysis of infrared and Raman spectra that is put forth in this thesis is based on the assumption that the normal modes of benzoic acid can be regarded as analogues of benzene and formic acid modes. The statement that modes are "analogues" means in practice that the normal coordinate displacements for benzene and formic acid can be used to predict the response of the benzoic acid modes to chemical and isotopic substitutions. This assumption is the usual basis of normal coordinate analyses of substituted benzenes. Justification of this assumption is found in the fact that the calculated displacements of modes of substituted benzenes resemble those of benzene itself in many cases. In some cases mixing of a ring and substituent mode creates a mode which is not an analogue. In such a case, the response of the mode to chemical and isotopic substitutions cannot be predicted from the displacement patterns of the pure ring and substituent group modes. For substituent groups that contain a small number of atoms, such cases are rare.

The out-of-plane modes for benzoic acid monomer can be constructed from those of benzene and formic acid. The former have been accurately calculated by a number of workers and the latter have been represented qualitatively by Statz and Lippert (1967). Qualitative representations of benzene and formic acid normal modes are shown in Figures 1 and 2, respectively.

Benzene has 9 out-of-plane modes. Formic acid has 2, the C-H hydrogen wag and the O-H hydrogen wag. This gives 11 modes whereas benzoic acid monomer is expected to have N-3 = 12. The additional mode comes from the replacement of the C-H hydrogen of formic acid by an extended mass, which has a moment of inertia. The new mode is described as the ring-carboxyl group torsion. The other composite modes of benzoic acid can be regarded as mixtures of the ring and carboxyl group modes. It is important to realize that the mixing of a ring mode with one derived from the carboxyl group always leads to two new modes. This occurs because there are two possible phase relationships between the ring and carboxyl group

FIGURE 1

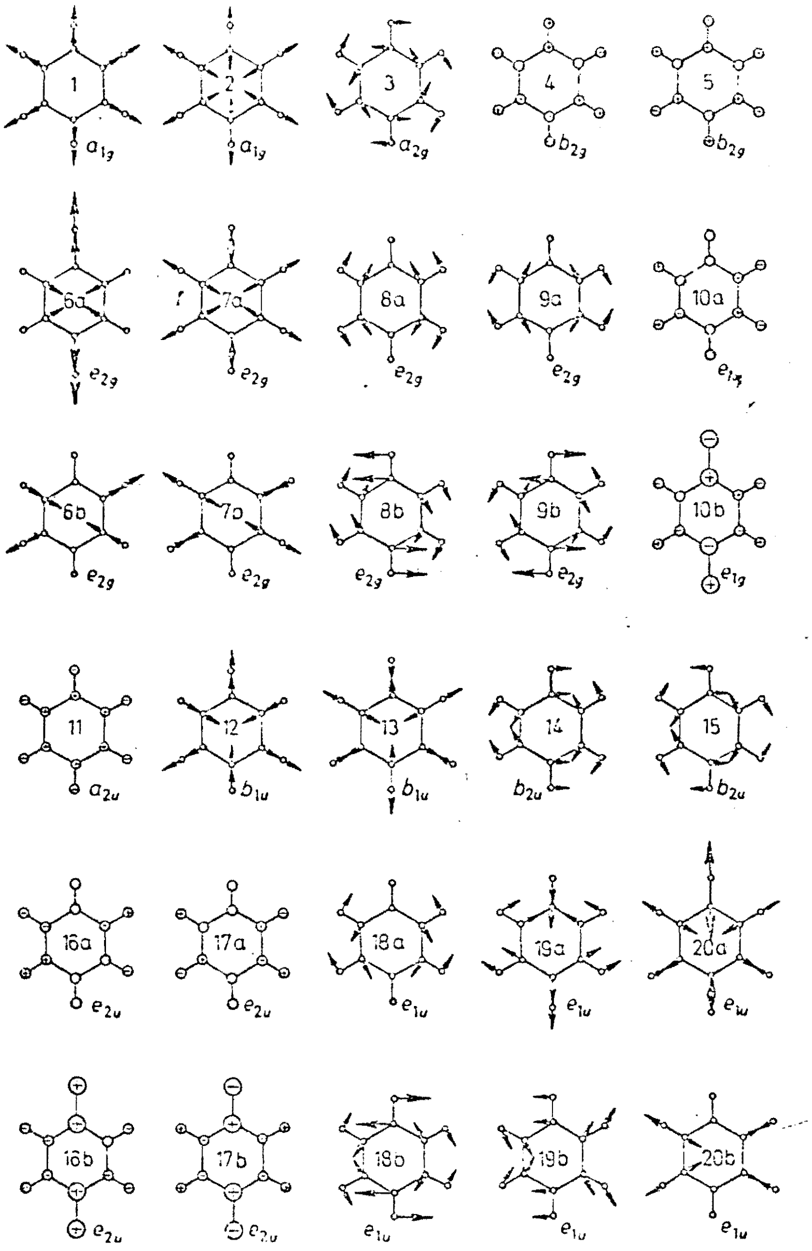

Schematic displacements for benzene normal modes (Taken from Varsanyi, 1969).

FIGURE 2

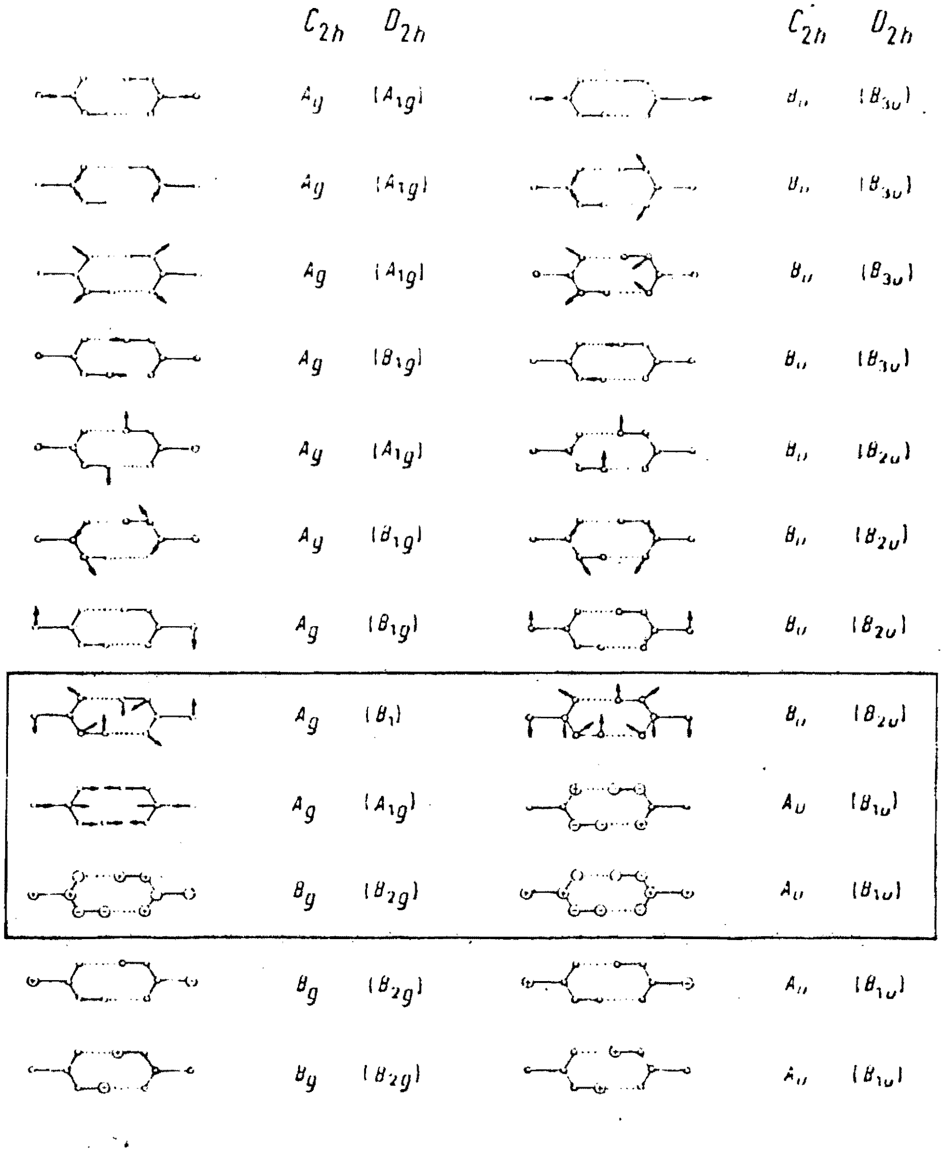

Schematic displacements for formic acid normal modes (Taken from Statz and Lippert, 1967).

modes. For example, the ring-carboxyl group out-of-plane wag is derived from a ring mode which involves the wagging of the hydrogen on the substituent carbon of the ring and from the C-H hydrogen wag of the carboxyl group. The two ways which these modes can be combined are shown in Figure 3. Appreciable mixing of modes is expected to occur when the modes have the same symmetry and approximately the same frequency.

The dimer out-of-plane modes consist of the monomer modes split into pairs in-phase and out-of-phase combinations, as illustrated in the above example) plus the H-bond out-of-plane modes. The H-bond modes involve the relative motions of the monomers as rigid bodies. These modes are shown in Figure 2 (boxed area).

Benzene has 21 in-plane modes and formic acid has 7, giving a total of 28. However, benzoic acid is expected to have 27. An inspection of the displacement patterns for formic acid shows that only the C-H stretching mode can combine with a benzene in-plane mode in such a way that only one phase relationship is possible. In this case, a formic acid mode and a benzene mode coalesce to form only one mode, reducing the total number to 27. No further reductions occur, since for all other formic acid in-plane modes, two phase relationships are possible when combined with a benzene in-plane mode.

FIGURE 3

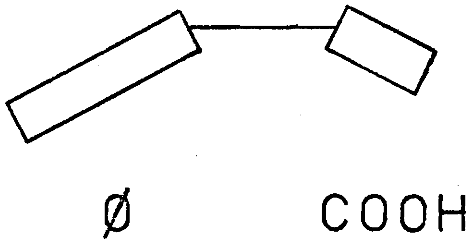

In-Phase Combination

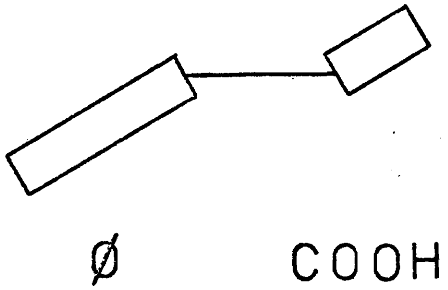

Out-of-Phase Combination

Schematic representations of in-phase and out-of-phase versions of the ring-carboxyl group out-of-plane wag mode for benzoic acid monomer.

The dimer in-plane modes consist of the 27 monomer in plane modes split into pairs (in-phase and out-of-phase combinations) plus three in-plane H-bond modes (see Figure 2) giving a total of 57.

C. X-Ray Data

An x-ray study of benzoic acid crystals at room temperature was carried out in 1955 by Sim, Robertson and Goodwin. Benzoic acid was found to form crystals of the monoclinic type with the unit cell dimensions:
$a = 5.52 \pm 0.02$ Å, $b = 5.14 \pm 0.02$ Å, $c = 21.90 \pm 0.05$ Å and $\beta = 97^{\circ}$. The unit cell contains two hydrogen-bonded dimers and the space group of the crystal is C_{2h}^{5} (Schoenflies notation).

Thus, benzoic acid is similar to many common organic molecules (*e.g.* napthalene, anthracene, *etc.*) which form monoclinic crystals and belong to the C_{2h}^{5} space group. The operators of this group are: E, $C_2(b)$, σ_{ac} , and i. $C_2(b)$ corresponds to a screw axis and σ_{ac} to a glide plane. A comparison of the multiplication tables for the C_{2h}^{5} space group and the C_{2h} point group shows that these groups are isomorphic. Figure 4 shows the location of the symmetry elements relative to the a and b axes of the unit cell. The two molecules of the unit cell are located at site 1 and site 2. Rotation by 180° around the screw-axis at a/4 moves the center of the molecule at

FIGURE 4

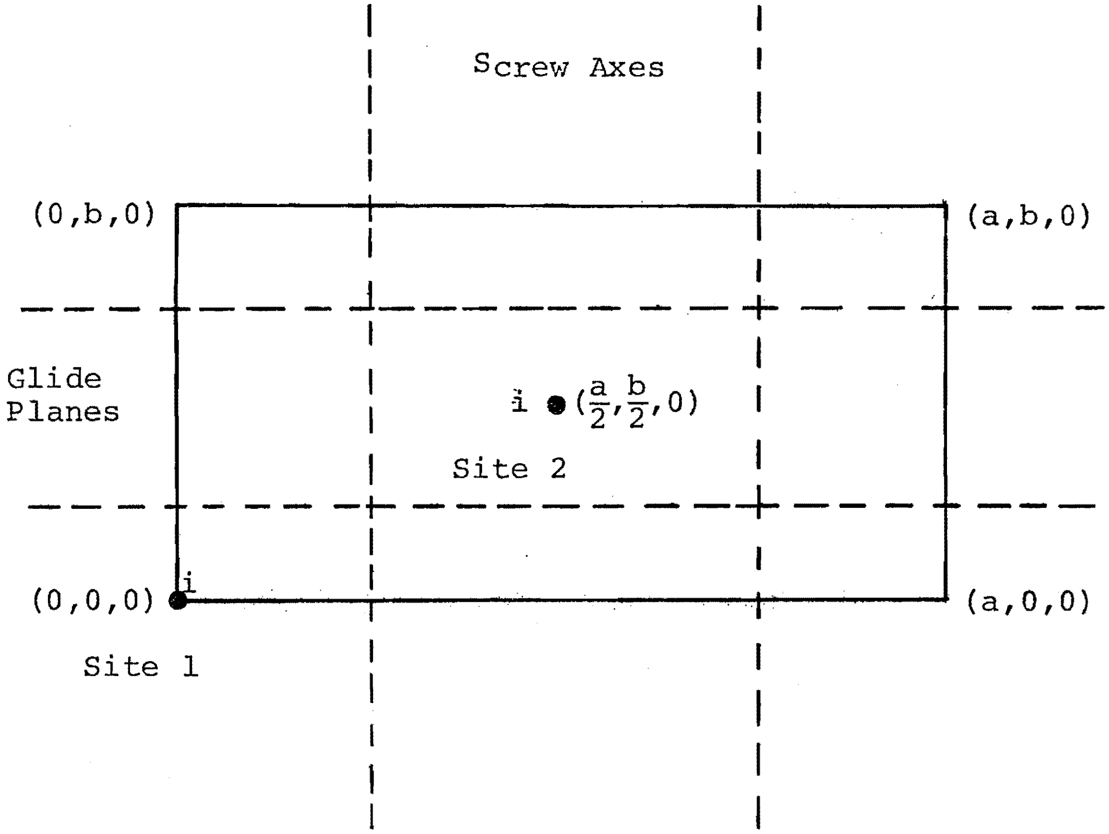

"i" denotes a center of inversion

Symmetry Elements for Unit Cell Belonging to

C_{2h}^{5} Space Group (Taken from Hochstasser, 1966).

site 1, (0,0,0) to (a/2,0,0). Then the screw translation shifts the molecule to (a/2,b/2,0), the coordinates of the center of the molecule at site 2. The centers of symmetry are at (0,0,0) and (a/2,b/2,0). The molecules located at these points have to be centrosymmetric, since these points are crystallographic centers of symmetry, and indeed the x-ray data shows that the benzoic acid dimer belongs to the C_i point group, within the limits of experimental error. Figure 5 shows the (0,1,0) and (1,0,0) projections of the unit cell.

Jeffrey and Sax (1963) in a review of x-ray studies of carboxylic acid dimers point out that planarity of the dicarboxylic acid dimer configuration is the exception rather than the rule. Usually, the carbon and two oxygens of one carboxyl group form a plane that is parallel but separated from the corresponding plane formed by the carbon and oxygens of the other carboxyl group. In the case of benzoic acid, the separation of the planes is 0.057 ± 0 Jeffrey and Sax suggest that the planar configuration has the lowest energy for the free molecule but that in the crystal, steric packing requirements for the rest of the molecule cause a deviation from planarity. If this line of reasoning is correct, it is likely that a greater separation of planes is present in the benzoic acid crystal at 4.2° K, since the unit cell is smaller at this temperature.

FIGURE 5

Arrangement of molecules in the benzoic acid crystal according to Sim, Robertson, and Goodwin (1955). The (100) and (010) projections are shown. The numbers next to the dashed lines give the carbon-carbon intermolecular distances. H-bonds are represented by unlabeled dashed lines and the boundaries of the unit cell in each projection are indicated by the rectangles.

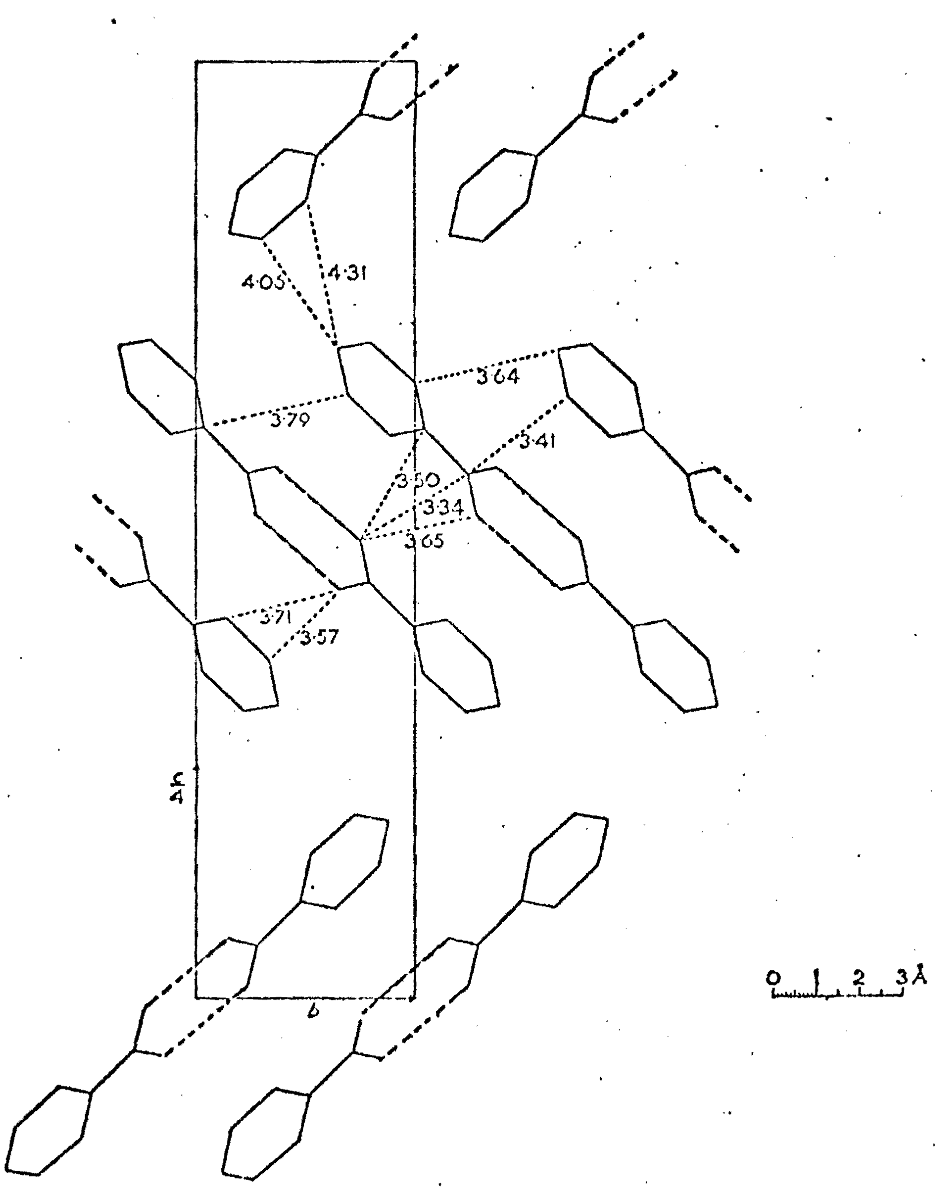
4·05
4·31
3·64
3·79
3·41
3·50
3·34
3·65
3·71
3·57
c/4
b
0 1 2 3 Å

(100)

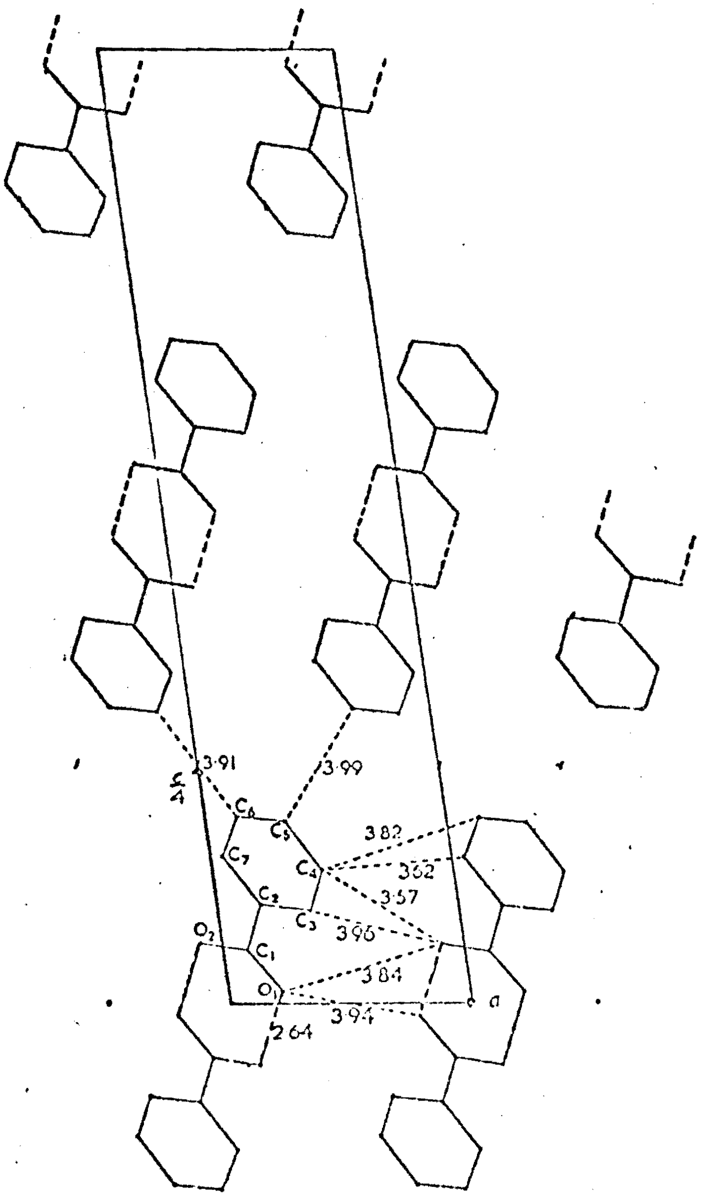
3·91
3·99
c/4
C6
C5
C7
C4
C2
C3
O2
C1
O1
3·82
3·62
3·57
3·96
3·84
3·94
2·64
a

(010)

Since the two benzene rings of the dimer belong to the same plane, it follows that the non-planarity of the carboxyl group prevents the dimer from belonging to the C_{2h} point group. Further the inequality of the C-0 and C=0 bond lengths (1.29 ± 0.021 Å and 1.25 ± 0.021 Å) prevents an accurately planar dimer from belonging to the D_{2h} point group. Presumably, the unequal C-0 and C=0 lengths require the O-H and H-bond lengths to be unequal as well.

Hayashi and coworkers (1966, 1974) have presented evidence that the measured difference between the C-0 and C=0 bond lengths is less than the true value. They postulate that two configurations of benzoic acid dimers are present in the crystal. These configurations differ in the location of the H-bonding protons, as shown in Figure 6. According to their data, the two configurations are separated by an energy barrier of 0.1 Kcal/mole, and the B configuration has the higher energy. Because of the small barrier, an appreciable fraction of the molecules will be in the B configuration at room temperature. This means that a corresponding fraction of the $C-0_2$ bonds will be double bonds. Thus, the measured $C-0_2$ bond length represents a weighted averaged of the C-0 and C=0 bond lengths. At 4.2° K, only the A configuration should be present in the crystal. Consequently, an x-ray measurement

FIGURE 6

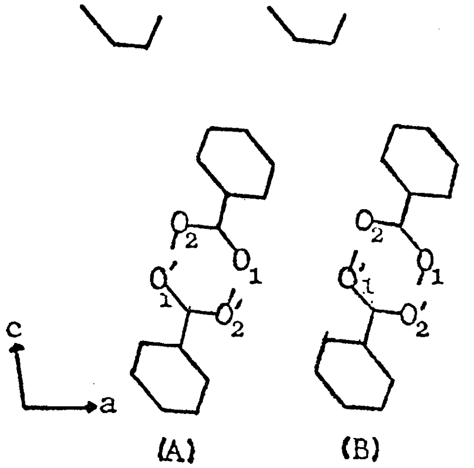

Different configurations of benzoic acid dimers in the pure crystal. (010) plane. (Taken from Hayashi and Kimura, 1966).

of the $C-O_2$ and $C-O_1$ bond lengths should reveal a larger difference in the lengths if Hayashi's hypothesis is correct. Further discussion of this hypothesis will be presented in Sections IID. and IIH.

In summary, the x-ray data shows that the symmetry of the benzoic acid dimer is accurately C_i and approximately C_{2h} or D_{2h}. It is important to realize that for the purpose of normal coordinate analysis, the symmetry has to be determined from the selection rules that are revealed in the Raman and infrared spectra. Furthermore, the symmetry "felt" by the molecule vibrating in one normal mode may be different from that felt in another mode. Accordingly, we will consider C_s and C_{2v} symmetry for benzoic acid monomer and C_i , C_{2h} and D_{2h} for the dimer.

Other important information provided by the x-ray data are the direction cosines relating the X, Y, and Z axes of the molecule to the a, b, and c' axes of the unit cell. The c' axis is perpendicular to the plane formed by the a and b axes. The angle between the c and c' axes is 7°. Table 1 gives the location of the X, Y, and Z axes of the dimer, and the direction cosines relative to these axes. The representations of the point groups considered in this study are shown in Table 2.

TABLE 1

Direction Cosines of Molecular Axes (X,Y,Z)
Relative to Unit Cell Axes (a,b,c').

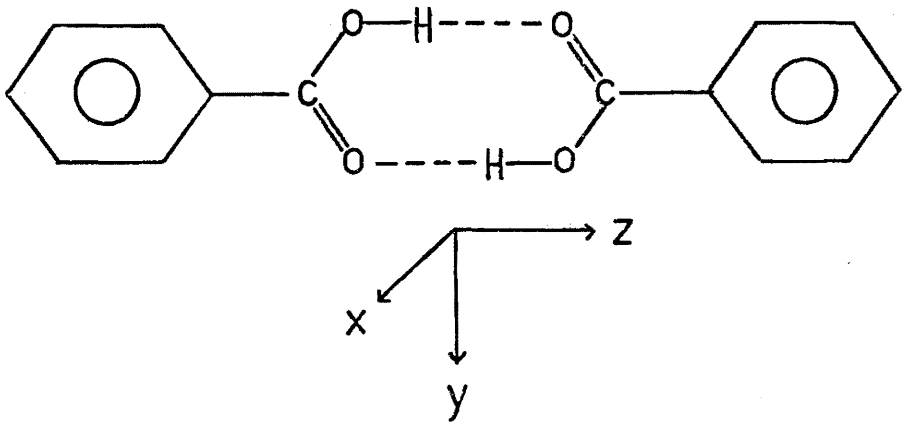

$\cos Z_a = 0.2118$	$Z_a = 77.8^\circ$
$\cos Z_b = 0.7189$	$Z_b = 44.0^\circ$
$\cos Z_{c'} = 0.6621$	$Z_{c'} = 48.5^\circ$
$\cos Y_a = -0.8236$	$Y_a = 145.5^\circ$
$\cos Y_b = -0.2666$	$Y_b = 103.7^\circ$
$\cos Y_{c'} = 0.5154$	$Y_{c'} = 59.0^\circ$
$\cos X_a = 0.5276$	$X_a = 58.2^\circ$
$\cos X_b = -0.6546$	$X_b = 130.9^\circ$
$\cos X_{c'} = 0.5420$	$X_{c'} = 57.2^\circ$

(Taken from Sim, Robertson, and Goodwin, 1955).

TABLE 2

C_i	E	i		
A_g	1	1	R_x, R_y, R_z	x^2, y^2, z^2 xy, xz, yz
A_u	1	−1	x, y, z	

C_{2h}	E	C_2	i	σ_h		
A_g	1	1	1	1	R_z	x^2, y^2, z^2, xy
B_g	1	−1	1	−1	R_x, R_y	xz, yz
A_u	1	1	−1	−1	z	
B_u	1	−1	−1	1	x, y	

z-axis =
perpendicular axis

C_{2v}	E	C_2	$\sigma_v(xz)$	$\sigma_v'(yz)$		
A_1	1	1	1	1	z	x^2, y^2, z^2
A_2	1	1	−1	−1	R_z	xy
B_1	1	−1	1	−1	x, R_y	xz
B_2	1	−1	−1	1	y, R_x	yz

z-axis = long axis

y-axis = perpendicular axis

x-axis = short axis

D_{2h}	E	$C_2(z)$	$C_2(y)$	$C_2(x)$	i	$\sigma(xy)$	$\sigma(xz)$	$\sigma(yz)$		
A_g	1	1	1	1	1	1	1	1		x^2, y^2, z^2
B_{1g}	1	1	−1	−1	1	1	−1	−1	R_z	xy
B_{2g}	1	−1	1	−1	1	−1	1	−1	R_y	xz
B_{3g}	1	−1	−1	1	1	−1	−1	1	R_x	yz
A_u	1	1	1	1	−1	−1	−1	−1		
B_{1u}	1	1	−1	−1	−1	−1	1	1	z	
B_{2u}	1	−1	1	−1	−1	1	−1	1	y	
B_{3u}	1	−1	−1	1	−1	1	1	−1	x	

axes same as
in Table 1

Character tables for C_i, C_{2h}, C_{2v}, and D_{2h} point groups. (Taken from Cotton, 1971).

D. Effects of Intra- and Inter-Molecular Interactions on the Infrared and Raman Spectra

1. Dimer Splitting

In the benzoic acid dimer, the monomers are coupled by two hydrogen bonds, which are relatively weak compared to the covalent bonds in the monomer. Because of the weak coupling, the dimer modes (except for the H-bond modes) can be regarded as in-phase and out-of-phase combinations of the monomer modes. If the H-bonds were sufficiently strong, the H-bond modes would have frequencies comparable to those of the monomer and accidental near degeneracies between H-bond and monomer modes would lead to mixing invalidating the analogue mode assumption mentioned in IIB. The in-phase modes will have gerade symmetry and will be only Raman active. The out-of-phase modes will have ungerade symmetry and will be only IR active. The magnitude of the coupling between monomers will be reflected in the difference between the IR and Raman frequencies of a given mode and is expected to vary from mode to mode. In particular, dimer splitting is expected to be greatest for modes which involve carboxyl group motion.

In addition to being analogues of the monomer modes, the dimer modes are expected to have a "memory" of the local symmetry felt by the monomer modes. For example, consider a hypothetical monomer mode which has zero amplitude at the carboxyl group atoms. A molecule vibrating in this mode will likely feel C_{2v} symmetry. Assume further that the mode belongs to the A_2 representation. Modes belonging to this representation are Raman active but not IR active. In this case, we expect the ungerade dimer mode to appear weakly in the IR spectrum even though it is group theoretically allowed. In short, we expect that weak coupling will allow local symmetry to prevail.

2. Fermi Resonance

Another complication of the spectra which results from intramolecular interaction is the phenomenon of Fermi resonance. This type of interaction occurs when a combination or overtone band is accidentally degenerate with a fundamental having the same symmetry, and is a result of the failure of the harmonic oscillator approximation. Fermi resonance splits or reduces the degeneracy, and the intensity of the combination band is enhanced at the expense of the intensity of the fundamental.

In addition to the group-theoretical requirement that the fundamental and combination modes have the same symmetry, there is the spatial requirement that both modes have appreciable amplitude in the same region of the molecule. An accidental degeneracy between a fundamental involving only carboxy group atoms and a combination mode involving only ring motion is therefore not expected to exhibit strong Fermi resonance.

The occurrence of Fermi resonance is expected to increase with the frequency of the fundamental because the density of combination states is greater at higher frequencies. Further, since deuterium substitution usually decreases the frequencies of the various modes, Fermi resonance occurs more frequently in deuterium substituted molecules. In other words, lowering the frequencies of the modes in effect compresses the spectrum into a smaller frequency range, increasing the density of states. This problem is expected to be most apparent in the spectrum of benzoic acid d_5.

3. Inversion Doubling and Configuration Splitting

In an isolated benzoic acid dimer, inspection shows that there are two possible configurations for the H-bonding protons. Both configurations are physically equivalent and should therefore have the same energy.

As early as 1938, Bushwell *et al.* suggested that the protons move in a potential well that has two minima separated by a barrier. Since the two configurations of protons are isoenergetic, the double-minimum potential can be constructed from two identical single-well potentials whose minima are separated by a distance q_o along the normal coordinate which corresponds to the gerade or in-phase motion of the protons. Because the potential wells are identical, the levels in one well are degenerate with those in the other. The application of degenerate perturbation theory splits the degenerate levels and leads to a double minimum potential well. Because the two minima are separated by a finite barrier, it is possible for the protons to shift from one minimum to another. One way this shift can be effected is by adding sufficient energy to the system to make the energy of the protons exceed the height of the barrier. Another way is for the protons to tunnel through the barrier. Calculation shows the rate of tunneling is inversely proportional to the magnitude of the splitting of the energy level. As observed for NH_3 (Herzberg, 1945, p. 224) and predicted for other systems (Wood, 1972), tunneling is drastically reduced by deuterium substitution. Bushwell _et al_. (1938) and others (Blinc and Hadzi, 1959, and references therein) have suggested that the complex structure of the O-H and O-D stretching bands in the IR spectrum of benzoic acid may be the result of tunneling splitting. However, in this connection, it is important to remember that in crystalline benzoic acid, the unequal C-0 and C=0 bond lengths and the non-planarity of the carboxyl group require motion of the oxygen atoms when the protons change from one configuration to another.

Since the oxygensmove with the hydrogens, deuterium substitution may not cause a large change in the reduced mass. Consequently, deuterium substitution may not lead to a large reduction of tunneling splitting. And indeed, the large reduced mass that results when the oxgyens are required to move may lead to a very slow tunneling rate, disallowing the hypothesis of Bushwell et al., at least for crystalline benzoic acid.

When a benzoic acid dimer is present in the crystal, it is not necessarily true that the two possible proton configurations will have the same energy. It is entirely possible for the crystal field to be asymmetric with respect to proton inversion, since the symmetry operations of the space group do not lead to the type of proton inversion that occurs with tunneling. When the two proton configurations are not isoenergetic, an asymmetric double well is formed by the resonance interaction. Initially, the levels of the two single wells are not exactly degenerate. However, the perturbation still causes the levels to spread apart. In this case, tunneling only causes a shift in the already separated levels, and the effect of deuterium substitution is to reduce the magnitude of the shift. This has the effect that the observed changes in the spectrum will appear less drastic than in the symmetrical case, where it is possible in principle, to see two bands coalesce into one upon deuterium substitution.

The possibility that the two configurations of protons may not be isoenergetic in the crystal was first noted by Hayashi and Kimura in 1966. These authors obtained the polarized infrared spectrum between 850 and 1800 cm^{-1}. They observed that some bands were resolved into pairs at low temperatures. For some pairs both members were found to have the same polarization, ruling out the possibility of factor group splitting. More surprising was the fact that as the temperature was lowered, one member of a pair became more intense and the other became less intense. As noted by Hayashi and Kimura, one possible explanation of this phenomenon is that the pair is due to Fermi resonance, with the temperature dependence resulting from changes in the energy difference between the fundamental and combination modes. The magnitude of this difference would be expected to change with temperature if the zero-order frequencies of the fundamental and combination modes possessed different temperature dependences. This possibility has been ruled out in a second paper by Hayshi and Umemura (1974). Their argument is based on a theory of Fermi resonance proposed by Miyazawa (1960) which requires the separation of a Fermi resonance pair to be smallest when the band areas are equal. Hayashi and Umemura find that the separation is smallest at room temperature where the band areas are unequal. Clearly, this argument is only as strong as the theory on which it is based. We have observed in the Raman bands at 79 and 88 cm^{-1} the same phenomena observed by Hayashi in the IR spectrum. In Section II I, we consider in detail the possibility that these phenomena are the result of Fermi resonances.

Hayashi and coworkers explain their observations by postulating the existence of the two configurations of benzoic acid molecules in the crystal. Their measurements show that these configurations are separated by an energy barrier of about 0.1 kcal/mole. According to their hypothesis, some but not all modes have different frequencies in one configuration than in another. This results in the band pairs for some modes. Reducing the temperature reduces the population of the higher energy configuration and increases the population of the other configuration by the same amount. This explains the change in relative intensities of the members of a band pair.

In Hayashi's spectrum the band pairs are associated with carboxylgroup modes and not with ring modes. This suggests that the two configurations differ with regard to carboxyl group atoms. Accordingly, Hayashi and coworkers have suggested that the two configurations correspond to the two possible configurations of protons in a dimer, relative to the crystal field. In this connection it must be remembered the non-planarity of the carboxyl group and the unequal C-0 and C=0 bond lengths require both in- and out-of-plane displacements of the oxygen atoms when the protons change from one configuration to another.

It is important to realize that the "hot bands" observed by Hayashi and coworkers are not the usual type of hot band. Normally, hot bands correspond to the transitions from an excited vibrational state. Reducing the temperature reduces the population of molecules in excited vibrational states so that transitions from these states are correspondingly reduced in intensity. The number of molecules in the zeroth vibrational state increases as the temperature is lowered and transitions from this level are increased accordingly. When this type of hot band is involved, lowering the temperature causes the disappearance of some bands and a more or less uniform increase in all of the other bands. The marked increase in a few bands and no others as the temperature is lowered cannot occur with this type of hot band.

In the case of Hayashi's model, however, such changes can occur. Let us consider for simplicity the case where the configuration splitting vanishes for all modes except one and where its magnitude is such that both bands are clearly resolved. Assume that the absolute absorption intensity for any mode is the same in either configuration and is unaffected by temperature. Then, as the temperature is lowered and molecules shift from one configuration to the other, no change in intensity will be observed for those bands that are not split. However, in the resolved pair one band will increase and the other will decrease. It is thus apparent that Hayashi's model is consistent with some bands becoming more intense as the temperature is lowered with most others being relatively unchanged in intensity.

4. Factor Group Splitting

Since the unit cell of the benzoic acid crystal contains two dimers it is necessary to consider the effect of any interaction between these two molecules on the normal modes. As pointed out previously, the space group of the crystal is C_{2h}^5 which consists of the operations E, $C_2(b)$, σ_{ac} , and i. $C_2(b)$ and σ_{ac} interchange sites 1 and 2 as shown previously. Only E and i leave a given site unchanged. This set of operations is a subgroup of the space group and is called the site group. The site group describes the symmetry of the crystal field seen by a given dimer. Since this field perturbs the dimer, the symmetry of a dimer in the crystal can be no higher than C_i. However, when one dimer is coupled to the other dimer in its unit cell, the symmetry of the coupled system must be considered. In particular, we have to consider the symmetry of the unit cell. The symmetry group of the unit cell is called the factor group. In the case of the space group C_{2h}^5, the factor group is C_{2h} (Craig & Walmsley 1968). Since the dimers in the unit cell are coupled, we have to consider the symmetry-adapted normal modes of the unit cell. These modes must belong to representations of the factor group. The representations of the site group C_i are correlated with those of the factor group in Figure 7. Appropriate symmetry groups for a free planar dimer are C_{2h} and D_{2h}. The representations of these groups are also correlated with those of the site group in Figure 7.

In treating the interaction between dimers in the unit cell, we assume what is called the oriented gas model. According to the model, the crystal in the zero order approximation is considered to be an oriented gas of non-interacting molecules. The interaction between the molecules is then included as a perturbation. The use of this model is feasible for so-called molecular crystals. In such crystals, the forces between molecules are small in comparison with the forces associated with covalent bonds. Thus the molecules retain their identity in the crystal and, in particular, the normal modes of the unit cell can be constructed from those of the free molecule.

FIGURE 7

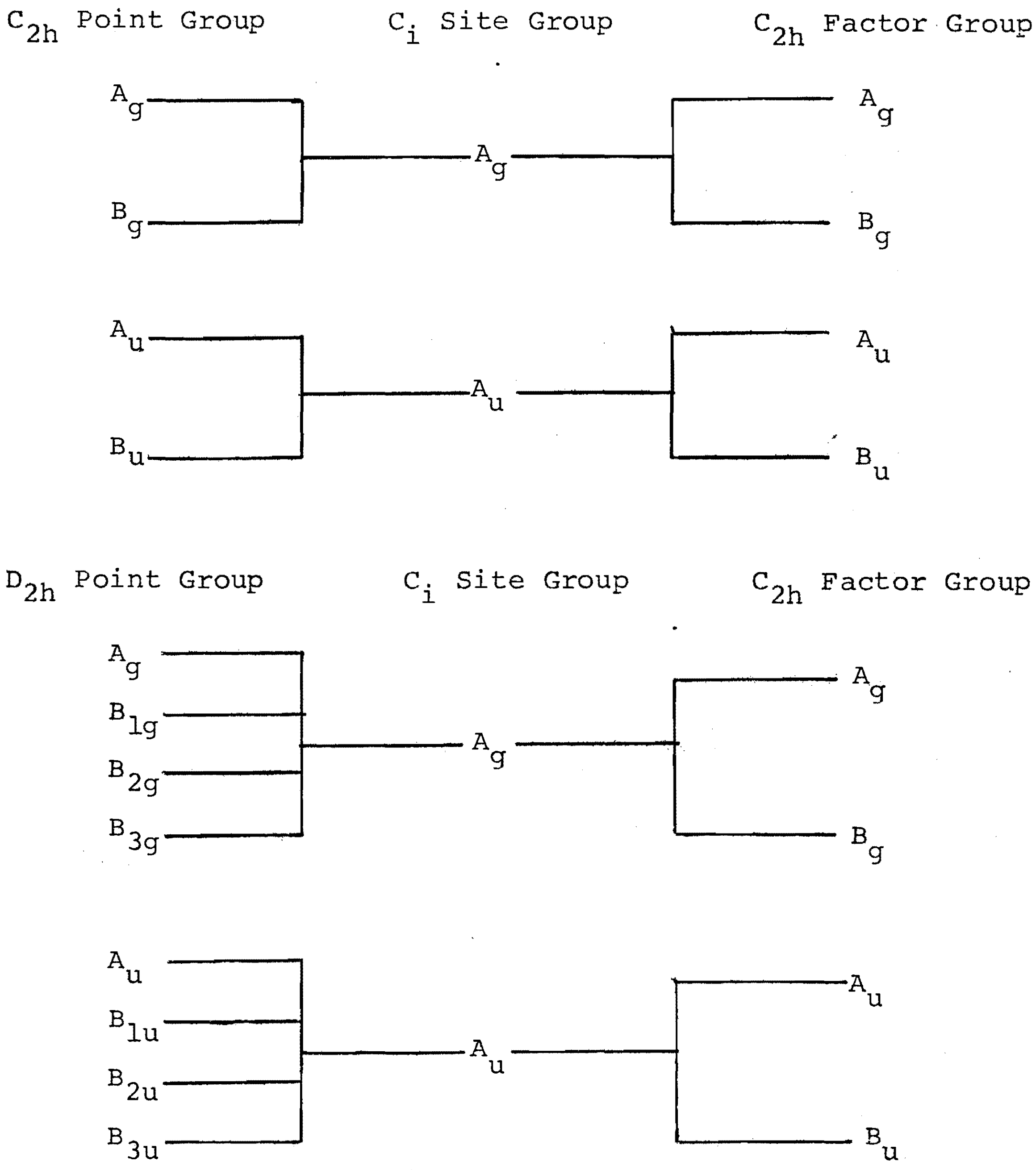

Correlation Diagrams for C_{2h} Factor Group, C_i Site Group and C_{2h} and D_{2h} Point Groups.

In the case of a molecule such as benzene, the oriented gas model is an excellent approximation as all of the bonds in benzene are strong compared to intermolecular forces. In the case of benzoic acid, this model has to be applied with care because the hydrogen bonds of the dimer are weaker than covalent bonds and may be comparable to intermolecular interactions. One consequence of this is that the lattice modes of the unit cell may have frequencies close to those of the H-bond modes, leading to mixing of lattice and H-bond modes of the same symmetry. This type of mixing yields modes which do not resemble those of the free dimer and in this case, the molecule would lose part of its identity when placed in the crystal.

The symmetry-adapted unit cell normal coordinates are constructed from the dimer normal coordinates as follows (Hochstrasser 1966, p. 303):

$$S(A_g) = 1/\sqrt{2}(Q_1(A_g) + Q_2(A_g)) \quad \text{or} \quad 1/\sqrt{2}(Q_1(B_g) + Q_2(B_g)$$

$$S(Bg) = 1/\sqrt{2}(Q_1(A_g) - Q_2(A_g)) \quad \text{or} \quad 1/\sqrt{2}(Q_1(B_g) - Q_2(B_g)$$

$$S(A_u) = 1/\sqrt{2}(Q_1(A_u) + Q_2(A_u)) \quad \text{or} \quad 1/\sqrt{2}(Q_1(B_u) + Q_2(B_u)$$

$$S(B_u) = 1/\sqrt{2}(Q_1(A_u) - Q_2(A_u)) \quad \text{or} \quad 1/\sqrt{2}(Q_1(B_u) - Q_2(B_u)$$

Thus, the unit cell modes are the in-phase and out-of-phase combinations of the dimer modes.

In addition to the unit cell modes derived from dimer vibrations, there are the unit cell modes derived from the rotations and translations of the dimers in the unit cell, the so-called lattice modes. Since each dimer has three rotational and three translational degrees of freedom, and since for each degree of freedom, an in-phase and an out-of-phase combination is possible, there are six rotational and six translational lattice modes. Three of the translational modes correspond to the in-phase combinations and are called acoustic modes. These modes are optically inactive (Davydov, 1962, page 15). Table 3 shows the character table for the C_{2h}^5 space group and the characters of the reducible representations of the lattice modes. Decomposing the characters of these representations, we find that $\Gamma(T) = 3A_u + 3B_u$ and $\Gamma(T_a) = A_u + 2B_u$. Hence, $\Gamma(T_o) = 2A_g + B_g$. For the rotational lattice modes we have $\Gamma(R) = 3A_g + 3B_g$. The six rotational lattice modes are Raman active and the three optically active translational modes are IR active.

When the factor group components of a mode are clearly resolved, measurement of the polarization properties is a clear-cut procedure. If the components are not resolved, then the stronger of the two components is expected to determine the qualitative polarization properties of the composite band.

TABLE 3

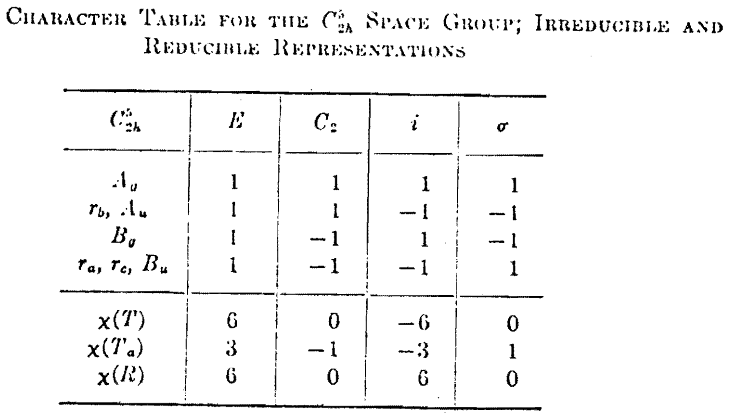

CHARACTER TABLE FOR THE C_{2h}^5 SPACE GROUP; IRREDUCIBLE AND REDUCIBLE REPRESENTATIONS

C_{2h}^5	E	C_2	i	σ
A_g	1	1	1	1
r_b, A_u	1	1	−1	−1
B_g	1	−1	1	−1
r_a, r_c, B_u	1	−1	−1	1
$\chi(T)$	6	0	−6	0
$\chi(T_a)$	3	−1	−3	1
$\chi(R)$	6	0	6	0

"T" denotes a translational lattice mode.

"T_a" denotes an acoustic translational lattice mode.

"T_O" (see text) denotes an optically active translational lattice mode.

Character table for the C_{2h}^5 space group (Taken from Davydov, 1962).

Because of the low site symmetry, each A-type and B-type dimer mode is correlated with both an A-type and a B-type factor group mode (see figure 7). However, in favorable cases, a knowledge of the intensity ratio of a factor group pair enables one to determine whether the corresponding dimer mode has A or B symmetry properties.

We first consider IR active vibrations. In order for a vibration to be IR active, the dipole moment must change as a result of the vibration. This change in dipole moment may be referred to as the vibration induced dipole moment, $\vec{e}$. The absolute intensity of an IR active mode for a free molecule is proportional to $\vec{e} \cdot \vec{e}$ (Herzberg 1945, p. 240). Let us suppose that the magnitude and direction of $\vec{e}$ relative to the dimer axes is known for the free molecule. In a unit cell mode we will have $\vec{e}_1$ for the molecule at site 1 and $\vec{e}_2$ for the molecule at site 2. Both $\vec{e}_1$ and $\vec{e}_2$ are identical relative to the respective sets of molecular axes. Davydov (1962, p. 21) has shown that in the context of the oriented gas model, the IR intensity of a unit cell mode is also proportional to $\vec{e} \cdot \vec{e}$, where $\vec{e}$ is equal to the sum of the free molecule dipole moments for the A_u mode and the difference for the B_u mode.

Since experimental measurements are made relative to the a, b, and c' axes of the crystal, it is necessary to express the vectors in terms of these axes. The available experimental data only deals with the case where the $\vec{E}$ vector of the light wave is parallel to the a-axis or the b-axis. Consequently, we calculate only $I(\omega_1)_b/I(\omega_2)_a$, where ω_1 is the frequency associated with the A_u mode and ω_2 with the B_u mode. $I(\omega_1)_b$ is the intensity of the A_u mode when the $\vec{E}$ vector is parallel to the b axis. Similarly, for $I(\omega_2)_a$. Also we consider only three directions of the dipole moment vector: $\vec{e}//\vec{x}$, $\vec{e}//\vec{y}$, and $\vec{e}//\vec{z}$, where $\vec{x}$, $\vec{y}$, and $\vec{z}$ are unit vectors along the axes of a dimer, and for simplicity, we assume that $\vec{e}$ is a unit vector. Using the direction cosines in Table 1, we calculate the following relationships: $\vec{e}//\vec{x}$:

$$(e_{x1} + e_{x2})_a = a_x - a_x = 0$$

$$(e_{x1} + e_{x2})_b = b_x + b_x = 2b_x$$

$$(e_{x1} + e_{x2})_{c'} = c'_x - c'_x = 0$$

$$(e_{x1} - e_{x2})_a = a_x + a_x = 2a_x$$

$$(e_{x1} - e_{x2})_b = b_x - b_x = 0$$

$$(e_{x1} - e_{x2})_{c'} = c'_x + c'_x = 2c'_x$$

Thus, $I(\omega_1)_b/I(\omega_2)_a = b_x^2/a_x^2 = (0.6546)^2/(0.5276)^2 = 1.5$ for $\vec{e}//\vec{x}$. Proceeding in exactly the same manner, we find that for $\vec{e}//\vec{y}$: $I(\omega_1)_b/I(\omega_2)_a = b_y^2/a_y^2 = (0.2366)^2/(0.8236)^2 = 0.1$, and for $\vec{e}//\vec{z}$: $I(\omega_1)_b/I(\omega_2)_a = b_z^2/a_z^2 =$

$(0.7189)^2/0.2118)^2 = 11.8$. Summarizing, we have: $\vec{e}//\vec{x}$ yields $A_u(b) > B_u(a)$; $\vec{e}//\vec{y}$ yields $B_u(a) >> A_u(b)$; and $\vec{e}//\vec{z}$ yields $A_u(b) >> B_u(a)$. We have expressed these results in terms of inequalties because experimental measurements are not expected to be highly accurate. Such factors as imperfect orientation and inhomogeneity of the crystal, imperfect polarization of the light, and unresolved bands having different polarization properties are some of the frequent sources of error in polarization measurements. Also, the direction cosines used in our calculations are determined from room temperature x-ray diffraction measurements; at 4.2° K, their values may be different.

In this treatment we have considered only the cases where $\vec{e}$ is parallel to one of the molecular axes. The reason for this is that only symmetry considerations are available for determining the direction of $\vec{e}$ for a given mode. In order for symmetry considerations to be useful, the symmetry has to be high enough that $\vec{e}$ is required to be accurately parallel to one of the molecular axes. For example, if the symmetry of the dimer is D_{2h}, it is a simple matter to determine the representation to which a mode belongs and then determine the polarization of the IR transition from the group theory table. For C_{2h} symmetry, the direction of $\vec{e}$ can be determined from an inspection of the displacement patterns, and as long as a $c_2(x)$ axis is present $\vec{e}$ will be parallel to one of the axes. In the case of C_i symmetry, it is not possible to use symmetry considerations to determine the direction of $\vec{e}$. As discussed in Section II C, the lowering of the dimer symmetry to C_i is caused by the deviation of the carboxyl group from the plane containing the benzene rings. Modes involving the oxygen atoms, such as the carbonyl stretch are likely to feel C_i symmetry. Since the plane containing the carboxyl group is inclined relative to the plane of the benzene rings, we expect the carbonyl stretch mode to generate a change in dipole moment that has an in-plane as well as an out-of-plane component, relative to the plane of the benzene rings. Since the relative magnitudes of these components cannot be determined, even qualitative polarization properties for this mode cannot be predicted. It is interesting to note that the polarization ratios for modes involving carboxyl group motion should be temperature dependent, since the inclination of the carboxyl group should change with temperature. This change should still be apparent after using temperature-corrected direction cosines. Modes not involving carboxyl group atoms should show constant polarization ratios when temperature-corrected direction cosines are used.

Since the H-bonding protons are in the region between the two inclined planes, it follows that their deviation from the plane of the benzene rings may be quite small and in any case smaller than the deviations of the oxygen atoms. Thus, a mode which has large amplitude at the hydrogen atoms and small amplitude at the oxygen atoms may feel C_{2h} symmetry. Such a mode would be the out-of-plane hydroxyl hydrogen wag. Benzene modes which have no amplitude at the 1 and 4 positions are expected to lead to benzene analogues which have little displacement at carboxyl group atoms. Hence these modes are expected to feel D_{2h} symmetry, allowing clear cut predictions of the relative intensities of the factor group components.

We now attempt to calculate the relative intensities of Raman active factor group components. In the free molecule, the intensity of a Raman active mode depends on the squares of the partial derivatives of the components of the polarizability tensor, where the partial derivatives are with respect to the normal coordinate in question. The tensor consisting of the partial derivatives of the polarizability can be referred to as the Raman tensor. Thus if $\vec{P}$ denotes the dipole moment induced by an external electric field $\vec{E}$ we have:

$$P_x = \alpha'_{xx}E_x + \alpha'_{xy}E_y + \alpha'_{xz}E_z$$

$$P_y = \alpha'_{yx}E_x + \alpha'_{yy}E_y + \alpha'_{yz}E_z$$

$$P_z = \alpha'_{zx}E_x + \alpha'_{zy}E_y + \alpha'_{zz}E_z$$

The Raman tensor α is given by:

$$\alpha = \begin{matrix} \partial\alpha'_{xx}/\partial Q & \partial\alpha'_{xy}/\partial Q & \partial\alpha'_{xz}/\partial Q \\ \partial\alpha'_{yx}/\partial Q & \partial\alpha'_{yy}/\partial Q & \partial\alpha'_{yz}/\partial Q \\ \partial\alpha'_{zx}/\partial Q & \partial\alpha'_{zy}/\partial Q & \partial\alpha'_{zz}/\partial Q \end{matrix}$$

The derivation that is presented here for benzoic acid is an adaptation of that given for napthalene and anthracene by Suzuki, <u>et</u> <u>al</u>., (1968). In the context of the oriented gas model, we assume that the polarizability of the unit cell is the sum of the free molecule polarizabilities of the two molecules in the unit cell: $\alpha'_{uc} = \alpha'_1 + \alpha'_2$. We write $\Delta\alpha'_{uc} = \alpha'_{uc}(Q_1,Q_2) - \alpha'_{uc}(0,00$, where Q_i is a normal coordinate of the molecule at site 1 and Q_2 is the corresponding coordinate for the molecule at site 2. $\Delta\alpha'_{uc}$ is approximately given by $\Delta\alpha'_{uc} = (\partial\alpha'_1/\partial Q_1)_0 Q_1 + (\partial\alpha'_2/\partial Q_2)_0 Q_2$. The components of the free molecule polarizability tensor have to be determined relative to the crystal axes, since experimental measurements are made in this reference frame. Relative to the a, b, c' reference frame, the free molecule Raman tensors are given by $T_1(\partial\alpha'_1/\partial Q_1)T_1^+$ and $T_2(\partial\alpha'/\partial Q_2)T_2^+$, where T_1 and T_2 are the matrices of direction cosines for the two sites of the unit cell. Further, since the observed bands in the Raman spectra correspond to unit cell normal modes, we need to express Q_1 and Q_2 in terms of the symmetry-adapted coordinates of the unit cell. As shown previously, $S(Ag) = 1/\sqrt{2}(Q_1+Q_2)$ and $S(B_g) = 1/\sqrt{2}(Q_1-Q_2)$. These equations can be rearranged to give $Q_1 = 1/\sqrt{2}(S(A_g) + S(B_g))$ and $Q_2 = 1/\sqrt{2}(S(A_g) - S(B_g))$ Substituting we obtain

$$\Delta\alpha'_{uc}=[(T_1\alpha_1T_1^\dagger+T_2\alpha_2T_2^\dagger)S(A_g) + (T_1\alpha_1T_1^\dagger-T_2\alpha_2T_2^\dagger)S(B_g)]1/\sqrt{2}.$$

Approximating $\alpha_{uc}(A_g)$ by

$\Delta\alpha'_{uc}/S(A_g)$ and $\alpha_{uc}(B_g)$ by $\Delta\alpha'_{uc}/S(B_g)$,

we obtain

$$\alpha_{uc}(A_g) = 1/\sqrt{2}[T_1\alpha_1T_1^\dagger+T_2\alpha_2T_2^\dagger] \text{ and}$$

$$\alpha_{uc}(B_g) = 1/\sqrt{2}[T_1\alpha_1T_1^\dagger-T_2\alpha_2T_2^\dagger].$$

When the matrices are multiplied out and combined we obtain:

$$\alpha_{uc}(A_g) = \begin{matrix} A_{aa} & 0 & A_{ac} \\ 0 & A_{bb} & 0 \\ A_{ac} & 0 & A_{cc} \end{matrix}$$

$$\alpha_{uc}(Bg) = \begin{matrix} 0 & A_{ab} & 0 \\ A_{ab} & 0 & A_{bc} \\ 0 & A_{bc} & 0 \end{matrix}$$

The components of these tensors have to be evaluated for each representation of the point group to which the dimer belongs. Table 4 shows the components for the D_{2h} point group. Most notable is the fact that the factor group intensity ratios for unit cell modes derived from non-totally symmetric dimer modes depend only on the direction cosines. For a molecule possessing C_{2h} symmetry, a B_g dimer mode leads to

$$A_{ab} = (c_z b_x + c_x b_z)\alpha_{zx} + (a_y b_x + a_x b_y)\alpha_{yx}$$

and $$A_{bc} = (c_z b_x + c_x b_z)\alpha_{zx} + (c_y b_x + c_x b_y)\alpha_{yx}.$$

Since the tensor components cannot be factored out, the factor group intensity ratio cannot be expressed in a way that depends only on the direction cosines, as was possible for D_{2h} symmetry.

E. Varsanyi Tables

Of great value in this normal coordinate analysis has been a recently published book by G. Varsanyi (1969) entitled Vibrational Spectra of Substituted Benzenes. Varsanyi has carefully considered and summarized results of the very large number of experimental and theoretical studies of the vibrational spectra of substituted benzenes. As a result others have been spared of this onerous and time consuming task. His summary takes the form of tables which show the expected frequency ranges of the benzene

TABLE 4

Elements of the derived polarizability tensors of naphthalene and anthracene crystals

		b_{1g}	b_{2g}	b_{3g}
A_g	A_{aa}	$2a_ua_w\alpha'_{uw}$	$2a_va_w\alpha'_{vw}$	$2a_ua_v\alpha'_{uv}$
	A_{bb}	$2b_ub_w\alpha'_{uw}$	$2b_vb_w\alpha'_{vw}$	$2b_ub_v\alpha'_{uv}$
	A_{cc}	$2c_uc_w\alpha'_{uw}$	$2c_vc_w\alpha'_{vw}$	$2c_uc_v\alpha'_{uv}$
	A_{ac}	$(a_uc_w + a_wc_u)\alpha'_{uw}$	$(a_vc_w + a_wc_v)\alpha'_{vw}$	$(a_uc_v + a_vc_u)\alpha'_{uv}$
B_g	A_{ab}	$(a_ub_w + a_wb_u)\alpha'_{uw}$	$(a_vb_w + a_wb_v)\alpha'_{vw}$	$(a_ub_v + a_vb_u)\alpha'_{uv}$
	A_{bc}	$(b_uc_w + b_wc_u)\alpha'_{uw}$	$(b_vc_w + b_wc_v)\alpha'_{vw}$	$(b_uc_v + b_vc_u)\alpha'_{uv}$

		a_g
A_g	A_{aa}	$a_u{}^2\alpha'_{uu} + a_v{}^2\alpha'_{vv} + a_w{}^2\alpha_{ww}$
	A_{bb}	$b_u{}^2\alpha'_{uu} + b_v{}^2\alpha'_{vv} + b_w{}^2\alpha'_{ww}$
	A_{cc}	$c_u{}^2\alpha'_{uu} + c_v{}^2\alpha'_{vv} + c_w{}^2\alpha'_{ww}$
	A_{ac}	$a_uc_u\alpha'_{uu} + a_vc_v\alpha'_{vv} + a_wc_w\alpha'_{ww}$
B_g	A_{ab}	$a_ub_u\alpha'_{uu} + a_vb_v\alpha'_{vv} + a_wb_w\alpha'_{ww}$
	A_{bc}	$b_uc_u\alpha'_{uu} + b_vc_v\alpha'_{vv} + b_wc_w\alpha'_{ww}$

Derived polarizability tensors for modes belonging to representations of the D_{2h} point group (Taken from Suzuki _et_ _al_., 1968).

analogues for various classes of substitutents. Since these ranges are based upon a particular set of molecules, it is always possible that the ranges will have to be enlarged as this set is enlarged. Consequently, we have not been surprised to find several modes which are slightly outside of the Varsanyi ranges. However, we have assumed, somewhat arbitrarily, that the sequence of modes predicted by the Varsanyi ranges is correct. While we have been able to make a consistent set of assignments that is in full agreement with the sequence required by the Varsanyi ranges, it is possible that other sets of assignments using the same criteria could be made which violate the Varsanyi sequence. This possibility has not been systematically investigated. The reader will understand why when he considers that if one has no expected ranges for the modes, then the number of logically possible sets of assignments for the 39 group - theoretically predicted modes of the monomer with 39 observed bands is $39! \sim 10^{18}$. Clearly, the use of the Varsanyi tables results in an enormous simplification.

In order to use the Varsanyi tables, it is necessary to determine if the substituent in question is "heavy" or "light". For Benzoic acid Varsanyi's criteria show that the carboxyl group is "light" for in-plane modes and "heavy" for out-of-plane modes. Table 5 shows the Varsanyi tables for light and heavy mono-substituted benzenes.

TABLE 5

FREQUENCY REGIONS OF DIFFERENT NORMAL VIBRATIONS OF BENZENE DERIVATIVES

Note: For in-plane vibrations "light" substituents are those whose first atom has atomic weight less than 25 except for $-CF_3$ and $-NSO$ which have to be classified as "heavy" substituents.

For out-of-plane vibrations "heavy" are all polyatomic substituents and monoatomic ones having atomic weight above 25. Polyatomic substituents in which free rotation is possible around the bond connecting the first "light" and *non-branching* atom with the ring, have to be considered as "light" substituents.

	monolight	monoheavy	1,4-dilight	1,4-diheavy	1-light-4-heavy	2,6-dilight	2,6-diheavy
1	620–830	1060–1100	720–860	1040–1100	1050–1100	650–750	1050–1140
2	3030–3070	3030–3070	3050–3085	3050–3085	3050–3085	3050–3095	3050–3080
3	1270–1331	1253–1275	1260–1313	1260–1310	1260–1310	1262–1297	1262–1297
4	680–700	680–700	665–735	680–730	665–735	675–700	675–700
5	970–1000	970–1000	240–380	910–970	910–970	930–990	930–1000
6a	300–530	650–710	330–510	680–810	720–840	450–550	640–710
6b	605–630	605–630	610–650	610–650	610–650	350–520	700–800
7a	3000–3060	260–420	1100–1270	150–330	240–400	3000–3050	250–400
7b	3030–3080	3000–3060	3030–3050	3030–3050	3030–3050	760–960	280–430
8a	1575–1614	1575–1614	1570–1628	1570–1628	1570–1628	1561–1608	1561–1608
8b	1562–1597	1562–1597	1552–1605	1552–1605	1552–1605	1591–1625	1591–1625
9a	1170–1181	1170–1181	1142–1190	1156–1190	1156–1190	230–360	140–200
9b	200–410	160–300	260–490	250–350	260–490	1145–1175	1145–1175
10a	810–850	810–860	800–840	790–850	790–850	860–920	190–220
10b	880–910	140–200	890–940	240–300	240–340	840–880	120–180
11	720–760	720–830	810–840	80–170	80–170	760–790	760–850
12	990–1010	990–1010	680–760	1060–1100	481–680	990–1010	990–1010
13	1100–1280	3020–3040	1100–1320	3050–3090	1100–1300	1120–1300	3000–3050
14	1300–1350	1300–1350	1240–1380	1240–1330	1240–1380	1250–1350	1250–1350
15	1150–1160	1150–1160	190–350	150–230	150–230	300–480	260–370
16a	390–420	390–420	380–420	380–420	380–420	460–600	460–600
16b	430–560	430–560	410–550	410–550	410–550	400–490	400–490
17a	940–980	940–980	940–980	930–990	930–990	220–280	890–950
17b	140–250	880–940	150–220	790–890	790–890	160–240	840–900
18a	1018–1030	1018–1030	1004–1022	1003–1022	1004–1022	1061–1091	1061–1091
18b	1065–1082	1065–1082	1085–1128	1100–1128	1100–1123	1082–1123	1082–1109
19a	1470–1515	1470–1515	1460–1530	1460–1530	1460–1530	1386–1467	1386–1467
19b	1440–1470	1440–1470	1370–1470	1370–1470	1370–1470	1460–1500	1460–1500
20a	3070–3110	3070–3110	3050–3090	360–550	3050–3090	3060–3120	3060–3120
20b	3020–3080	3020–3080	3020–3120	3020–3120	3020–3120	3030–3095	3030–3095

(Taken from Varsanyi, 1969).

F. Experimental Procedures

1. Synthesis of Isotopically Substituted Benzoic Acids

The synthesis of benzoic acid $4d_1$ is described in Section IIIB. Benzoic acid d_5 was obtained from Merck Sharpe & Dohme.

Benzoic acid $1d_1$ was prepared by dissolving zone refined benzoic acid in a large excess of MeOD (Diaprep, 99%), and then evaporating the methanol. To prevent contamination from moisture in the air, all manipulations were carried out in a dry box or else in a sealed glass sublimator. The dry box was purged with nitrogen gas that was dried by passage through a fresh P_2O_5 column. The nitrogen atmosphere in the box was stirred by a small fan, and several large evaporating dishes containing fresh P_2O_5 were placed in the box to aid in maintaining a moisture-free atmosphere.

The solution of benzoic acid in MeOD (240 mg in 20 ml) was prepared in the dry box and added to a Kontes Bantam sublimator which was modified so that the cold-finger functioned as an inlet for N_2 gas. The N_2 inlet (previously water inlet for cold-finger) and the vacuum port were fitted with teflon stopcocks. After the methanol solution was added to the sublimator, the teflon stopcocks were closed and the unit was removed from the dry box and attached to a source of dry N_2 gas. The passage of N_2 gas through the sublimator evaporated the methanol in a reasonable period of time. D_2O was not used because of difficulties in evaporation. After evaporation, the stopcocks were closed and the unit was put back into the dry box. An additional 20 ml of MeOD was added and the evaporation step was repeated. The modified cold-finger was then replaced with a standard cold-finger and the unit was removed from the dry box and attached to a vacuum system. After sublimation was complete the vacuum port stopcock was closed and the unit was put back into the dry box. The interior of the sublimator was brought up to atmospheric pressure by opening the stopcock inside of the dry box.

2. Purification Procedures

All compounds except benzoic acid $1d_1$ were extensively zone refined as described in Section IIIB. Benzoic acid $1d_1$ was purified by sublimation as described above. The zone refined compounds were found to be of sufficient purity for phosphorescence work. Also, these compounds were free of fluorescent impurities to the extent that fluorescence was essentially undetectable under the normal conditions of Raman spectrocopy (*vide infra*). The $1d_1$ material was found to exhibit slight fluorescence under these conditions. These impurities were presumably picked up from the methanol used for deuterium exchange. In this regard, D_2O would be superior to MeOD since it would likely contain fewer fluorescent impurities.

3. Isotopic Purity

Because of the high resolution and large signal-to-noise ratio characteristic of the Raman spectra obtained in this study, it is necessary to consider the isotopic purity of the samples carefully. The isotopic purity of the d_5 compound was 99% as shown by mass spectroscopy. The remaining 1% was composed of d_4 , d_3 , d_2 , d_1 and d_o, most of it being d_4 and very little being d_o. The purity of the $4d_1$ compound was found to be 98.5% by mass spectroscopy, and the Raman data confirms this measurement. The purity of the $1d_1$ samples could not be readily determined by mass spectroscopy since these compounds cannot be handled in room air. The $1d_1$ Raman spectrum shows that the d_o impurity is about 3%. Naturally, in the crystal the d_o molecules are almost all present as partsof mixed d_0-$1d_1$ dimers.

We must also be concerned with the natural abundances of C^{13} and O^{18}. The natural abundance of C^{13} is 1.11%. For O^{18} it is 0.2% and for O^{17}, 0.04%. The probability that a molecule having 7 carbons will have at least one C^{13} atom is 7.77%. This fact is readily revealed in the mass spectrum of benzoic acid. The probability that a given molecule will have two C^{13} atoms is $(.0777)^2$, etc. Since the shift caused by a C^{13} atom is one position may be the same as that caused by a C^{13} atom in another position, the C^{13} bands can have appreciable intensities, provided that they are resolved. According to Herzberg (1945, p. 368) shifts as large as 10 cm^{-1} have been observed for benzene skeletal deformations. Smaller shifts are expected for other types of ring modes. In the section on assignments we will present evidence that some bands are definitely due to the pressure of C^{13} atoms. In other cases, it will not be possible to distinguish between factor group components and C^{13} side bands because polarization data is not available. Shifts due to O^{18} have not been identified as there is no way of distinguishing them from C^{13} shifts. We feel that those bands which are suspected to be the result of isotopic impurity are most likely due to C^{13}, since this atom is more than 25 times as abundant as O^{18}.

4. Sample Preparation

Raman samples were pressed pellets of 100% benzoic acid. These pellets were prepared with a standard die and press normally used for KBr pellets. The pressure was 12,000 pounds per square inch. Pressed and unpressed benzoic acid samples gave the same spectrum at room temperature. For benzoic acid ld_1 the sample was transferred from the sublimator to the pellet die in the dry box. After the die was sealed, it was removed from the dry box and the pellet was pressed. The pellet was then removed from the die and transferred to the liquid helium dewar in the dry box. The dewar was sealed and removed from the dry box. After it was set up in the Raman spectrometer, it was unsealed and quickly (about 3 seconds) attached to the vacuum system, which was immediately turned on in order to prevent exposure of the sample to room air.

Infrared samples were prepared by mixing benzoic acid with KBr in an agate mortar and pestle. Pellets were prepared with a standard die and press using a pressure of 12,000 pounds per square inch. The concentration of benzoic acid in KBr was about 0.2% in most cases. For benzoic acid $1d_1$, the benzoic acid powder and KBr were mixed in the dry box. The quantity of benzoic acid added to the KBr was estimated by eye rather than weighed. The remainder of the procedure was identical to that used for Raman $1d_1$ samples.

5. Instrumentation

Raman spectra were obtained with a Carey Model 82 Raman spectrometer. This instrument, which is undoubtedly a state-of-the-art design, uses a triple monochromator, which eliminates Rayleigh light to the point that one can easily obtain Raman spectra to within 5-7 cm^{-1} of the laser line using powdered samples. The sensitivity of the instrument allowed the determination of benzoic acid spectra having a high signal-to-noise ratio with spectral bandwidths as small as 0.5 cm^{-1}, with a 1 watt argon laser (Coherent Radiation Model 52C).

Normally, the 5145 Å line was used instead of the 4880 Å line because of fewer problems with plasma lines.

Infrared spectra were obtained with a Perkin Elmer Model 225 infrared spectrometer. This instrument, which was intended for research purposes, possesses severe limitations. First, the spectra are given as Percent Transmission rather than in Absorbance, which makes visual interpretation of the spectra difficult. Secondly, the expanded scale readout is such that the total range of the instrument cannot be covered with a single degree of expansion. A more serious problem is that all of the light from the source passes through the sample before it enters the monochromator. This causes sample heating, which is particularly a problem with low temperature spectra. Further, the light from the source is focused in a plane that coincides with the <u>edge</u> of the sample compartment. When using a liquid helium dewar in the sample compartment, the sample cannot be located in the focal plane of the source beam. Consequently, severe vignetting of the beam occurs, greatly reducing the available signal-to-noise ratio.

Another problem was created by the use of KBr pellets instead of single crystals. Because of scattering from the KBr, the 100% baseline intensity decreases as the wavelength decreases. Since the apparent peak height for a given percent transmission decreases as the baseline intensity decreases, it is more difficult to evaluate the spectra. Also, the KBr caused an asymmetric broadending of the bands, the greatest broadening occurring at the low frequency end of a band. Symmetric, gaussian bands are obtained with single crystals, and the baseline change due to scattering appears to be less.

For infrared and Raman spectra at low temperatures, an Air Products Model LT-3-110 Cryotip dewar was used. This dewar is of the cold-finger type that allows the windows to remain at room temperature. For Raman work, the windows were of fused quartz, and for IR work, CsI windows were used. Pressed pellets were used for all experiments. The pellet was inserted into a copper pellet holder. An indium o-ring was used to achieve good thermal contact between the pellet and the holder. The pellet holder was attached to the coldfinger of the dewar. A gold-cobalt thermocouple and a Keithley digital voltmeter were used to monitor the temperature of the coldfinger. Since the energy absorbed due to Raman scattering is extremely small, it is believed that sample temperature and cold-finger temperature were nearly equal in the Raman experiments. For the infrared experiments, sample heating undoubtedly made the sample warmer than the cold-finger. The magnitude of the temperature difference is unknown.

G. Infrared and Raman Spectra

This section contains the infrared and Raman spectra obtained in this study as well as reproductions of some infrared spectra that have appeared in the literature.

The spectra obtained in this study have been transferred by hand onto tracing paper and then reduced with a reduction xerox machine. Since tracing cannot accurately represent the high frequency components of the noise that appear in the spectra, it should be understood that noise has been represented in a stylized manner. Although the Raman chart paper and tracing paper possessed nominally identical grids a small mismatch was sometimes observed. Consequently, accurate frequencies should be sought in the tables rather than the spectra.

The tables accompanying the spectra contain a number of extremely weak bands which are not discussed in the sections on assignments. We have included these bands for the benefit of future studies of combination bands. It should be realized that the weakest of these bands have signal-to-noise ratios that are close to unity and may therefore be noise. Also some bands, which are very broad or asymmetric, may actually consist of a number of superimposed bands that are unresolved.

Since the IR spectra obtained in this study do not exhibit the unusually high resolution and signal-to-noise ratio found in the Raman spectra, expanded scale versions of the IR spectra are not presented. However, frequencies can be read more accurately in the expanded scale spectra; consequently, these spectra were consulted in preparing the tables of IR frequencies. The Raman and IR frequencies are believed to be accurate to within ± 1 to ± 2 cm^{-1}. The best available evidence for this is the fact that bands corresponding to modes expected to show zero dimer splitting agree to within ± 2 cm^{-1}.

For benzoic acid d_o , $4d_1$, and d_5 both high and low sensitivity Raman spectra are presented. In the low sensitivitiy spectra almost all bands are on scale, while in the high sensitivity spectra the gain has been increased by about an order of magnitude in order to reveal very weak bands. The strongest bands are more than a thousand times as intense as the weakest bands observed. A high sensitivity spectrum of benzoic acid $1d_1$ could not be obtained because of fluorescent impurities. The Raman spectra along with corresponding IR spectra are given in Figures 8-18. Figures 19-23 contain previously published IR spectra that are referred to in the sections on assignments. Figure 24 presents selected regions of the Raman spectra of benzoic acid d_o taken at 298° K, 77° K, and 4.2° K.

FIGURE 8

Raman Spectrum of Benzoic Acid d_o

Carey Model 82 Raman Spectrometer

Temperature = 4.2^o K

Spectral Bandwidth = 0.5 cm^{-1}

Scan Rate = 0.25 cm^{-1}/second

Pen Period = 1.0 second

Sensitivity = 1.5×10^4 counts per second full scale

Laser Wavelength = 5145 Å

Laser Power = 740 milliwatts

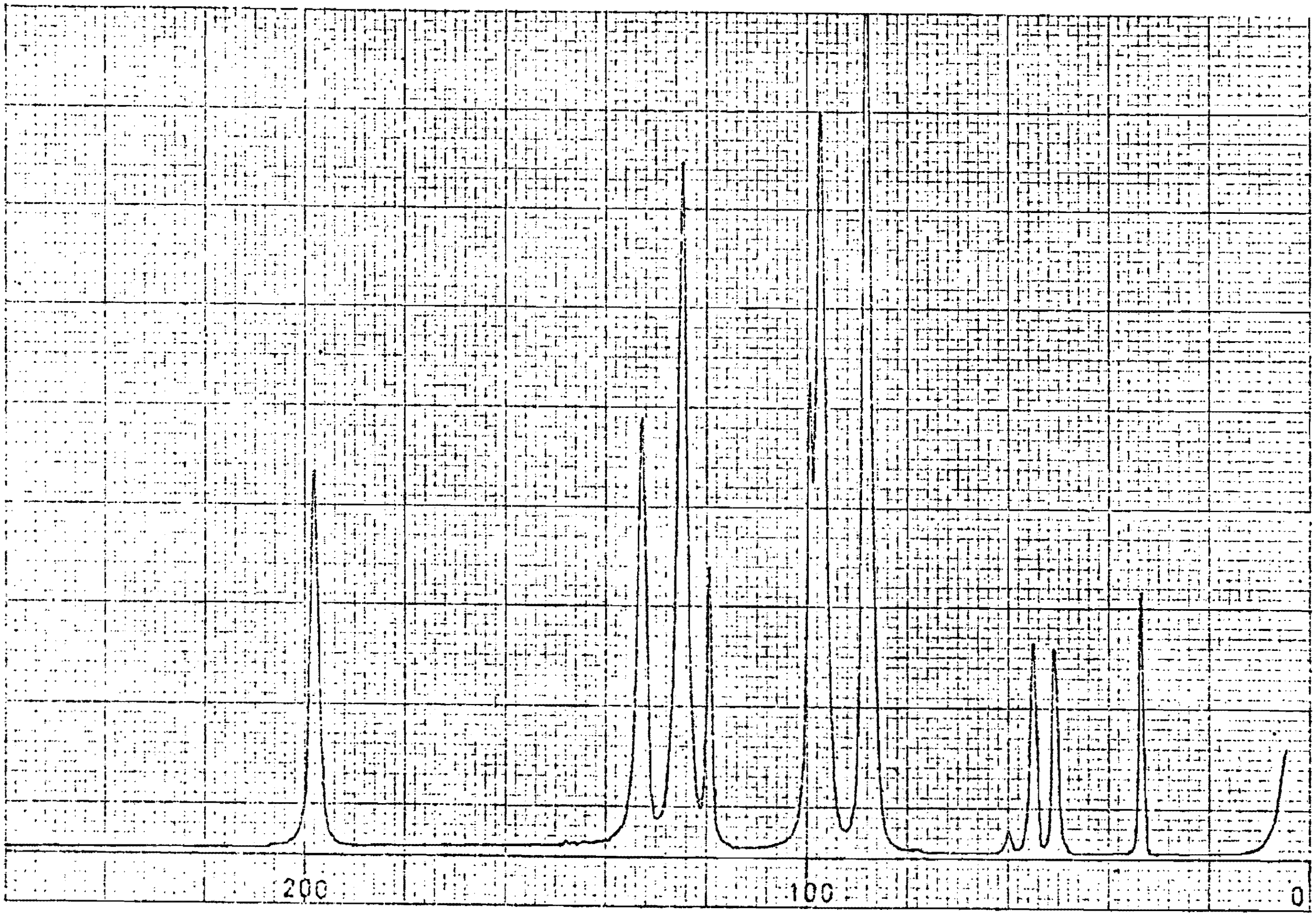
200
100
0

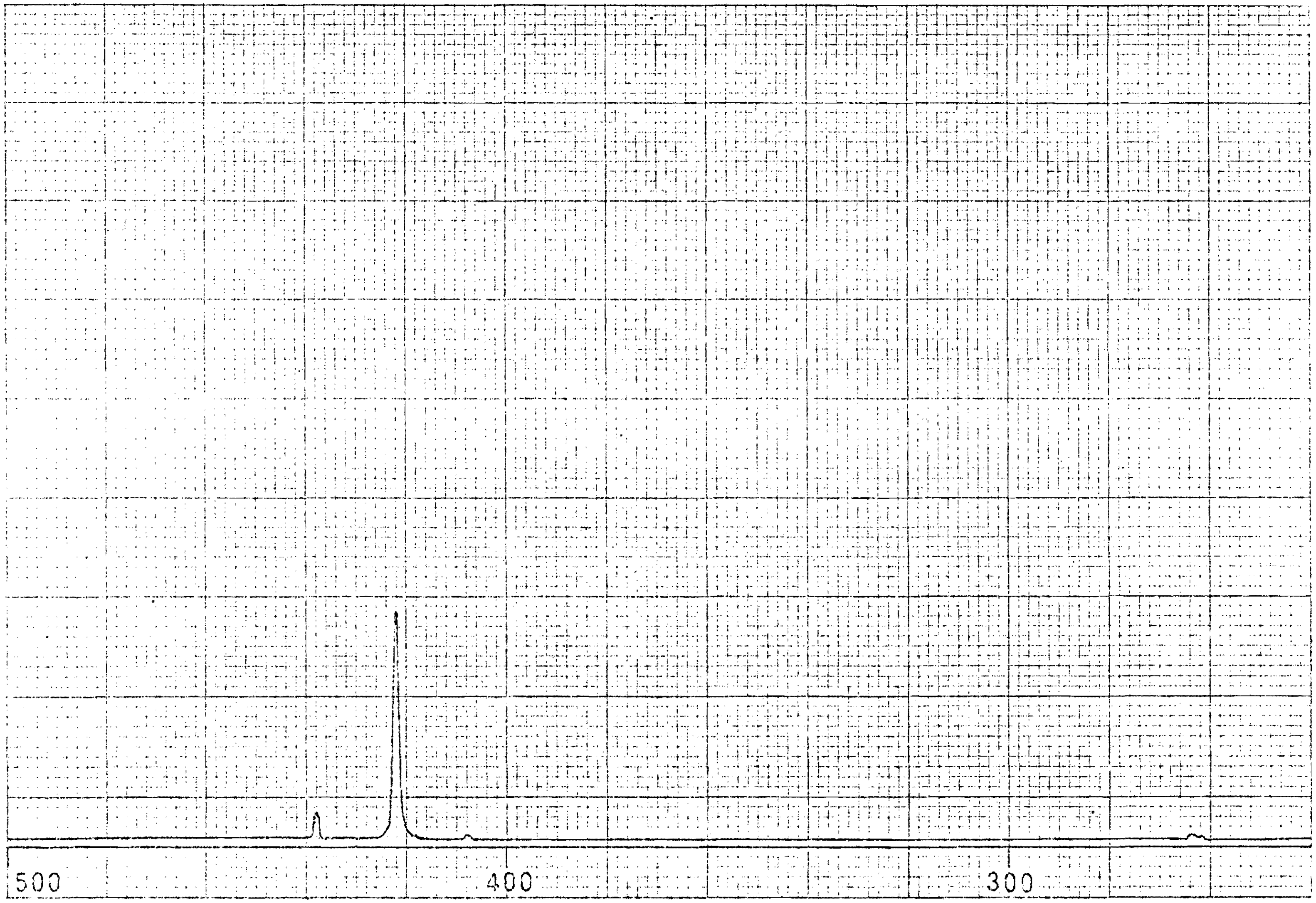
500
400
300

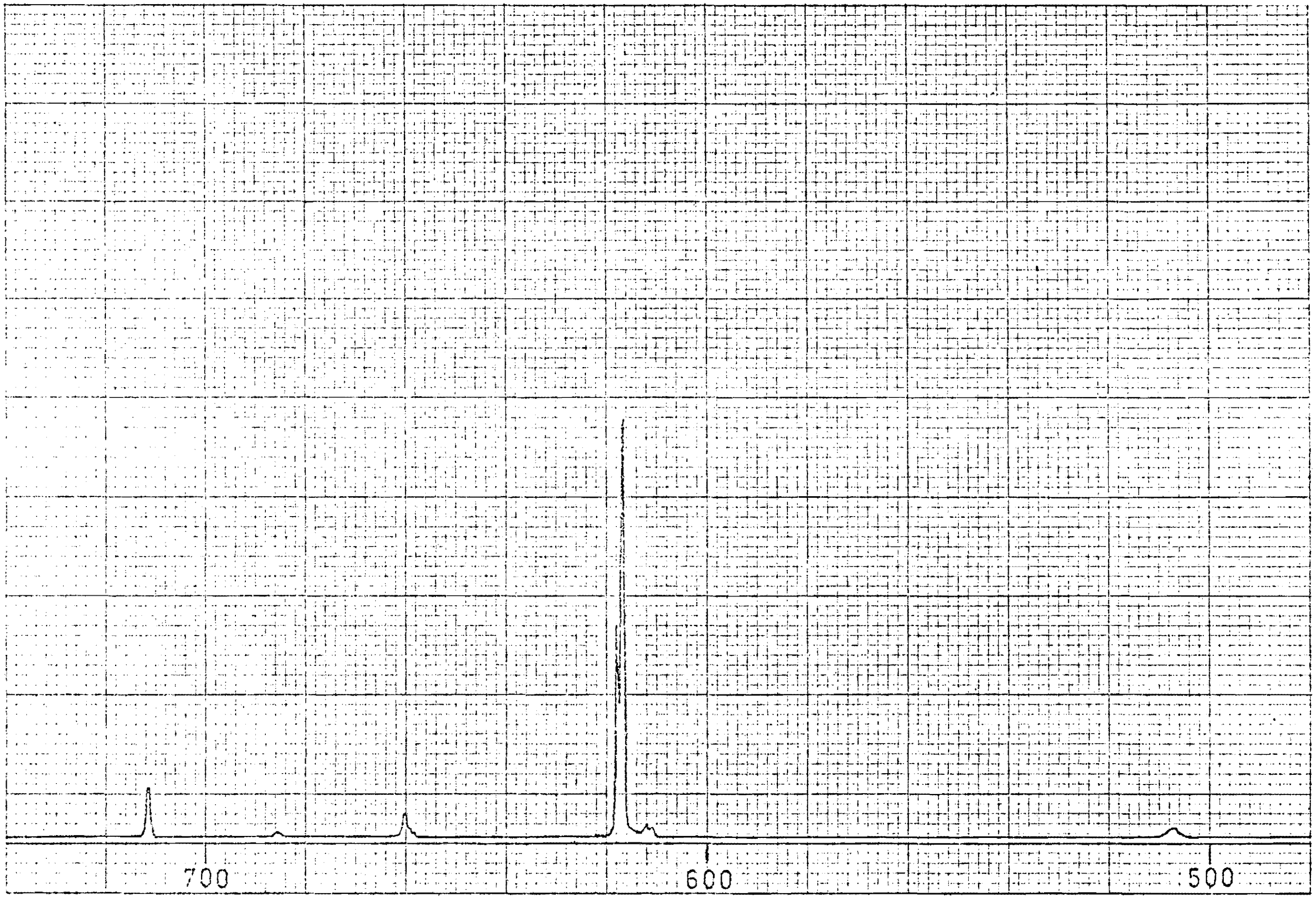
700
600
500

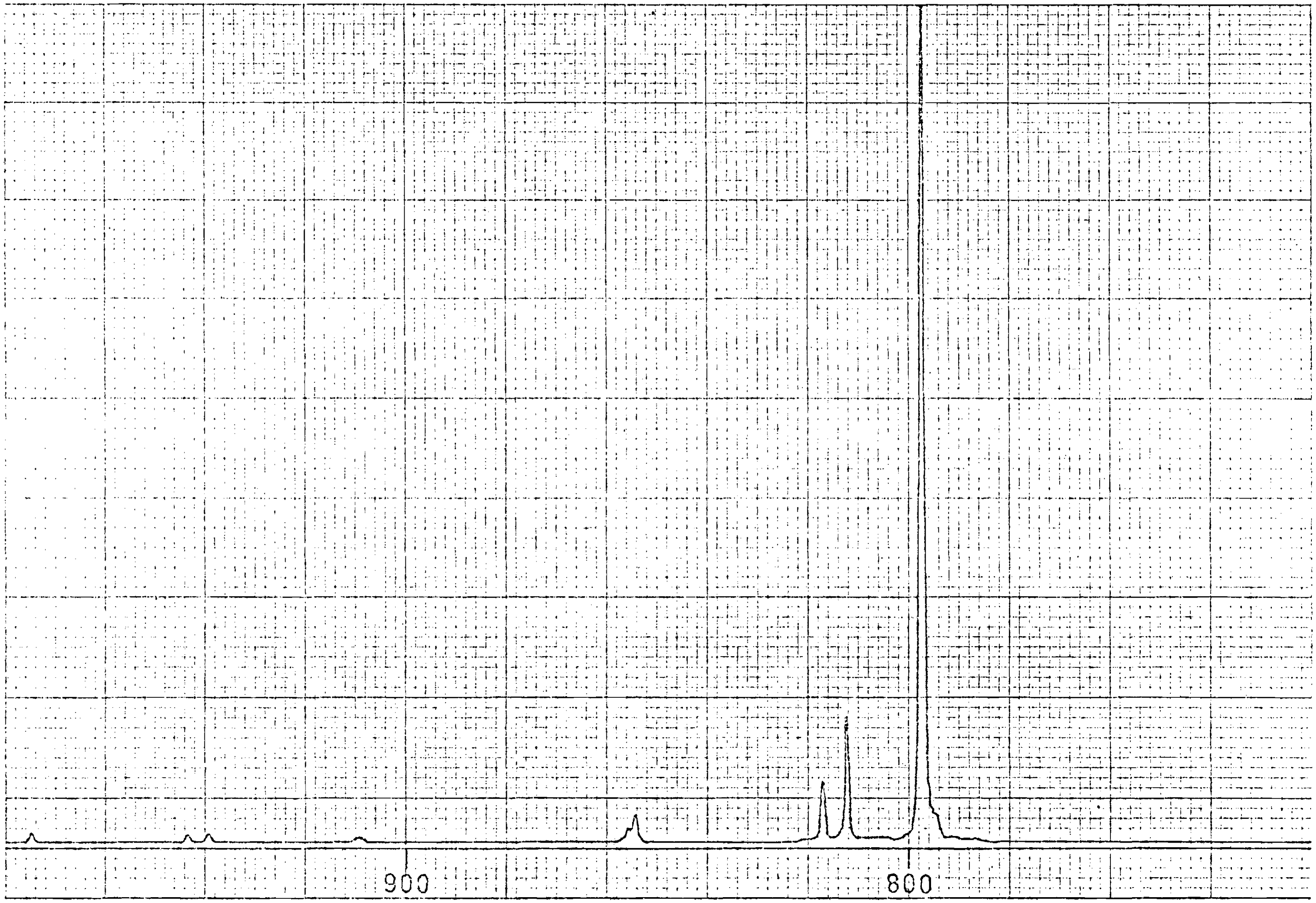
900
800

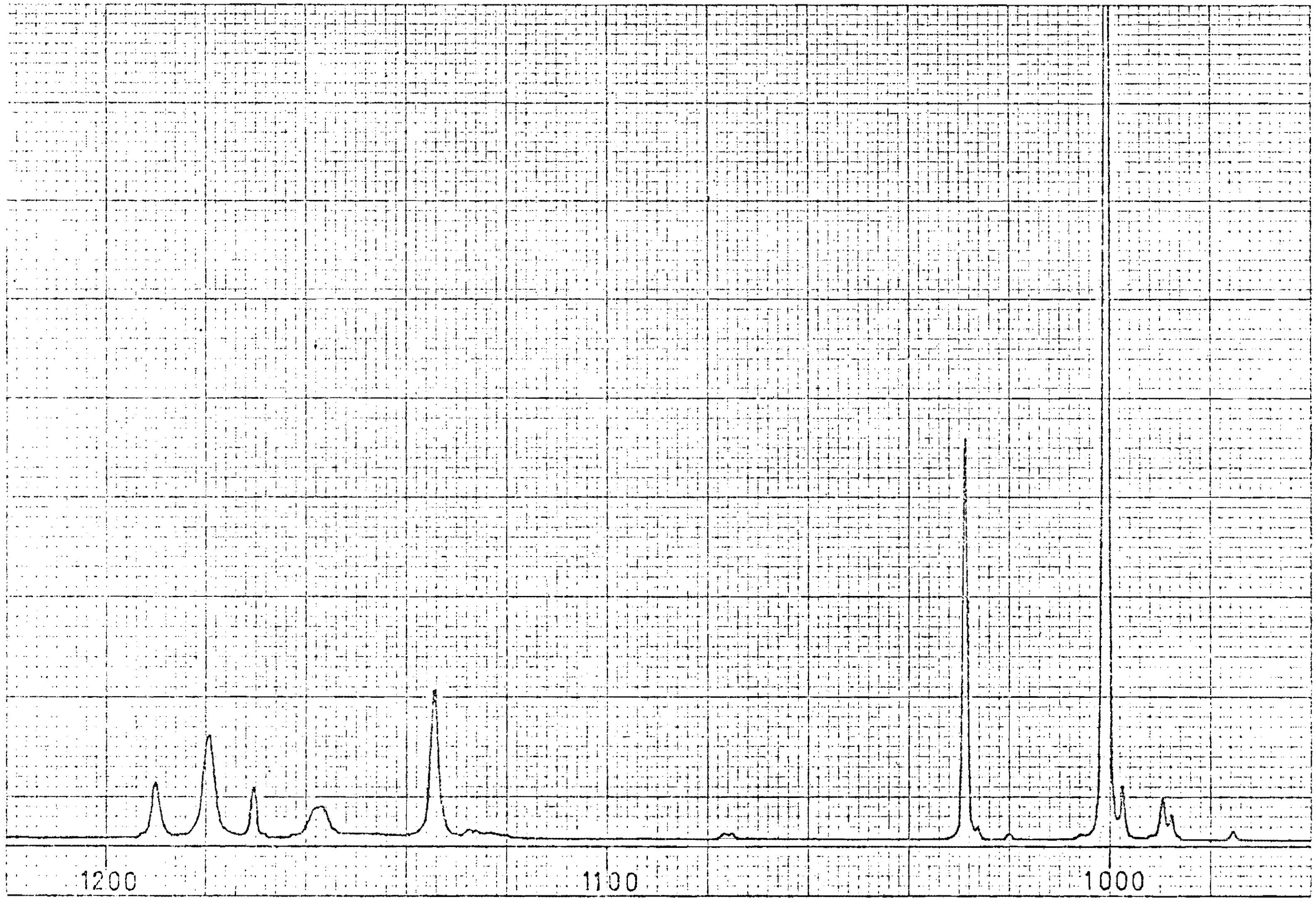
1200
1100
1000

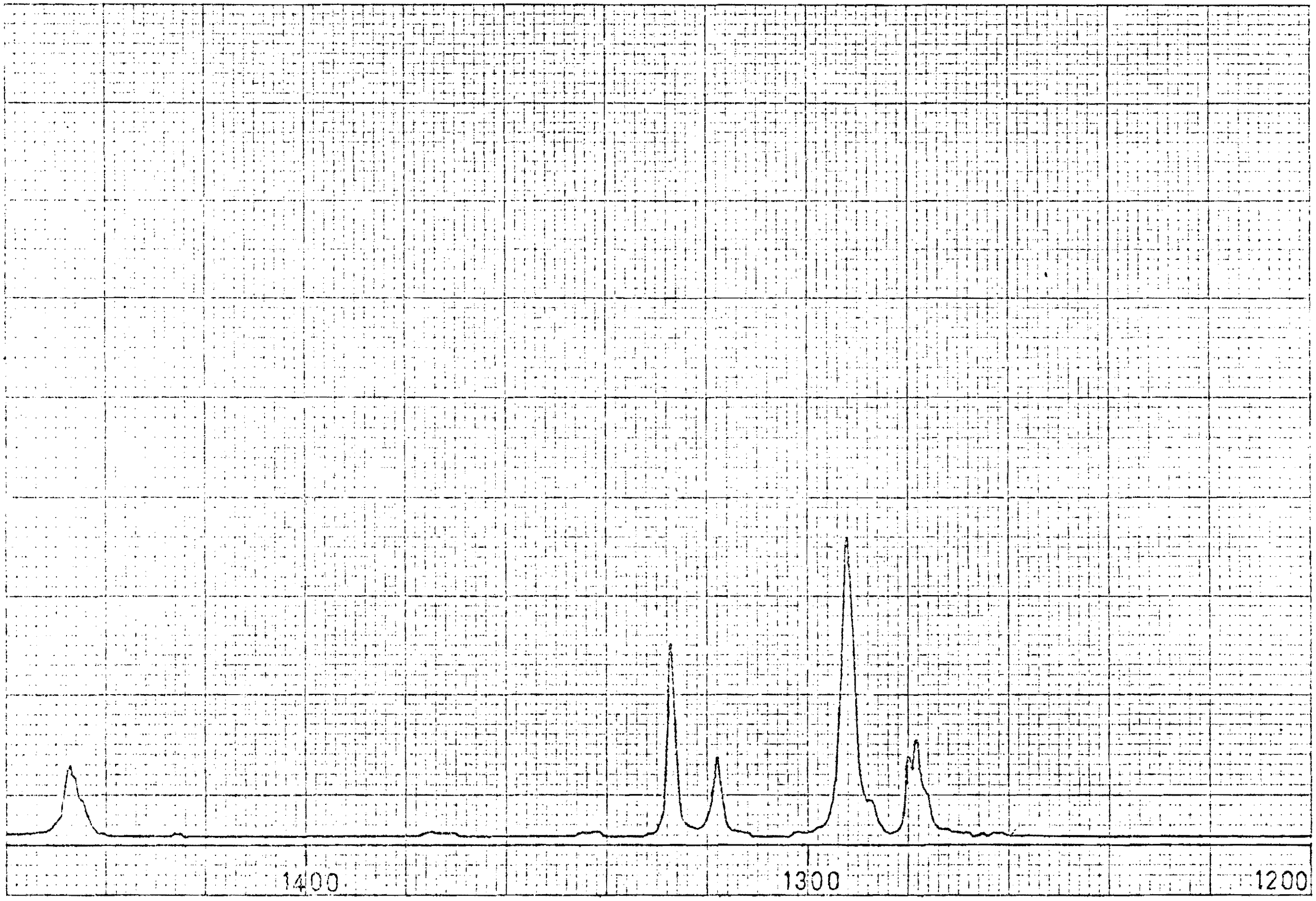
1400
1300
1200

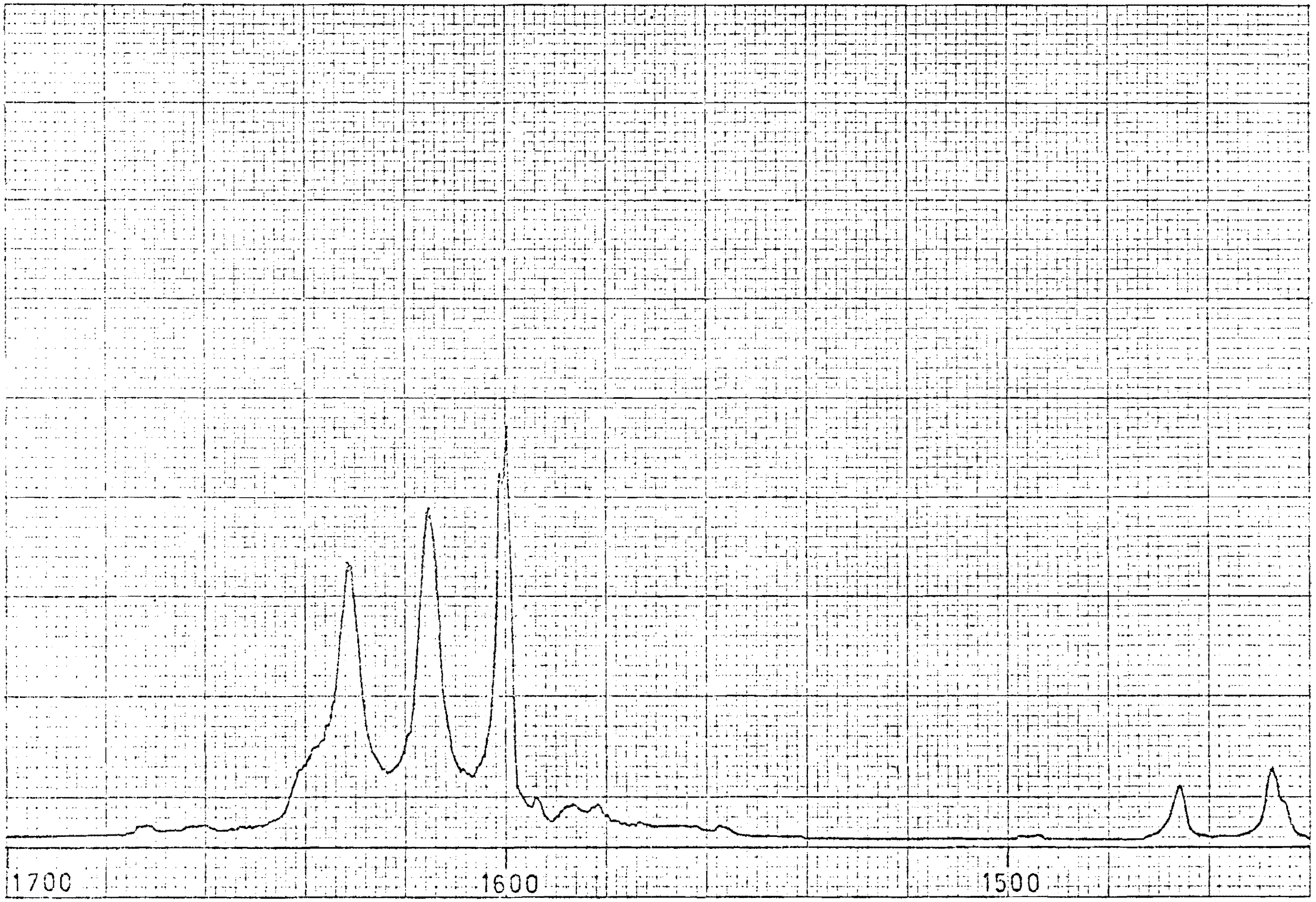
1700
1600
1500

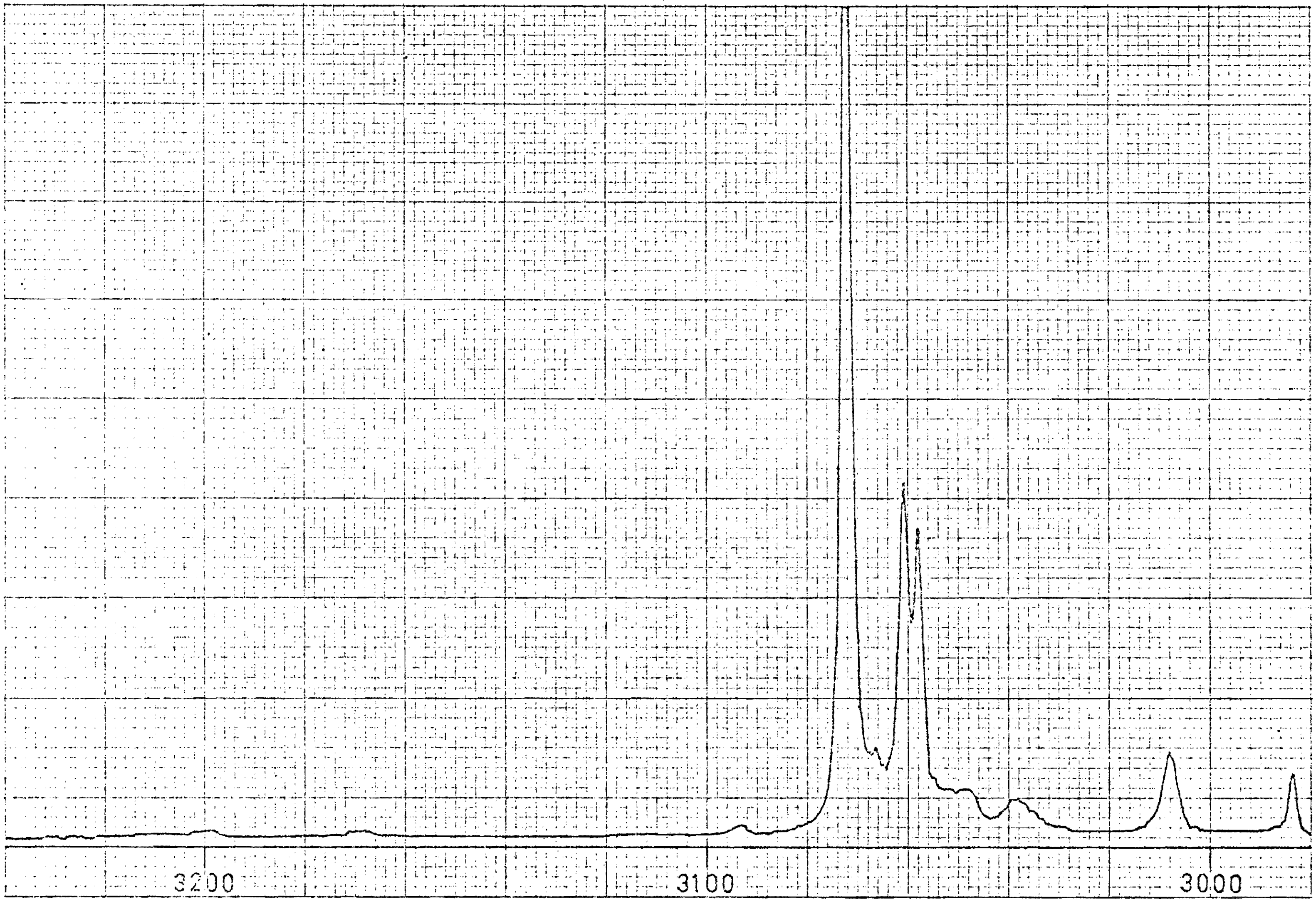
3200
3100
3000

FIGURE 9

Raman Spectrum of Benzoic Acid d_o

Carey Model 82 Raman Spectrometer

Temperature = 4.2^o K

Spectral Bandwidth = 0.5 cm^{-1}

Scan Rate = 0.25 cm^{-1}/second

Pen Period = 2.0 seconds

Sensitivity = 3×10^3 counts per second full scale

Laser Wavelength = 5145 Å

Laser Power = 640 milliwatts

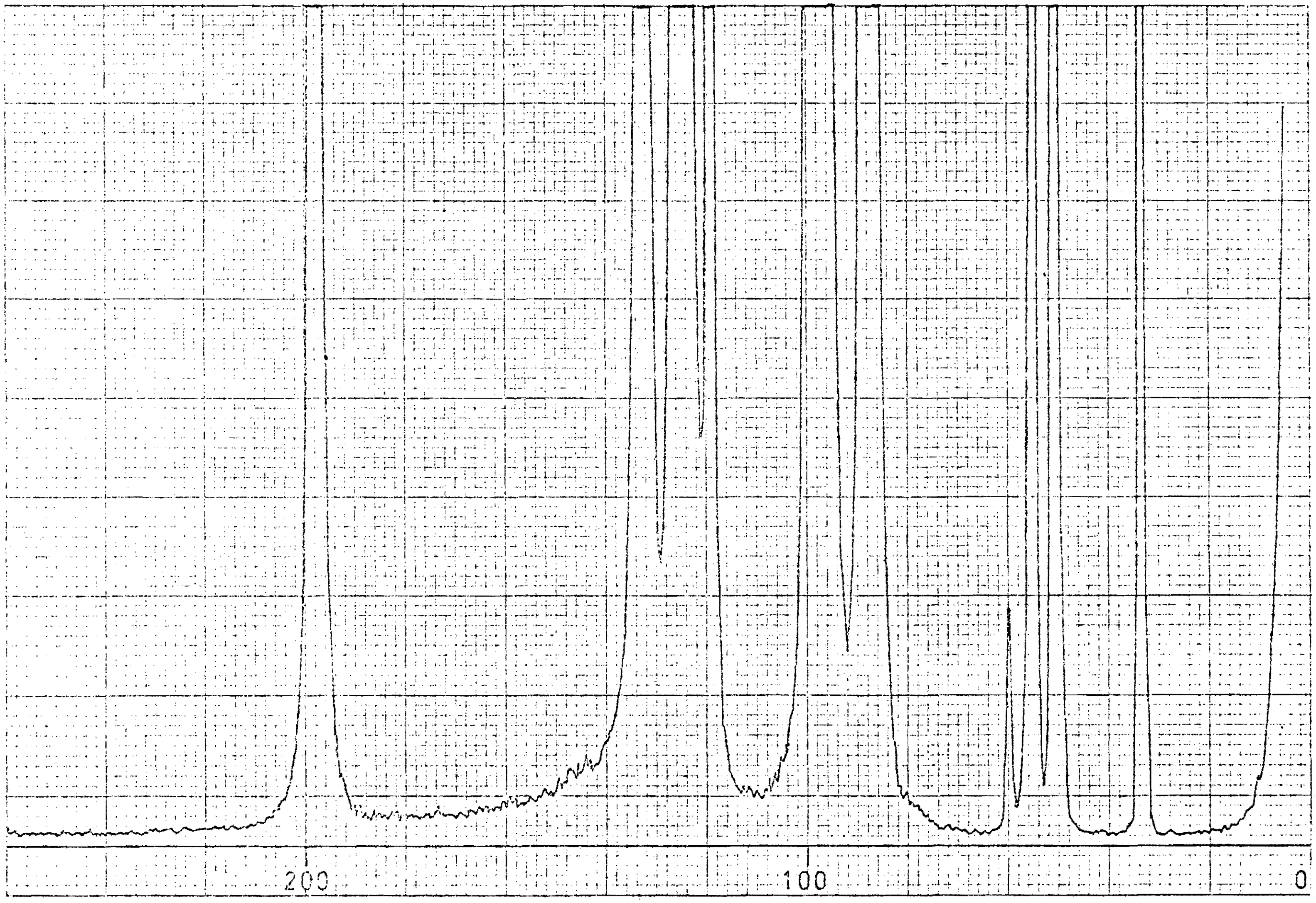
200
100
0

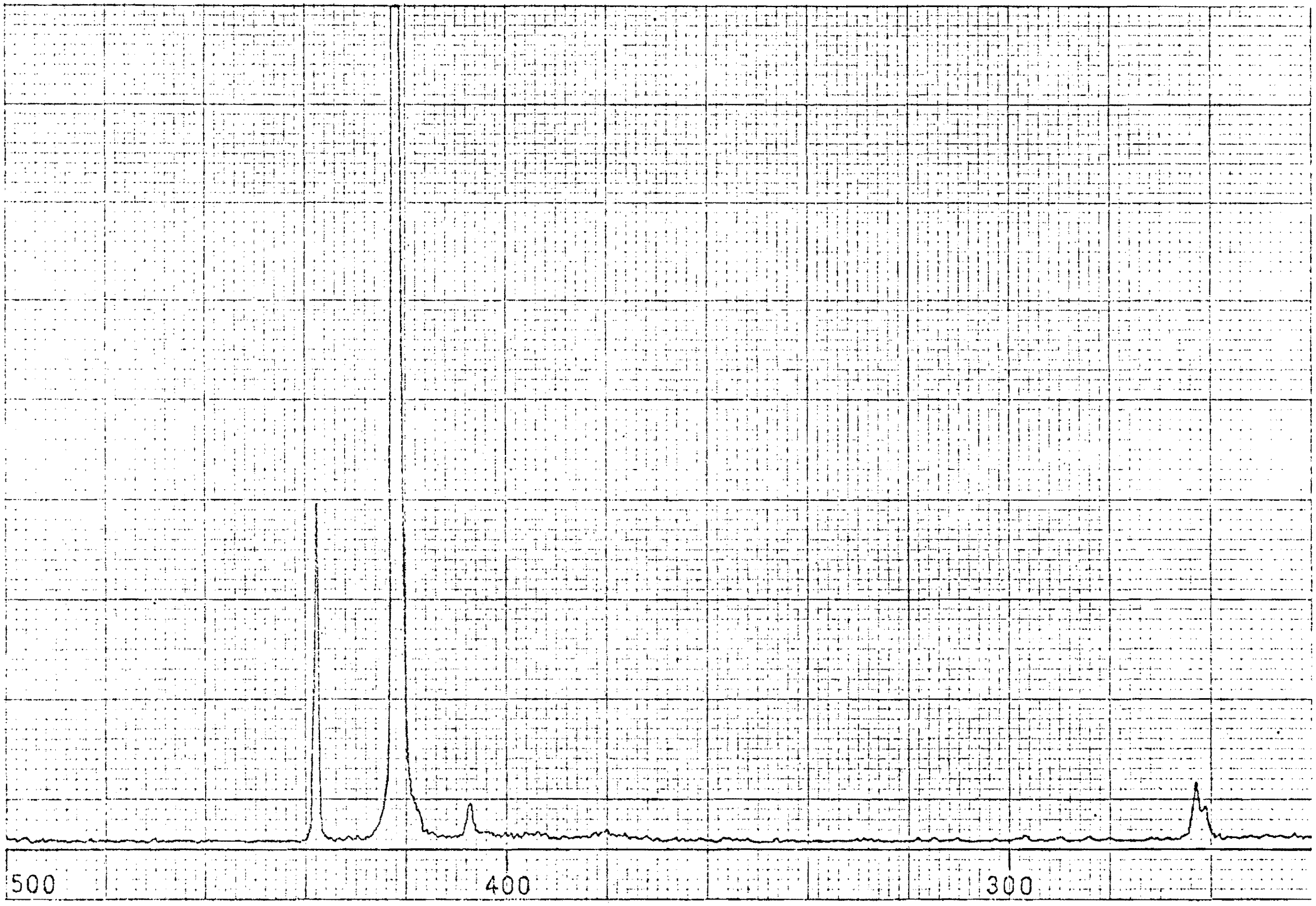
500
400
300

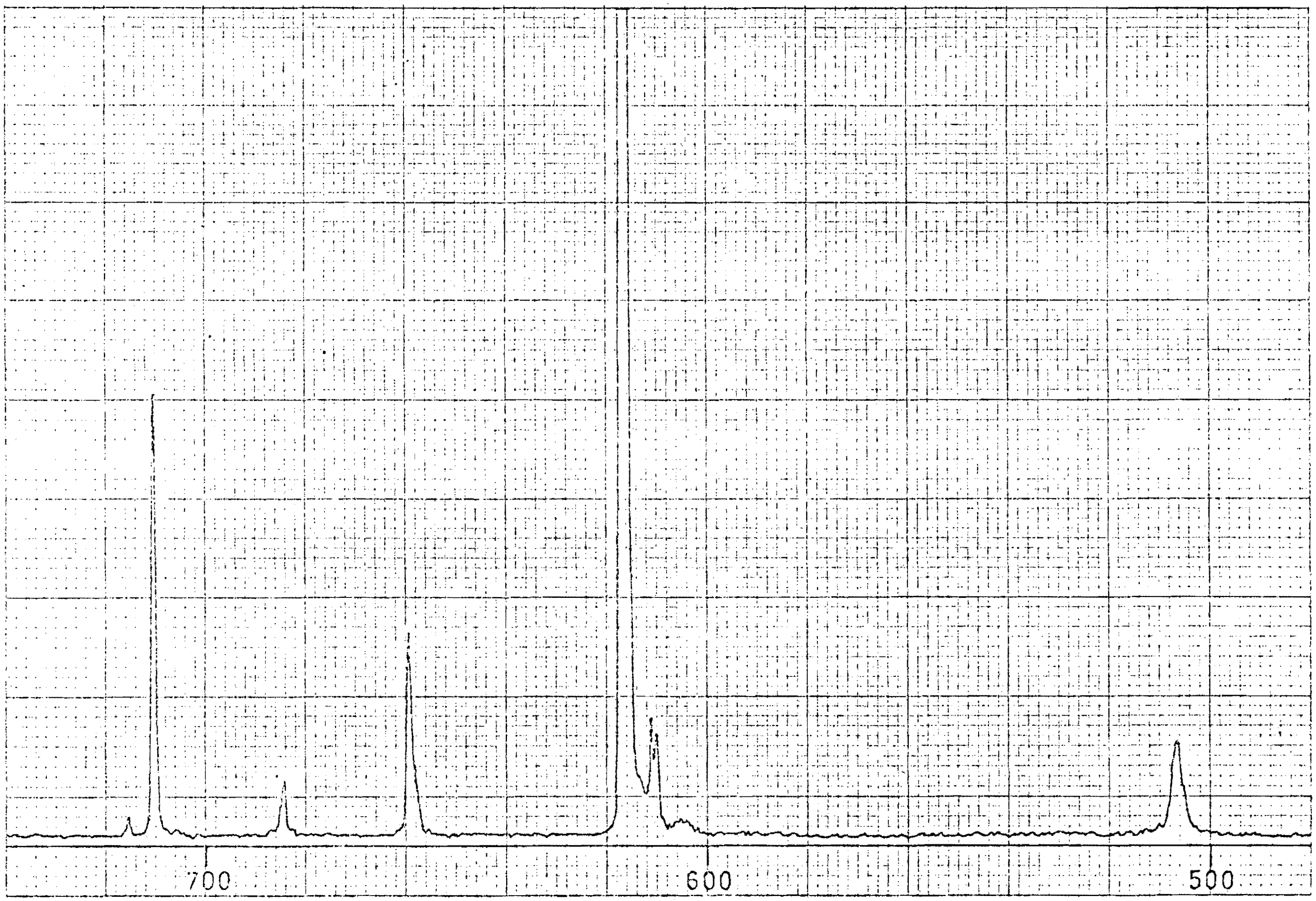
700
600
500

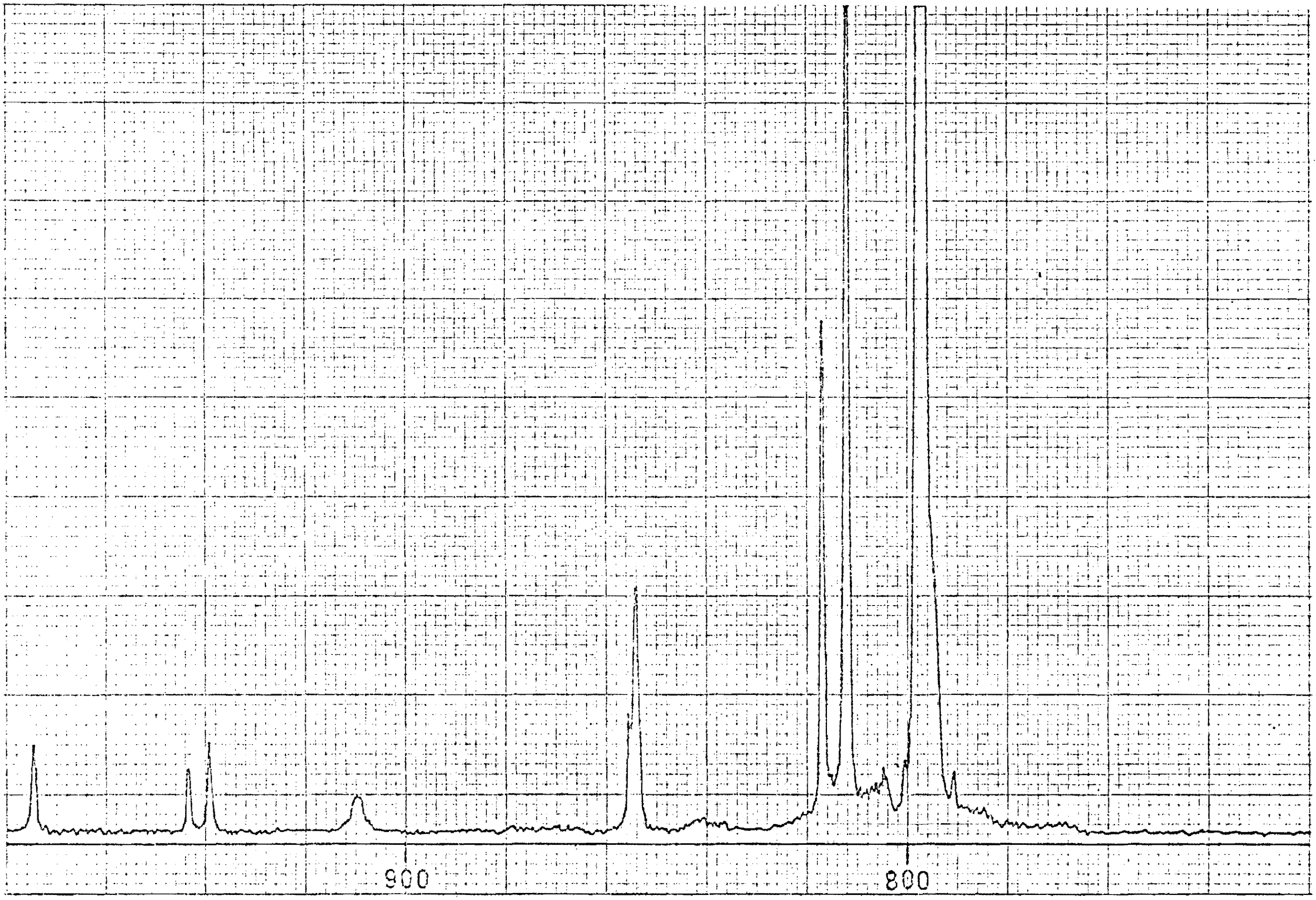
900
800

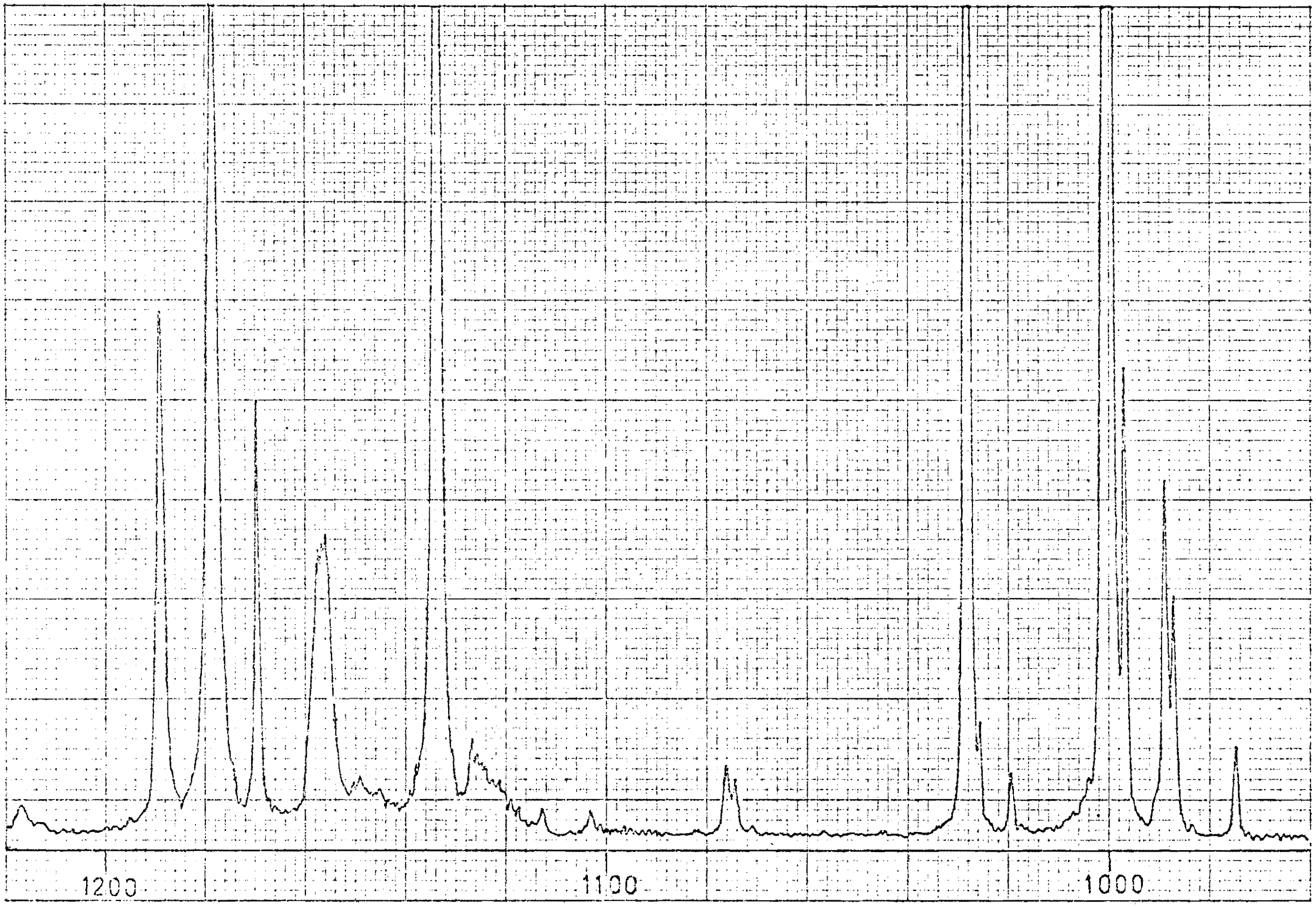
1200
1100
1000

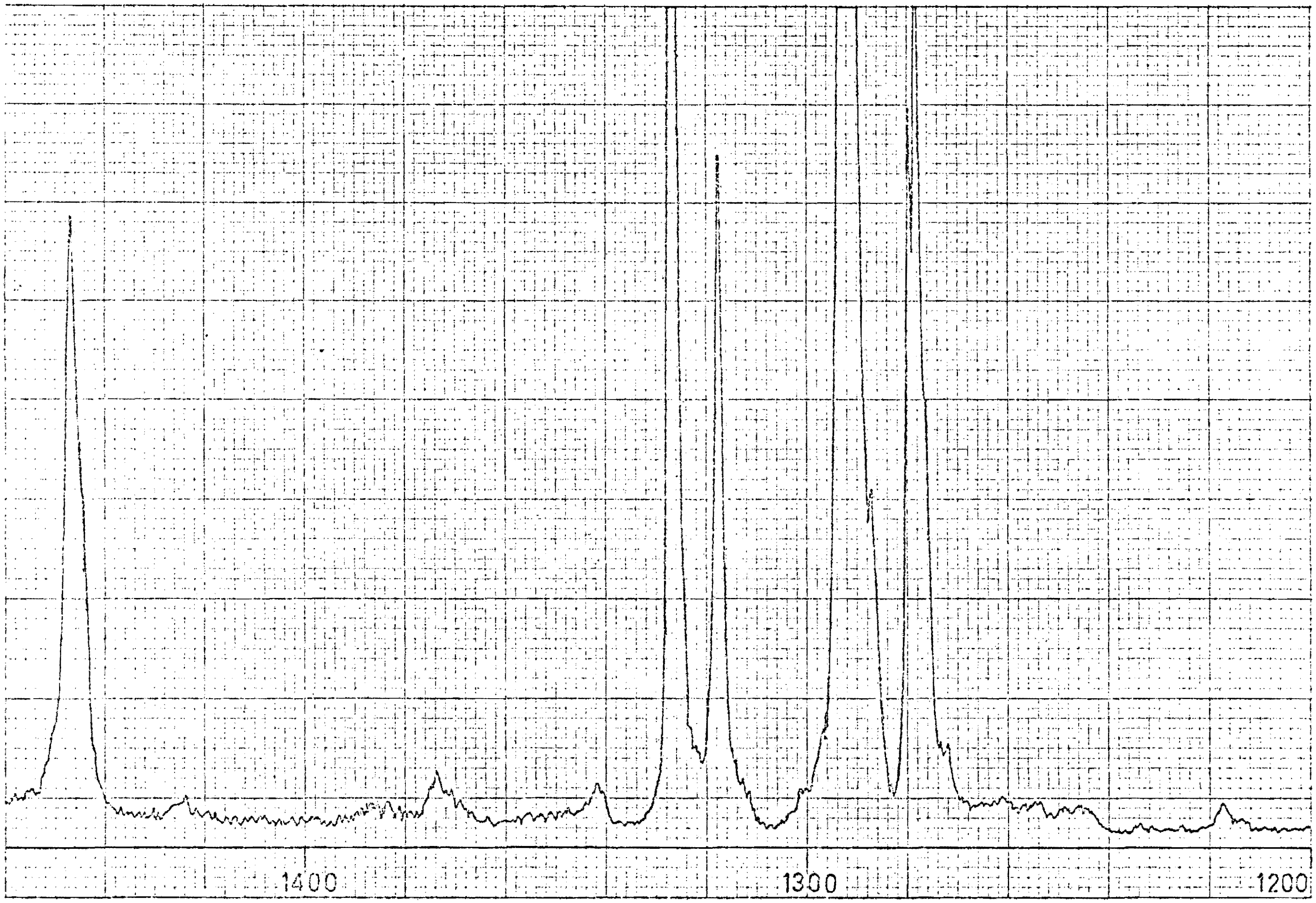
1400
1300
1200

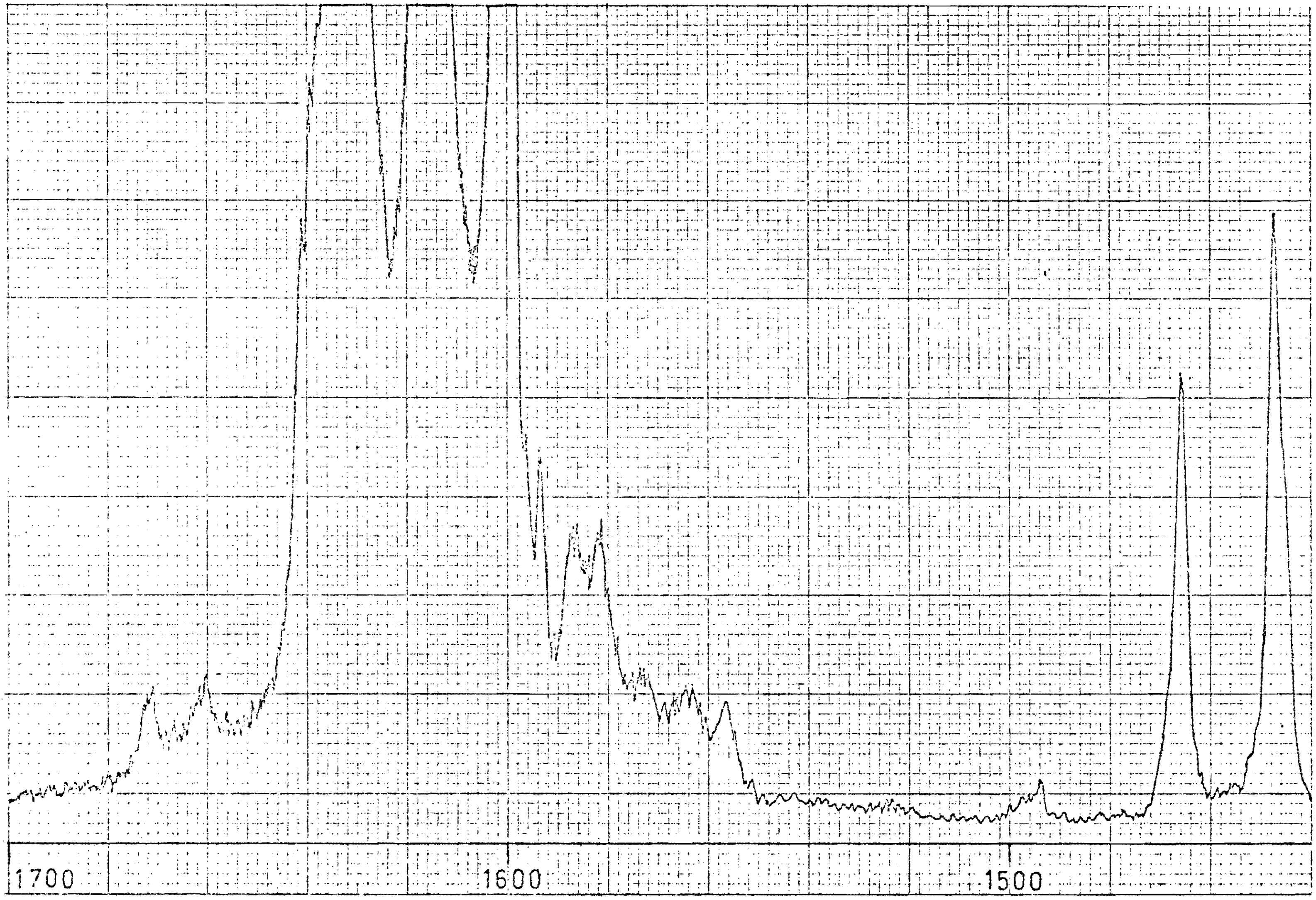
1700
1600
1500

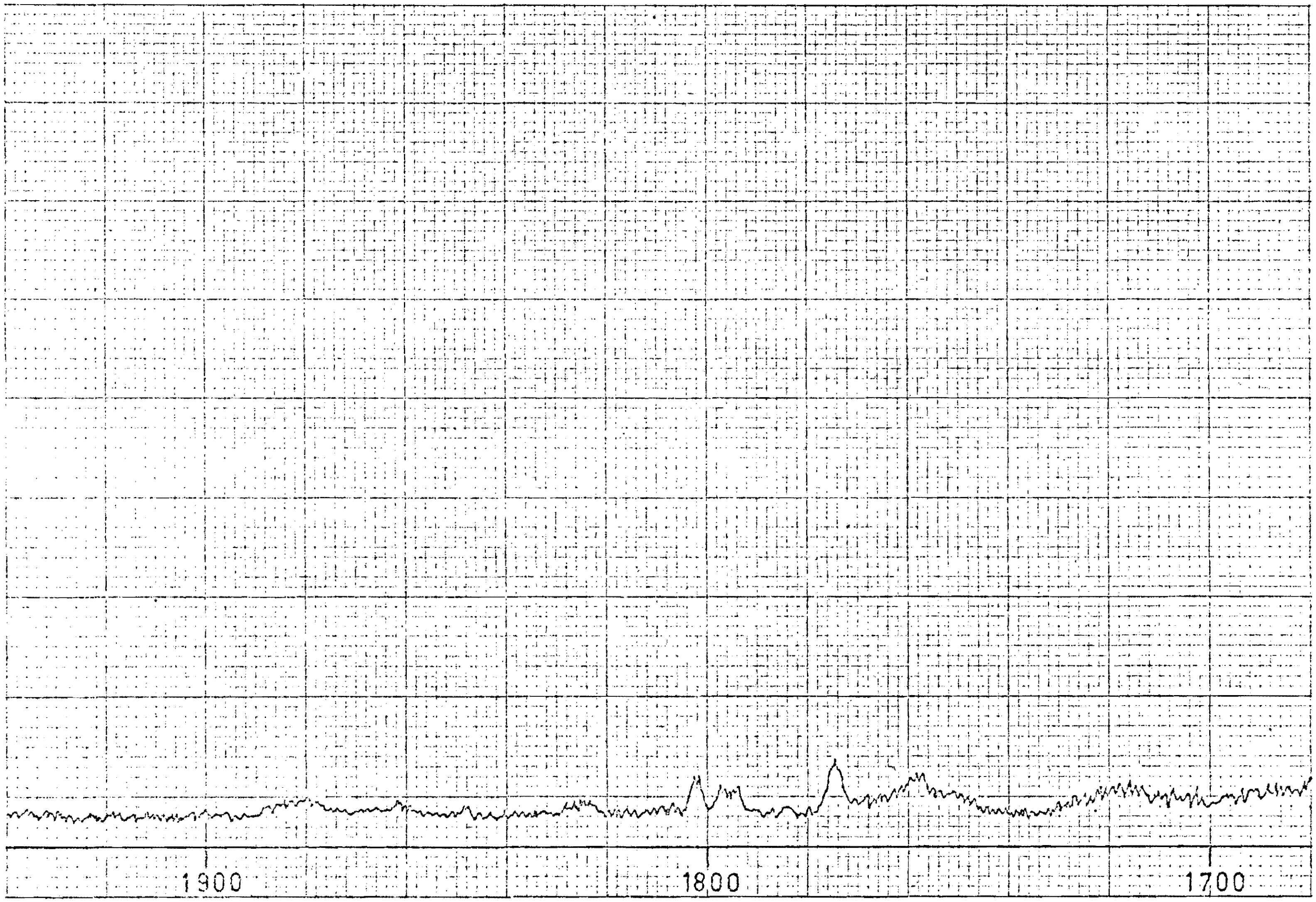
1900
1800
1700


2100
2000
1900

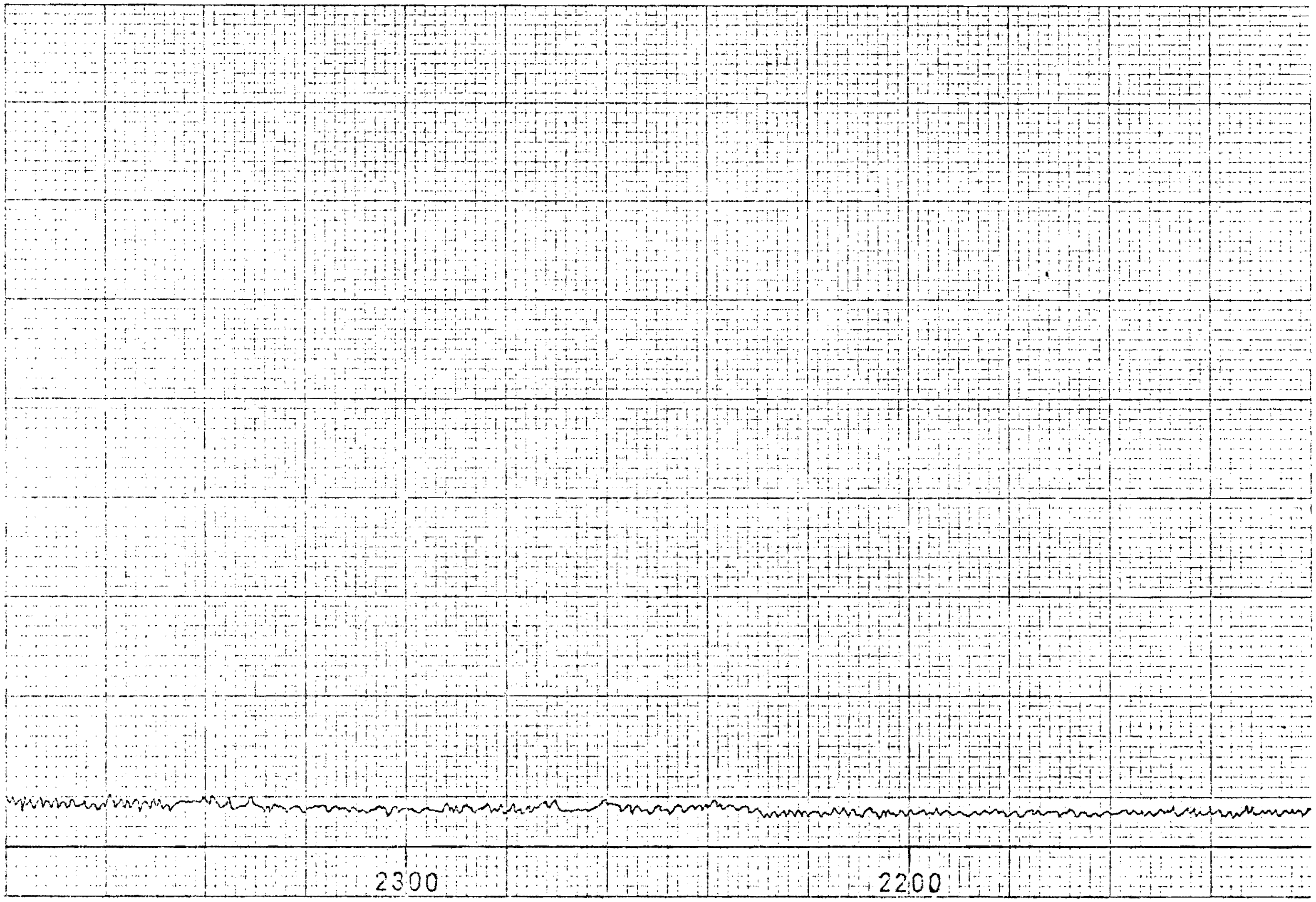
2300
2200

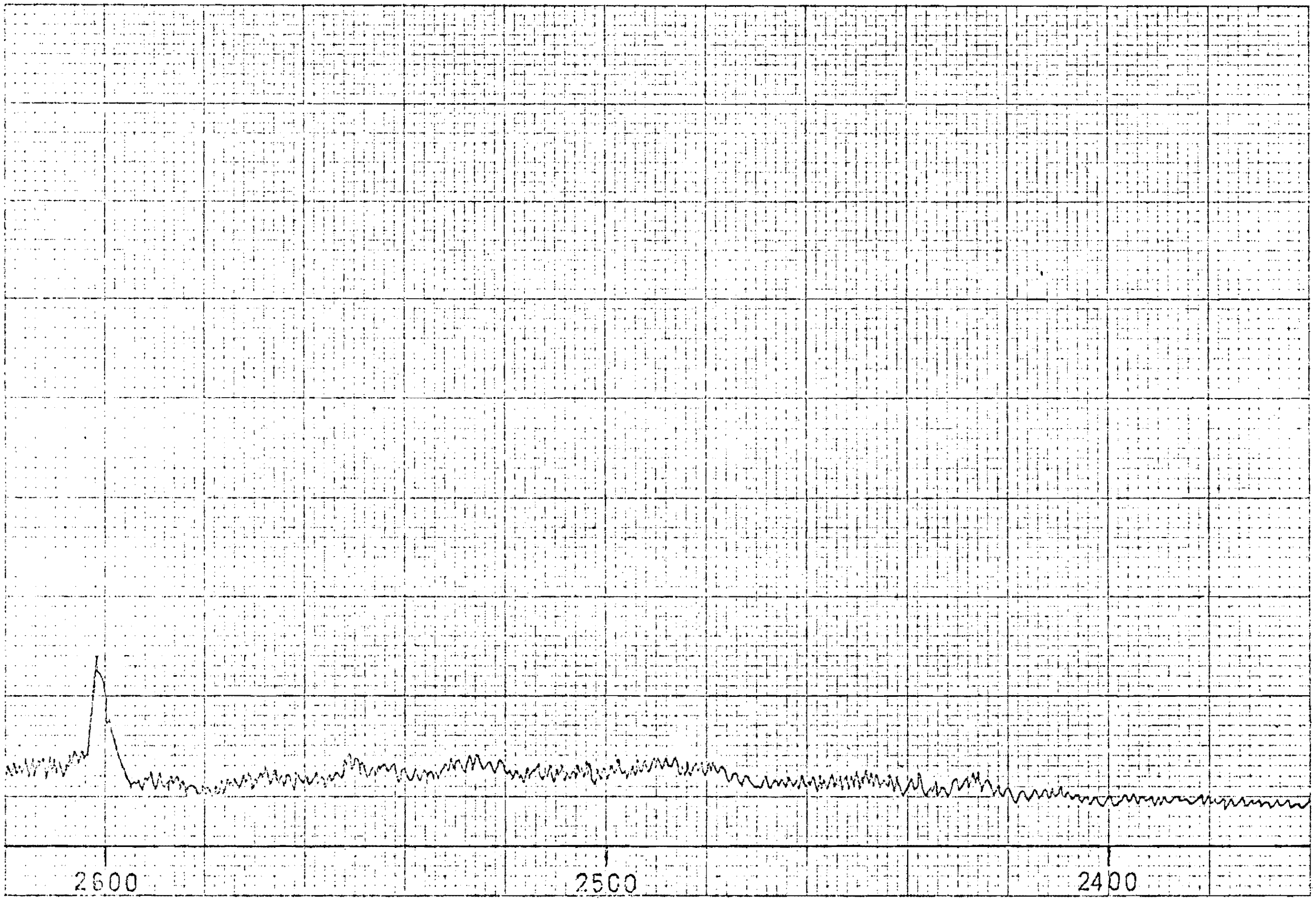

2600
2500
2400

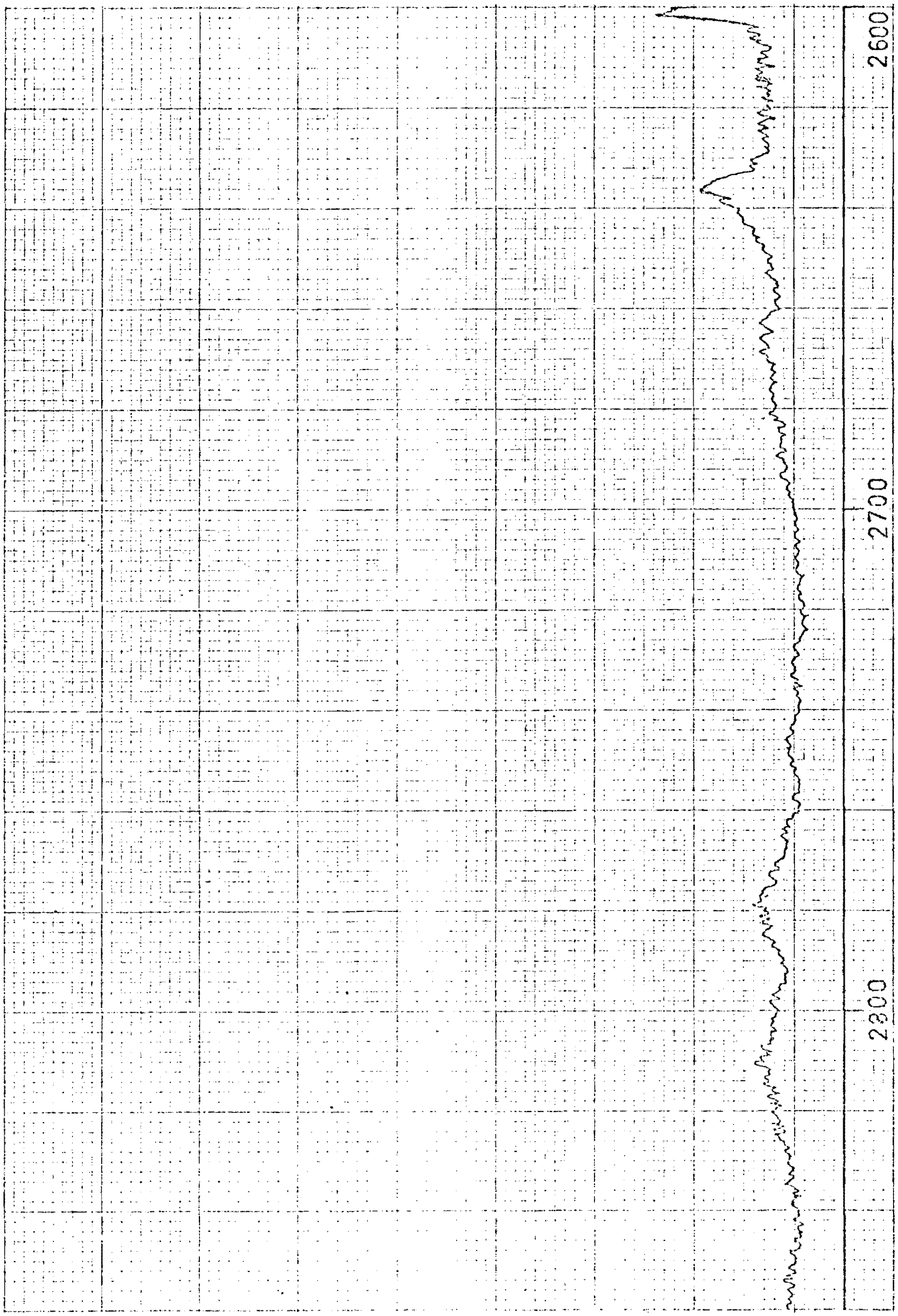
2600
2700
2300

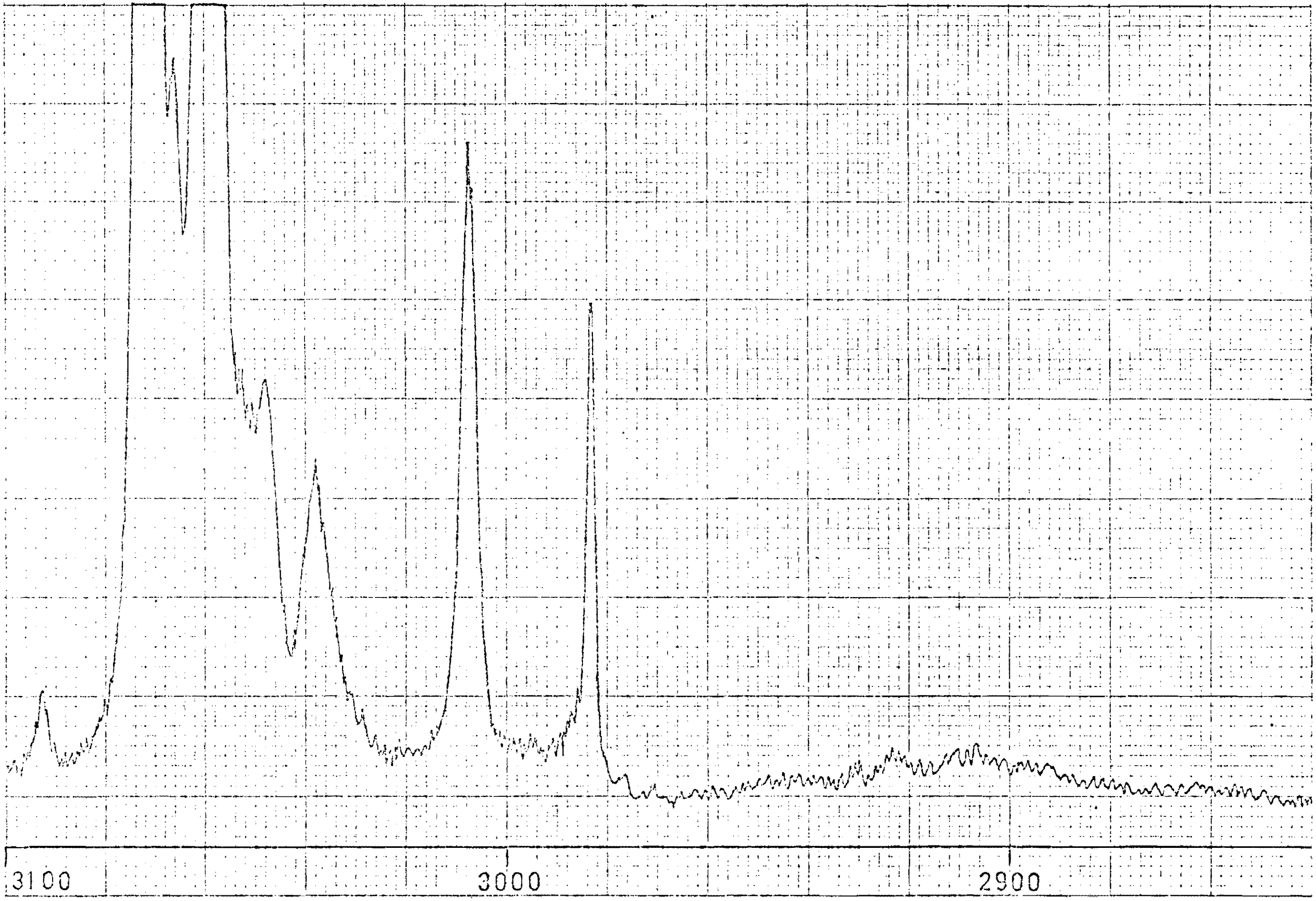
3100
3000
2900

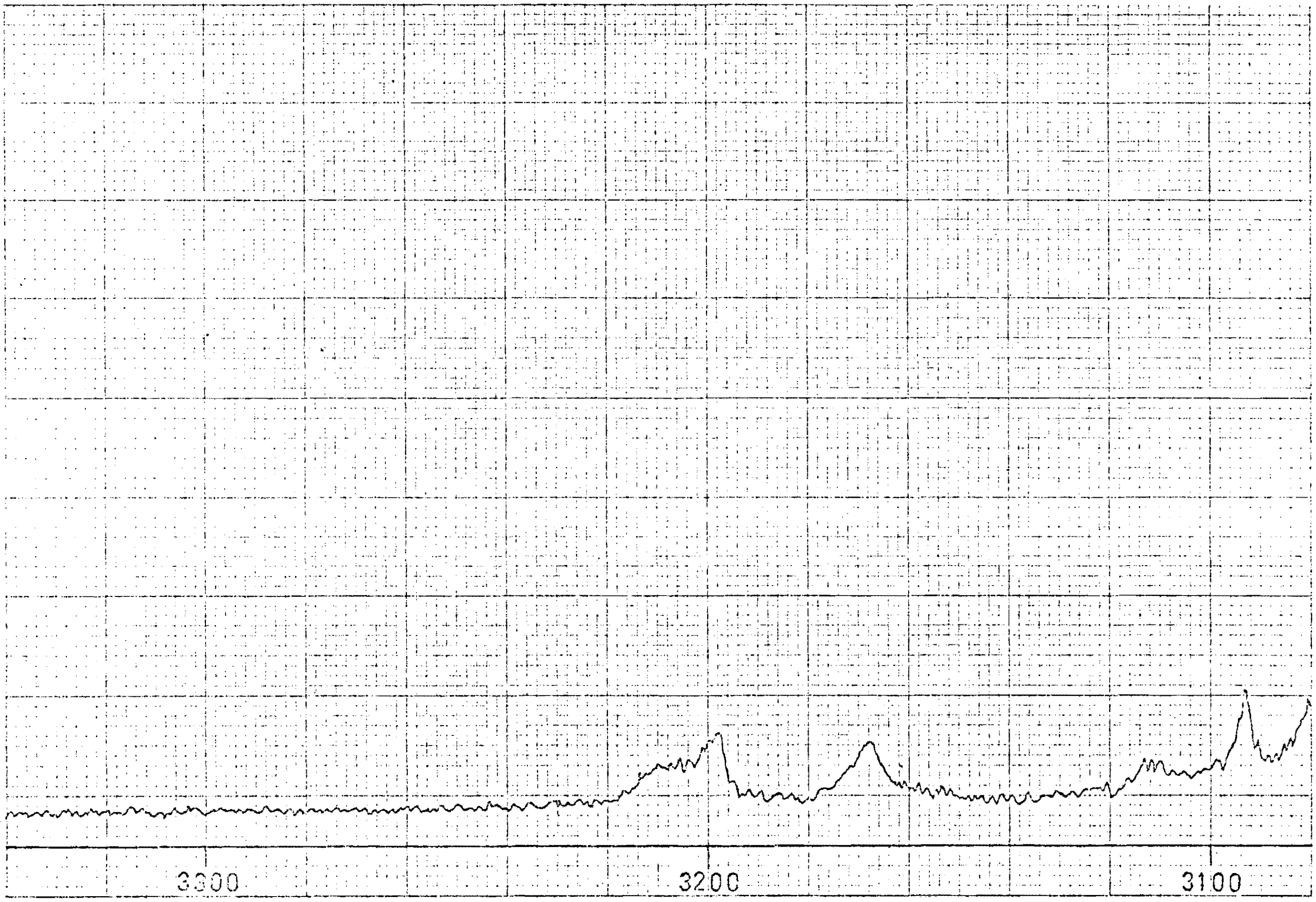
3300
3200
3100

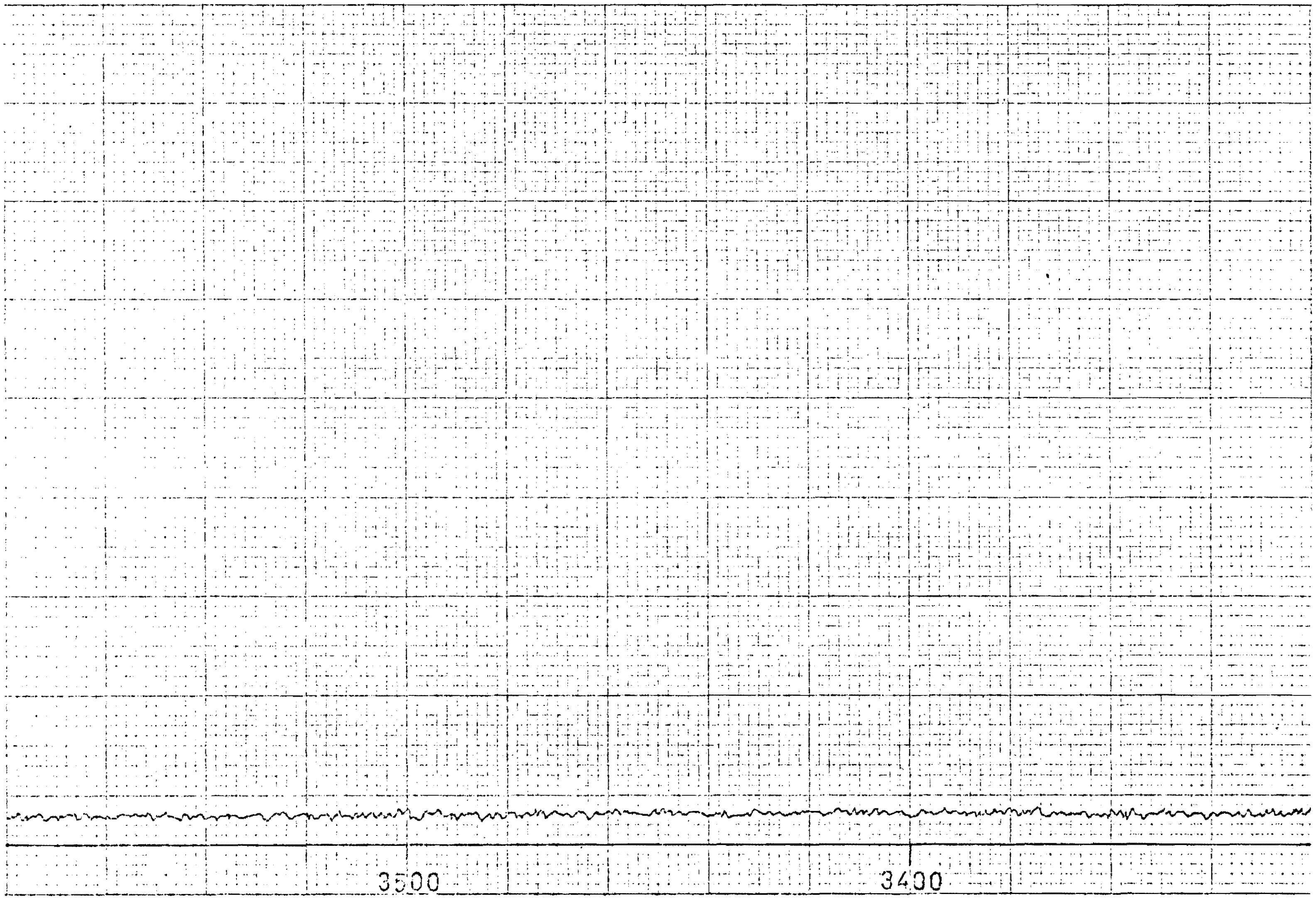
3500
3400

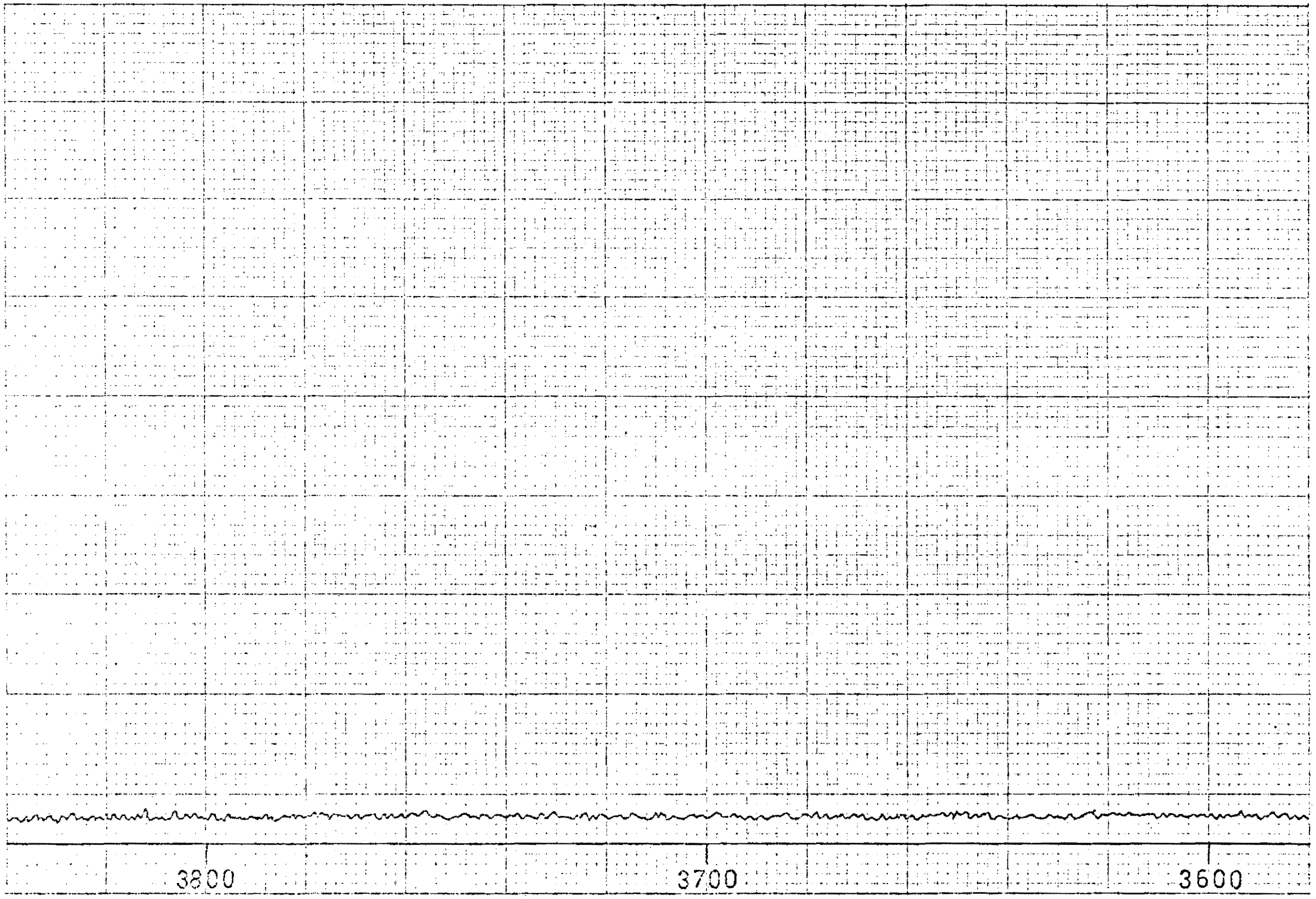
3800
3700
3600

TABLE 6

This table contains the frequencies and peak heights of bands in the Raman spectra shown in Figures 8 and 9. Peak heights are given relative to an arbitrary unit of intensity.

Band Number	Frequency (cm^{-1})	Peak Height	Comments
1	33.6	26.0	
2	51.0	20.4	
3	55.2	20.9	
4	60.0	2.4	
5	88.0	90.0	
6	97.5	74.4	
7	99.0	46.9	shoulder
8	119.5	28.0	
9	124.7	69.0	
10	132.7	43.0	
11	198.0	37.5	
12	261.5	0.40	shoulder
13	263.5	0.68	
14	407.5	0.44	
15	422.0	26.4	
16	438.0	4.04	
17	505.5	0.54	shoulder
18	506.8	1.13	
19	605.0	0.18	broad
20	610.0	1.2	
21	611.2	1.38	
22	613.5	0.18	shoulder
23	616.0	43.0	
24	617.5	21.3	
25	658.5		very weak shoulder
26	659.5	2.40	
27	684.6	0.66	
28	710.5	5.34	
29	716.0	0.22	
30	767.0	0.07	
31	769.0	0.10	
32	783.0	0.12	
33	791.0	0.36	
34	795.0		weak, unresolved shoulder
35	797.4	95.0	
36	800.5		weak shoulder
37	804.5	0.42	
38	812.0	1.44	
39	817.0	5.76	
40	837.0	0.06	

Table 6 (Continued)

Band Number	Frequency (cm^{-1})	Peak Height	Comments
41	841.0	0.10	
42	854.0	2.94	
43	855.5	1.38	
44	909.8	0.42	
45	939.4	1.08	
46	943.5	0.78	
47	975.0	1.08	
48	983.5	0.12	
49	987.4	2.82	
50	989.0	4.26	
51	991.0		unresolved shoulder
52	997.0	5.52	shoulder
53	1000.5	>105	
54	1019.8	0.66	
55	1026.0	0.78	shoulder
56	1028.3	40.0	
57	1071.0	0.12	
58	1074.5	0.66	
59	1076.0	0.84	
60	1103.0	0.24	
61	1113.0	0.24	
62	1122.0	0.54	
63	1127.0	0.84	
64	1134.0	1.74	
65	1145.5	0.18	
66	1149.5	0.24	
67	1157.0	3.18	
68	1170.0	4.98	
69	1179.0	10.40	
70	1189.5	6.72	
71	1196.0	0.12	
72	1214.0	0.12	
73	1218.0	0.30	
74	1234.0	0.12	
75	1246.0	0.24	
76	1249.0	0.24	
77	1254.0	0.24	
78	1261.5	0.18	
79	1272.0	0.30	
80	1276.0		unresolved shoulder
81	1278.5	10.4	
82	1280.0	8.64	
83	1287.0	3.96	
84	1292.0	30.0	
85	1301.0	0.18	
86	1318.0	8.16	

Table 6 (Continued)

Band Number	Frequency (cm^{-1})	Peak Height	Comments
87	1327.0	19.5	
88	1342.0	0.42	
89	1369.0	0.30	
90	1371.0	0.42	
91	1374.0	0.54	
92	1384.0	0.12	
93	1386.0	0.12	
94	1424.0	0.24	
95	1426.0	0.18	
96	1445.0		unresolved shoulder
97	1447.0	7.32	
98	1466.0	5.40	
99	1494.0	0.42	
100	1498.0	0.24	
101	1524.0	0.12	
102	1538.5	0.12	
103	1543.0	0.12	
104	1546.0	0.12	
105	1555.0	0.12	
106	1557.0	0.66	
107	1563.0	0.72	
108	1565.0	0.72	
109	1573.0	0.42	
110	1581.5	1.80	
111	1586.5	1.68	
112	1593.5	2.16	
113	1599.7	41.0	
114	1601.0	36.0	
115	1615.0	33.0	
116	1631.0	27.0	
117	1660.0	1.02	
118	1663.0	0.12	unresolved shoulder
119	1671.0	0.96	
120	1673.0	0.84	
121	1718.0	0.24	
122	1751.0	0.12	
123	1758.0	0.30	
124	1775.0	0.48	
125	1794.0	0.30	
126	1797.5	0.30	
127	1802.5	0.42	
128	1824.0	0.12	
129	1827.0	0.12	
130	1848.0	0.12	
131	1994.0	0.24	
132	2028.0	0.12	
133	2055.0	0.12	
134	2261.0	0.12	

Table 6 (Continued)

Band Number	Frequency (cm^{-1})	Peak Height	Comments
135	2272.0	0.12	
136	2331.0	0.12	
137	2427.0	0.18	
138	2480.0	0.18	
139	2498.0	0.24	
140	2521.0	0.12	
141	2526.0	0.12	
142	2530.0	0.12	
143	2544.0	0.12	
144	2550.0	0.24	
145	2599.0	0.78	shoulder
146	2601.5	1.44	
147	2636.0	1.08	
148	2728.0	0.12	
149	2746.0	0.12	
150	2764.0	0.24	
151	2773.0	0.42	
152	2779.0	0.54	
153	2785.0	0.48	
154	2798.0	0.12	
155	2811.0	0.48	
156	2892.0	0.12	
157	2898.0	0.12	
158	2907.0	0.18	
159	2912.0	0.18	
160	2923.0	0.24	
161	2931.0	0.18	
162	2971.0	0.12	
163	2977.0	0.18	
164	2983.5	6.0	
165	2995.0	0.12	
166	3007.5	0.79	
167	3038.5	2.88	
168	3048.5	3.96	shoulder
169	3058.0	31.0	shoulder
170	3060.5	35.5	
171	3066.5	1.74	shoulder
172	3072.0	>105	
173	3093.0	0.84	
174	3113.0	0.30	
175	3168.0	0.72	
176	3198.0	0.84	
177	3210.0	0.48	

FIGURE 10

Raman Spectrum of Benzoic Acid $4d_1$

Carey Model 82 Raman Spectrometer

Temperature = 4.2° K

Spectral Bandwidth = 0.5 cm^{-1}

Scan Rate = 0.25 cm^{-1}/second

Pen Period = 1.0 second

Sensitivity = 2 x 10^4 counts per second
full scale

Laser Wavelength = 5145 Å

Laser Power = 500 milliwatts

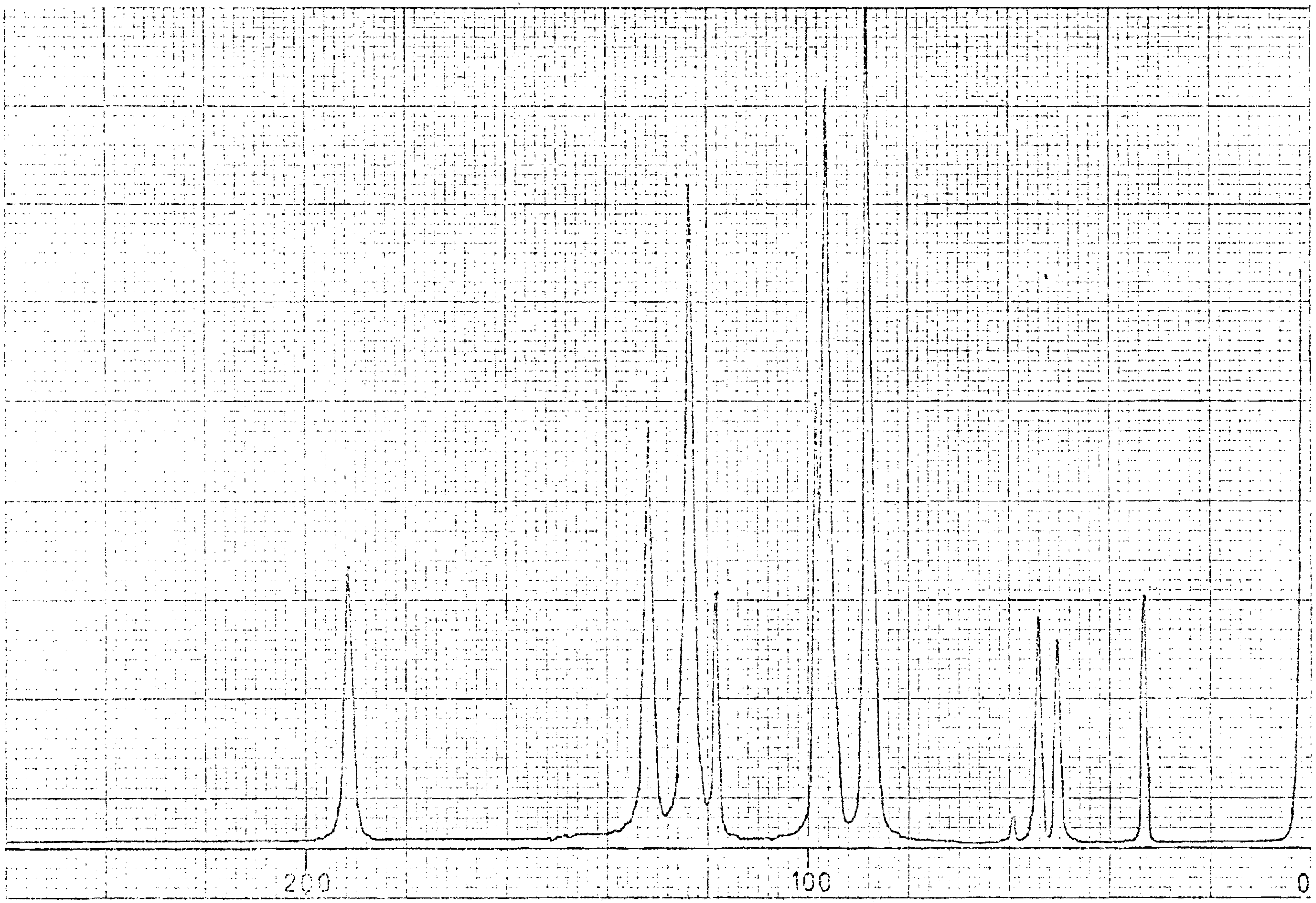
200
100
0

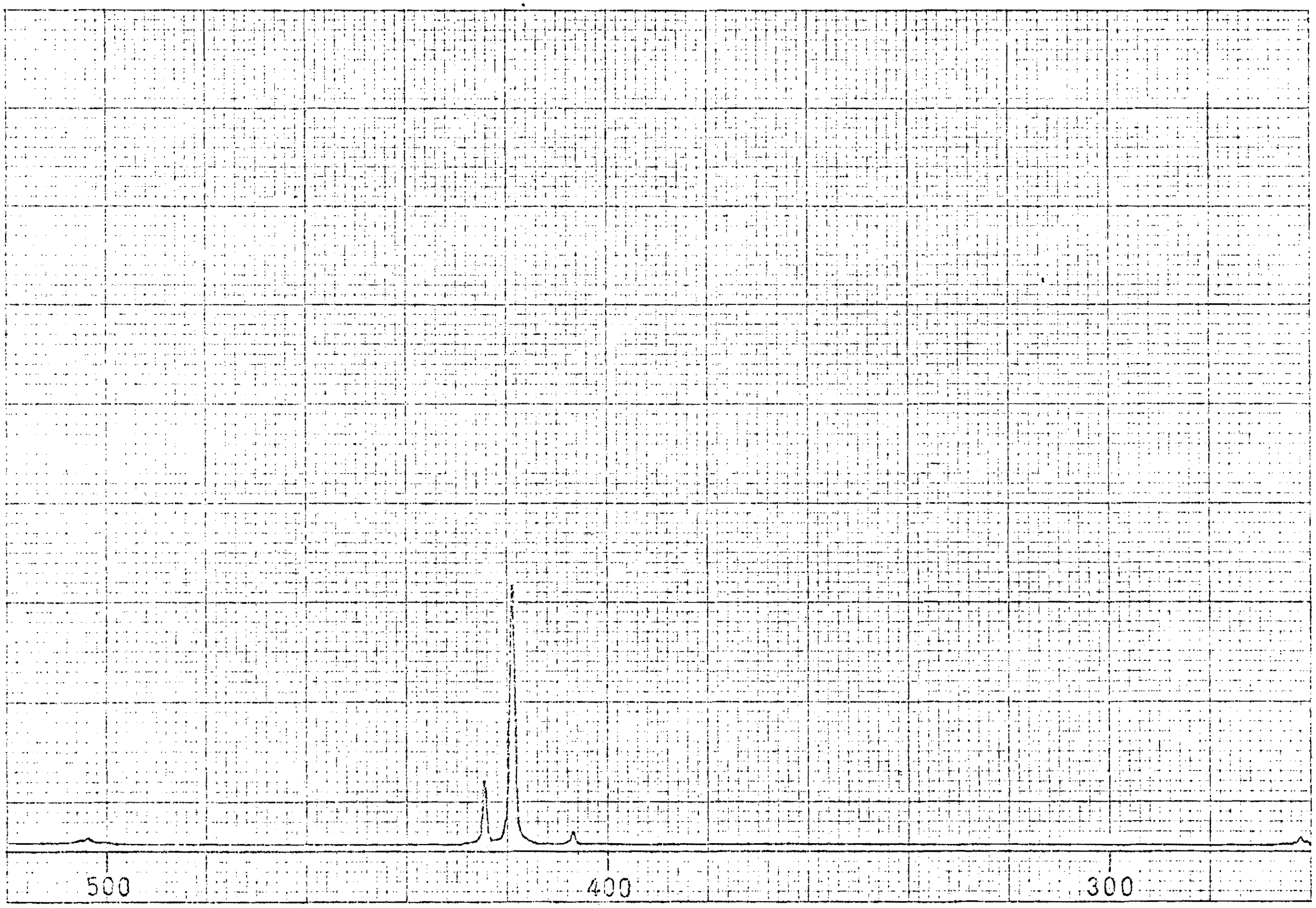
500
400
300

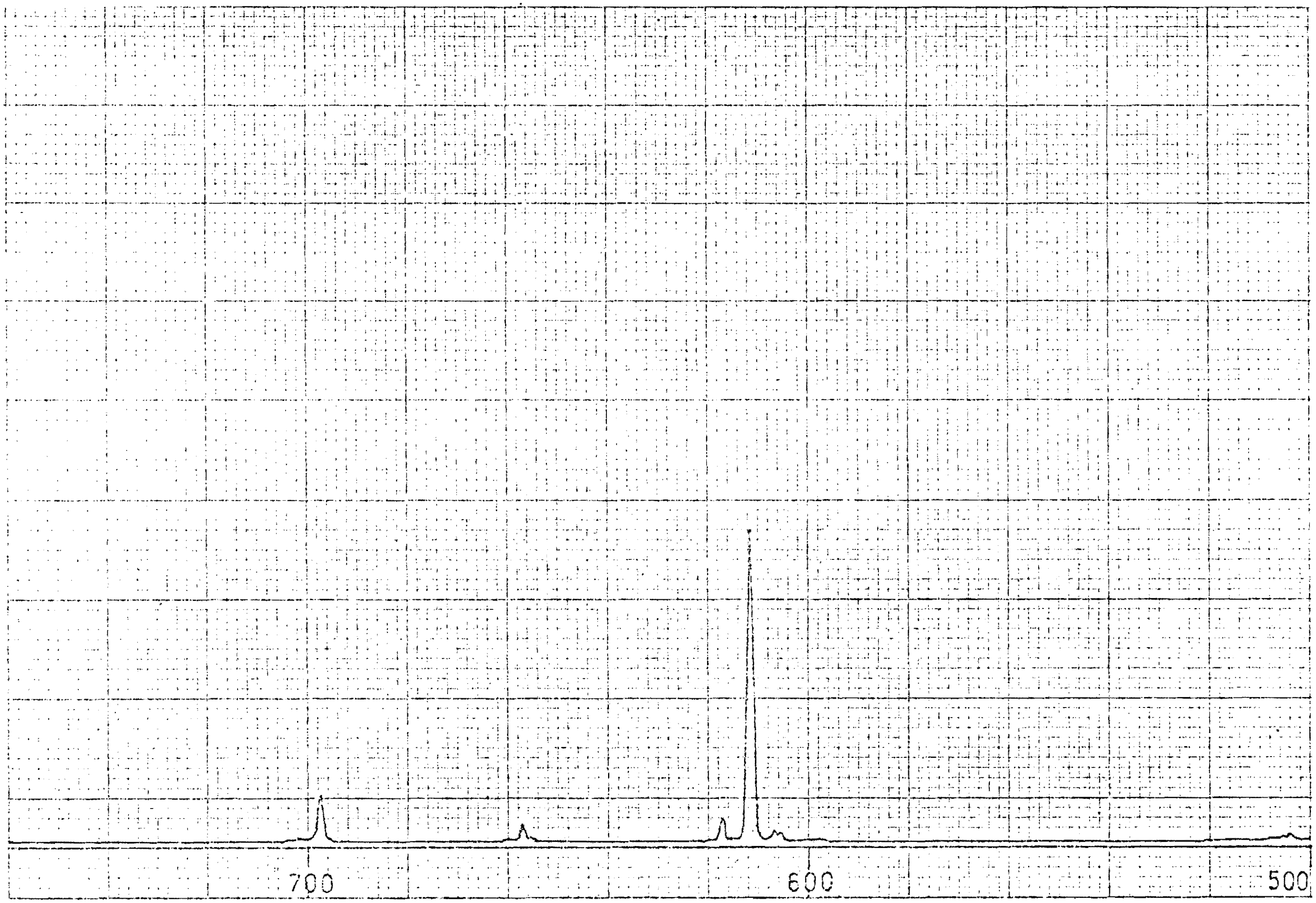
700
600
500

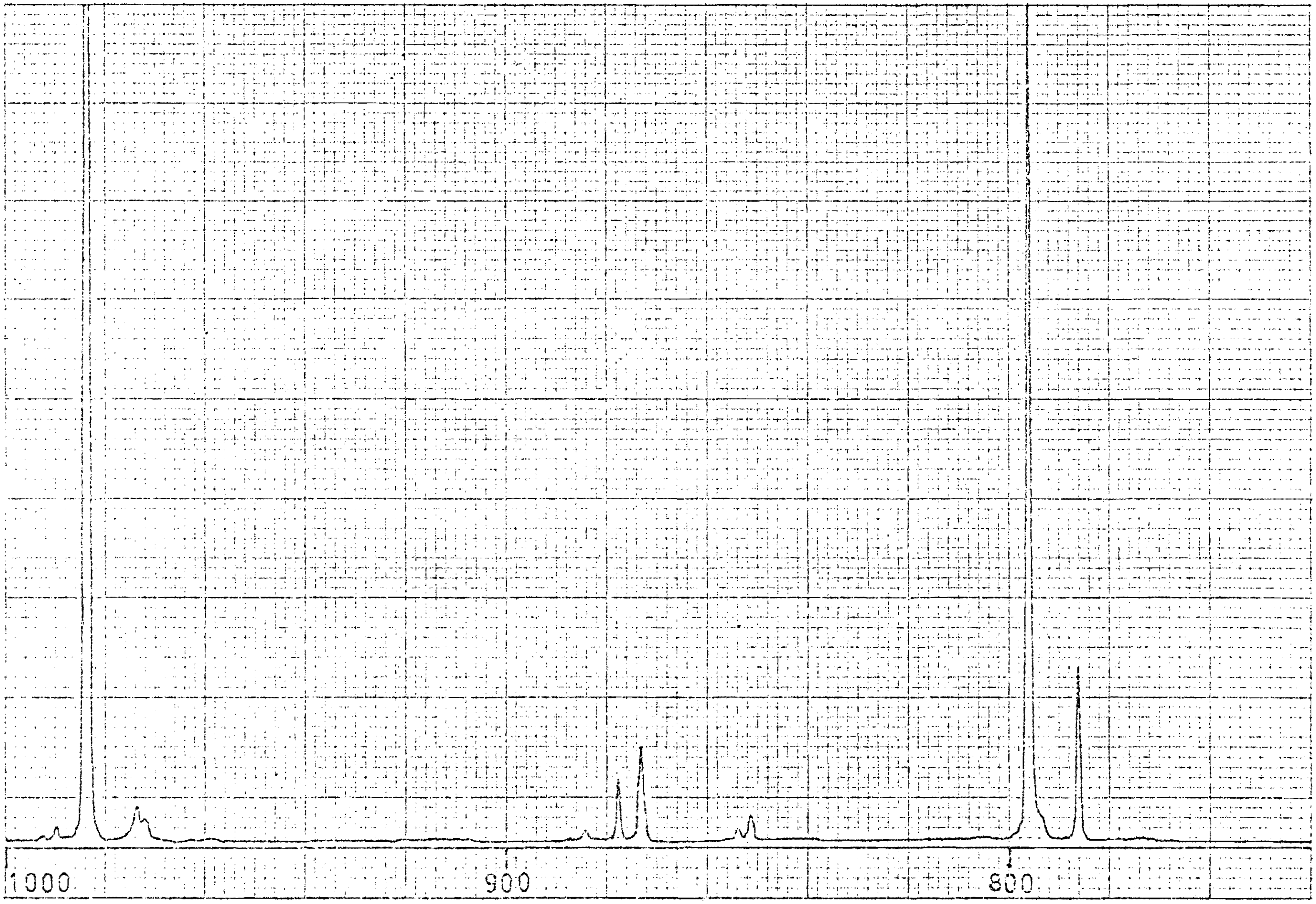
1000
900
800

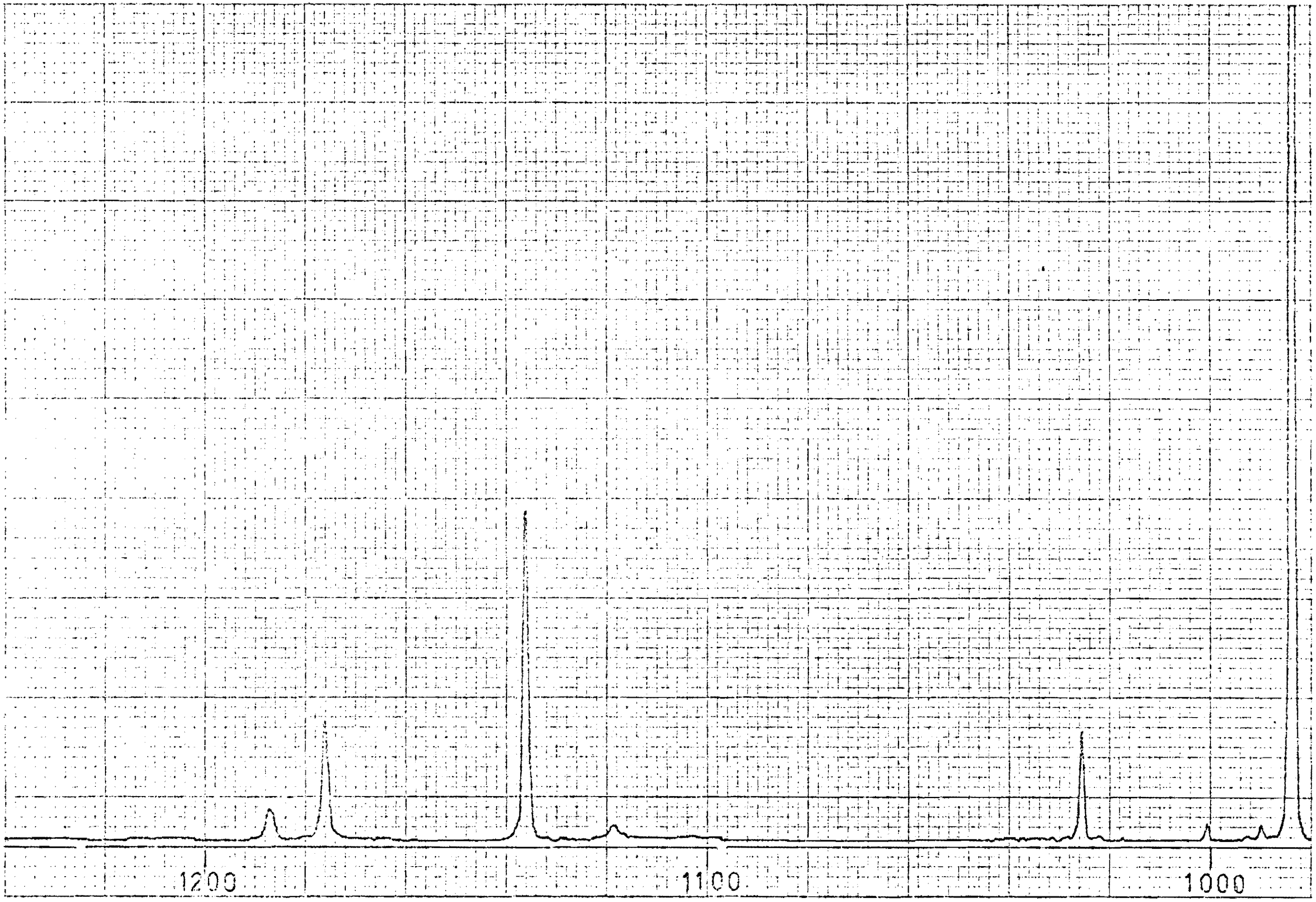
1200
1100
1000

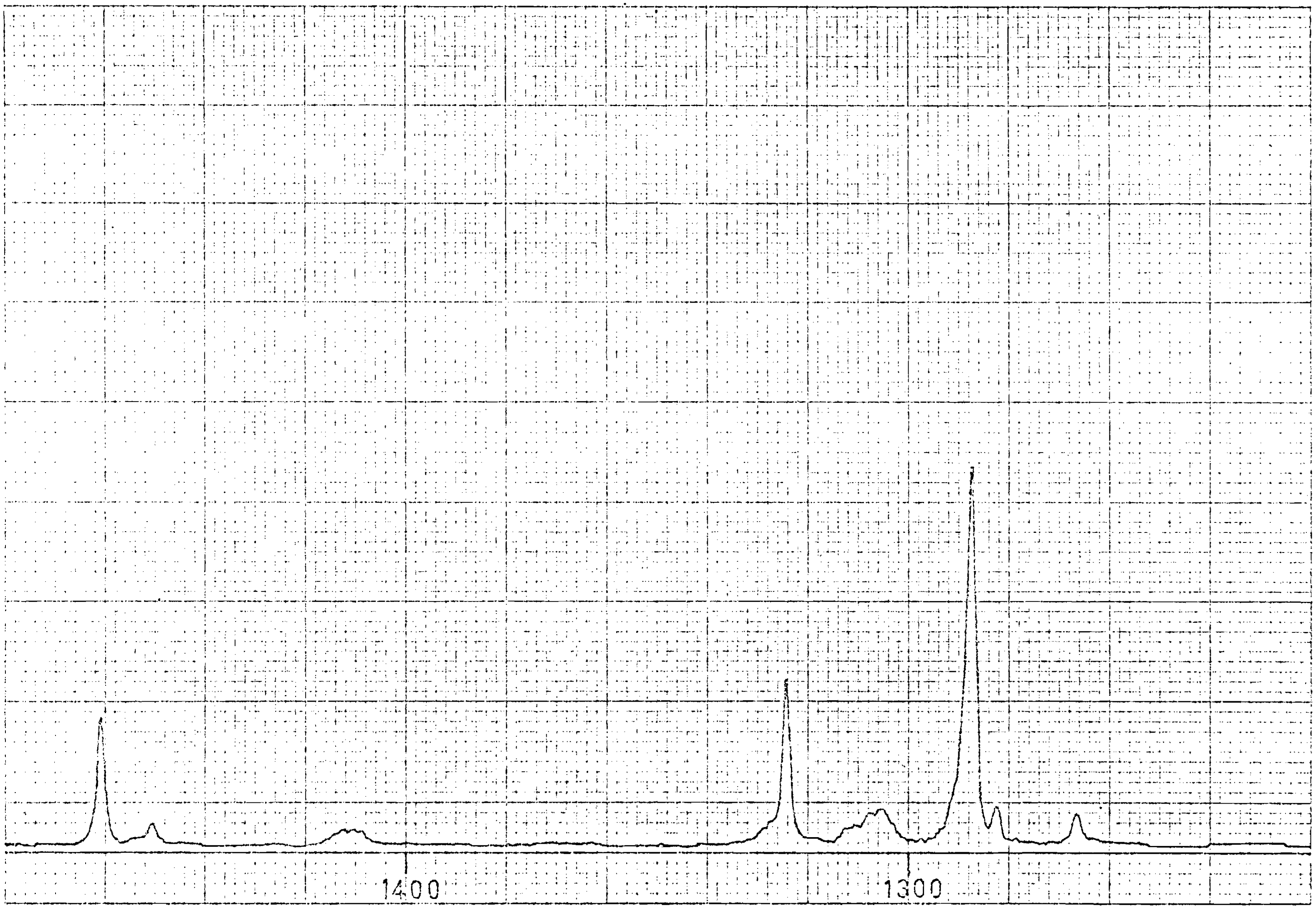
1400
1300

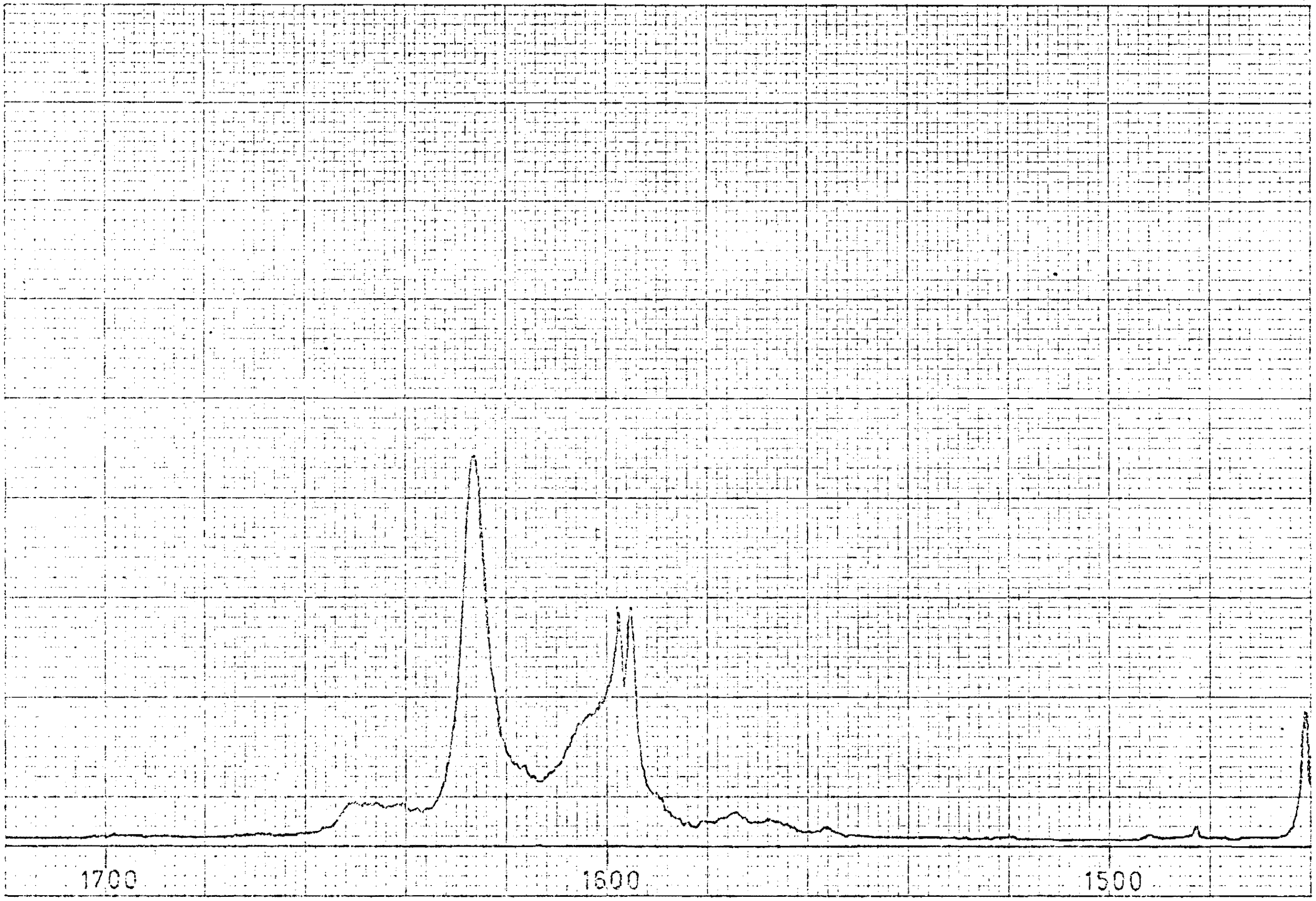
1700
1600
1500

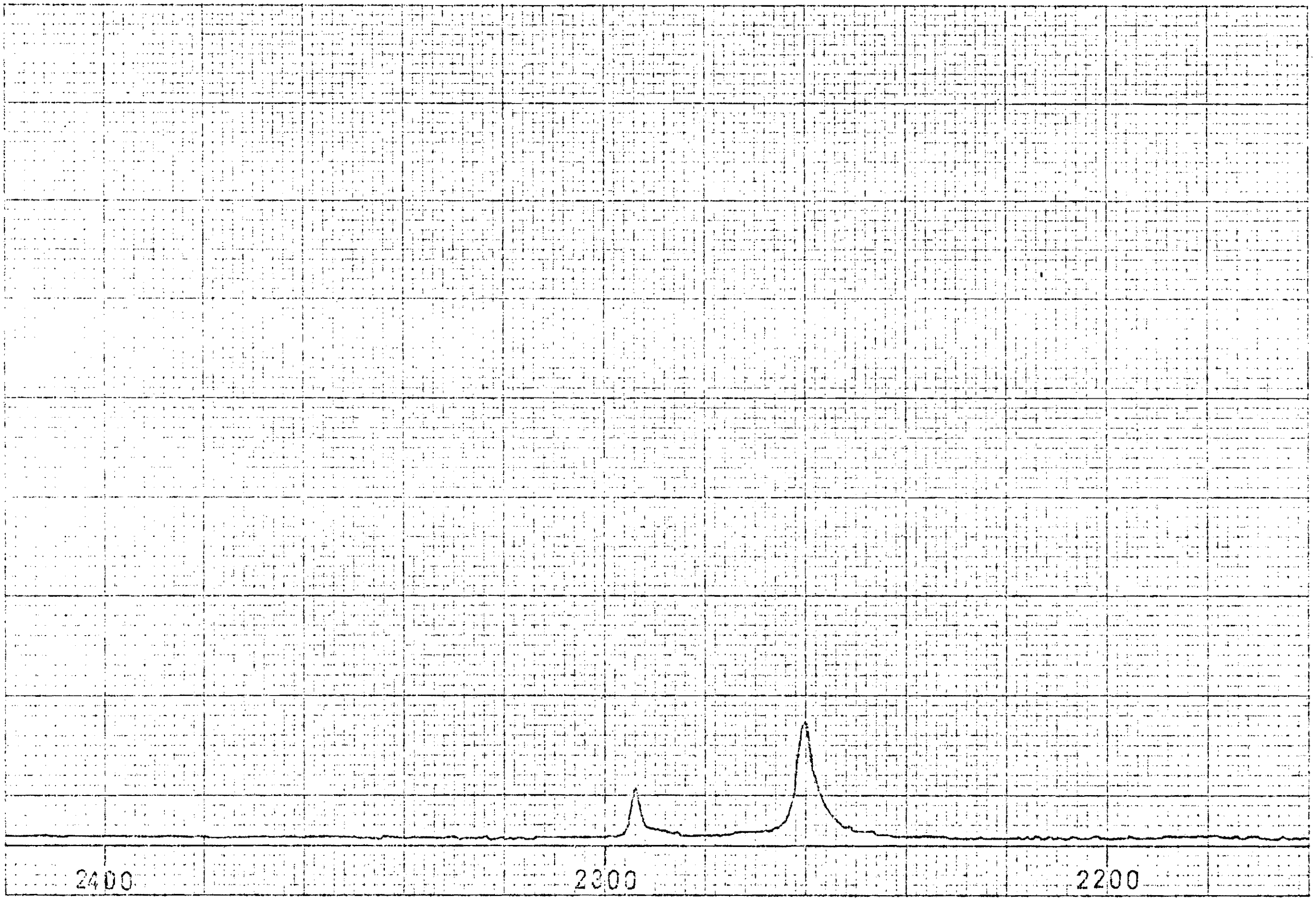
2400
2300
2200

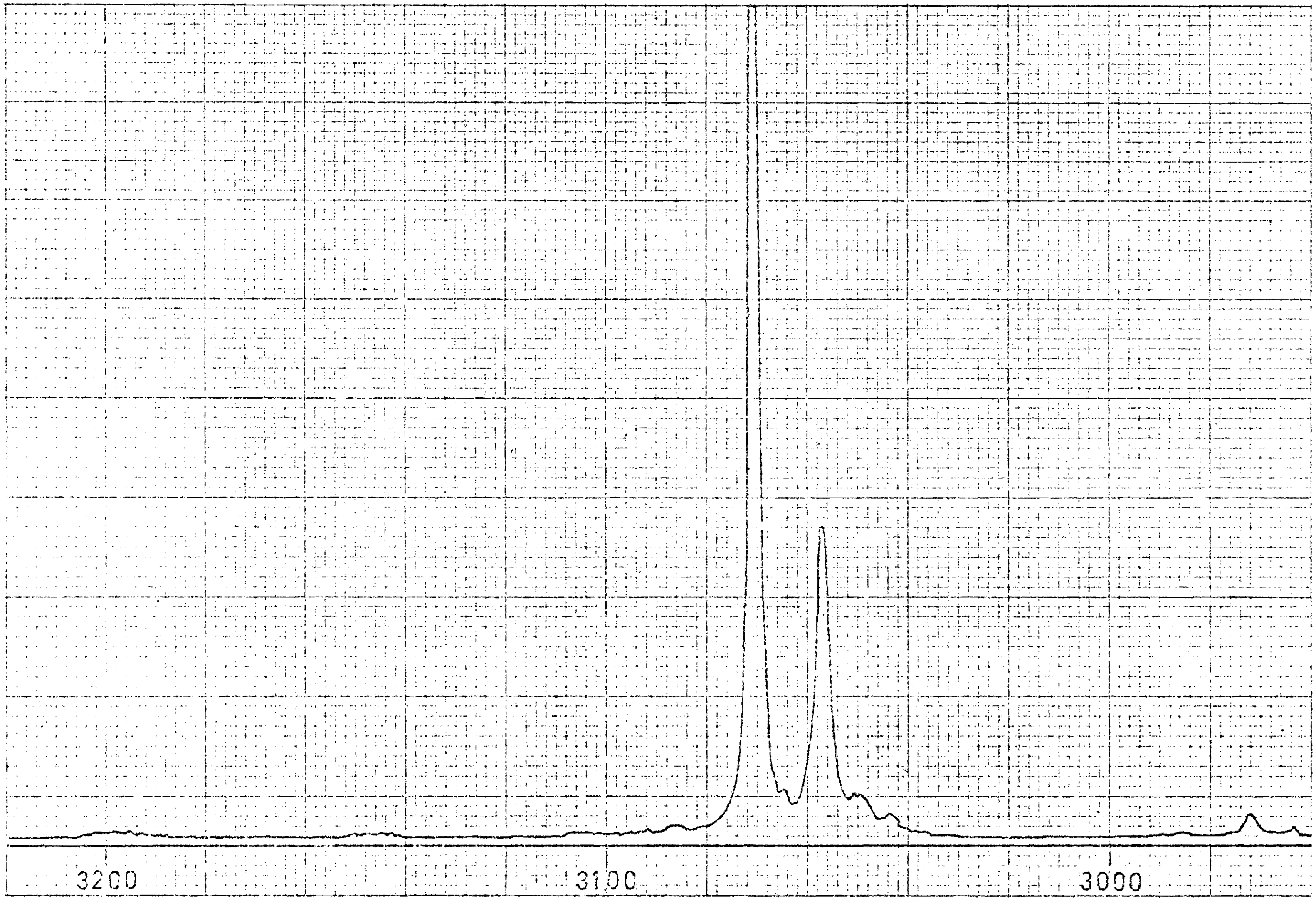
3200
3100
3000

FIGURE 11

Raman Spectrum of Benzoic Acid $4d_1$

Carey Model 82 Raman Spectrometer

Temperature = 4.2° K

Spectral Bandwidth = 0.4 cm^{-1}

Scan Rate - 0.5 cm^{-1}/second

Pen Period = 2.0 seconds

Sensitivity = 2×10^3 counts per second

Laser Wavelength - 5145 Å

Laser Power = 500 milliwatts

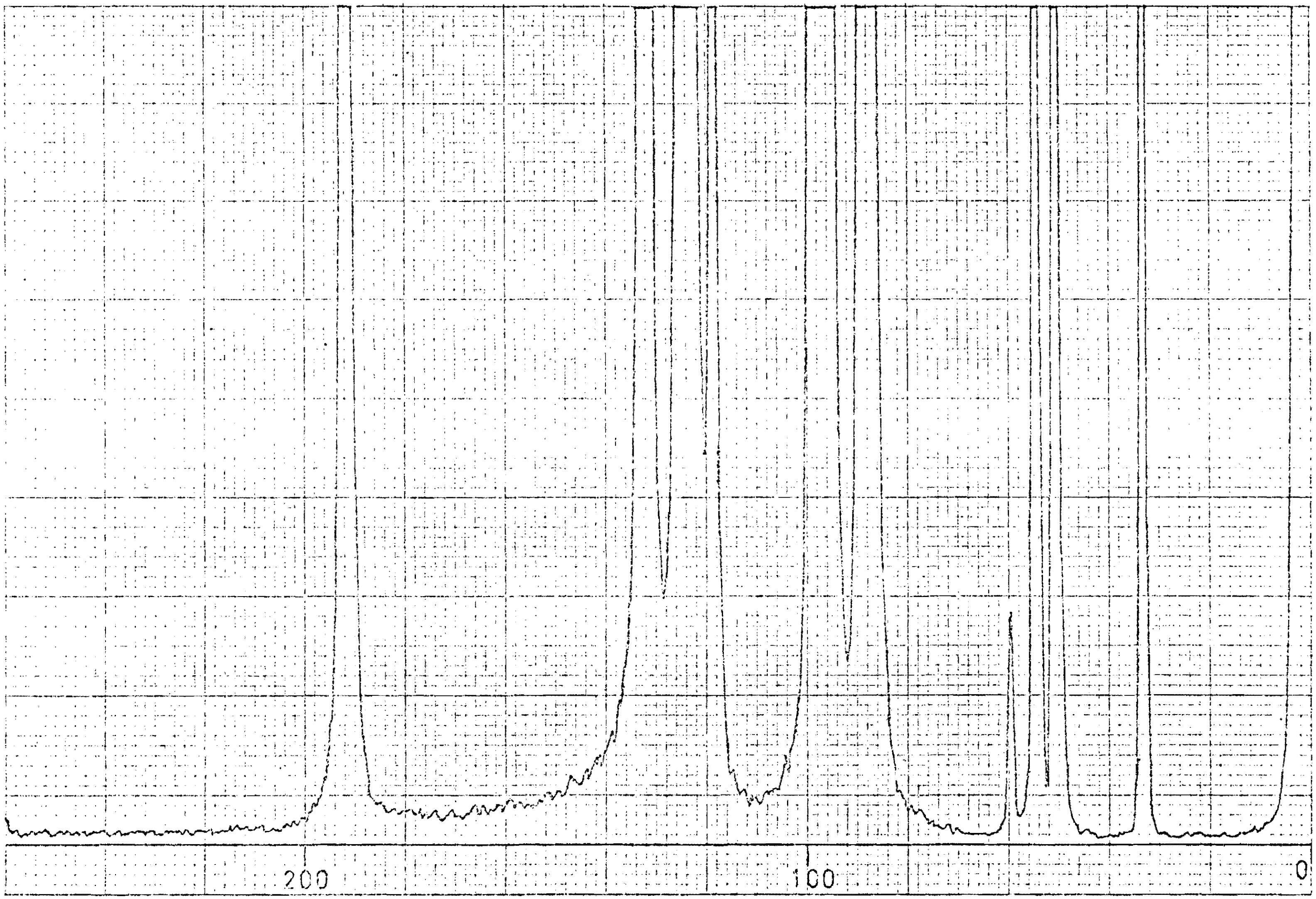
200
100
0

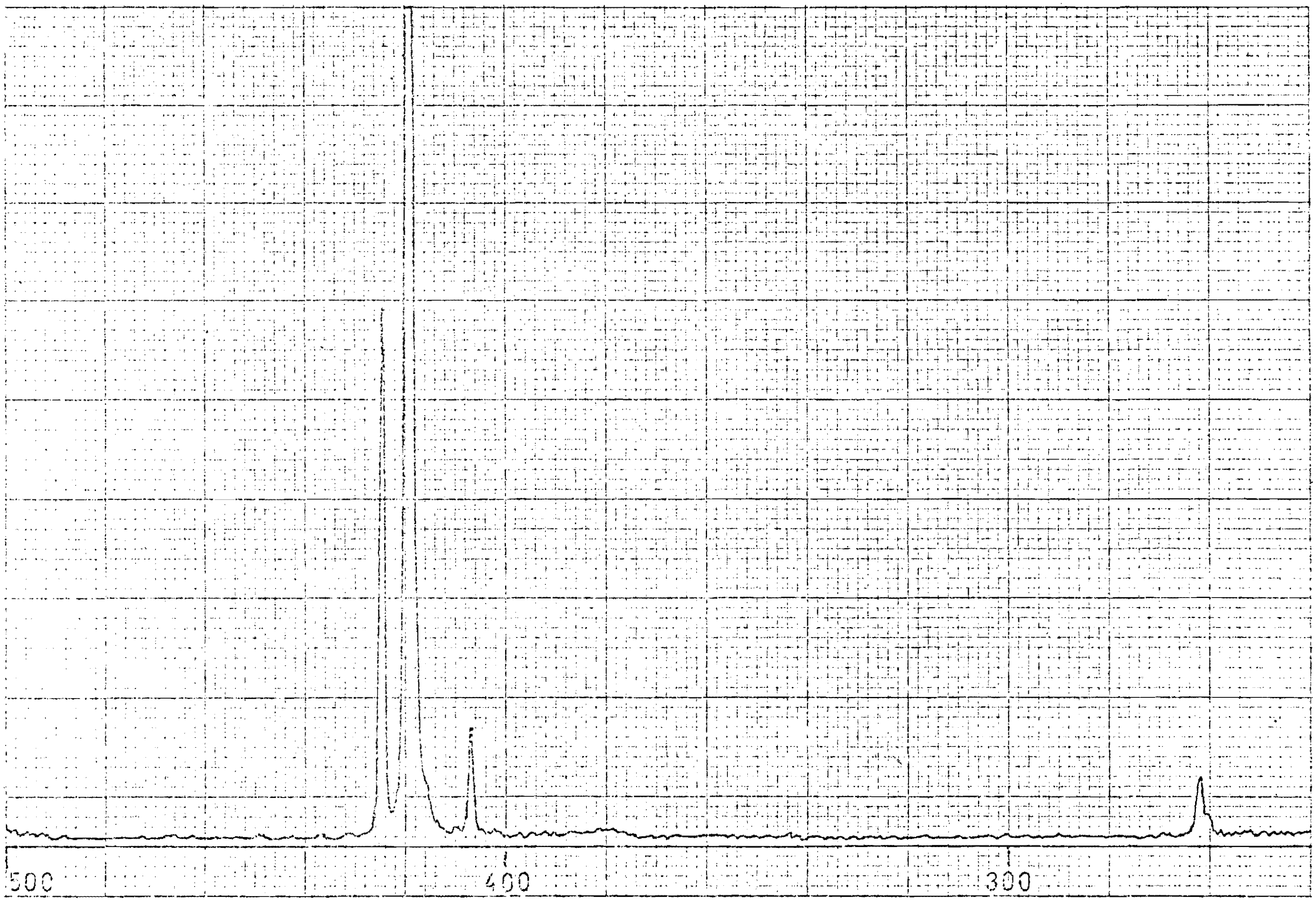
500
400
300

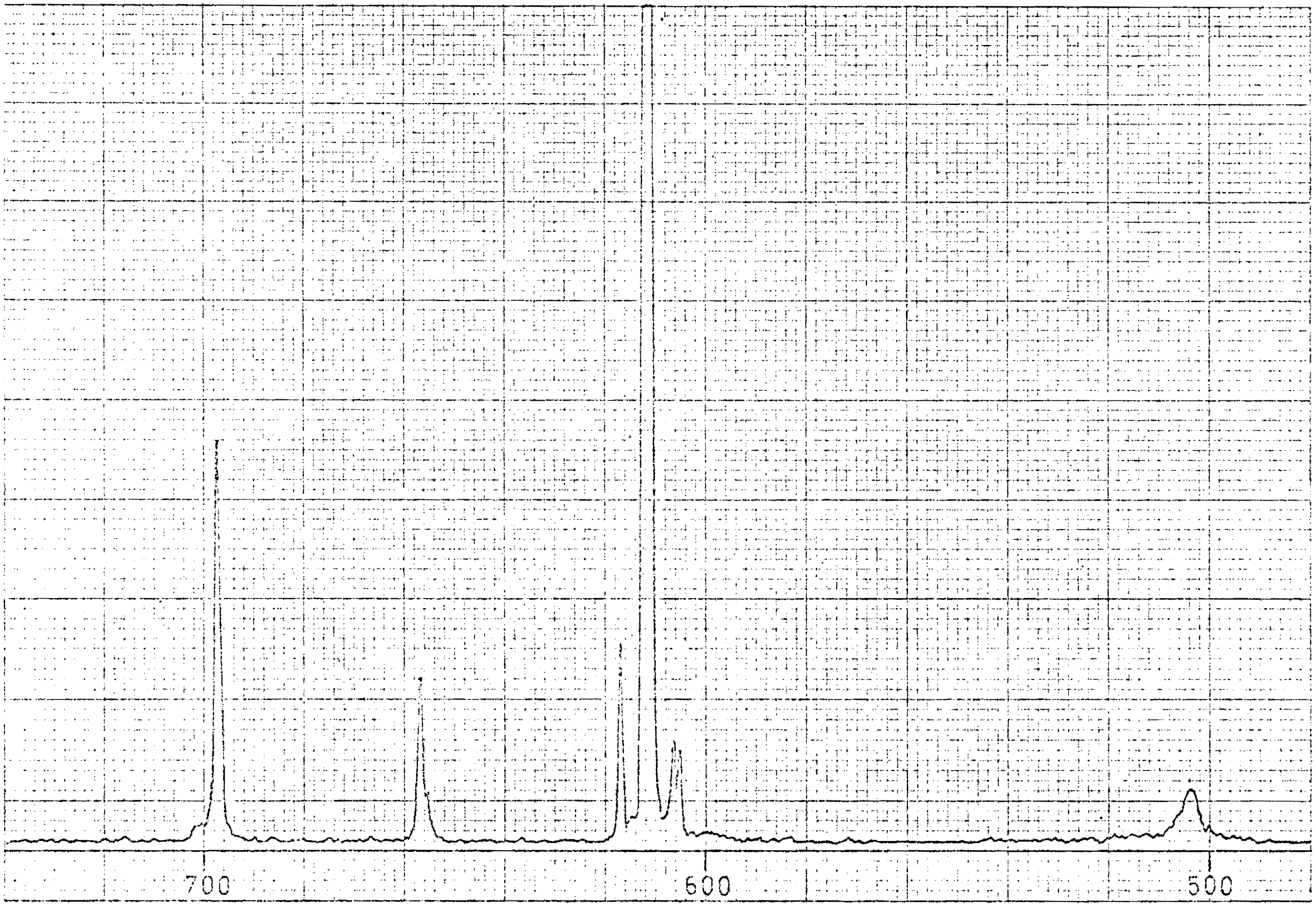
700
600
500

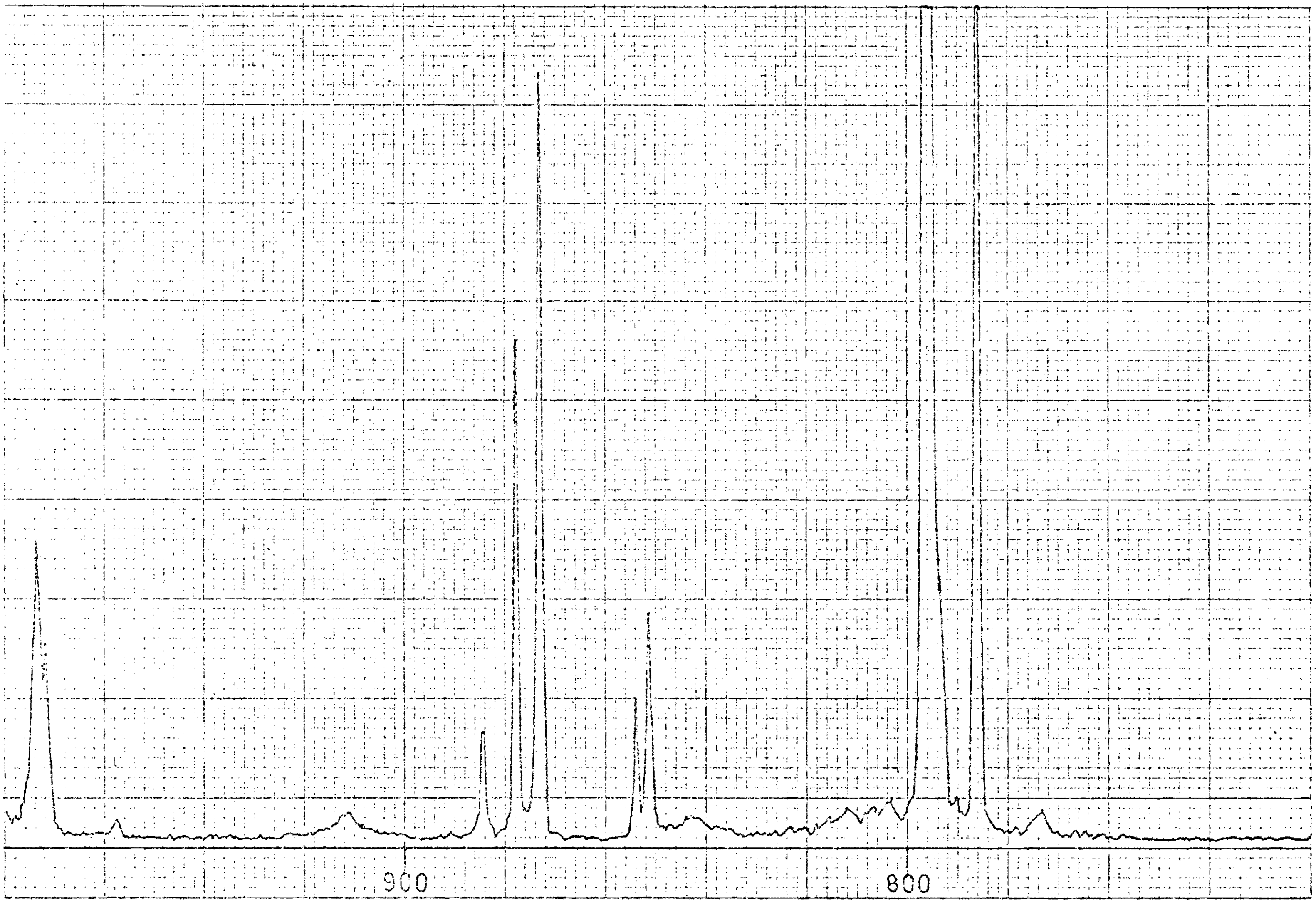
900
800

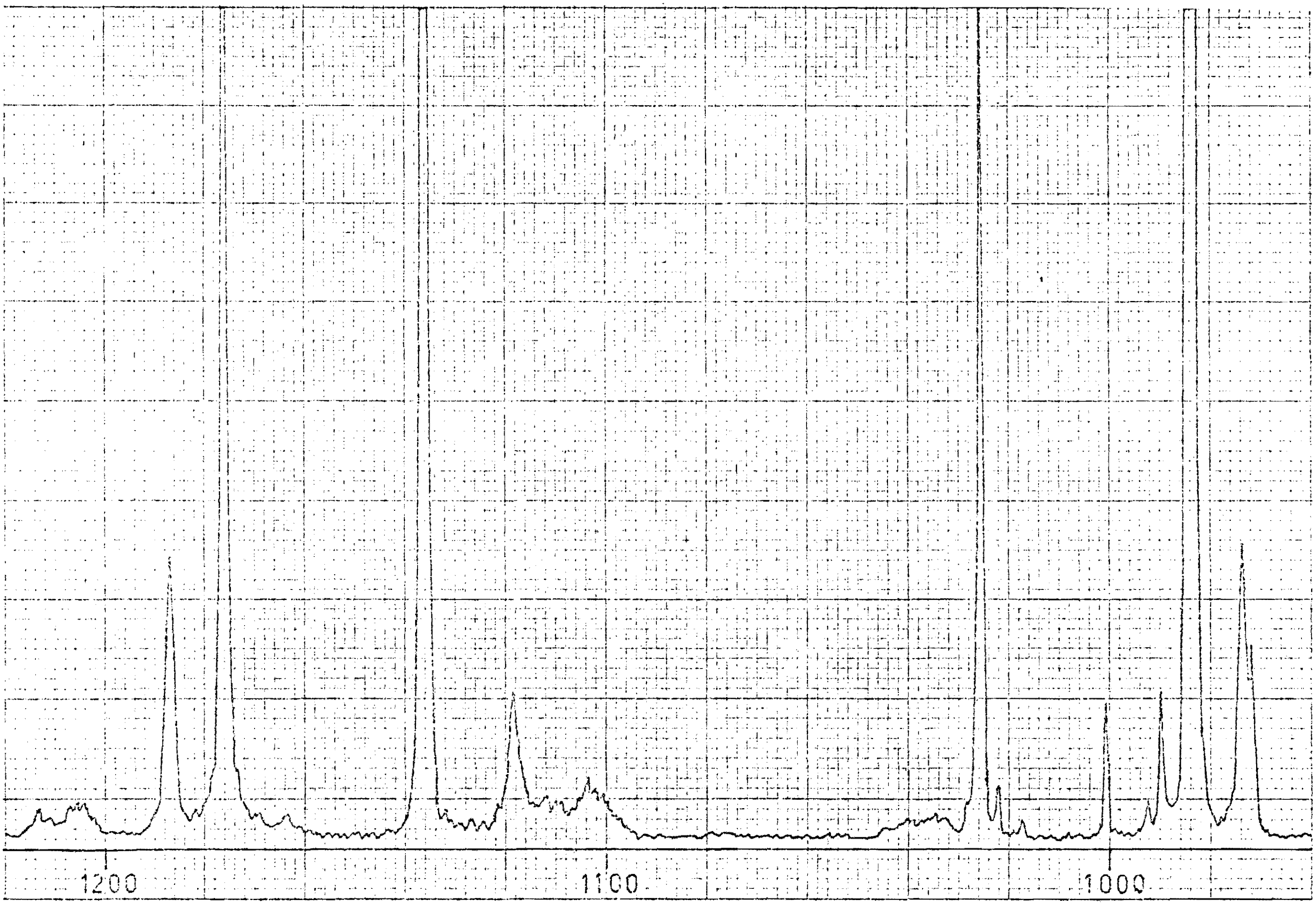
1200
1100
1000

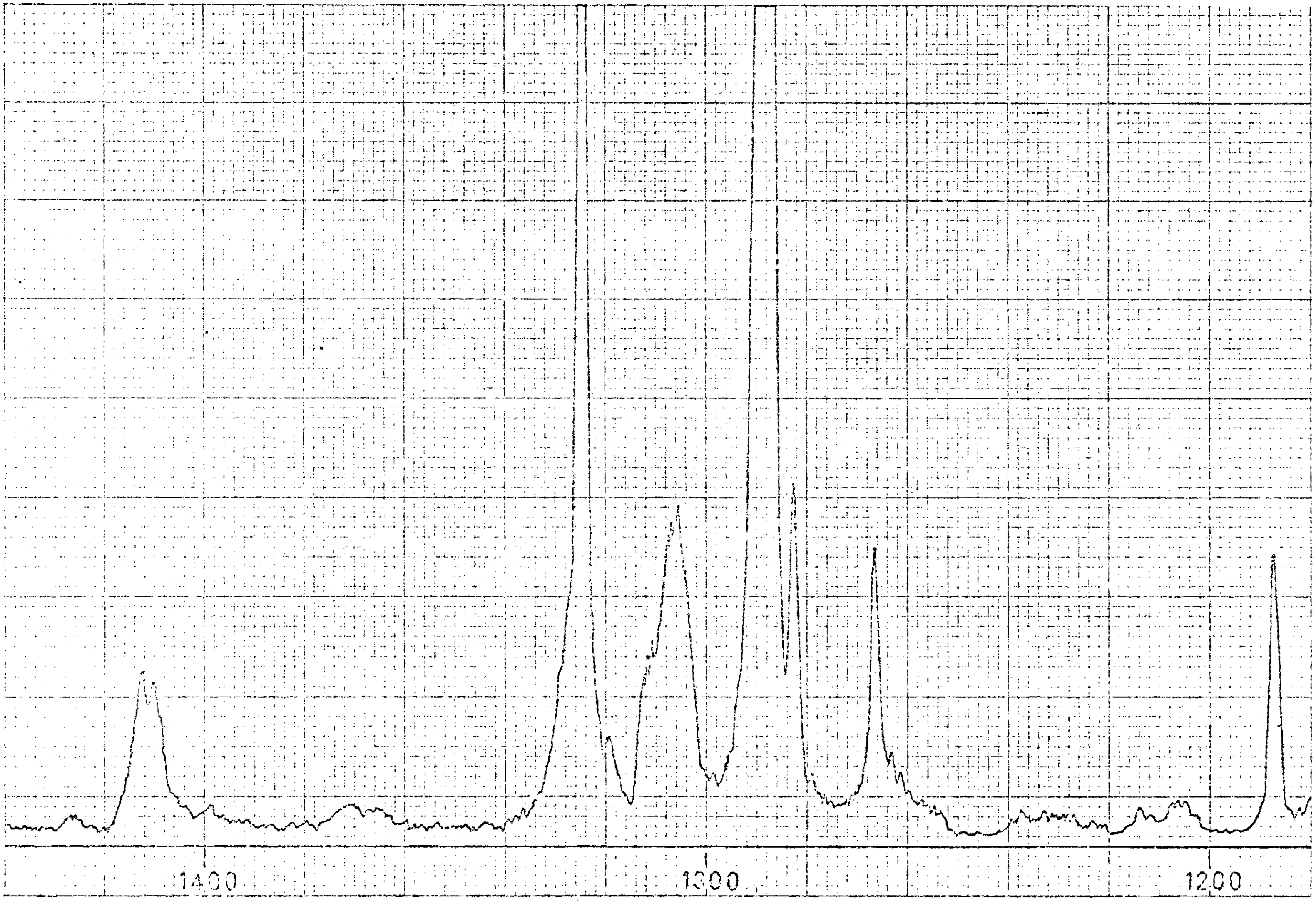
1400
1300
1200

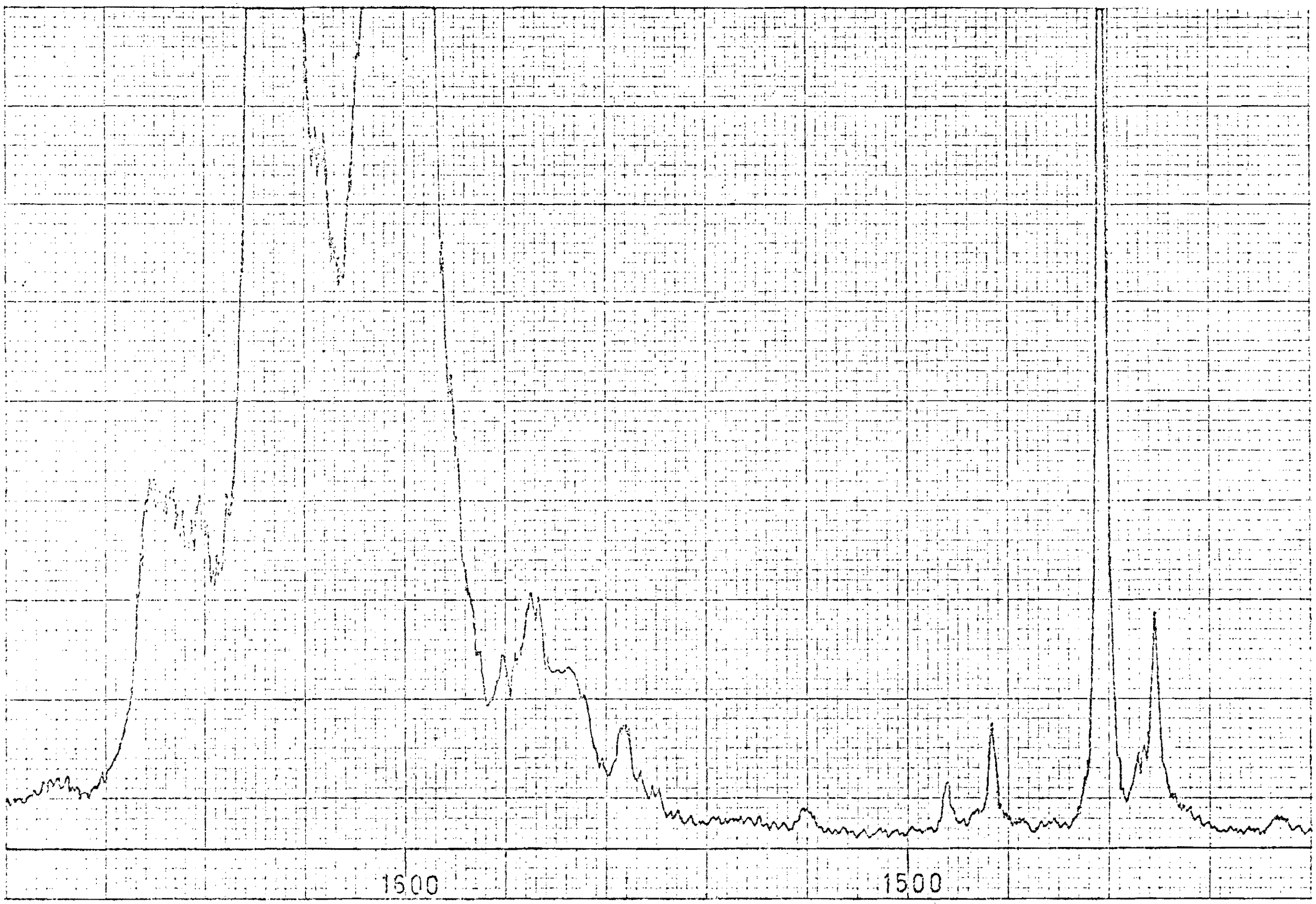

1600
1500

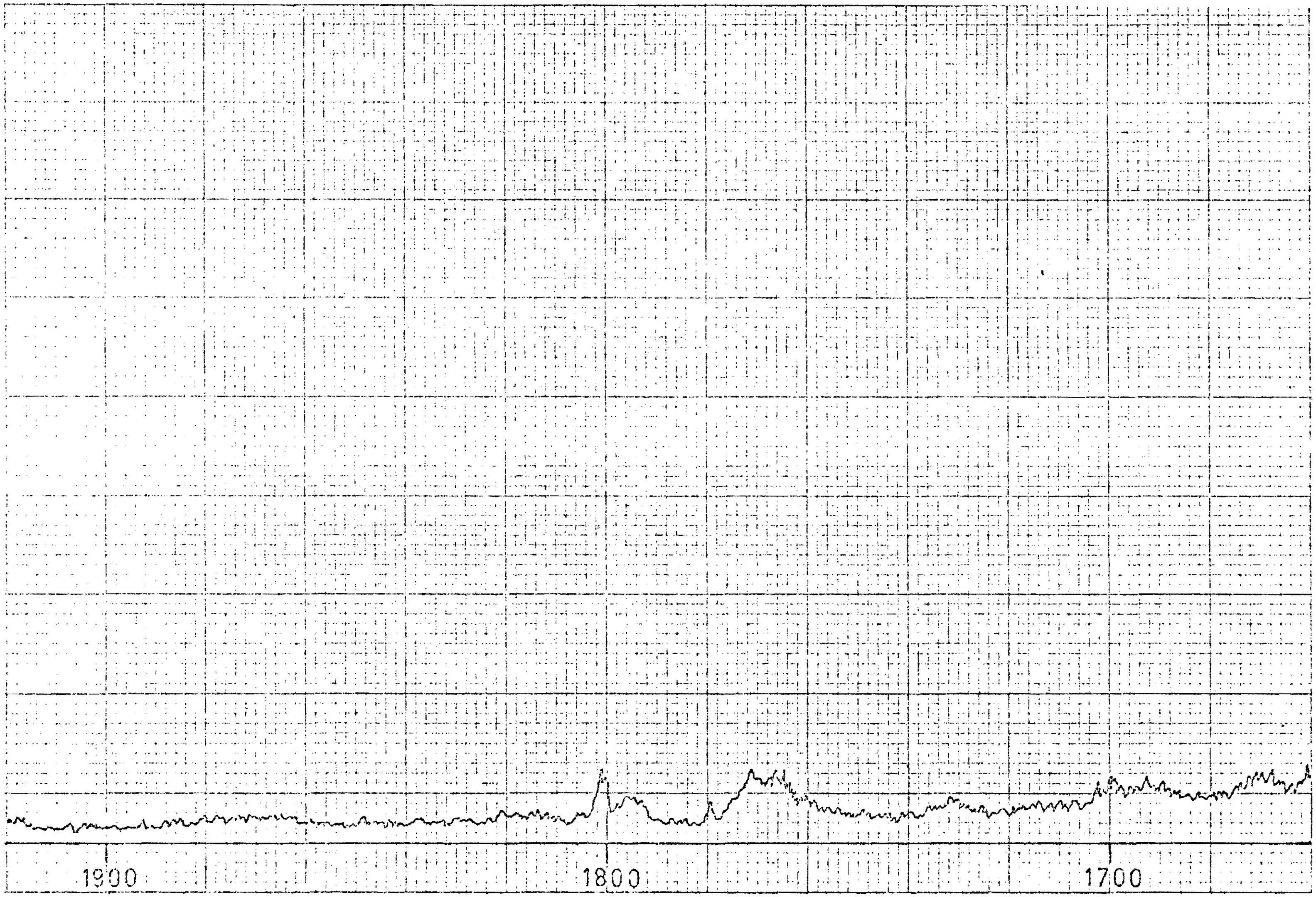
1900
1800
1700


2100
2000
1900

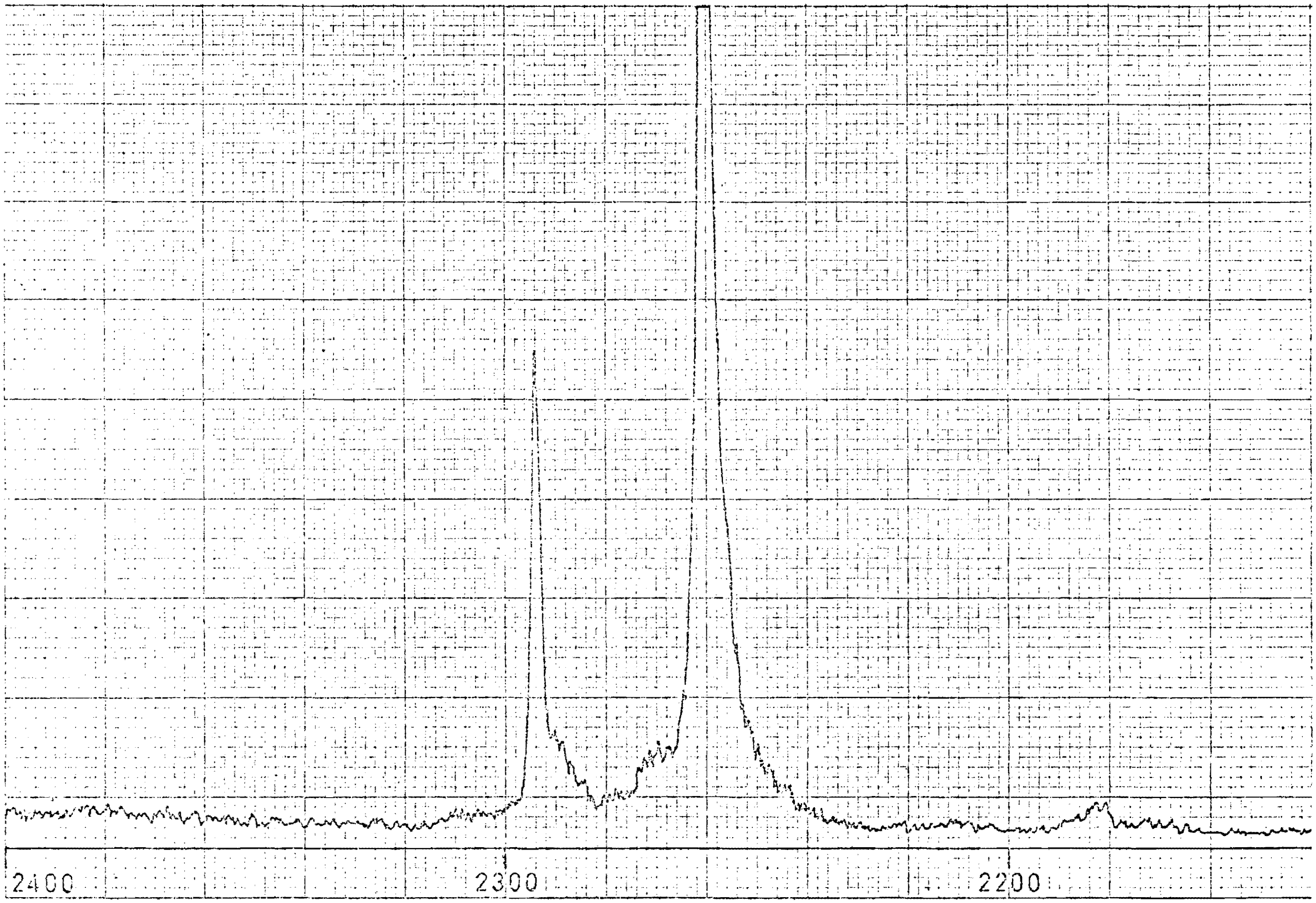
2400
2300
2200

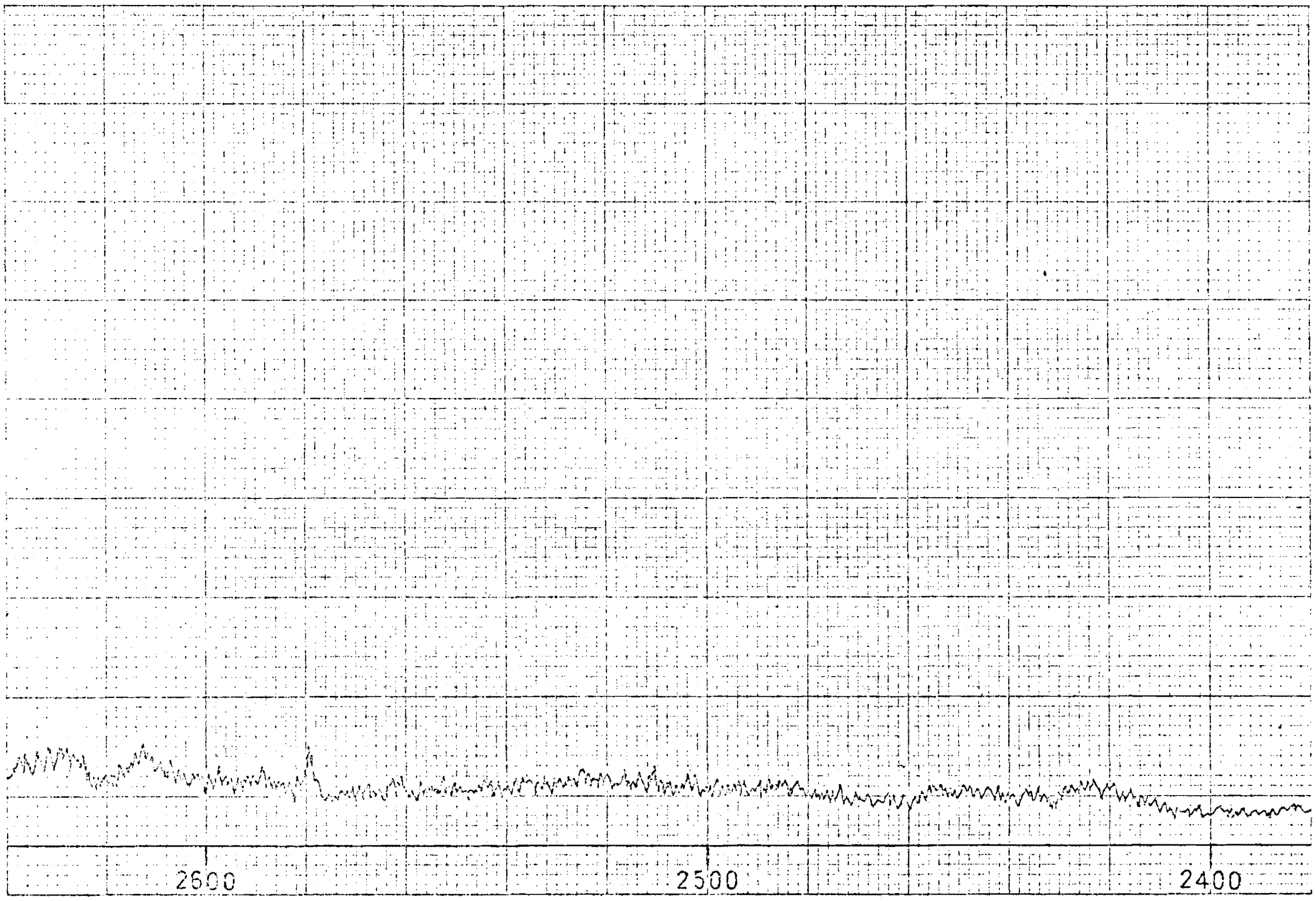
2600
2500
2400

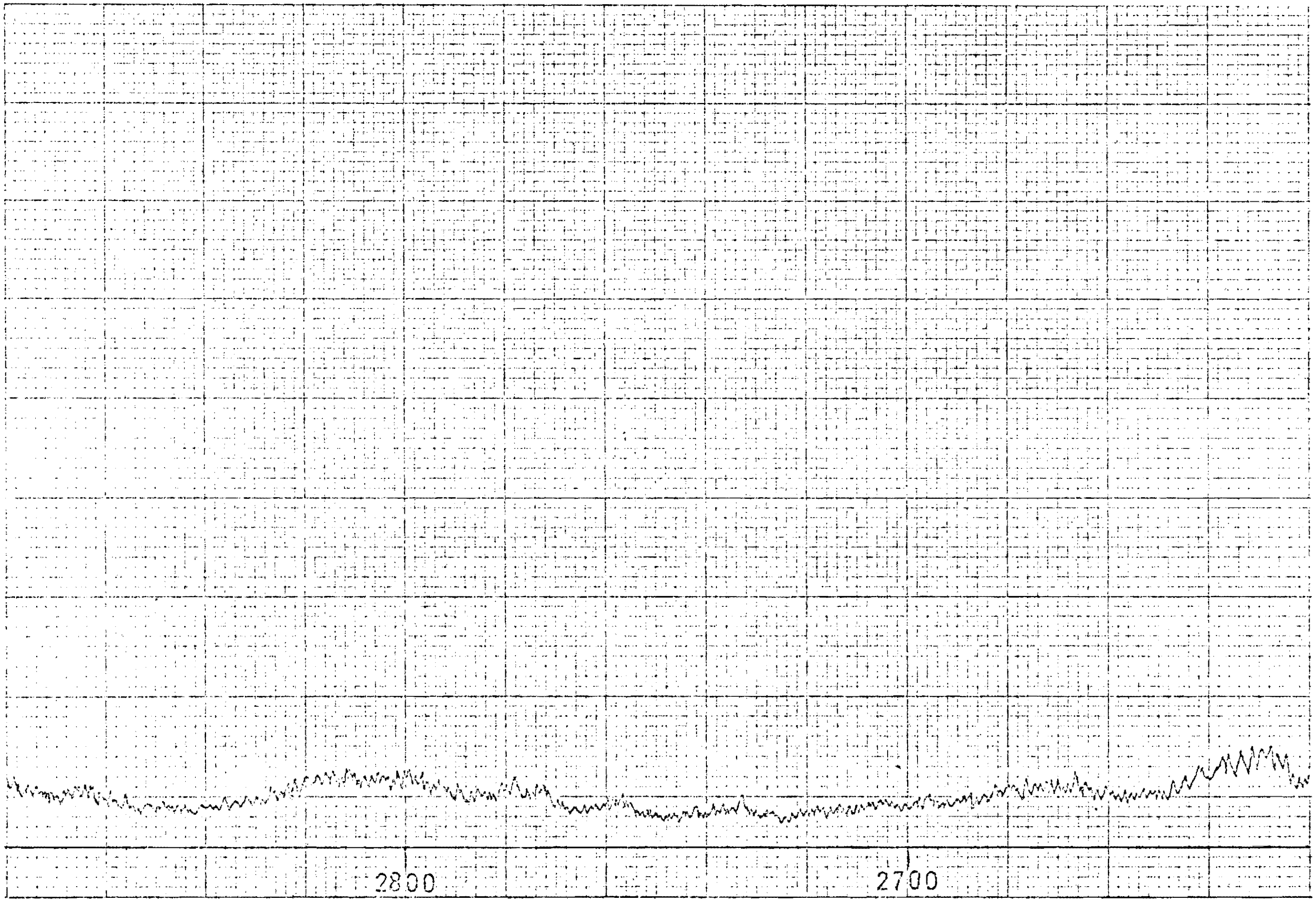
2800
2700

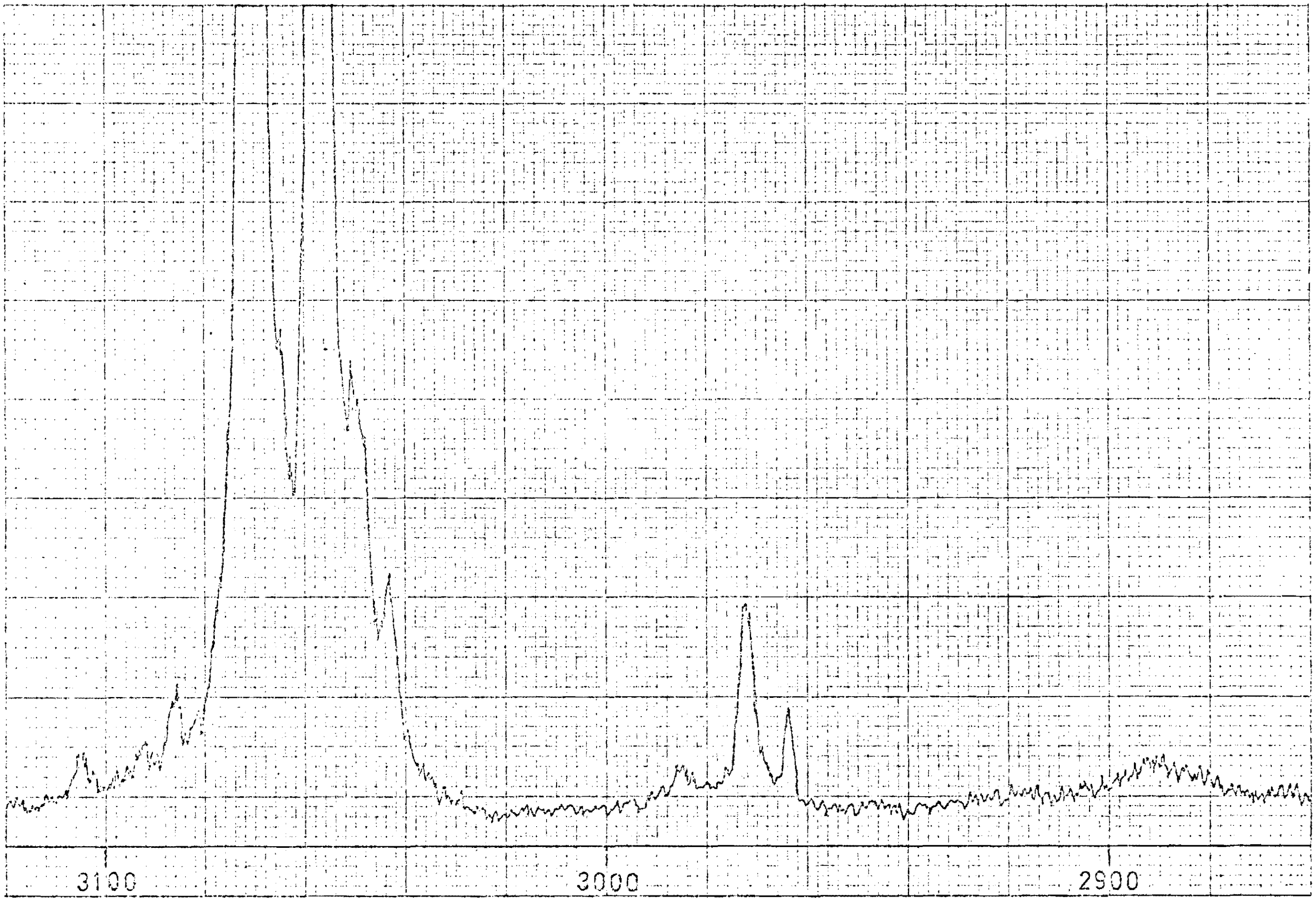
3100
3000
2900

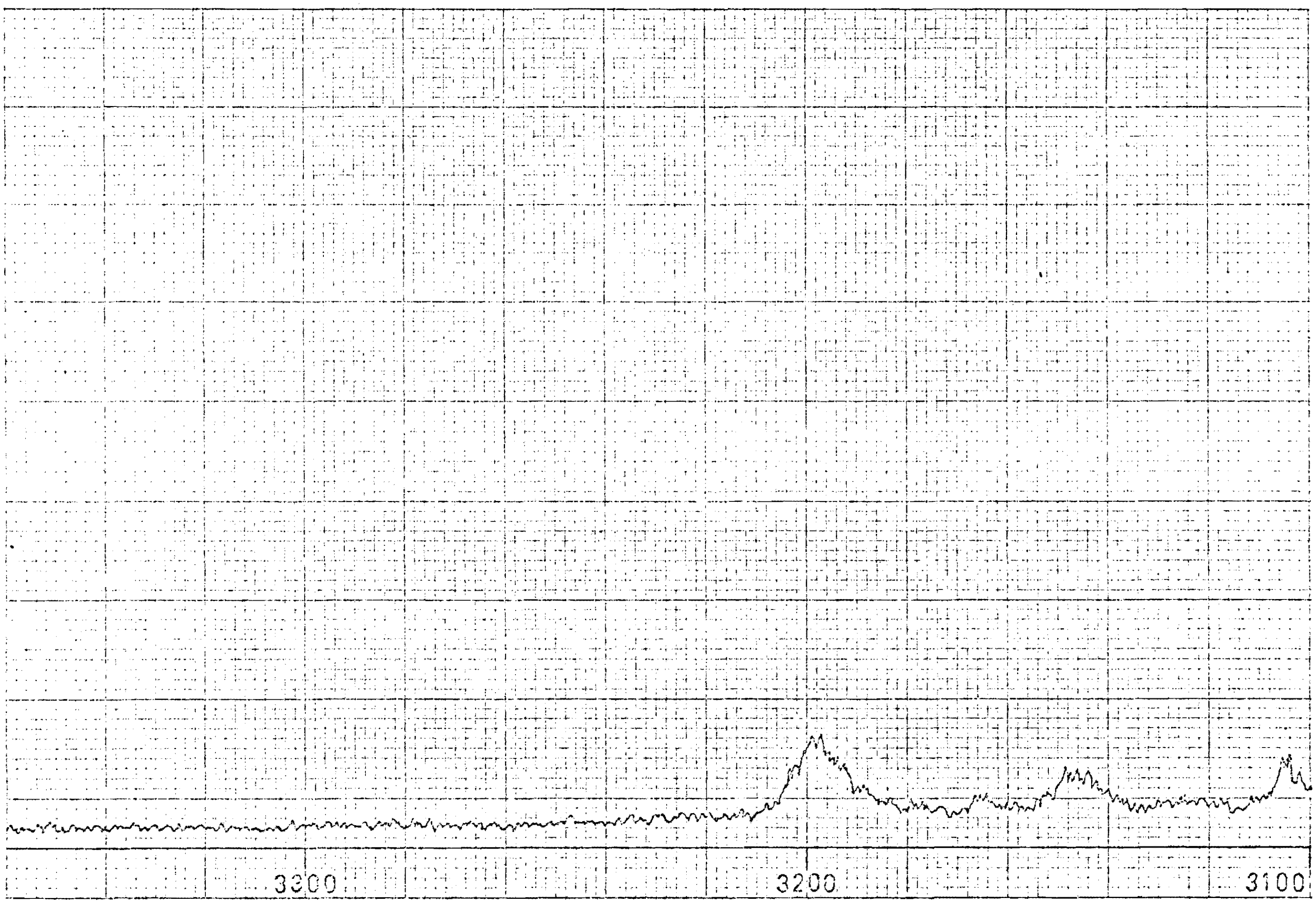
3300
3200
3100

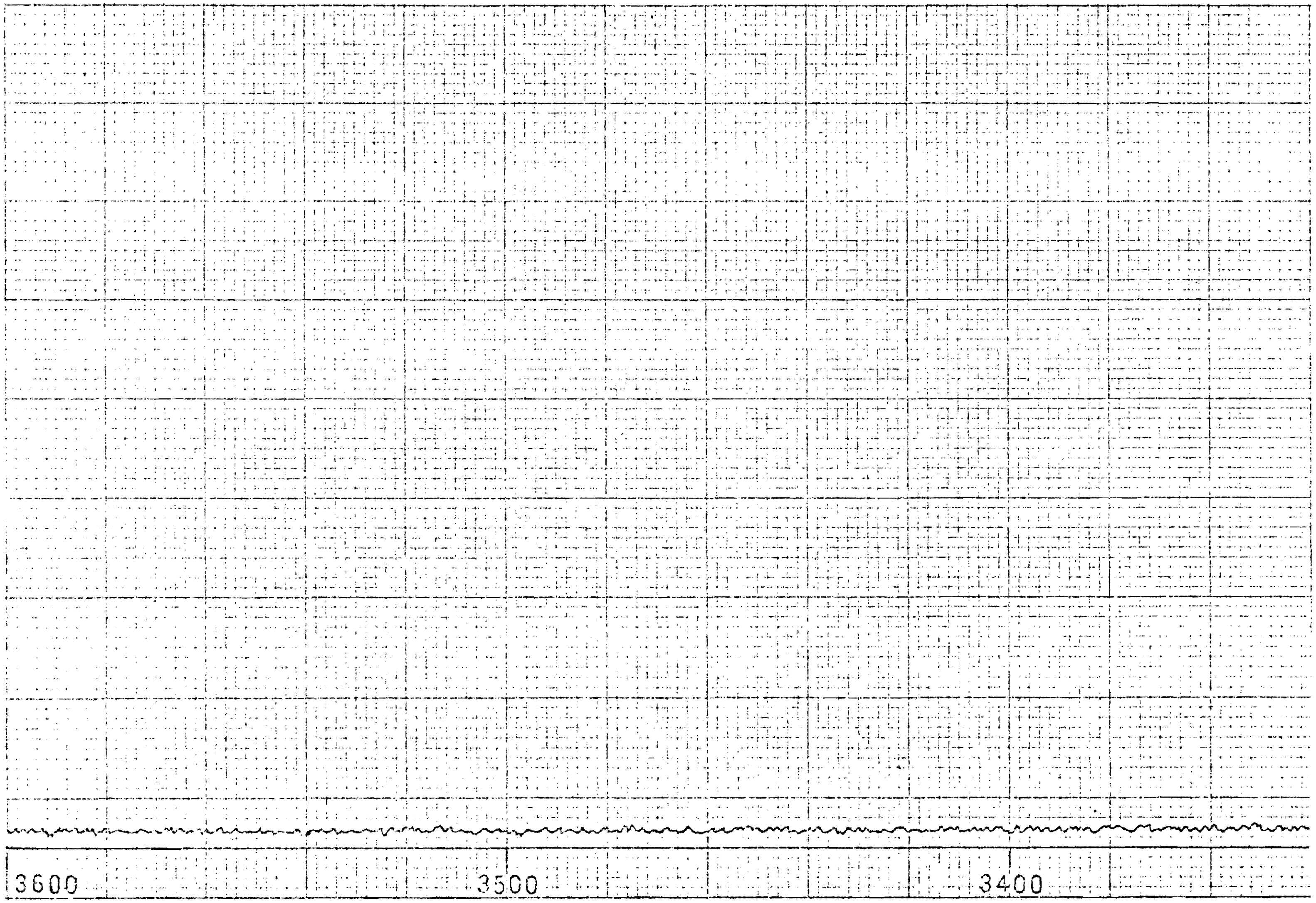
3600
3500
3400

TABLE 7

This table contains the frequencies and peak heights of bands in the Raman spectra shown in Figures 10 and 11. Peak heights are given relative to an arbitrary unit of intensity.

Band Number	Frequency (cm^{-1})	Peak Height	Comments
1	33.7	25.0	
2	51.0	20.0	
3	54.8	22.0	
4	60.0	2.50	
5	88.5	89.0	
6	96.9	76.0	
7	98.9	45.0	shoulder
8	119.0	25.0	
9	124.0	66.0	
10	132.5	42.0	
11	192.2	27.5	
12	260.7	0.24	shoulder
13	262.7	0.72	
14	380.5	0.96	
15	407.3	1.32	
16	415.5		unresolved shoulder
17	420.0	26.0	
18	425.0	6.42	
19	504.5	0.60	
20	506.5		unresolved shoulder
21	599.5	0.06	
22	605.5	.84	
23	607.0	1.2	
24	612.3	31.5	
25	612.8		unresolved shoulder
26	615.0	0.06	
27	617.3	2.34	
28	656.0	0.54	
29	657.0	1.92	
30	697.8	5.16	
31	701.5	0.18	
32	773.5	0.30	
33	775.5	0.24	
34	779.3	0.12	
35	786.5	17.0	
36	790.5	0.12	
37	794.5		unresolved shoulder
38	796.8	88.0	
39	803.0	0.36	
40	807.0	0.24	

Table 7 (Continued)

Band Number	Frequency (cm^{-1})	Peak Heights	Comments
41	811.5	0.30	
42	837.0	0.12	
43	843.0	0.24	
44	852.0	2.82	
45	854.5	1.68	
46	870.0	0.06	
47	873.5	9.30	
48	878.0	6.00	
49	881.0	0.12	
50	895.0	1.26	
51	911.5	0.42	
52	958.3	0.18	
53	972.7	2.28	
54	974.3	0.36	
55	985.3	>105	
56	990.5	14.5	
57	993.2	0.36	
58	1001.0	1.62	
59	1018.0	0.24	
60	1022.5	0.60	
61	1026.2	11.2	
62	1029.0		unresolved shoulder
63	1035.0	0.24	very broad
64	1043.0	0.18	very broad
65	1076.0	0.06	
66	1079.5	0.06	unresolved shoulder
67	1101.0	0.66	
68	1104.0	0.12	
69	1109.5	0.12	
70	1112.0		unresolved shoulder
71	1118.0	1.74	
72	1119.0	0.06	
73	1122.0	0.12	
74	1125.0	0.12	
75	1127.5	0.12	
76	1132.5	0.12	
77	1137.0	32.5	
78	1164.2	0.30	
79	1170.0	0.30	
80	1174.0		unresolved shoulder
81	1176.5	12.4	
82	1182.5	0.06	
83	1187.7	3.24	
84	1203.0	0.06	
85	1206.0	0.36	
86	1212.0	.12	

Table 7 (Continued)

Band Number	Frequency (cm^{-1})	Peak Heights	Comments
87	1214.5	.42	
88	1222.5	0.06	very broad
89	1230.0	0.24	very broad
90	1239.0	0.12	broad
91	1255.0	0.36	very broad
92	1261.5	0.12	shoulder
93	1263.5	0.18	shoulder
94	1267.0	3.48	
95	1279.3	0.30	
96	1283.0	4.26	shoulder
97	1287.8	37.5	
98	1298.5	0.06	
99	1303.5	3.96	
100	1307.5	3.6	shoulder
101	1311.0		unresolved shoulder
102	1312.0		unresolved shoulder
103	1319.5	0.72	shoulder
104	1325.0	16.5	
105	1328.0		unresolved shoulder
106	1329.5		unresolved shoulder
107	1365.0	0.24	
108	1371.5	0.24	
109	1391.0	0.24	
110	1404.0	0.12	broad shoulder
111	1410.5	0.18	
112	1413.0	1.92	
113	1427.0	0.18	
114	1451.0	2.70	
115	1453.5	0.18	shoulder
116	1554.7	0.24	shoulder
117	1461.5	13.0	
118	1471.5	0.12	broad
119	1478.5	0.18	broad
120	1483.5	1.32	
121	1487.0	0.12	shoulder
122	1491.0		unresolved shoulder
123	1492.0	0.60	
124	1520.5	0.36	
125	1550.5	0.18	
126	1556.5	0.72	
127	1567.5	0.60	broad shoulder
128	1574.0	1.68	shoulder

Table 7 (Continued)

Band Number	Frequency (cm^{-1})	Peak Heights	Comments
129	1575.5	1.80	
130	1580.5	0.48	
131	1585.5		unresolved shoulder
132	1587.5		unresolved shoulder
133	1589.5		unresolved shoulder
134	1591.0		unresolved shoulder
135	1592.5		unresolved shoulder
136	1596.0	23.0	
137	1598.0	22.0	
138	1605.0	6.0	broad shoulder
139	1616.5		unresolved shoulder
140	1618.0		unresolved shoulder
141	1627.0	39.0	
142	1633.5		unresolved shoulder
143	1641.0	0.78	
144	1646.5		unresolved shoulder
145	1650.5	3.60	
146	1670.0	0.24	very broad
147	1693.0	0.12	
148	1700.0	0.30	
149	1732.0	0.24	
150	1736.0	0.12	
151	1766.0	0.66	broad
152	1772.0	0.66	broad
153	1780.0	0.30	
154	1795.0	0.30	broad
155	1801.0	0.60	
156	2182.0	0.18	
157	2188.0	0.06	
158	2255.0		unresolved shoulder
159	2260.5	12.0	
160	2270.5	0.36	very broad
161	2282.5	0.06	shoulder
162	2287.5	0.06	shoulder
163	2290.0	0.06	shoulder
164	2294.5	5.76	
165	2305.0	0.12	
166	2310.0	0.12	
167	2414.0	0.06	very broad

Table 7 (Continued)

Band Number	Frequency (cm^{-1})	Peak Heights	Comments
168	2425.0	0.24	very broad
169	2455.0	0.30	very broad
170	2479.5	0.48	
171	2613.0	0.36	
172	2630.0	0.48	very broad
173	2757.5	0.18	
174	2773.0	0.24	
175	2779.0	0.18	
176	2808.0	0.48	very broad
177	2865.0	0.24	
178	2890.0	0.54	very broad
179	2964.0	1.20	
180	2968.0	1.20	broad shoulder
181	2992.5	2.52	
182	2985.0	0.48	
183	3043.0	1.44	
184	3050.0	1.80	unresolved shoulder
185	3057.5	31.50	
186	3065.0	1.32	
187	3071.0	>105	
188	3081.5	0.24	
189	3086.0	0.66	
190	3092.5	0.36	
191	3103.5	0.54	
192	3147.0	0.48	broad
193	3153.0	0.24	
194	3166.0	0.18	
195	3198.0	1.08	

FIGURE 12

Raman Spectrum of Benzoic Acid d_5

Carey Model 82 Raman Spectrometer

Temperature - 4.2° K

Spectral Bandwidth = 0.5 cm^{-1}

Scan Rate = 0.25 cm^{-1}/second

Pen Period = 1.0 second

Sensitivity = 2×10^4 counts per second

Laser Wavelength = 5145 Å

Laser Power (not recorded)

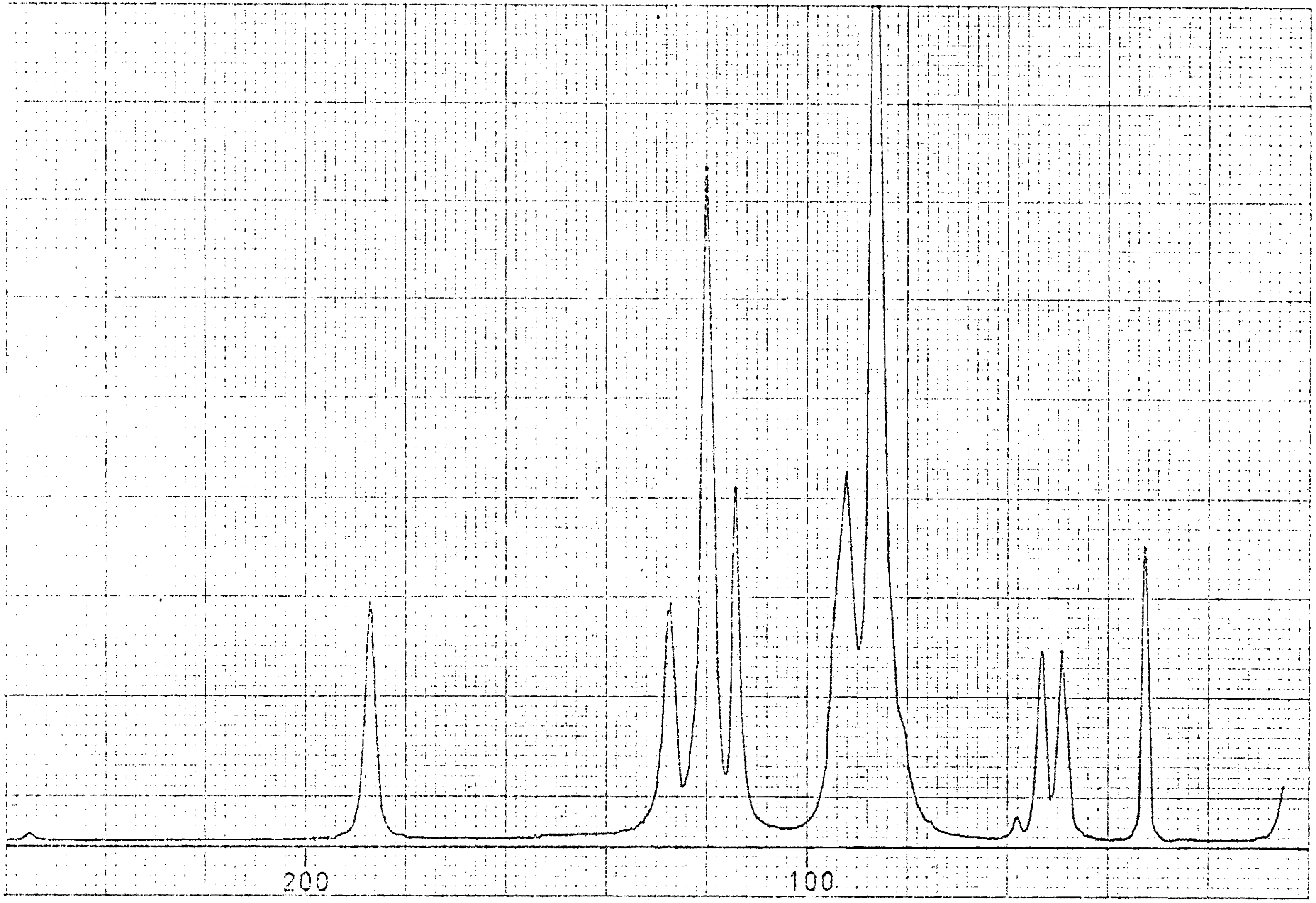
200
100

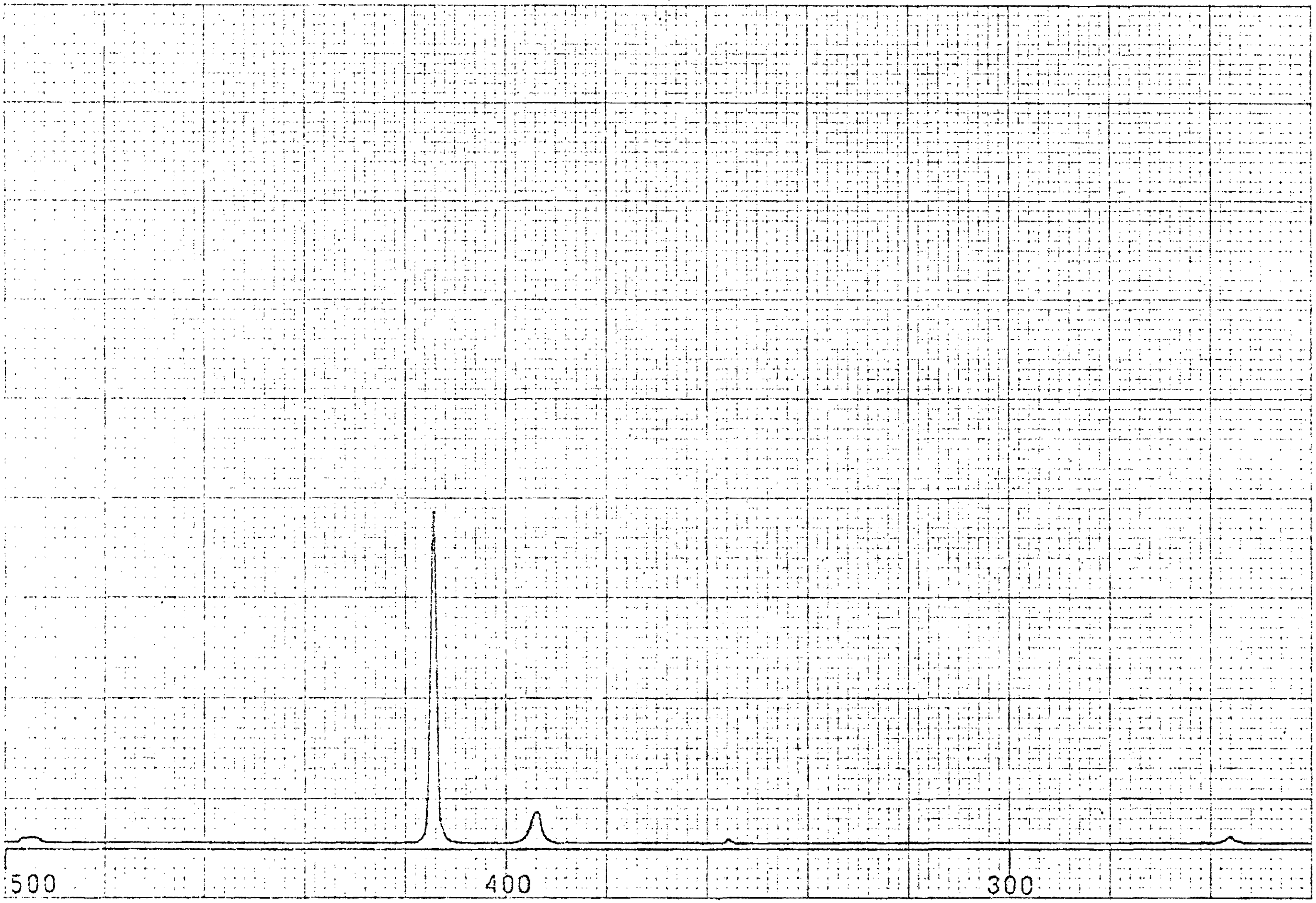
500
400
300

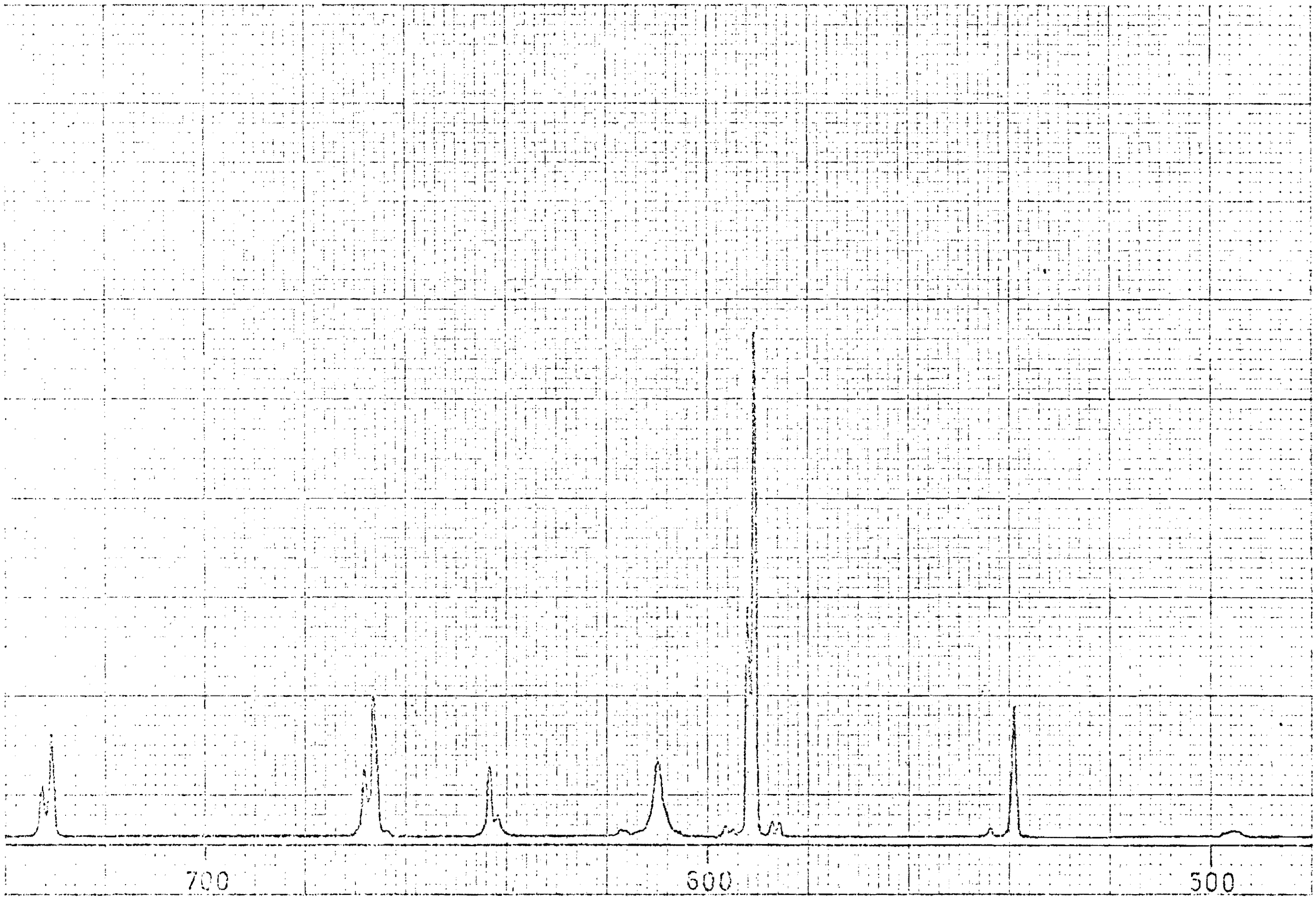
700
600
500

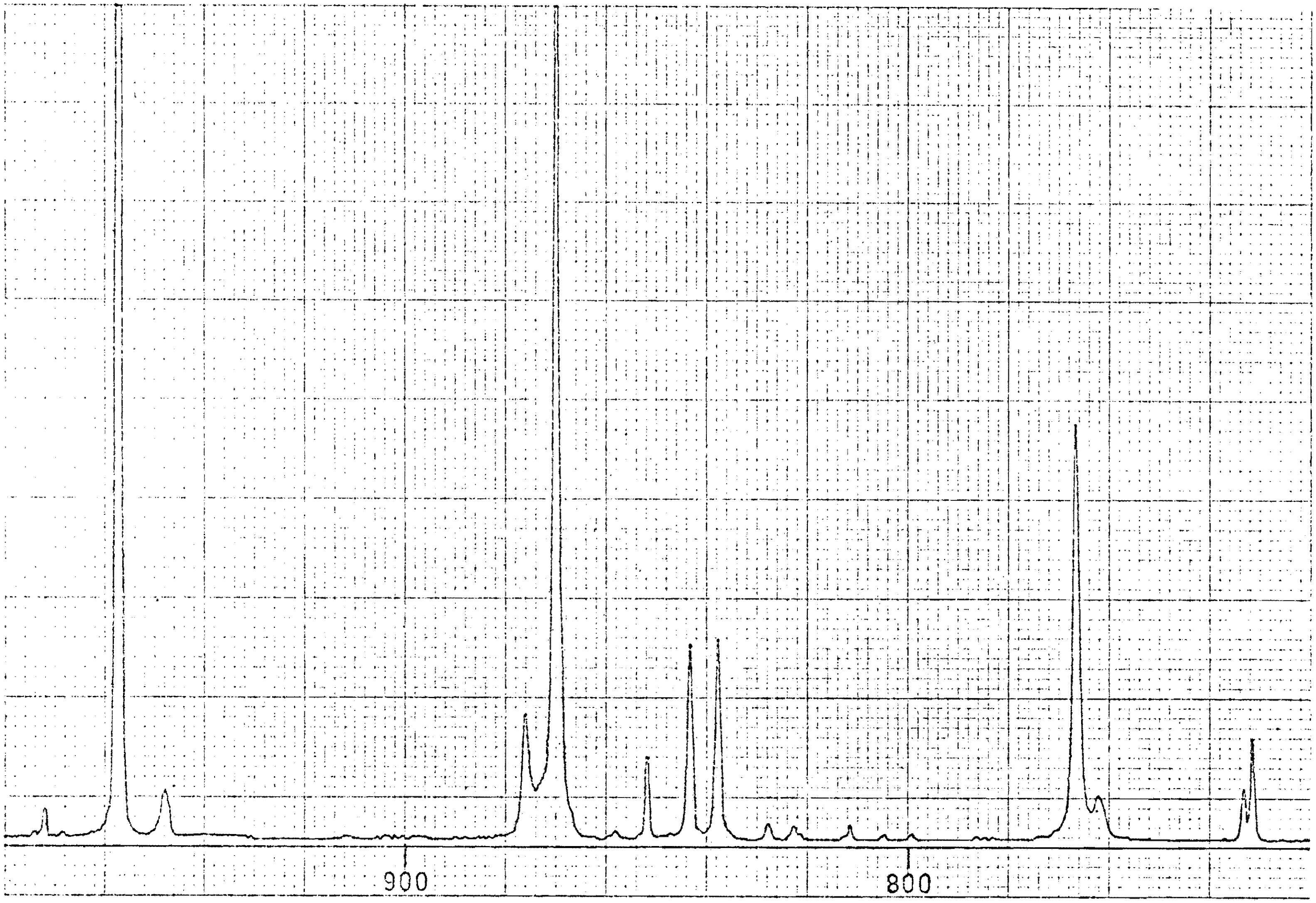
900
800

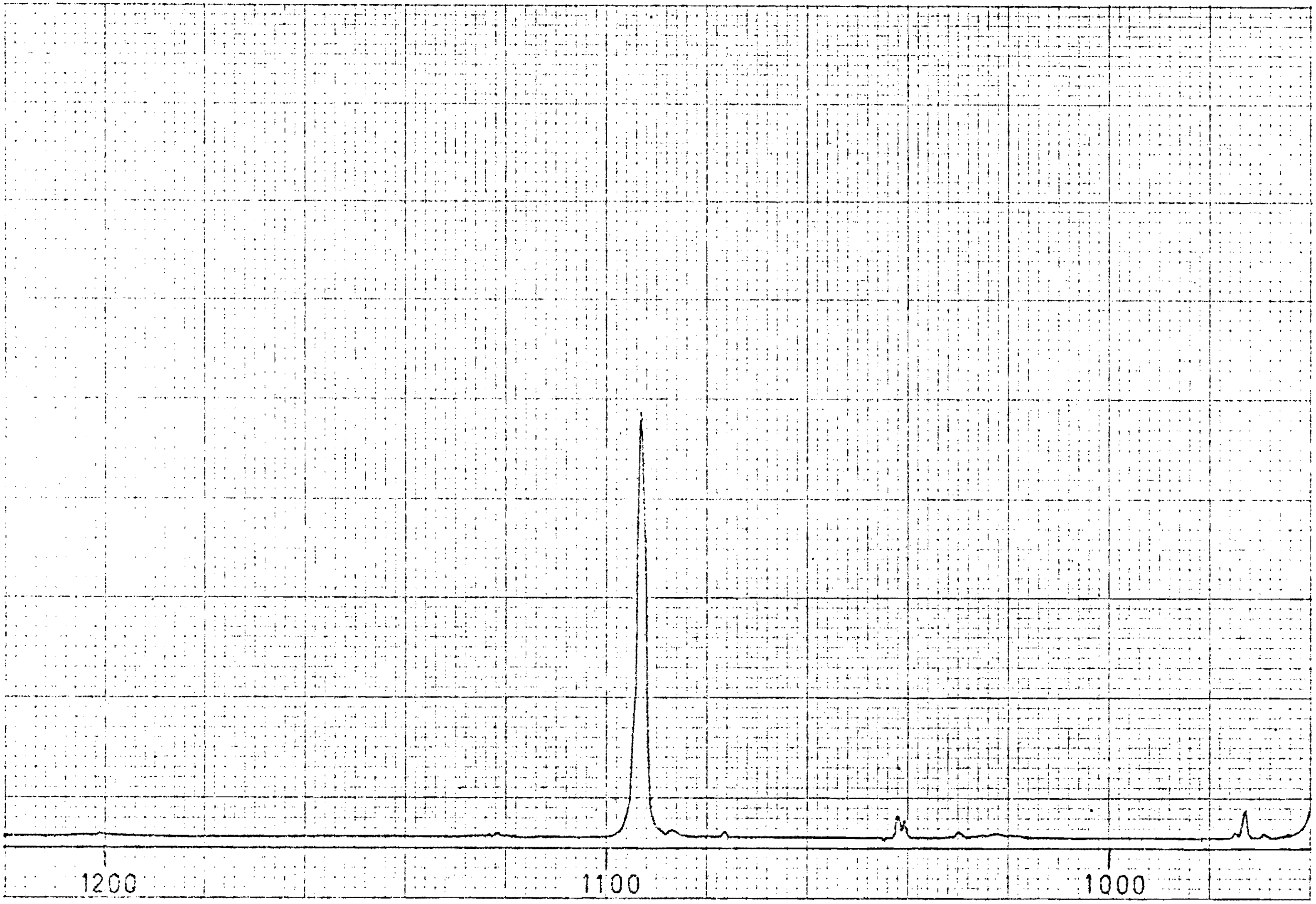
1200
1100
1000

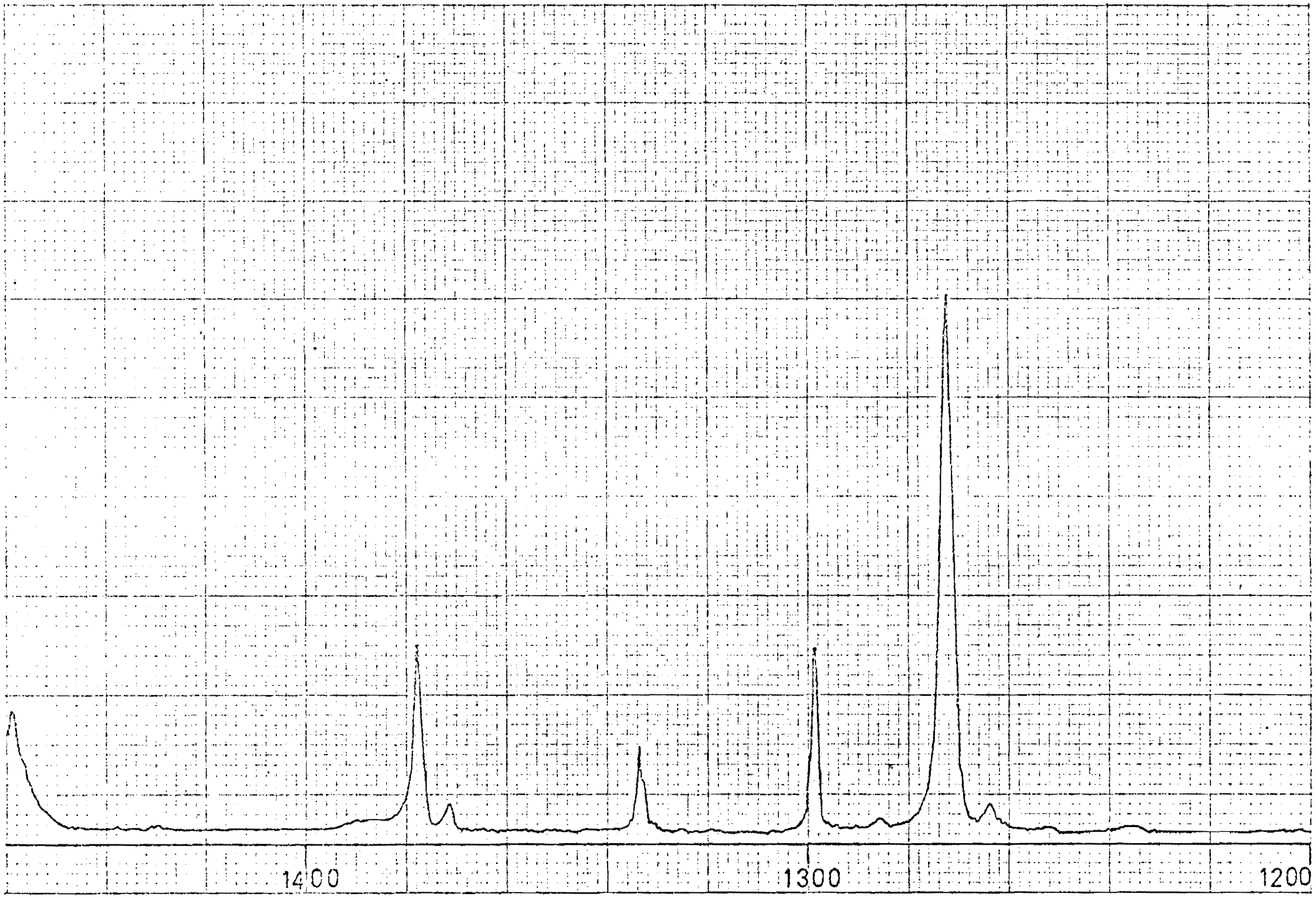
1400
1300
1200

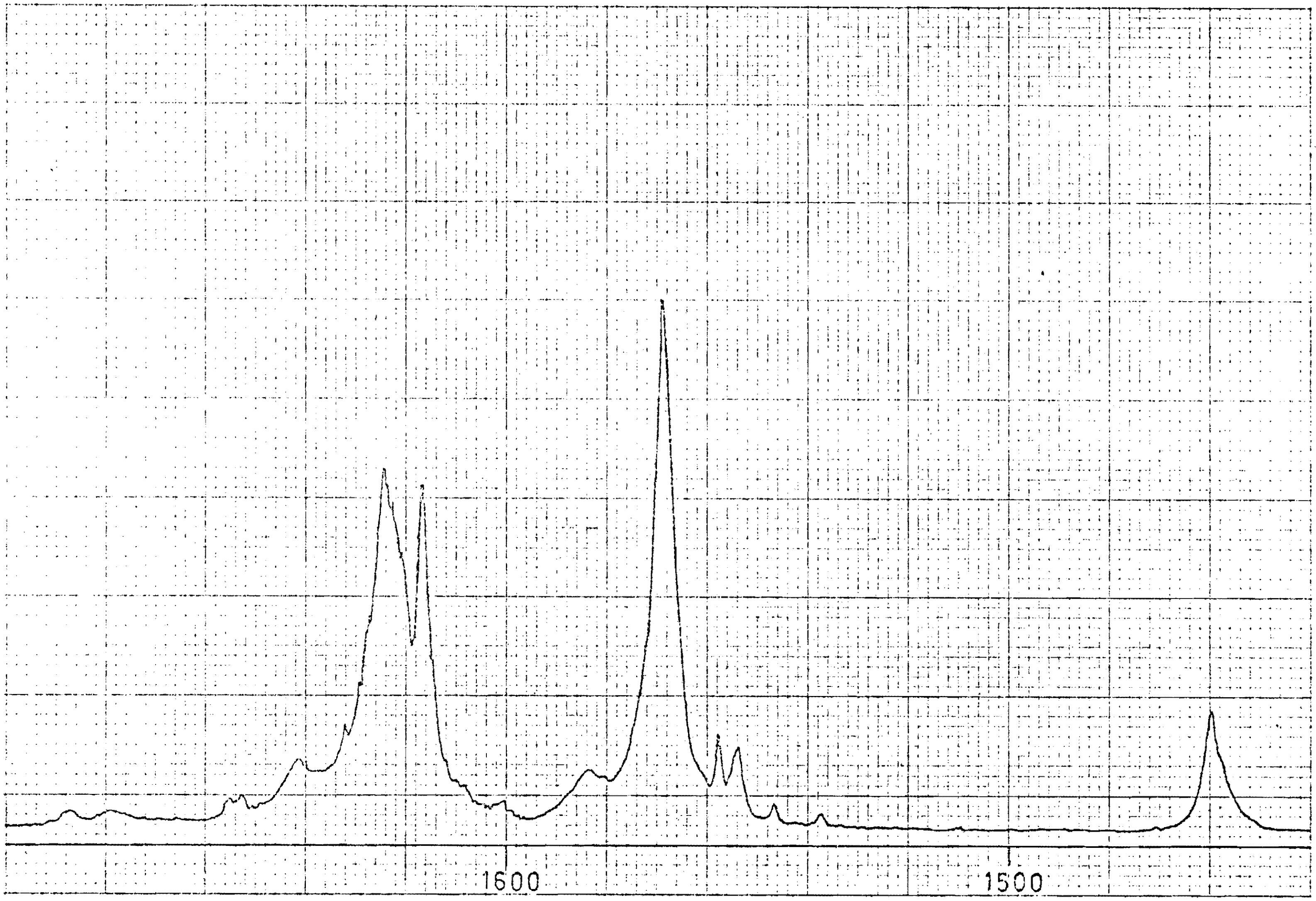
1600
1500

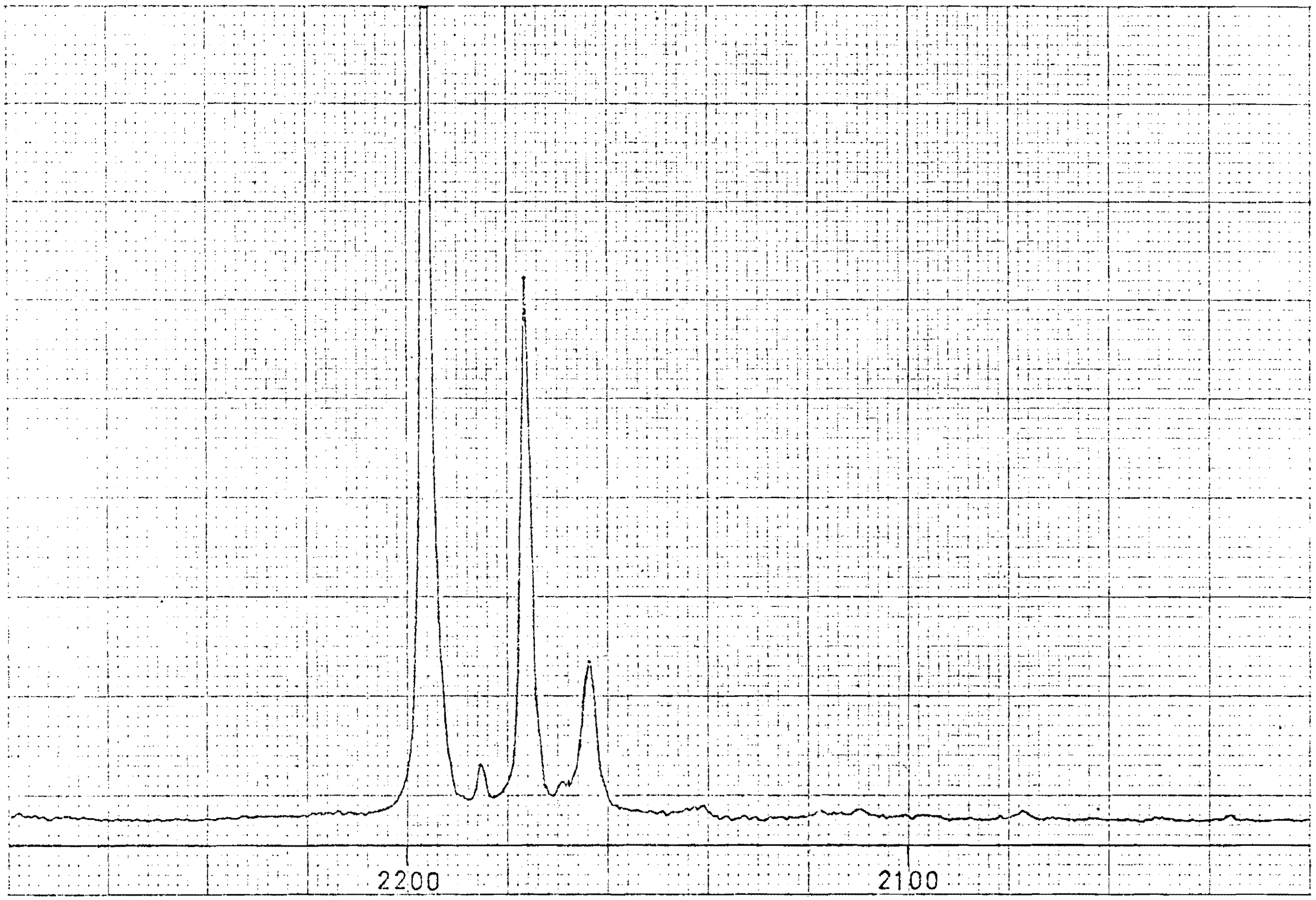
2200
2100

FIGURE 13

Raman Spectrum of Benzoic Acid d_5

Carey Model 82 Raman Spectrometer

Temperature = 4.2° K

Spectral Bandwidth = 0.5 cm^{-1}

Scan Rate = 0.25 cm^{-1}/second

Pen Period = 2.0 seconds

Sensitivity - 2 x 10^3 counts per second
full scale

Laser Wavelength = 5145 Å

Laser Power = 380 milliwatts


200
100
0

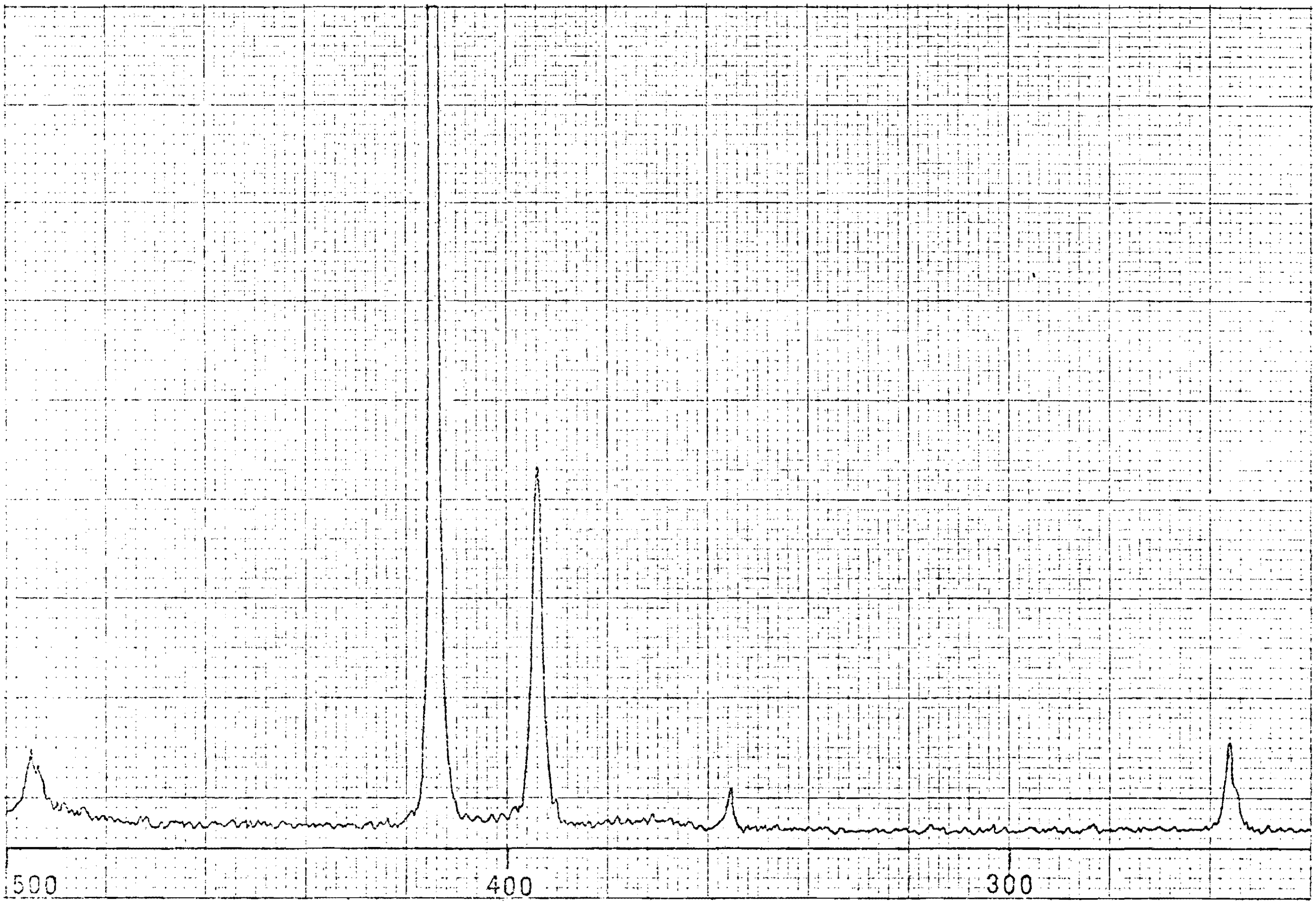
500
400
300

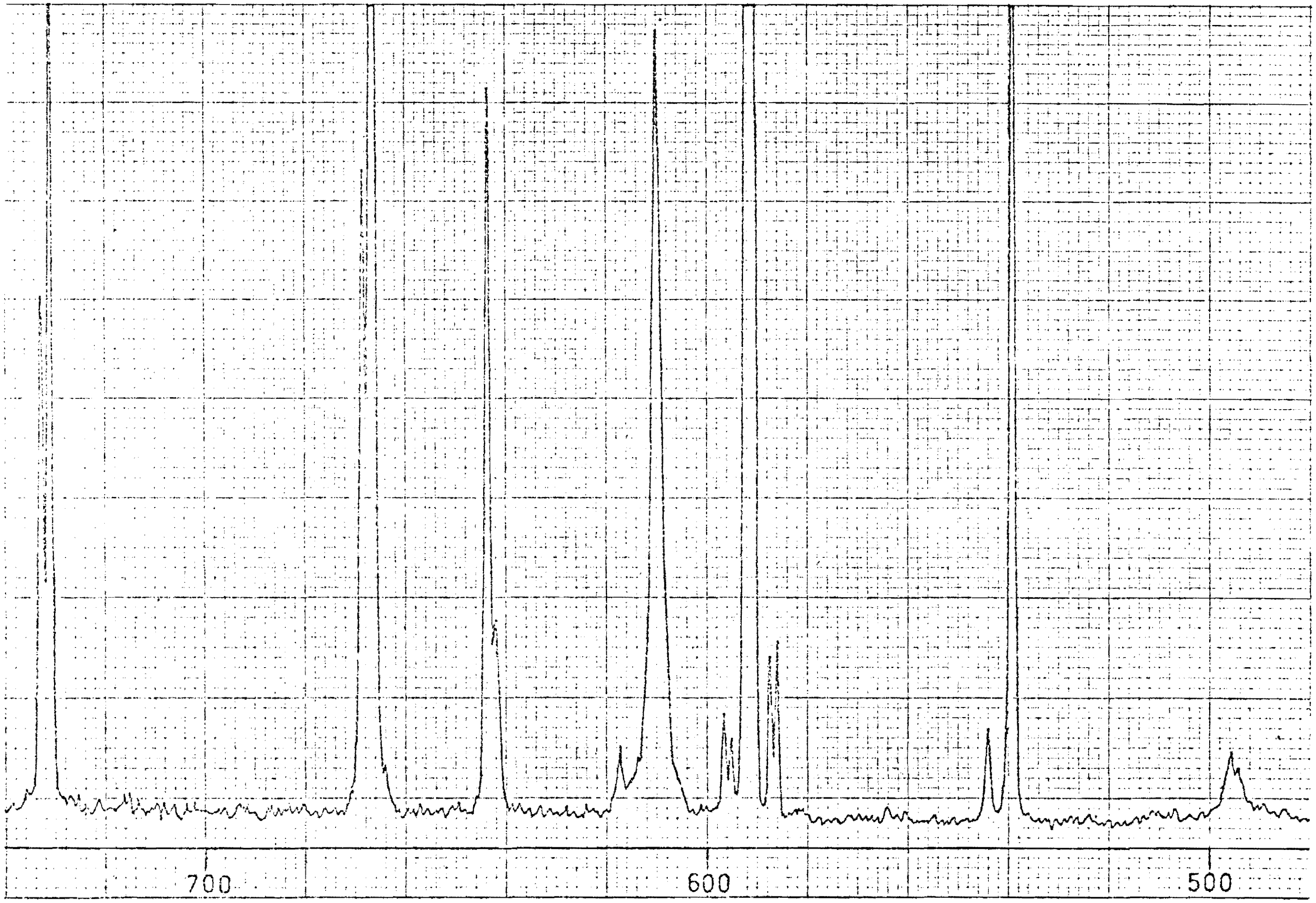
700
600
500

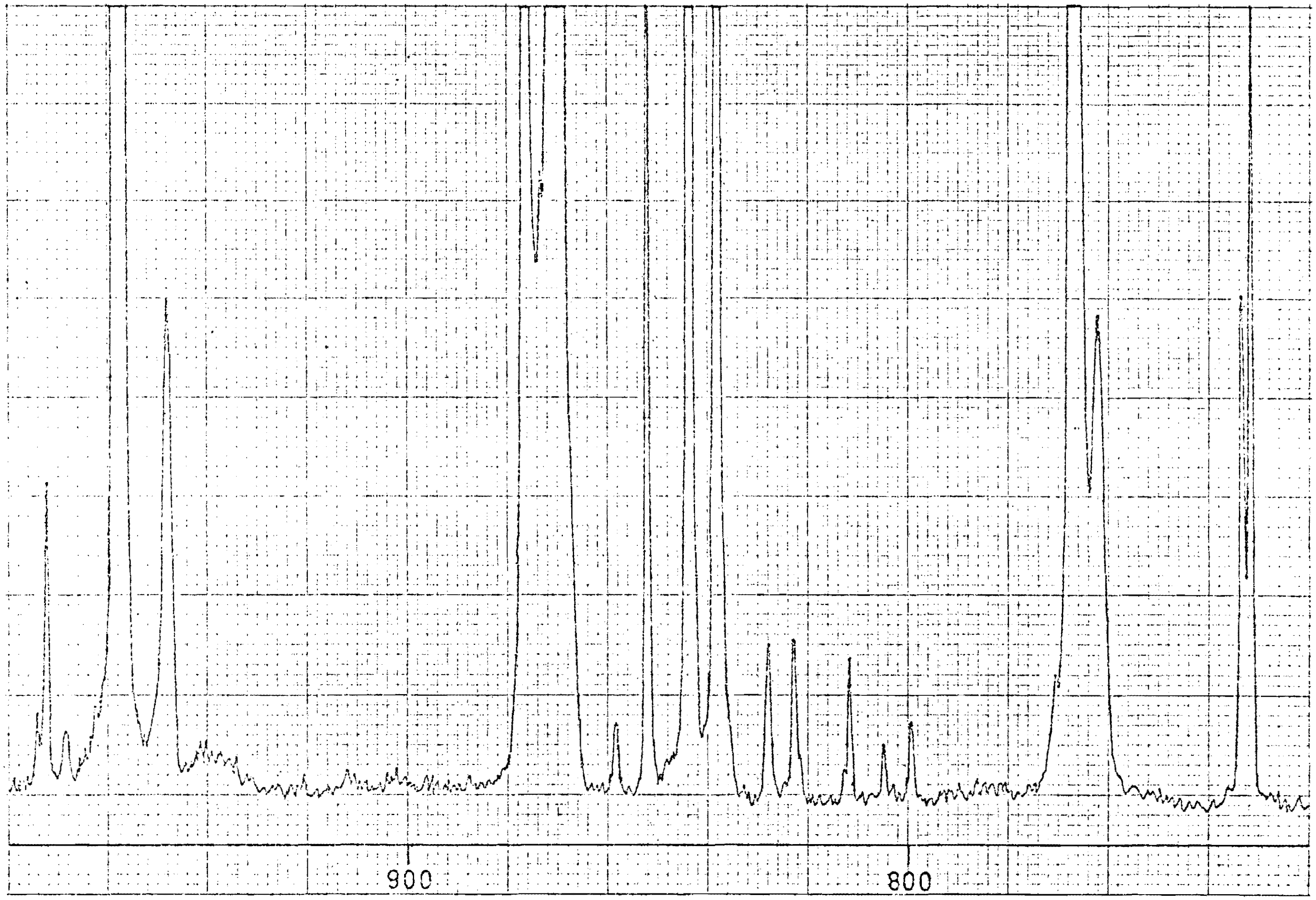
900
800

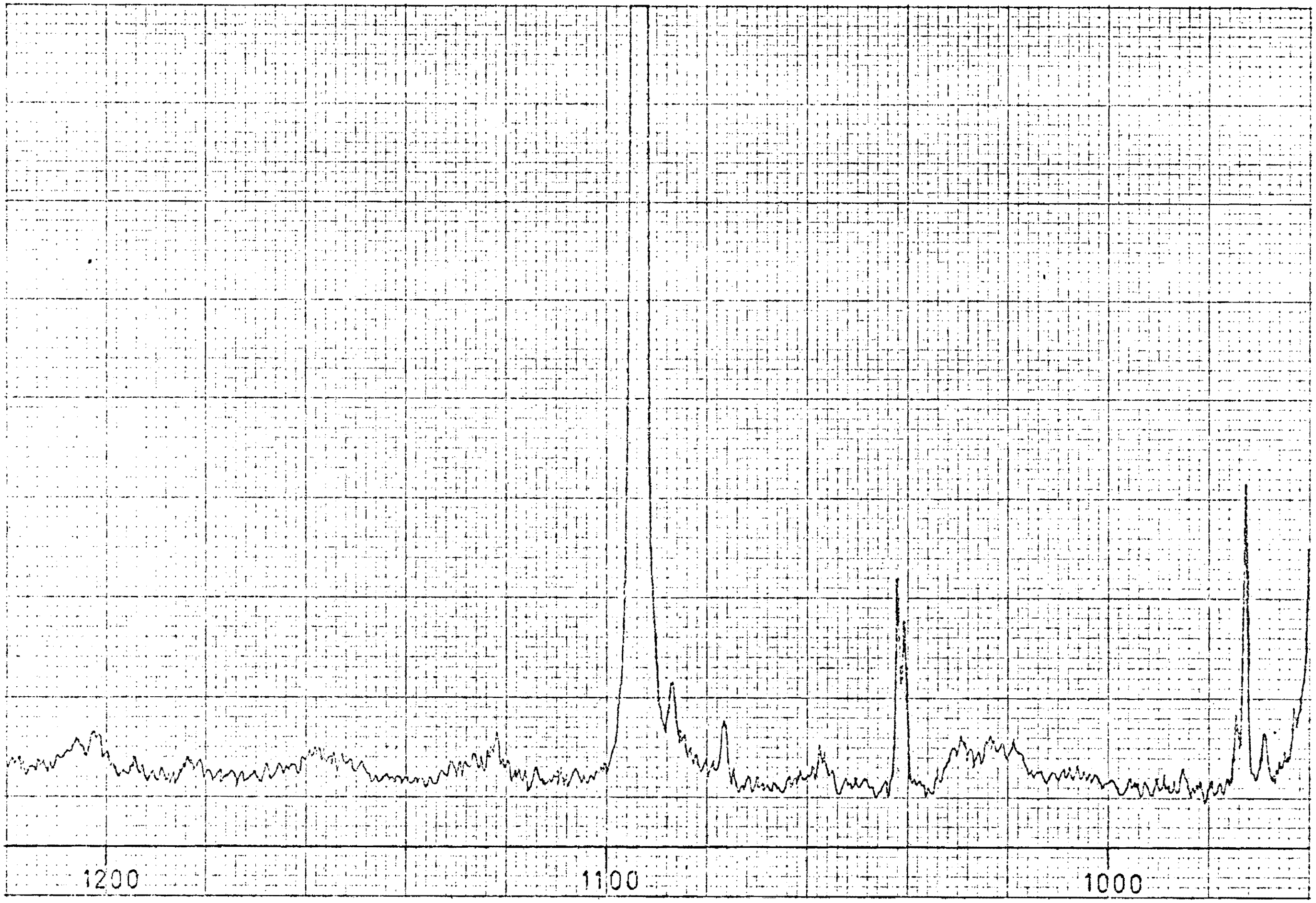
1200
1100
1000

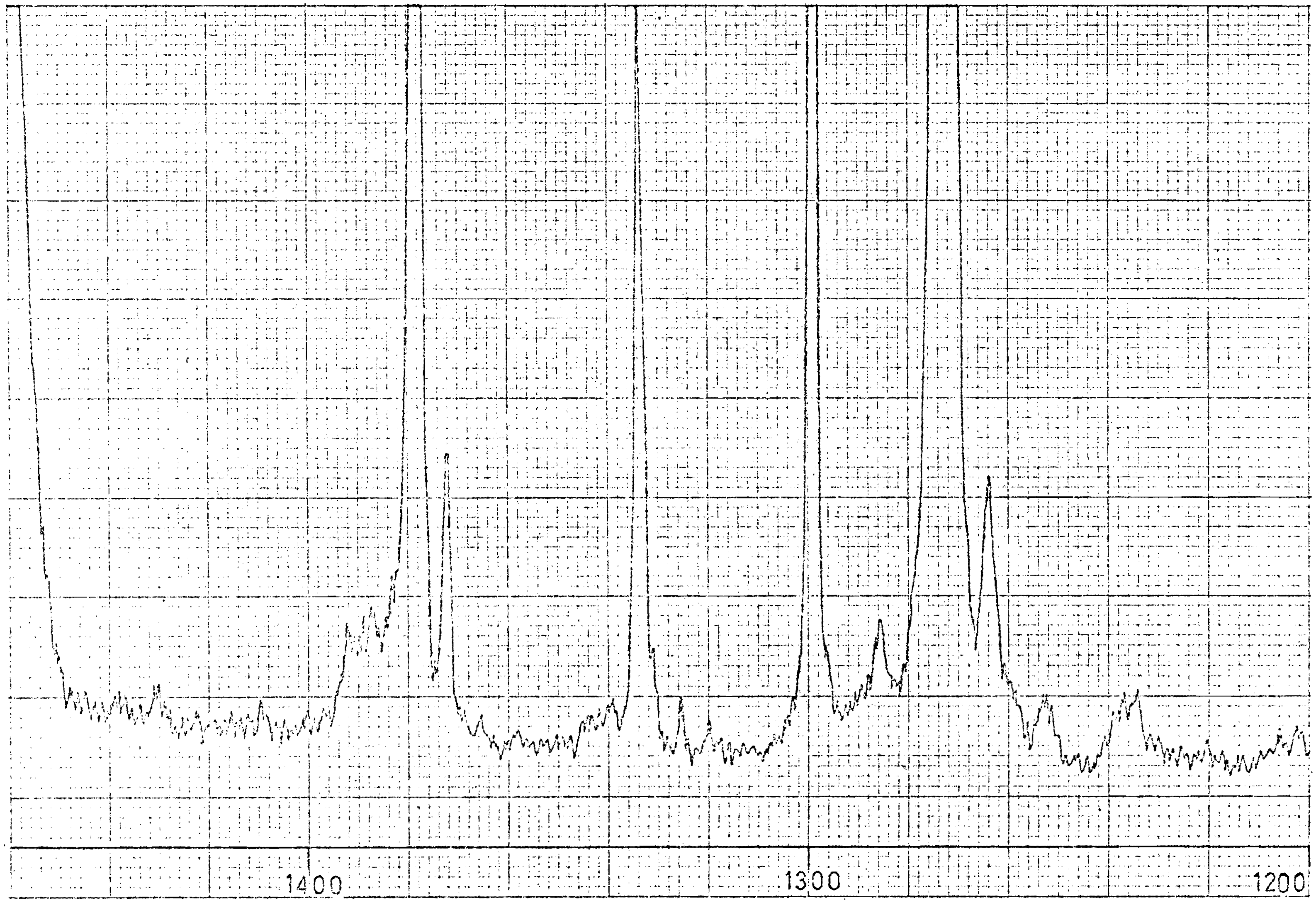
1400
1300
1200

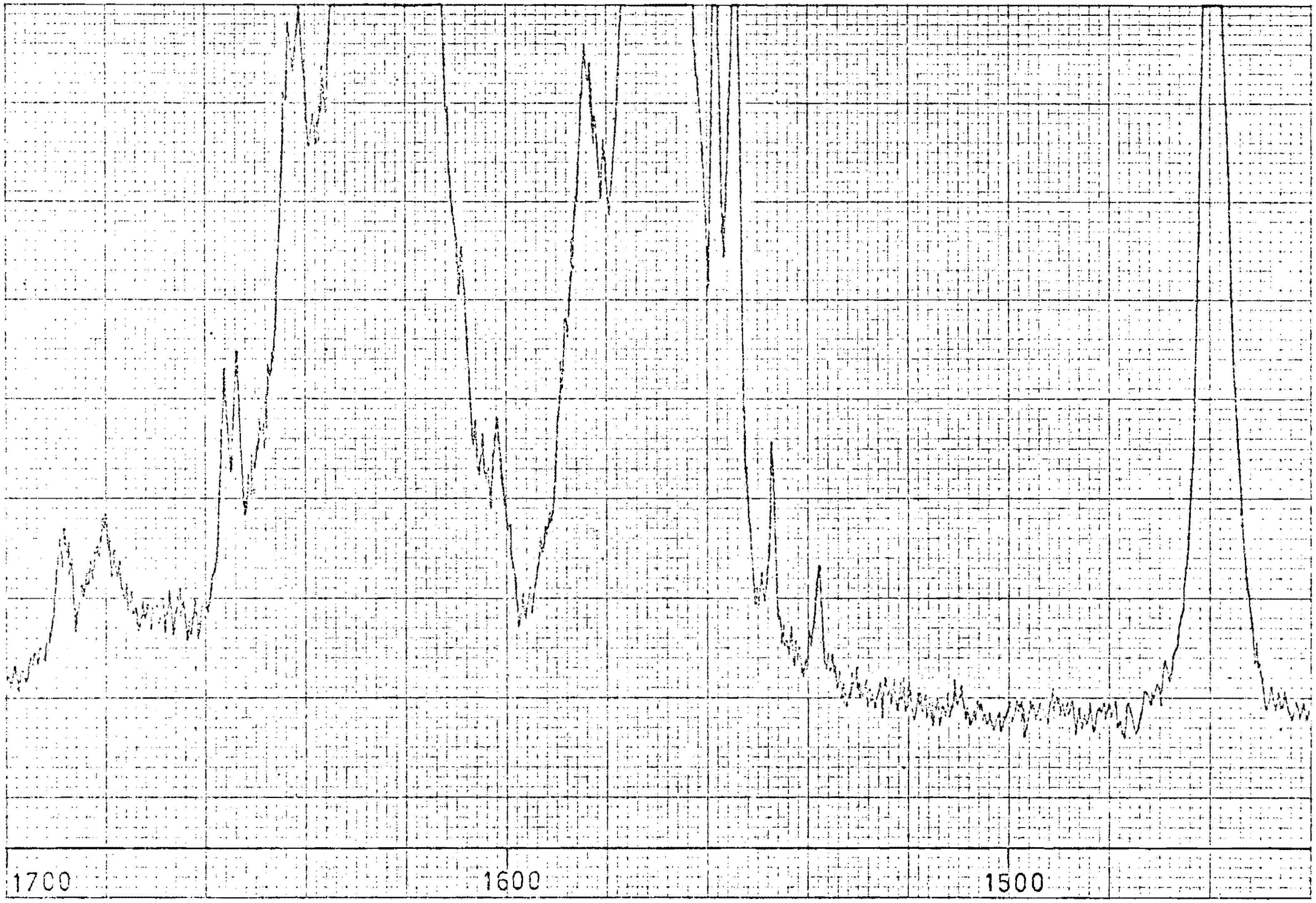
1700
1600
1500

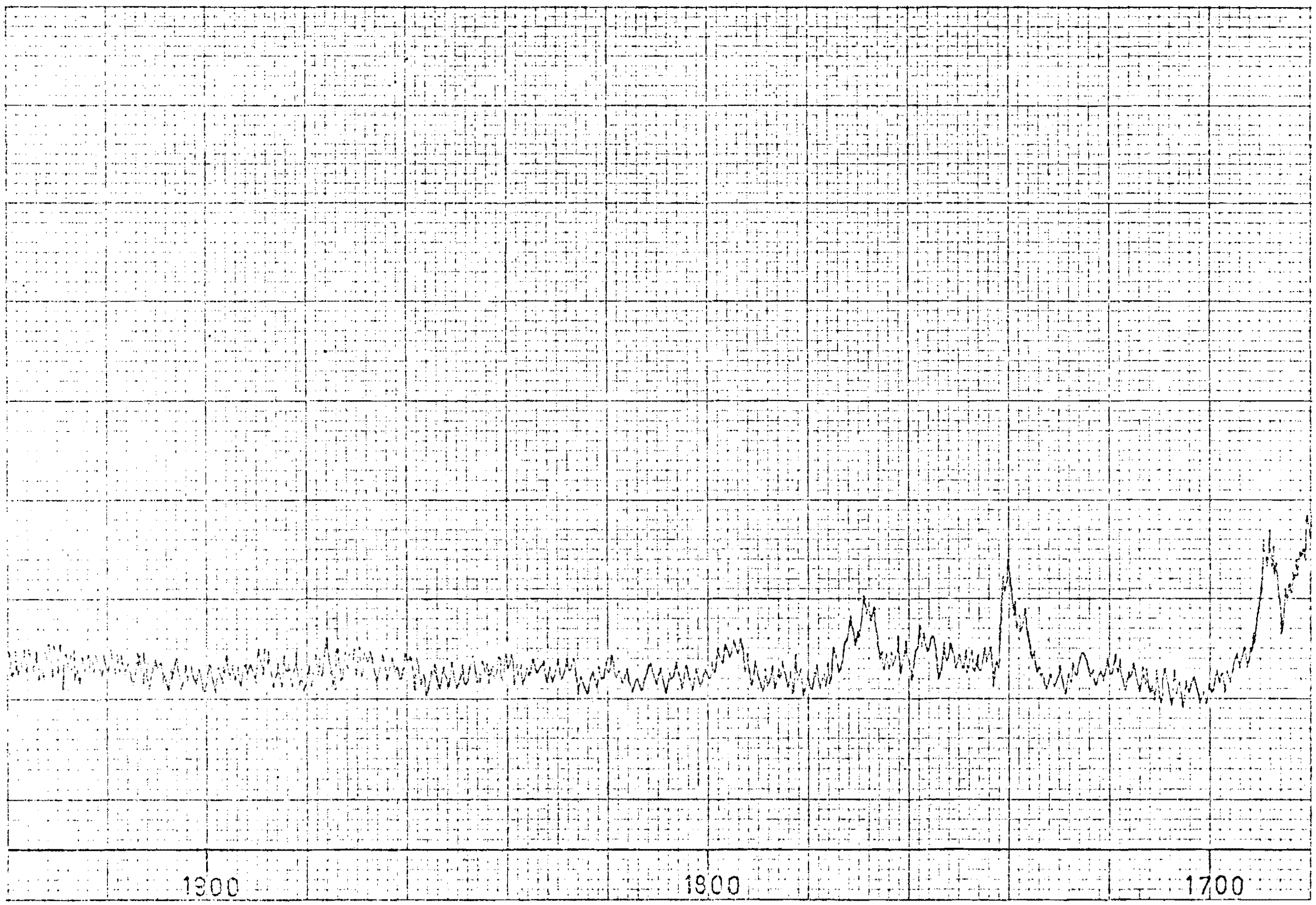
1900
1900
1700

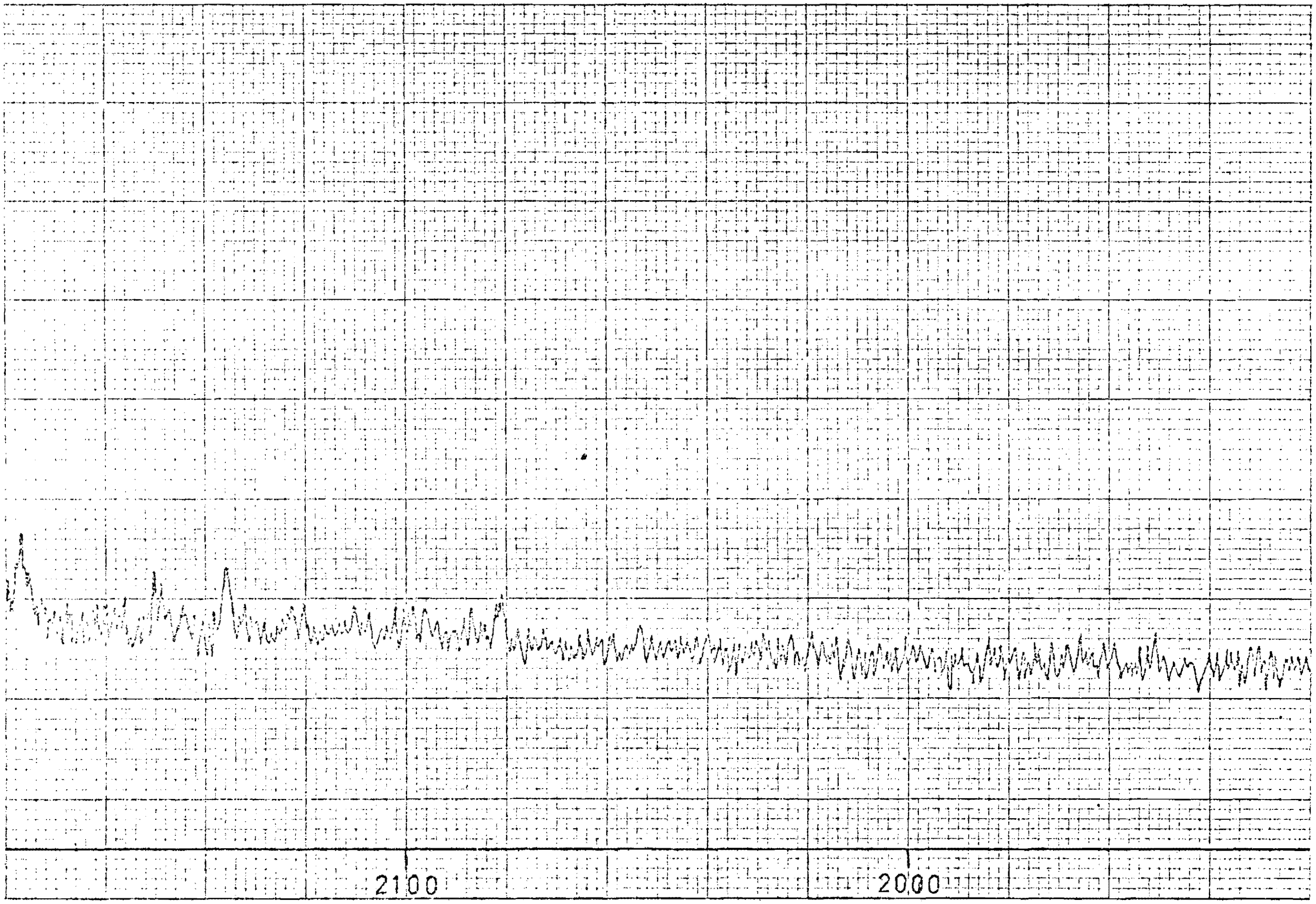
2100
2000

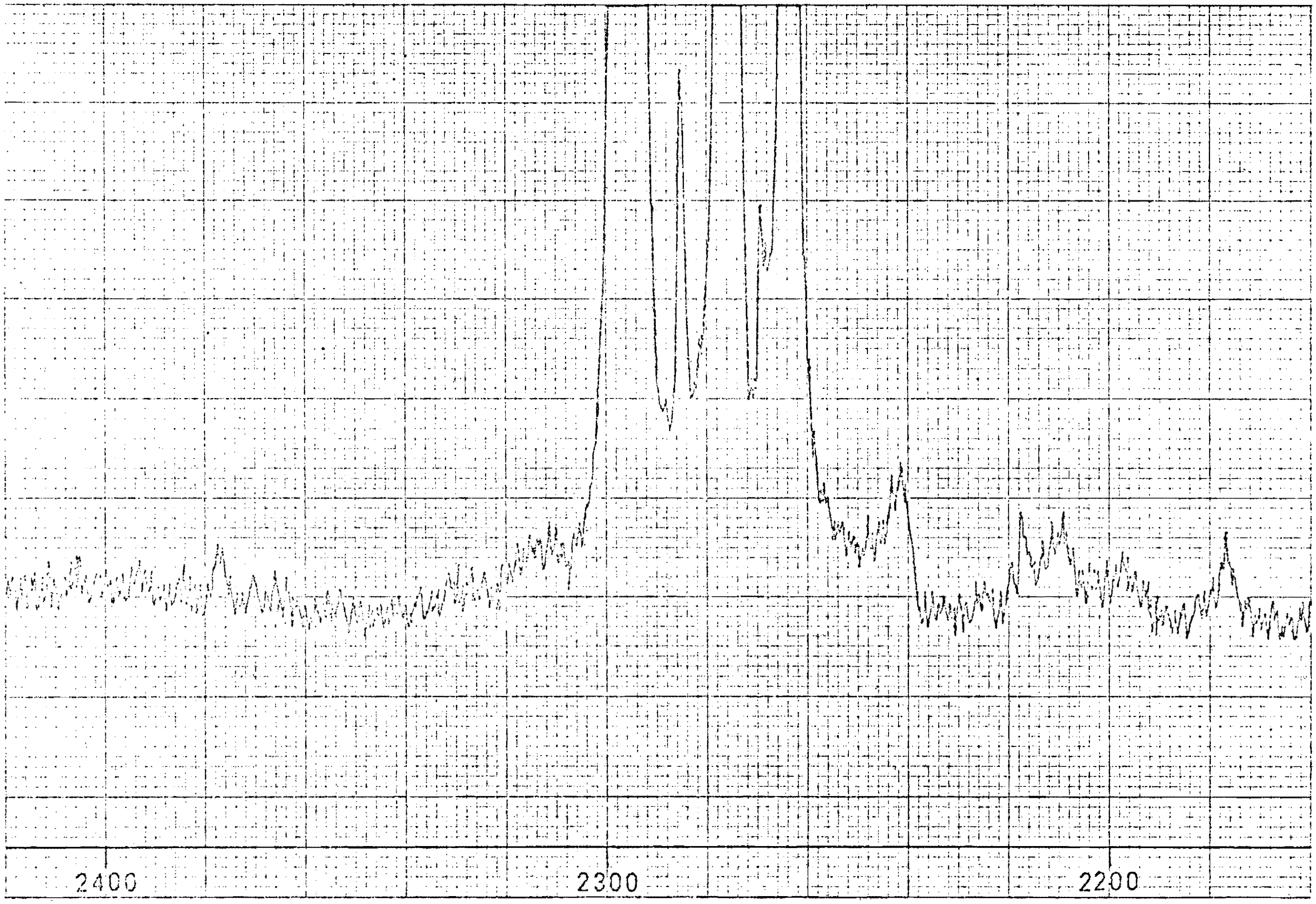
2400
2300
2200

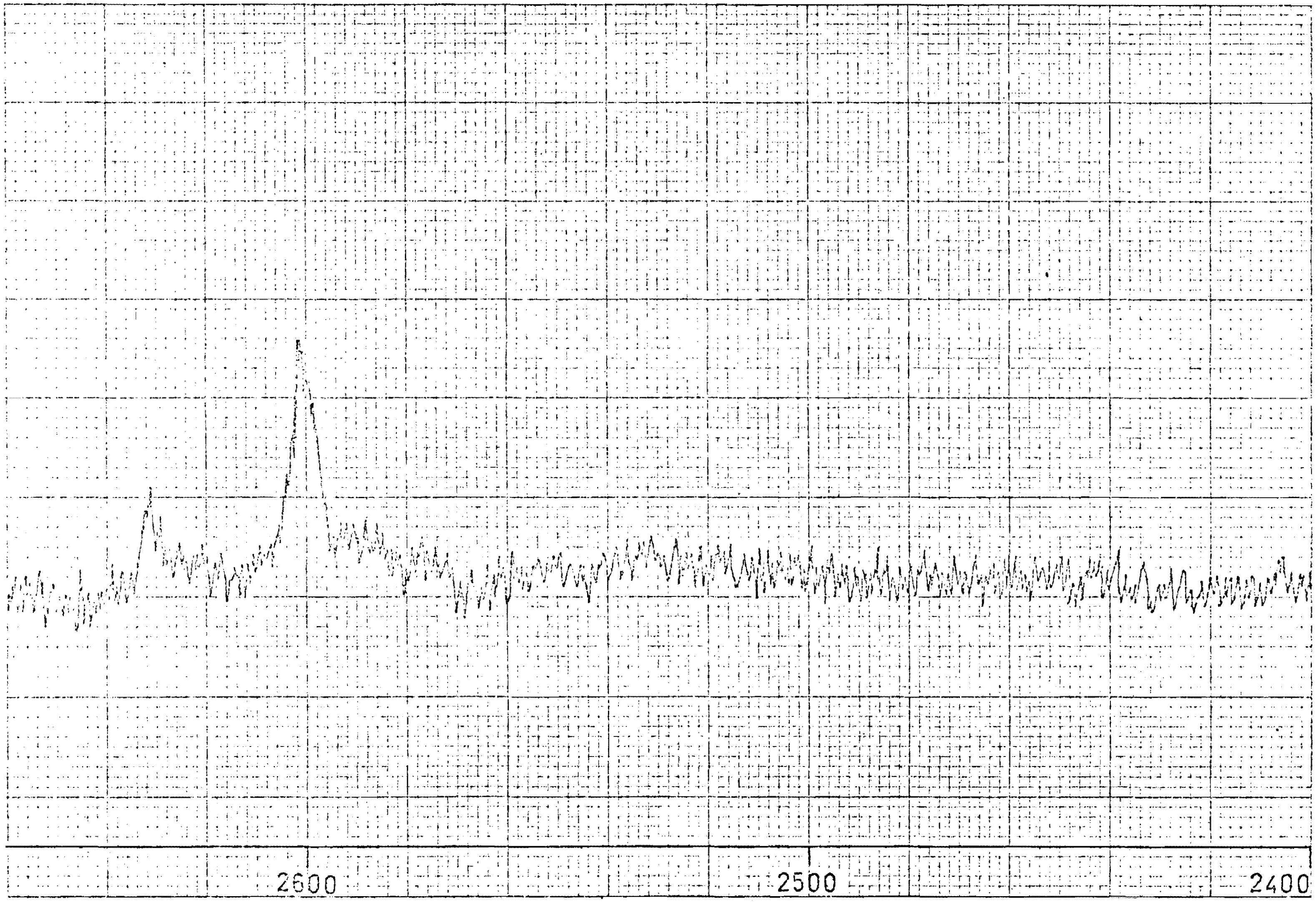
2600
2500
2400

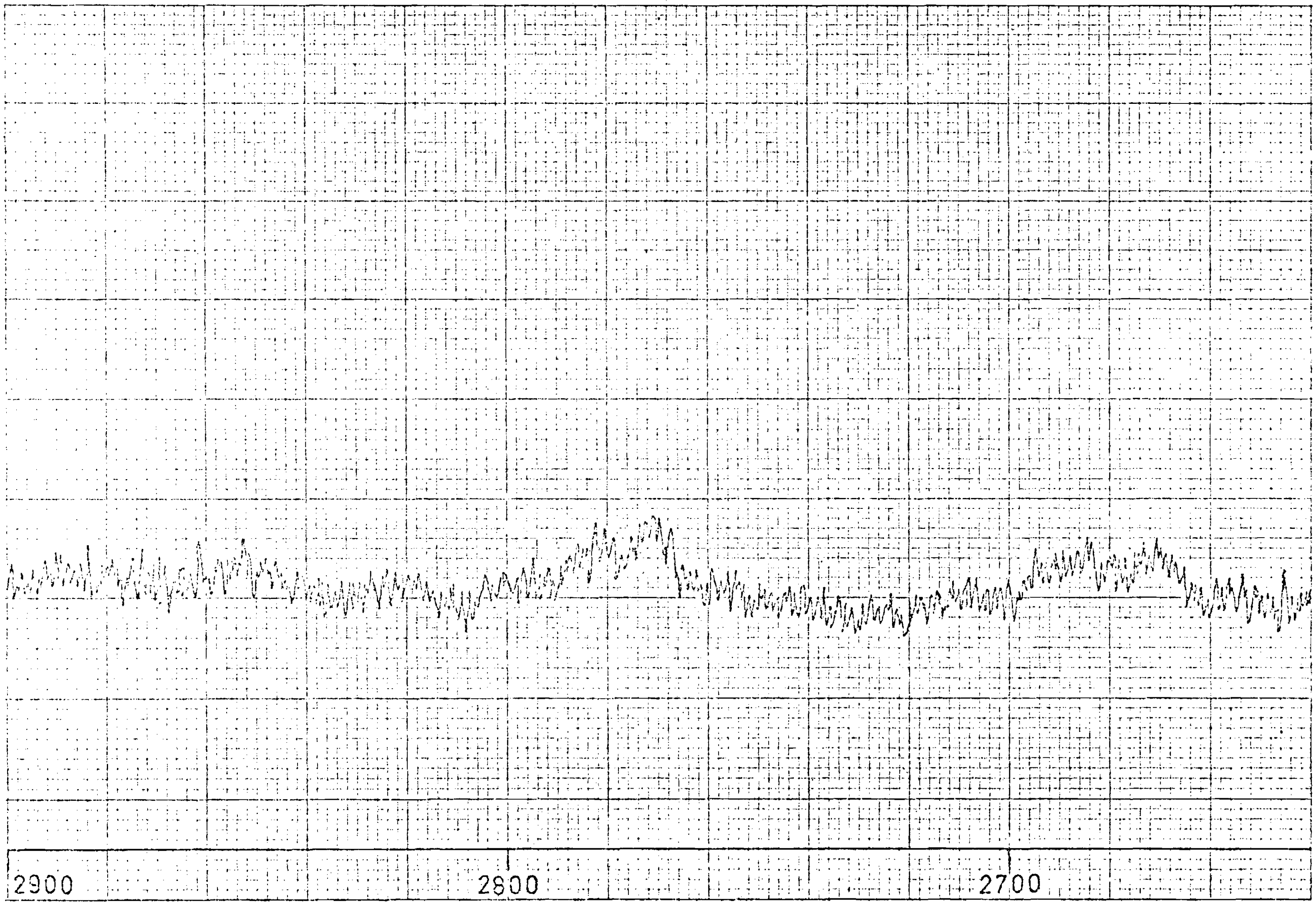
2900
2800
2700

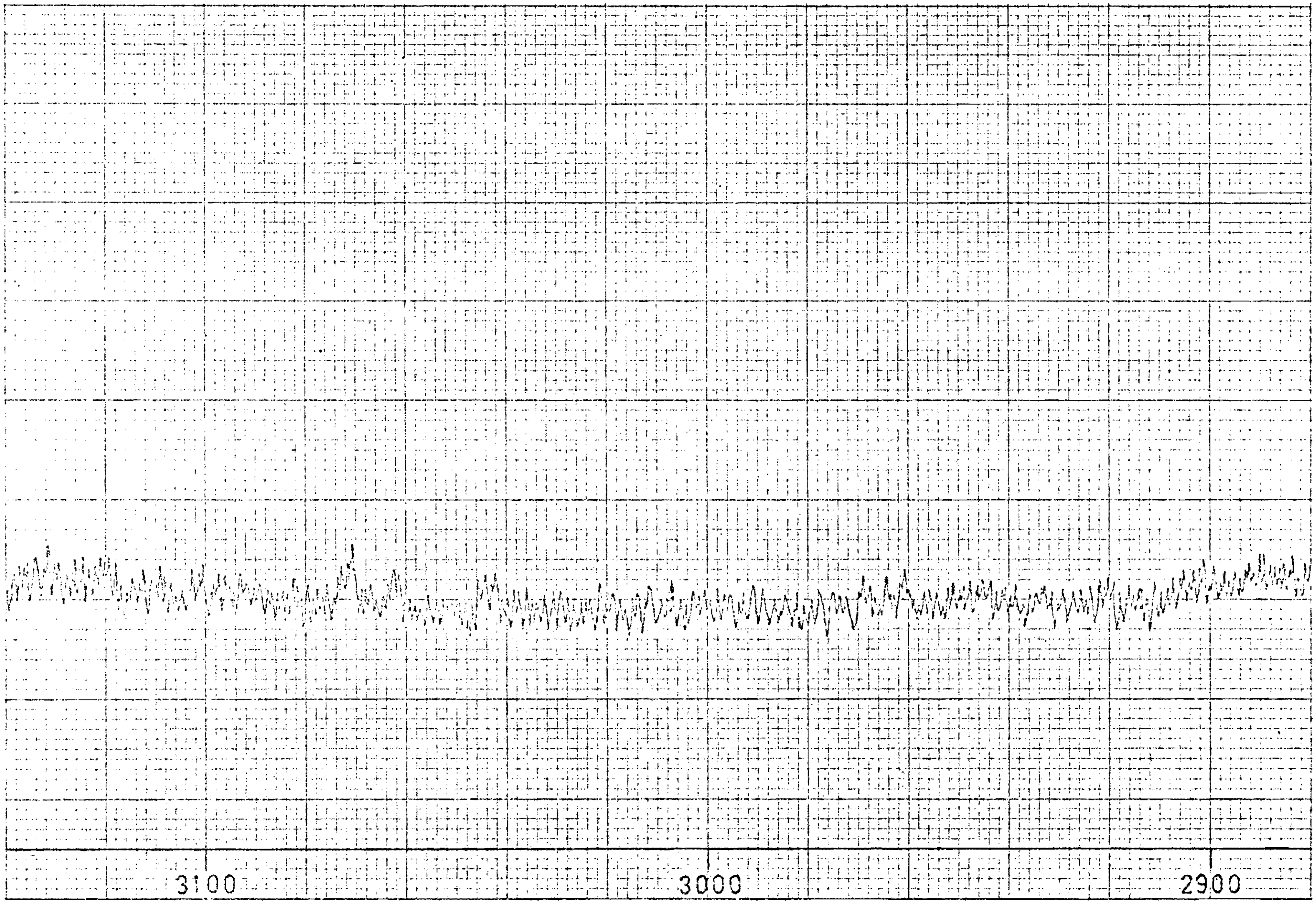
3100
3000
2900

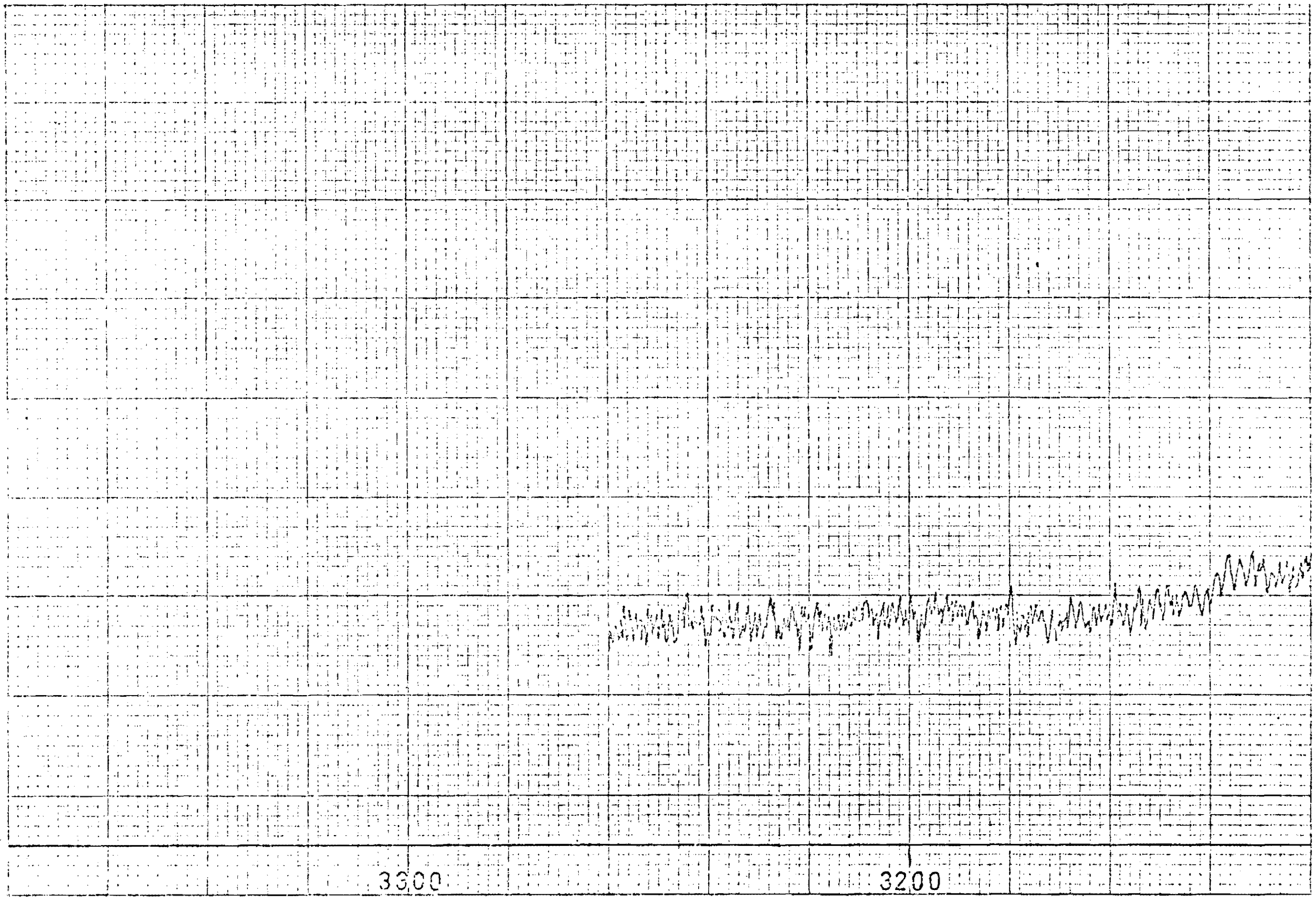
3300
3200

TABLE 8

This table contains the frequencies and peak heights of bands in the Raman spectra shown in Figures 12 and 13. Peak heights are given relative to an arbitrary unit of intensity.

Band Number	Frequency (cm^{-1})	Peak Height	Comments
1	32.8	29.5	
2	49.5	19.0	
3	53.5	19.0	
4	58.5	1.80	
5	81.0		unresolved shoulder
6	83.6	96.0	
7	92.5	37.0	
8	94.5		unresolved shoulder
9	114.5	35.0	
10	120.3	68.5	
11	128.0	23.0	
12	187.8	23.5	
13	255.0	0.40	shoulder
14	256.2	0.85	
15	356.0	0.40	
16	391.0	0.20	
17	394.5	0.36	
18	415.0	33.3	
19	495.5	0.60	
20	539.5	0.13	
21	544.2	0.95	
22	586.2	0.17	
23	587.5	0.16	
24	591.2	51.0	
25	592.4	23.0	
26	595.5	0.70	
27	596.8	0.10	
28	610.3	0.80	
29	617.5	0.60	
30	642.5	0.20	shoulder
31	644.0	0.73	
32	667.0	14.0	
33	669.0	6.7	
34	731.5	10.3	
35	733.4	5.0	
36	762.0	4.8	
37	766.8	42.0	
38	770.8		unresolved shoulder
39	799.5	0.80	
40	805.0	0.60	

Table 8 (Continued)

Band Number	Frequency (cm^{-1})	Peak Height	Comments
41	811.8	0.15	
42	813.0	0.30	shoulder
43	822.0		shoulder
44	823.0	0.17	
45	828.2	0.16	
46	833.0	0.05	
47	838.4	20.0	
48	843.8	20.0	
49	852.3	0.82	
50	858.7	0.65	
51	867.5		unresolved shoulder
52	870.3	93.00	
53	877.0	12.50	
54	902.5	0.10	
55	912.0	0.15	
56	921.0	0.10	
57	927.0	0.10	
58	935.0		unresolved shoulder
59	941.0	0.40	
60	948.5	4.90	
61	957.5	>105	
62	963.2	0.30	shoulder
63	969.0	0.50	
64	972.8	3.10	
65	975.0	0.70	
66	985.5	0.20	
67	1006.0	0.20	very broad
68	1019.0	0.50	
69	1023.5	0.55	
70	1029.5	0.50	
71	1038.0	0.10	
72	1041.0	1.80	
73	1042.0	2.25	
74	1057.0	0.30	
75	1077.0	0.60	
76	1087.5	0.60	
77	1093.5	42.50	
78	1122.0	0.50	
79	1126.0	0.20	
80	1130.0	0.10	very broad
81	1149.0	0.10	very broad
82	1158.0	0.25	very broad
83	1183.0	0.15	
84	1194.0	0.05	
85	1202.0	0.40	
86	1206.0	0.35	
87	1220.5	0.10	

Table 8 (Continued)

Band Number	Frequency (cm^{-1})	Peak Height	Comments
88	1234.5	0.70	
89	1237.0	0.70	
90	1247.0	0.05	
91	1253.0	0.50	
92	1259.0	0.30	shoulder
93	1264.5	2.20	
94	1272.5	54.5	
95	1279.0		unresolved shoulder
96	1286.0	0.90	
97	1296.0		unresolved shoulder
98	1299.0	1.80	
99	1320.0	0.30	
100	1325.5	0.50	
101	1331.5		unresolved shoulder
102	1334.2	7.90	
103	1339.5	0.30	
104	1344.0	0.20	
105	1358.5	0.10	
106	1365.5	0.10	
107	1372.5	2.50	
108	1378.5	18.5	
109	1384.0		unresolved shoulder
110	1387.5	0.80	
111	1392.5	0.60	
112	1409.0	0.20	
113	1422.5	0.10	
114	1430.5	0.40	
115	1438.0	0.20	
116	1459.5	12.0	
117	1510.0	0.20	
118	1530.5	0.20	
119	1538.0	1.05	
120	1547.2	1.85	
121	1554.5	8.40	
122	1558.5	10.0	
123	1568.5	50.0	unresolved
124	1569.3	53.0	
125	1574.0		unresolved shoulder
126	1584.5	3.00	
127	1602.0	1.80	
128	1617.0	34.0	
129	1621.0		unresolved shoulder

Table 8 (Continued)

Band Number	Frequency (cm^{-1})	Peak Height	Comments
130	1623.0		unresolved shoulder
131	1625.0		unresolved shoulder
132	1628.0		unresolved shoulder
133	1630.0		unresolved shoulder
134	1633.0	2.00	
135	1641.2	4.00	
136	1643.5	4.00	unresolved
137	1654.0	2.10	
138	1656.5	2.10	
139	1680.0	1.40	
140	1688.5	0.80	
141	1726.0	0.15	
142	1737.5	0.50	shoulder
143	1740.5	1.10	
144	1769.0	0.60	
145	1771.0	0.40	
146	1796.0	0.30	
147	2081.0	0.45	
148	2136.0	0.65	
149	2150.0	0.40	
150	2177.0	0.80	
151	2197.5	0.40	
152	2210.5	0.70	
153	2219.5	0.90	
154	2242.0	1.30	
155	2264.0	16.0	
156	2269.7	1.70	
157	2276.4	54.5	
158	2285.8	3.50	
159	2296.5	>105	
160	2377.5	0.40	
161	2601.0	2.30	
162	2631.5	1.00	
163	2671.0	0.50	very broad
164	2690.0	0.50	very broad
165	2772.0	0.70	broad
166	2781.0	0.50	broad
167	3131.0	0.40	broad
168	3136.0	0.40	broad

FIGURE 14

Raman Spectrum of Benzoic Acid $1d_1$

Carey Model 82 Raman Spectrometer

Temperature = 4.2° K

Spectral Bandwidth = 0.5 cm^{-1}

Scan Rate = 0.5 cm^{-1} second

Pen Period = 1.0 second

Sensitivity - 4 $x10^4$ counts per second
full scale

Laser Wavelength = 5145 Å

Laser Power = 1000 milliwatts

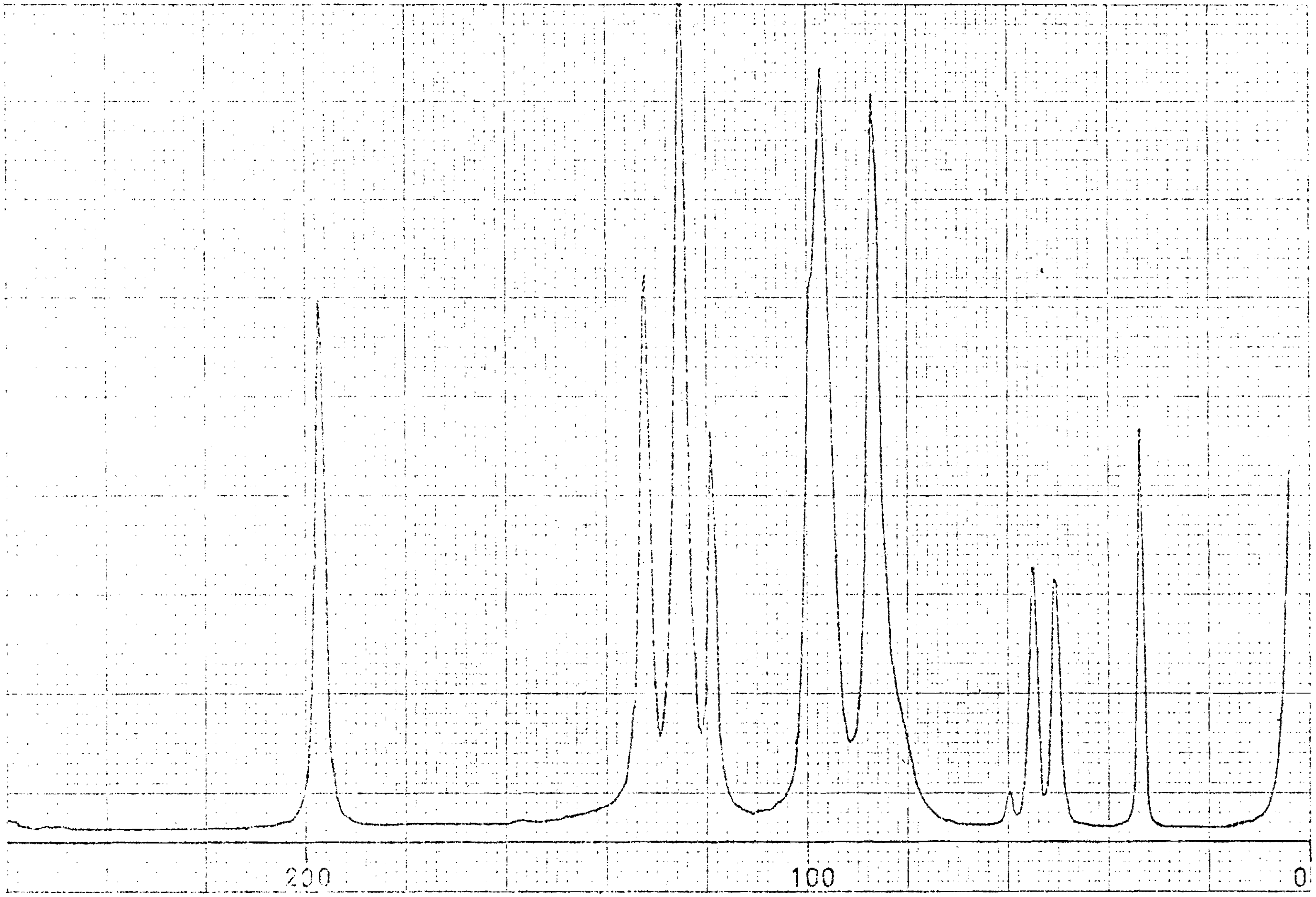
200
100
0

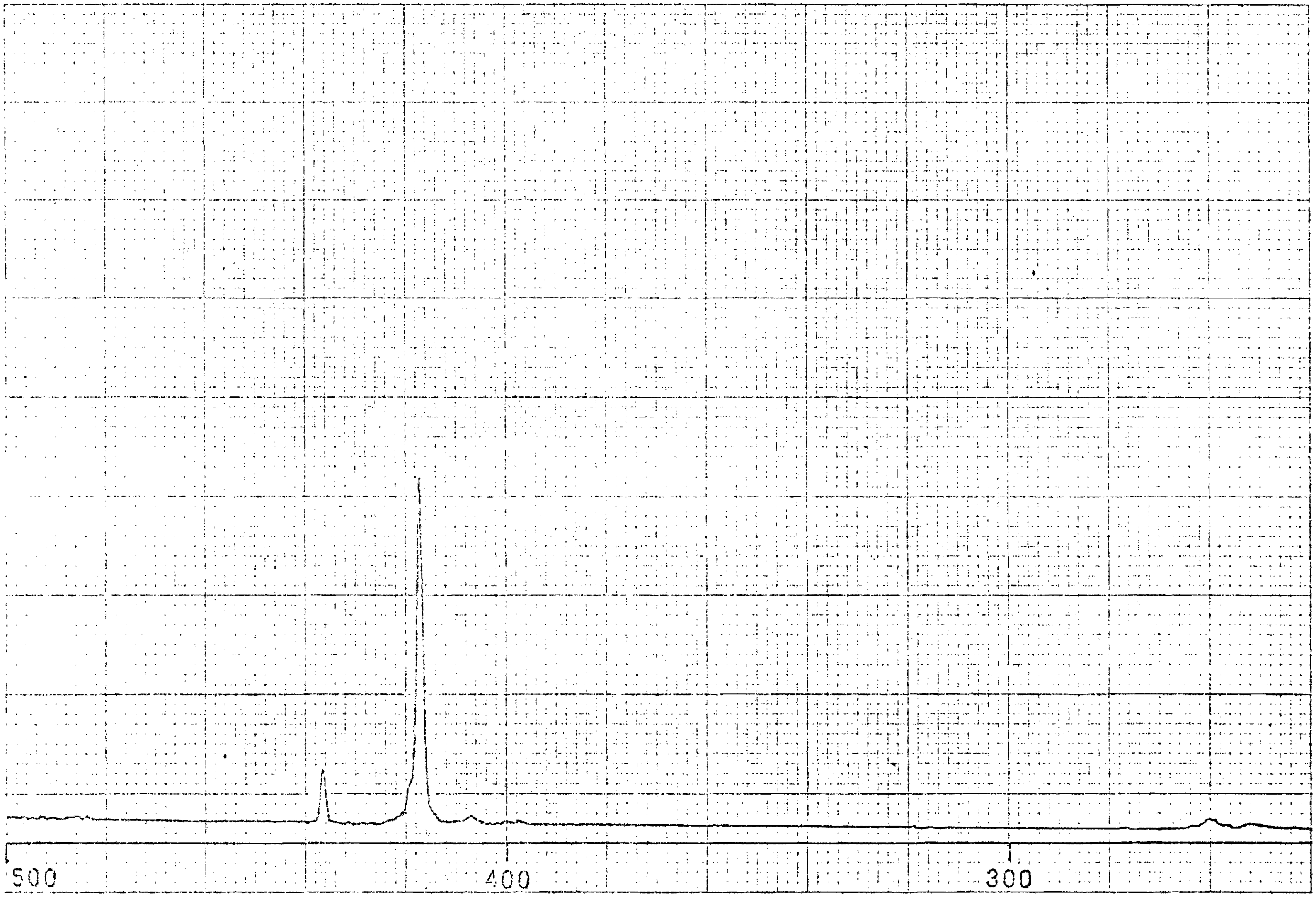
500
400
300

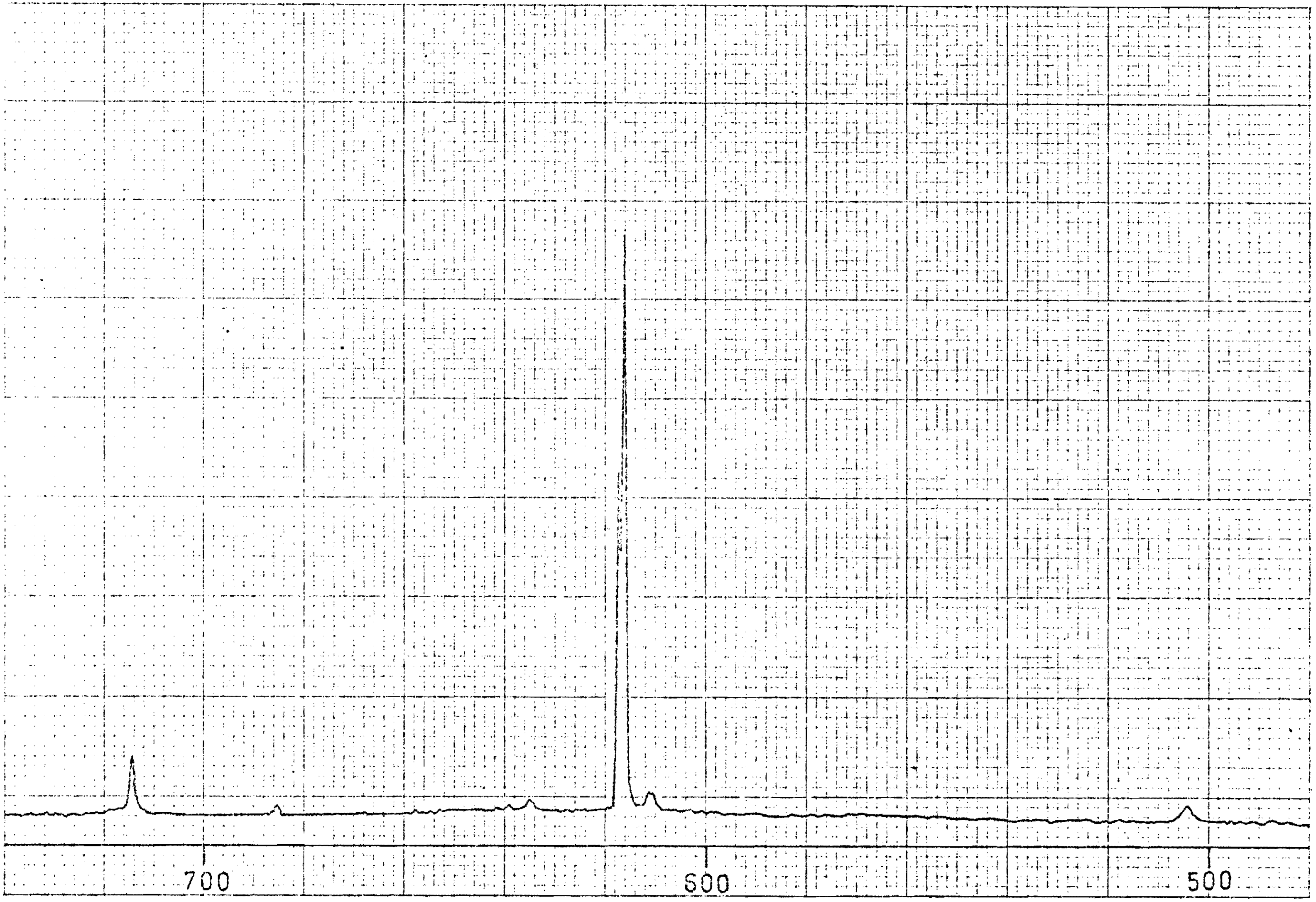
700
600
500

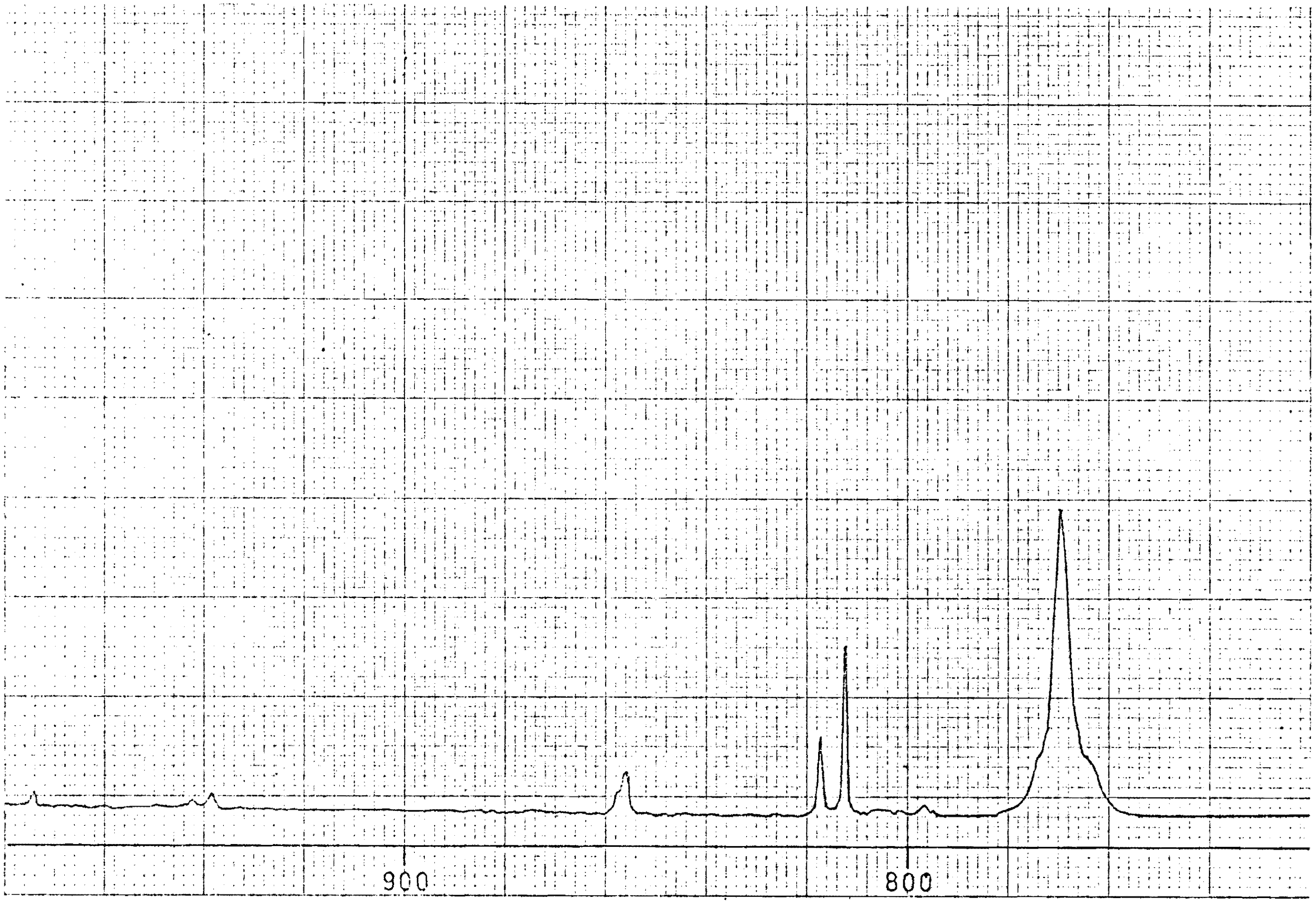
900
800

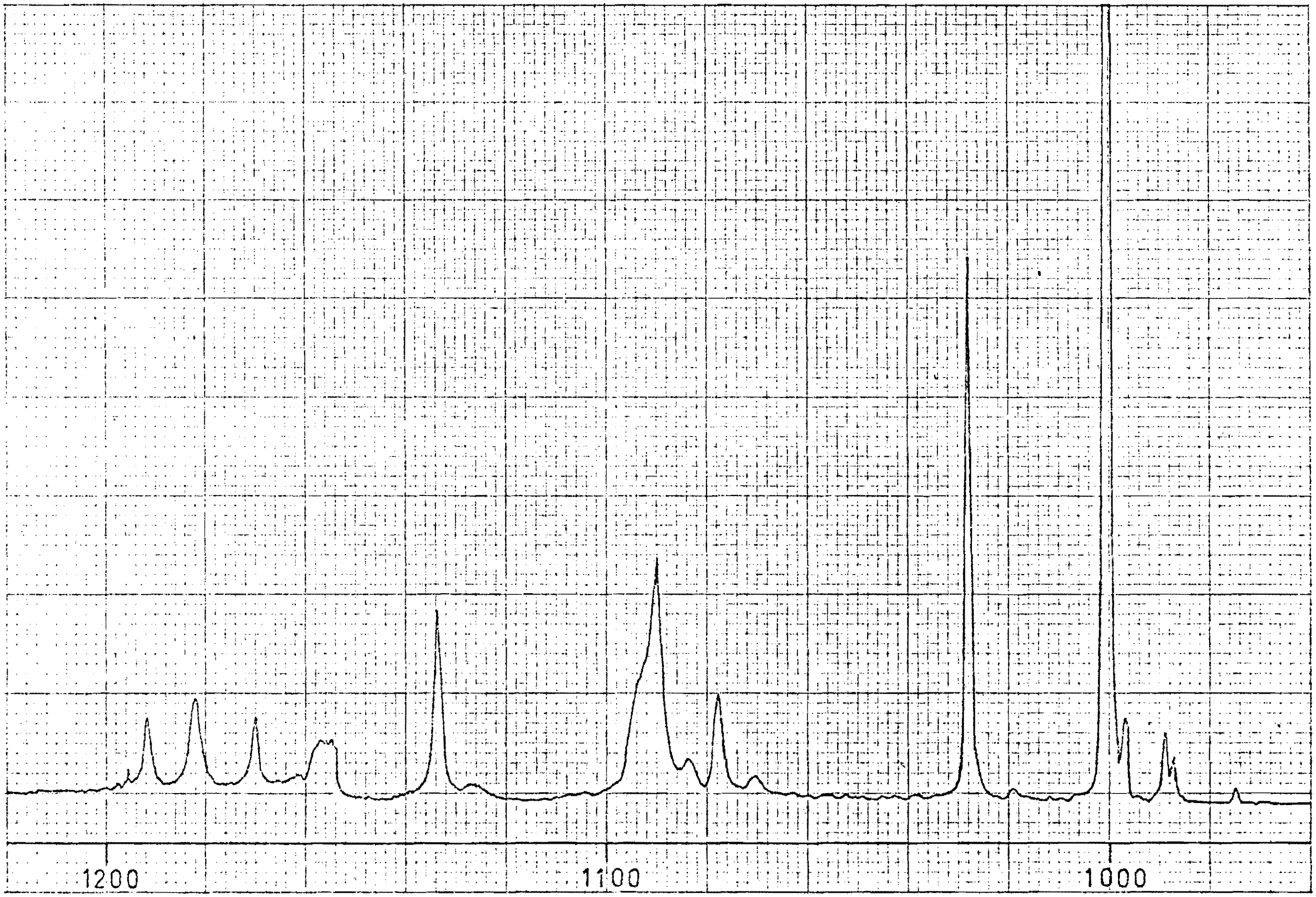
1200
1100
1000

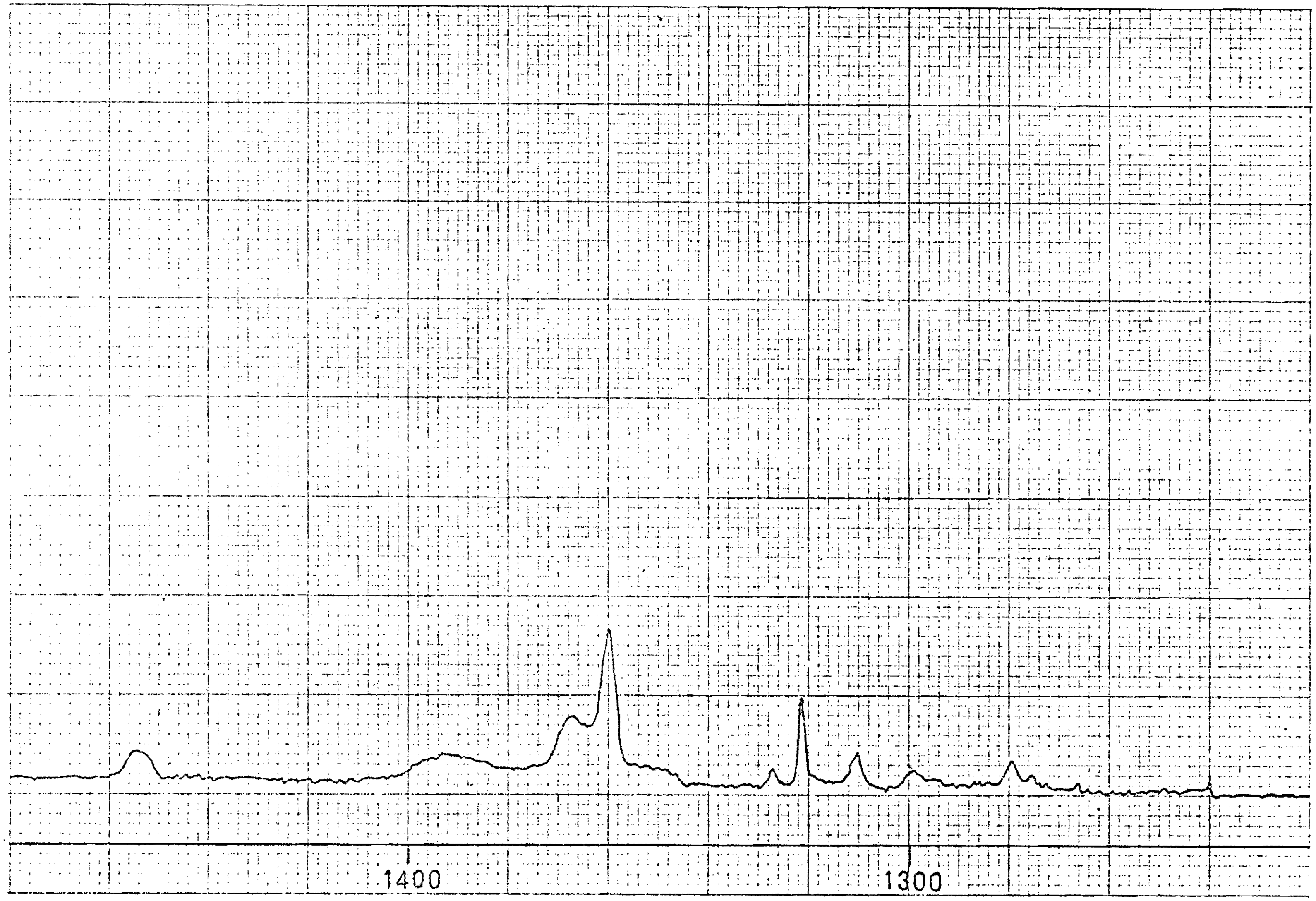
1400
1300

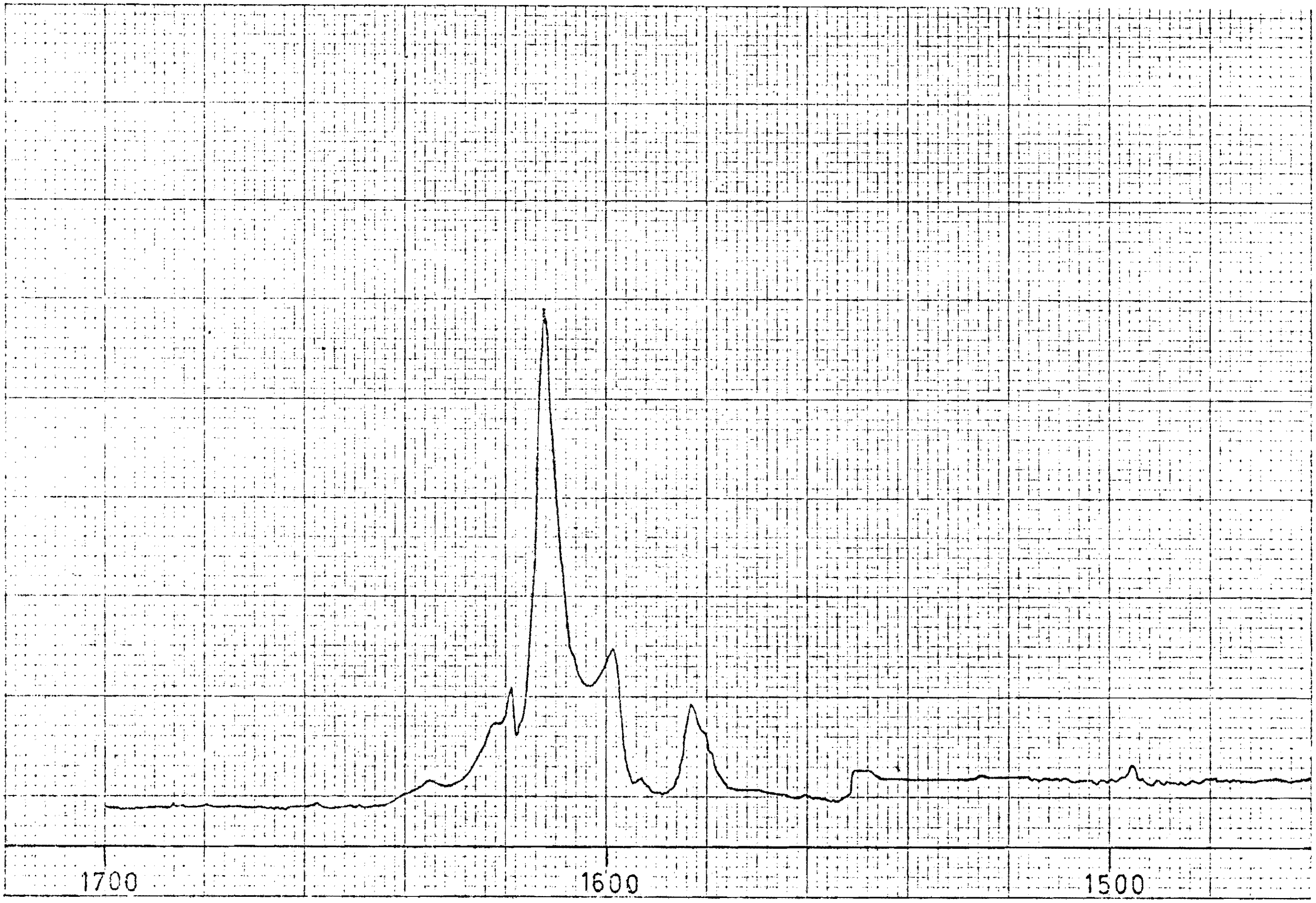
1700
1600
1500


3000
2900
2800

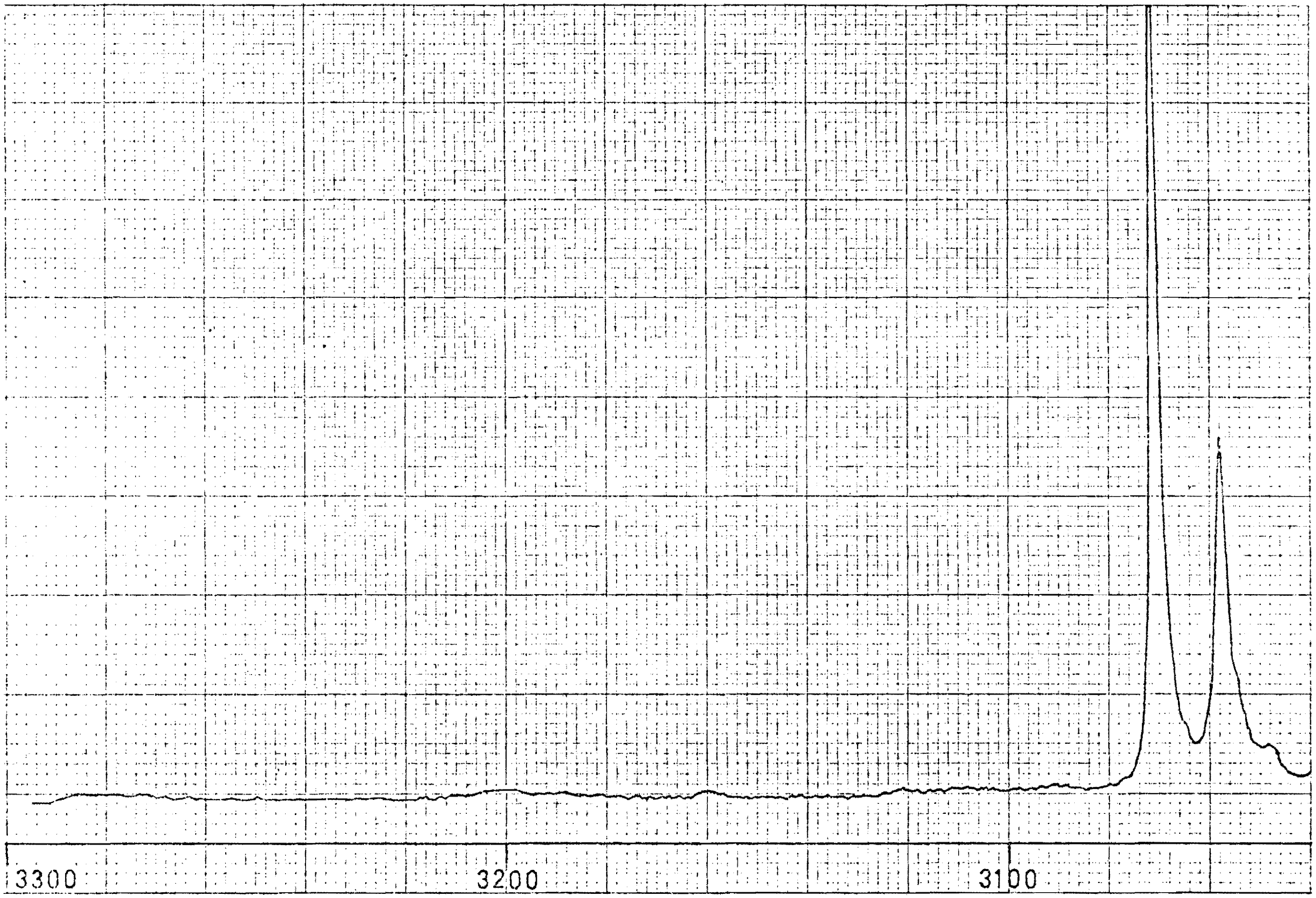
3300
3200
3100

TABLE 9

This table contains the frequencies and peak heights of bands in the Raman spectrum shown in Figure 14. Peak heights are given relative to an arbitrary unit of intensity.

Band Number	Frequency (cm^{-1})	Peak Height	Comments
1	33.8	40.0	
2	51.0	25.0	
3	55.2	26.0	
4	60.0	3.0	
5	80.0		unresolved shoulder
6	87.2	73.0	
7	97.4	77.0	
8	99.5		unresolved shoulder
9	119.5	34.5	
10	125.5	86.0	
11	132.5	55.0	
12	197.8	53.0	
13	253.0	0.3	
14	260.0	0.5	
15	408.0	0.5	
16	418.0	35.0	
17	420.0		unresolved shoulder
18	437.0	5.5	
19	504.5	1.5	
20	610.5	1.5	
21	611.8	1.5	
22	616.4	58.0	
23	617.5	34.0	shoulder
24	635.4	1.0	
25	686.0	1.0	
26	714.7	6.0	
27	763.0		unresolved shoulder
28	769.8	31.0	
29	797.0	1.3	
30	812.8	17.0	
31	817.5	8.0	
32	856.5	4.0	
33	858.0	2.5	
34	939.0	1.5	
35	943.0	1.0	
36	975.0	1.5	
37	987.5	4.5	
38	989.0	7.0	
39	997.0	8.5	
40	1000.5	>105	
41	1019.5	1.0	

Table 9 (Continued)

Band Number	Frequency (cm^{-1})	Peak Height	Comment
42	1028.2	55.0	
43	1971.0	1.5	
44	1078.2	9.5	
45	1084.2	2.5	
46	1090.5	24.0	
47	1094.0		shoulder
48	1127.5	1.5	
49	1134.2	19.0	
50	1157.0	5.5	
51	1170.5	6.5	
52	1182.5	9.5	
53	1192.7	7.5	
54	1196.0	1.5	
55	1240.0	1.0	
56	1266.5	1.5	
57	1273.0	1.0	
58	1275.5	1.0	
59	1280.0	2.5	
60	1295.0	0.7	
61	1300.0	2.0	
62	1310.5	4.0	
63	1322.0	8.5	
64	1327.5	1.5	
65	1351.0	2.0	
66	1360.5	15.0	
67	1368.0	5.0	
68	1392.0	2.5	
69	1455.0	3.0	
70	1496.0	2.0	
71	1579.5		unresolved shoulder
72	1581.0		unresolved shoulder
73	1583.5	9.0	
74	1593.8	1.0	
75	1599.0	14.5	
76	1613.0	49.5	
77	1619.5	6.0	
78	1623.0	3.0	
79	1636.0	1.5	
80	1640.0	0.5	
81	2946.0	0.5	
82	2984.5	4.5	
83	3008.5	6.5	
84	3029.0	0.5	

Table 9 (Continued)

Band Number	Frequency (cm^{-1})	Peak Height	Comment
85	3037.5	4.5	
86	3048.0	2.0	
87	3054.0		unresolved shoulder
88	3058.0	35.5	
89	3065.0		unresolved shoulder
90	3072.5	86.0	
91	3091.0	0.3	
92	3121.5	0.5	
93	3160.0	0.5	
94	3189.0	0.3	
95	3201.0	0.5	

FIGURE 15

Infrared Spectrum of Benzoic Acid d_o

Perkin Elmer Model 225 Infrared Spectrometer

Temperature = 4.2° K

Sample: 0.5 milligrams of Benzoic Acid d_o
in 300 milligrams of KBr

Reference: 300 milligrams of KBr + Screen

Pen Period = 3.0 seconds

Suppression = 2

Scan Speed = 3

Slit Program = 4.5

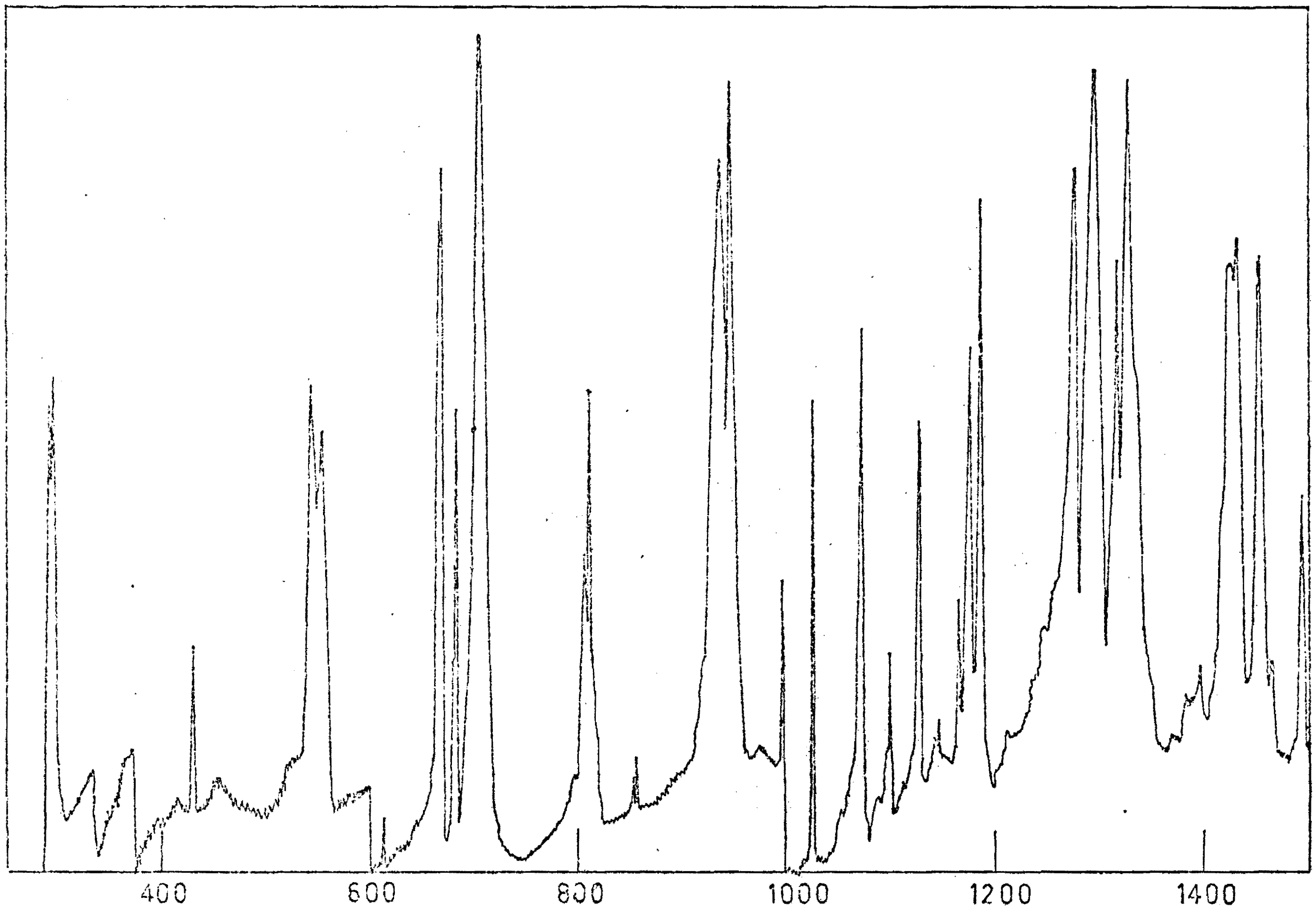
400
600
800
1000
1200
1400

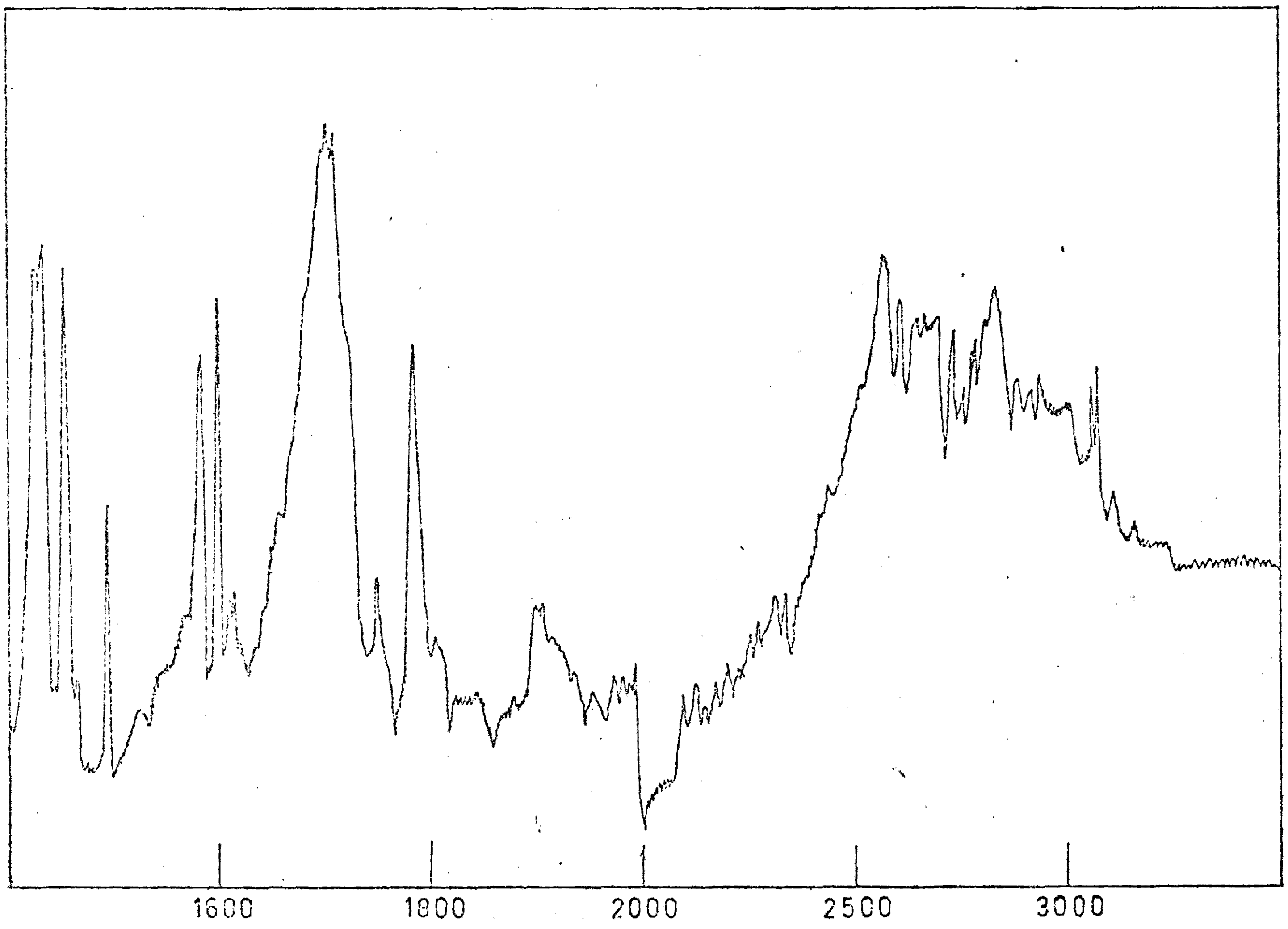
1600
1800
2000
2500
3000

TABLE 10

This table contains the frequencies and qualitative relative intensities of bands in the IR spectrum shown in Figure 15. The frequencies given in this table have been taken from an expanded scale version of the spectrum in Figure 15, since frequencies can be determined more accurately in the expanded scale spectrum.

Band Number	Frequency (cm^{-1})	Intensity	Comments
1	286.0	strong(s)	
2	294.0	s	
3	431.0	weak (w)	
4	546.0	s	
5	557.0	s	
6	626.0	w	
7	667.0	medium (m)	shoulder
8	669.5	s	unresolved
9	671.5	s	
10	683.0	w	shoulder
11	685.0	m	
12	694.0	w	shoulder
13	697.0		shoulder
14	708.0	s	
15	710.5	s	unresolved
16	797.0	w	
17	809.0	m	
18	813.5	m	
19	817.0	m	
20	858.0	w	
21	938.5	s	
22	941.5	m	shoulder
23	948.0	s	
24	962.0	w	
25	999.5	m	
26	1026.0	m	
27	1071.0	w	shoulder
28	1073.5	m	shoulder
29	1075.2	s	
30	1101.8	m	
31	1129.8	s	
32	1148.0	w	
33	1151.5	w	
34	1156.5	w	
35	1168.8	m	
36	1178.5	s	
37	1188.0	s	
38	1276.0	w	shoulder
39	1278.5	s	
40	1280.0	s	
41	1287.5	m	

Table 10 (Continued)

Band Number	Frequency (cm^{-1})	Intensity	Comments
42	1298.0	s	
43	1313.0	w	shoulder
44	1329.5	s	
45	1337.5	m	shoulder
46	1418.5	w	shoulder
47	1426.0	s	
48	1432.5	s	
49	1437.0	w	shoulder
50	1453.5	s	
51	1456.5	w	shoulder
52	1466.5	m	
53	1496.0	m	
54	1584.5	s	
55	1602.0	s	
56	1705.0	s	very broad
57	1710.0	w	shoulder
58	1723.0	w	shoulder
59	1752.0	m	
60	1785.0	s	
61	1795.0	w	shoulder
62	1903.5	m	very broad
63	1937.0	w	
64	1975.0	w	
65	1994.5	w	
66	2096.0	w	
67	2204.0	w	
68	2584.0	s	
69	2610.0	s	
70	2724.0	w	shoulder
71	2737.0	s	
72	2757.0	w	
73	2773.5	m	
74	2787.0	m	
75	3058.0	w	shoulder
76	3061.0	w	
77	3067.0	w	
78	3072.0	m	

FIGURE 16

Infrared Spectrum of Benzoic Acid 4d_1

Perkin Elmer Model 225 Infrared Spectrometer

Temperature = 4.2° K

Sample: 0.65 milligrams of Benzoic Acid 4d_1
in 300 milligrams of KBr

Reference: 300 milligrams of KBr + Screen

Pen Period = 3.0 seconds

Suppression = 0

Scan Speed = 4

Slit Program 4.5

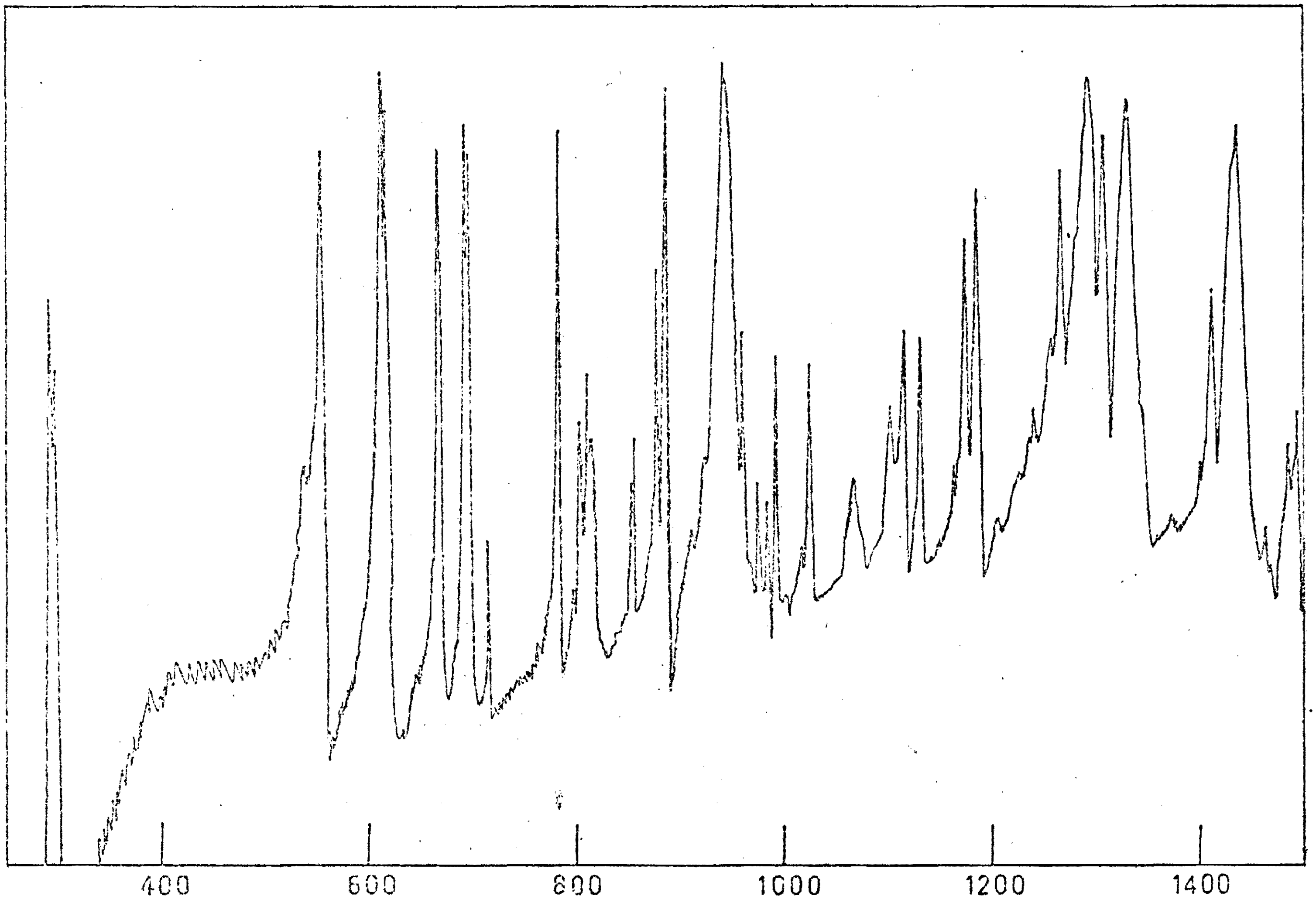
400
600
800
1000
1200
1400

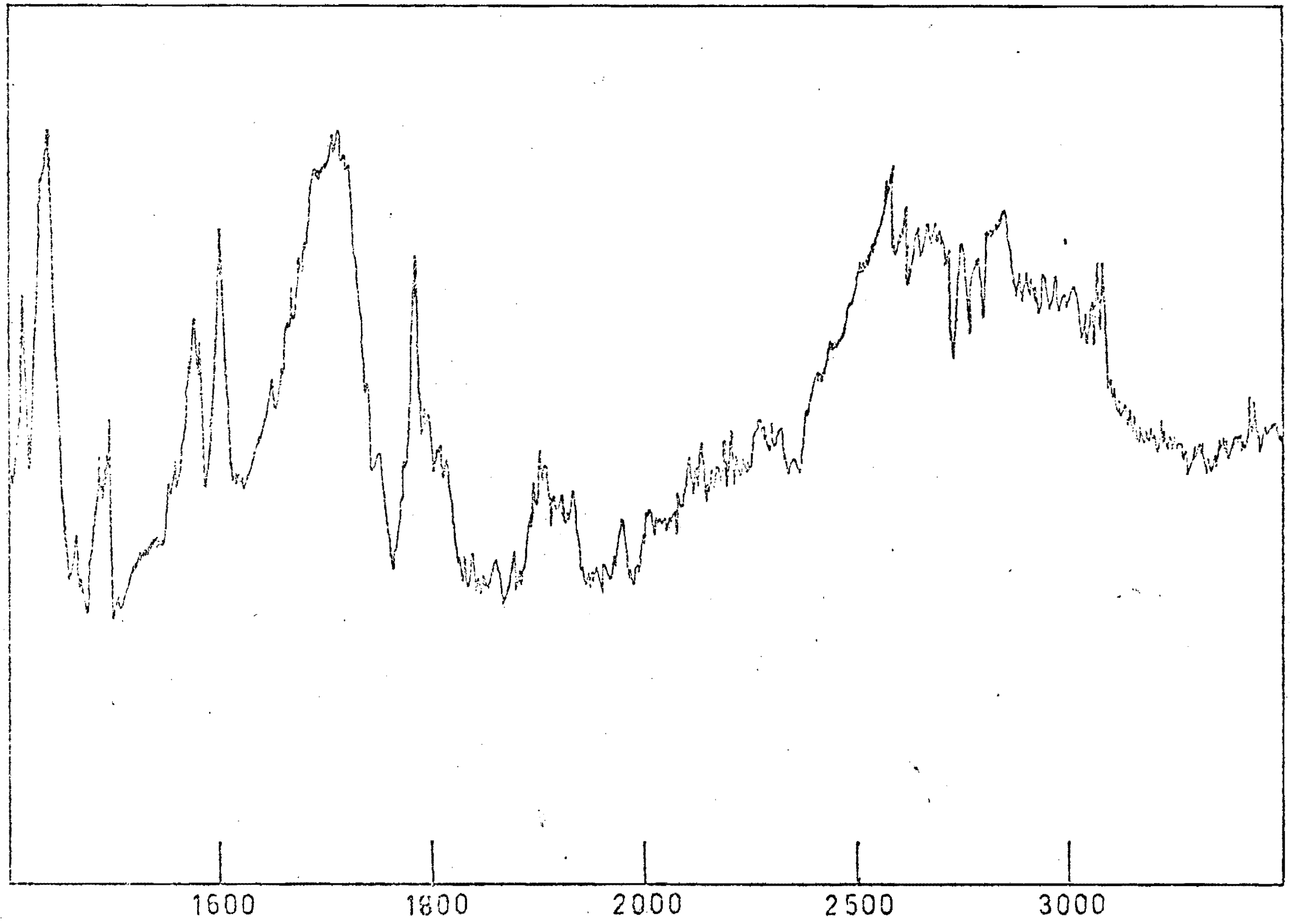
1600
1800
2000
2500
3000

TABLE 11

This table contains the frequencies and qualitative relative intensities of bands in the IR spectrum shown in Figure 16. The frequencies given in this table have been taken from an expanded scale version of the spectrum in Figure 16, since frquencies can be determined more accurately in the expanded scale spectrum.

Band Number	Frequency (cm^{-1})	Intensity	Comments
1	290.6	strong (s)	
2	295.2	s	
3	537.0	medium (m)	shoulder
4	553.5	s	
5	555.0	s	shoulder
6	611.5	s	
7	615.5	s	
8	645.0	weak (w)	
9	666.5	s	
10	668.0	s	
11	692.5	s	
12	694.0	s	
13	710.5	w	
14	715.5	m	
15	768.5	w	
16	773.0	w	
17	779.9	w	shoulder
18	783.5	s	
19	797.0	w	
20	804.2	m	
21	810.5	m	
22	814.0	m	
23	853.5	m	
24	855.8	m	
25	878.0	m	
26	886.5	s	
27	944.0	s	
28	959.5	m	
29	975.5	m	
30	983.5	m	
31	993.0	m	
32	1017.0	w	
33	1026.0	m	
34	1067.0	m	
35	1171.0	w	shoulder
36	1102.0	m	
37	1113.0	w	shoulder
38	1116.5	m	
39	1124.0	w	
40	1127.0	w	
41	1131.5	m	
42	1139.5	w	
43	1171.0	w	shoulder

Table 11 (Continued)

Band Number	Frequency (cm^{-1})	Intensity	Comments
44	1175.3	m	
45	1182.5	m	shoulder
46	1240.0	w	
47	1258.0	m	broad shoulder
48	1266.0	m	
49	1281.5	w	shoulder
50	1293.0	s	
51	1306.0	s	
52	1329.5	s	
53	1371.0	w	
54	1397.0	w	
55	1411.0	m	
56	1422.5	w	shoulder
57	1427.5	m	shoulder
58	1433.5	s	
59	1437.0	m	shoulder
60	1444.5	w	shoulder
61	1449.0	w	
62	1452.5	w	
63	1462.0	w	
64	1467.0	w	
65	1474.5	w	
66	1483.5	m	
67	1493.0	m	
68	1562.5	w	shoulder
69	1567.0	w	shoulder
70	1573.5	m	
71	1579.0	m	
72	1597.0	s	
73	1600.0	m	unresolved
74	1602.5	w	shoulder
75	1604.0	w	shoulder
76	1690.0	m	shoulder
77	1710.0	s	
78	1720.0	w	shoulder
79	1782.0	m	
80	1795.0	m	broad
81	1806.0	m	broad
82	1903.0	m	broad
83	1931.0	w	
84	1974.0	w	shoulder
85	1976.5	w	
86	2576.0	s	very broad
87	2608.0	s	very broad
88	2665.0	s	
89	2737.0	strong	very broad
90	2764.0	m	broad
91	2776.0	strong	broad
92	3058.0	m	
93	3063.0	w	
94	3071.5	m	

FIGURE 17

Infrared Spectrum of Benzoic Acid d_5

Perkin Elmer Model 225 Infrared Spectrometer

Temperature = 4.2° K

Sample: 0.5 milligrams of Benzoic acid d_5
in 300 milligrams of KBr

Reference: 300 milligrams of KBr + Screen

Pen Period = 3.0 seconds

Suppression = 0

Scan Speed = 3

Slit Program = 4.5

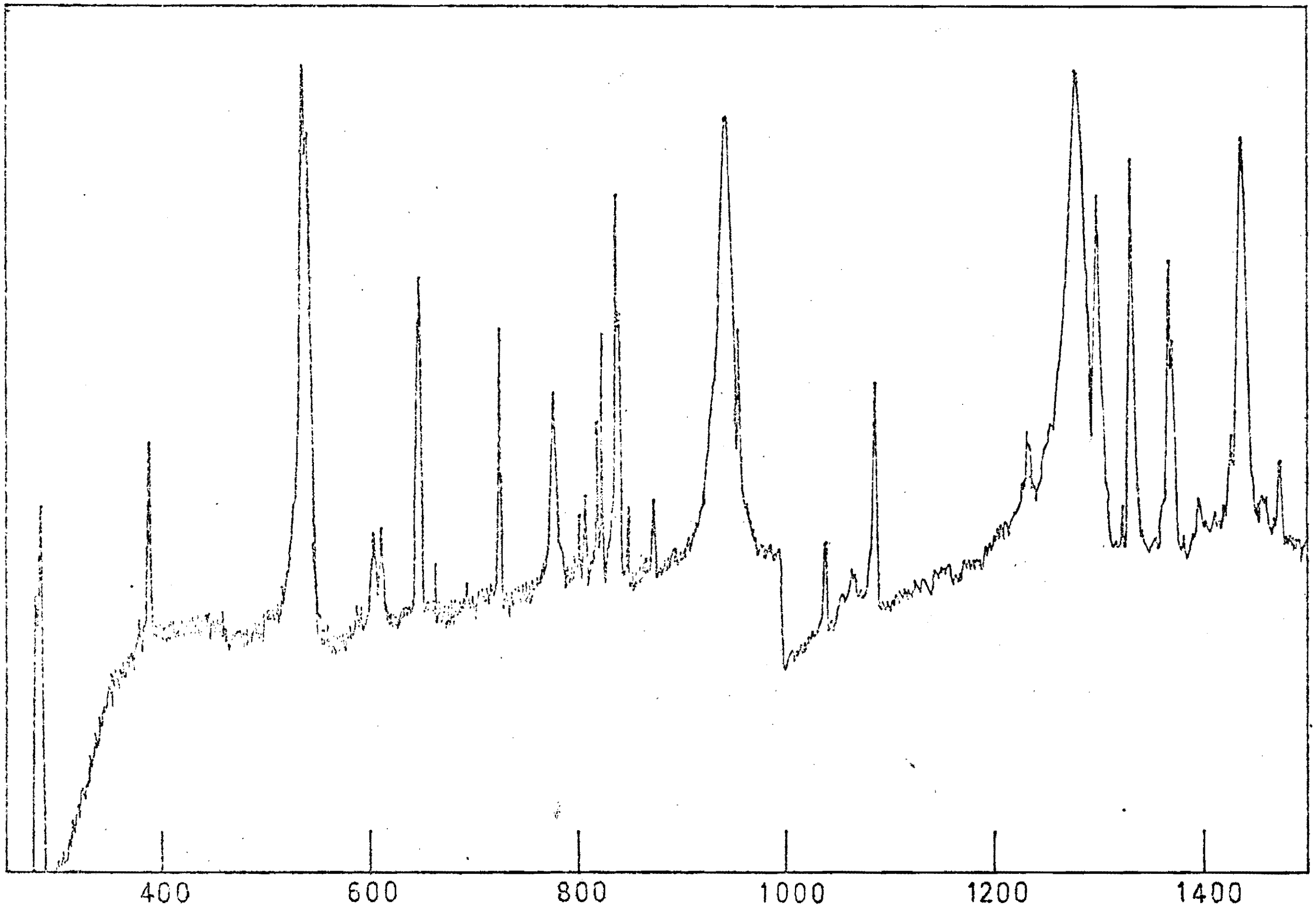
400
600
800
1000
1200
1400

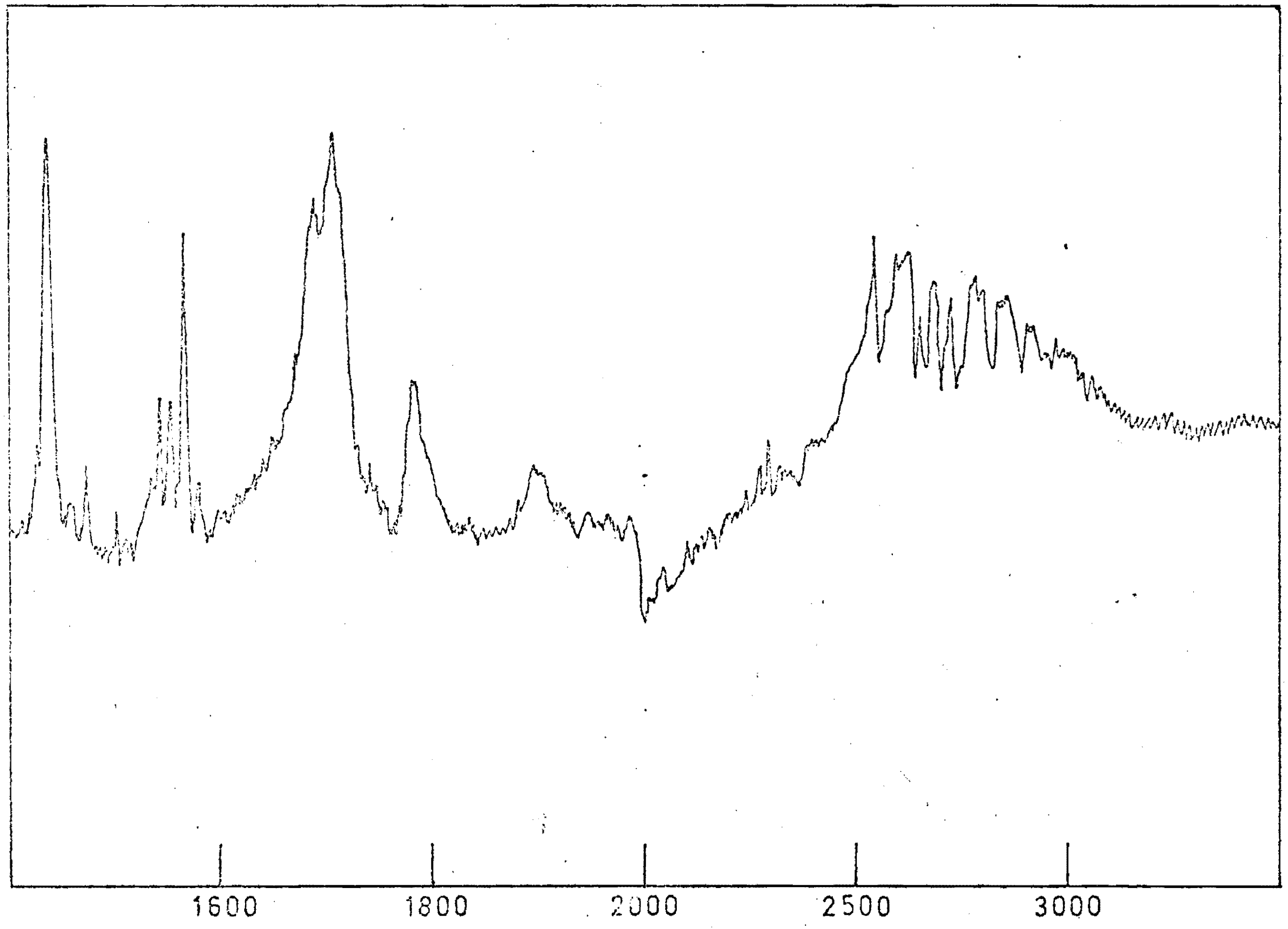
1600
1800
2000
2500
3000

TABLE 12

This table contains the frequencies and qualitative relative intensities of bands in the IR spectrum shown in Figure 17. The frequencies given in this table have been taken from an expanded scale version of the spectrum shown in Figure 17, since frequencies can be determined more accurately in the expanded spectrum.

Band Number	Frequency (cm^{-1})	Intensity	Comments
1	281.0	strong (s)	
2	285.0	s	
3	391.0	medium (m)	
4	538.0	s	
5	541.0	s	shoulder
6	590.0	weak (w)	
7	592.5	w	
8	605.5	w	
9	613.0	w	
10	648.5	m	
11	650.5	m	
12	728.3	m	
13	729.8	w	shoulder
14	780.0	m	
15	785.0	w	
16	805.0	w	
17	810.2	w	
18	822.0	w	
19	827.0	w	
20	840.5	s	
21	843.8	m	shoulder
22	852.0	w	
23	876.5	w	
24	933.0	w	shoulder
25	946.0	s	
26	958.0	m	
27	1041.0	m	
28	1044.0	m	
29	1086.0	w	shoulder
30	1089.0	s	
31	1234.0	w	
32	1236.5	w	shoulder
33	1262.5	w	shoulder
34	1280.0	s	
35	1292.0	w	shoulder
36	1300.2	s	
37	1305.5	m	shoulder
38	1311.5	w	shoulder
39	1325.0	w	
40	1331.0	w	shoulder
41	1333.6	s	

Table 12 (Continued)

Band Number	Frequency (cm^{-1})	Intensity	Comments
42	1370.0	s	
43	1373.5	s	
44	1385.0	w	
45	1398.5	w	
46	1423.0	w	
47	1428.5	w	shoulder
48	1436.5	m	shoulder
49	1438.5	s	
50	1459.0	w	
51	1463.5	w	
52	1472.5	w	shoulder
53	1475.0	w	
54	1500.5	w	shoulder
55	1503.5	w	
56	1538.0	w	
57	1546.0	m	
58	1553.5	w	
59	1556.5	w	
60	1568.8	s	
61	1582.0	w	
62	1606.0	w	very broad
63	1620.0	w	
64	1653.0	w	
65	1687.5	m	shoulder
66	1691.0	s	very broad
67	1709.0	s	very broad
68	1714.0	m	shoulder
69	1743.5	w	broad
70	1784.0	s	very broad
71	1899.0	w	very broad
72	2050.5	w	very broad
73	2276.0	w	
74	2296.0	w	
75	2545.0	s	very broad
76	2633.0	s	
77	2658.0	m	very broad
78	2680.0	s	very broad
79	2727.0	s	very broad
80	2082.0	m	very broad
81	2822.0	w	

FIGURE 18

Infrared Spectrum of Benzoic Acid $1d_1$

Perkin Elmer Model 225 Infrared Spectrometer

Temperature = 4.2° K

Sample: 0.8 milligrams (estimated) of Benzoic acid $1d_1$ in 300 milligrams of KBr

Reference: 300 milligrams of KBr + Screen

Pen Period = 3.0 seconds

Suppression = 2

Scan Speed (not recorded)

Slit Program = 4.5

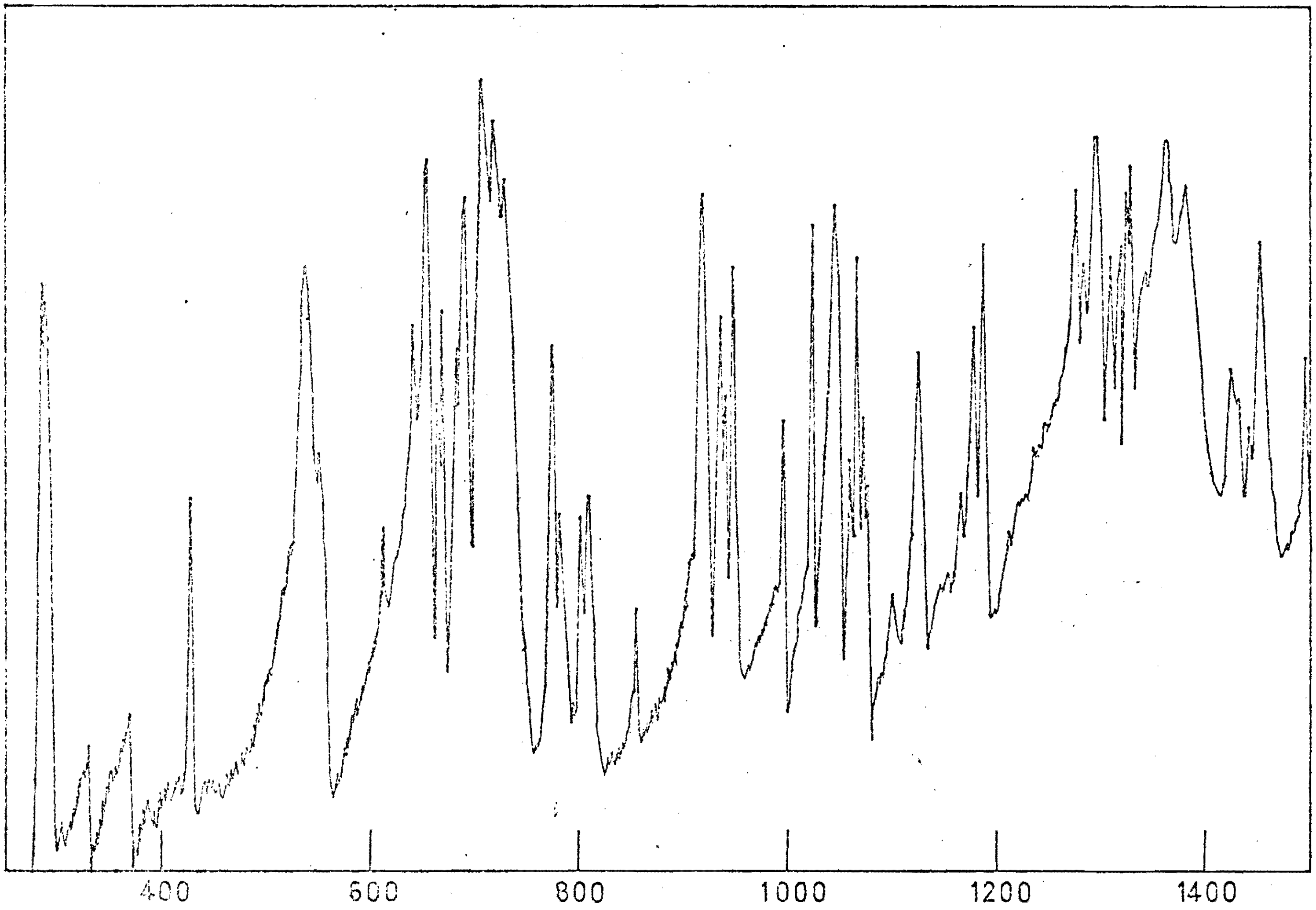
400
600
800
1000
1200
1400

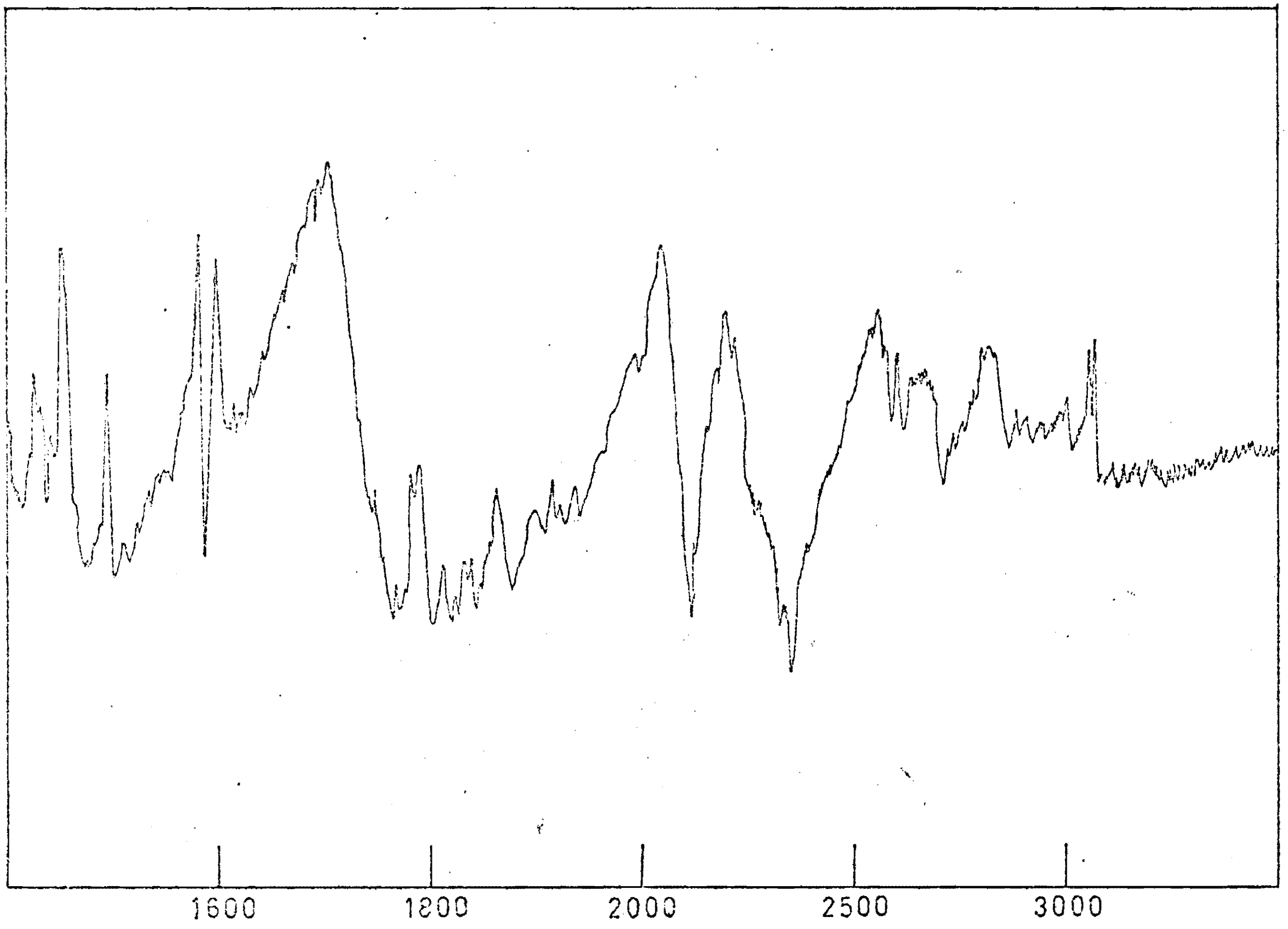
1600
1800
2000
2500
3000

TABLE 13

This table contains the frequencies and qualitative relative intensities of bands in the IR spectrum shown in Figure 18. The frequencies given in this table have been taken from an expanded scale version of the spectrum in Figure 18, since frequencies can be determined more accurately in the expanded scale spectrum.

Band Number	Frequency (cm^{-1})	Intensity	Comments
1	287.5	strong (s)	
2	291.0	s	
3	431.0	medium (m)	
4	540.5	s	
5	554.0	m	
6	616.0	weak (w)	
7	644.0	w	
8	657.0	s	
9	667.0	m	
10	671.0	m	
11	686.0	m	
12	692.0	s	
13	694.0	s	
14	710.0	s	
15	720.5	s	
16	732.0	s	
17	778.0	s	
18	786.0	s	
19	805.5	m	
20	811.0	m	
21	814.0	m	
22	853.0	w	shoulder
23	854.0	w	
24	923.0	s	
25	939.5	s	
26	944.0	m	
27	951.0	s	
28	999.5	s	
29	1026.0	w	unresolved shoulder
30	1028.0	s	
31	1044.0	m	shoulder
32	1046.0	s	broad
33	1063.5	m	
34	1069.5	s	
35	1075.5	m	
36	1077.0	w	
37	1103.0	w	
38	1120.0	w	shoulder
39	1127.5	s	
40	1129.5	s	shoulder
41	1169.0	w	
42	1179.5	m	

Table 13 (Continued)

Band Number	Frequency (cm^{-1})	Intensity	Comments
43	1190.0	s	
44	1238.0	w	
45	1279.0	s	
46	1285.5	w	
47	1298.0	s	
48	1302.0	s	shoulder
49	1308.0	w	shoulder
50	1311.5	m	
51	1319.0	w	shoulder
52	1320.0	m	
53	1327.0	s	
54	1330.0	s	
55	1338.0	w	
56	1345.0	w	
57	1365.0	s	very broad
58	1383.5	s	very broad
59	1396.0	w	shoulder
60	1403.0	w	
61	1427.0	m	
62	1433.0	m	
63	1443.3	w	
64	1454.0	s	
65	1496.0	m	
66	1585.0	s	
67	1601.5	s	
68	1617.0	w	
69	1705.0	s	very broad
70	1786.0	m	broad
71	1792.0	m	broad
72	1814.0	w	broad
73	1865.0	m	very broad
74	1917.0	w	
75	1938.0	w	very broad
76	2127.0	w	broad
77	2202.0	s	very broad
78	2224.0	m	very broad
79	2584.0	m	broad
80	2611.0	m	very broad
81	2984.0	w	
82	3008.5	w	
83	3049.0	w	
84	3060.0	m	
85	3072.5	m	

FIGURE 19

Polarized Infrared Spectra of Benzoic Acid d_o

These spectra were kindly supplied by Dr. R. Zwarich

Temperature: 298° K

Sample: Benzoic Acid d_o crystal grown between NaCl disks.

Orientation: Angle between b-axis (extinction axis) and slit of spectrometer = 45°. Spectrum represented by solid line was obtained with light polarized perpendicular to b-axis. Spectrum represented by broken line was obtained with light polarized parallel to b-axis.

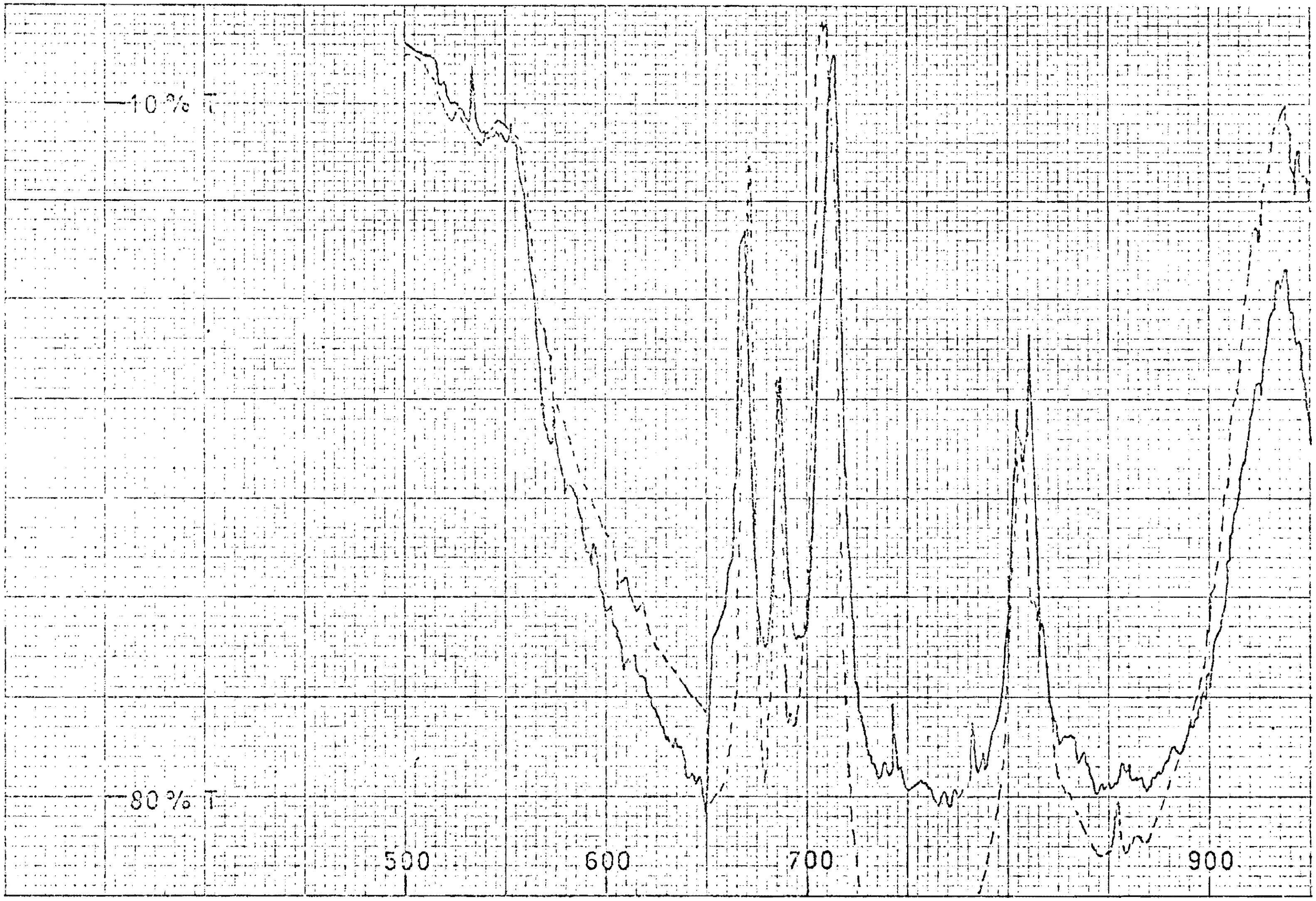
10 % T
80 % T
500
600
700
900

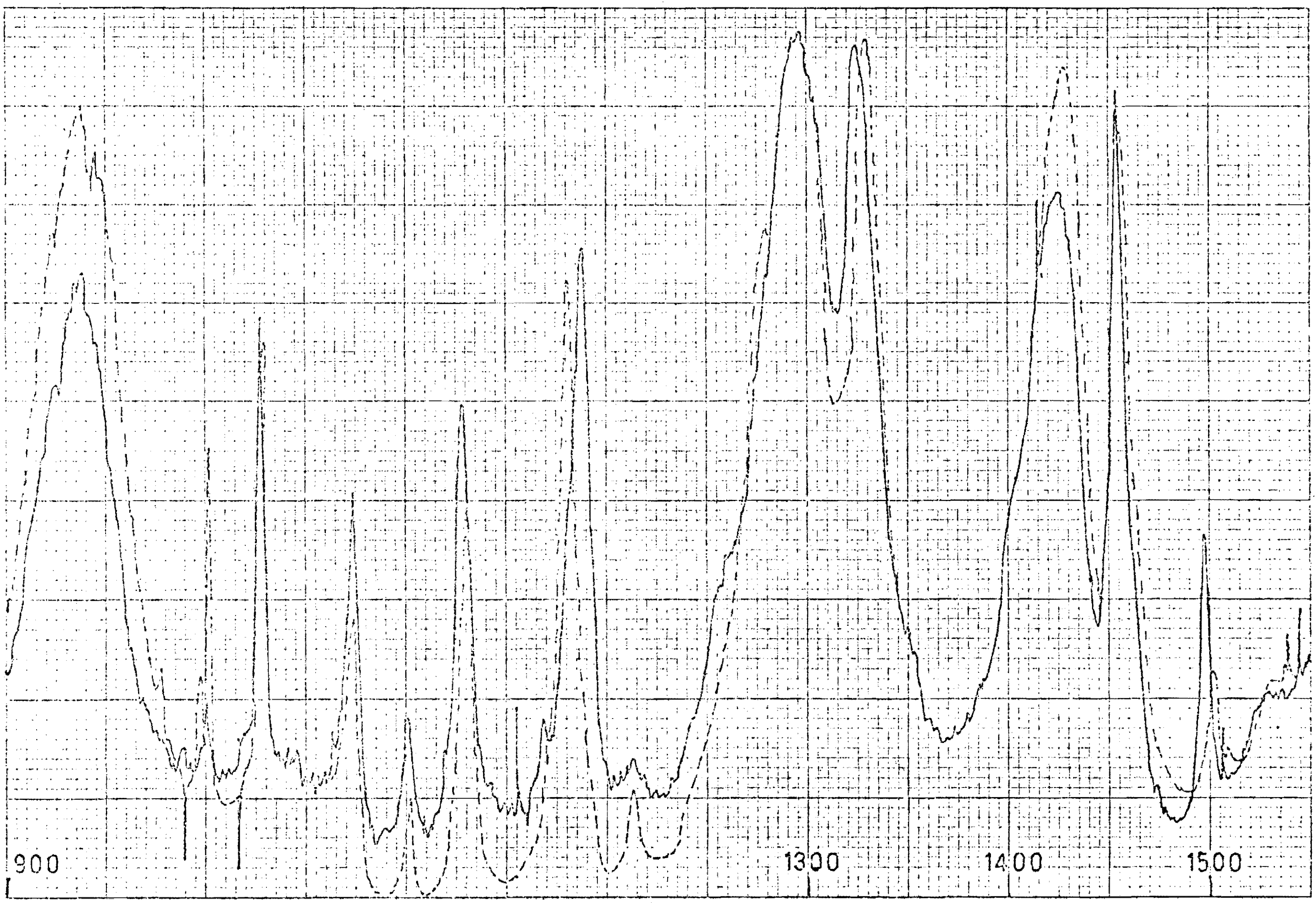
900
1300
1400
1500

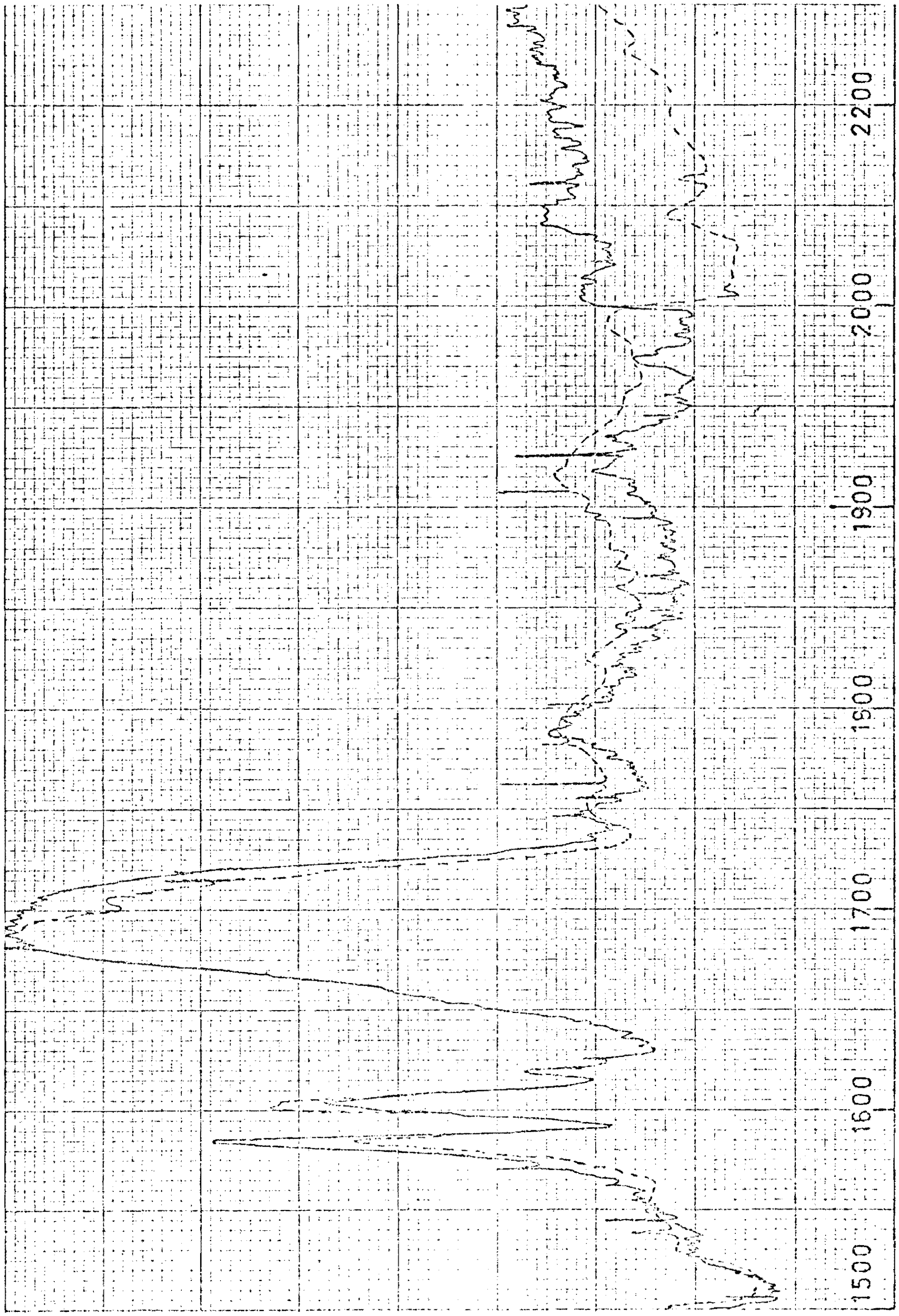
1500
1600
1700
1500
1900
2000
2200

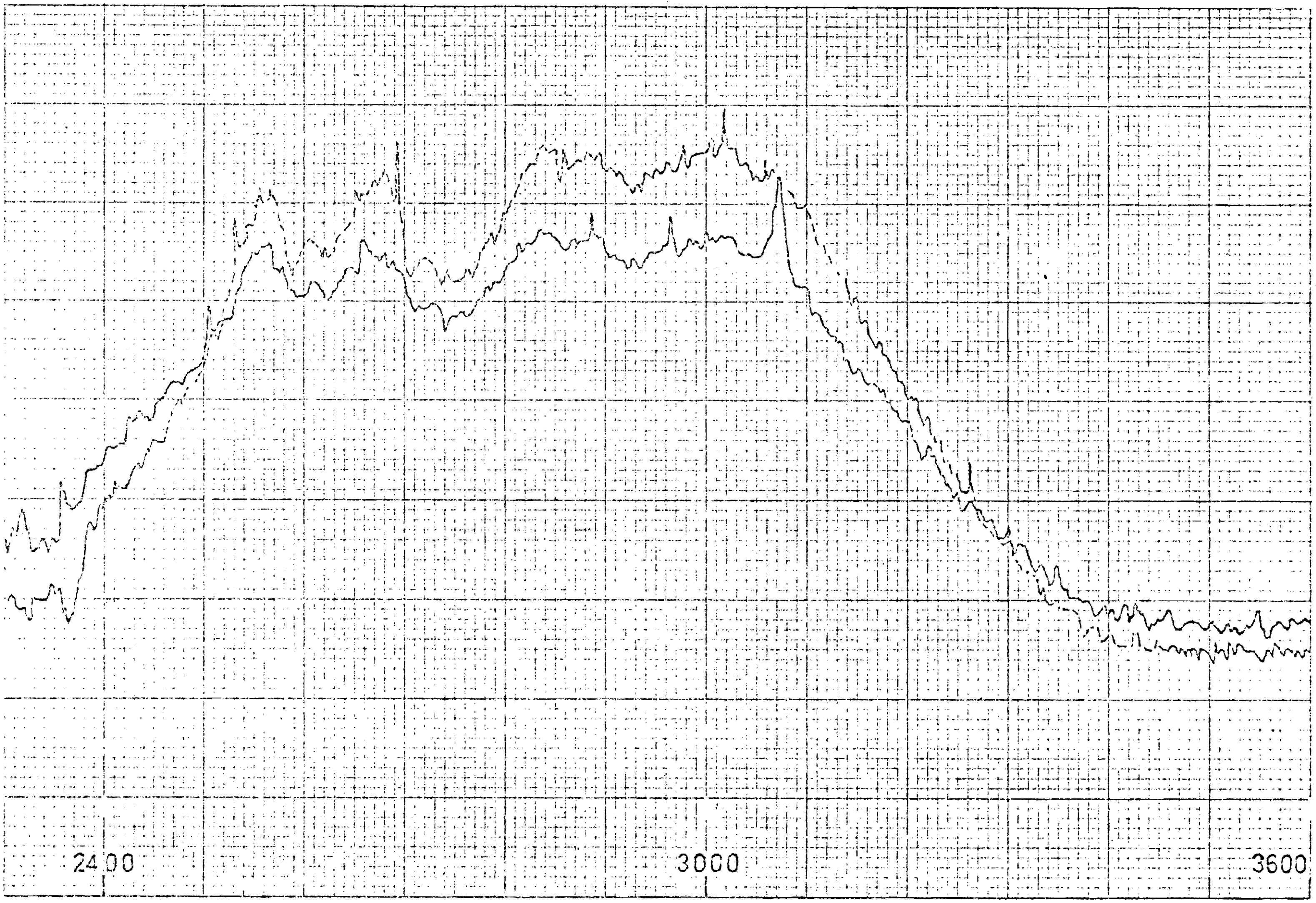
2400
3000
3600

FIGURE 20

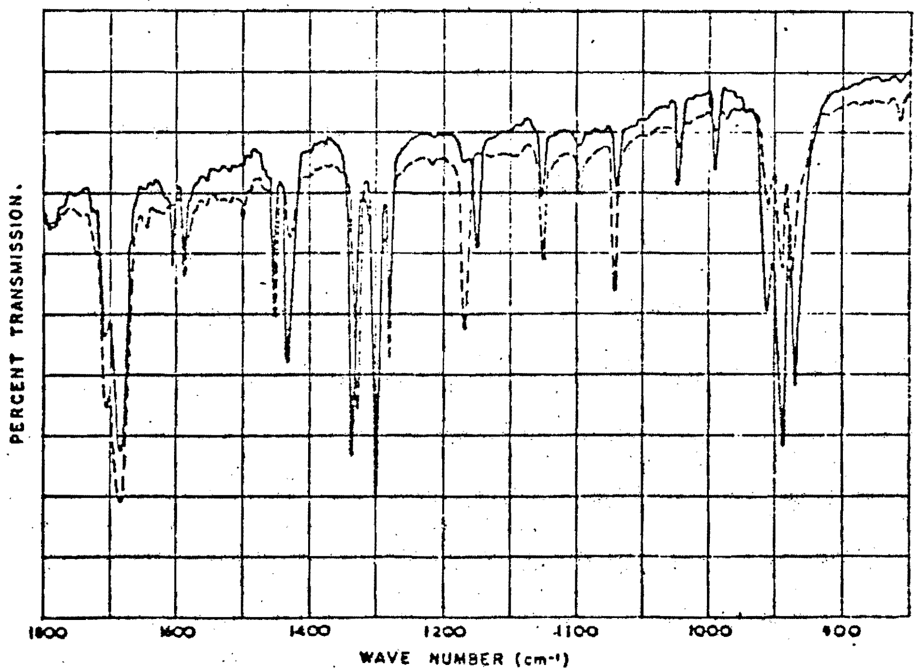

Polarized infrared spectra of benzoic acid at −150°C.

—— *E* vector parallel to *b* axis.

······ *E* vector perpendicular to *b* axis.

Polarized infrared spectra of benzoic acid d_0 at -150° C. (Taken from Hayashi and Kimura, 1966)

FIGURE 21

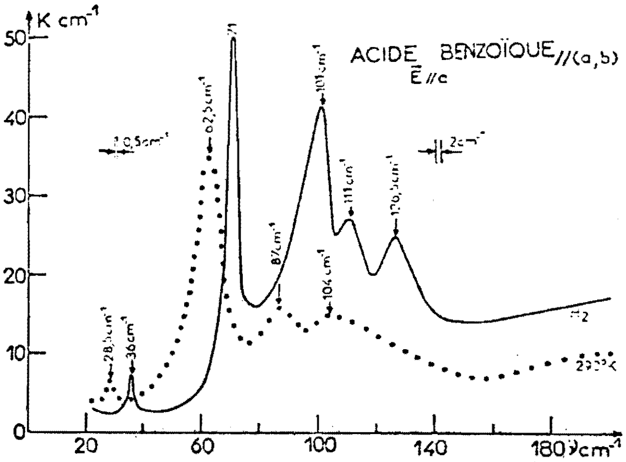

— Spectre d'absorption d'une lame d'acide benzoïque taillée parallèlement au plan de clivage, à la température ordinaire et à la température de l'hydrogène liquide. Le champ électrique **E** est orienté parallèlement à l'axe **a**.

Nous observons des maximums d'absorption à 28,5, 62,5, 87 et 104 cm^{-1} à 290 °K et 36, 71, 101, 111 et 126,5 cm^{-1} à la température de l'hydrogène liquide.

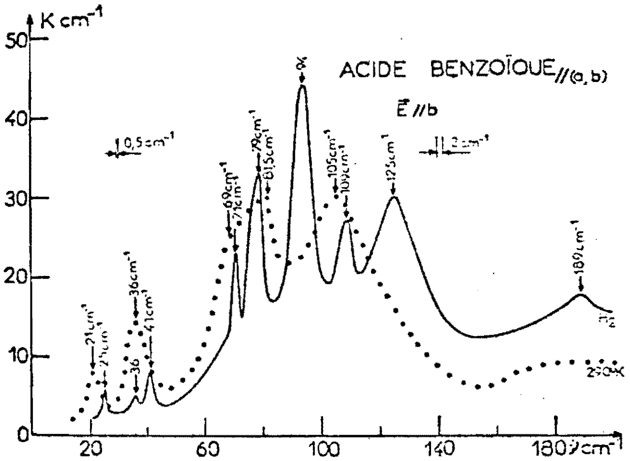

— Spectre d'absorption d'une lame d'acide benzoïque taillée parallèlement au plan de clivage, à la température ordinaire et à la température de l'hydrogène liquide. Le champ électrique **E** est orienté parallèlement à l'axe **b**. Nous observons des maximums d'absorption à 21, 36, 69, 81,5 et 105 cm^{-1} à 290 °K et à 25, 36, 41, 71, 79, 94, 109, 125 et 189 cm^{-1} à la température de l'hydrogène liquide.

Polarized far infrared spectra of benzoic acid d_o at 25° K (Taken from Wyncke et al., 1968)

FIGURE 22

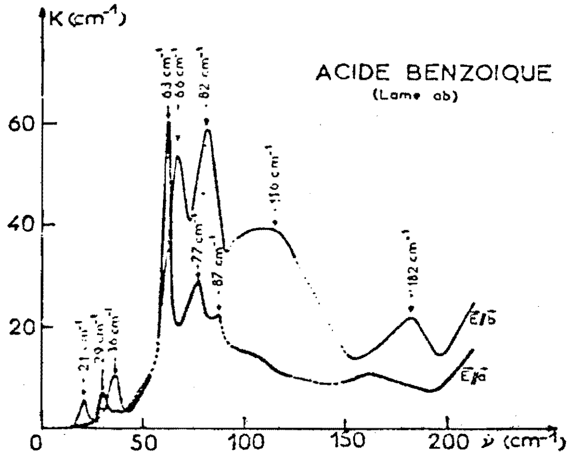

— Spectre d'absorption d'une lame d'acide benzoïque taillée parallèlement au plan de clivage avec le champ électrique polarisé successivement suivant les deux lignes neutres. Pour **E** parallèle à l'axe **b** d'ordre 2, les maximums d'absorption s'observent à 21, 36, 66, 82, 116 et 182 cm^{-1}. Pour **E** parallèle à la direction **a**, le maximum d'absorption s'observe à 63 cm^{-1}.

Polarized far infrared spectra of benzoic acid d_o at 298^o K (Taken from Wyncke et al., 1968)

FIGURE 23

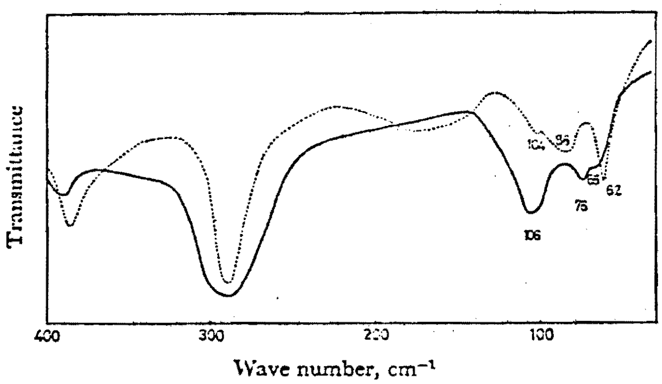

Polarized far-infrared spectra of benzoic acid single crystals.

······Electric vector parallel to the *b*-axis

——Electric vector perpendicular to the *b*-axis (parallel to the *a*-axis)

Polarized far infrared spectra of benzoic acid d_o at 298° K (Taken from Meshitsuka _et al_., 1972).

FIGURE 24

Selected regions of benzoic acid d_o Raman spectra taken at 298, 77, and 4.2^o K. The temperature dependence of the linewidths of a pure ring mode (R), a carboxyl group mode (C), an H-bond mode (H), and a lattice mode (L) are compared.

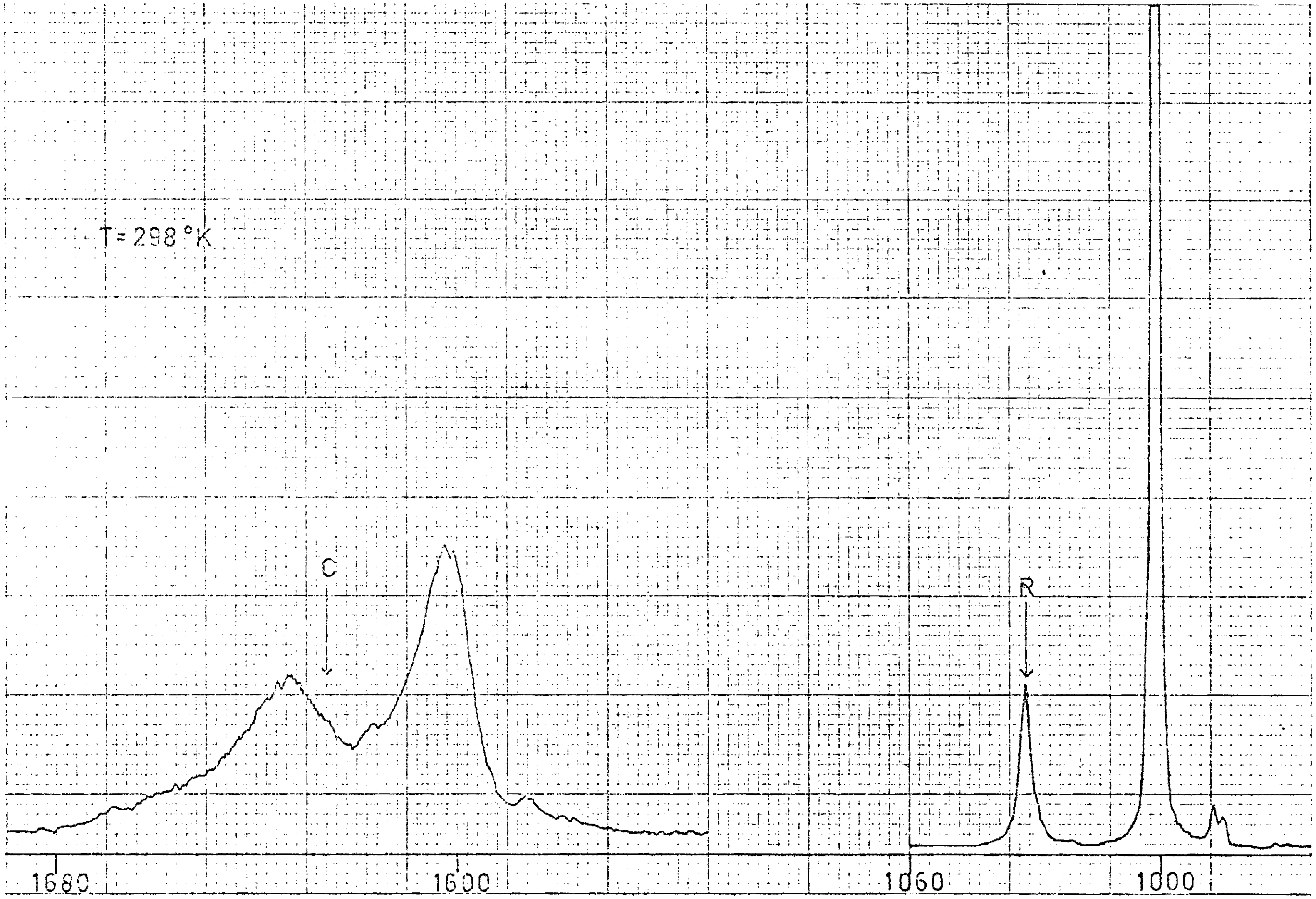

T = 298 °K
C
R
1680
1600
1060
1000

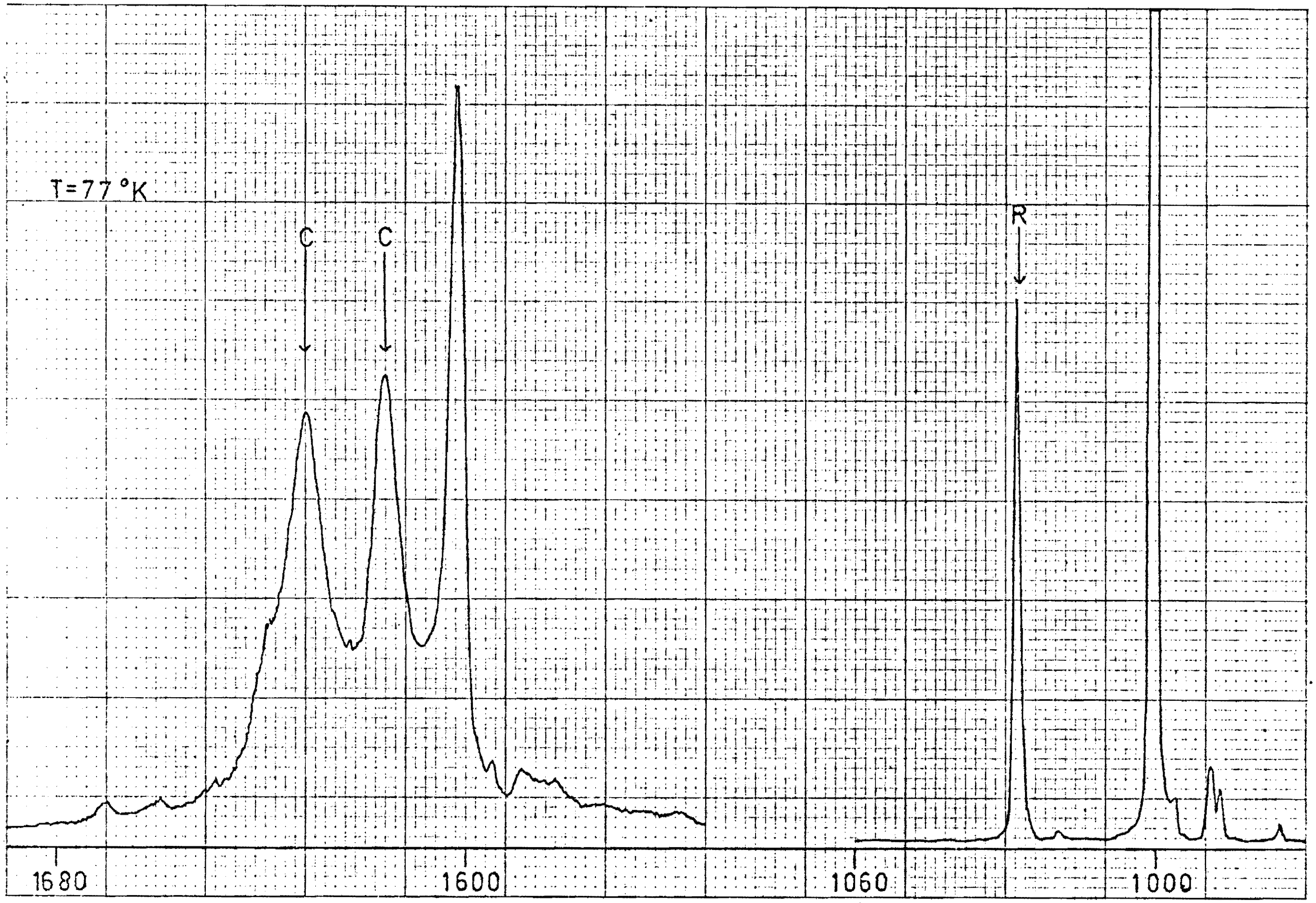
T=77°K
C
C
R
1680
1600
1060
1000

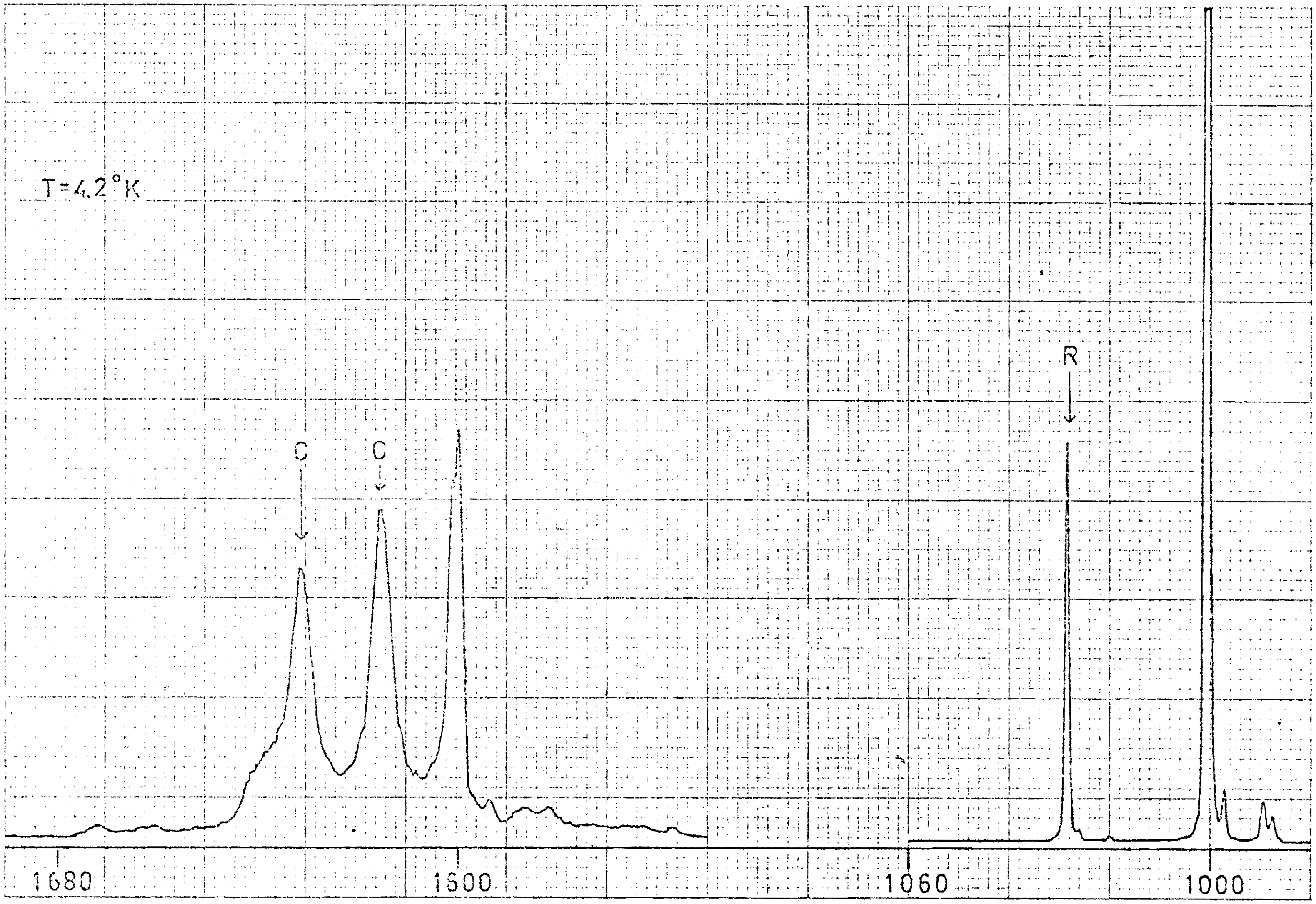
T=4.2°K
C
C
R
1680
1500
1060
1000

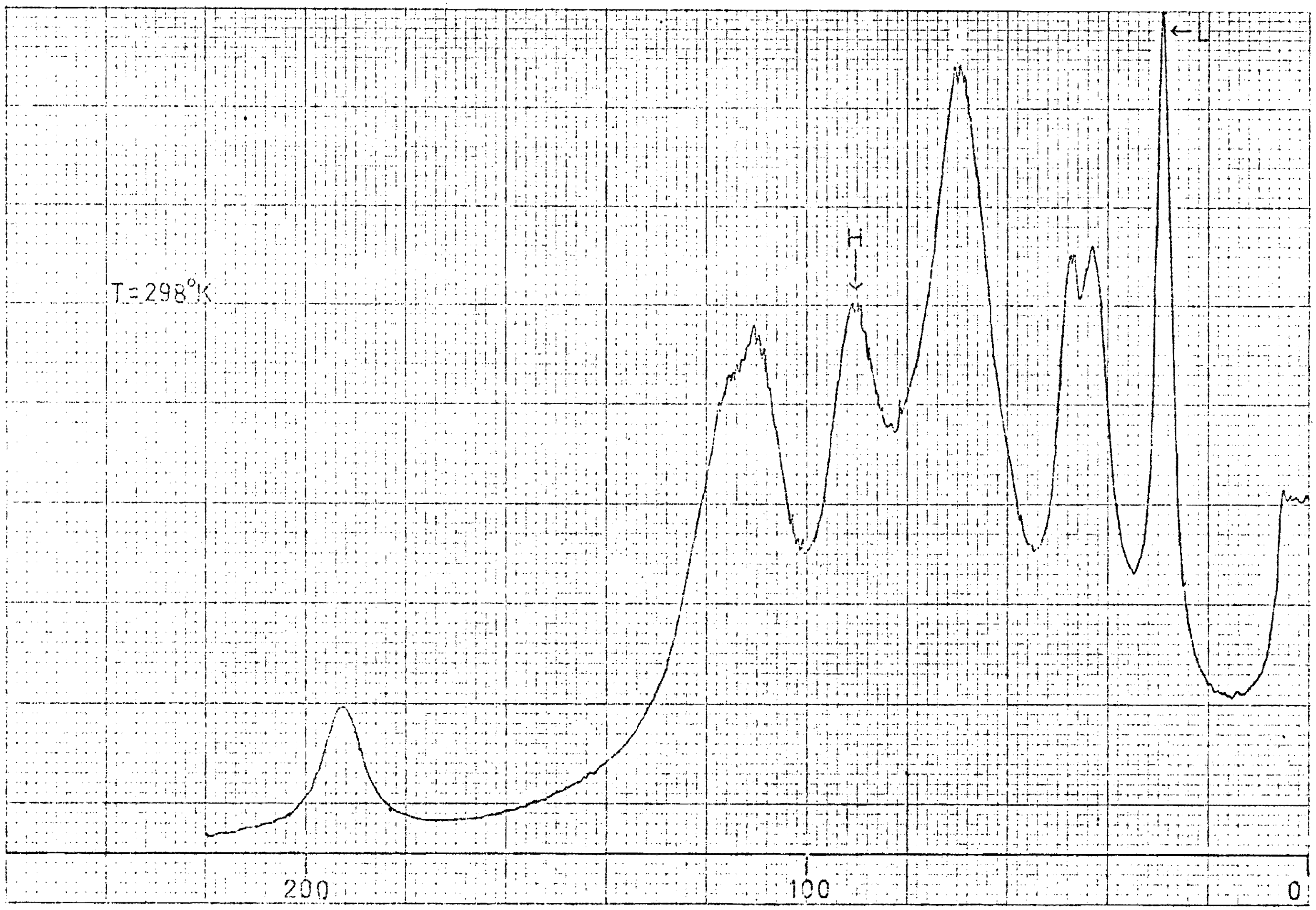
L
H
T=298°K
200
100
0

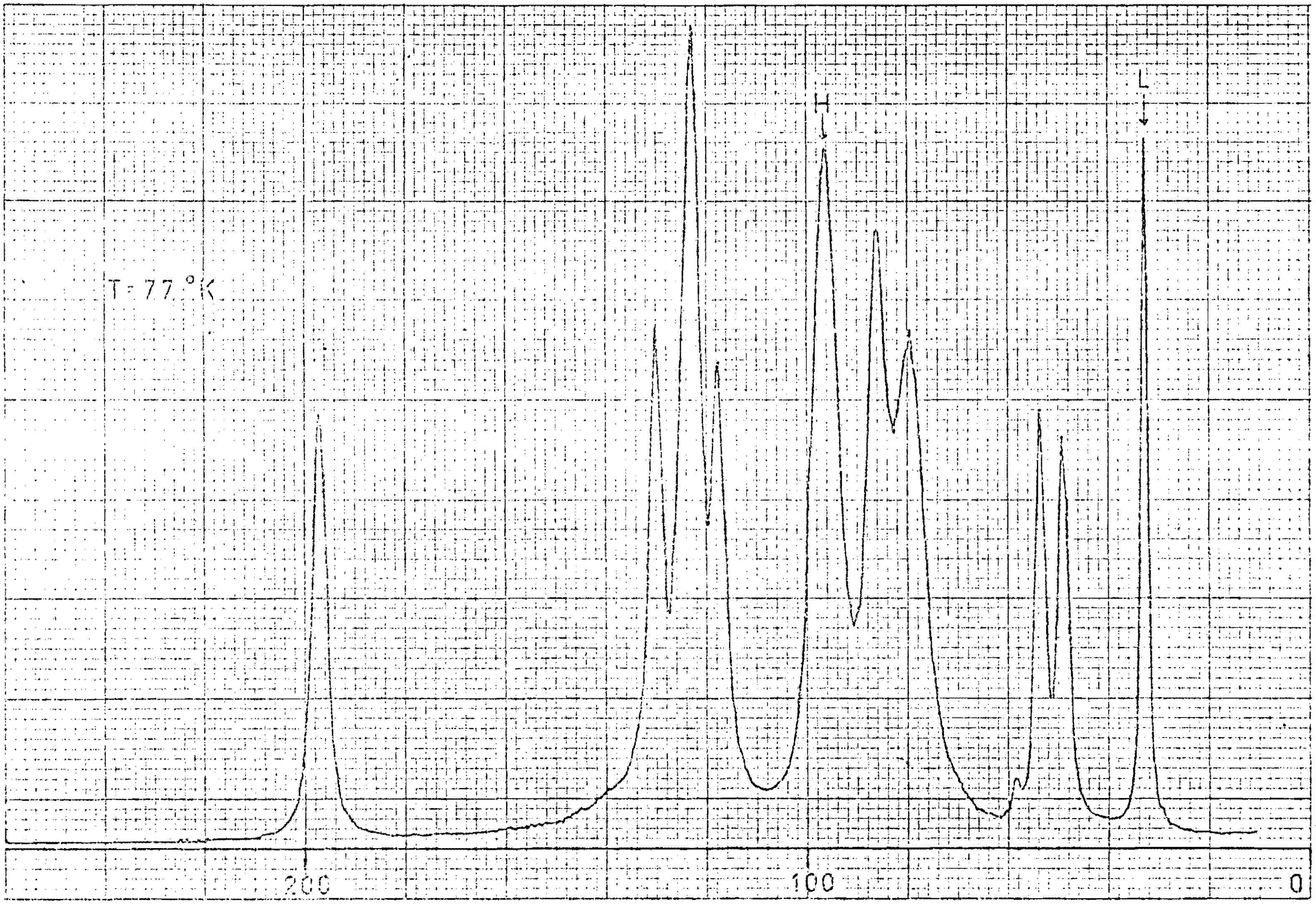
T=77°K
H
L
200
100
0

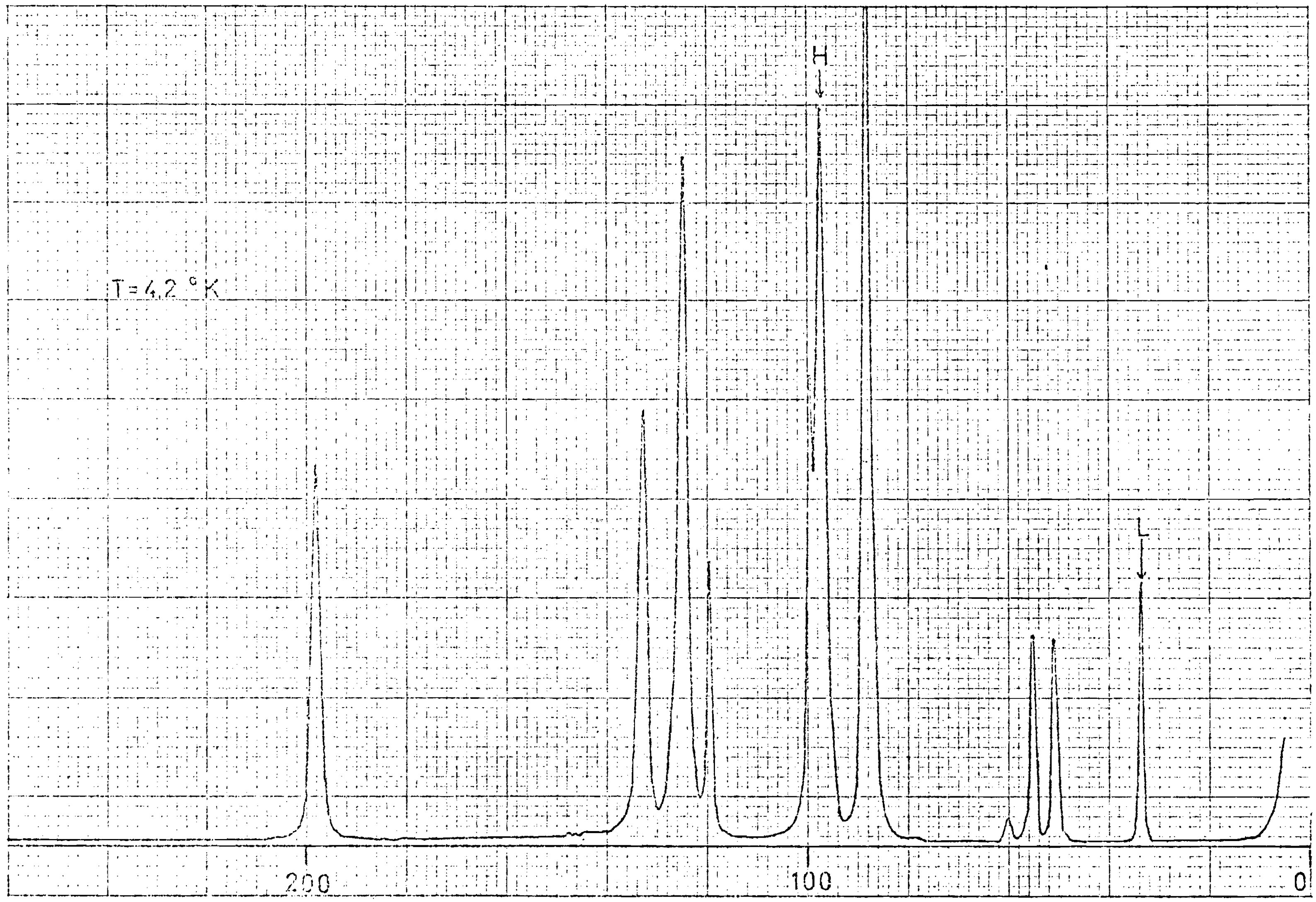
H
L
T=4.2 °K
200
100
0

H. Assignments

1. Out-of-Plane Benzene Analogues

We first consider the assignment of out-of-plane modes that are benzene analogues. This group includes all out-of-plane modes except the ring-carboxyl group torsion, the O-H out-of-plane wag, and the H-bond out-of-plane modes.

In making the assignments we follow a systematic procedure. First, those bands which are in or near the appropriate Varsanyi range are determined. Then the displacement pattern for the corresponding benzene mode is consulted in order to determine whether or not the frequency of the benzene analogue should be sensitive to $d_o \rightarrow 4d_1$ substitution. Bands which do not show the appropriate $d_o \rightarrow 4d_1$ shifts are excluded from further consideration. Next we determine the point group that is appropriate for the mode under consideration. This is first done for the monomer. If local symmetry is expected to prevail, then local symmetry selection rules are used to predict whether the mode should be strong or weak in the IR and Raman spectra. Shifts for $d_o \rightarrow 1d_1$ and $d_o \rightarrow d_5$ substitutions are used to support arguments concerning the appropriateness of using local symmetry. Next the appropriate point group for the dimer mode is determined. Then symmetry considerations are used to determine the direction of the vibration induced dipole moment for the IR active version of the dimer mode. This information is used to predict the intensity ratio of the factor group pair, as discussed in Section IID. These predictions are compared with available polarization data. For IR bands we consult the polarized absorption spectra obtained at -150° C by Hayashi and Kimura (1966) which extend from 850 to 1800 cm^{-1}, and the room temperature spectra obtained by Zwarich, which extend from 650-3000 cm^{-1}. Unfortunately, polarized Raman spectra of oriented crystals are not available except in the range below 200 cm^{-1}. However, depolarization ratios for benzoic acid dimer in solution have been obtained by Baum (1974).

Another criterion used in making the assignments is the intensity change for IR active modes upon $d_o \rightarrow 4d_1$ substitution. Whether the intensity is expected to increase or decrease is determined by considering the vibration induced dipole for the monomer to be the sum of the vibration induced dipoles associated with each C-H group of the ring. In some cases, symmetry allows a clear-cut prediction of the intensity changes while in others one must make assumptions about the relative magnitudes of the dipoles associated with the various C-H groups.

Another, very important criterion used in assigning the out-of-plane modes is based upon the phosphorescence spectrum of benzoic acid. As will be discussed in detail in Chapter III, the phosphorescence spectrum contains a set of bands which are highly sensitive to environmental perturbations. In some matrices they are intense and in others weak. At least two of the modes in this set (ν_4 and ν_{16a} can be firmly assigned as out-of-plane modes entirely on the basis of infrared and Raman data. Since the modes in this set increase or decrease in intensity as a group when the environment is changed, we assume that they are all out-of-plane. This assumption is supported by the success of the model used to account for the presence of these modes. This model, which involves Herzberg-Teller coupling between $n\pi^*$ and $\pi\pi^*$ states, requires all of the environmentally sensitive modes to be out-of-plane. This is discussed in detail in Chapter III. Having justified our assumption, we return to the Raman and infrared spectra with the knowledge that certain modes are out-of-plane. This sorting between in-plane and out-of-plane modes greatly reduces the number of sets of possible assignments. It is important to realize that no circularity is involved in using Raman and IR data to interpret phosphorescence data and then using phosphorescence data to interpret IR and Raman spectra, because different modes are involved in each case.

Mode ν_{16a}: The Varsanyi range is 390-420 cm^{-1}. In the d_o Raman spectrum, two weak bands appear at 407.5 and 438.0 cm^{-1}, and a medium band appears at 422.0 cm^{-1}. No other Raman bands appear between 265.0 and 507.0 cm^{-1}. In the d_oIR spectrum, a single weak band appears at 433 cm^{-1}. No other IR bands appear between 388.0 and 540.0 cm^{-1}. For $d_o \rightarrow 4d_1$ substitution the following shifts are observed:

Raman	IR
$d_o \rightarrow 4d_1$	$d_o \rightarrow 4d_1$
407.5 → 407.5	
422.0 → 419.0	
438.0 → 424.5	433 → missing

An inspection of the benzene displacement pattern for ν_{16a} (see Fig. 1) shows no amplitude at the 1 and 4 positions. Hence the benzene analogue should be $d_o \rightarrow 4d_1$ insensitive, This eliminates the Raman band at 438.0 cm^{-1} and the IR band at 433.0 cm^{-1}, since the disappearance or reduction in intensity is inconsistent with small amplitude in the 4 position. The remaining candidates are the Raman bands at 407.5 and 422.0 cm^{-1}.

Since the benzene displacement pattern shows no amplitude at the 1 and 4 positions, we expect the benzene analogue to have little amplitude at the carboxyl group atoms. Hence, this mode is expected to feel C_{2v} symmetry at the level of the monomer. In this point group, ν_{16a} belongs to the A_2 representation. Consequently, it should be Raman active and IR inactive. Since the mode does not likely involve appreciable carboxyl group motion, we expect the dimer interaction to be weak, allowing monomer symmetry to prevail. Our failure to observe a $d_o \rightarrow 4d_1$ insensitive IR mode in the Varsanyi range for ν_{16a} is consistent with this expectation.

The depolarization ratio for the Raman band at 422.0 cm^{-1} is 0.09, consistent with a totally symmetric mode. Thus, the only remaining candidate is the band at 407.5 cm^{-1}.

As argued above, ν_{16a} should not involve carboxyl group motion. This implies that it should be $d_o \rightarrow 1d_1$ insensitive. Consistent with this expectation is the observed shift from 407.5 cm^{-1} to 408.0 cm^{-1}. At the same time, this mode should be highly sensitive to $d_o \rightarrow d_5$ substitution. A shift of 51.5 cm^{-1} is observed. The band at 422 cm^{-1} shows a shift of only 7 cm^{-1}, suggesting that this band corresponds to a mode involving appreciable carboxyl group motion.

All the data are fully consistent with the assignment of ν_{16a} to the weak Raman band at 407.5 cm^{-1}. We consider this a firm assignment. Note that the factor group component is either unresolved or too weak to be observed.

Mode ν_{16b}: The Varsanyi range is 430-560 cm^{-1}. The Raman bands in this range are at 438.0, 503.0, and 507.0 cm^{-1}. In the d_o IR spectrum, there are bands at 433.0, 546 cm^{-1}, and 557 cm^{-1}. An inspection of the benzene displacement pattern shows large amplitude at the 1 and 4 positions. Hence we expect $d_o \rightarrow 4d_1$ sensitivity. The following shifts are observed:

Raman			IR		
d_o	→	$4d_1$	d_o	→	$4d_1$
438.0	→	424.5	433.0	→	Missing
505.0	→	504.0	543.0	→	537.0
507.0	→	506.0	553.5	→	554.0

The bands at 505.0, 507.0, and 553.5 cm^{-1} are eliminated as possible candidates. Since no polarization data is available, it is difficult to discriminate among the remaining bands. However, the phosphorescence data shows that the 438 cm^{-1} band is an out-of-plane mode. Unfortunately, this data does not allow the conclusion that the band at 543.0 cm^{-1} is not an out-of-plane mode. None the less, a firm conclusion can be drawn, since there is no other Varsanyi range for an out-of-plane mode to which the band at 438 cm^{-1} can belong. Consequently, we firmly assign ν_{16b} to 438.0 cm^{-1} in the Raman and 433.0 cm^{-1} in the IR. No factor group splitting is observed for either band.

Mode ν_{10a}: The Varsanyi range is 810-860 cm^{-1}. The Raman bands in this range are at 812.0, 817.0, 854.1 and 855.8 cm^{-1}. The IR bands are at 809.0, 814.0 817.0, 856.0, and 858.0 cm^{-1}. An inspection of the benzene displacement pattern shows no amplitude at the 1 and 4 positions. Hence we expect ν_{10a} to be $d_o \rightarrow 4d_1$ insensitive. The following shifts are observed:

Raman	IR
$d_o \rightarrow 4d_1$	$d_o \rightarrow 4d_1$
812.0 → 786.2	809.0 → 804.0
817.0 → missing	814.0 → 783.0
854.1 → 851.8	817.0 → 814.0
855.8 → 854.0	856.0 → 853.0
	858.0 → 856.0

The bands at 812.0, 814.0 and 817.0 (Raman only) cm^{-1} are eliminated as possible candidates.

Since the benzene mode has no amplitude at the 1 and 4 positions, we expect the monomer analogue mode to feel C_{2v} symmetry. In this point group, ν_{10a} belongs to the A_2 representation and is thus IR inactive and Raman active. Since this mode should not involve appreciable carboxyl group motion, we expect weak coupling, allowing local symmetry to prevail. Thus the IR dimer mode should be weak. Further, the absence of carboxyl group motion should cause the dimer mode to feel D_{2h} symmetry. In this point group, the Raman active dimer mode belongs to the B_{3g} representation and the IR mode to the B_{1u} representation, requiring the free-dimer IR transition to be accurately perpendicular to the plane of the molecule. As shown in Section IID this polarization leads to $I(B_u)_a/I(A_u)_b \sim \frac{2}{3}$.

On the basis of intensity, the IR bands at 809.0 and 817.0 cm^{-1} are unlikely candidates for ν_{10a}, while the much weaker bands at 856.0 and 858.0 cm^{-1} are more acceptable. Further, since ν_{10a} at the monomer level should be Raman active and IR inactive, we expect to observe its Raman active version. The Raman and IR active modes should have nearly equal frequencies, since a small dimer splitting is expected for modes not involving carboxyl group motion. The bands at 809.0 and 817.0 cm^{-1} have no obvious Raman counterparts at nearby frequencies so these bands are firmly rejected as candidates for ν_{10a}. The bands at 856.0 and 858.0, however, are fully acceptable as far as intensity and dimer splitting are concerned.

Hayashi's polarization data shows B_u slightly greater than A_u which is the reverse of what is expected for ν_{10a}. However, Zwarich's spectrum shows $A_u \geq B_u$, as required. Since his spectrum appears to have the higher signal-to-noise ratio, we are more confident of his data. Except for marginal cases Zwarich's data is in agreement with that of Hayashi.

It thus appears that ν_{10a} can be firmly assigned to the Raman pair at 854.1 and 855.8 cm^{-1} and the IR pair at 856.0 and 858.0 cm^{-1}. The pairs of bands are assumed to be factor group partners. Since the members of each pair are of comparable intensity, it is unlikely that the splitting is due to C^{13} impurity.

Mode ν_{17a}: The Varsanyi range is 940-980 cm^{-1}. The only Raman bands between 856.0 cm^{-1} and the very strong band at 1000.5 cm^{-1} are at 910.0, 938.5, 943.8, and 975.0 cm^{-1}. In the d_o IR spectrum, the only bands between 856.0 and 980.0 cm^{-1} are two very strong bands at 938.0 and 948.0 cm^{-1}. An inspection of the benzene displacement pattern for ν_{17a} shows no amplitude at the 1 and 4 positions, implying $d_o \rightarrow 4d_1$ insensitivity. For $d_o \rightarrow 4d_1$, the following shifts are observed:

Raman	IR
$d_o \rightarrow 4d_1$	$d_o \rightarrow 4d_1$
910.0 → 912.0	
939.5 → 873.6	938.0 → 878.0, 886.0
943.8 → 878.1	948.0 → 944
975.0 → 975.0 or 958.0 ?	

These shifts eliminate all bands except the weak Raman bands at 910.0 and 975.0 cm^{-1} and the very strong IR band at 948.0 cm^{-1}. Because another band shifts to 975.0 cm^{-1} in the $4d_1$ spectrum, it is not clear whether the original band is unshifted or whether it shifts to 958.0 cm^{-1}.

Since the benzene mode has no amplitude at the 1 and 4 positions, the benzene analogue is expected to involve little carboxyl group motion. Hence, it should feel C_{2v} symmetry at the monomer level, and since the dimer interaction is expected to be small for modes not involving carboxyl group motion, we expect local symmetry to prevail at the dimer level. And for the same reason we also expect the dimer splitting to be small.

In the C_{2v} point group, ν_{17a} belongs to the A_2 representation making it Raman active and IR inactive. On this basis, the very strong IR band at 948.0 cm^{-1} is eliminated as a possible candidate. Other data show that this mode corresponds to the O-H out-of-plane wag.

For $d_o \rightarrow 1d_1$ substitution, the band at 975.0 cm^{-1} undergoes no observable shift, while the band at 910.0 cm^{-1} either undergoes a large shift or else becomes too weak to be detected. On this basis, the band at 910.0 cm^{-1} is rendered an unlikely candidate for ν_{17a}. For $d_o \rightarrow d_5$

substitution, the band at 910.0 cm^{-1} shows no shift, while the band at 975.0 cm^{-1} undergoes a large shift. This suggests that the band at 910.0 cm^{-1} corresponds to a carboxyl group mode. In any case, it is rigorously eliminated as a candidate for ν_{17a}. It should be noted that this band is also outside of the Varsanyi range for ν_{17a}.

Additional support for the assignment of ν_{17a} to the band at 975.0 cm^{-1} is found in the fact that no IR counterpart of this band is observed, as expected for an A_2 monomer mode.

All of the data are fully consistent with the assignment of ν_{17a} to the Raman band at 975.0 cm^{-1}. The only questionable point concerns the behavior of this band for $d_o \rightarrow 4d_1$ substitution. Because of this uncertainty, we regard this assignment as highly probable but not firm.

Mode ν_5 : The Varsanyi range is 970-1000 cm^{-1}. The Raman bands in this range are at 975.0 (already assigned), 987.5, 989.2, 997.0,and 1000.5 cm^{-1}. The only IR band in this range is 999.5 cm^{-1}. An inspection of the benzene displacement pattern shows that this mode has equal amplitude at all positions. Hence we expect ν_5 to be $d_o \rightarrow 4d_1$ sensitive. For $d_o \rightarrow 4d_1$ substitution the following shifts are observed:

Raman	IR
$d_o \to 4d_1$	$d_o \to 4d_1$
987.5 → 972.0	
989.2 → 974.0	976.0
997.0 → ?	
1000.5 → 983.5	999.5 → 984.0

Clearly, all modes are possible candidates on the basis of these shifts.

The band at 1000.5 cm^{-1} is the strongest band in the Raman spectrum and has a depolarization ratio of 0.03. This band is definitely a totally symmetric, in-plane mode and is firmly assigned to ν_{12}, as will be shown later. Since the IR band at 999.5 undergoes a similar shift, we assume this band to correspond to the IR active version of ν_{12}. Further support for this assumption comes from the polarization data of Hayashi which is consistent with assignment of this band to ν_{12}. Thus, the only remaining candidates are the Raman bands at 989.5, 989.2, and 997.0 cm^{-1}.

To differentiate among the remaining candidates, it is necessary to consult the phosphorescence data. This data shows that the pair at 987.5 and 989.2 cm^{-1} correspond to an out-of-plane mode. Since the only range for an out-of-plane mode to which this pair can belong is that for ν_5, we firmly assign ν_5 to 987.5 and 989.2 cm^{-1}. It is interesting to note that while the d_o IR band is not observed, the $4d_1$ IR band is observed at 976.0 cm^{-1}.

We assume that the bands at 987.5 and 989.2 are factor group partners, since they are of comparable intensity.

Mode ν_{17b}: The Varsanyi range is 880-940 cm^{-1}. The Raman bands in this range which have not been assigned previously are at 939.5 and 944.0 cm^{-1}. In the IR, the only bands in this region are at 939.0 and 941.0 cm^{-1}. These bands, which are barely resolved, form a strong band that is located adjacent to the strong band at 948.0 cm^{-1}. The latter band can be firmly assigned to the O-H out-of-plane wag, as will be discussed later. The benzene displacement pattern shows that the ν_{17b} analogue mode should be $d_o \rightarrow 4d_1$ sensitive. For $d_o \rightarrow 4d_1$ substitution, the following shifts are observed:

Raman	IR
$d_o \rightarrow 4d_1$	$d_o \rightarrow 4d_1$
939.0 → 873.6	939.0 → 878.0
944.0 → 871.5	941.0 → 886.0

These shifts are consistent with the expectations for ν_{17b}. For $d_o \rightarrow 1d_1$ substitution, we observe the following shifts:

Raman	IR
$d_o \rightarrow 1d_1$	$d_o \rightarrow 1d_1$
939.5 → 938.0	939.0 → 939.0
944.0 → 943.0	941.0 → 944.0

These shifts have been presented to support the correlation of the d_o Raman bands at 939.5 and 944.0 cm^{-1} with the IR bands at 939.0 and 941.0 cm^{-1}. An inspection of the spectra shows that this correlation is not straightforward. The d_o IR bands form a single very intense band, while the $1d_1$ bands at 939.0 and 944.0 cm^{-1} are of medium intensity. This large reduction in intensity is inconsistent with a frequency shift of 1.5 cm^{-1}. In addition, the $1d_1$ spectrum shows a strong band at 923.0 cm^{-1} and a band at 951.0 cm^{-1} of medium intensity. One interpretation, which we favor, is that one or both of the bands at 923.0 and 951.0 cm^{-1} are combination bands in Fermi resonance with the bands at 939.0 and 944.0 cm^{-1}. This would account for the reduction in intensity of these last bands. Another possibility is that the bands at 939.0 and 944.0 cm^{-1} correspond to the H-wag mode for d_o - $1d_1$ mixed dimers that are present as an impurity. In our opinion, the observed intensity is too large for this interpretation to be correct, but quantitative data is not available so a firm opinion is not possible. A third possibility is that the intensity of the d_o bands at 939.0 and 941.0 is really no greater than in the $1d_1$ spectrum, with the apparent peak height being due in part to a superimposed combination band in Fermi resonance with the H-wag mode at 948.0 cm^{-1}. No doubt, other possibilities can be conceived. Because of the uncertainty about the IR bands at 939.0 and 941.0, the assignment of these bands to ν_{17b} is considered probable but not firm. However, the Raman bands at 939.5 and 944.0 cm^{-1} can be firmly assigned to ν_{17b}. Because of their comparable intensities, we assume that the members of the Raman and IR band pairs are factor group partners.

Mode $\nu_{10b}(+)$: The Varsanyi range is 140-200 cm^{-1}. This mode can be described as the ring-carboxyl group out-of-plane wag. With a heavy monoatomic substituent, the benzene mode simply drops to a low frequency; no new modes result. However, as discussed in Section IIB the replacement of the ring hydrogen by the carboxyl group leads to the formation of two ring-carboxyl group wagging modes, which can be regarded as the in-phase and out-of-phase combinations of the ring and carboxyl group motions. We denote these modes as $\nu_{10b}(+)$ (in-phase) and $\nu_{10b}(-)$ (out-of-phase). Our physical intuition suggests that $\nu_{10b}(+)$ should be lower in frequency than $\nu_{10b}(-)$. However, no firm conclusion is possible. In what follows, we arbitrarily associate $\nu_{10b}(+)$ with the Varsanyi range given for ν_{10b}. The range for $\nu_{10b}(-)$ is not known. This mode will be assigned later by elimination.

The only Raman band in the Varsanyi range is at 198.0 cm^{-1} (4.2° K). Its counterpart in the IR is at 189.0 cm^{-1} (25° K). If this mode does not involve appreciable motion of the oxygen atoms relative to the carboxyl ring as a whole, then it should feel D_{2h} symmetry. In this point group, the IR active version of the mode belongs to the B_{1u} representation which requires the transition in the free dimer to be accurately polarized along the perpendicular axis. This requires $A_u > B_u$. The polarization data of Wyncke *et al.* shows that the band at 189.0 cm^{-1} meets this requirement.

Since the ring-carboxyl group in-plane bend is expected to have a frequency similar to its out-of-plane counterpart, it is important to make certain that these bands are not confused. As will be shown later, the in-plane bend is at 293, 297 cm^{-1} in the IR spectrum. This band pair is distinguished from its out-of-plane counterpart by the polarization data of Meshitsuka *et al.*, which is consistent with a dimer mode whose transition dipole moment is parallel to the short axis of the dimer.

This assignment of $\nu_{10b}(+)$ is considered highly probable but not firm on account of the uncertainty of D_{2h} symmetry for this mode.

Mode ν_4. The Varsanyi range is 680-700 cm^{-1}. In the d_o Raman spectrum, the only band in this range is at 685.5 cm^{-1}. The only IR bands in this range are at 683.0 and 685.0 cm^{-1}. An inspection of the benzene displacement pattern shows that the analogue mode should be $d_o \rightarrow 4d_1$ sensitive. For $d_o \rightarrow 4d_1$ substitution the following shifts are observed.

Raman	IR
$d_o \rightarrow 4d_1$	$d_o \rightarrow 4d_1$
685.5 → 617.5	683.0 → 611.0
	685.0 617.0

These shifts are consistent with the expectation for ν_4. No polarization data is available for the IR bands.

Primarily on the basis of Varsanyi range and $d_o \rightarrow 4d_1$ shifts we assign ν_5 to 685.5 cm^{-1} in the Raman spectrum and to 683.0 and 685.0 cm^{-1} in the IR spectrum. The band at 683.0 cm^{-1} is sufficiently weak compared to the band at 685.0 cm^{-1}, that it is not possible to determine whether this band is a factor group partner or a C^{13} band.

Modes ν_{11} and $\nu_{10b}(-)$: The Varsanyi range for ν_{11} is 720-830 cm^{-1}. The range for $\nu_{10b}(-)$ is unknown. Not counting the O-H out-of-plane wag, the ring-carboxyl group torsion and the out-of-plane H-bond modes, these are the only two out-of-plane modes not yet assigned. Fortunately, on the basis of phosphorescence data, we know that the Raman bands at 710.0 and 812.0 cm^{-1} are out-of-plane modes. The IR counterparts of the Raman bands are at 708.0, 710.0, and 812.0 cm^{-1}. All bands show $d_o \rightarrow 4d_1$ sensitivity. Consequently, these bands cannot be distinguished on the basis of frequency shifts. To make a firm distinction between these bands, it is necessary to consider the change in intensity caused by $d_o \rightarrow 4d_1$ substitution.

An inspection of the benzene displacement pattern for ν_{11} shows that the displacement of each C-H group is in the same direction as the others. Consequently the out-of-plane components of the vibration induced dipole moments of the individual C-H groups all point in the same direction. In benzene, the sum of the in-plane components is zero by symmetry. For $d_o \rightarrow 4d_1$ substitution we expect reduced amplitude at the 4 position causing the vibration induced dipole moment associated with this position to become smaller. This should lead to a smaller total induced dipole moment, which should in turn, lead to a decrease in intensity.

For $d_o \rightarrow 4d_1$ substitution, we observe a decrease in the intensity of the IR band pair at 708.0, 710.0 cm^{-1} and an increase in the intensity of the 812.0 cm^{-1} band. On this basis we firmly assign ν_{11} to the 708.0, 710.0 cm^{-1} band pair in the IR spectrum and to the Raman band at 710.0 cm^{-1}. The IR bands are assumed to be factor group partners on the basis of their comparable intensity.

By the process of elimination, $\nu_{10b}(-)$ is assigned to the Raman and IR bands, both at 812.0 cm^{-1}.

Assignment of out-of-plane benzene analogues are listed in Table 14.

2. In-Plane Benzene Analogues

Mode ν_{12} : The Varsanyi range is 990-1010 cm^{-1}. The Raman bands in this range are at 997.0 and 1000.4 cm^{-1}. In the IR spectrum the only band in this range is at 999.5 cm^{-1}.

Varsanyi notes that normal coordinate calculations for monosubstituted benzenes show that ν_{12} has its dominant amplitudes at the 2, 4, and 6 positions, with the other positions having negligible amplitudes. This mode is always very strong in the Raman spectrum and is usually weak in the IR, for monosubstituted benzenes. Since this mode has a significant amplitude at the 4 position we expect it to be sensitive to $d_o \rightarrow 4d_1$ substitution.

For $d_o \rightarrow 4d_1$ substitution we observe the following shifts:

Raman	IR
$d_o \rightarrow 4d_1$	$d_o \rightarrow 4d_1$
997.0 → 990.0,993.0(?)	
1000.5 → 983.8	999.5 → 983.5

The bands at 999.5 and 1000.5 cm^{-1} undergo shifts which are consistent with the expectations for ν_{12}. The small shift observed for the band at 997.0 cm^{-1} makes this band an unlikely candidate for ν_{12}. Also, this band is extremely weak while ν_{12} is expected to be very strong in the Raman spectrum. We tend to regard this band as a combination band enhanced by Fermi resonance with the strong fundamental at 1000.5 cm^{-1}, although it may be a factor group partner or C^{13} band associated with this fundamental.

Since there is negligible amplitude at the 1 position we expect ν_{12} to involve little carboxyl group motion, allowing D_{2h} symmetry to prevail. In this point group, the IR active version of ν_{12} belongs to the B_{1u} representation, requiring the transition to be accurately long-axis polarized.

As shown in Section IID, a long-axis polarized transition requires $A_u >> B_u$. Hayashi's polarization data shows that the 999.5 cm^{-1} band has $A_u >> B_u$ as required. Also the small dimer splitting ($\sim 1\ \text{cm}^{-1}$) is consistent with the absence of carboxyl group motion as is the fact that the bands at 1000.5 and 999.5 cm^{-1} are insensitive to $d_o \rightarrow 1d_1$ substitution. Furthermore $d_o \rightarrow d_5$ substitution causes a 40 cm^{-1} shift in this band, indicating that it is predominantly a ring mode. We thus firmly assign ν_{12} to 1000.5 cm^{-1} in the Raman spectrum and 999.5 cm^{-1} in the IR spectrum. No factor group splitting is observed.

Mode ν_{6a}. The Varsanyi range is from 300 to 530 cm^{-1}. This range is for all monosubstituted benzenes. However, if the substituent has two atoms of atomic weight higher than 10, ν_{6a} will be found below 500. And if free rotation about the C-X bond is hindered, the range is 300-450 cm^{-1}. It is the last range that applies to benzoic acid. The Raman band at 422.0 cm^{-1} is the only band in this range that has not previously been assigned. Our IR spectrum shows no obvious counterpart to this band. However, Statz and Lippert (1967) and Meshitsuka et al. (1972) observe a band at 388.0 cm^{-1} which may be the IR counterpart of the band at 422.0 cm^{-1} despite the large frequency difference.

The displacement pattern for the benzene mode shows no amplitude for the hydrogens at the 2, 3, 5, and 6 positions, and appreciable amplitude for the hydrogen at the 4 position. Consequently, we expect ν_{6a} to be sensitive to $d_o \rightarrow 4d_1$ substitution and relatively insensitive to $4d_1 \rightarrow d_5$ substitution.

For $d_o \rightarrow 4d_1$ and $4d_1 \rightarrow d_5$ substitutions we observe:

Raman	Raman
$d_o \rightarrow 4d_1$	$4d_1 \rightarrow d_5$
422.0 → 419.4	419.4 → 414.7

As expected, the $4d_1 \rightarrow d_5$ shift is quite small. However, this is not strongly convincing because of the very small $d_o \rightarrow 4d_1$ shift. The smallness of the $d_o \rightarrow d_5$ shift suggests that this mode involves appreciable carboxyl group motion. Monomer modes which involve carboxyl group motion are expected to show larger dimer splitting because of strong coupling between the monomer modes. Thus, it is understandable that there is no observable IR counterpart in the immediate vicinity of 420 cm^{-1}. Further, it becomes more plausible, that the 388.0 cm^{-1} band is the IR counterpart of the Raman band at 422.0 cm^{-1} band. Additional evidence for this contention can be found in the data of Statz and Lippert which shows that the 388 band shifts to 380 cm^{-1} in the spectrum of the $CO^{18}O^{18}H$ isotope. This indicates that the 388 cm^{-1} band has appreciable carboxyl group motion, as required for the counterpart of the Raman band at 422.0 cm^{-1}. We therefore firmly assign the bands at 388.0 and 422.0 cm^{-1} to $\nu_{6a} + \nu_{COOH}$. ν_{COOH} will be assigned in the section on carboxyl group modes.

Mode ν_{6b}. The Varsanyi range is 605-630 cm^{-1}. The Raman bands in this range are at 610.0, 611.5, 616.0 and 617.5 cm^{-1}. In the IR spectrum the only band in this range is at 616.0 cm^{-1}. An inspection of the benzene displacement pattern shows that the benzene analogue should be $d_o \rightarrow 4d_1$ insensitive.

For $d_o \rightarrow 4d_1$ substitution we observe the following shifts:

Raman	IR
$d_o \rightarrow 4d_1$	$d_o \rightarrow 4d_1$
610.0 → 605.5	
611.5 → 607.0	
610.0 → 616.0	616.0 → ?
617.0 → 617.5	

All of these shifts are consistent with the expectation for ν_{6b}. The weak band expected to be at 616 cm^{-1} in the $4d_1$ IR spectrum is probably obscured by a very strong band that shifts into the same region.

Since this mode has no amplitude at the 1 and 4 positions, we expect it to have little amplitude at the carboxyl group atoms. Consequently, it should feel D_{2h} symmetry and exhibit small dimer splitting.

In the D_{2h} point group the Raman active version of ν_{6b} belongs to the B_{2g} representation. Since it is non-totally symmetric, it should have a large depolarization ratio (>6/7).

Baum's data shows that the band at 616.0 cm^{-1} has a depolarization ratio of .71, which is reasonable for a non-totally symmetric mode. The IR counterpart of the mode is at 616.0 cm^{-1}, which is consistent with the expectation of small dimer splitting.

The weak pair of bands at 610.0 and 611.5 are of comparable intensity. Consequently, it is likely that they are factor group partners. The same conclusion holds for the pair of bands at 616.0 and 617.5 cm^{-1}. According to Varsanyi, ν_{6b} is usually of medium intensity in the Raman spectrum. On this basis the factor group pair at 616.0 and 617.5 cm^{-1} is chosen over the pair at 610.0 and 611.5 cm^{-1} as the best candidate for ν_{6b}. All of the data are fully consistent with this assignment, which we regard as firm. The pair at 610.0 and 611.5 cm^{-1} undergoes shifts identical to those of the stronger pair for all of the isotopic substitutions considered in this study. This fact, together with the frequency difference (6 cm^{-1}) and intensity ratio (1/42) suggest that the weaker pair is a C^{13} version of the stronger pair.

Similar frequency shifts for $C^{12} \rightarrow C^{13}$ substitution are observed for benzene skeletal deformation modes. We, therefore, assign the pair of bands at 610.0 and 611.5 cm^{-1} as a C^{13} version of ν_{6b}. This assignment is considered highly probable.

Mode ν_{18a}. The Varsanyi range is 1018-1030 cm^{-1}. The Raman bands in this range are at 1019.8, 1025.8, and 1028.0 cm^{-1}. The first two bands are very weak and the third is of medium intensity. In the IR spectrum, the only band in this range is at 1028.0 cm^{-1} and is of medium intensity.

An inspection of the displacement pattern for ν_{18a} in benzene shows that this mode has no amplitude at the 1 and 4 positions. Hence we expect the analogue mode to be $d_o \rightarrow 4d_1$ insensitive and to involve little carboxyl group motion. The absence of carboxyl group motion should make the mode insensitive to $d_o \rightarrow 1d_1$ substitution and strongly sensitive to $d_o \rightarrow d_5$ substitution. It also should lead to weak coupling between monomers, causing the dimer splitting to be small. Finally, the absence of carboxyl group motion leads us to expect that the mode will feel D_{2h} symmetry. In the D_{2h} point group, the IR active dimer mode belongs to the B_{1u} representation which requires that the transition be accurately long-axis polarized. This in turn requires $A_u >> B_u$.

For $d_o \rightarrow 4d_1$, $d_o \rightarrow 1d_1$ and $d_o \rightarrow d_5$ substitutions, we observed the following shifts:

Raman	IR
$d_o \rightarrow 4d_1$	$d_o \rightarrow 4d_1$
1019.8 → 1016.3	
1025.8 → 1022.5	
1028.0 → 1025.8	1028.0 → 1028.0
$d_o \rightarrow 1d_1$	$d_o \rightarrow 1d_1$
1019.8 → 1019.8	
1016.3 → 1015.5	
1028.0 → 1028.0	1028.0 → 1028.0
$d_o \rightarrow d_5$	$d_o \rightarrow d_5$
1019.8 → 858.7	
1025.8 → 867.5	
1028.0 → 870.5	?

All of these shifts are fully consistent with the expectations for ν_{18a}. The shifts for $d_o \rightarrow d_5$ substitution are somewhat uncertain, but the data definitely shows large shifts for this substitution.

Hayashi's polarization data shows that $A_u >> B_u$ for the 1028 cm^{-1} band as required. Finally, Baum's measured depolarization ratio for the 1028.0 cm^{-1} Raman band is .01, which is consistent with a totally symmetric mode. In the D_{2h} point group (and lower symmetry groups as well), the Raman active version of ν_{18a} belongs to the A_g representation. Thus, all of the data are completely consistent with the assignment of ν_{18a} to 1028.0 cm^{-1} in the Raman spectrum and 1028.0 cm^{-1} in the IR spectrum. This is considered a firm assignment. The very weak Raman bands at 1019.8 and 1025.8 are most likely C^{13} versions of ν_{18a}. At most one of these bands may be a factor group partner of the 1028.0 band, but the very weak intensity relative to the 1028.0 band suggests that this is unlikely.

Mode ν_{18b}. The Varsanyi range is 1065 - 1082 cm^{-1}. The Raman bands in this range are at 1074.5 and 1076.5 cm^{-1}. In the IR spectrum the only bands in this range are at 1073.5 and 1075.5 cm^{-1}.

An inspection of the benzene displacement pattern, shows amplitude at all positions. Consequently the benzene analogue is expected to be $d_o \rightarrow 4d_1$ sensitive

For $d_o \rightarrow 4d_1$ substitution, the following shifts are observed:

Raman	IR
$d_o \rightarrow 4d_1$	$d_o \rightarrow 4d_1$
1974.5 → 990.0	1073.5 → (?)
1076.5 → 992.5	1075.0 → 993.0

Thus, these bands show the $d_o \rightarrow 4d_1$ sensitivity required for ν_{18b}. Since the benzene mode has amplitude at the 1 position, the benzene analogue may involve appreciable carboxyl group motion. However, the small dimer splitting ($\sim$1 cm^{-1}) suggests that such motion is not appreciable. On this basis, it seems worthwhile to consider the application of D_{2h} symmetry to this mode. In the D_{2h} point group, the IR active dimer mode belongs to the B_{2u} representation, and the transition should be polarized in-plane along the short axis, requiring $B_u >> A_u$. Hayashi's polarization data shows the bands at 1073.5 and 1075.5 cm^{-1} to have $B_u >> A_u$, as required. We therefore firmly assign ν_{18b} to 1074.5 and 1076.5 cm^{-1} in the Raman and 1073.5 and 1075.5 cm^{-1} in the IR spectrum. In the Raman spectrum, where the band pair is more clearly resolved, the members of the pair are of comparable intensity suggesting that they are factor group partners, rather than one member being due to C^{13}.

Mode ν_{15}. The Varsanyi range is 1150 - 1160 cm^{-1}. The only Raman band in this range is at 1156.8 cm^{-1}. In the IR spectrum, there are no bands in this range. Slightly outside of the Varsanyi range is a Raman band at 1170.0 cm^{-1} and an IR band at 1163.0 cm^{-1}.

An inspection of the benzene displacement pattern shows that this mode has amplitude at the 1 and 4 positions. Consequently, this mode should be $d_o \rightarrow 4d_1$ sensitive and may involve carboxyl group motion.

We observe for $d_o \rightarrow 4d_1$ substitution the following shifts:

Raman	IR
do → $4d_1$	$d_o \rightarrow 4d_1$
1156.0 → 1103(?)	
1170.0 → 1118.5	1168.5 → 1116.0

These shifts are consistent with the expectation for ν_{15}. Most likely, the IR band at 1168.5 cm^{-1} is the counterpart of the Raman band at 1170.0 cm^{-1}, rather than the band at 1156.8 cm^{-1}.

If we assume C_{2v} symmetry for the monomer, which may not be justified, ν_{15} belongs to the A_1 representation which makes the mode both Raman and IR active at the level of the monomer. If the molecule involves carboxyl group motion and therefore feels a symmetry lower than C_{2v}, there will still be no group-theoretical restrictions on IR activity. Therefore we expect ν_{15} to appear in both the Raman and IR spectra. This expectation makes the band at 1156.8 an unlikely candidate for ν_{15}. We therefore assign ν_{15} with high probability to 1170.0 cm^{-1} in the Raman spectrum and 1168.5 cm^{-1} in the IR spectrum.

This is not a firm assignment, however, because it is somewhat outside the Varsanyi range and the nature of the 1156.8 cm^{-1} band is not known. The IR band at 1168.5 cm^{-1} is not visible in Hayashi's polarized absorption spectrum. However, Zwarich's data shows that $B_u >> A_u$ for this band as required for a B_{2u} mode in the D_{2h} point group.

Mode ν_{9a}. The Varsanyi range is 1170 - 1181 cm^{-1}. The only Raman band in this range is at 1179 cm^{-1}. Slightly outside the range is a band at 1190 cm^{-1}. The only IR bands in or close to the Varsanyi range are at 1178.5, and 1189.0 cm^{-1}.

The benzene displacement pattern shows that this mode has zero amplitude at the 1 and 4 positions. Consequently, we expect the benzene analogue mode to be $d_o \rightarrow 4d_1$ insensitive and to involve little carboxyl group motion. The small carboxyl group motion leads us to expect C_{2v} symmetry at the monomer level, D_{2h} at the dimer level, and a small dimer splitting. We also expect the mode to be strongly $d_o \rightarrow d_5$ sensitive and $d_o \rightarrow 1d_1$ insensitive.

For $d_o \rightarrow 4d_1$ substitution we observe the following shifts:

Raman	IR
$d_o \rightarrow 4d_1$	$d_o \rightarrow 4d_1$
1179.0 → 1176.3	1178.5 → 1175.0
1190.0 → 1187.5	1189.0 → 1186.5

It is clear that all bands show the $d_o \rightarrow 4d_1$ insensitivity expected for ν_{9a}.

In the C_{2v} point group, ν_{9a} belongs to the A_g representation. Hence this mode should be both IR and Raman active at the monomer level. In the D_{2h} point group, the Raman active dimer mode belongs to the A_g representation and should have a small depolarization ratio. The IR active mode belongs to the B_{1u} representation requiring the transition to be accurately long-axis polarized. The depolarization ratio measured by Baum for the 1179.0 band is 0.1, as expected for ν_{9a}. In solution the 1190.0 cm^{-1} band is not observed. Hayashi's polarization data shows that the 1178.5 cm^{-1} band has A_u symmetry and the 1189.0 cm^{-1} band has B_u symmetry with $B_u > A_u$.

However, Zwarich's data has $A_u \geq B_u$ as required. As explained previously, we consider Zwarich's data more reliable.

The reasons for assuming that the bands at 1179.0 and 1190.0 cm^{-1} and those at 1178.5 and 1189.0 cm^{-1} are factor group pairs are that the 1190.0 band does not appear in solution and that no other $d_o \rightarrow 4d_1$ insensitive band is predicted to be in this region by the Varsanyi ranges. Also, the polarized IR spectrum shows that the bands at 1178.5 and 1189.0 cm^{-1} have different symmetries, which rules out Fermi resonance. Therefore, we firmly assign ν_{9a} to the Raman bands at 1179.0 and 1190.0 cm^{-1} and the IR bands at 1178.5 and 1189.0 cm^{-1}.

Modes ν_3 and ν_{14}. The Varsanyi ranges are 1270-1331 cm^{-1} and 1300-1350 cm^{-1}, respectively. Between 1260 and 1340 cm^{-1} in the Raman spectrum, there are two strong bands and two bands of medium intensity. As will be discussed later, the strong band at 1291.8 cm^{-1} is firmly assigned to a carboxyl group mode. We are thus faced with three bands and two expected fundamentals in this range. The weak band at 1317.8 cm^{-1} and the strong band at 1327.1 cm^{-1} are sharp, symmetrical bands and have every appearance of being fundamentals. The medium intensity band at 1278.3 cm^{-1} is broad and has at least two shoulders. The broadness of this band suggests that it may be a combination band. In order for a combination band to have medium intensity, it is necessary for its intensity to be enhanced by Fermi resonance. For $d_o \rightarrow 4d_1$ substitution we observe 1291.8 → 1287.5 cm^{-1} and 1278.3 → 1266.5 cm^{-1}. Thus the energy gap between the bands has increased from 13.5 cm^{-1} to 21.0 cm^{-1}. If Fermi resonance were occurring between the 1278.3 cm^{-1} band and the 1291.8 cm^{-1} band, we would expect this increase in energy gap to break or reduce the Fermi resonance interaction. We find that the 1287.5 cm^{-1} band is more intense than the 1291.8 cm^{-1} band and the 1266.5 band is much weaker than the 1278.3 cm^{-1} band. Thus the intensity changes support the assignment of the 1278.3 cm^{-1} band as a Fermi resonance enhanced combination band. In the d_o and 4 d_1 IR spectra, exactly similar phenomena are observed. In the $1d_1$ and d_5 spectra the counterparts of the 1278.3 cm^{-1} band are either very weak or missing. Finally, Hayashi's polarization data shows that both of these bands have the same polarization properties, as required for Fermi resonance. We therefore consider it highly probable that the 1278.3 cm^{-1} band is a combination band enhanced by Fermi resonance with the fundamental at 1291.8 cm^{-1}.

At this point we are left with two predicted fundamentals and two observed fundamentals. Both of these modes show amplitude at the 1 and 4 positions.

Hence we do not expect $d_o \rightarrow 4d_1$ shifts to discriminate between these modes. Hayashi's polarization data shows that the bands are oppositely polarized. This raises the question of whether these modes are factor group partners, rather than separate fundamentals.

For $d_o \rightarrow d_5$ substitution, we observe the following shifts:

Raman	IR
do → d_5	$d_o \rightarrow d_5$
1317.0 → 1298.0	1319.0 → 1300.0
1327.1 → 1333.0, 1333.9	1330.0 → 1333.5

A similar pattern is observed for $d_o \rightarrow 4d_1$ substitution. The fact that one band shifts much more than the other is incompatible with the hypothesis that these modes are factor group partners. Therefore these bands must correspond to different fundamentals.

Since the band at 1327.2 cm^{-1} involves appreciable carboxyl group motion, this mode will not feel D_{2h} symmetry. Hence the expected polarization properties cannot be determined and polarization data cannot be used to determine whether ν_3 or ν_{14} goes with one or the other band. All that can be said is that the band at 1327.1 cm^{-1} corresponds to ν_3 or ν_{14} mixed with appreciable carboxyl group mode character, and that the band at 1317.8 cm^{-1} corresponds to either ν_{14} or ν_3.

Mode ν_{19b}. The Varsanyi range is 1440-1470 cm^{-1}. The Raman bands in this range are at 1445.0, 1447.4 and 1465.7 cm^{-1}. In the IR spectrum there are bands at 1453.5 and 1466 cm^{-1}. An inspection of the benzene displacement pattern shows that this mode should have appreciable $d_o \rightarrow 4d_1$ sensitivity.

For $d_o \rightarrow 4d_1$ and $d_o \rightarrow d_5$ substitutions, we observe the following shifts:

Raman	IR
$d_o \rightarrow 4d_1$	$d_o \rightarrow 4d_1$
1445.0 → 1410.0	1453.5 → 1411.0
1447.0 → 1412.5	
1465.7 → 1461.0	1466.0 → 1462.0
$d_o \rightarrow d_5$	
1445.0 → 1371.9	
1447.0 → 1378.1	
1465.7 → 1465.7	

All bands show the expected shifts for $d_o \rightarrow 4d_1$ substitution except the band at 1465.7 cm^{-1}. The $d_o \rightarrow d_5$ shift for this band shows that it is primarily a carboxyl group mode. On this basis this band is definitely eliminated from further consideration. Consequently ν_{19b} is firmly assigned to the Raman bands at 1445.0 and 1447.4 cm^{-1} and the IR band at 1453.5 cm^{-1}. Polarization data was not considered in this assignment because the bands at 1445.0 and 1447.4 cm^{-1} show marked $d_o \rightarrow 1d_1$ sensitivity.

Mode ν_{19a}. The Varsanyi range is 1470-1515 cm^{-1}. The only IR band in this range is at 1496 cm^{-1}. The Raman bands in this range are at 1494.0 and 1496.0 cm^{-1}.

An inspection of the qualitative displacement pattern for ν_{19a} in benzene shows amplitude at the 1 and 4 positions. However, the displacement pattern calculated by Duniker and Mills (1968) shows that these are small. Hence we expect only low sensitivity to $d_o \rightarrow 4d_1$ substitution.

For $d_o \rightarrow 4d_1$ and $d_o \rightarrow 1d_1$ substitution we observe the following shifts:

Raman	IR
$d_o \rightarrow 4d_1$	$d_o \rightarrow 4d_1$
1494.0 → 1483.0	? → 1483.0
1496.0 → 1493.0	1496.0 → 1493.0
$d_o \rightarrow 1d_1$	$d_o \rightarrow 1d_1$
1494.0 → ?	
1496.0 → 1496.0	1496.0 → 1496.0

The $d_o \rightarrow 4d_1$ shifts are all consistent with the expectations for ν_{19b}. All bands are insensitive to $d_o \rightarrow 1d_1$ substitution.

The small dimer splitting and the $d_o \rightarrow 1d_1$ insensitivity suggest that D_{2h} symmetry, may be appropriate for this mode. However, for $d_o \rightarrow d_5$ substitution we observe 1496.0 $cm^{-1} \rightarrow$ 1472.0 or 1475.0 cm^{-1}. On a percentage basis, this is a small $d_o \rightarrow d_5$ shift and indicates appreciable carboxyl group motion. Consequently D_{2h} (and C_{2h}) symmetry is ruled out and the polarization data can not be reliably considered. Primarily on the basis of Varsanyi range and $d_o \rightarrow 4d_1$ shifts we firmly assign ν_{19a} to 1496.0 cm^{-1} in the IR spectrum and to 1494.0 and 1496.0 cm^{-1} in the Raman spectrum. One rather puzzling feature of this mode is the large increase in what is apparently factor group splitting for $d_o \rightarrow 4d_1$ substitution. The basis of this large increase is not understood.

Mode ν_{8a}. The Varsanyi range for this mode is 1575 - 1614 cm^{-1}. The IR bands in this range are at 1584.0 and 1601.0 cm^{-1}. In the Raman spectrum there are weak bands at 1581.5, 1586.5, 1593.0 cm^{-1} and a strong pair at 1599.7 and 1601.0 cm^{-1}.

An inspection of the displacement pattern for the benzene mode shows that the analogue mode should be $d_o \rightarrow 4d_1$ insensitive. For $d_o \rightarrow 4d_1$ substitution we observe the following shifts:

Raman	IR
$d_o \rightarrow 4d_1$	$d_o \rightarrow 4d_1$
1581.5 → 1567.0	1584.0 → 1567.0,1574.0, 1579.0
1586.5 → 1574.0	
1593.5 → 1580.0	
1599.7 → 1595.7	
1601.0 → 1597.8	1601.0 → 1597.0,1600.0

All bands are eliminated from further consideration except those at 1599.7 and 1601.0 cm^{-1}.

Since the benzene mode has no amplitude at the 1 position it is unlikely that the analogue mode involves carboxyl group motion. This contention is supported by the small dimer splitting and the insensitivity of this mode to $d_o \rightarrow 1d_1$ substitution. For $d_o \rightarrow d_5$ substitution the 1601.0 cm^{-1} band shifts at least 30 cm^{-1}, consistent with a mode that is predominantly a ring mode. On this basis we expect the dimer mode to feel D_{2h} symmetry. In the D_{2h} point group the IR active mode belongs to the B_{1u} representation and the transition has to be accurately long-axis polarized, requiring $A_u > B_u$. Hayashi's polarization data shows that the IR band at 1601.0 cm^{-1} has $A_u >> B_u$. The Raman active mode belongs to the A_g representation and should have a small depolarization ratio. Baum's measured depolarization ratio is 0.50, which is large for a totally symmetric mode but not above the theoretical limit of 6/7. Also others (Cleveland, 1945) have observed similar depolarization ratios for ν_{8a} in other monosubstituted benzenes. We therefore firmly assign ν_{8a} to 1599.7 and 1601.0 cm^{-1} in the Raman spectrum and 1601.0 cm^{-1} in the IR spectrum.

While the assignment of this mode is clear, the changes in Raman intensity upon $d_o \rightarrow 4d_1$ substitution and $d_o \rightarrow 1d_1$ substitution are among the more perplexing features of the entire spectrum. In the d_o Raman spectrum, ν_{8a} is a strong band and shows two barely resolved factor group components separated by about 1 cm^{-1}. In the $4d_1$ spectrum the intensity is markedly ($\sim$50%) reduced and the two components are now separated by about 2 cm^{-1}. This reduction in Raman intensity is surprising in view of the small amplitude expected at the 4 position for ν_{8a}. The IR band at 1601.0 cm^{-1} does not show a drastic change for $d_o \rightarrow 4d_1$ substitution. In the $4d_1$ spectrum, the band is of about the same intensity and is only somewhat broadened. We are inclined to attribute the reduced intensity of ν_{8a} in the $4d_1$ Raman spectrum to a Fermi resonance between ν_{8a} and $\nu_{6b} + \nu_{12}$. In the d_o spectrum, $\nu_{6b} + \nu_{12}$ should be located at 617.0 + 1000.5 = 1617.5 cm^{-1}. In the $4d_1$ spectrum the combination shifts to 983.8 + 613.0 =

1596.8 cm^{-1}. Clearly the condition of accidental near degeneracy is fulfilled. Also Fermi resonance is observed in benzene between $\nu_1 + \nu_6$ and ν_8 (Brodersen and Langseth, 1956). ν_1 and ν_{12} are closely related vibrations having the same symmetry. In addition all three modes are predominantly ring modes, which meets the spatial requirement for Fermi resonance discussed in Section IID2. It is therefore very likely that the band at 1595.7 cm^{-1} in the $4d_1$ spectrum is the combination band associated with $\nu_{12} + \nu_{6b}$. The intensity of this band is markedly enhanced by Fermi-resonance with the band at 1597.8 cm^{-1} (ν_{8a}) whose intensity is accordingly reduced. This Fermi resonance can not occur in the d_o spectrum since ν_{8a} = 1600.5 cm^{-1} and $\nu_{6b} + \nu_{12}$ = 1617.5 cm^{-1}, leading to a much larger energy gap. Fermi resonance between ν_{8a} and $\nu_{12} + \nu_{6b}$ is apparently weak in the IR spectrum, since the intensity of ν_{8a} is relatively unchanged by $d_o \rightarrow 4d_1$ substitution. We are unable to explain this difference between the IR and Raman spectra.

In the $1d_1$ spectrum, ν_{8a} is even weaker than in the $4d_1$ spectrum. The band appears at 1599 cm^{-1}, indicating that the intensity rather than the frequency has been changed by $1d_1$ substitution. In the $1d_1$ IR spectrum, ν_{8a} is broadened but not weakened. Thus as in the case of $d_o \rightarrow 4d_1$ substitution, the unusual behavior is confined to the Raman spectrum. As before we interpret the loss of intensity to Fermi resonance with a combination band. An inspection of the $1d_1$ Raman spectrum shows that the broad unresolved pair at 1583.5, and 1581.0 cm^{-1} is markedly enhanced in intensity. The 1583.5 cm^{-1} peak of this broad band apparently corresponds to the weak band at 1586.5 cm^{-1} in the d_o spectrum. In the d_o spectrum, the weak bands at 1586.5 and 1581.5 cm^{-1} are of comparible intensity, while in the $1d_1$ spectrum the 1581.5 cm^{-1} band appears as a weaker shoulder on the band at 1583.5 cm^{-1}. We assume that the combination band which enters into Fermi resonance with ν_{8a} is at 1586.5 cm^{-1} in the d_o spectrum and 1583.5 cm^{-1} in the $1d_1$ spectrum. Since a comprehensive study of combination bands has not been carried out, it is not possible to give a firm assignment of these combination bands.

Mode ν_{8b}. The Varsanyi range is at 1562-1597 cm^{-1}. The only IR band in this range is at 1584.0 cm^{-1}. In the Raman spectrum there are weak bands at 1557.0, 1564.0, 1573.0, 1581.5, 1586.5, and 1593.0 cm^{-1}.

The displacement pattern for ν_{8b} in benzene shows that the analogue mode should be $d_o \rightarrow 4d_1$ sensitive. The Raman band at 1557.0 cm^{-1} shifts only 1 cm^{-1} for

$d_o \rightarrow 4d_1$ substitution and is eliminated from further consideration. As indicated in the discussion for ν_{8a}, the Raman bands at 1586.5 and 1593.0 cm^{-1} are most likely combination bands. Intensity comparison suggests that the Raman band at 1581.5 cm^{-1} shifts to 1574.0 cm^{-1} upon $d_o \rightarrow 4d_1$ substitution. The IR band at 1584.0 cm^{-1} also probably shifts to 1574.0 cm^{-1}. It is accompanied by two side bands at 1567.0 and 1579.0 cm^{-1}, which are probably combination bands enhanced by Fermi resonance with the stronger band at 1574.0 cm^{-1}. It is not possible to determine the $d_o \rightarrow 4d_1$ shifts of the d_o Raman bands at 1564.0 and 1573.0 cm^{-1}. Probably these bands are burried under the new stronger bands that appear at 1577.0 and 1574.0 cm^{-1} in the $4d_1$ spectrum.

Although ν_{8b} in benzene has amplitude at the 1 position, insensitivity to $d_o \rightarrow 1d_1$ substitution, small dimer splitting (seen clearly in the $4d_1$ spectra) as well as a large sensitivity to $d_o \rightarrow d_5$ substitution suggest that D_{2h} symmetry may be appropriate for this mode. In the D_{2h} point group, ν_{8b} belongs to the B_{2u} representation, making the transition short-axis polarized which, in turn, requires $B_u > A_u$. Hayashi's polarization data shows that the band at 1584.0 cm^{-1} has $B_u > A_u$, as required for ν_{8b}.

We thus firmly assign ν_{8b} to the IR band at 1584.0 cm^{-1} and tentatively to the Raman band at 1581.5 cm^{-1}. The Raman assignment is not firm because of the confusion created by the nearby combination bands.

Mode $\nu_{9b}(+)$. The Varsanyi range is 200-410 cm^{-1}. According to Varsanyi, in monosubstituted benzenes, this mode becomes the ring-carboxyl group in-plane bend. As discussed in Section IIB, there are in-phase and out-of-phase combinations of this mode. Our physical intuition suggests that the in-phase combination will have the lower frequency. However, no definite statement can be made. In what follows, we arbitrarily assume that the Varsanyi range for "ν_{10b}" applies to $\nu_{10b}^{(+)}$.

The only Raman bands in this range not previously assigned are at 261.5 and 263.0 cm^{-1}. In the IR spectrum, the only bands in this range are at 293.0 and 297.0 cm^{-1}.

Since this mode must involve carboxyl group motion, the application of D_{2h} or even C_{2h} symmetry may be unjustified. Realizing that it may be weak evidence, we nonetheless consider the application of D_{2h} symmetry. In the D_{2h} point group, the IR active mode belongs to the B_{2u} representation making the transition short-axis polarized. This in turn requires $B_u > A_u$. The polarization data of Meshitsuka et al (1972) shows that the bands at 293.0 and 297.0 cm^{-1} have $B_u > A_u$, while the band at 388 cm^{-1} has $A_u > B_u$.

For $d_o \rightarrow 1d_1$, $d_o \rightarrow 4d_1$ and $d_o \rightarrow d_5$ substitutions we observe the following shifts:

Raman	IR
$d_o \rightarrow 1d_1$	$d_o \rightarrow 1d_1$
261.5 → 253.0	293.0 → 287.0
263.0 → 260.0	297.0 → 292.0
$d_o \rightarrow 4d_1$	$d_o \rightarrow 4d_1$
261.5 → 260.0	293.0 → 291.0
263.0 → 262.0	297.0 → 295.0
$d_o \rightarrow d_5$	$d_o \rightarrow d_5$
261.5 → 255.0	293.0 → 281.0
263.0 → 256.0	297.0 → 285.5

These shifts are consistent for a mode which involves both ring and carboxyl group motion.

The dimer splitting of about 30 cm^{-1} is consistent with a mode involving appreciable carboxyl group motion. On the basis of the Varsanyi range we assign ν_{9b} (+) to 261.5 and 263.0 cm^{-1} in the Raman spectrum and 293.0 and 297.0 cm^{-1} in the IR spectrum. This assignment is considered highly probable rather than firm on account of the uncertainty of using D_{2h} symmetry to interpret the polarization data.

Mode ν_{13}. The Varsanyi range is 1100-1280 cm^{-1}. According to Varsanyi, in monosubstituted benzenes with light substituents, this mode becomes the C-X stretching mode. Since this mode has a very large range, we have waited until all other modes expected in this range have been assigned. Except for extremely weak bands, the only remaining Raman band in this range is at 1134.0 cm^{-1}. In the IR spectrum, the only remaining bands are at 1130.0 and 1102.0 cm^{-1}. The latter band, which is weak in the IR spectrum, apparently corresponds to an extremely weak Raman band at 1102.0 cm^{-1}.

The displacement pattern for ν_{13} in benzene shows amplitude at the 1 and 4 positions. However, normal coordinate calculations by Whiffen (1956) for monosubstituted benzenes show that the 2,4 and 6 positions have small amplitude and the other positions large amplitude. This behavior of ν_{13} upon monosubstitution parallels the behavior of ν_1. In monosubstitution benzenes, ν_1 has large amplitudes at the 1, 3 and 5 positions and negligible amplitudes at the other positions. ν_1 is strongly substituent sensitive and insensitive to $d_o \rightarrow 4d_1$ substitution. Accordingly, we expect ν_{13} to behave similarly for these substitutions. Indeed, the large Varsanyi range for ν_{13} indicates its strong substituent sensitivity.

For $d_o \rightarrow 4d_1$, $d_o \rightarrow 1d_1$ and $d_o \rightarrow d_5$ substitution we observe the following shifts:

Raman	IR
$d_o \rightarrow 4d_1$	$d_o \rightarrow 4d_1$
1134.0 → 1136.5	1130.0 → 1132.0
1103.0 → 1103.0	1102.0 → 1102.0
$d_o \rightarrow 1d_1$	$d_o \rightarrow 1d_1$
1134.0 → 1134.0	1130.0 → 1128.0
1103.0 → ?	1102.0 → 1103.0
$d_o \rightarrow d_5$	$d_o \rightarrow d_5$
1134.0 → 1093.0	1030.0 → 1089.0
1103.0 → ?	1103.0 → ?

The $d_o \rightarrow 4d_1$ shifts are all consistent with the expectations for ν_{13}. According to Varsanyi, ν_{13} is insensitive to $d_o \rightarrow 1d_1$ substitution. The observed shifts are also consistent with this expectation. The large shifts for $d_o \rightarrow d_5$ substitution show that these bands do not correspond to pure carboxyl group modes, as required. Also the 41 cm^{-1} shift observed for the band at 1134.0 cm^{-1} is almost identical to the shift observed for ν_{12} for $d_o \rightarrow d_5$ substitution.

The C-X stretching mode is likely to involve internal motion of the substituent group X. Consequently, one cannot reliably assume that this mode will feel

D_{2h} or even C_{2h} symmetry. It is therefore not possible to use polarization data to support the assignment of ν_{13}. However, the polarization data is useful in another connection. Hayashi's polarized IR spectrum shows that the bands at 1102.0 and 1130.0 cm^{-1} have the same polarization properties. This implies that these bands cannot be factor group partners.

According to Varsanyi, ν_{13} is usually strong in both the IR and Raman spectra of monosubstituted benzenes. On this basis the bands at 1134.0 and 1130.0 cm^{-1} are clearly selected as the best candidates for ν_{13}. (The Raman band at 1134.0 cm^{-1} is more than fifty times as intense as the band at 1130 cm^{-1}). Thus, on the basis of intensity and Varsanyi range we firmly assign ν_{13} to 1134.0 cm^{-1} in the Raman spectrum and 1130.0 cm^{-1} in the IR spectrum. No factor group splitting is observed. The weak bands at 1102.0 and 1130.0 cm^{-1} are most likely combination bands, since no other fundamentals are expected in this range.

Modes ν_1 and $\nu_{9b}(-)$. The Varsanyi range for ν_1 is 620-830 cm^{-1}. The range for $\nu_{9b}(-)$ is unknown. The only unassigned Raman bands in the range for ν_1 are a very strong band at 797.4 cm^{-1}, a weak band at 817.0 cm^{-1}, and very weak bands at 658.0 and 659.5 cm^{-1}. The only IR bands in the range for ν_1 are at

670.0, 672.0, 795.5, 809.0 and 817.0 cm^{-1}.

Varsanyi notes that normal coordinate calculations for monosubstituted benzenes show that ν_1 has large amplitudes at the 1, 3, and 5 positions and negligible amplitudes at the other positions. We therefore expect this mode to be $d_o \rightarrow 4d_1$ insensitive and strongly substituent sensitive. The substituent sensitivity is also indicated by the rather large range for this mode. According to Varsanyi, ν_1 is usually strong in the Raman spectra of monosubstituted benzenes.

For $d_o \rightarrow 4d_1$ substitution, we observe the following shifts:

Raman	IR
$d_o \rightarrow 4d_1$	$d_o \rightarrow 4d_1$
797.4 → 796.3	797.5 → 796.5
658.0 → 655.5	670.0 → 666.0
659.5 → 657.0	672.0 → 668.0
817.0 → ?	809.0 → 804.0
	817.0 → 814.0

The Raman band at 817.0 cm^{-1} is eliminated from further consideration as a candidate for ν_1. This band evidently does not correspond to the IR band at 817.0 cm^{-1} which does not shift for $d_o \rightarrow 4d_1$ substitution. The Raman bands at 658.5 and 659.5 cm^{-1} correspond to the IR bands at 670.0 and 672.0 cm^{-1} as indicated by their similar shifts. This is a large dimer splitting and indicates appreciable carboxyl group motion. The nature of the IR band at 817.0 cm^{-1} is not known, but Zwarich's polarization data shows that it has the same polarization properties as the band at 809.0 cm^{-1}. Therefore, these bands are not factor group partners. Most likely these bands are combination bands. Zwarich's data shows that these bands cannot be in Fermi resonance with the out-of-plane mode at 812.0 cm^{-1} ($\nu_{10b}(-)$) since the latter band has opposite polarization properties. Also the band at 812.0 cm^{-1} shifts to 784.0 cm^{-1} for $d_o \rightarrow 4d_1$ substitution, while the bands at 809.0 and 817.0 cm^{-1} are essentially unshifted ($\sim$5 cm^{-1}) and unchanged in intensity. The most compelling reason for assuming that these bands correspond to combination modes is the fact that all fundamental expected in this region are best accounted for with other bands. The Raman band at 817.0 cm^{-1} is also not understood. As noted previously it is not a counterpart of either of the bands at 809.0 and 817.0 cm^{-1} since it disappears upon $d_o \rightarrow 4d_1$ substitution. For the same reason it is also unlikely that it is a factor group partner of either the band at 812.0 cm^{-1} or the band at 797.4 cm^{-1}. Most likely it is a combination band in Fermi resonance with one of these bands. These assignments of combination bands must be regarded as tentative until a comprehensive study of combination bands is carried out.

The Raman band at 797.1 cm^{-1} is about 40 times as intense as the bands at 658.0 and 659.5 cm^{-1}. Since ν_1 should be a strong Raman band according to Varsanyi, it is clear that the best choice for ν_1 is the Raman band at 797.4 cm^{-1} and its IR counterpart at 797.5 cm^{-1}. All observed shifts for isotopic substitutions are consistent with this assignment. In addition the measured depolarization ratio for the 797.5 cm^{-1} band is .02, a low value as expected for ν_1.

By elimination, $\nu_{9b}(-)$ is assigned to the Raman bands at 658.0 and 659.5 cm^{-1} and the IR bands at 672.0 and 679.0 cm^{-1}. Since $\nu_{9b}(-)$ is expected to involve both ring and carboxyl group motion we expect it to be sensitive to $d_o \rightarrow d_5$ substitution and to show a large dimer splitting. For $d_o \rightarrow d_5$ substitution, we observe the following shifts:

Raman	IR
$d_o \rightarrow d_5$	$d_o \rightarrow d_5$
658.0 → 642.5	670.0 → 648.0
659.5 → 644.0	672.0 → 650.0

These shifts and the observed dimer splitting are fully consistent with the expectations for $\nu_{9b}(-)$.

It should be noted that while the range for $\nu_{9b}(-)$ is unknown, it is not expected to have a high frequency. Consequently, we assume that it cannot be confused with the carboxyl group modes expected to lie in the

1300-1700 cm^{-1} range. On the other hand it could be confused with the 0-C=0 scissor mode which is expected to have a lower frequency. As we will show later, this mode is assigned to 557.0 cm^{-1} in the IR spectrum and 504.0 cm^{-1} in the Raman spectrum. $\nu_{9b}(-)$ was not assigned to these bands because they are insensitive to $d_o \rightarrow 4d_1$ substitution.

We regard the assignments for ν_1 and $\nu_{9b}(-)$ as firm since all the data are consistent with these assignments.

At this point, the only in-plane benzene analogues which have not been assigned are the C-H stretching modes, which are expected to be in the vicinity of 3000 cm^{-1}. Since the O-H stretching mode also occurs in this region, it is appropriate to consider the assignment of this mode with those of the C-H stretching modes.

An inspection of the Varsanyi ranges (Table 5) for the C-H stretching modes shows that all ranges overlap except those for ν_2 and ν_{20b} and those for ν_{7a} and ν_{20a}. The displacement patterns for benzene show that modes ν_{7b} and ν_{20b} have zero amplitude at the 1 and 4 positions. Normal coordinate calculations for monosubstituted benzenes by Baily <u>et al</u>. (1946) show that ν_{20a} also has no amplitude at the 1 and 4 positions.

On this basis, we expect to observe three modes that are $d_o \rightarrow 4d_1$ insensitive.

The C-H stretching modes are much higher in frequency than all of the carboxyl group modes except the O-H stretching mode. Consequently, we expect that this mode is the only carboxyl group mode that will be mixed with the C-H stretching modes. Unless a C-H stretching mode is sensitive to $d_o \rightarrow 1d_1$ substitution, we conclude that it involves no significant carboxyl group motion.

The d_o Raman spectrum at 4.2° K shows six bands whose sharpness and intensity suggest that they are fundamentals. The d_o IR spectrum in this region shows a broad, relatively structureless conglomeration of bands in the region of 3000 cm^{-1}. Four individual bands can be discerned. The Raman and IR bands together with their $d_o \rightarrow 4d_1$ shifts are given below.

Raman	IR
$d_o \rightarrow 4d_1$	$d_o \rightarrow 4d_1$
3072.0 → 3071.0	3072.0 → 3071.5
3066.0 → 3065.5	3067.0 (?) → 3063.0(?)
3060.5 → 2972.0	3061.0 → ?
3058.0 → 3057.5	3058.0 → 3058.0
3008.0 → 2260.0	
2983.0 → 2293.5	

The bands at 3072.0, 3066.0 and 3058.0 cm^{-1} are clearly candidates for ν_{7b}, ν_{20b}, and ν_{20a}.

For $d_o \rightarrow 1d_1$ substitution, the only Raman band affected is at 3060.5 cm^{-1}. In the $1d_1$ spectrum, this band cannot be identified. The IR band at 3061.0 cm^{-1} behaves in a similar fashion.

At this point it is necessary to decide which bands correspond to the C-H stretching modes. Candidates for ν_{7b} , ν_{20b} , and ν_{10a} have already been specified. For ν_2 and ν_{7a}, there are three choices in the Raman spectrum: 3060.5, 3008.0 and 2983.0 cm^{-1}. For $d_o \rightarrow 4d_1$ substitution the last two bands shift more than 700 cm^{-1}. These shifts are reasonable for modes having large amplitude at the 4 position. They are unreasonable for a combination band. A combination band would involve two or three fundamentals located below 1700 cm^{-1}. These fundamentals never shift more than 50 cm^{-1} for $d_o \rightarrow 4d_1$ substitution. Therefore we would expect a combination band in the vicinity of 3000 cm^{-1} to shift less than 150 cm^{-1} for $d_o \rightarrow 4d_1$ substitution. Thus the bands at 2983.0 and 3008.0 cm^{-1} must be fundamentals. On the otherhand, the band at 3060.5 cm^{-1} shifts 88.5 cm^{-1} for $d_o \rightarrow 4d_1$ substitution, which is reasonable for a combination band. We therefore conclude that the only candidates for ν_2 and ν_{7a} are the bands at 2983.0 and 3008.0 cm^{-1}.

To proceed further, we have to consult Zwarich's polarized IR spectrum taken at room temperature. This spectrum shows little structure in the 3000 cm^{-1} region. However, a band at 3073.0 cm^{-1} can be discerned. This band has $B_u >> A_u$. Assuming D_{2h} symmetry, the IR active versions of ν_{20b} and ν_{7b} should belong to the B_{2u} representation, which requires $B_u >> A_u$ as observed. At this point we are left with the following possible assignments.

Raman	IR	Assignment
3072.0	3072.0	ν_{20b} or ν_{7b}
3066.0	3067.0	ν_{20a} ,ν_{20b} , or ν_{7b}
3058.0	3058.0	ν_{20a} , ν_{20b}, or ν_{7b}
3008.0		ν_2 or ν_{7a}
2983.5		ν_2 or ν_{7a}

It is not possible to specify the assignments more completely on the basis of the available data. The Varsanyi ranges are of little aid because most ranges overlap considerably. For example, the band at 3072.0 cm^{-1} is in the ranges for both ν_{20b} and ν_{7b}. Mode ν_{20a} should be between 3070 and 3110 cm^{-1} according to

Varsanyi. Our data show that ν_{20a} is either at 3066.0 or 3058.0 cm^{-1}. This discrepancy is not significant since it is unreasonable to expect the boundaries of the Varsanyi ranges to be accurate to a few tenths of a percent. All of the Raman bands which are insensitive to $d_o \rightarrow 4d_1$ substitution are in the range for ν_{7b}, so no discrimination can be made for this mode. The band at 2983.0 cm^{-1} is somewhat below the ranges for ν_{7a} and ν_2. However, this is not surprising since these modes are expected to be substituent sensitive. A more complete assignment of the C-H stretching modes must await further experimental study.

The IR active version of the dimer O-H stretching mode has been shown by a number of workers to correspond to the strong broad band that extends from 2500 cm^{-1} to 3000 cm^{-1}. Davies and Sutherland (1938) have convincingly argued that this band consists of the O-H stretching fundamental and numerous combination bands in Fermi resonance with the fundamental. The basis of this interpretation is the observation that the monomer O-H stretching mode is a relatively sharp band. Davis and Sutherland further suggest that the combination bands in Fermi resonance with the O-H stretching fundamental involve the H-bond modes. In their view, the absence of these modes in the monomer, accounts for the sharpness of the monomer band.

Most previous studies of the O-H stretching mode have considered the spectra of benzoic acid in solution. The solution spectra show four prominent bands for benzoic acid d_o. The $1d_1$ spectrum shows only two prominent bands. In the d_o crystal spectrum at room temperature, four broad bands can also be discerned. However, in the crystal spectrum, these bands are much less resolved. At 4.2^o K the d_o crystal spectrum shows about ten bands between 2500 and 3000 cm^{-1}. The $1d_1$ spectrum at 4.2^o K shows two strong bands at 2050.0 and 2200.0 cm^{-1}, each band having several weak shoulders. Weaker bands between 2500 and 3000 cm^{-1} are probably associated with d_o impurity. The d_o Raman spectrum at 4.2^o K shows two weak bands at 2601.5 and 2636.0 cm^{-1}. In the d_5 spectrum, bands of similar intensity are found at 2601.5 and 2632.0 cm^{-1}. This insensitivity to $d_o \rightarrow d_5$ substitution is consistent with these bands being associated with pure carboxyl group modes. For $d_o \rightarrow 1d_1$ substitution these bands apparently shift to 2040.0 and 2197.0 cm^{-1}. These frequencies are almost identical to the $1d_1$ IR frequencies. It therefore appears that the Raman bands at 2601.5 and 2636.0 cm^{-1} are associated with the O-H stretching mode. It remains to be determined whether these bands are factor group partners or whether one is a combination band in Fermi resonance with the fundamental. Since the $1d_1$ crystal and solution IR spectra both show two bands, the possibility of the bands being factor group partners is ruled out, And since the $1d_1$ Raman bands are clearly the counterparts of the $1d_1$ IR bands, the same conclusion holds for the $1d_1$ Raman bands. We assume that this conclusion can be extended to the pair of bands in the d_o spectrum. The possibility that one of the bands at 2601.5 and 2636.0 cm^{-1} is a combination band is supported by the shifts observed for $d_o \rightarrow 4d_1$ substitution. The band at 2601.5 cm^{-1} shifts to 2612.5 cm^{-1} and becomes weaker. The band at 2636.0 cm^{-1} also becomes weaker and probably shifts to 2630.0 cm^{-1} (very broad). We interpret these shifts and intensity changes to the presence of a new Fermi resonance involving a combination band at 2579.0 cm^{-1}. We assume that this band enters into Fermi resonance with the band at 2612.5 cm^{-1}. This Fermi resonance most likely competes with the Fermi resonance between the combination band at 2630.0 cm^{-1} and the band at 2612.5 cm^{-1}, which we assume to be the O-H stretching fundamental. The red shift of the 2636.0 cm^{-1} d_o band upon $d_o \rightarrow 4d_1$

substitution is consistent with a weakening of the Fermi resonance between this band and the band at 2601.5 cm^{-1}. On the other hand, the blue shift of the 2601.5 cm^{-1} band upon $d_o \rightarrow 4d_1$ substitution is consistent with the appearance of the Fermi resonance between this band and the band at 2579.0 cm^{-1}. This interpretation must be considered tentative until a comprehensive analysis of combination bands is carried out.

To summarize, we assign the O-H stretching mode to 2601.5 cm^{-1} in the Raman spectrum and to the cluster of bands between 2500 and 3000 cm^{-1} in the IR spectrum. It is interesting to note the small dimer splitting observed for the O-H stretching mode in the $1d_1$ IR and Raman spectra. Other carboxyl group modes show much larger dimer splittings. We are unable to offer an explanation of this small dimer splitting. Assignments given in this section are listed in Table 15.

3. Midrange Carboxyl Group Modes

At this point the only midrange modes which have not yet been assigned are those associated with the carboxyl group. These modes are the O-C=0 "scissor" the out-of-plane H-wag, the O-H in-plane bend, the C-O stretching mode, and the C=0 stretching mode. The only other carboxyl group modes are the O-H stretching mode, assigned in the previous section, and the H-bond modes, which are located below 200 cm^{-1}.

Hadzi and Sheppard (1953) have studied the IR spectra of a number of carboxylic acids and have established ranges for three of the carboxyl group modes. By the nature of their sorting procedure, only modes which are sensitive to $d_o \rightarrow 1d_1$ substitution have been specified. Fortunately, one of the molecules they studied was benzoic acid. According to their room temperature IR data, the following frequencies correspond to carboxyl group modes:

d_o	$1d_1$
1420	1367
1287	1042
935	648

In our IR spectra, taken close to 4.2 °K, the frequencies of these carboxyl group modes are as follows:

d_o	$1d_1$
1425.0,1433.0	1365.0
1298.0	1048.0
948.0	657.0

Some of these frequency shifts have been interpreted by Hayashi to be due to the presence of two configurations of benzoic acid in the crystal, the relative populations of which are temperature dependent. This has been discussed in detail in Section IID 3.

In the Raman spectrum, the counterpart of the bands at 1425.0 and 1433.0 cm^{-1} (one is probably a combination band) is at 1465.7 cm^{-1}. The large dimer splitting is consistent with a carboxyl group mode. The Raman counterpart of the 1298.0 cm^{-1} band is at 1292.0 cm^{-1} and that of the 948.0 cm^{-1} band is at 910.0 cm^{-1}.

According to Hadzi and Sheppard, the bands at (1425.0 or 1433.0) and 1298.0 cm^{-1} must both be assigned to mixtures of the C-O stretching and O-H bending modes. The reason for this is that both modes show marked $d_o \rightarrow ld_1$ sensitivity.

The band at 948.0 cm^{-1} is assigned by Hadzi and Sheppard to the out-of-plane H-wag mode. However, these authors do not supply compelling evidence that this mode is not the O-H in-plane bend. One argument that this mode is not the O-H in-plane bend can be based on the fact that the bands 1298.0 cm^{-1} and 1425.0 or 1433.5 cm^{-1} correspond to mixed modes. Because of the marked $d_o \rightarrow ld_1$ sensitivity one component of the mixture must be either the O-H in-plane bend or the O-H out-of-plane wag. Since the other component is the C-O stretch, an in-plane mode, only the O-H in-plane bend could be involved in the mixing. Here we are assuming that the molecule has a plane of symmetry.

Since the carboxyl group modes may experience C_i symmetry, which does not distinguish between in-plane and out-of-plane modes, this argument is not convincing. Compelling evidence that the bands at 948.0 cm^{-1} (IR) and 910.0 cm^{-1} (R) correspond to an out-of-plane mode is furnished by the phosphorescence data which shows that the band at 910.0 cm^{-1} corresponds to an out-of-plane mode. An this basis we firmly assign the out-of-plane H-wag to 910.0 cm^{-1} in the Raman spectrum and its IR counterpart at 948.0 cm^{-1}.

According to Hadzi and Sheppard, the O-C=0 scissor mode is a lower frequency mode usually found below 700 cm^{-1} and is more substituent sensitive than the other carboxyl group modes. They note that this band is relatively insensitive to $d_o \rightarrow 1d_1$ substitution. These contentions are apparently based upon physical intuition. Clearly, the possibility that a carboxyl group mode such as the C-0 stretching mode might lie in the region below 700 cm^{-1} must be eliminated. Unfortunately, we have been unable to find any argument more compelling than "physical intuition" to support the contention that the scissor mode occurs below 700 cm^{-1}. However, we have found an IR band at 557.0 cm^{-1} which shifts to 540.0 or 537.0 cm^{-1} upon $d_o \rightarrow d_5$ substitution. Its Raman counterpart is at 504.0 cm^{-1} and shifts to 496.0 cm^{-1}. In the room temperature spectrum, the IR band has the characteristic appearance of a carboxyl group mode. However, a shift of 17 cm^{-1} is somewhat large for a pure carboxyl group mode in this frequency range. As noted previously, ν_{6a} at 422.0 cm^{-1} (R) and 388.0 cm^{-1} (IR) is mixed with a carboxyl group mode. Since it should be mixed with a nearby mode of appropriate symmetry, it appears likely that ν_{6a} is mixed with the scissor mode. In this case, the IR band at 557.0 cm^{-1} and the Raman band at 504.0 cm^{-1} would correspond to a mode which consists of the scissor mode mixed with a small amount of ν_{6a} character. In this way, the $d_o \rightarrow d_5$ sensitivity of those bands would be explained. Thus, in agreement with the expectations of Hadzi and Sheppard, we assign the scissor mode to the bands at 504.0 cm^{-1} (R) and 557.0 cm^{-1} (IR). This assignment is not firm since there is no rigorous basis by which the scissor mode can be distinguished from other carboxyl group modes. There is also the uncertainty concerning the mixing of the scissor mode with ν_{6a}.

The only remaining midrange carboxyl group mode is the C=0 stretching mode. This mode is well known to be located in the vicinity of 1700 cm^{-1}. Hayashi has shown that at temperatures close to 4.2^{o} K (i.e. when only one configuration is present in the crystal) the $C = 0$ stretching mode is located at 1710.0 cm^{-1}.

Our Raman spectrum shows two strong, so far unassigned bands at 1615.0 and 1631.0 cm^{-1}. Both bands are of comparable intensity. These bands are likely the Raman counterpart of the IR band at 1710.0 cm^{-1}. The large dimer splitting is consistent with the large coupling expected for carboxyl group modes. One possibility is that the two Raman bands are factor group partners. Another is that the band pair is the result of inversion doubling. A third possibility is that one of the bands is a combination band enhanced by Fermi resonance with the other band which would be the funadmental associated with the C=0 stretch.

For $d_o \rightarrow 4d_1$ substitution, we observe only one band at 1627.0 cm^{-1}, which is distinctly more intense than either of the bands in the d_o spectrum. The disappearance of one of the bands for $d_o \rightarrow 4d_1$ substitution rigorously rules out the possibility of inversion doubling since this substitution should have no effect whatever on inversion doubling. Further, it is hard to imagine how $d_o \rightarrow 4d_1$ substitution could have any effect, let alone a drastic effect on the factor group splitting associated with a carboxyl group mode. Therefore the only possibility remaining is that one of the bands is a combination band enhanced by Fermi resonance. For $d_o \rightarrow 1d_1$ substitution, we also observe only one strong band at 1612.8 cm^{-1} and for $d_o \rightarrow d_5$ substitution, we observe two bands at

1625.0 and 1617.0 cm^{-1}. The 1617.0 cm^{-1} band has about one third the area of the 1625.0 cm^{-1} band.. Both bands have the same peak height.

As noted in Section IID a combination band must have amplitude in the same region of the molecule as the fundamental. Thus we would expect that the combination band that enters into Fermi resonance with the C=0 stretching mode must be a combination of two carboxyl group modes or perhaps a carboxyl group mode and a ring mode.

Since a complete study of combination bands has not been carried out, it is not possible at this time to make an assignment of the combination band that interacts with the C=0 stretching fundamental. Nonetheless, we regard it as highly probable that 1631.0 cm^{-1} corresponds to the C=0 stretching fundamental and 1615.0 cm^{-1} is a combination band. The 1631.0 band is chosen as the fundamental since the $4d_1$ frequency is 1627.0 cm^{-1}. If Fermi resonance were not present in the d_o spectrum, we would expect the d_o and $4d_1$ spectra to have the same C=0 stretching frequency. The only reason this assignment is not regarded as firm is that the combination band has not been assigned.

Assignments for midrange carboxyl group mode are listed in Table 16.

TABLE 14

This table contains assignments for out-of-plane benzene analogues. In those cases where two Raman or two IR frequencies are listed for a single mode, the two frequencies are believed to correspond to factor group partners. Only assignments for benzoic acid d_o and $4d_1$ are given. Question marks indicate uncertainties that are discussed in the text. "N.O." is an abbreviation for "not observed". Frequencies are given in wavenumbers.

Mode	R(d_o)	IR(d_o)	R($4d_1$)	IR($4d_1$)
$\nu_{10b}^{(+)}$	198.0	189.0	192.2	N.O.
ν_{16a}	407.5	N.O.	407.5	N.O.
ν_{16b}	438.0	433.0	424.5	N.O.
ν_4	685.5	683.0, 685.0	617.5	611.0, 617.0
ν_{11}	710.0	708.0 710.0	698.0	692.5 696.0,
$\nu_{10b}^{(-)}$	812.0	812.0	786.7	783.5
ν_{10a}	854.1, 855.8	856.0 858.0	851.8, 854.0	853.0, 856.0
ν_{17b}	939.5, 944.0	930.0, 941.0	871.0, 873.6	878.0, 886.0
ν_{17a}	975.0	N.O.	975.0(?)	N.O.
ν_5	987.5, 989.2	N.O.	972.0, 974.0	976.0

TABLE 15

This table contains assignments for in-plane benzene analogues and the O-H stretching mode. In those cases where two Raman or the IR Frequencies are listed for a single mode, the two frequencies are believed to correspond to factor group partners. Only assignments for benzoic acid d_0 and $4d_1$ are given. Question marks indicate uncertainties that are discussed in the text. "N.O." is an abbreviation for "Not Observed". Frequencies are given in wavenumbers.

Mode	$R(d_o)$	$IR(d_o)$	$R(4d_1)$	$IR(4d_1)$
$\nu_{9b}(+)$	261.5, 263.0	293.0, 299.0	260.0 262.0	291.0, 295.0
ν_{6a}	422.0	388.0	419.4	N.O.
ν_{6b}	616.0 617.5	616.0	616.0 617.5	N.O.
$\nu_{9b}(-)$	658.0 659.0	670.0 672.0	656.0 657.0	668.0, 667.0
ν_1	797.4	797.5	796.3	796.5
ν_{12}	1000.5	999.5	983.8	983.5
ν_{18a}	1028.0	1028.0	1025.8	1028.0
ν_{18b}	1074.5, 1076.5	1073.5, 1075.5	990.0, 992.5	993.0
ν_{13}	1134.0	1130.0	1136.5	1132.0
ν_{15}	1170.0	1168.5	1118.5	1116.0
ν_{9a}	1179.0, 1190.0	1178.5, 1189.0	1176.3, 1187.5	1175.0, 1186.5
ν_3 or ν_{14}	1317.0	1319.0	1306.0	1306.0
ν_{14} or ν_3	1327.1	1330.0	1324.5	1329.0
ν_{19b}	1445.0, 1447.4	1453.5 1453.5	1410.0 1412.5	1411.0
ν_{19a}	1494.0 1496.0	1396.0	1483.0 1492.0	1483.0 1493.0

Table 15 (Continued)

Mode	$R(d_o)$	$IR(d_o)$	$R(4d_1)$	$IR(4d_1)$
ν_{8a}	1599.7, 1601.0	1601.0,	1595.7, 1597.8	1597.0, 1600.0
ν_{8b}	1581.5	1584.0	1574.0	1574.0
O-H stretch	2601.5	2500-3000	2612.5	2500-3000
ν_2 or ν_{7a} (?)	2983.0	N.O.	2260.0	N.O.
ν_2 or ν_{7a} (?)	3008.0	N.O.	2293.0	N.O.
ν_{20a}, ν_{20b}, or ν_{7b} (?)	3058.0	3058.0	3057.5	3058.0
ν_{20a}, ν_{20b}, or ν_{7b} (?)	3066.0	3067.0(?)	3065.5	3063.0(?)
ν_{20b} or ν_{7b}	3072.0	3072.0	3071.0	3071.5

TABLE 16

This table contains assignments for midrange carboxyl group modes. The $4d_1$ assignments included in this table have not been discussed in the text. However, their determination is straightforward. Frequencies are given in wavenumbers.

Mode	$R(d_o)$	$IR(d_o)$	$R(4d_1)$	$IR(4d_1)$
out-of-plane H-wag	910.0	948.0	911.5	944.0
O-C=0 scissor	504.0	557.0	504.5	553.5
C-0 stretch + 0-H bend	1292.0	1298.0	1288.0	1293.0
O-H bend + C-0 stretch	1465.7	1425.0 or 1433.0	1461.5	1433.5
C=O stretch	1631.0	1710.0	1627.0	1710.0

4. Low Frequency Modes

In this section we present assignments of modes located below 200 cm^{-1}. The modes in this region are the lattice modes and H-bond modes. Qualitative displacement patterns for the H-bond modes are shown in Figure 2 (boxed area).

Before considering the spectra obtained in this study, it is appropriate to examine the results of previous investigations. Far infrared spectra of benzoic acid have been obtained by a number of workers. Room temperature solution spectra have been reported by Statz and Lippert (1968) and Meshitsuka et al. (1972). These spectra show almost no structure below 200 cm^{-1}. The earliest crystal spectrum (unpolarized) was obtained by Genzel and Weber (1959). This spectrum, which was actually analyzed and published by Maier and Schifferdecker (1962) shows very poor resolution, most likely as a result of instrumentation problems. A more recent spectrum by Delorme (1964) shows even less structure. In this case, the sample consisted of benzoic acid powder dispersed in polyethylene. High quality unpolarized spectra of benzoic acid (crystal or powder?) were obtained by Stanevich in 1964. In his spectrum, the instrumental resolution exceeded the inherent resolution of the bands.

In 1968 Wyncke *et al.* obtained the polarized far infrared spectra of single, oriented crystals at 25° K (see Figure 21). The spectra were presented in terms of absorbance rather than % transmission, and the instrument resolution was indicated in each region of the spectrum. From an experimental point of view, this study is the best that has been published so far. More recently, polarized far infrared spectra have been obtained by Meshitsuka *et al.* (1972) at room temperature (see Figure 22). These spectra are presented in terms of percent transmission. Instrumental resolution was not specified, but in view of the broadness of the observed bands, it was poor.

Wyncke and coworkers observed three weak, sharp bands at 25, 36, and 41 cm^{-1} (25° K). The polarization properties of these bands indicated that the corresponding modes belong to the A_u, B_u, and A_u representation, respectively. The remaining bands below 180 cm^{-1} are broader and can very plausibly be grouped together as factor group pairs. On this basis, Wyncke *et al.* concluded that the broad bands were associated with H-bond modes and the low frequency modes were lattice modes. Group theory predicts three IR active lattice modes (see Section IID4). Because they believed that there should be 1 A_u and 2 B_u lattice modes, Wyncke and coworkers concluded that the band at 25 cm^{-1} was due to an impurity and that the missing B_u mode was located in the extreme infrared, outside of the region covered by their spectrometer. However, in reality group theory predicts 1 B_u and 2 A_u lattice modes (Darydow 1962, page 15 and Section IID4 of this thesis). Thus, there is no conflict between theory and experiment.

In the study by Meshitsuka et al., great effort was made to verify the orientation of the crystal, using x-ray diffraction techniques. These authors were led to make this careful determination because they regarded their polarized spectra to be in better agreement with the spectra obtained by Wyncke et al. (Fig.23) if the a and b axes specified by the latter authors were interchanged. In our opinion, there are significant differences between the spectra regardless of how the a and b axes are assigned. First of all, the sharp, weak bands at 21, 29, and 36 cm^{-1} which appear in Wyncke's spectra are missing in the spectra obtained by Meshitsuka. The most likely explanation for this is that the spectral band width of Meshitsuka's instrument was much larger than the 0.5 cm^{-1} bandwidth of the instrument used by Wyncke. Consistent with this is the fact that all bands in Meshitsuka's spectra are broader and less resolved than the corresponding bands in Wyncke's spectra. Also the relative intensities are reversed in some cases. For example, the broad band at 106 cm^{-1} in Wyncke's spectrum is less intense (according to peak height) than the sharp bands at 66 and 82 cm^{-1}. In Meshitsuka's spectrum the sharp bands appear weaker than the broad band. This is what is expected when the instrumental band width is made larger than the intrinsic width of the sharp bands but not larger than the width of the broad band which is about 20 cm^{-1} wide. Too large an instrumental bandwidth is especially a problem when obtaining spectra with polarized light, because overlapping or adjacent bands having different polarization properties are observed simultaneously. This causes erroneous polarization ratios, false peak locations, and incorrect relative intensities. We regard it as very likely that poor resolution is the cause of the differences between the spectra obtained by Wyncke and Meshitsuka. We therefore conclude that Meshitsuka's data presents no hard evidence that the a and b axes were misassigned in Wyncke's study. Moreover, Meshitsuka's data contains good, if not firm, evidence that the a and b axes are assigned in the same way in both studies. Wyncke's spectra at 25° K shows that the band at 189.0 cm^{-1} is a single band and is at least 40 cm^{-1} away from any other band. Since there are no overlapping or nearby bands, the only effect of too large a spectral band width is to broaden and reduce the peak height of the band. This occurs to an equal extent for both orientations of the polarized light. Wyncke's data shows that the 189.0 cm^{-1} band is strongest when the E vector of the light wave is parallel to the b axis. In Meshitsuka's spectrum, a broad but definite "bump" in the region of 190 cm^{-1} appears when $\vec{E}\parallel\vec{b}$. When $\vec{E}\parallel\vec{a}$ the base line is flat. Thus, the spectra of Meshitsuka and Wyncke are qualitatively in agreement as far as the isolated band at 189.0 cm^{-1} is concerned. This is good evidence that the a and b axes were assigned identically in both studies. The spectra obtained by Wyncke and coworkers seem to constitute a nearly definitive study of the far infrared absorption spectrum. of benzoic acid d_o.

The first Raman spectrum for the region below 200 cm^{-1} was obtained by Maier and Schifferdecker in 1962. Polarized light and oriented single crystals were used for benzoic acid d_o. Unpolarized spectra were obtained for benzoic acid $1d_1$. The spectra were well-resolved and eight bands were observed, the number predicted by group theory being twelve.

The most recent Raman study of the region below 200 cm^{-1} was carried out by Colombo and Furic in 1971. These authors used a laser source which allows polarized Raman spectra to be obtained with enormously greater ease than with conventional light sources. All bands predicted by group theory were thought to be observed, and the temperature dependence of the bands over the range from 200 to 350^{o} K was used to separate lattice modes from dimer modes. The basic idea of the temperature dependence approach for sorting lattice and H-bond modes is that the force constants which determine the frequencies of the lattice modes depend upon the distances between the atoms of one dimer and those of the other dimer in the unit cell. Since the size of the unit cell changes with temperature, the force constants for the lattice modes change accordingly. On the otherhand force constants associated with covalent bonds are expected to be much less temperature dependent. For the H-bond modes, the force constants are much weaker than those associated with covalent bonds and a clear separation between the temperature dependence of the H-bond modes and the lattice modes is not expected. However, it was Colombo and Furics supposition that some difference should be apparent in the responses of the two types of modes to temperature changes.

As noted by Meshitsuka _et al._, the assignments of Columbo and Furic are unconvincing. These authors also report that Colombo and Furic have subsequently revised their assignments on the basis of a normal coordinate calculation. Rather than speculate on the possible reasons why the temperature dependence approach may be unreliable for benzoic acid, we will later present evidence for a sorting of lattice and H-bond modes that is different from the sorting presented by Colombo and Furic.

Figure 2 presents qualitative displacement patterns for carboxylic acid dimers as given by Statz and Lippert (1968). In these displacement patterns, the substituent group is represented as a point mass. Since the benzene ring in benzoic acid is not a point mass, a new mode arises, which is called the ring-carboxyl group torsion. Qualitative displacements for this mode and the H-bond torsion are shown in Figure 25.

It is interesting to note that neither Colombo and Furic nor Meshitsuka _et al._ have considered the monomer torsion. Since this mode should be in the same region as the H-bond modes, this neglect is unpermissible. Further, since the monomer torsion and H-bond torsion have the same symmetry and may have similar frequencies one must consider the possibility that these modes are mixed.

FIGURE 25

Monomer Torsion Mode

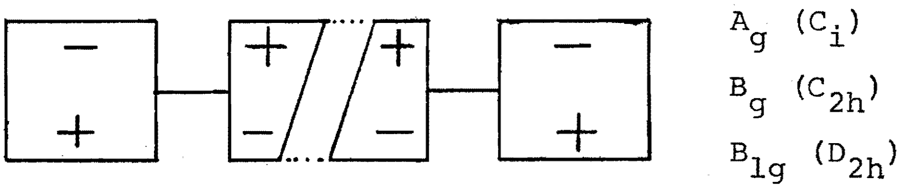

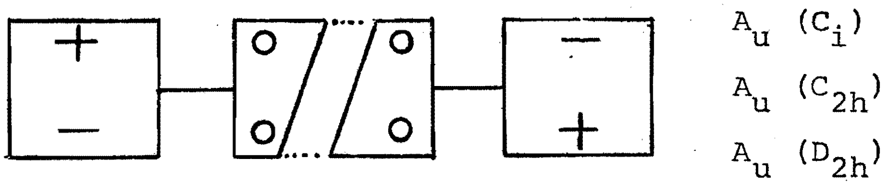

H-Bond Torsion Mode

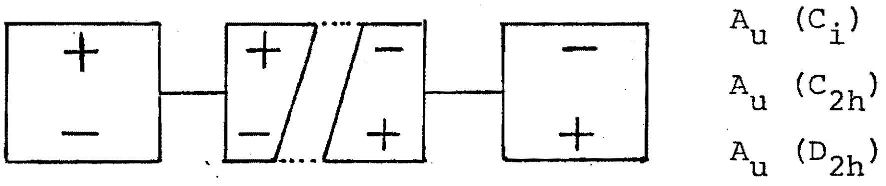

Schematic displacements for H-bond and monomer torsion modes.

As shown in Figure 2 Statz and Lippert give the representations of the modes for the C_{2h} and D_{2h} point groups. The H-bond torsion (boxed area) is shown to belong to the B_{1u} representation of the D_{2h} point point group. This is an error. In order for a mode to belong to any D_{2h} representation, the O-H and H-bond lengthsmust be equal and the protons must have zero amplitude. Inspection shows that the H-bond torsion actually belongs to the A_u representation. Modes belonging to this representation are optically inactive. The spectrum of Wyncke et al. shows four factor group pairs. This is exactly what is expected if the monomer torsion and all of the ungerade H-bond modes are active. Since none of the observed factor group pairs is especially weak compared to the others it follows that D_{2h} symmetry is not appropriate for the H-bond modes. This is not surprising in view of the non-planarity of the carboxyl group and the unequal C-O bond lengths, particularly if the true difference in bond lengths is much greater than the measured difference as suggested by Hayashi and Kimura.

At this point it is appropriate to consider the Raman spectra obtained in this study. For the time being, we restrict our attention to the spectra obtained at 4.2° K. In Section III we will discuss the spectra obtained at higher temperatures. Initially, it was our hope that a comparison of the d_o, $1d_1$, $4d_1$, and d_5 spectra would yield considerable insight into the low frequency modes. This expectation was not realized because the observed shifts for isotopic substitutions proved to be small compared to the bandwidths of the low frequency modes. Also the interpretation of the shifts is complicated by factor group splitting. Increasing the mass or moment of inertia of the molecule not only reduces the frequency of a mode at the dimer level, but also reduces the amplitude of vibration. A reduction in amplitude can affect the magnitude of the factor group splitting which will also lead to a frequency shift.

An inspection of the d_o spectrum shows four sharp (1.5 cm^{-1} FWHM) bands at 33.6, 50.9, 55.1, and 60.0 cm^{-1}. Another sharp band appears at 119.5 cm^{-1}. The four remaining bands are somewhat broader (2.2 cm^{-1}). As will be discussed in Section II I, the linewidths of the sharp bands are less temperature dependent than those of the broad bands.

If the lattice modes are not mixed with the H-bond modes or the monomer torsion, then the dimers will move as rigid bodies when vibrating in a lattice mode. Consequently, we would expect no observable change in a pure lattice mode for $d_o \rightarrow 1d_1$ substitution. This substitution should only cause a very small change in the moments of inertia of the dimer.

Table 17 shows the frequency shifts, linewidth changes, and intensity changes for $d_o \rightarrow 1d_1$ substitution. It is shown that $d_o \rightarrow 1d_1$ substitution increases the linewidths of all bands by about 50%. This suggests that the lattice and H-bond modes are mixed together. The only bands which show experimentally significant frequency shifts for $d_o \rightarrow 1d_1$ substitution are those at 88.0 and 124.7 cm^{-1}. We regard this as good evidence that these bands correspond to modes that are predominantly H-bond modes. Both have linewidths of about 2.2 cm^{-1}.

On the basis of linewidth, the low frequency bands can be divided into two groups. One group consists of 4 or possibly 5 bands having a linewidth slightly greater than 2 cm^{-1}. The other group consists of bands having linewidths less than 1.5 cm^{-1}. Since two of the broad bands appear to correspond to modes that are predominantly H-bond modes, we regard it reasonable to assume that all of the broad bands correspond to modes that are predominantly H-bond modes and that the sharp bands correspond to modes that are basically lattice modes or else the monomer torsion. In other words, we associate broadness with modes that involve

TABLE 17

This table contains frequencies, bandwidths, and peak heights of bands below 150 cm^{-1} in the Raman spectra of benzoic acid d_o and ld_1 at 4.2° K. Question marks refer to bands not completely resolved.

d_o			ld_1		
$\nu(cm^{-1})$	$\Delta\nu(cm^{-1})$	Peak Heights	$\nu(cm^{-1})$	$\Delta\nu(cm^{-1})$	Peak Height
33.6	1.0	27.0	33.8	1.5	36.0
50.9	1.3	20.5	51.0	2.1	23.0
55.1	1.3	21.0	55.2	2.1	24.0
60.0	1.0	2.5	60.0	1.5	2.5
88.0	2.2	91	87.2	3.2	67.0
97.4	2.2(?)	74	97.4	?	73.0
99.3	(?)	47.5(?)	99.5	?	53.0(?)
119.5	1.2	28	119.3	1.5	35.0
124.7	2.2	69	125.4	3	75.0
132.8	2.2	43	132.5	2.9	49.0

a stretching of the H-bond In making this correlation we are assuming that the mixing of H-bond and lattice modes is small.

One of the sharp bands (119.5 cm^{-1}) is well separated from the remainder which are below 60 cm^{-1}. We regard the band at 119.5 cm^{-1} as the best candidate for the monomer torsion. In benzaldehyde this mode occurs at about 111 cm^{-1}. It seems quite unlikely that the benzoic acid monomer mode could have a frequency one-half of this value. The monomer torsion in the dimer is expected to have a frequency very close to the monomer value since the equivalent force constant and reduced moment of inertia for the dimer are both twice the monomer values. It therefore appears that the 119.5 cm^{-1} band is the most likely candidate for the monomer torsion.

The remaining sharp bands at 60 cm^{-1} and below are thus assigned to the lattice modes. Group theory predicts six Raman lattice modes. However, only four bands are observed, Given six observed bands there are 6! = 720 ways the assignments can be made. We now consider the shifts in the bands due to $d_o \rightarrow 4d_1$ substitution:

d_o			$4d_1$		
ν	$\Delta\nu$	Peak Height	ν	$\Delta\nu$	Peak Height
33.6	1.0	27.0	33.2	1.2	25.0
50.9	1.3	20.5	50.5	1.2	20.5
55.1	1.3	21.0	54.3	1.2	23.0
60.0	1.0	2.5	59.5	1.2	2.5

The apparent frequency shifts in all of the bands except the 55.1 band are due to an error in setting the zero position of the Raman wavenumber scale to the laser line. When the d_o and $4d_1$ spectra are superimposed, all bands coincide exactly except the 55.1 cm^{-1} band, which shows a shift of about 0.4 cm^{-1}. In the Raman spectrum, only rotational lattice modes are active so we need to be concerned solely with changes in the moments of inertia that are caused by $d_o \rightarrow 4d_1$ substitution. The moment of inertia about the long axis of the molecule should be unaffected by $d_o \rightarrow 4d_1$ substitution. The other two moments of inertia should however be affected. We can therefore firmly say that the 55.1 cm^{-1} band cannot correspond to the lattice mode that involves rotation about the long axis. This reduces the number of possible sets of assignments from 720 to 480 if we assume that 55.1 cm^{-1} corresponds to a single band rather than a superimposed pair of bands. For a superimposed pair, the number of possible sets is reduced to 288. Since it is reasonable to expect both members of a factor group pair to respond similarly to an isotopic substitution, we regard it likely that the 55.1 cm^{-1} band consists of a superimposed pair of factor group partners, since no other lattice mode shows a measurable shift upon $d_o \rightarrow 4d_1$ substitution. Here, as elsewhere, we assume that all resolved lattice modes are sufficiently intense to be observed. We emphasize that the S/N ratio in our spectra was large enough to detect bands an order of magnitude weaker than the weak band at 60 cm^{-1}. Because the coupling between dimers is weak we do not expect factor group partners to differ greatly in intensity. In other words we expect weak coupling to permit the degree of local allowness to determine the intensity of both factor group components of a unit cell mode.

The forces that oppose the rotation of a given dimer in the crystal about one of its axes are generated by the interaction of the dimer with the other molecules in the crystal. The magnitude of these interactions is reflected in the frequency of rotation about the axis in question. The sum of the interactions between the dimer and its unit cell partner should be less than the sum of the interactions between the dimer and all of the other molecules in the crystal. On this basis we expect the magnitude of the factor group splitting to be significantly less than the zero order frequency of the lattice mode in question.

consider it unlikely that either of the bands at 51.0 and 60.0 cm^{-1} is a factor group partner of the band at 33.6 cm^{-1}. In this case the 33.6 cm^{-1} band would consist of two factor group partners superimposed. By elimination, the bands at 51.0 and 60.0 cm^{-1} are thus required to be factor group partners.

We regard it plausible to assume that the restoring force generated by a small angular displacement about the short axis of the dimer would be nearly equal to the restoring force generated by an angular displacement of the same magnitude about the axis perpendicular to the plane of the dimer. Since the moments of inertia about these axes are nearly the same, it follows that the rotational lattice modes associated with these axes should be close together in frequency. No prediction can be made about the relative frequency of the other lattice mode. Since the average frequencies of the factor group pairs at (55.2, 55.2 cm^{-1}) and (51.0, 60.0 cm^{-1} are almost equal and are well separated from the pair at (33.6, 33.6 cm^{-1}), we assign the pair at (33.6, 33.6 cm^{-1}) to the R_z (long axis) lattice mode and the other pairs to the R_x and R_y lattice modes. Since it is not possible to specify the R_x and R_y modes exactly, we are left with two possible sets of assignments for the lattice modes. Our data does not allow any further discrimination of the Raman lattice modes.

The remaining five bands must be assigned to H-bond modes. Six bands are predicted by group theory. Consequently, we must determine which of the observed Raman bands consists of an unresolved factor-group pair. For $d_o \rightarrow d_5$ substitution we observe that the d_o bands at 97.5 and 99.0 cm^{-1} are greatly reduced (70%) in the d_5 spectrum. This suggests that both of these bands are closely related and may thus be a factor group pair. Since the band at 88.0 cm^{-1} is well-separated from the bands at 124.7 and 132.7 cm^{-1}, we regard this band as the most likely choice for the band that consists of an unresolved factor group pair. By elimination, the bands at 124.7 and 132.7 cm^{-1} are assigned as a factor group pair. For $d_o \rightarrow d_5$ substitution, the band at 88.0 cm^{-1} shifts to 86.6 cm^{-1} and a weak shoulder appears at 81.0 cm^{-1}. A similar shoulder appears in the $1d_1$ Raman spectrum. These facts give good support to the assumption that the d_o band at 88.0 cm^{-1} is a composite band. Having grouped the observed bands into factor group pairs, the number of possible assignments is now 3. The data does not allow further specification.

At this point it is appropriate to return to the infrared spectrum. As noted by Wyncke et al., the infrared bands between 70 and 130 cm^{-1} can plausibly be grouped into factor group pairs as follows:

(71.0, 79.0; $B_u >> A_u$), (94.0, 101.0; $A_u > B_u$), (109.0, 111.0; $A_u > B_u$), and (125.0, 126.5; $A_u > B_u$). In this region, we expect the H-bond in-plane bend, the H-bond torsion, the monomer torsion, and the H-bond out-of-plane bend. If we assume C_{2h} symmetry, the transition for the first mode should be accurately short-axis polarized. The transition moments of the other modes should be polarized perpendicular to the molecular plane. These free-dimer polarizations require $B_u >> A_u$ for the first mode and $A_u > B_u$ for the remainder, which is precisely what the spectrum shows. Unfortunately, no other, independent data is available to support the appropriateness of C_{2h} symmetry. Although emphasizing the uncertainty of C_{2h} symmetry, we will proceed with the remainder of the assignments under the assumption that C_{2h} symmetry prevails at the dimer level.

To proceed further, it is necessary to resort to physical intuition. We regard it as likely that the force constant for the monomer torsion will be larger than the effective force constant for the H-bond torsion. A straight-forward calculation of the reduced moments of inertia for these modes shows that the reduced moment of inertia for the H-bond torsion is the larger of the two. Thus, on the basis of force constant and moment of inertia considerations, we conclude that the H-bond torsion should be lower in frequency than the monomer torsion.

An inspection of the dimer splittings for the higher frequency modes of benzoic acid shows that sometimes the gerade mode has the higher frequency and sometimes the reverse occurs. We therefore are unable to predict whether the gerade version of the monomer torsion will be higher or lower in frequency than the ungerade mode. If the ungerade frequency is lower than the gerade frequency, then only one set of IR assignments is possible:

In-plane Bend	(71.0, 79.0)	$B_u >> A_u$
H-bond torsion	(94.0, 101.0)	$A_u > B_u$
Monomer Torsion	(109.0, 111.0)	$A_u > B_u$
Out-of-Plane Bend	(125.0, 126.5)	$A_u > B_u$

If the ungerade frequency is higher than the gerade frequency, then two sets of IR assignments are possible:

In-Plane Bend (71.0,79.0)	In-Plane Bend (71.0,79.0)
H-bond torsion (94.0,101.0)	Out-of-Plane Bend (94.0,101.0)
Out-of-Plane bend (109.0,111.0)	H-bond torsion (109.0,111.0)
Monomer torsion (125.0,126.5)	Monomer torsion (125.0,126.5)

The IR active lattice modes are at 25.0, 36.0, and 41.0 cm^{-1}. T_z (long axis) corresponds to 26.0 cm^{-1}. T_x and T_y, which cannot be distinguished experimentally, correspond to 25.0 and 41.0 cm^{-1}.

At this point we are left with 6 possible sets of assignments of IR bands below 180 cm^{-1}. A more complete specification of the assignments must await further experimental study.

I. Temperature Dependent Aspects of the Spectra

We now consider the temperature dependent aspects of the Raman spectra obtained in this study. Figure 24 shows selected regions of the Raman spectra of benzoic acid d_o at 298° K, 77° K, and 4.2° K. A number of phenomena require explanation. The low frequency H-bond modes are broad (5-10 cm^{-1}) at room temperature and become much sharper (2 cm^{-1}) at 4.2° K. Mid-frequency modes involving carboxyl group motion show a similar behavior. On the other hand pure ring modes are relatively sharp (2-3 cm^{-1}) at room temperature and are only somewhat sharper (1-1.5 cm^{-1}) at 4.2° K. Lattice modes have linewidths of about 4 cm^{-1} at room temperature and about 1.5 - 2 cm^{-1} at 4.2° K. It is interesting to note that lattice modes resemble ring modes rather than H-bond modes.

At room temperature kT is about 200 cm^{-1}. This means that many transitions occur from molecules that are in an excited vibrational state. At 4.2° K, kT is about 3 cm^{-1}. Since the lowest frequency mode in benzoic acid has a frequency of about 30 cm^{-1}, the number of molecules in an excited vibrational state at this temperature is negligible (e^{-10}).

Let us write a schematic vibrational wavefunction for benzoic acid as follows:

$$\chi(q_R, q_C, q_L, q_{HB1}, q_{HB2}) =$$

$$\chi^i(q_R)\chi^j(q_C)\chi^k(q_L)\chi^l(q_{HB1})\chi^m(q_{HB2}) \;,$$

where q_R refers to a ring mode, q_C to a carboxyl group mode, q_L to a lattice mode, q_{HB1} to an H-bond mode and q_{HB2} to a different H-bond mode. The superscripts represent vibrational quantum numbers. In writing the total vibrational wavefunction as a product of wavefunctions, each involving only one normal corrdinate, we have in effect assumed that the harmonic oscillator approximation holds exactly. An important consequence of the harmonic oscillator approximation is that a transition associated with one normal coordinate is independent of the vibrational quantum numbers associated with the other normal coordinates. For example the transition $\chi(00000) \rightarrow \chi(00001)$ should have the same energy and probability as $\chi(00030) \rightarrow \chi(00031)$. On the otherhand, if the harmonic oscillator approximation does not hold exactly, the vibrational wavefunctions can be written as linear combinations of the zero-order harmonic wavefunctions. Once mixing occurs, it is no longer necessary that the above transitions have the same energy. In order words, the transition energy and probability associated with one approximate normal coordinate may depend on the vibrational quantum numbers of the other approximate normal coordinates.

Since anharmonicity increases with the amplitude of vibration, we expect it to increase with vibrational quantum number. At room temperature, kT is such that significant thermal population of levels having vibrational quantum numbers greater than 1 is possible only for modes whose fundamentals are less than about 200 cm^{-1}. Since there are twenty-three observed fundamentals in benzoic acid below 200 cm^{-1}, a large variety of vibrational excited states will be populated at room temperature. These excited states will involve primarily excitations of lattice and H-bond modes. The introduction of anharmonicity leads to the possibility that molecules in different initial vibrational excited states will have different energies for the $0 \rightarrow 1$ transition of a given mode. Thus, anharmonicity could be a source of the increase in linewidth that occurs when the temperature is raised from 4.2° K to 298° K.

There is also another type of broadening that arises as a result of anharmonicity. For exact harmonic wavefunctions, transitions of the form $\chi(00000) \longrightarrow \chi(00001)$ should be isoenergetic with sequences of the form $\chi(0\ 0\ 0\ 0\ n) \rightarrow \chi(0\ 0\ 0\ 0\ n{+}1)$. However, anharmonicity introduces unequal spacing and sequence bands will not necessarily be isoenergetic. Clearly, sequence broadening could be an important source of the room temperature linewidths of low frequency modes.

A third type of broadening may arise as a result of the uncertainty principle. At room temperature, a large fraction of the transitions are occurring from excited vibrational states, which arise as a result of thermal population. It is conceivable that these excited states could have lifetimes sufficiently short to account for at least part of the observed line widths on the basis of the uncertainty principle [$\Delta E(\mathrm{cm}^{-1}) \cdot \Delta t(\mathrm{seconds}) \geq 2.7 \times 10^{-12}$ sec cm^{-1}].

For completeness, we include the possibility of Doppler broadening, which is normally encountered in the spectra of molecules in the gaseous state. In a crystal, Doppler broadening arises as a result of the translational lattice modes, and would increase with the vibrational quantum numbers of the lattice modes.

Fortunately, the data allow a discrimination among the possible sources of linewidth. If uncertainty broadening were the main source of the increase in linewidth that occurs when the temperature is increased from 4.2° K to 298° K, all types of modes would be affected equally. This is not observed. As discussed previously, pure ring modes and carboxyl group modes have different linewidths and are affected to different degrees by changes in temperature. Consequently, we conclude that uncertainty broadening is not a dominant source of the increase in linewidth that results when the temperature is raised. By a similar argument Doppler broadening can also be eliminated.

Sequence broadening can only account for the increase in linewidth of the low frequency modes, since the higher frequency modes are not significantly populated at room temperature. In particular, the increase in linewidth of the carboxyl group modes cannot be the result of sequence broadening.

Thus, for the carboxyl group modes, we are left with anharmonicity broadening as a possible source of the increase in linewidth that occurs when the temperature is raised from 4.2° K to 298° K. This type of broadening arises from a mixing of zero-order harmonic wavefunctions. The perturbation, H', responsible for the mixing is the sum of the third and higher order terms in the Taylor series expansion of the potential energy function. Using our schematic vibrational wavefunction for benzoic acid we can write the types of matrix elements that will lead to mixing as follows:

$\langle \chi^{i}(q_R) | H' | \chi^{j}(q_C) \rangle$, $\langle C | H' | HB \rangle$, $\langle HB | H' | L \rangle$,

$\langle R | H' | HB \rangle$, $\langle R | H' | L \rangle$, and $\langle C | H' | L \rangle$. Overlap considerations favor $\langle C | H' | HB \rangle$ matrix elements and disfavor all others except $\langle HB | H' | L \rangle$, for which no qualitative prediction can be made since the degree of mixing of these modes at the zero-order level is not known. These overlap considerations are consistent with the data, which shows that the carboxyl group modes and H-bond modes have comparable linewidths and exhibit a similar temperature dependence. The data also shows that the lattice and pure ring modes are sharper and exhibit a smaller temperature dependence. On this basis, we suggest that anharmonicity broadening is the main source of the increase in linewidth of the carboxyl group modes as the temperature is raised from 4.2° K to 298° K. In the case of the H-bond modes, sequence broadening may also play a role. We are unable to specify the source of the increase in linewidths of the ring and lattice modes. Also, we have not attempted to account for the intrinsic linewidth observed at 4.2° K.

In this discussion we have restricted our attention to the Raman spectra. The same general conclusions should hold for the IR spectra. However, we have not considered these spectra since they show an asymmetric broadening that is a artifact caused by the use of KBr pellets. Also combination bands enhanced by Fermi resonance appear more frequently in the IR spectra. Consequently, the widths of strong IR bands are apparently increased by the presence of shoulders corresponding to combination bands in Fermi resonance with the fundamental. The presence of this type of broadening makes it difficult to assess the roles of anharmonicity broadening and other sources of linewidth.

The most striking temperature dependence of the low frequency Raman spectrum is associated with the band at 69.5 cm^{-1} (298° K) (see Figure 24). At room temperature, this band is a single strong band that is symmetric in shape. As the temperature is lowered, it splits into two bands, both of which increase in frequency. At 77° K, one band is at 80.0 cm^{-1} and the other at 86.5 cm^{-1}. At this temperature, the band at 86.5 cm^{-1} is the stronger. At higher temperatures, the intensity ratio is reversed. When the temperature is lowered to 4.2° K, the lower frequency band disappears and the second becomes the most intense band below 200 cm^{-1}. Its frequency at this temperature is 88.0 cm^{-1}. These phenomena are identical to those observed by Hayashi and coworkers for midfrequency carboxyl group modes. As discussed in Section IIC and IID3 these authors have proposed that two configurations of benzoic acid dimer (see Figure 6) exist in the crystal and that the relative populations of these configurations are temperature dependent. A competing interpretation is that the phenomena are the result of Fermi resonance between combination bands and fundamentals. In benzoic acid there are seven bands below 70 cm^{-1}. An inspection of the possible combination frequencies shows that the observed phenomena might be rationalized in terms of Fermi resonances. Thus our data does not allow a discrimination between Hayashi's hypothesis and the interpretation based on Fermi resonance.

It is interesting to consider whether the Raman active carboxyl group modes show the same temperature dependence observed by Hayashi and coworkers for their IR active counterparts. In this connection, it should be realized that the behavior of the IR active C=0 stretching mode offers the clearest evidence for Hayashi's two configuration model. The other midrange carboxyl group modes offer less conclusive evidence.

An inspection of the Raman spectra taken at 4.2° K, 77° K, and 298° K shows that only the mixed O-H bending, C-O stretching modes show a temperature dependence similar to their IR active counterparts. Most notably, the temperature dependence of the C=O stretching fundamental does not resemble that of its IR active counterpart. The out-of-plane H-wag mode is apparently too weak and broad to be observed in the Raman spectra at 77° K and above, so this mode cannot be compared with its IR counterpart. The mixed O-H bending, C-O stretching modes at 1323.0 and 1298.0 cm^{-1} (298° K) exhibit a temperature dependence that is in reasonable agreement with their IR counterparts. However, only the band at 1323.0 cm^{-1} shows the splitting and intensity changes that support Hayashi's two configuration model. Thus, the only Raman bands which show a temperature dependence that supports Hayashi's model are at 1323.0 cm^{-1} and 69.5 cm^{-1}.

It is clear that the Raman data obtained in this study does not offer the evidence necessary for a conclusive test of Hayashi's model. In our opinion, the most conclusive way to test this model would be to carry out an x-ray study of the benzoic acid crystal at 4.2° K.

J. Recommendations for Future Studies

The most important goal of a future study of the infrared and Raman spectra of benzoic acid should be the attainment of polarized spectra using oriented crystals at 4.2° K. This study has demonstrated that a dramatic clarification of the spectra results when the sample is cooled to 4.2° K. Additional clarification should result from the use of polarized light and single crystals at this temperature.

In addition to the isotopes employed in this study, we recommend the use of benzoic acid 1,4d_2. This isotope, which is easy to synthesize, should be useful in clarifying the assignments of ν_{17a} and ν_{17b} Benzoic acid d_6 should be useful in tracking the shifts that result from $d_0 \rightarrow d_5$ substitution. Isotopic substitutions in the carboxyl group should also be useful.

In this study, a number of bands have been tentatively assigned as combination bands enhanced by Fermi resonance. These assignments could be made firm by a comprehensive analysis of combination bands using isotope shifts and polarization data. In our opinion this goal should have a high priority in a future study.

Of special importance is the exact structure of the benzoic acid crystal at temperatures close to 4.2° K. Since cryostats are now available that can maintain a sample at temperatures as low as 7° K for long periods of time using only small quantities of helium gas, high resolution x-ray studies are economically feasible. A knowledge of the crystal structure at low temperatures would provide a rigorous test of Hayashi's hypothesis that two configurations of benzoic acid dimer exist in the crystal. It would also yield accurate direction cosines, which are needed to calculate polarization ratios for spectra obtained at low temperatures. Further, a measurement of the non-planarity of the carboxyl group would be of great value in interpreting the phosphorescence spectra (see Section III E).

The only published IR spectrum of benzoic acid vapor (Hadzi and Pintar 1958) was apparently obtained with a low resolution spectrometer. It would be desirable to obtain high resolution IR and Raman spectra of benzoic acid vapor, particularly in the region below 200 cm^{-1}.

In this study we have proposed that the increase in linewidth that is observed when the temperature is raised from 4.2° K to room temperature is due to an increase in the number of molecules in vibrational excited states. This hypothesis could be rigorously tested by selectively populating the various low frequency vibrational excited states and measuring the changes in the Raman or IR frequencies. Selective population of the lowest vibrational excited states could be achieved by careful adjustment of the temperature. Another method would be to maintain the temperature at 4.2° K and use a tunable far IR laser to achieve selective population. Such lasers should be available in the near future.

CHAPTER III

AN ANALYSIS OF THE LOWEST TRIPLET STATE OF BENZOIC ACID

A. A Summary of Previous Studies of Benzoic Acid Phosphorescence Emission

The earliest study of benzoic acid phosphorescence was carried out by von Kowalski in 1911. The phosphorescence of benzoic acid in ethanol was measured at 90° K. The origin of the emission was at 3660 Å. In their classic paper associating phosphrescence emission with the triplet state, Lewis and Kasha (1944) measured the phosphorescence emission of benzoic acid in EPA at 90° K. The origin of the emission was at 3672 Å. McClure in 1949 measured the phosphorescence lifetime of benzoic acid in EPA at 77° K and found it to be 2.5 ± .2 seconds. A series of papers on benzoic acid phosphorescence were published by Pyatnitskii in 1941, 1948, and 1949. He observed the origin of the emission to be at 4050 Å. As demonstrated by Kanda, Shimada, and Takenoshita (1963) and noted by Lower and El Sayed (1966) in their review paper, the emission observed by Pyatnitskii was due to an impurity. In 1961 Teplyakov and Grosul obtained the phosphorescence spectrum of benzoic acid in n-nonane at 90° K. They noted that the spectrum was better resolved in nonane than in other solvents.

The first study in which vibrationally resolved spectra were obtained and an analysis of the vibrations presented was carried out by Kanda, Shimada, and Takenoshita in 1963. These authors found that the spectrum of benzoic acid in benzene was well-resolved at 90° K. They observed intense ring out-of-plane modes and concluded that benzoic acid was distorted in the benzene lattice. Since only ring modes were observed, the lowest triplet state was considered to be a pure benzenoid state and was assigned as ^3L_a by analogy with benzene. Also in 1963, Levshin and Rebane studied the phosphorescence emission of benzoic acid and some of its salts. In agreement with Kanda _et al._, they concluded that the lowest triplet state was a pure benzenoid state.

In 1967, Nurmukhametov _et al._ attempted to explain the phosphorescence of benzoic acid using benzaldehyde as a starting point. They reasoned that substitution of the hydroxyl group should increase the transition energies of the $n\pi^*$ states, causing $^1n\pi^*$ to be closer to $^1\pi\pi^*$ than in benzaldehyde. The red tail of the $S_o \rightarrow S_1$ transition was thought to correspond to $^1n\pi^*$. $^3n\pi^*$ was assumed to lie between $^1\pi\pi^*$ and $^3\pi\pi^*$ in order to account for the absence of fluorescence, _vida infra_.

Maria and McGlynn in 1970 studied the phosphorescence of the series of acids $\emptyset$-$(CH_2)_n$-COOH and some of their salts. Unlike Levshin and Rebane, these authors found that lifetime of the salts were different from those of the corresponding acids. On this basis they argued that the lowest triplet state of benzoic acid extended over the carboxyl group. They also argued that the spectra obtained by Kanda _et al._ (1963) were not sufficiently resolved to exclude the presence of carboxyl group modes, which should be active if the triplet state has density in the region of the carboxyl group. Using the composite molecule approach these authors calculated that the lowest triplet state could be represented in terms of the lowest benzenoid ($^1b_{1u}$) and $\pi\pi^*$ carboxyl group triplet states as follows: $^3\Psi = 0.72\ ^3\Psi_{\emptyset} + 0.68\ ^3\Psi_{COOH}$. The ideas of Maria and McGlynn will be discussed in more detail in Section E.

In 1972 Tornson and El Bayoumi studied the phosphorescence of the series of acids $\emptyset\text{-}(CH_2)_n\text{-}X$, where $X = CH_3$, COOH , OH, NH_2 , and $COOC_2H_5$. Quantum yield measurements allowed the determination of radiative lifetimes. On the basis of their results, these authors suggested that intramolecular charge transfer from the ring to the COOH group played an important role in benzoic acid. However, a detailed description of the role of charge transfer was not presented. The ideas of Tournon and El Bayoumi will be discussed in more detail in Section III E.

Baba and Kitamura in 1972 studied the emission of benzoic acid in methylcyclohexane-isopentane glass at 77° K. These authors were the first to report the fluorescence spectrum of benzoic acid. In their opinion both monomer and dimer were present in the hydrocarbon glass at 77° K. The monomer was found to be non-fluorescent while the fluorescence quantum yield of the dimer was found to be 0.25. These authors proposed an energy level scheme similar to that proposed by Nurmukhametov (1967). Unlike Nurmukhametov, they assumed $^{1}n\pi^{*}$ to be above $^{1}\pi\pi^{*}$. The absence of fluorescence in the monomer was attributed to the presence of $^{3}n\pi^{*}$ below $^{1}\pi\pi^{*}$. In the dimer $^{3}n\pi^{*}$ was assumed to be above $^{1}\pi\pi^{*}$, allowing fluorescence to occur. Baum (1974) has definitely shown that the "monomer" considered by Baba and Kitamura is actually a complex involving a hydrogen-bonding impurity in the solvent and a benzoic acid monomer. Except for the nature of the monomer, the conclusions of Baba and Kitamura are otherwise unaltered. The result of Baba and Kitamura will be discussed in more detail in Section III D.

B. Experimental Procedures

Purification of Benzene

Benzene was purified by a chlorination procedure developed by R. E. Smalley (Baum, 1974). The basis of this procedure is that impurities in benzene are chlorinated more rapidly than benzene itself. After chlorination the chlorinated impurities as well as any chlorinated benzenes are separated from benzene by fractional distillation. This separation is efficient because the chlorinated compounds have boiling points which are much higher than that of pure benzene.

Chlorination was carried out in a 2 liter 3-neck flask having 24/40 ground joints. The starting material was spectroquality benzene (1 liter) obtained from Matheson Coleman & Bell Inc. Chlorine gas (obtained from Merck and Co. Inc.) was introduced into the liquid through a gas dispersion tube (fritted tip). This tube was connected to a chlorine tank by means of Teflon tubing. A 500 watt quartz-iodine tungsten lamp was placed next to the flask. The light and flask were surrounded with aluminium foil in order to focus the light into the flask. The lamp was connected to a variac set at 60 volts. At the beginning of the procedure the system was purged with helium gas. Then the flow rate of the chlorine gas was adjusted so that the characteristic yellow color remained in the flask when exposed to the light from the tungsten lamp. No stirring was necessary as the liquid boiled vigorously, apparently due to the absorption of light from the lamp. Because of the vigorous boiling, the flask was fitted with a large bore condenser. The chlorination was carried out for approximately 2 hours. The length of time necessary depends of course, on the amount of impurities initially present in the benzene. Clearly a high purity starting material is desirable. After chlorination, the flask was flushed with helium gas. This did not remove the yellow-green color. However, when the aluminum foil was removed and the flask exposed to room light for a period of time, the color disappeared.

After the liquid was free of color, out-gassed (450° C) "Boileezers" were added to the flask, which was then attached to a vacuum-jacketed distillation column 85 cm long and 1 cm inside diameter. The column was packed with stainless steel Heli Pak spirals (#3013) obtained from Podbelniak, Inc. The magnetically operated distilling head was fitted with a Teflon stopcock and no grease was used in the entire system. Teflon sleeves (Kontes Glass Co. #K676000) were used on the 24/40 ground joints. The reflux ratio was controlled automatically by a Flexopulse timing unit (Eagle Signal

Corp.). Soon after boiling began, the solution became tan in color and finally a golden brown. After distillation was stopped and the flask cooled to room temperature, a substantial amount of precipitate was found in the flask. The material in the flask had the characteristic smell of chlorobenzene. The first 100 ml collected were discarded and the next 400 ml were retained as the pure fraction; the remaining 500 ml were not passed through the column.

After distillation, the benzene was passed through an alumina column. The upper portion of this column was neutral alumina ($Al_2 0_3$). The bottom portion was basic alumina ($(Al_2 0_3$ with Na sites). Both kinds of alumina were of the W200 grade manufactured by M. Woelm. This column was out-gassed at 450° C in a tube furnance with N_2 gas predried by a "Drierite" ($CaS0_4$) column. The first 50 ml of the eluate were put through the column again.

In order to check the spectroscopic purity of the benzene passed through the alumina column, an open cell was filled with eulate and frozen within the next 5 minutes. The phosphorescence spectrum of this material at 4.2° K showed very little if any emission that could be ascribed to toluene or benzoic acid. However, some long lifetime impurities were present. The impurity spectrum consisted of a broad "bump" with 4 or 5 spikes extending above the bump. Since the lifetimes of these impurities were of the order of several seconds, it is unlikely that they were chlorinated compounds. This means that either the chlorination procedure was not carried far enough, or else new impurities were picked up in the distillation column or the alumina column. To check the possibility of the alumina column having trace amounts of organic compounds on it, the column was placed in a tube furnace at 450° C and oxygen gas was passed through it for 3 hours in order to oxidize any organic substances that might have been present. Previous to the oxygen treatment, helium gas was passed through the column at 450° C for 12 hours in order to drive out any moisture adsorbed on the alumina. This procedure eliminated the spikes seen in the phosphorescence spectrum previously. The broad bump however, remained. It should be emphasized that this emission was quite negligible compared with the emission obtained when a sample is deliberately dissolved in the benzene. Therefore, the benzene obtained after chlorination, distillation and alumina chromatography was considered adequately pure for use in phosphorescence spectroscopy at 4.2^{0} K.

This procedure for purifying benzene was carried out only once. For future work the following modifications are recommended:

1. The tube used to introduce chlorine and helium should be fitted with an all-glass check valve.

2. Stainless steel spirals should not be used in the distillation column as it is not possible to clean them with chromic acid. Instead glass helices should be used in order that the entire system can be cleaned with chromic acid.

3. The column used for alumina chromatography should be made of Vycor in order that the activation of the column can be carried out above the melting point of pyrex, say 700° C. This higher temperature would allow more effective oxidation of organic substances present on the alumina.

4. The helium (or nitrogen) gas used to dry the column should be predried by a P_2O_5 column before entering the alumina column. This would ensure that the gas entering the alumina column is free of moisture.

Purification of Benzoic Acid d_o

Benzoic Acid was purified by zone melting according to the general principles described by W. G. Pfann (1959) and H. Schildknecht (1966). Zone melting was carried out in a zone refiner manufactured by Princeton Organics. This device is of conventional design, except for the fact that tubes from 25 mm to about 4 mm in diameter can be used. The starting material used was "Benzoic Acid, Primary Standard, 99.99% Pure", obtained from J. T. Baker Chemical Co. Tubes were cleaned in chromic acid cleaning solution and thoroughly rinsed in distilled water and dried at 120° C. Benzoic acid powder was poured into the tube and melted in the presence of air. Alternate pouring and melting was carried out until the proper amount of material was in the tube. Then the tube was sealed under air at atmospheric pressure with a standard glass blowing torch. This caused the decomposition of a small amount of benzoic acid at the end of the tube. Accordingly this end was made the bottom end in the zone refiner since in vertical zone refiners, impurities are swept to the bottom of the tube. Zone melting was carried out for a minimum of 80 passes and usually more than a hundred.

The purity of zone refined benzoic acid was assayed in three ways: (1) Vibrational frequencies observed in the phosphorescence spectra were found to be in excellent agreement with those obtained by Raman and infrared spectroscopy. (2) Excitation of benzoic acid powder at room temperature with UV light too low in energy to excite the singlet state of benzoic acid was used to determine the presence of fluorescent impurities. Excitation was carried out with a nitrogen laser at 3371 Å and an AH-6 mercury arc followed by a Spex 1/4 meter Czerny-Turner grating monochromator (3200-3600 Å). This procedure showed no visible fluorescence at the pure end of the zone refiner tube and bright blue fluorescence at the impure end. A sample of zone refined benzoic acid obtained from Princeton Organics showed faint blue fluorescence, and a sample obtained from Aldrich Chemical Co. showed no visible fluorescence. However, all three samples gave essentially identical phosphorescence spectra. (3) The absence of fluorescent impurities absorbing in the visible region of the spectrum was verified with a Carey 82 Raman Spectrometer. Raman spectra of zone refined benzoic acid at 4.2° K showed a "zero base line" at 3000 cm^{-1} from the laser line (5145 Å or 4880 Å) under the normal conditions of Raman spectroscopy. Samples which are not carefully purified regularly show fluorescence under these conditions.

Purification of Benzoic Acid d_5

This compound was obtained from Merck Sharp and Dohme of Canada Ltd. A preliminary purification was carried out by vaccum sublimation in a Kontes Bantam sublimator. This procedure revealed a tan-colored impurity that sublimed less readily than benzoic acid. A second sublimination revealed a lesser amount of this impurity, indicating that sublimination was not particularly effective in removing this impurity. Due to high cost, only 5 grams of material were purchased. This made it necessary to use a small diameter tube for zone melting. The use of a small diameter tube (4 mm outside diameter) was complicated by the formation of bubbles in the tube which acted as "bottlenecks" against impurity transport. In spite of this, effective purification was achieved, as indicated by agreement of vibrational frequencies in phosphorescence, Raman, and infrared spectra. Isotopic purity was checked by mass spectroscopy and found to be 99% pure as specified by the manufacturer.

Purification of Benzoic Acid $4d_1$

This material was synthesized in the laboratory. Crude purification was carried out by sublimation in a large sublimator constructed in the laboratory. A tan-colored impurity was also found in this material. Like the similar impurity found in benzoic acid d_5 (probably synthesized by the same procedure), sublimation was only partially effective. Sublimation was continued until the material appeared white to the eye. Then it was extensively zone refined ($\sim$100 passes). Purity was verified by the same procedures used for benzoic acid d_o. Isotopic purity of this compound was determined by mass spectroscopy, which showed about 1.5% benzoic acid d_o impurity.

Purification of Paraflurobenzoic Acid

Parafluorobenzoic acid 99% pure was obtained from Aldrich Chemical Co. Inc. and extensively zone refined (100 passes). The upper portion of the tube was then cut away from the bottom half and wrapped in heavy duty aluminum foil and smashed with a hammer. The particles of glass and parafluorobenzoic acid were placed in a sublimator and sublimed, separating the glass from the paraflurobenzoic acid. The sublimed material was then zone refined for another 100 passes. Purity was checked by the same procedure used for unfluorinated benzoic acid.

Purification of Methyl Benzoate

The starting material was obtained from Matheson Coleman and Bell and was specified to have a melting range of -12 to -10° C. Some of the material was purified by vacuum distillation in a completely sealed all-glass two-step distillation apparatus. In other cases, the compound was passed through a column containing neutral and basic alumina and then zone refined in a laboratory-constructed zone refiner. Purity was determined as usual.

Purification of n-Nonane

Chromatoquality n-nonane was obtained from Matheson Coleman and Bell. This material was supplied with a batch chromatogram and was specified to have 99^+ mole per cent purity. Further purification was carried out by alumina chromatography. Spectroscopic purity was assessed by the absence of detectable phosphorescence under the conditions normally used for benzoic acid.

Synthesis of Benzoic Acid $4d_1$

Benzoic acid $4d_1$ of high isomer and isotopic purity was needed in order to facilitate assignment of combination bands in the phosphorescence spectra and fundamentals in the Raman and infrared spectra. In order to achieve high isomer purity, zone refined 1,4-dibromobenzene was obtained from Aldrich Chemical Co. Inc. Using a Grignard reaction, bromobenzene $4d_1$ was prepared. Benzoic acid $4d_1$ was prepared by a second Grignard reaction.

Numerous attempts were made to prepare Bromobenzene $4d_1$ of high isotopic purity using the conventional procedures for Grignard reactions. None of these attempts yielded an isotopic purity higher than about 93%. A successful procedure, suggested by

Dr. J. San Filippo, was developed which employed methyl magnesium bromide as a water scavenger.

Diethyl ether (anhydrous, Fischer Scientific) was distilled from lithium aluminum hydride under a N_2 atmosphere, the N_2 gas being dried with a column of fresh P_2O_5, 25 mm in diameter and 30 cm in length. Excess pressure was released by a mercury bubbler. Glassware having 24/40 ground joints were used. No grease was used in the system. The distillate was collected under N_2 gas in an Erlenmeyer flask having a 24/40 ground joint. The flask was exposed to air for only a second when disconnected from the distillation apparatus.

Magnesium turnings (Matheson Coleman & Bell, "For Grignard Reactions") were dried overnight at 120° C in a drying oven.

All glassware was cleaned in chromic acid cleaning solution, thoroughly rinsed in distilled water, and dried overnight at 120° C.

The reaction was carried out in a dry box, continuously purged with N_2 gas dried by P_2O_5. Several large evaporating dishes containing fresh P_2O_5 were placed in the dry box and the atmosphere in the box was stirred by a plastic fan.

To a 500 ml flask (one-neck) 125.5 g of 1,4-dibromobenzene were added. In the dry box, 250 ml of dry ether were added and the flask capped with a glass 24/40 stopper. To a second flask (1000 ml, 3-neck) 15.8 grams of magnesium and a large Teflon covered magnetic stirring bar were added. In the dry box, 50 ml of dry ether were added. A Friedric condenser (chosen for high efficiency) was attached to the flask and all holes were capped. To each flask about 35 ml of methyl magnesium bromide were added. After the cessation of bubbling, the flasks were capped and then tilted and rotated in order to expose as much of the surface area of the glass as possible to the methyl magnesium bromide. Unfortunately, it was not possible to get the methyl magnesium bromide into the upper portions of the condenser. For future work, it is recommended that the methyl magnesium bromide be added through the condenser. The addition of more methyl magnesium bromide (about 12 ml) to the flasks yielded no bubbles, confirming the absence of H_2O. Only slight bubbling was initially observed in the flask containing 1,4-dibromobenzene. Substantial bubbling was observed in the flask containing magnesium. The flasks were kept capped as much as possible, the pressure build-up due to methane liberation being occasionally released. After this water scavenging procedure was completed, the flasks were connected by a U-tube. A 24/40 joint was inserted at the midpoint of the U-tube in order that one flask could be titled while the other remained stationary. This joint was fitted with Teflon sleeve (Kontes Glass Co. #K67000) in order to have a freely rotating grease-free joint. After the system was completely capped, the dry box was opened and the system was removed and attached to a rack in the fume hood. A source of N_2 gas dried by P_2O_5 was quickly attached along with a mercury bubbler. By tilting the flask the ether solution of 1,4-dibromobenzene could be transfered slowly into the flask containing magnesium and ether without opening the system to the external air (which possessed ∿ 100% relative humidity due to a violent thunder storm in progress). The reaction proceeded spontaneously. The rate of addition of 1,4-dibromobenzene was controlled to prevent excessive reflux in the condensor. When all of the 1,4-dibromobenzene was added, the reaction mixture was stirred for one hour. After the scavenging procedure was completed and the flasks capped, but before the dry box was opened, a previously unopened bottle of D_2O (Aldrich Chemical Co, 99.7% isotopic purity) was opened and 10 ml of D_2O were poured into the dropping funnel. The top and bottom ends of the funnel were capped and the Teflon stopcock opened.

The funnel was then vigorously shaken in order that the D_2O come in contact with as much of the glass surface as possible. The D_2O was then drained out and replaced with 50 ml of fresh D_2O. After the funnel was capped (24/40 stopper at top and 50 ml flask (24/40 joint) at bottom), the dry box was opened as described previously.

After the Grignard reaction mixture had been stirred for one hour, the flask was placed in an ice bath and allowed to cool down to about 5° C (estimated, not measured). The dropping funnel was then quickly attached and D_2O was slowly added with vigorous stirring to break-up clumps of magnesium salts as much as possible. This is necessary to prevent unreacted Grignard reagent from being occluded inside of the clumps. After the D_2O was added, the reaction mixture was stirred for one hour. Then 40 ml more of D_2O were quickly added to dropping funnel in room air and added to the flask. This last step was probably unnecessary as the initial amount of D_2O was already a large excess.

The reaction mixture was then treated with 10% H_2SO_4 until the magnesium salts were dissolved (about 650 ml were used). A separatory funnel (Teflon stopcock) was used to separate the organic layer from the aqueous layer. The organic layer was washed with 10% Na_2CO_3 to remove any acid. After separation of the aqueous layer, the organic layer was distilled at atmospheric pressure in a small distillation column. About 100 ml of ether came off first; then about 3.6 ml of $C_6H_4D_2$ (78-80° C boiling range) came off. The column was allowed to cool to room temperature. A vacuum pump and an N_2 gas bleed were attached. The pressure was adjusted to 25 mm Hg and the heating mantle was turned on (50 volts). Residual liquid in the condenser from the first disstillation was quickly evaporated. The first material collected had a boiling range of 60-63° C at 26 mm Hg pressure. No other material was collected. After the flask cooled, the material not distilled formed a solid. Assuming 100% purity of the distillate, which weighed 58.2 grams, 0.37 mole were collected. This constitutes a yield of 68 moles % which is reasonable for this reaction. The yield of 1,4-benzene d_2 was 7%. The isotopic purity of the product was found to be 98.5% by mass spectroscopy! This high degree of isotopic purity indicates that the use of methyl magnesium bromide is an excellent means of removing water in Grignard reactions.

Benzoic acid $4d_1$ was prepared by the carbonation of the Grignard reagent of bromobenzene $4d_1$. The procedure followed was that due to Hussey (1951). The conventional procedure is to pour the Grignard reagent onto dry ice exposed to air. Because of the exposure to oxygen and water, the yield is less than optimum. Hussey's procedure involves forcing the Grignard reagent through a filter tube with dry N_2 gas onto an ether slurry of crushed dry ice in a flash that is connected to a mercury bubbler. Thus, air is excluded from the system. The only appreciable moisture present is that adsorbed on the crushed dry ice. Hussey claimed a yield of about 89%, which was verified by our experience. A high yield in the carbonation step was desirable on account of the high cost of the 1,4-dibromobenzene used to prepare bromobenzene $4d_1$.

Ether was distilled from lithium aluminum hydride. To a 3-neck, 1 liter flask, 13.6 g. of magnesium and 250 ml of ether were added. This flask was fitted with a Friedrich condensor. A mercury bubbler and N_2 source were also attached. 57.5 grams of Bromobenzene $4d_1$ + 65 ml of ether were added to a dropping funnel. The material in the dropping funnel was slowly added to the flask (over a period of one hour) in order to prevent excessive refluxing. After the reaction was complete, the Grignard reagent was forced with N_2 pressure into a second flask containing a slurry of crushed ice (250 ml ether, 600 g CO_2). After the reaction mixture had warmed to about 10° C, about 200 ml of 50% HCl (6 Normal) were added. The ether layer was recovered with a separatory funnel and evaporated. The acid layer, containing magnesium salts, was discarded. The crude product was purified by five sublimations followed by extensive zone refining. After the carbonation step, the isotopic purity was again checked and found to be the same as that of the bromobenzene $4d_1$. The chemical purity was checked with the same methods used for benzoic acid d_o.

Sample Preparation

In initial runs, open vycor cells were employed. These cells were made from vycor tubing by blowing a bubble and then flattening the bubble with tongs. The cells were cleaned in chromic acid cleaning solution, rinsed and dried at 120° C. Final cleaning consisted of heating in an oxygen-natural gas flame until the cell appeared white hot when viewed through glasses designed for working quartz. Contaminants of the vycor appeared as "hot spots" when heated. Prolonged heating often removed these spots. During the heating procedure the cell as supported by a small quartz rod inserted into its interior. For final runs, a sealed cell was used. This cell was made from rectangular quartz tubing attached to a pyrex-to-quartz graded seal. The rectangular section of the cell was about one inch long. This type of cell was cleaned as above, except that the pyrex section and the graded seal were not heated white hot.

For solid solutes, a small particle of material (weighed on a Metlar Balance) was placed in the cell. Then the proper amount of solvent was added and the cell attached to the vacuum line with a Swagelok Union made of 316 stainless steel and having Teflon ferrules. Prior to attachment of the cell, the vacuum line was pumped down with a Welch 1402 mechanical pump and liquid nitrogen added to the cold trap. The system including Swagelok fittings, were flamed with a Bunsen burner. Between the cold trap and the sample, the system was grease-free, employing a single stopcock sealed by viton-O-rings. Before applying the vacuum, the sample was frozen with liquid nitrogen. Then the system was pumped down to the limit of the pump. Next the stopcock was closed and the sample allowed to warm to room temperature. Usually, vigorous bubbling was observed. The sample was again frozen and the system evacuated. As before, the stopcock was closed and the system warmed to room temperature. Much less bubbling was observed during the second thaw. The sample was frozen again and the system extensively evacuated.

With the sample immersed in liquid nitrogen, the sample cell was sealed with a standard glass blowing torch.

Experimental Arrangements for Phosphorescence Spectroscopy

Low resolution phosphorescence spectra (polarized and unpolarized) at 77° K were obtained using an Hitachi-Perkin Elmer MPF3 Fluorimeter. This instrument employs a Xenon source followed by single Czerny-Turner monochromater for excitation. For observation of emission a single Czerny turner monochromator and photomultiplier tube are employed. Spectral bandpass for emission and excitation monochromator is indicated directly on dials calibrated in nanometers. The sample cell, liquid nitrogen dewar, chopper and polarizers comprise an integrally designed phosphorescence attachment.

This instrument was also used to obtain low resolution excitation spectra of benzoic acid d_o and p-fluorobenzoic acid.

High resolution phosphorescence spectra at 4.2° K were obtained with a Spex Model 1702 3/4 Meter Czerny Turner monochormator fitted with a Model 6256S photomultiplier tube made by Emitronics Inc. The output of the photomultiplier was measured with a Model 414S Keithley picoammeter and recorded with a Model 7101B

Hewlet Packard recorder. The instrument used a 102 x 102 mm, 1200 groove/mm. grating blazed at 5000 Å, made by Jobin-Yvon. Excitation was achieved with a AH-6 high pressure mercury arc. Light from the source was filtered by a 10 cm cell containing Ni_2SO_4. Excitation and emission light were separated using a Becquerel chopper. The exciting light was made to impinge on the side of the sample facing the monochromator. A standard glass and quartz liquid helium dewar was used.

Samples (as many as six) were mounted on an aluminum strip with Scotch Brand (3M Co) electrical tape. The metal strip was suspended in the liquid helium with a polystyrene rod. The tape exhibited no detectable phosphorescence under the conditions of the experiments. In many cases, however, it was completely covered with aluminium foil. Supracil lenses were used to focus the excitation and emission light. The object and image distance were made equal so that these lenses gave a magnification of 1. Care was taken to align the optics so that the grating was properly filled with light. Final optical alignment was done photoelectrically.

The sensitivity of this system was marginal for phosphorescence spectroscopy of benzoic acid. Due to the highly resolved spectra exhibited by benzoic acid, it is necessary to use narrow slits (30-100 μ, dispersion of monochromator = 11 Å/mm). The use of narrow slits required long time constants (3-30 seconds) on the electrometer, which necessitated long scans. But the scanning time was restricted due to the moderately rapid photodecomposition of benzoic acid and the resulting loss of phosphorescence intensity. Thus, in some cases the observed resolution was slightly instrument limited.

C. Phosphorescence Spectra

In this study we have obtained the phosphorescence spectra of fourteen different guest-host systems. These spectra are shown in Figures 26 through 39. Frequencies and assignments of vibronic bands are given in Tables 18 through 31. Vibrationally resolved spectra have been obtained for all systems. In this section we consider the general features of these spectra.

Benzoic Acid in Benzene

This system was observed by Kanda *et al*. (1963) to yield moderately resolved spectra at 90° K. We find that lowering the temperature to 4.2° K yields a substantial increase in resolution. The spectra obtained by photoelectric detection were limited by instrumental resolution. However, the spectra obtained by Baum (1974) with a high resolution spectrograph show linewidths of the order of 1 cm^{-1}.

The phosphorescence of benzoic acid in benzene (polycrystalline) is characterized by a strong origin and several strong totally symmetric vibrations. The strongest of these vibrations are ν_{12} and ν_{8a}. ν_{9a} is somewhat weaker but still prominent. All of these vibrations form progressions. Two and three quanta of ν_{12} and two quanta of ν_{8a} can be observed. A recent study by Haaland and Nieman (1973) shows that these vibrations are also prominent in the phosphorescence spectrum of toluene.

Since benzoic acid can exist as a monomer or dimer in nonpolar solvents, such as benzene, it is important to determine which species is responsible for the phosphorescence emission. The spectrum of benzoic acid in polycrystalline benzene shows only one origin. All vibronic bands can be explained relative to this origin. Consequently, we conclude that the emission is due predominantly to only one species. As shown in Chapter II, vibrational modes involving carboxyl group motion show appreciable dimer splitting. If the emission comes from monomers the frequencies of the modes will be the averages of the Raman and IR frequencies observed for the dimer. Since, in several cases, the dimer splitting is more than 30 cm^{-1}, there will be large differences between monomer and dimer frequencies for these cases. One of the modes found to exhibit a large dimer splitting is ν_{6a} (422.0 cm^{-1} (R) and 388.0 cm^{-1} (IR). Fortunately, the 422.0 cm^{-1} band is observed in the phosphorescence spectrum of benzoic acid benzene. As expected, it is the totally symmetric mode that is built on the allowed origin. This provides convincing evidence that dimer emission is being observed.

As noted previously, the spectra of benzoic acid and toluene are similar with regard to the strong totally symmetric modes. However, unlike toluene benzoic acid shows a number of intense out-of-plane modes. In toluene, the out-of-plane modes are generally weak (<15% of origin intensity); only ν_{16b} and ν_5 occur with medium intensity (35% and 29% of origin intensity, respectively). In benzoic acid, the strongest of the out-of-plane modes are comparable to ν_{8a} and ν_{12}. The out-of-plane modes which can be observed in the spectrum are: $\nu_{10b}(+)$ (Raman frequency), ν_{16a}, ν_{16b}, ν_4, ν_{11}, $\nu_{10b}(-)$, ν_{10a}, out-of-plane H-wag (Raman frequency), ν_{17b}, ν_{17a}, and ν_5. Noteworthy, is the fact that the Raman frequencies appear for $\nu_{10b}(+)$ and the H-wag mode. The strongest modes in benzene host are ν_{11} and $\nu_{10b}(-)$. The only carboxyl group mode, the H-wag mode, is relatively weak. In general, most of the out-of-plane activity is associated with ring vibrations. Most notable is the fact that while even quanta of strong in-plane modes can readily be found in the spectra, even quanta of the out-of-plane modes cannot.

It is important to determine the percentage of the total intensity that is associated with carboxyl group modes. Not counting the H-bond modes, the following carboxyl group modes appear in the spectrum: $\nu_{10b}(+)$, ν_{6a} out-of-plane H-wag, ν_{13}, $\nu_{9b}(-)$, C-0 stretching + 0-H bending mode at 1298.0 cm^{-1} and possibly the C-0 stretching + 0-H bending mode at 1449.0 cm^{-1}, and the C=0 stretching mode at 1637.0 cm^{-1}. It is important to realize that ν_{6a}, ν_{13}, and $\nu_{9b}(-)$ involve appreciable ring motion and may be active by virtue of this motion. The other modes, particularly the C=0 stretch, are thought to be relatively pure carboxyl group modes. These fundamentals are also components of combination bands. Below 200 cm^{-1} there are modes which might be the ring-carboxyl group torsion and the H-bond in plane bend. However, the assignments of these modes are not on a firm basis and furthermore, these modes are environment sensitive. Thus, it is questionable whether these modes appear.

The measurement of the percentages of the total intensity that contribute by the various kinds of modes is complicated by the relatively rapid photodecomposition of benzoic acid (∿50% in 50 minutes) and the net spectral response of the spectrometer. Because the photographic recording observes all wavelengths simultaneously, we tend to regard these measurements as more reliable than those obtained photoelectrically. Baum's photographic data indicates that 45% of the intensity is associated with out-of-plane modes, 9%

with carboxyl group in-plane modes and 46% with in-plane ring modes.

In order to facilitate the assignment of combination bands, the phosphorescence spectra of benzoic acid $4d_1$ and d_5 in benzene were also obtained. Unfortunately, the discrimination offered by this approach is somewhat mitigated by the inaccuracy of the wavelength counter on the Spex 1702 monochromator. In some cases, the error in the vibrational frequency was estimated to be $\pm$ 10 cm^{-1}. An uncertainty this large increases the number of possible assignments for a given band. Wavelengths in Baum's photographic data are expected to be much more accurate since they are measured relative to iron and neon lines. The assignments of combination bands given in this thesis are based upon a consideration of both the photoelectric data and Baum's photographic data.

Benzoic Acid in n-Nonane

The goal of this study has been to determine intrinsic molecular properties of benzoic acid. It is therefore important to identify the effects of the environment on the spectra. This is best done by obtaining the spectra in a variety of hosts having different properties. The main problem with this procedure is the difficulty of finding hosts which give vibrationally resolved spectra. Normally, these hosts are discovered by trial and error, guided by physical intuition. However, a methodical procedure for finding hosts that yield sharp spectra was discovered in 1963 by Sh'polskii. According to Sh'polski sharp spectra of an aromatic molecule will be obtained in a normal alkane matrix when the length of the alkane is the same as that of the aromatic molecule. Application of the rule to benzoic acid shows that n-nonane should be the correct Sh'polskii solvent. And indeed, well-resolved phosphorescence spectra are obtained in this host.

The general features of the phosphorescence emission in this host are similar to those seen in the benzene spectrum. ν_{12} and ν_{8a} are the strongest bands in the spectrum although the intensity of ν_{12} relative to the origin is somewhat less than in benzene. ν_{6a} is missing in this spectrum. This is definitely confirmed by consulting the spectra of benzoic acid d_5 in n-nonane which shows ν_{16a} and ν_{16b} shifted to the expected values for $d_o \rightarrow d_5$ substitution. Since no other fundamentals are close to ν_{6a} we conclude that ν_{6a} does not appear in the nonane spectrum. Also ν_1, which was weak to medium in benzene is missing in the nonane spectrum. Like ν_{6a} this mode involves appreciable carboxylgroup motion.

In nonane host bands corresponding to out-of-plane modes are in general weaker than in benzene, the strongest being about 50% as intense as ν_{12} and about 30% as intense as the origin. The three strongest out-of-plane bands are of comparable intensity and are ν_{11}, $\nu_{10b}(-)$ and ν_{10a}. ν_{10a} was relatively much less (∿50%) intense in the benzene spectrum. The mixed O-H bending + C-0 stretching mode at 1298.0 cm^{-1} in benzene is missing in the nonane spectrum and the C=0 stretching mode at 1634.0 cm^{-1} (in nonane) is barely visible. As noted previously ν_{6a} , which contains appreciable carboxyl group motion is also missing. Thus, we conclude that bands associated with carboxyl group modes are, in general, weaker in nonane than in benzene. A similar conclusion holds for the out-of-plane modes.

We also obtained the spectra of benzoic acid $4d_1$ and d_5 in n-nonane for the purpose of making firm assignments of combination bands. Except for benzoic acid d_o, photographically recorded spectra for nonane host are not available for comparison.

Benzoic Acid d_o in Benzoic Acid d_5

In the two previous cases, nonpolar solvents were employed as hosts. Clearly, it is desirable to determine if the properties of the spectra depend on polarity. For this purpose, benzoic acid d_5 was chosen as a host since sharp spectra are generally obtained when a deuterated analogue is used as a host.

In the mixed isotopic crystal the predominant emitting species is expected to be the d_o — d_5 mixed dimer. For the mole ratio of 8/1000 used in our experiments, the percentage of d_o - d_o dimers is expected to be negligible. Since the dimer is no longer homogeneous, the modes of one half of the dimer are not degenerate with those of the other half. This means that the dimer splitting observed in the Raman and IR spectra may not be observed in the phosphorescence spectrum. However, pure carboxyl group modes, such as the out-of-plane H-wag mode are still expected to be degenerate since $d_o \rightarrow d_5$ substitution does not change the frequency of these modes. Therefore, we expect the same dimer splitting of the H-wag mode that was observed in d_o - d_o dimers to be observed in d_o - d_5 dimers. For ring modes having negligible carboxyl group motion, the dimer splitting in the homogeneous dimer was observed to be less than 1 cm^{-1}. Consequently the interaction between these modes in the mixed dimer is also expected to be comparably small. For example, ν_{12} in d_5 - d_5 is 960 cm^{-1} and in d_o - d_o ν_{12} is 1000.5 cm^{-1}. In the vibrational spectra of mixed d_o - d_5 we expect to observe both 960.0 and 1000.5 cm^{-1}, each being negligibly perturbed by the other. On the other hand it is possible that a d_5 monomer mode will be degenerate or nearly degenerate with a different d_o mode of the same symmetry type. If both modes involve carboxyl group motion then appreciable coupling is expected and new frequencies may be observed in the $d_o - d_5$ vibrational spectra.

The phosphorescence spectrum of mixed $d_o - d_5$ dimers is, in general, similar to the spectra of $d_o - d_o$ dimers in benzene and n-nonane. The origin is strong and the strongest in-plane modes are ν_{8a} and ν_{12}. The frequencies of these modes are identical ($\pm$ 1 cm^{-1} using Baum's photographic data) to the $d_o - d_o$ Raman frequencies obtained at 4.2^o K. No $d_5 - d_5$ frequencies are observed, except possibly those which are identical to $d_o - d_o$ frequencies, and this occurs only for modes which are pure carboxyl group modes. On this basis we conclude that the excited state from which the emission occurs is localized on the d_o portion of the $d_o - d_5$ mixed dimer.

No bands are present which can be ascribed to ν_{6a} and ν_1. The C=0 stretching mode, if present in the spectrum, is weak relative to ν_{8a}. The out-of-plane modes are as intense as they are in benzene, but the strongest are ν_{11} , $\nu_{10b}(+)$, and ν_{10a}. This pattern resembles the spectrum for nonane host where ν_{10a} is strong and is unlike the spectrum for benzene host, where ν_{10a} is of weak-to-medium intensity.

Parafluorobenzoic Acid in Benzoic Acid

In this system the host is benzoic acid and the guest in parafluorobenzoic acid (∿1 mole %). However, the emission does not originate from the guest molecule. Rather, the emission originates from guest induced defects in the host crystal. That the emission comes from benzoic acid rather than parafluorobenzoic acid is readily verified by examining the vibrational frequencies that appear in the phosphorescence spectrum. Parafluorobenzoic acid has vibrational frequencies that are markedly different from those of benzoic acid Tables 21 & 27. That the omission does not come from natural defects in the crystal is indicated by the different origins. The origin of guest-induced defect emission is at 3694.0 Å while the origin of the natural defect emission is at 3673 Å Baum, 1974). We think it most likely that the emission is coming from mixed dimers and assume that the benzoic acid half of the mixed dimer is perturbed by its parafluorobenzoic acid mate so that its triplet level is below the exciton level of the crystal. Because the K_a of p-fluorobenzoic acid is greater than unsubstituted benzoic acid, the hydrogen bonds will be stronger in the mixed dimer than in a homogeneous unsubstituted dimer. As shown by Baum, (1974), hydrogen bonding to the carbonyl group causes a red shift of the phosphorescence origin while hydrogen bonding of identical strength to the hydroxyl group causes a blue shift, but to a less extent. Therefore, we expect a net red shift as a result of the greater H-bond strength in the dimer. This is consistent with what is observed. Natural defect emission from a d_o crystal and d_o - d_5 emission from a mixed isotopic crystal have their origin at 3673.0 Å and 3672.3 Å, respectively, while the induced defect emission has its origin at 3694.0 Å. Note that the only difference between natural and guest-induced defects is the presence of the fluorine atom at one end of the dimer. The surrounding environment should be very similar in both cases as far as dispersion forces are concerned. We are, therefore, inclined to regard the shift in origin as due almost entirely to the change in H-bond strength.

It is worth noting that this approach for obtaining vibrationally resolved spectra is different from the widely practiced mixed crystal technique originated by McClure in 1954. In his technique the guest molecule has an energy level that is below the exciton level of the host. Either the guest is excited directly or else the host is excited and the excitation transferred to the traps created by the guest molecules. This approach is superior because it allows singlet absorption measurements to be made in addition to emission measurements. With the guest-induced defect technique singlet absorption measurements are not possible. Nonetheless, we regard this technique to be a useful adjunct to the conventional technique. In both cases, sharp spectra occur because the guest substitutes into the host lattice in a regular way. We are aware of only one previous case in which guest-induced defects have been used to obtain sharp spectra (ElSayed 1972). In our opinion this technique deserves more frequent exploitation.

The phosphorescence emission from defects induced by parafluorobenzoic acid doped into polycrystalline benzoic acid can be succinctly described as being very similar to the emission from benzoic acid in n-nonane. Even the origin are very close to each other (3694.0 Å and 3701.5 Å). The comparison made between the spectra for nonane and benzene hosts applies in all of its details to the guest-induced defect spectrum.

Benzoic Acid in Cyclohexane Carboxylic Acid

Cyclohexane carboxylic acid was suggested as a suitable host for benzoic acid by Dr. Koyanagi. The crystal structure of cyclohexane carboxylic acid is unknown. In view of the highly resolved spectrum obtained with this host, benzoic acid apparently substitutes well into the lattice. Because it is a saturated molecule, its triplet exciton level is expected to be well above the triplet level of benzoic acid. Also the saturated ring weakens the K_a to 1.26×10^{-5} as opposed to 6.3×10^{-5} for benzoic acid.

The phosphorescence of benzoic acid doped into single crystal of cyclohexane carboxylic acid has been obtained at 4.2° K by Baum 1974). This spectrum is markedly different from the spectra discussed so far. The major difference is a large reduction in the intensity of the out-of-plane modes. In benzene host, the out-of-plane intensity is 45% of the total intensity while in cyclohexane carboxylic acid host, it reduces to about 9%. ν_{16a} appears weakly at 405.0 cm^{-1}. A weak-to-medium band appears at 425.0 cm^{-1}, which is probably ν_{6a}. The uncertainty concerning this band derives from the altered H-bond strengths and the breaking of the degeneracy that exists in homogeneous dimers. The unperturbed monomer frequency is estimated to be at $(422.0 + 388.0)/2 = 405.0\ \mathrm{cm}^{-1}$. But this mode involves appreciable carboxyl group motion so it may be altered by the different H-bonding environment. Since all other ring out-of-plane modes agree <u>very closely</u> with the Raman frequencies we would expect ν_{16b} to be located at $438.0\ \mathrm{cm}^{-1}$. On this basis we regard it as unlikely that the $425.0\ \mathrm{cm}^{-1}$ band corresponds to ν_{16b}. $\nu_{9b}(-)$ (C-X in-plane bend) appears very weakly and ν_1 appears with medium intensity. As in all the other hosts, the origin, ν_{8a} and ν_{12} are the strongest bands of the spectrum.

The strongest out-of-plane modes are ν_{11}, $\nu_{10b}(-)$ and ν_{10a}. All are of weak of medium intensity. The carbonyl stretching frequency will likely be different because of the different H-bond environment but if it appears in the spectrum at all, it appears very weakly.

It should be noted that in benzene, nonane, mixed isotopic crystal, and parafluorobenzoic acid, the H-bonding environment of a benzoic acid monomer has been approximately the same in all cases. The change in H-bond environment is apparently the major difference between cyclohexane carboxylic acid host and the others.

Parafluorobenzoic Acid in Nonane

So far we have considered the effects of differing environments on the phosphorescence emission of benzoic acid. We now consider the effects of substituent groups. Nonane was chosen as the host for parafluorobenzoic acid because this solvent is the Sh'polskii solvent for the molecule, and a resolved spectrum was obtained. Since a thorough normal coordinate analysis for this molecule was not carried out, we limit our consideration to the out-of-plane modes and other general features of the spectrum. The out-of-plane modes and ν_1 have been assigned using the Varsanyi tables and the phosphorescence frequencies (see Table 27).

The origin of the spectrum is strong as are modes ν_1 and ν_{8a}, which are located at 960 cm^{-1} and 1618 cm^{-1}. In this respect, the spectrum resembles that of benzoic acid.

Five out-of-plane modes can be identified: ν_{10b}, ν_{16a}, ν_{16b}, ν_4, and ν_{10a}. The intensity of ν_{10b} is about 50% of the origin, ν_{10a} about 8% and the others about 25%. Thus, the intensity of the out of plane modes relative to the origin is much less than observed for benzoic acid in all matrices except cyclohexane carboxylic acid. As for benzoic acid, there is no evidence for multiple quanta of the out-of-plane modes.

Parafluorobenzoic Acid in Cyclohexane Carboxylic Acid

Since the out-of-plane modes in benzoic acid were weakened in cyclohexane carboxylic acid, we also used this host with parafluorobenzoic acid. In this case, the host was in a polycystalline state and the spectrum is not as highly resolved as Baum's single crystal spectrum. Similar broadening was observed for benzoic acid in polycrystalline cyclohexane carboxylic acid. Nonetheless, a vibrationally resolved spectrum was obtained. This spectrum showed the same weakening of the out-of-plane modes that was observed for benzoic acid. The intensity of ν_{10b} is reduced from 50% of the origin to 14% and the other modes are reduced to about 4% or less. On the other hand the intensities of ν_{8a} and ν_1 are essentially unchanged relative to the origin. In short, the behavior of parafluorobenzoic acid in cyclohexane carboxylic acid parallels that of benzoic acid in the same host.

Methyl Benzoate in Benzene

As discovered by Kanda, *et al* (1963), methyl benzoate in benzene yields a moderately resolved spectrum at 90° K. We have found that the spectrum becomes highly resolved at 4.2° K. The general features of the methyl benzoate spectrum, as noted by Kanda and coworkers, are similar to those of benzoic acid. The origin is strong and the dominant in-plane modes of the spectrum are ν_{12} and ν_{8a}, although ν_{12} is somewhat weaker than in the benzoic acid spectra. The photoelectric spectrum shows two bands at 420 and 450 cm^{-1}. The more highly resolved and more accurate spectrum obtained by Baum shows three bands at 412, 420, and 443 cm^{-1}. The bands at 412 and 443 are readily identified as ν_{16a} and ν_{16b}, respectively. The band at 420 cm^{-1}, however, is somewhat perplexing. Presumably, this band corresponds to ν_{6a}. However, the frequency of this mode in the Raman spectrum is 362 cm^{-1}. While some phosphorescence frequencies have been observed to differ as much as 10 to 15 cm^{-1} from Raman values, a shift of 58 cm^{-1} is hard to accept. The phosphorescence band at 420 is sharp and strong (50% of origin intensity). It cannot be a combination band since all bands of lower frequency are significantly weaker. If this band were a different a site or an impurity one would expect to see bands built upon this origin. However, all other observed bands can be rationalized relative to the strong origin at 3620 Å. Therefore, the nature of this band remains a mystery. ν_1 appears at 822 cm^{-1} (frequency taken from Baum's photographic data) with weak-to-medium intensity.

The ring-carboxyl group wag appear at 219 cm^{-1} which is in good agreement with Raman value of 218 cm^{-1} (298^{o} K). The intensity of this mode is greater than in the benzoic acid spectra. The strongest out-of-plane modes are ν_{11} and $\nu_{10b}(-)$. These bands are as intense as the origin and ν_{8a}. ν_{10a} is relatively weak, being about 25% of the intensity of the origin. Multiple quanta of the out-of-plane modes are not present in the spectrum.

The carboxyl stretching mode appears at 1730 cm^{-1} with weak to medium intensity. It thus appears that the appearance of ν_{6a} (422?) , ν_{1} , and the carbonyl stretching mode, along with the weak appearance ν_{10a} resembles benzoic acid in benzene, rather than benzoic acid in nonane.

In summary, the phosphorescence emission of methyl benzoate in benzene shows the same general features that are present in the spectrum of benzoic acid in benzene. Most notably, the intense out-of-plane modes are present in both spectra.

Benzoic Acid in Methyl Benzoate and Parafluorobenzoic Acid in Methyl Benzoate

Since the out-of-plane modes in benzoic acid were found to exhibit a strong environmental dependence, an attempt was made to determine if a similar dependence existed for the out-of-plane modes in methyl benzoate. The guest-induced defect method was used in this attempt. Three spectra were obtained using benzoic acid and two using parafluorobenzoic acid, as the guest. Although these systems yielded resolved spectra in all five cases, several origins appeared in each spectrum. The relative intensities of these origins vary greatly among the spectra. One possibility is that the various origins are due to different sites which are differently populated in the various spectra. Another possibility is that the origins are due to impurities. In two of the spectra methyl benzoate was purified by alumina and silica gel chromatography, and vacuum distillation. For the third spectrum, zone refined methyl benzoate was used. Zone refined benzoic acid and parafluorobenzoic acid were used in all cases. Table 32 p.440) shown the possible origins observed in the five spectra. All bands to the blue of the strongest origin are considered origins and all bands to the red in the immediate vicinity of the origin that are significantly stronger than normally expected for this region and which do not correspond to known vibrational frequencies are listed as possible origins. For those origins indicated by an asterisk there is a band in the spectrum which can be assigned as ν_{12} built upon the origin in question. It should be realized that these bands can also be regarded as combination bands. A number of conclusions can be drawn from the data presented in Table 32. First, it is unlikely that most of the bands listed in the table are associated with impurities because most origins that appear in I, II and III also appear in IV and V. The zone refined material is far less likely to contain impurities than the vacuum distilled material. Secondly, the bands which we have called "origins" are most likely associated with sites that are differently populated in the various spectra. The best evidence comes from spectra IV and V. These spectra were obtained with the same sealed sample two days apart. When spectrum V was obtained it was noticed that some portions of the sample were "glossy" and while other portions showed the characteristic appearance of a polycrystalline sample. We regard it as most likely that the difference between the two spectra are due to the "glossy" composition of the sample used to obtain spectrum V, which showed little vibrational structure. When methyl benzoate was being zone refined, it was noticed that it had a tendency to form a glass. This tendency was eliminated by adding a small quanity of alumina, which fell to the bottom of the tube and acted as a seed. Presumably the same technique could be used with the spectroscopic samples. A second possibility is that the extra origins observed in spectrum V are photoproducts that were produced when spectrum IV was being obtained. This is unlikely, because the extra origins produced appear in spectrum I and II which were exposed to light only once.

Furthermore, it is important to realize that some of the bands listed in Table 32 may be vibronic bands rather than origins. Most likely the band occurring at 3733.0 Å corresponds to ν_{6b}(616 cm^{-1}) built upon the origin at 3648.0 Å. The best evidence for this is that the 3757.5 Å band also corresponds to ν_{6b} built on 3672.0 Å. The only reason these bands (3733.0 and 3757.5 Å) are included in the table is that they are extremely strong for a vibronic band (150% as intense as the origin). The "best" spectra to consider in detail are III and IV because III has only two origins of significant intensity and IV has only one. The presence of intense, multiple origins greatly complicates the assignments of fundamentals and combintion bands.

The band systems built upon the two origins in spectrum III are identical. That is, the same frequencies and intensity pattern occur in both systems. Benzoic acid and methyl benzoate have similar triplet energy levels and too similar vibrational frequencies to make an obvious decision whether emission is coming from methyl benzoate or benzoic acid molecules.

We assume that the emission is coming from guest-induced defects that consist of methyl benzoate-benzoic acid complexes. If we neglect the intense ν_{6b} vibration, the frequencies and intensity pattern of spectrum VI closely resembles that of spectrum IV. Since the vibrational frequencies for parafluorobenzoic acid are markedly different from those of methyl benzoate, it is certain that the emission is not from parafluorobenzoic acid in spectrum IV. We thus regard it as likely that the emission observed in spectrum III comes from methyl benzoate molecules (complexed with benzoic acid molecules). Definitive proof of this fact will have to await further experimental investigation.

The most striking feature of this spectrum (III) is the weakness of the out-of-plane modes. The intensity of $\nu_{10b}(-)$ is about 25% of the origin intensity whereas for methyl benzoate in benzene its intensity is comparable to that of the origin. The other out-of-plane modes are about 10% (or less) as intense as the origin. It thus appears that the out-of-plane modes in methyl benzoate have the same environmental dependency as those in benzoic acid. As discussed previously, for benzoic acid the hydrogen bonding environment seems to be the parameter which has the greatest effect on the intensity of the out-of-plane modes. The same is probably true for methyl benzoate since it is very likely that the complex is held together by a hydrogen bond. The strong in-plane modes in spectrum IV are ν_{12} and ν_{8a} and their intensities relative to the origin are the same as for methyl benzoate in benzene.

As for spectrum III, a striking feature of spectrum IV is the weakness of the out-of-plane modes. In this spectrum, these modes are slightly less intense than in spectrum III. Since there is no uncertainty about the emitting species in this case, this spectrum constitutes better evidence that the out-of-plane modes in methyl benzoate possess the same environmental sensitivity as those in benzoic acid.

Another striking feature of spectrum IV is the presence of a band at 619 cm^{-1} (ν_{6b}) which is as intense than the origin. This band is definitely not an origin associated with a different site or an impurity origin. It combines with ν_{8a}, the next strongest band in the spectrum. This combination band (strong and broad) appears at 2220 cm^{-1} (1600 + 619 = 2219). The intensity of this band is greater than all other fundamentals, even ν_{12}. It therefore cannot be a combination of any of these weaker bands. The band at 2220 cm^{-1} can not be accounted for except as the above combination. We regard this a good evidence that the band at 619 cm^{-1} is a vibronic band. Two and three quanta are unequivocally absent in the spectrum.

The presence of an intense ν_{6b} band can also be found in spectra I and II. In both cases, the vibration is built upon the origin at 3648.0 Å. Since the intense ν_{6b} band appears when either benzoic acid or parafluorobenzoic acid is used as a guest, it might appear at first sight that the defect or trap responsible for the emission is a natural defect rather than a guest-induced defect. This possibility is made improbable by the fact that the origin for the benzoic acid system is at 3648.0 Å while that for the parafluorobenzoic acid system is at 3672.0 Å.

The intensities of the strong in plane modes ν_{8a} and ν_{12} in Spectrum IV resemble those of spectrum III.

The data presented here for benzoic acid and parafluorobenzoic acid in methyl benzoate must be regarded as preliminary and tentative on account of the difficulties encountered in obtaining reproducible spectra.

FIGURE 26

Phosphorescence Spectrum of Benzoic Acid d_o in Polycrystalline Benzene

Spex 1702 3/4 Meter Monochromator

Concentration	:	∿ 10^{-3} molar
Slit Width	:	75 μ, 75 μ
Sensitivity	:	$3x10^{-7}$ amperes full scale
Time Constant	:	0.3 seconds
Scan Rate	:	20 Å/minute
Temperature	:	4.2 °K

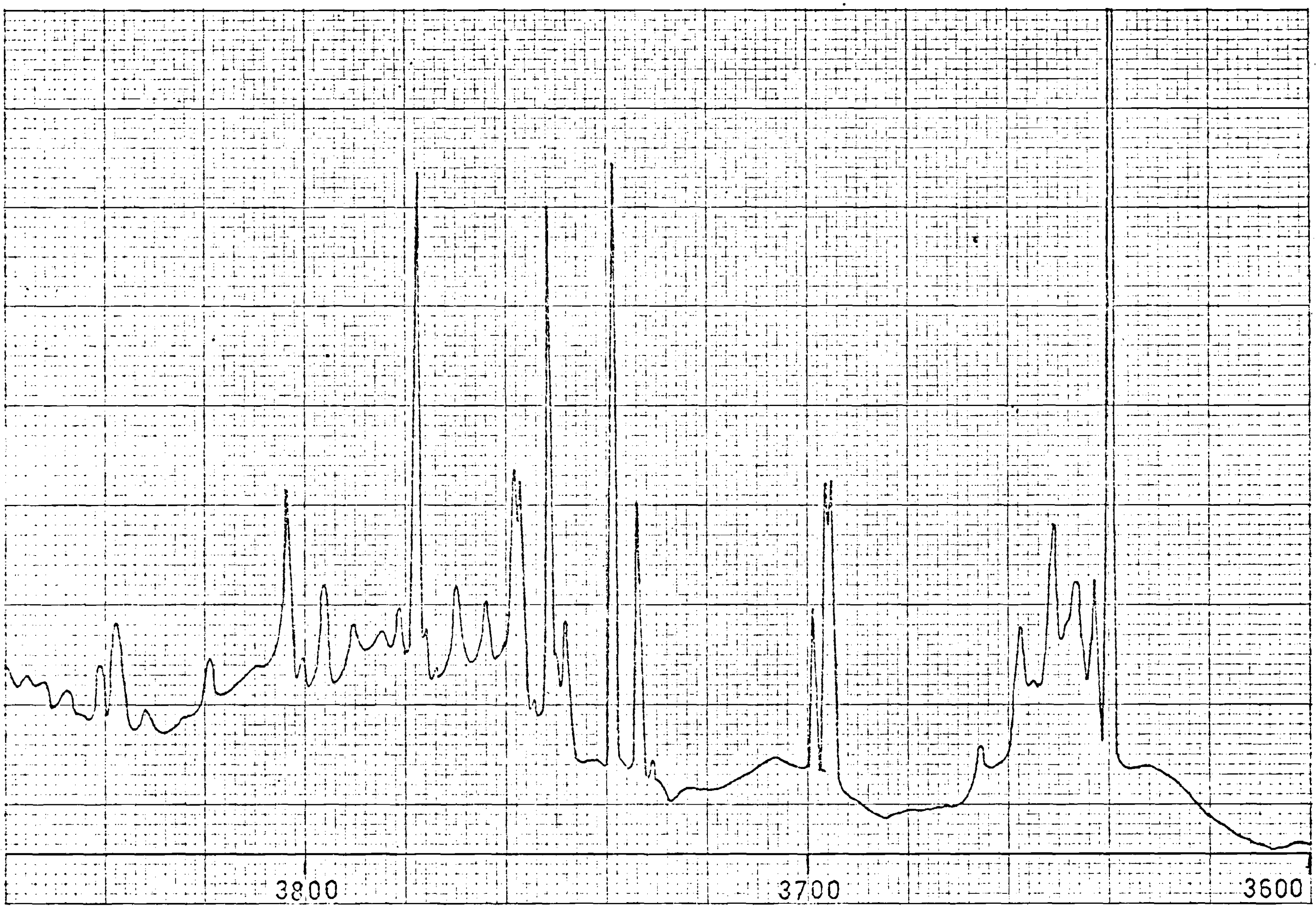
3800
3700
3600

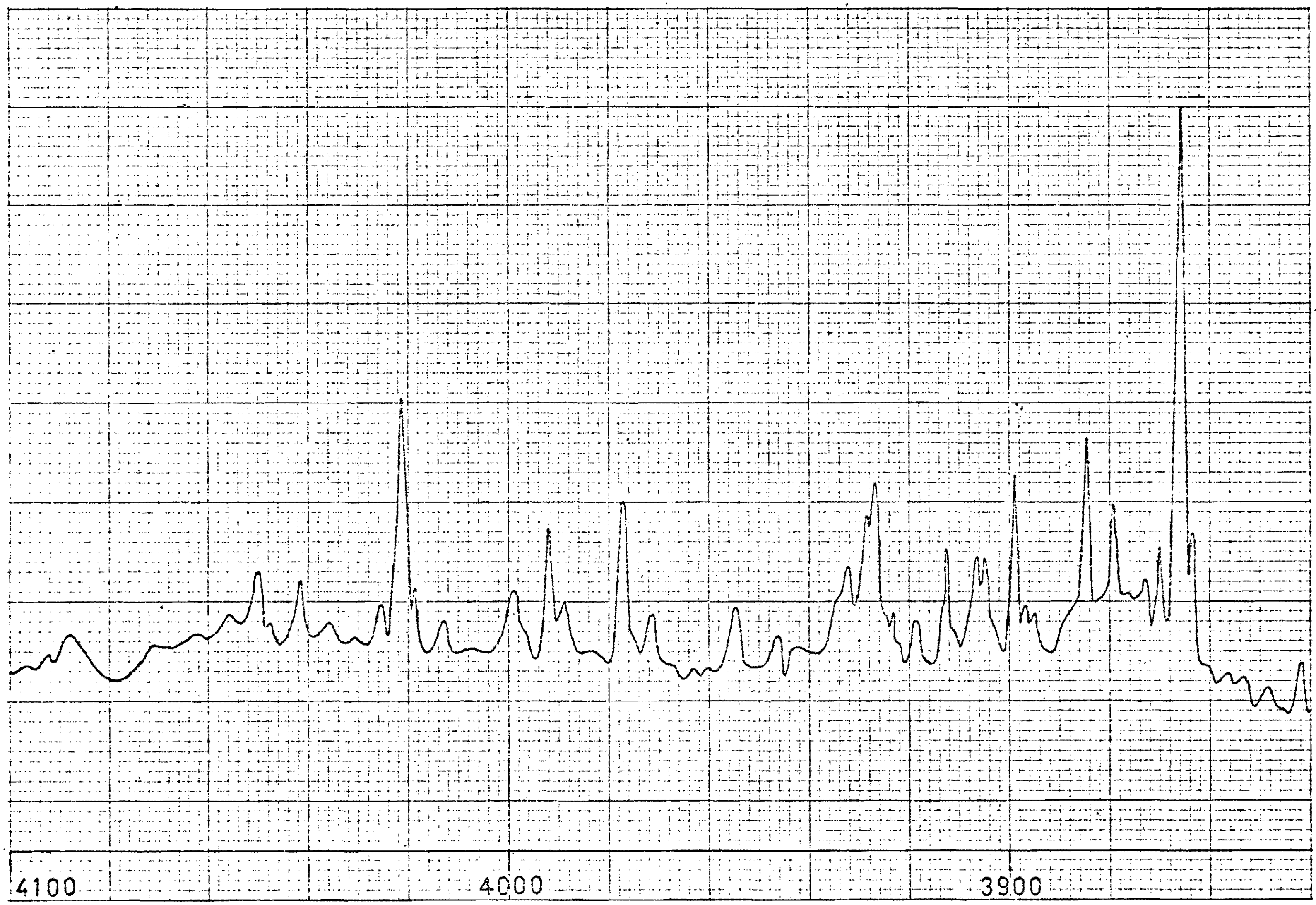
4100
4000
3900

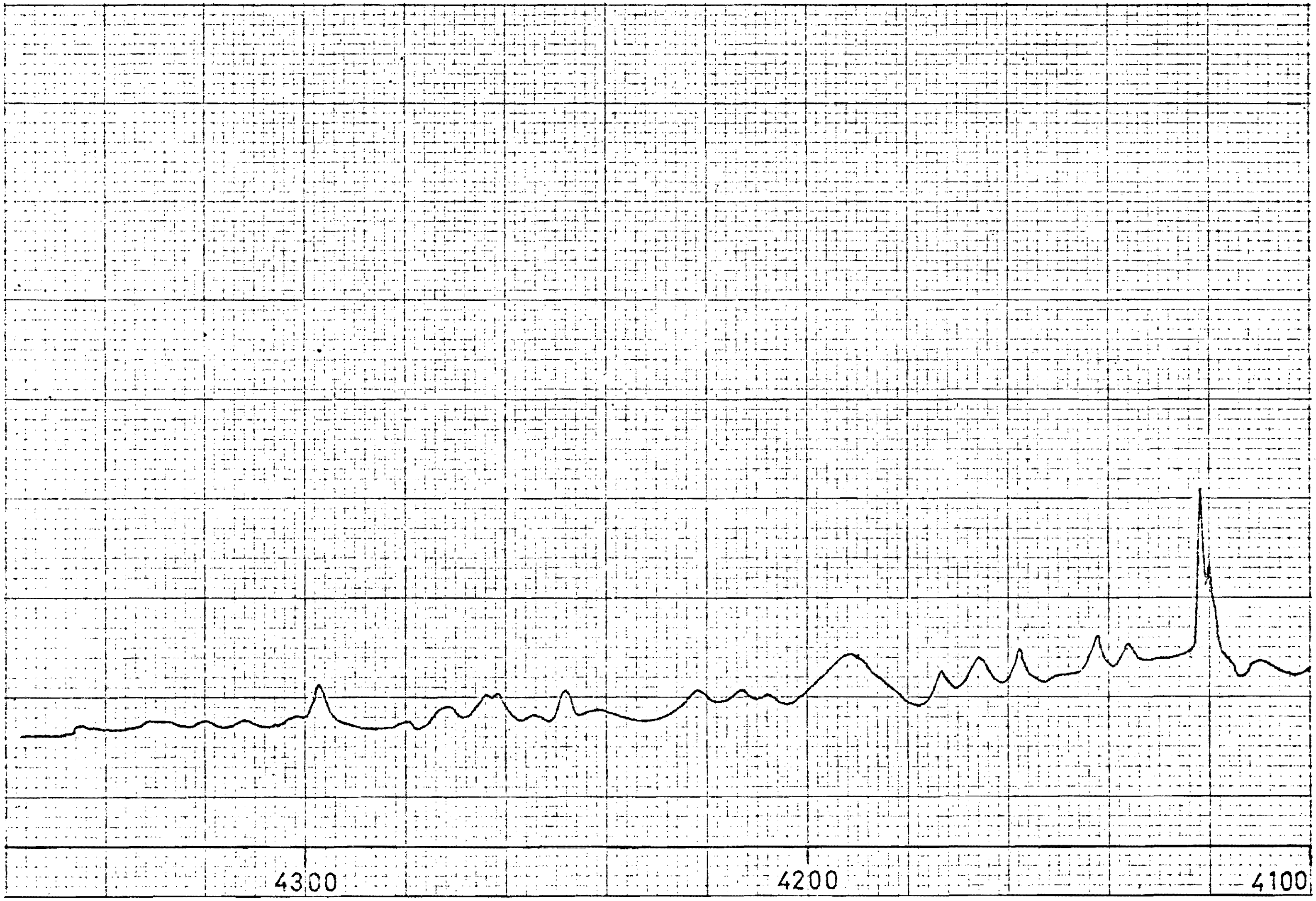
4300
4200
4100

TABLE 18

This table contains the frequencies, relative intensities and assignments of bands in the spectrum shown in Figure 26. The assignments are based upon a consideration of the photoelectric spectra obtained in this study, as well as Baum's more accurate photographic data. Only the most probable assignments are given. For some bands, particularly combination bands, alternate assignments are possible. Average frequencies are given for Raman factor group pairs and all Raman frequencies are rounded off to the nearest wavenumber. Actual Raman frequencies are given only for fundamentals. For combination bands sums of phosphorescence frequencies are given - s = strong, w = weak, and vw = very weak.

λ(Å)	ν(cm^{-1})	$\Delta\nu$(cm^{-1})	Intensity	Assignment	Raman Freq.(cm^{-1})	Deviation (cm^{-1})
3639.5	27469	0	s	origin		
3643.0	27442	27	w	lattice (or side)		
3646.5	27416	53	w	lattice		
3651.0	27382	87	m	H-bond		
3655.0	27352	117	vw	Monomer torsion	119	2
3657.5	27333	136	w	H-bond		
3666.0	27270	199	w	$\nu_{10b}(+)$	198	1
3695.5	27052	417	m	ν_{16a}	408	9
3696.5	27045	424	m	ν_{6a}	422	2
3699.0	27027	449	m	ν_{16b}	438	11
3730.5	26798	671	w	$\nu_{9b}(-)$	659	12
3734.0	26773	696	m	ν_4	686	10
3738.0	26745	724	s	ν_{11}	710	14
3748.5	26670	799	w	ν_1	797	2
3752.0	26645	824	s	$\nu_{10b}(-)$	812	12
3758.0	26602	867	m	$\nu_{10a}(-)$	855	12
3758.5	26599	870	m	+ ν_{10b} lattice	865	5
3764.5	26556	913	w	H-wag	910	3
3770.5	26514	955	w	ν_{17b}	942	13
3776.5	26472	997	w	ν_5	989	8
3778.0	26462	1007	s	ν_{12}	1001	6
3782.0	26434	1035	w	ν_{18a}	1028	7
3785.0	26413	1056	vw	ν_{12} + lattice	1060	4
3791.0	26371	1098	vw	ν_{12} + H-bond	1094	4

Table 18 (Continued)

3797.0	26329	1140	w	ν_{13}	1134	6
3801.0	26301	1168	vw	ν_{15}	1170	2
3804.5	26277	1192	m	ν_{9a}	1185	7
3820.0	26171	1298	w	C-O stretch + O-H bend	1292	6
3833.0	26082	1387	vw	$\nu_{9a} + \nu_{10b}(+)$	1391	4
3839.0	26041	1428	w	$\nu_{12} + \nu_{6a}$	1431	3
3842.0	26020	1449	w	ν_{19b}	1446	3
3849.0	25973	1496	vw	ν_{19a}	1495	1
3853.0	25946	1523	vw	$\nu_{11a}+\nu_{1}$	1523	0
3857.0	25920	1549	vw	$\nu_{16} + \nu_{13}$	1547	2
3863.5	25876	1593	w	ν_{8b}	1582	11
3866.0	25859	1610	s	ν_{8a}	1600	10
3870.0	25832	1637	w	C=O stretch	1631	6
3873.0	25812	1657	w	ν_{8a} + lattice	1663	6
3879.5	2576	1700	w	$\nu_{12} + \nu_{4}$	1703	3
3884.5	25736	1733	m	$\nu_{12} + \nu_{11}$	1731	2
3895.0	25667	1802	vw	$\nu_{12} + \nu_{1}$	1806	4
3899.0	25640	1829	m	$\nu_{12} + \nu_{10b}(-)$	1831	2
3905.0	25601	1868	w	$\nu_{12} + \nu_{10a}$	1874	6
3906.5	25591	1878	w	$\nu_{9a} + \nu_{4}$	1888	10
3912.5	25552	1917	w	ν_{12} + H-wag	1920	3
3919.0	25506	1963	w	$\nu_{12} + \nu_{17b}$	1962	1
3927.0	25,458	2011	m	$2\nu_{12}$	2014	3
3929.0	25,445	2024	m	$\nu_{8a} + \nu_{6a}$	2034	10
3932.0	25,425	2044	w	$\nu_{8a} + \nu_{6b}$	2059	15
3946.5	25,332	2137	w	$\nu_{12} + \nu_{13}$	2034	3
3955.0	25,277	2192	w	$\nu_{12} + \nu_{9a}$	2199	7
3971.5	25,172	2297	W	$\nu_{8a} + \nu_{4}$	2306	9
3977.5	25,134	2335	m	$\nu_{8a} + \nu_{11}$	2334	1
3989.0	25,062	2407	w	$\nu_{8a} + \nu_{1}$	2409	2
3992.0	25,040	2429	w	$\nu_{8a} + \nu_{10b}(-)$	2434	5

3999.5	24,996	2473	w	$\nu_{8a}+\nu_{10a}$	2477	4
4013.5	24,909	2560	w	$\nu_{8a}+\nu_{17b}$	2565	5
4019.0	24,875	2594	w	$\nu_{12}+\nu_{8b}$	2600	6
4022.0	24,856	2613	m	$\nu_{12}+\nu_{8a}$	2617	4
4026.0	24,832	2637	w	$\nu_{8a}+\nu_{18a}$	2645	8
4036.5	24,767	2702	w	$2\nu_{12}+\nu_{4}$	2710	8
4042.0	24,733	2736	w	$2\nu_{12}+\nu_{11}$	2738	2
4051.0	24,678	2791	w	$\nu_{8a}+\nu_{9a}$	2799	8
4057.0	24,642	2827	vw	$2\nu_{12}+\nu_{10b}(-)$	2826	1
4072.5	2 ,548	2921	vw	$\nu_{12}+\nu_{11}+\nu_{9a}$	2920	1
4089.0	2 ,449	3020	w	$3x\nu_{12}$	3021	1
4111.0	24,318	3151	vw	$\nu_{8a}+\nu_{11}+\nu_{10b}(-)$	3158	7
4120.0	24,265	3204	vw	$\nu_{8a}+\nu_{8b}$	3203	1
4122.0	24,253	3216	m	$2\nu_{8a}$	3220	4
4136.0	24,171	3298	vw	$2\nu_{8a}$ + H-bond	3307	9
4142.0	24,136	3333	vw	$\nu_{12}+\nu_{8a}+\nu_{11}$	3341	8
4158.0	24,043	3426	vw	$\nu_{12}+\nu_{8a}+\nu_{1}$	3416	10
4166.0	23,997	3472	vw	$\nu_{12}+\nu_{10a}+\nu_{8a}$	3484	12
4173.5	23,954	3515	vw	$\nu_{8a}+\nu_{9a}+\nu_{11}$	3526	11
4191.0	23,854	3615	w	$2\nu_{12}+\nu_{8a}$	3624	9
4222.0	23,679	3790	vw	$\nu_{12}+\nu_{8a}+\nu_{9a}$	3802	12
4248.5	23,531	3938	vw	$2\nu_{8a}+\nu_{11}$	3944	6
4264.5	23,443	4020	vw	$4\nu_{12}$	4028	8
4298.0	23,260	4209	w	$2\nu_{8a}+\nu_{12}$	4227	18
4412.0	22,659	4810	vw	$3\nu_{8a}$	4830	20

FIGURE 27

Phosphorescence Spectrum of Benzoic Acid $4d_1$ in Polycrystalline Benzene

Spex 1702 3/4 Meter Czerny Turner Monochromator

Concentration : $\sim 10^{-3}$ molar
Slit Width : 44 μ, 44 μ
Sensitivity : 3×10^{-8} amperes full scale
Time Constant : 1.0 second
Scan Rate : 20 Å/minute
Temperature : 4.2° K

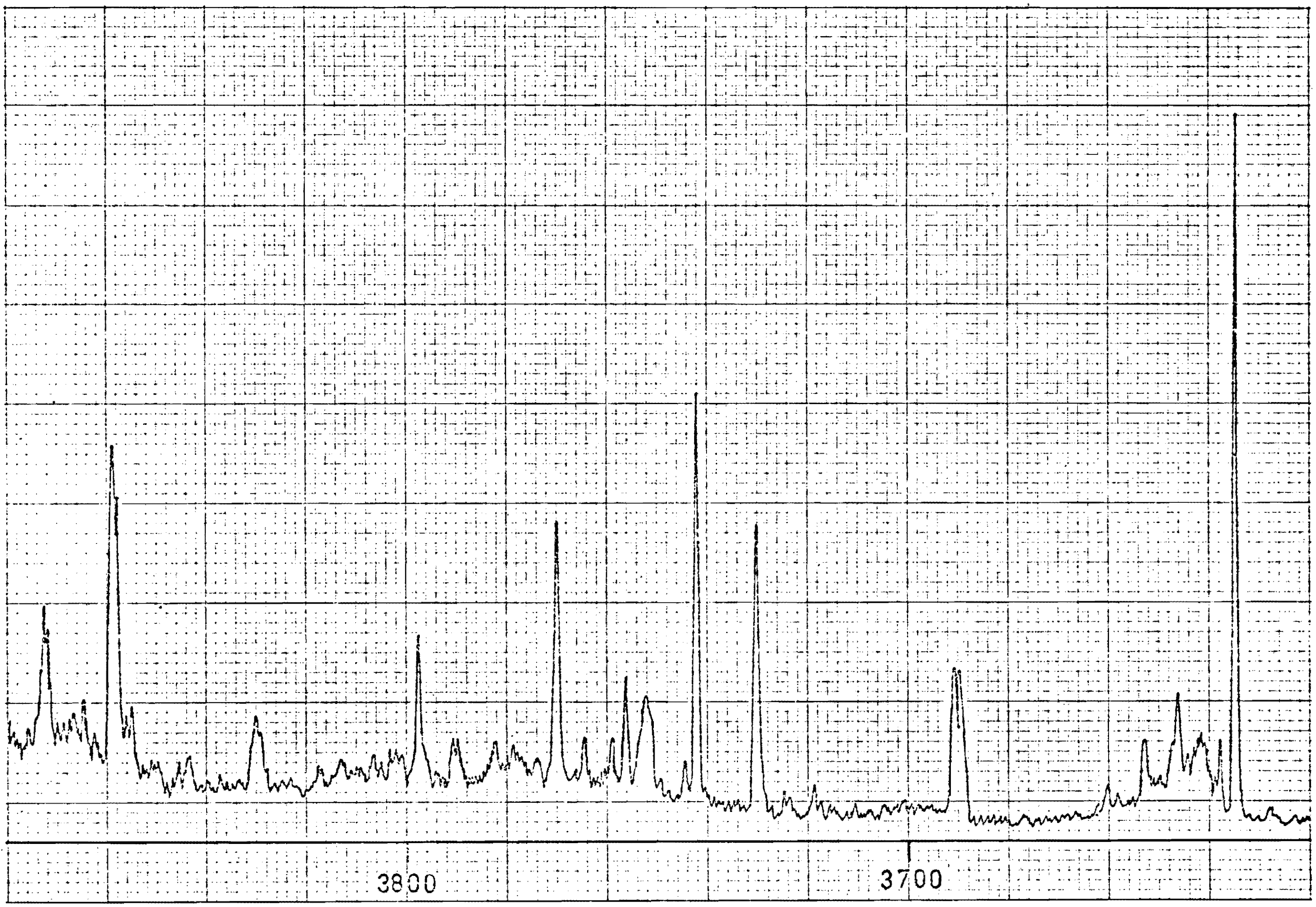
3800
3700

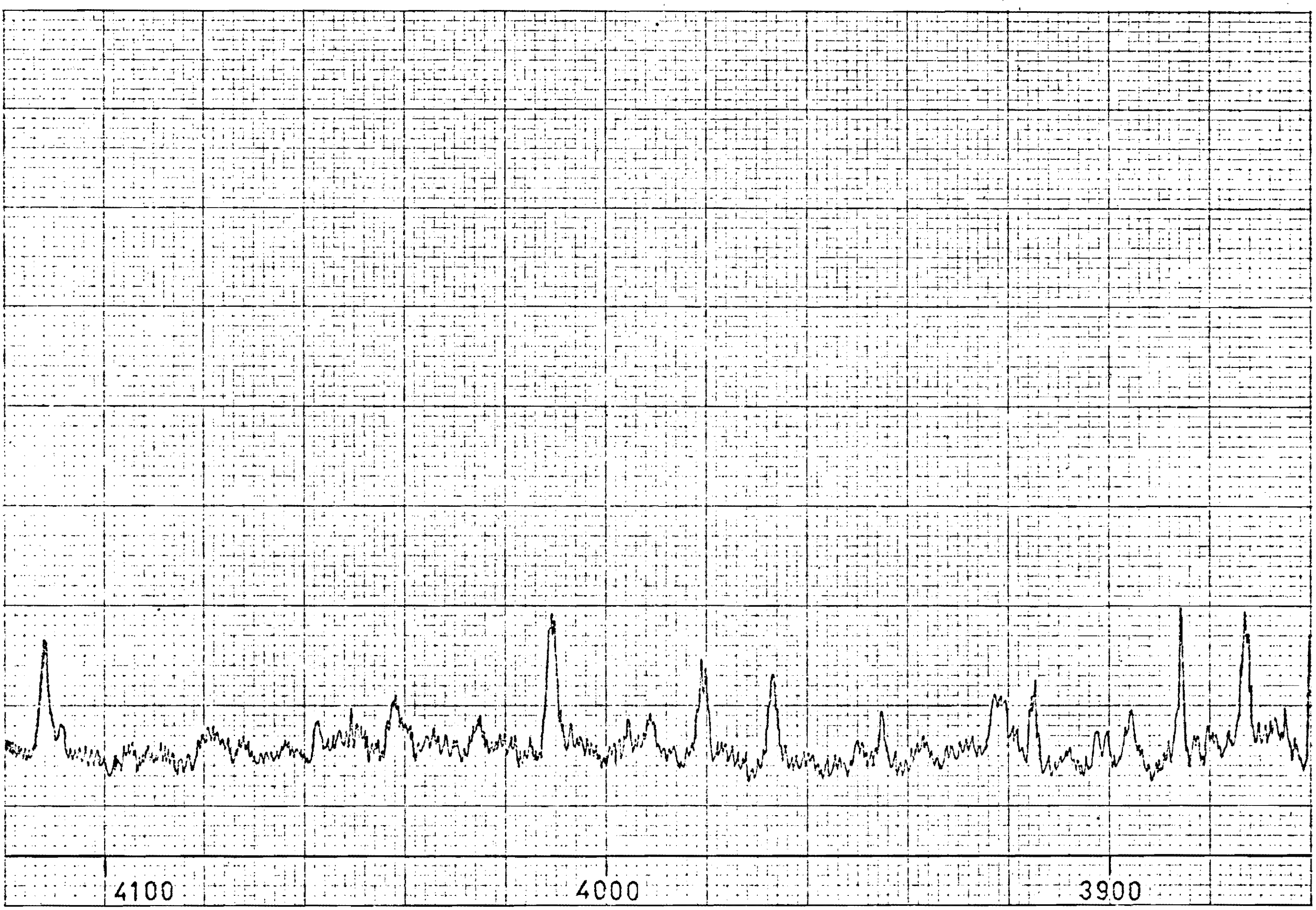
4100
4000
3900

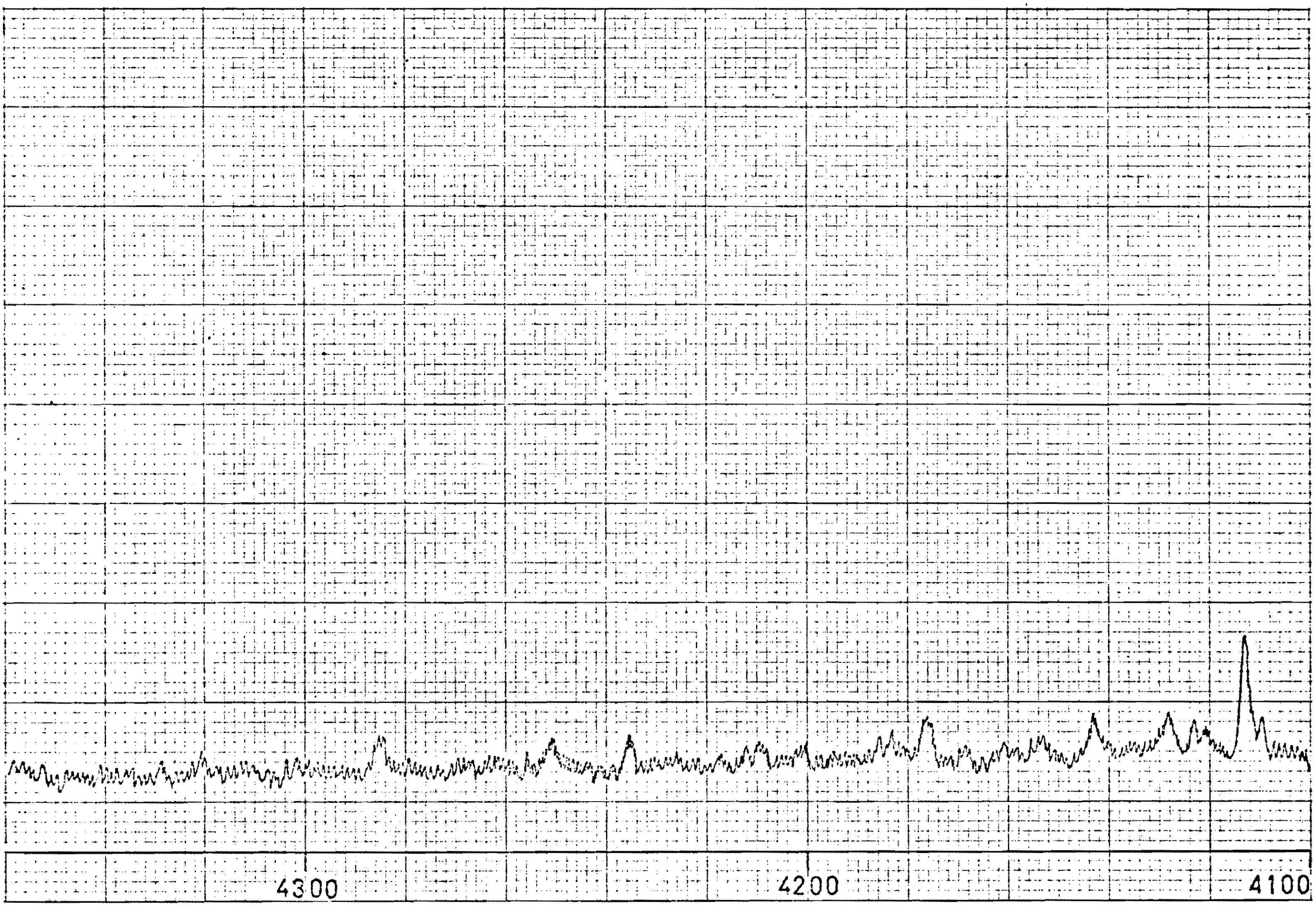
4300
4200
4100

TABLE 19

This table contains the frequencies, relative intensities, and assignments of bands in the spectrum shown in Figure 27. The assignments are based upon a consideration of the photoelectric spectra obtained in this study, as well as Baum's more accurate photographic data. Only the most probable assignments are given. For some bands, particularly combination bands, alternate assignments are possible. Average frequencies are given for Raman factor group pairs and all Raman frequencies are rounded off to the nearest wavenumber. Actual Raman frequencies are given only for fundamentals. For combination bands sums of phosphorescence frequencies are given. s = strong, w = weak, and vw = very weak.

λ(Å)	ν (cm^{-1})	Δν (cm^{-1})	Intensity	Assignment	Raman Freq. (cm^{-1})	Deviation (cm^{-1})
3645.5	27506	0	s	Origin	0	
3637.5	27484	22	w	site (or lattice)		
3641.5	27453	53	w	lattice		
3646.0	27420	86	m	H-bond		
3647.5	27408	98	vw	H-bond		
3650.5	27386	120	w	monomer torsion	119	1
3653.0	27367	139	vw	H-bond		
3660.5	27311	195	vw	$10b^{(+)}$	192	3
3690.5	27089	417	m	ν_{6a}&ν_{16a}	408 & 419	9 & 2
3691.5	27082	424	m	ν_{16b}	425	1
3719.0	26881	625	w	ν_4	618	7
3724.5	26842	664	w	$\nu_{9b}^{(-)}$	657	7
3730.0	26802	704	s	ν_{11}	698	6
3742.0	26716	790	s	$\nu_{10b}^{(-)}$	788	2
3745.0	26695	811	w	site+$\nu_{10b}^{(-)}$	812	1
3750.0	26659	847	vw	ν_{11}+H-bond	843	4
3751.7	26641	865	m	ν_{10a}	853	12
3756.5	26613	893	m	ν_{17b}	872	21
3759.0	26595	911	w	H-wag	912	1
3765.0	26553	953	w	ν_{10a}+H-bond	951	2
3770.0	26518	988	s	ν_{12}	984	4
3774.5	26486	1020	w	site+ν_{12}	1010	10
3779.5	26455	1051	w	ν_{12}+lattice	1041	10
3783.0	26427	1079	w	ν_{12}+H-bond	1074	5
3791.0	26371	1135	w	ν_{13}	1137	2

Table 19 (Continued)

3798.5	26319	1187	m	ν_{9a}	1182	5
3829.0	26109	1397	m	$\nu_{12}+\nu_{16a}$	1405	8
3830.5	26099	1407	m	$\nu_{12}+\nu_{6a}$	1405	2
3844.0	26007	1499	w	ν_{19a}	1488	1
3851.0	25960	1546	w	$\nu_{13}+\nu_{16a}$	1552	6
3856.5	25923	1583	w	$\nu_{9a}+\nu_{16a}$	1604	21
3858.5	25909	1597	s	ν_{8a}	1597	0
3863.5	25876	1630	vw	C=0 stretch	1627	3
3873.0	25812	1694	m	$\nu_{12}+\nu_{11}$	1692	2
3883.5	25743	1763	vw	$\nu_{13}+\nu_{4}$	1760	3
3885.5	25729	1777	m	$\nu_{12}+\nu_{10b}(-)$	1776	1
3896.0	25660	1840	m	$\nu_{12}+\nu_{10a}$	1853	13
3901.0	25627	1879	m	$\nu_{12}+\nu_{17b}$	1881	2
3902.5	25617	1889	w	$\nu_{9a}+\nu_{11}$	1891	2
3908.5	25578	1928	w	$\nu_{10b}(-)+\nu_{13}$	1923	5
3915.5	25532	1974	m	$2\nu_{12}$	1976	2
3922.0	25490	2016	m	$\nu_{8a}+\nu_{16a}$	2014	2
3929.0	25445	2061	vw	$2\nu_{12}$+H-bond	2062	1
3931.5	25428	2078	vw	$\nu_{9a}+\nu_{17b}$	2080	2
3936.0	25399	2107	vw	$2\nu_{12}$+H-bond	2115	8
3938.0	25386	2120	vw	$\nu_{12}+\nu_{13}$	2123	3
3945.5	25339	2167	m	$\nu_{12}+\nu_{9a}$	2175	8
3950.0	25309	2197	vw	$\nu_{12}+\nu_{10b}(-)+\nu_{6a}$	2193	4
3960.0	25245	2261	vw	$\nu_{8a}+\nu_{9b}(-)$	2261	0
3967.0	25201	2305	m	$\nu_{8a}+\nu_{11}$	2301	4
3981.0	25112	2394	m	$\nu_{8a}+\nu_{10b}(-)$	2387	7
3991.5	25046	2460	vw	$\nu_{8a}+\nu_{10a}$	2462	2
3996.0	25018	2488	vw	$\nu_{12}+\nu_{11}+\nu_{10b}(-)$	2482	6
4010.5	24928	2578	m	$\nu_{12}+\nu_{8a}$	2585	7
4015.5	24896	2610	vw	ν_{12}+C=0 stretch	2618	8

Table 19 (Continued)

4019.0	24875	2631	vw	$\nu_{12}+\nu_{8a}$ + lattice	2638	7
4026.0	25832	2674	w	$2\nu_{12}+\nu_{11}$	2680	6
4035.0	24776	2730	w	$\nu_{8a}+\nu_{11}+\nu_{6a}$	2718	12
4040.0	24746	2760	vw	$2\nu_{12}+\nu_{10b}(-)$	2766	6
4043.0	24727	2779	w	$\nu_{8a}+\nu_{9a}$	2784	5
4050.5	24681	2825	vw	$\nu_{12}+\nu_{13}+\nu_{11}$	2827	2
4058.0	24636	2870	vw	$\nu_{12}+\nu_{9a}+\nu_{11}$	2879	9
4073.0	24542	2964	vw	$3\nu_{12}$	2964	0
4080.0	24503	3003	vw	$\nu_{12}+\nu_{8a}+\nu_{16b}$ or $\nu_{12}+\nu_{8a}+\nu_{6a}$	3002	1
4096.0	24407	3099	vw	$\nu_{8a}+\nu_{11}+\nu_{10b}(-)$	3091	8
4104.0	24360	3146	vw	$2\nu_{12}+\nu_{9a}$	3163	17
4112.5	24309	3197	m	$2\nu_{8a}$	3194	3
4120.0	24265	3241	vw	$2\nu_{8a}$+lattice	3247	6
4127.0	24221	3285	w	$\nu_{12}+\nu_{8a}+\nu_{11}$	3289	4
4143.0	24127	3379	w	$\nu_{12}+\nu_{8a}+\nu_{10b}(-)$	3375	4
4153.5	24069	3437	w	$\nu_{8a}+\nu_{13}+\nu_{11}$	3436	1
4161.0	24026	3480	w	$\nu_{12}+\nu_{8a}+\nu_{17b}$	3478	2
4176.0	23937	3569	w	$2\nu_{12}+\nu_{8a}$	3573	4
4185.0	23888	3618	vw	$2\nu_{8a}+\nu_{16a}$	3611	7
4202.0	23792	3714	w	$\nu_{12}+\nu_{8a}+\nu_{13}$	3720	6
4210.0	23746	3760	w	$\nu_{12}+\nu_{8a}+\nu_{9a}$	3772	12
4234.5	23609	3897	w	$2\nu_{8a}+\nu_{11}$	3898	1
4251.0	23517	3989	w	$2\nu_{8a}+\nu_{10b}(-)$	3984	5
4285.5	23328	4178	m	$2\nu_{8a}+\nu_{12}$	4182	4
4320.0	23142	4364	vw	$2\nu_{8a}+\nu_{9a}$	4381	17
4360.0	22929	4577	w	$2\nu_{8a}+\nu_{12}+\nu_{16a}$	4599	22
4402.0	22711	4795	vw	$3\nu_{8a}$	4791	4

FIGURE 28

Phosphorescence Spectrum of Benzoic Acid d_5 in Polycrystalline Benzene

Spex 1702 3/4 Meter Czerny Turner Monochromator

Concentration: $\sim 10^{-3}$ molar

Slit Width : 30 μ, 30 μ

Sensitivity : 1×10^{-7} amperes full scale

Time constant: 1.0 second

Scan Rate : 20 Å/minute

Temperature : 4.2° K

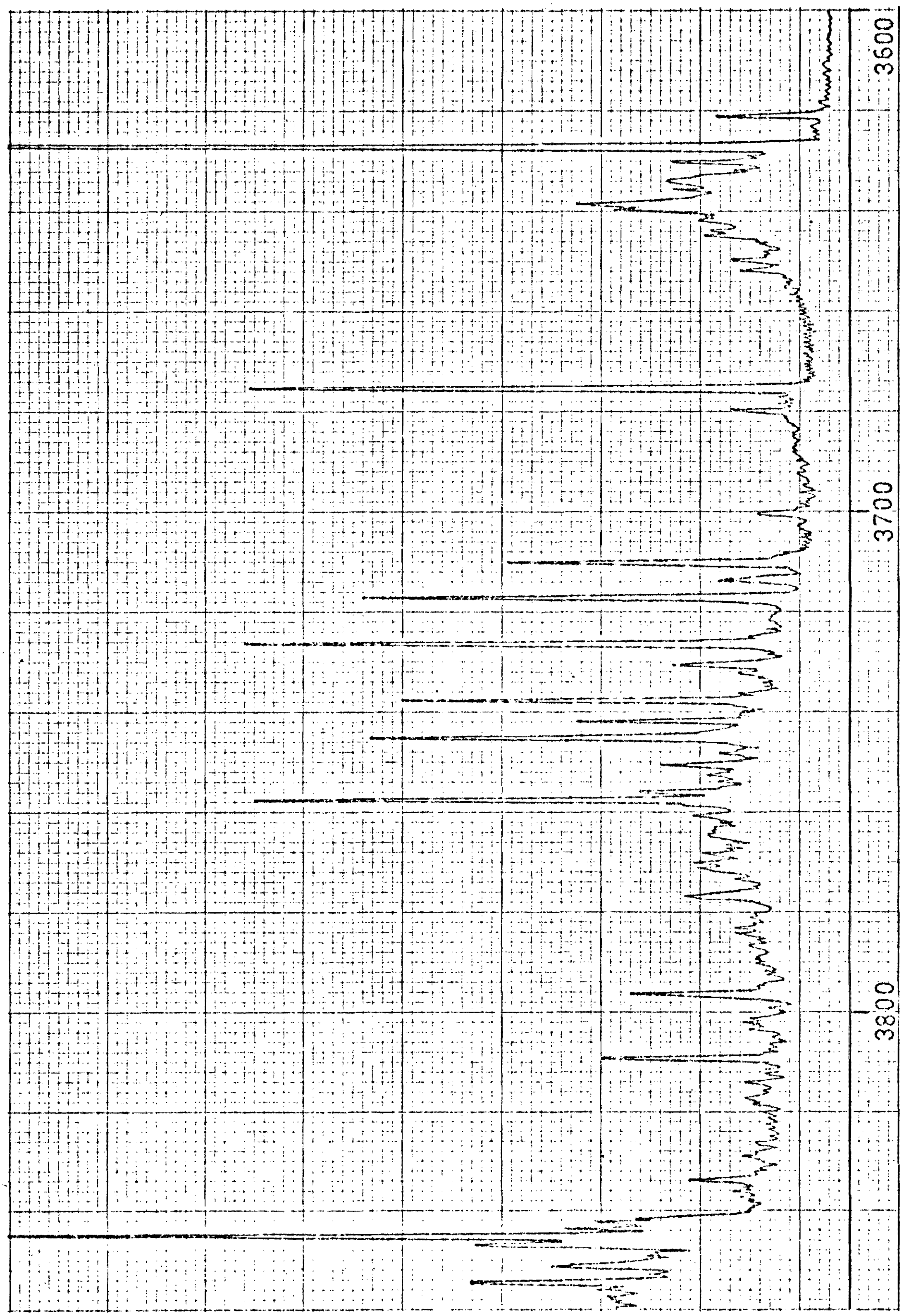
3600
3700
3800

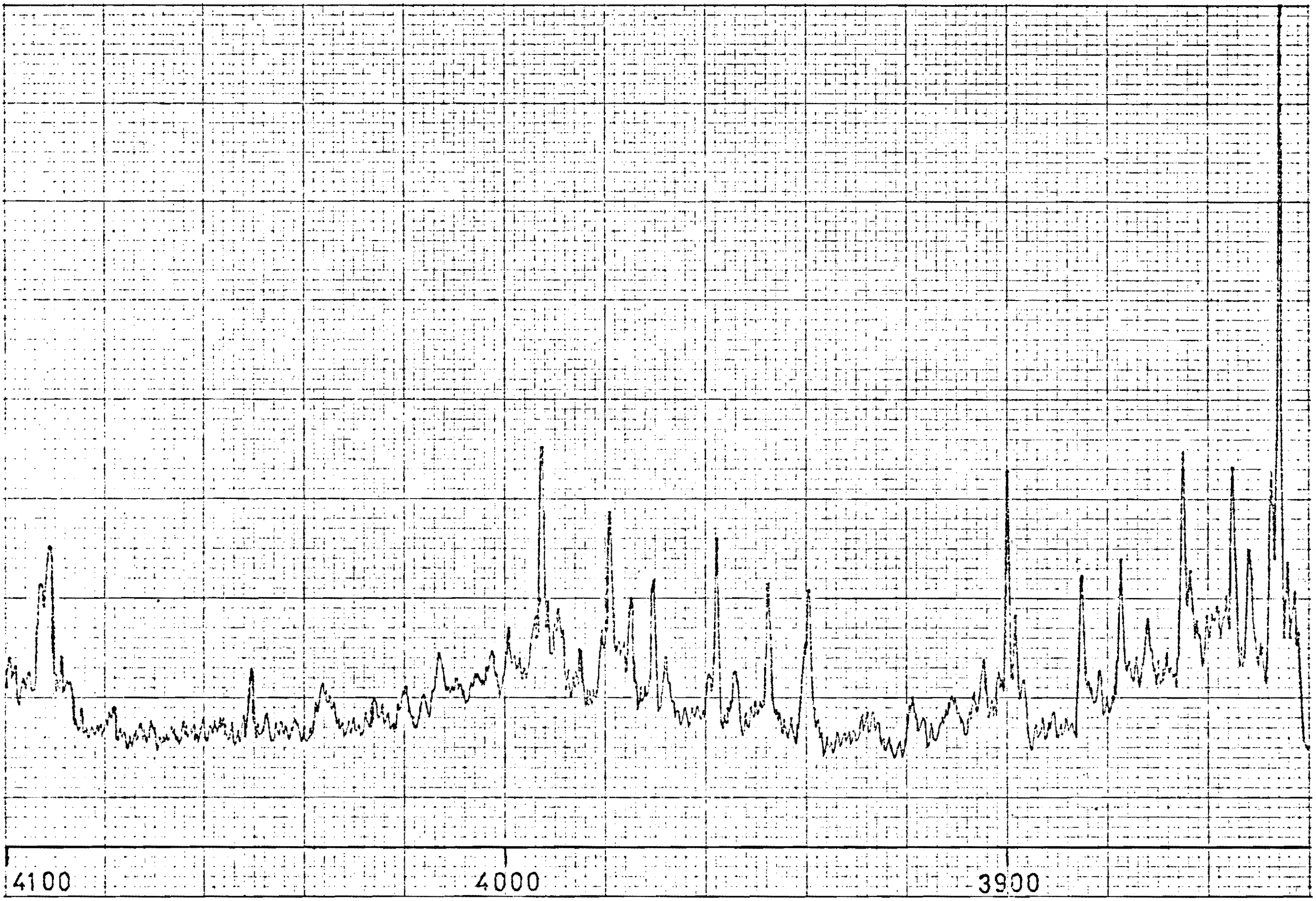
4100
4000
3900

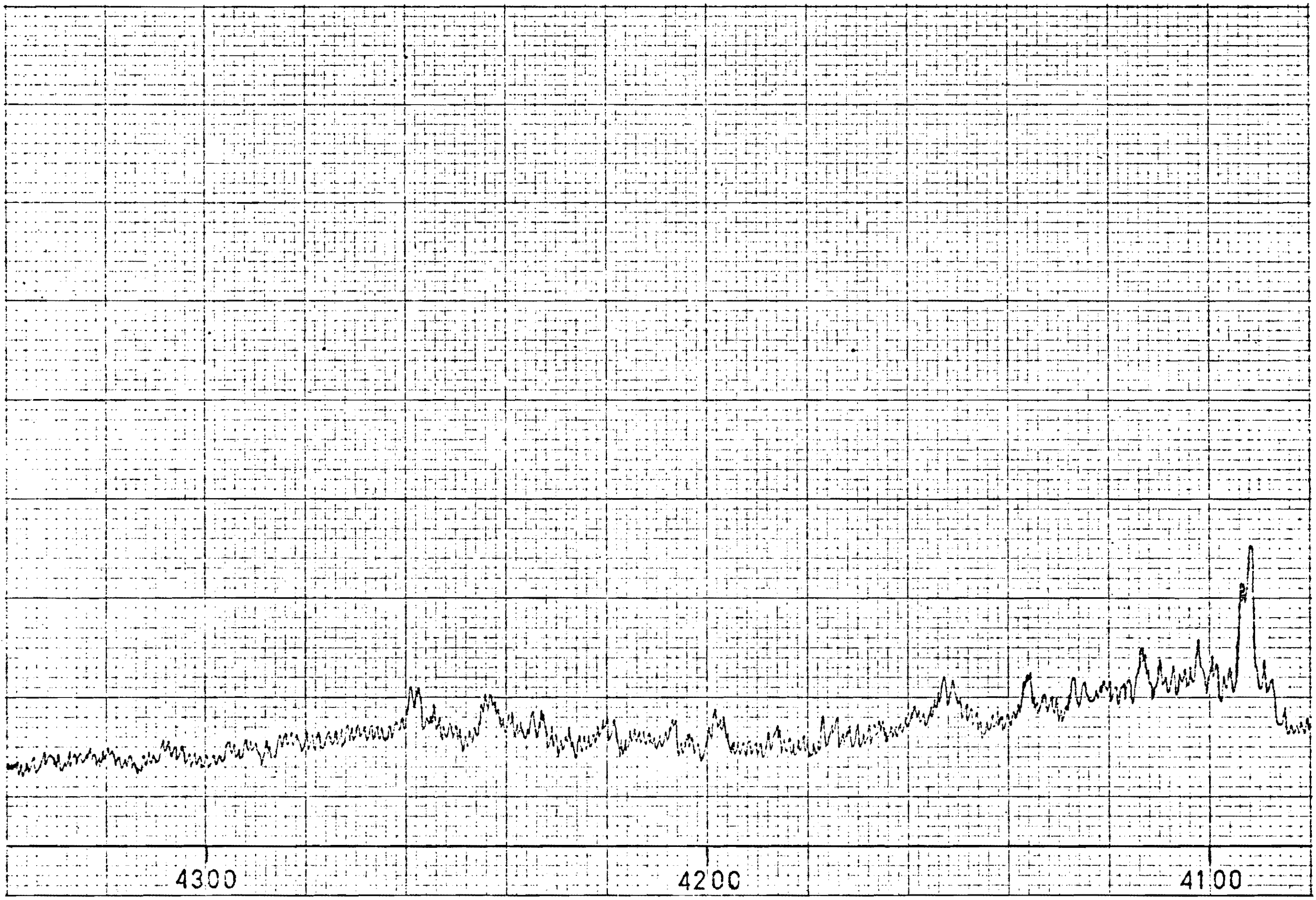
4300
4200
4100

TABLE 20

This table contains the frequencies, relative intensities, and assignments of bands in the spectrum shown in Figure 28. The assignments are based upon a consideration of the photoelectric spectra obtained in this study, as well as Baum's more accurate photographic data. Assignments of most d_5 Raman and infrared bands are uncertain. Only those assignments which are considered firm or highly probable are given. Since most fundamentals are unassigned assignments of combination bands has not been attempted. Average frequencies are given for Raman factor group pairs and all Raman frequencies are rounded off to the nearest wavenumber. s = strong, w = weak, and vw = very weak.

λ(Å)	ν(cm^{-1})	$\Delta\nu$(cm^{-1})	Intensity	Assignment	Raman Freq.(cm^{-1})	Dev.(cm^{-1})
3621.0	27609	-42	w	site		
3626.5	27567	0	s	origin		
3630.0	27540	27	w	site(or lattice)		
3633.5	27514	53	w	lattice		
3635.5	27499	68	vw	lattice		
3638.5	27476	91	m	H-bond		
3639.5	27469	98	vw	H-bond		
3641.5	27453	114	vw	monomer torsion	119	5
3644.5	27431	136	vw	H-bond		
3649.5	27393	174	vw			
3652.0	27374	193	vw	$\nu_{10b}(+)$	118	5
3675.0	27203	364	s	ν_{16a}	356	8
3680.0	27166	401	w	ν_{16b} & ν_{6a}	394 & 415	7 & 14
3700.5	27016	551	vw			
3710.5	26943	624	s			
3714.0	26918	649	w			
3717.0	26896	671	s			
3726.5	26827	740	s			
3731.0	26795	772		ν_1	767	5
3738.0	26745	822	s			
3742.0	26716	851	m			
3745.5	26691	876	s			
3748.5	26670	897	w			
3751.0	26652	915	w	H-wag	913	2
3756.5	26613	954	w			
3757.5	26606	961	s	ν_{12}	958	3
3761.0	26581	986	vw			
3765.0	26553	1014	vw			
3770.0	26514	1053	vw			
3777.0	26469	1098	w			
3797.0	26329	1238	m			
3802.5	26291	1276	vw			

(Table 20 Continued)

3809.5	26243	1324	m			
3814.0	26212	1355	vw			
3818.0	26184	1383	vw			
3829.5	26106	1461	vw			
3834.5	26072	1495	w			
3842.5	26017	1550	w			
3844.0	26007	1560	w			
3845.0	26000	1567	s	ν_{8a}	1569	2
3847.5	25984	1583	m			
3851.5	25957	1610	w			
3855.5	25933	1634	m	C=0 stretch	1625	9
3863.5	25876	1691	vw			
3864.5	25869	1698	m			
3872.0	25819	1748	vw			
3877.0	25786	1781	w			
3881.5	25756	1811	vw			
3885.0	25733	1834	w			
3896.5	25657	1910	vw			
3898.5	25644	1923	w			
3900.0	25634	1933	m			
3901.5	25624	1943	vw			
3904.5	25604	1963	vw			
3911.0	25562	2005	vw			
3919.0	25510	2057	vw			
3928.0	25451	2116	vw			
3939.5	25377	2190	m			
3947.5	25325	2242	m			
3954.5	25281	2286	w			
3957.5	25261	2306	m			
3968.0	25195	2372	vw			
3970.5	25179	2388	w			
3975.0	25150	2417	w			
3979.5	25122	2445	m			
3885.0	25087	2480	vw			
3989.5	25059	2508	w			
3993.0	2 037	2530	m			
4000.0	24993	2574	vw			
4003.0	25974	2593	vw			
4013.5	24909	2658	w			
4020.0	25860	2698	vw			
4036.5	24769	2800	w			
4051.0	24678	2889	w			
4079.0	24509	3058	vw			
4089.0	24449	3118	vw			
4091.5	24434	3133	m			
4093.0	24425	3142	w			
4113.0	24306	3261	vw			
4136.0	24171	3396	vw			
4152.5	24075	3492	w			
4198.0	23814	3753	vw			
4244.0	23556	4011	w			
4259.0	23473	4094	w			
4372.0	22866	4701	w			

FIGURE 29

Phosphorescence Spectrum of Benzoic Acid d_o in
Polycrystalline n-Nonane

Spex 1702 3/4 Meter Czerny Turner Monochromator

Concentration: $\sim 10^{-3}$ molar
Slit Width : 40 μ, 40 μ
Sensitivity : 3×10^{-7} amperes full scale
Time Constant: 0.3 seconds
Scan Rate : 20 Å/minute
Temperature : 4.2° K

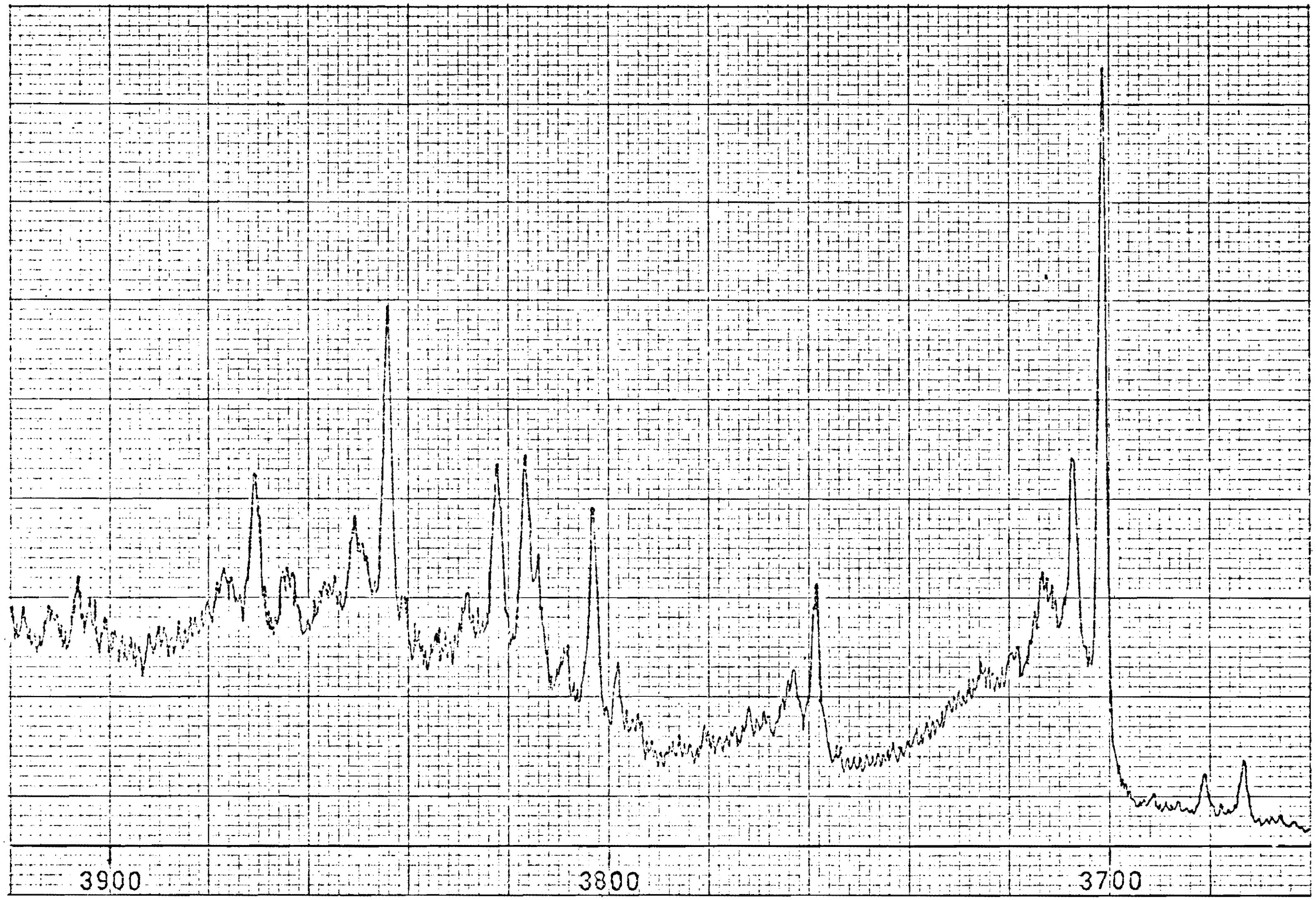
3900
3800
3700

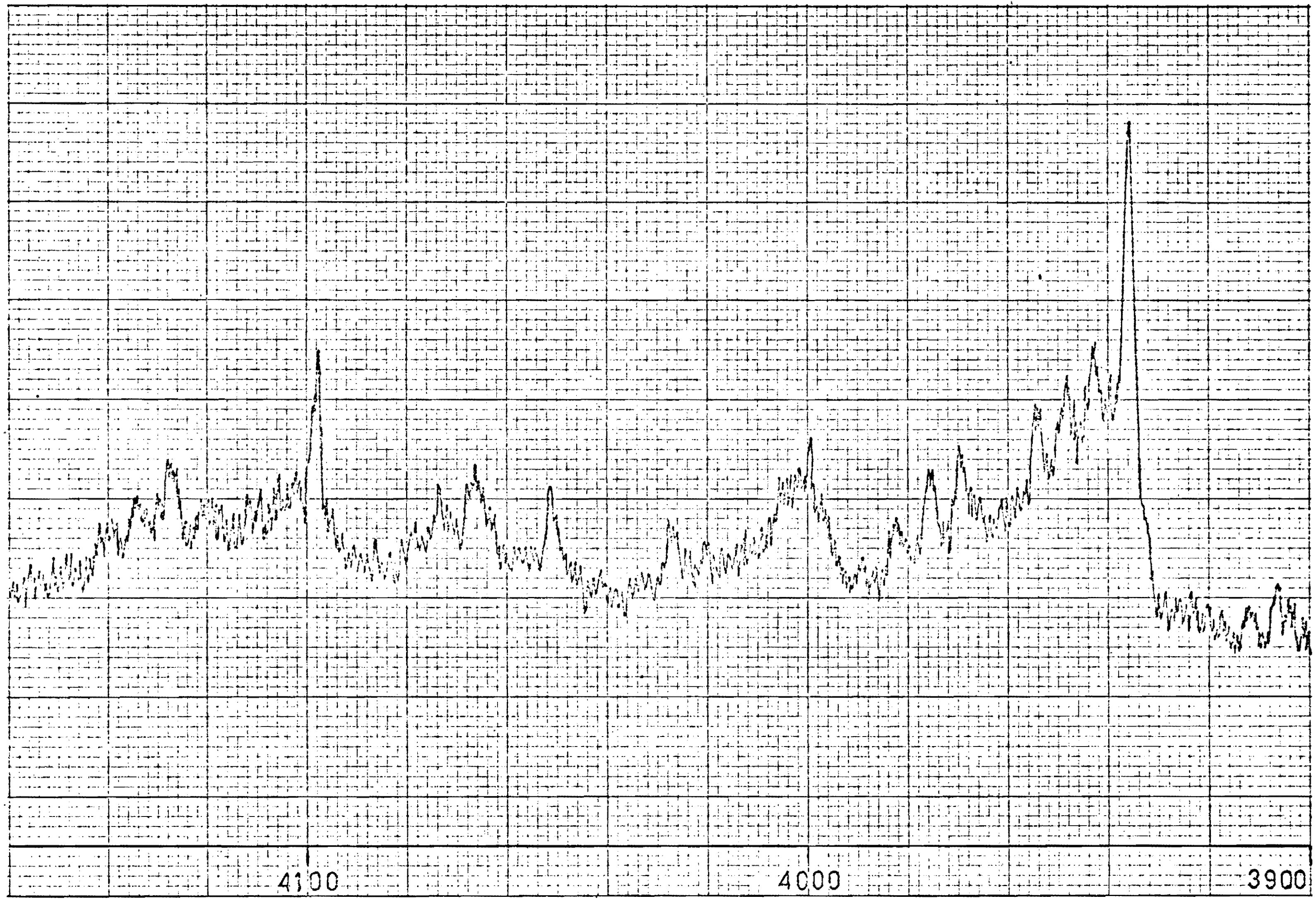
4100
4000
3900

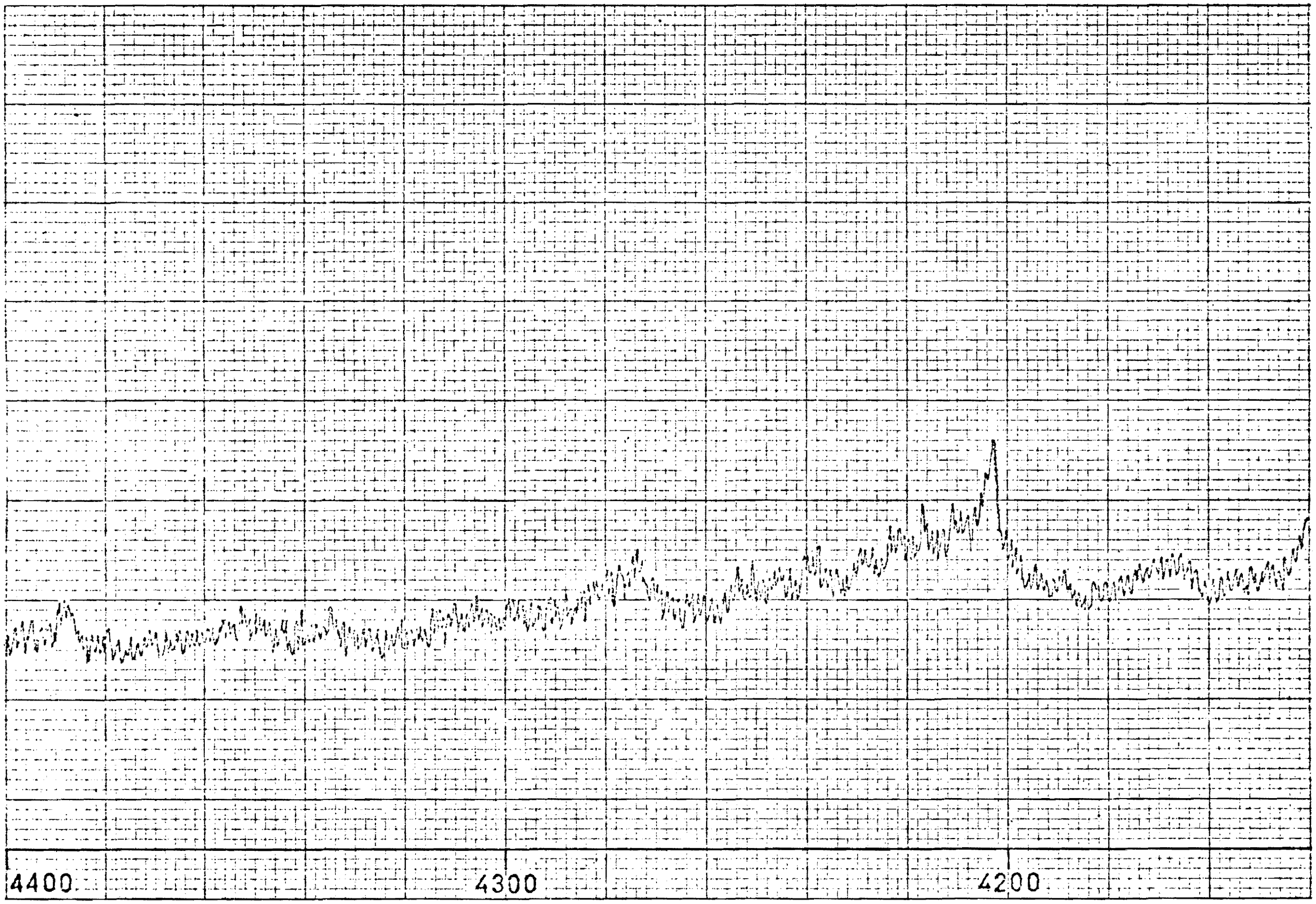
4400
4300
4200

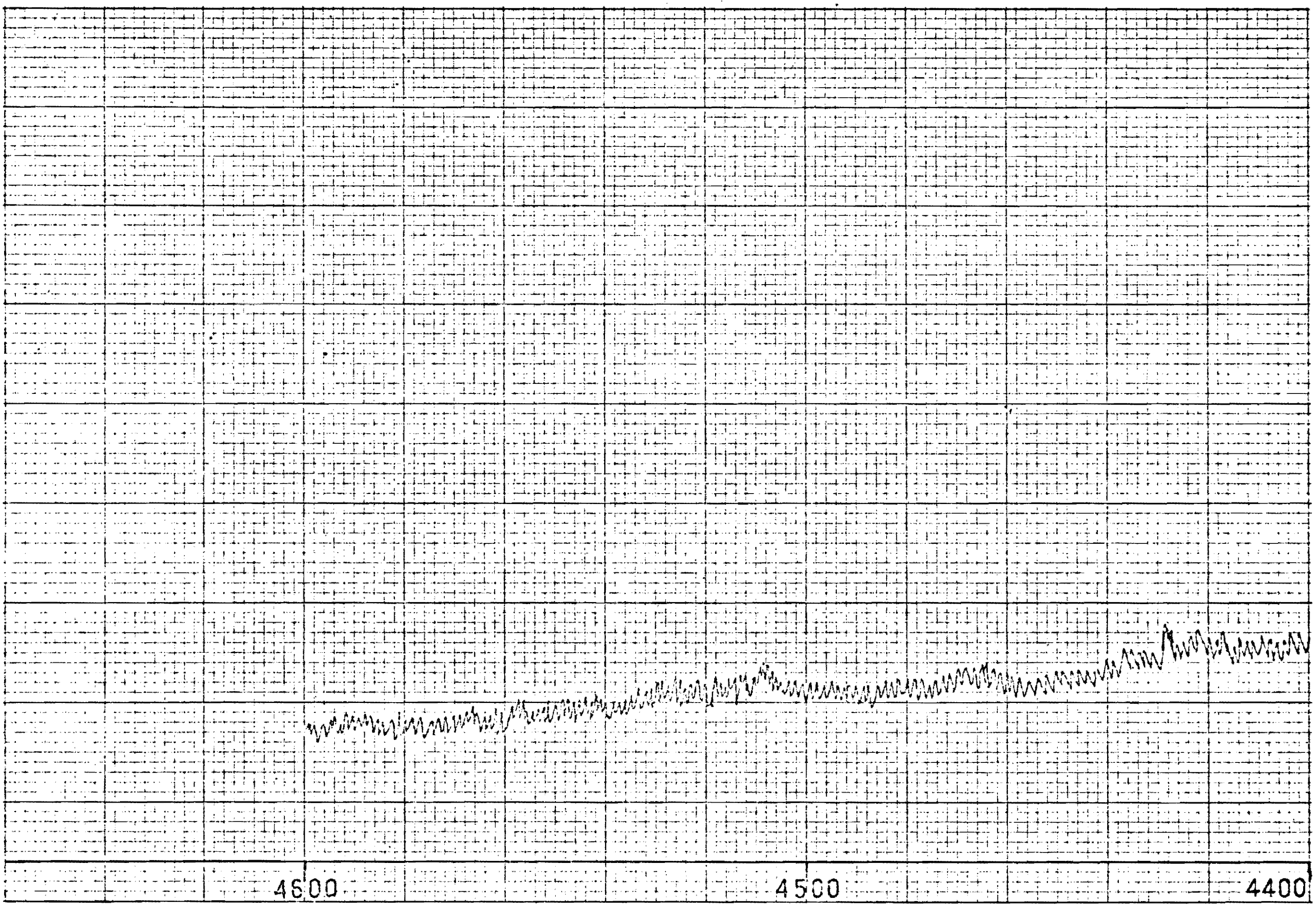
4600
4500
4400

TABLE 21

This table contains the frequencies, relative intensities, and assignments of bands in the spectrum shown in Figure 29. The assignments are based upon a consideration of the photoelectric spectra obtained in this study, as well as Baum's more accurate photographic data. Only the most probable assignments are given. For some bands, particularly combination bands, alternate assignments are possible. Average frequencies are given for Raman factor group pairs and all Raman frequencies are rounded off to the nearest wavenumber. Actual Raman frequencies are given only for fundamentals. For combination bands sums of phosphorescence frequencies are given. s = strong, w = weak, and vw = very weak.

λ(Å)	ν(cm^{-1})	$\Delta\nu$(cm^{-1})	Intensity	Assignment	Raman Freq. (cm^{-1})	Deviation (cm^{-1})
3673.5	27214	-206	w	site		
3681.5	27155	-147	w	site		
3691.5	27082	- 74	vw	site		
3701.5	27008	0	s	origin		
3707.5	26965	43	m	lattice		
3713.5	26921	87	w	H-bond		
3719.5	26878	130	vw	H-bond		
3726.0	26831	177	vw	site+H-bond		
3759.0	26595	413	m	ν_{16a}	408	5
3763.5	26563	445	w	ν_{16b}	438	7
3772.5	26500	508	vw	scissor	504	4
3795.0	26343	665	vw	$\nu_{9b}(-)$	659	6
3798.0	26322	686	w	ν_4	686	0
3803.5	26284	724	m	ν_{11}	710	14
3809.0	26246	762	w	ν_{11}+site	767	5
3814.0	26212	796	w	ν_1	797	1
3817.0	26191	817	m	$\nu_{10b}(-)$	812	5
3822.5	26153	855	m	ν_{10a}	855	0
3828.5	26113	895	w	ν_{10a}+site	898	3
3841.0	26028	980	vw	ν_5	988	8
3844.5	26004	1004	s	ν_{12}	1001	3
3849.0	25973	1035	vw	ν_{18a}	1028	7
3851.0	25960	1048	w	ν_{12}+site	1044	4
3856.0	25926	1082	vw	ν_{12}+site	1091	9
3864.0	25873	1135	w	ν_{13}	1134	1
3871.0	25826	1182	m	ν_{9a}	1185	3
3877.0	25786	1222	w	ν_{9a}+site	1228	6

Table 21 (Continued)

3907.0	25588	1420	vw	$\nu_{12}+\nu_{16a}$	1417	3
3912.0	25555	1453	vw	$\nu_{12}+\nu_{16b}$	1449	4
3936.0	25399	1609	s	ν_{8a}	1601	8
3943.0	25354	1654	w	ν_{8a}+site	1652	2
3948.5	25319	1689	w	ν_{8a}+site	1696	7
3954.5	25281	1727	w	$\nu_{12}+\nu_{11}$	1728	1
3970.0	25182	1826	w	$\nu_{12}+\nu_{10b}{}^{(-)}$	1821	5
3976.0	25144	1864	w	$\nu_{12}+\nu_{10a}$	1859	5
3982.5	25103	1905	w	$\nu_{9a}+\nu_{11}$	1906	1
3989.5	25059	1949	vw	$\nu_{12}+\nu_{10a}$ +site	1946	3
4000.0	25993	2015	m	$2\nu_{12}$	2008	7
4005.0	24962	2046	w	$2\nu_{12}$+site	2051	5
4020.0	24866	2142	vw	$\nu_{12}+\nu_{13}$	2139	3
4027.0	25825	2183	w	$\nu_{12}+\nu_{9a}$	2186	3
4033.5	25785	2223	vw	$\nu_{12}+\nu_{9a}$ +site	2229	6
4041.5	24736	2272	vw	$2\nu_{13}$	2270	2
4047.0	24703	2305	vw	$\nu_{8a}+\nu_{4}$	2295	10
4052.0	24672	2336	w	$\nu_{8a}+\nu_{11}$	2333	3
4066.5	24584	2424	w	$2\nu_{12}+\nu_{16a}$	2421	3
4074.0	24539	2469	w	$\nu_{8a}+\nu_{10a}$	2464	5
4098.0	24395	2613	m	$\nu_{12}+\nu_{8a}$	2613	0
4120.0	24265	2743	vw	$\nu_{8a}+\nu_{13}$	2744	0
4127.5	24221	2787	w	$\nu_{8a}+\nu_{9a}$	2791	4
4135.0	24177	2831	vw	$2\nu_{12}\mp\nu_{10b}{}^{(-)}$	2825	6
4140.0	24148	2860	vw	$2\nu_{12}+\nu_{10a}$	2863	3
4167.0	23991	3017	vw	$\nu_{12}+\nu_{8a}$ $+\nu_{16a}$	3026	9
4189.0	23865	3143	vw	$2\nu_{12}+\nu_{13}$	3143	0
4203.0	23786	3222	m	$2\nu_{8a}$	3218	4
4211.0	23741	3267	vw	$2\nu_{8a}$+site	3265	2
4217.0	23707	3301	vw	$\nu_{12}+\nu_{8a}+\nu_{4}$	3299	2

Table 21 (Continued)

4222.0	23679	3329	vw	$\nu_{12}+\nu_{8a}+\nu_{11}$	3337	8
4239.0	23584	3424	vw	$\nu_{12}+\nu_{8a}$ $+ \nu_{10b}{}^{(-)}$	3430	6
4246.0	23545	3463	vw	$\nu_{12}+\nu_{8a}+\nu_{10a}$	3468	5
4253.0	23506	3502	vw	$\nu_{8a}+\nu_{9a}+\nu_{11}$	3515	13
4274.0	23391	3617	w	$2\nu_{12}+\nu_{8a}$	3617	0
4509.0	22172	4836	w	$3\nu_{8a}$	4827	9

FIGURE 30

Phosphorescence Spectrum of Benzoic Acid $4d_1$ in Polycrystalline n-Nonane

Spex 1702 3/4 Meter Czerny Turner Monochromator

Concentration : $\sim 10^{-3}$ molar
Slit Width : 38 μ, 38 μ
Sensitivity : 1×10^{-7} amperes full scale
Time Constant : 1.0 second
Scan Rate : 20 Å/minute
Temperature : 4.2° K

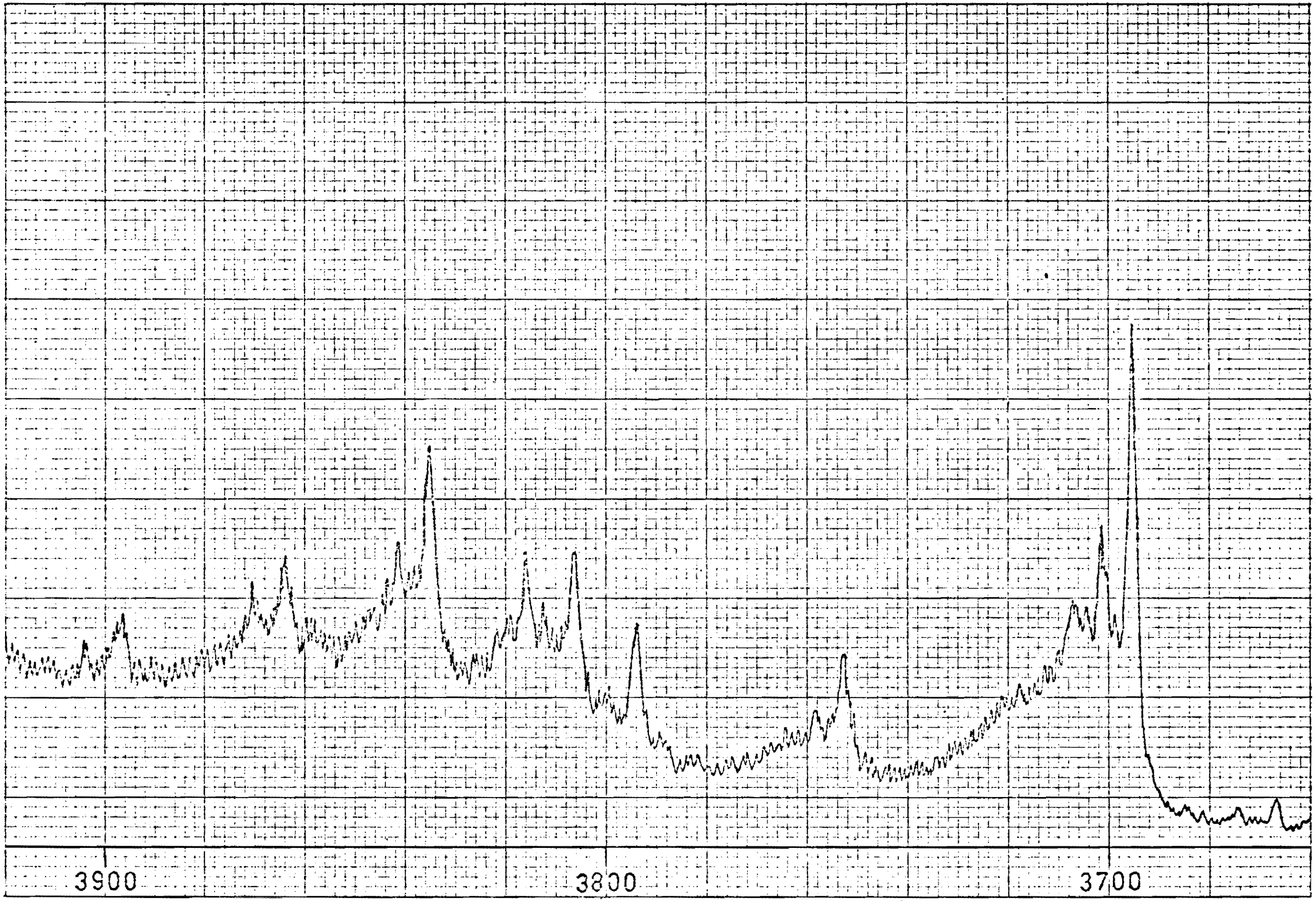
3900
3800
3700

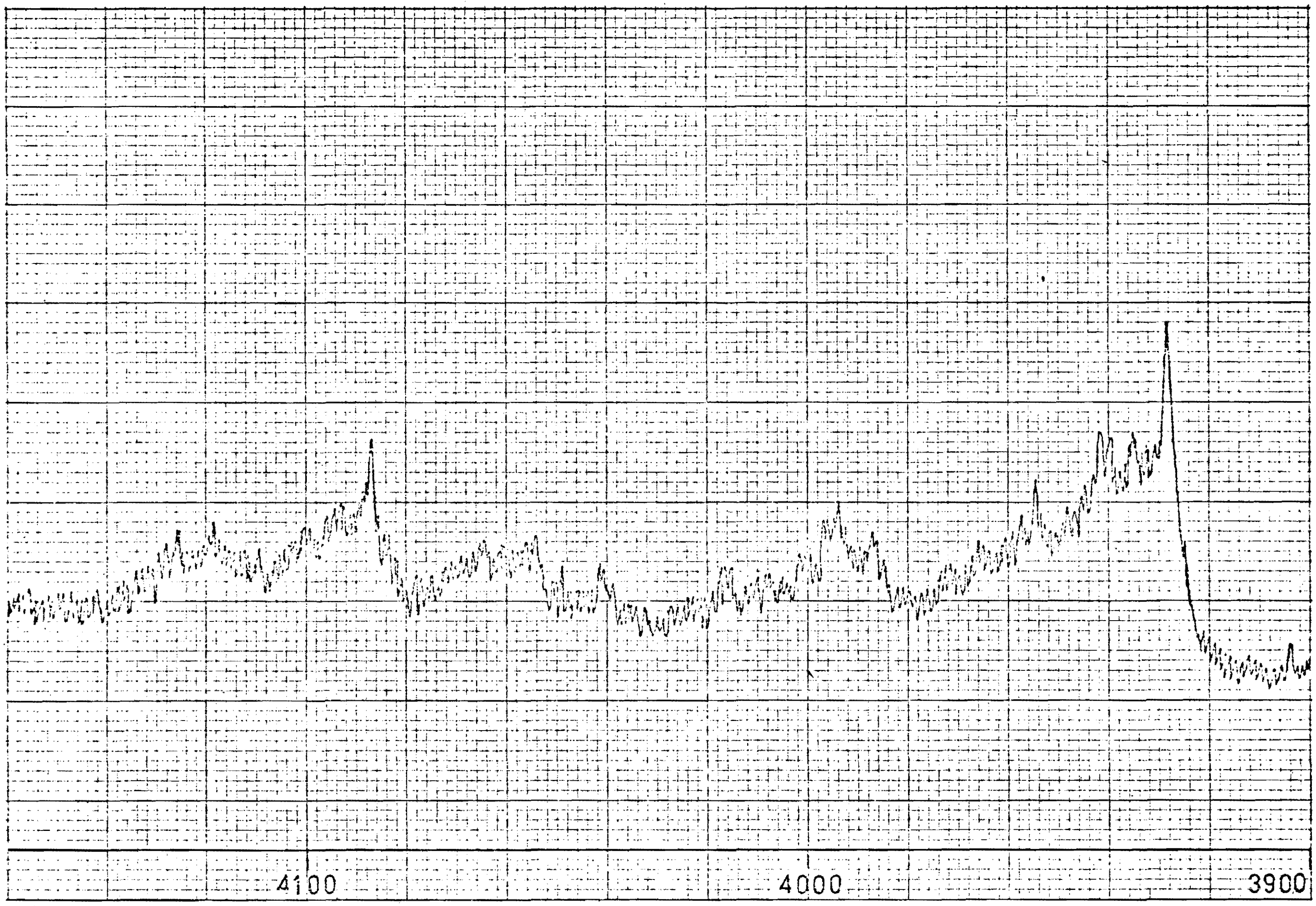
4100
4000
3900

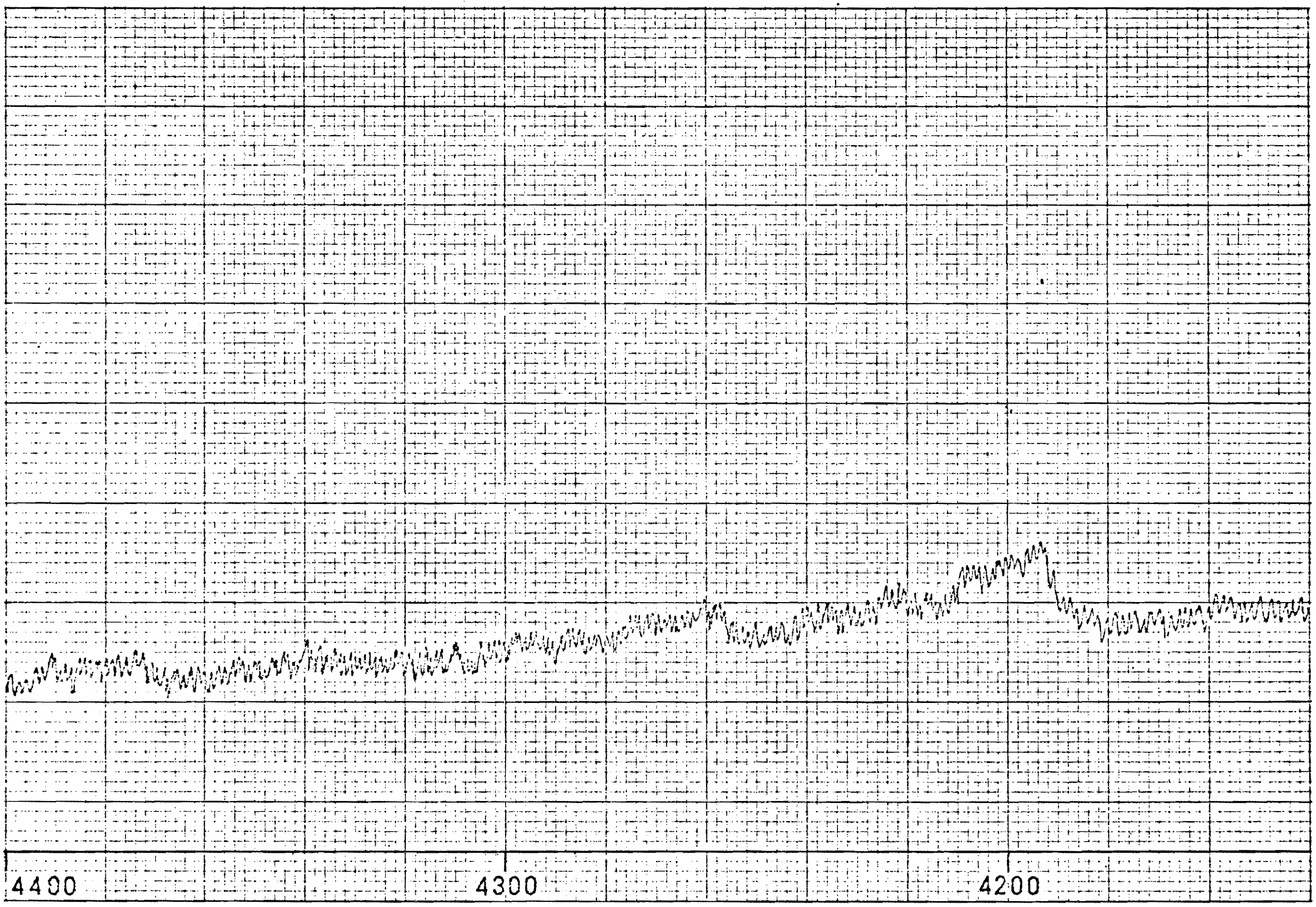
4400
4300
4200

TABLE 22

This table contains the frequencies, relative intensities, and assignments of bands in the spectrum shownin Figure 30. Only the most probable assignments are given. For some bands, particularly combination bands, alternate assignments are possible. Average frequencies are given for Raman factor group pairs and all Raman Frequencies are rounded off to the nearest wavenumber. Actual Raman frequencies are given only for fundamentals. For combination bands sums of phosphorescence frequencies are given. s = strong, w = weak, and vw = very weak.

λ (Å)	ν(cm^{-1})	Δν(cm^{-1})	Intensity	Assignment	Raman Freq. (cm^{-1})	Deviation (cm^{-1})
3695.5	27052	0	s	Origin		
3699.0	27027	25	vw	site (or lattice)		
3701.5	27008	44	m	lattice		
3704.5	26987	65	vw	lattice		
3707.0	26968	84	vw	H-bond		
3753.0	26638	414	m	ν_{16a}		
3759.0	26595	457	vw	ν_{16a}+lattice	458	1
3789.0	26385	667	vw	$\nu_{9b}(-)$	657	10
3794.0	26350	702	m	ν_{11}	698	4
3800.0	26308	744	vw	ν_{11}+lattice	746	2
3806.5	26263	785	m	$\nu_{10b}(-)$	787	2
3812.5	26222	830	vw	ν_{10b}+lattice	829	1
3816.0	26198	854	m	ν_{10a}	853	1
3835.5	26065	987	s	ν_{12}	984	3
3841.5	26024	1028	w	ν_{18a}	1026	2
3864.0	25873	1179	m	ν_{9a}	1182	3
3870.5	25829	1220	w	ν_{9a}+lattice	1223	3
3897.5	25650	1402	w	ν_{19b}	1411	9
3904.0	25608	1444	vw	ν_{19b}+site	1446	2
3928.5	25448	1604	s	ν_{8a}	1597	7
3935.5	25403	1649	vw	ν_{8a}+lattice	1648	1
3942.0	25361	1691	w	$\nu_{12}+\nu_{11}$	1689	2
3954.5	25281	1771	w	$\nu_{12}+\nu_{10b}(-)$	1772	1
3966.0	25207	1845	vw	$\nu_{8a}+\nu_{10a}$	1841	4
3987.0	25074	1978	vw	$2\nu_{12}$	1974	4
3994.0	25031	2021	w	$\nu_{8a}+\nu_{16a}$	2018	3

Table 22 (Continued)

3996.5	25015	2037	vw	$\nu_{10a}+\nu_{9a}$	2033	4
4016.0	24894	2159	w	$\nu_{12}+\nu_{9a}$	2166	7
4041.0	24739	2313	w	$\nu_{8a}+\nu_{11}$	2306	7
4054.0	24660	2452	vw	$\nu_{8a}+\nu_{10a}$	2458	6
4087.0	24461	2591	m	$\nu_{8a}+\nu_{12}$	2591	0
4093.0	24425	2627	w	$\nu_{8a}+\nu_{18a}$	2632	5
4100.0	24383	2669	vw	$\nu_{8a}+\nu_{12}$ +H-bond	2675	6
4119.0	24271	2781	w	$\nu_{8a}+\nu_{9a}$	2783	2
4126.0	24230	2822	w	$\nu_{8a}+\nu_{9a}$ +lattice	2827	5
4193.0	23843	3209	m	$2\nu_{8a}$	3208	1
4207.0	23763	3289	w	$2\nu_{8a}$+H-bond	3292	3

FIGURE 31

Phosphorescence Spectrum of Benzoic Acid d_5 in Polycrystalline n-Nonane

Spex 1702 3/4 Meter Czerny Turner Monochromator

Concentration : $\sim 10^{-3}$ molar
Slit Width : 38 μ, 38 μ
Sensitivity : 1×10^{-7} amperes full scale
Time Constant : 1.0 second
Scan Rate : 20 Å/minute
Temperature : 4.2° K

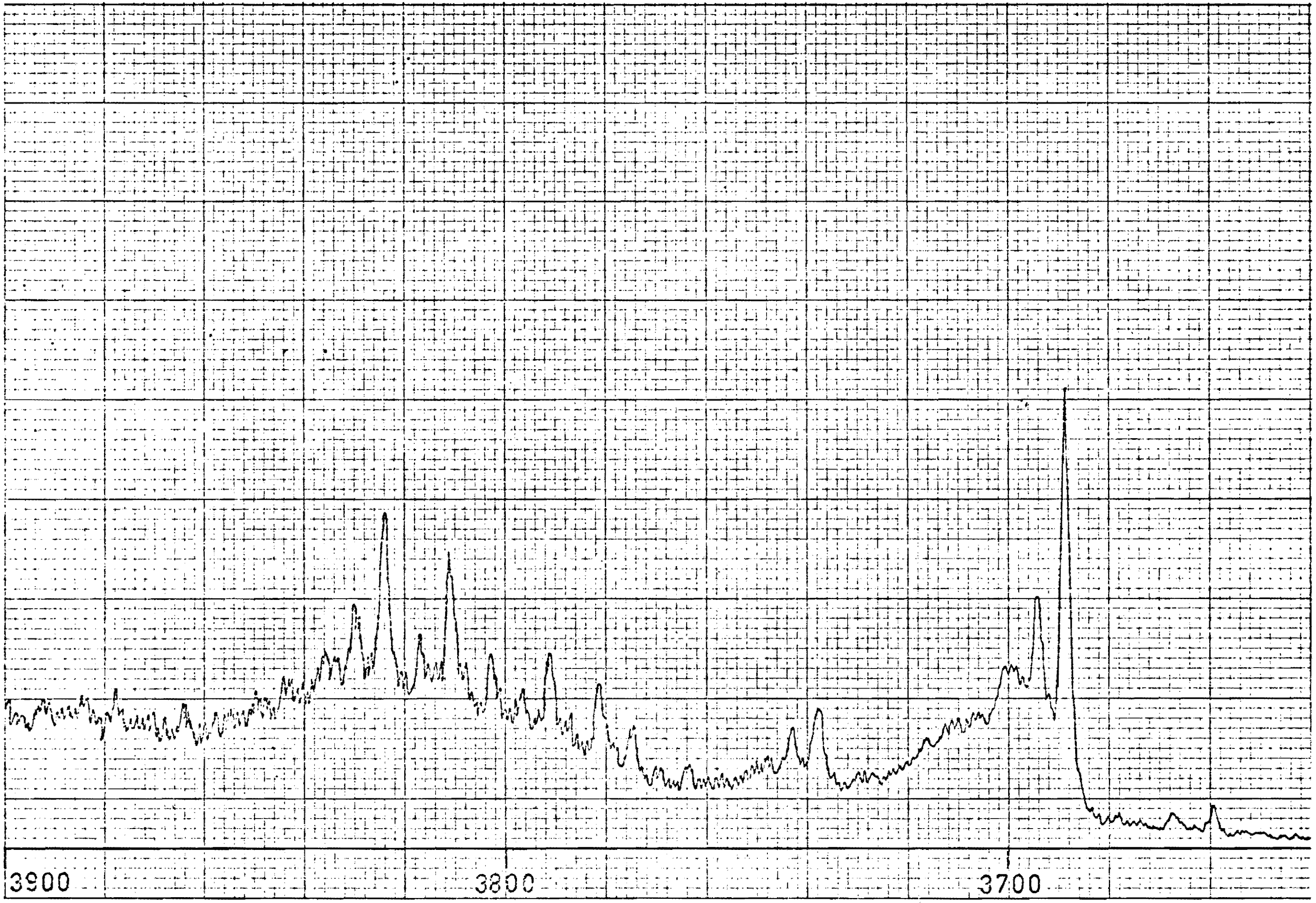
3900
3800
3700

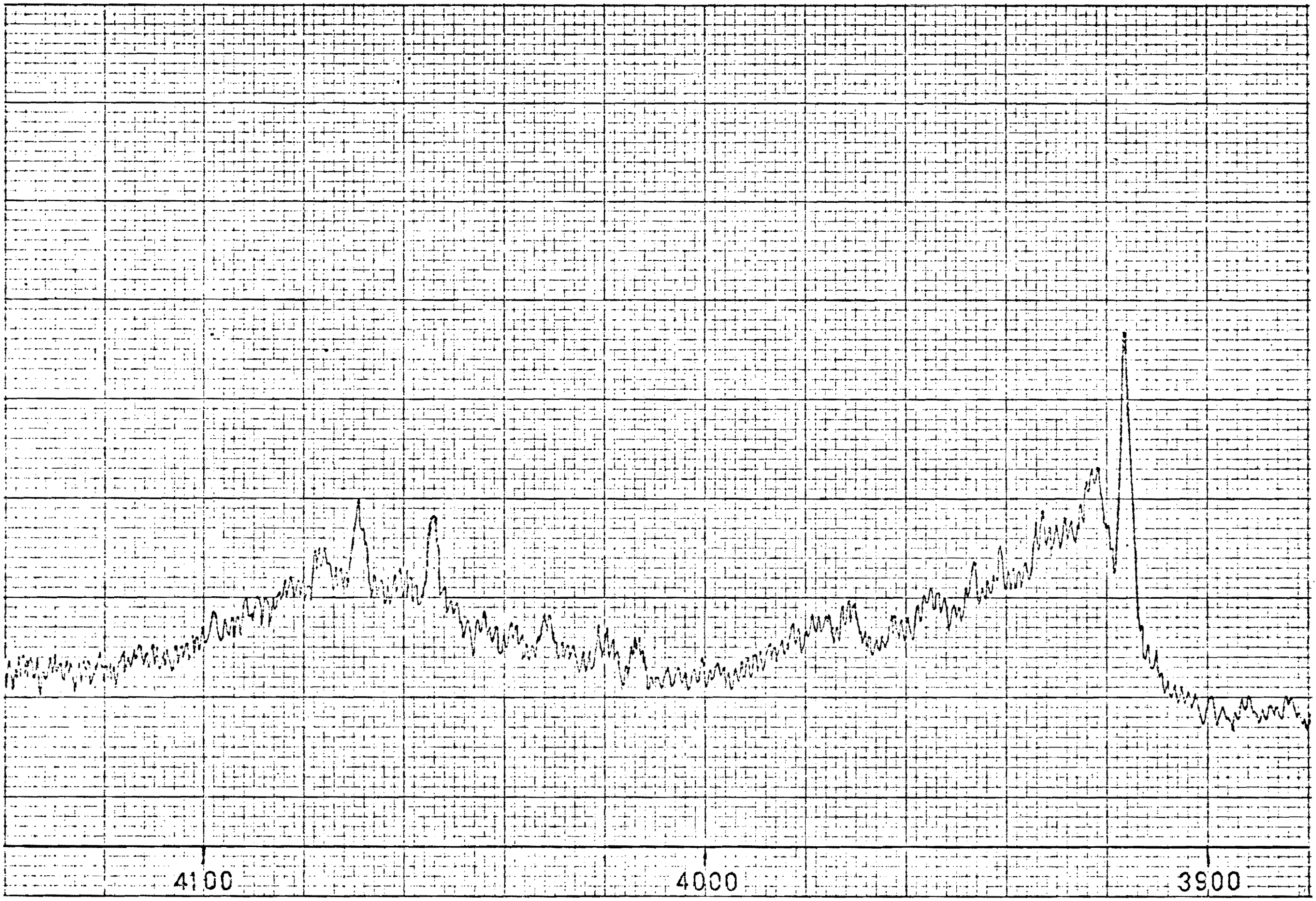
4100
4000
3900

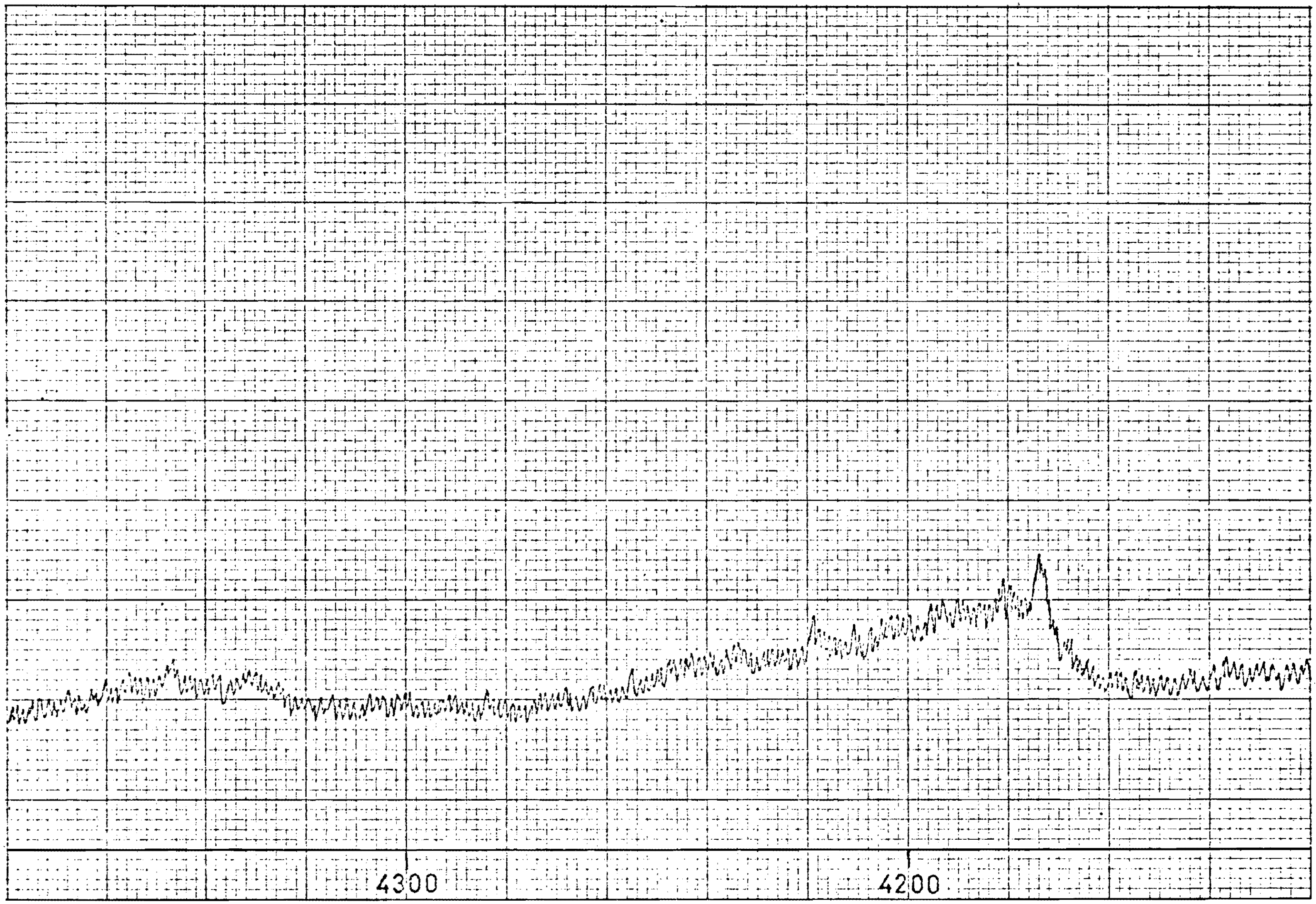
4300
4200

TABLE 23

This table contains the frequencies, relative intensities, and assignments of bands in the spectrum shown in Figure 31. Assignments of most d_5 Raman and IR bands are uncertain. Only those assignments which are considered firm or highly probable are given. Since most fundamentals are unassigned, assignment of combination bands has not been attempted. Average frequencies are given for Raman factor group pairs and all Raman frequencies are rounded off to the nearest wavenumber. s = strong, w = weak, and vw = very weak.

λ(Å)	ν(cm^{-1})	$\Delta\nu$(cm^{-1})	Intensity	Assignment	Raman Freq.(cm^{-1})	Dev. (cm^{-1})
3688.5	27104	0	s	origin		
3694.0	27063	41	m	lattice		
3699.5	27023	81	w	H-bond		
3766.0	26976	128	vw	H-bond		
3712.0	26932	172	vw	H-bond + lattice	169	3
3716.0	26903	201	vw			
3737.5	26748	356	m	ν_{16a}	356	0
3743.0	26709	395	w	ν_{16b}	394	1
3747.0	26680	424	vw	ν_{6a}	422	2
3763.5	26563	541	w			
3768.0	26532	572	vw			
3774.5	26486	618	w			
3781.0	26441	663	m			
3796.5	26333	771	w	ν_1	767	4
3802.5	26291	813	w			
3807.5	26257	847	vw			
3811.0	26232	872	m			
3817.0	26191	913	w	H-wag	913	2
3824.0	26143	961	s	ν_{12}	958	3
3829.5	26106	998	m			
3835.5	26065	1039	vw			
3864.0	25873	1231	vw			
3877.5	25783	1321	vw			
3884.0	25739	1365	vw			
3892.0	25686	1418	vw			
3916.5	25526	1578	s	8a	1569	9
3922.5	25487	1617	m			
3933.0	25419	1685	vw			
3941.5	25364	1740	w			
3946.5	25332	1772	w			
3956.0	25271	1833	vw			
3962.0	25233	1871	vw			
3971.0	25175	1929	w			

Table 23 (Continued)

4013.0	24912	2192	w
4020.0	24869	2235	w
4031.5	24798	2306	w
4054.0	24660	2444	m
4060.5	24621	2483	vw
4069.5	24566	2538	m
4076.0	24527	2577	w
4173.5	23954	3150	m
4181.0	23911	3193	vw
4219.0	24696	3408	vw
4321.0	2 136	3968	vw
4347.0	22998	4106	vw

FIGURE 32

Phosphorescence Spectrum of Benzoic Acid d_o in Polycrystalline Benzoic Acid d_5

Spex 1702 3/4 Meter Czerny Turner Monochromator

Concentration : ∿0.8 mole percent
Slit Width : 20 μ, 20 μ
Sensitivity : 3×10^{-7} amperes full scale
Time Constant : 0.3 seconds
Scan Rate : 20 Å/minutes
Temperature : 4.2° K

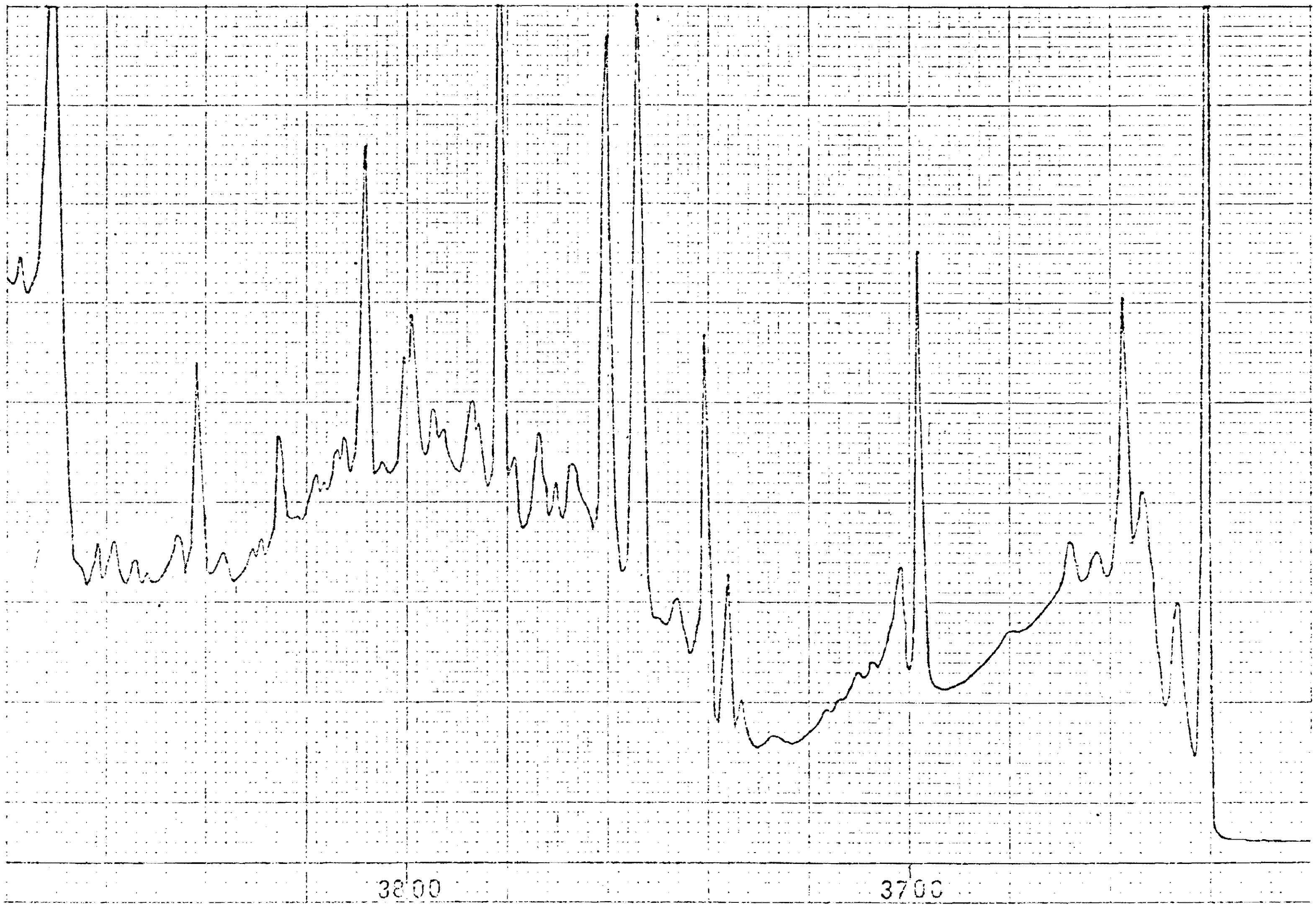
3800
3700

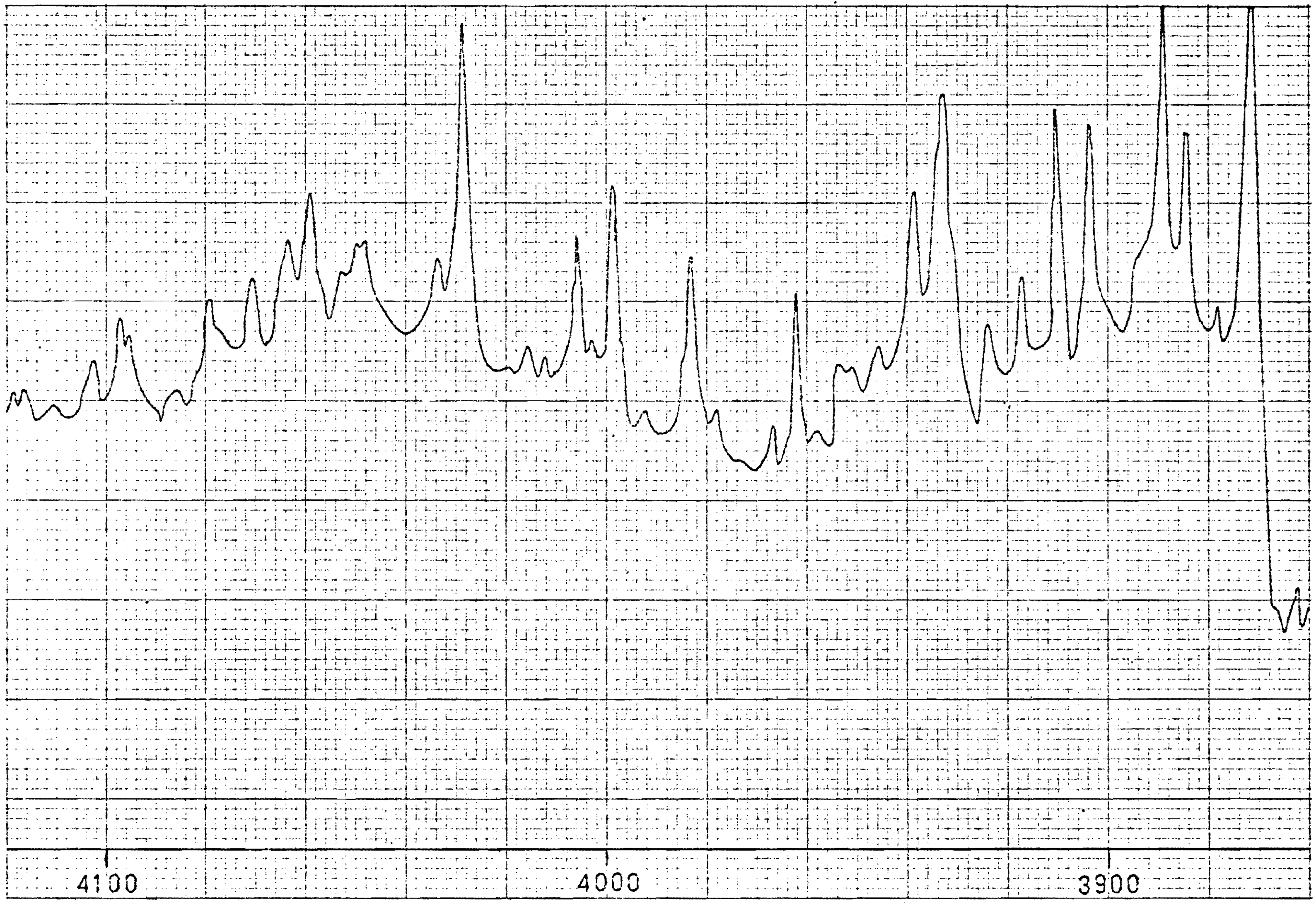
4100
4000
3900

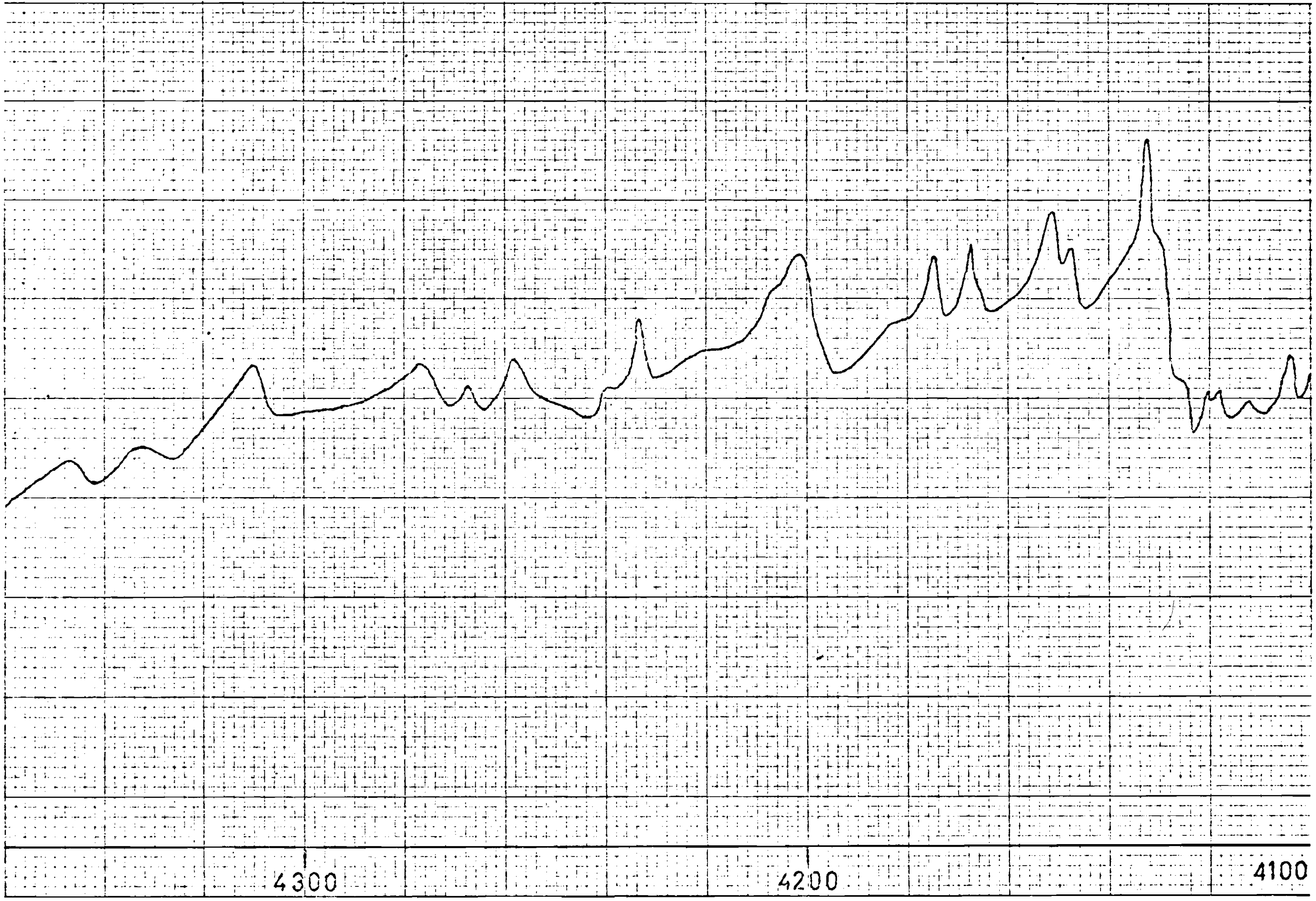
4300
4200
4100


4500
4400

TABLE 24

This table contains the frequencies, relative intensities, and assignments of bands in the spectrum shown in Figure 22. The assignments are based upon a consideration of the photoelectric spectra obtained in this study as well as Baum's more accurate photographic data. Only the most probable assignments are given. For some bands, particularly combination bands, alternate assignments are possible. Average frequencies are given for Raman factor group pairs and all Raman frequencies are rounded off to the nearest wavenumber. Actual Raman frequencies are given only for fundamentals. For combination bands sums of phosphorescence frequencies are given. s = strong, w = weak, and vw = very weak.

λ(Å)	ν(cm^{-1})	$\Delta\nu$(cm^{-1})	Intensity	Assignment	Raman Freq.(cm^{-1})	Deviation (cm^{-1})
3670.6	27236	0	s	origin		
3676.5	27192	44	m	lattice		
3683.0	27144	92	w	H-bond		
3687.5	27111	125	m	monomer torsion (MT)	119	6
3693.0	27071	165	vw	MT+lattice	169	4
3698.5	27030	206	w	$\nu_{10b}(+)$	198	8
3728.0	26816	420	s	ν_{16a}	408	12
3732.0	26788	448	w	ν_{16b}	438	10
3740.5	26727	509	vw	scissor	504	5
3764.0	26560	676	w	$\nu_{9b}(-)$	659	17
3766.5	26546	690	m	ν_{4}	686	4
3771.0	26511	725	s	ν_{11}	710	15
3777.0	26469	767	w	ν_{11}+lattice	769	2
3784.5	26416	820	s	$\nu_{10b}(-)$	812	8
3791.0	26371	865	s	ν_{10a}	855	10
3797.5	26326	910	vw	H-wag	910	0
3804.5	26277	959	w	ν_{17b}	942	17
3809.5	26243	993	vw	ν_{5}	988	5
3812.5	26222	1014	s	ν_{12}	1001	13
3816.0	26198	1038	vw	ν_{18a}	1028	10
3818.0	26184	1052	w	ν_{12}+lattice	1058	6
3823.5	26147	1089	vw	ν_{18b}	1075	14
3830.0	26099	1137	m	ν_{12}+MT	1133	7
3831.5	26092	1144	vw	ν_{13}	1134	10
3839.0	26041	1195	s	ν_{9a}	1185	10
3856.0	25926	1310	w	ν_{9a}+MT	1320	10

Table 24 (Continued)

3860.0	25899	1337	vw	ν_{14} or ν_3	1327	10
3867.5	25849	1387	vw	$\nu_{9a}+\nu_{10b}(+)$	1401	14
3872.5	25816	1420	m	$\nu_{12}+\nu_{16a}$	1434	14
3876.5	25789	1447	w	$\nu_{12}+\nu_{16b}$	1462	15
3885.5	25733	1503	vw	ν_{19a}	1495	8
3901.5	25624	1612	s	ν_{8a}	1601	11
3915.0	25536	1700	m	$\nu_{12}+\nu_4$	1700	0
3919.0	25510	1726	m	$\nu_{12}+\nu_{11}$	1739	13
3934.0	25412	1824	m	$\nu_{12}+\nu_{10b}(-)$	1834	10
3941.0	25367	1869	m	$\nu_{11}+\nu_{13}$	1869	0
3948.0	25322	1914	w	$\nu_{9a}+\nu_{11}$	1920	6
3954.5	25281	1955	w	$\nu_{12}+\nu_{17b}$	1973	18
3963.0	25226	2010	s	$2\nu_{12}$	2028	18
3965.0	25214	2022	w	$\nu_{8a}+\nu_{16a}$	2032	10
3969.0	25188	2048	m	$\nu_{8a}+\nu_{16b}$	2060	12
3984.0	25093	2143	vw	$\nu_{12}+\nu_{13}$	2158	15
3993.0	25037	2199	m	$\nu_{12}+\nu_{9a}$	2209	10
4014.0	24906	2330	m	$\nu_{8a}+\nu_{11}$	2337	7
4030.0	24810	2426	m	$\nu_{8a}+\nu_{10b}(-)$	2432	6
4037.0	24764	2472	m	$\nu_{8a}+\nu_{10a}$	2477	5
4043.5	24724	2512	vw	$\nu_{12}+\nu_{19a}$	2517	5
4047.0	24703	2533	vw	$\nu_{14}+\nu_{9a}$	2522	11
4059.5	25627	2609	s	$\nu_{12}+\nu_{8a}$	2626	17
4080.0	24503	2733	w	$\nu_{8a}+\nu_{13}$	2756	23
4090.0	24443	2793	m	$\nu_{8a}+\nu_{9a}$	2807	14
4095.0	24413	2823	w	$2\nu_{12}+\nu_{10b}(-)$	2948	25
4129.0	24212	3024	w	$\nu_{12}+\nu_{8a}+\nu_{16a}$	3046	22
4163.0	24014	3222	m	$2\nu_{8a}$	3224	2
4182.0	23905	3331	w	$\nu_{12}+\nu_{8a}+\nu_{11}$	3351	20
4198.0	23814	3422	w	$\nu_{12}+\nu_{8a}+\nu_{10}(-)$	3446	24
4232.0	23623	3613	m	$2\nu_{12}+\nu_{8a}$	3640	27
4264.5	23446	3790	w	$\nu_{12}+\nu_{8a}+\nu_{9a}$	3821	31
4342.0	23024	4212	m	$\nu_{12}+2\nu_{8a}$	4238	26
4460.0	22415	4821	w	$3\nu_{8a}$	4836	15

FIGURE 33

Phosphorescence Spectrum of Parafluorobenzoic Acid in Polycrystalline Benzoic Acid d_o

Spex 1702 3/4 Meter Czerny Turner Monochromator

Concentration: ∿1 mole percent

Slit Width : 45 μ, 45 μ

Sensitivity : 1×10^{-7} amperes full scale

Time Constant: 1.0 second

Scan Rate : 20 Å/minute

Temperature : 4.2° K

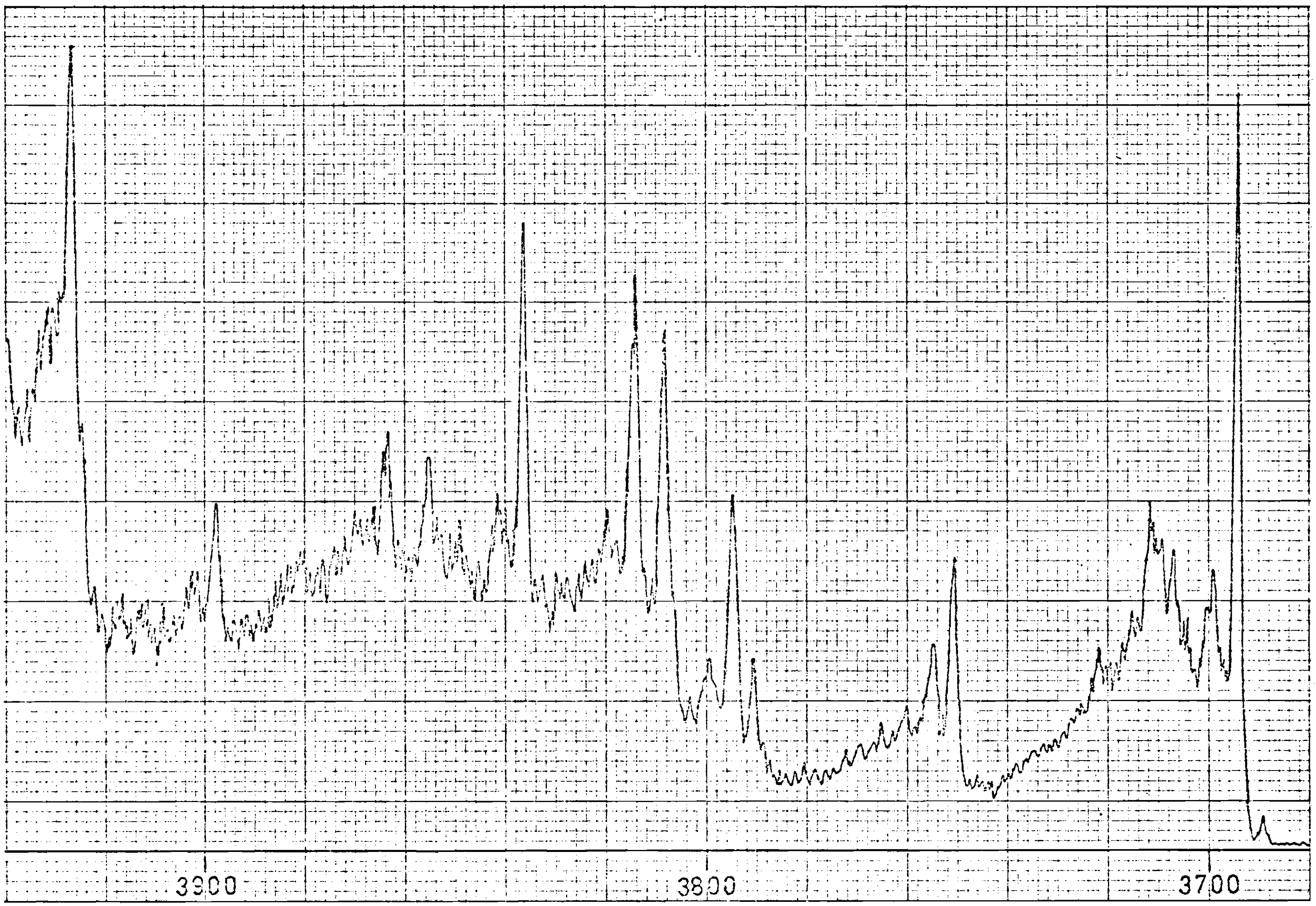
3900
3800
3700

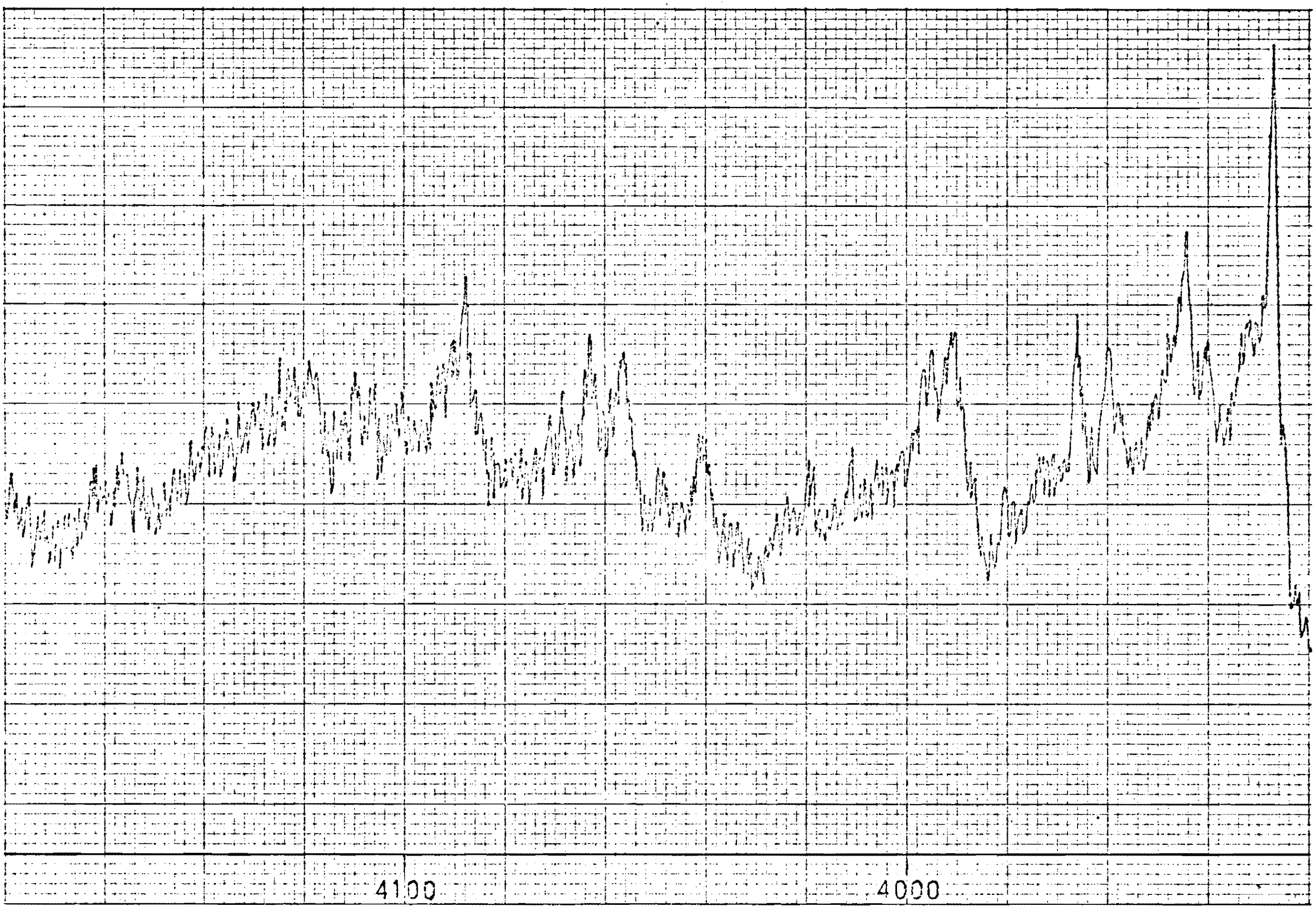
4100
4000

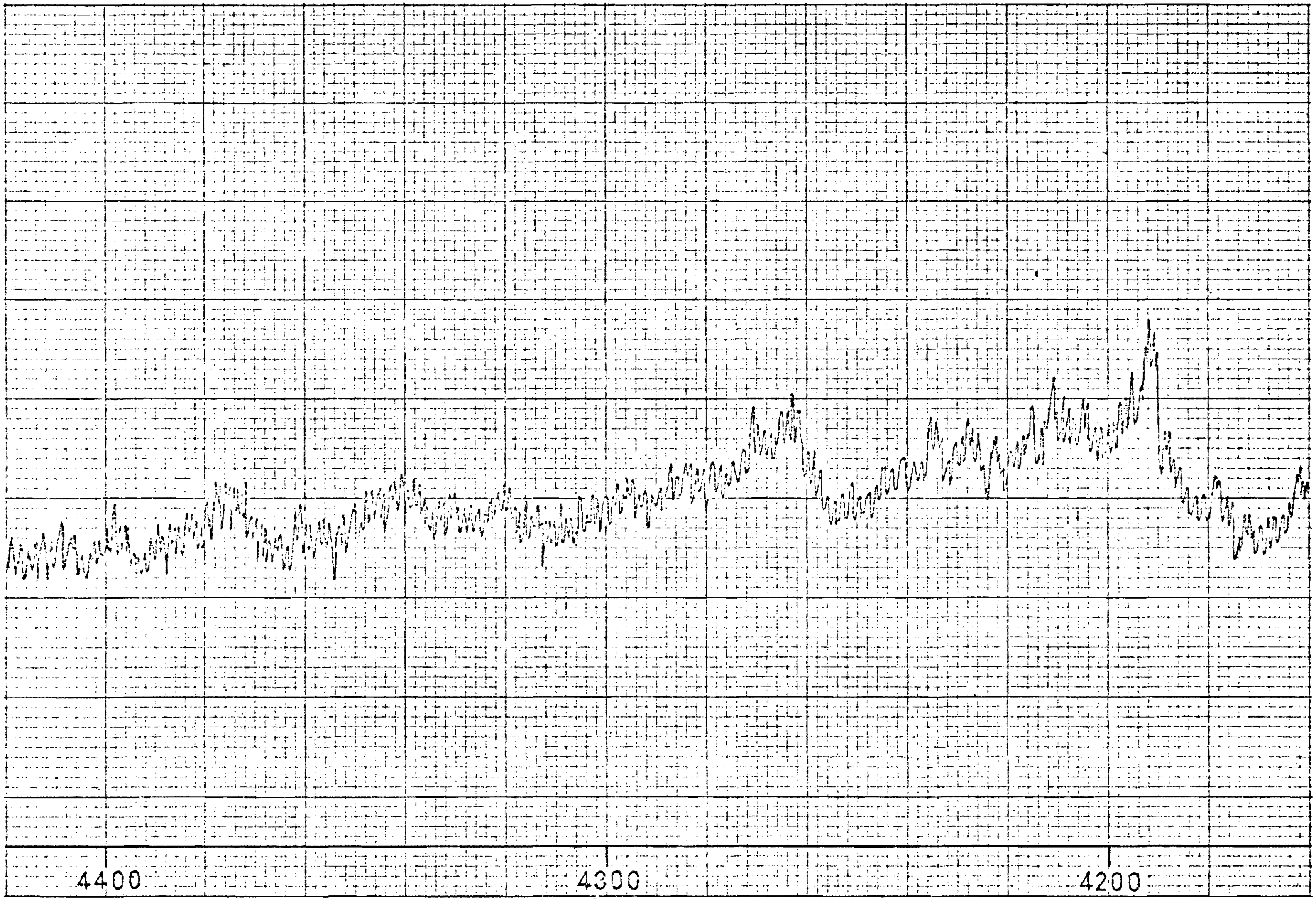
4400
4300
4200

TABLE 25

This table contains the frequencies, relative intensities, and assignments of bands in the spectrum shown in Figure 23. Only the most probable assignments are given. For some bands, particularly combination bands, alternate assignments are pssible. Average frequencies are given for Raman factor group pairs and all Raman frequencies are rounded off to the nearest wavenumber. Actual Raman frequencies are given only for fundamentals. For combination bands sums of phosphorescence frequencies are given. s = strong, w = weak, and vw = very weak.

λ(Å)	ν(cm^{-1})	Δν(cm^{-1})	Intensity	Assignment	Raman Freq. (cm^{-1})	Deviation (cm^{-1})
3689.0	27100	-37	vw	site		
3694.0	27063	0	s	origin		
3699.5	27024	39	m	lattice		
3707.0	26968	95	m	H-bond		
3710.0	26947	116	w	monomer Torsion (MT)	119	3
3712.0	26932	131	m	H-bond		
3722.0	26860	203	w	$\nu_{10b}(+)$	198	5
3751.0	26652	411	m	ν_{16a}	408	3
3755.0	26624	439	m	ν_{16b}	438	1
3790.5	26374	689	m	ν_4	686	3
3794.5	26346	717	s	ν_{11}	710	7
3799.5	26312	751	w	ν_{11}+lattice	756	5
3805.5	26250	813	s	$\nu_{10b}(-)$	812	1
3814.0	26212	851	s	ν_{10a}	855	4
3820.0	26171	892	w	ν_{10a}+lattice	890	2
3836.5	26058	1005	s	ν_{12}	1001	4
3841.5	26024	1039	w	ν_{18a}	1028	11
3848.5	25977	1086	vw	ν_{18a}+lattice	1078	8
3855.5	25930	1133	w	ν_{13}	1134	1
3864.0	25873	1190	m	ν_{9a}	1185	5
3870.0	25832	1231	vw	ν_{9a}+lattice	1229	2
3881.0	25759	1304	vw	ν_{9a}+MT	1306	2
3897.5	25650	1413	m	$\nu_{12}+\nu_{16a}$	1416	3
3902.5	25617	1446	w	$\nu_{12}+\nu_{16b}$	1444	2
3927.0	25458	1605	s	ν_{8a}	1601	4
3932.0	25425	1638	vw	ν_{8a}+lattice	1644	6
3940.0	25374	1689	w	$\nu_{12}+{}_{4}$	1691	2

Table 25 (Continued)

3944.0	25348	1715	s	$\nu_{12}+\nu_{11}$	1722	7
3960.0	25245	1818	vw	$\nu_{12}+\nu_{10b}(-)$	1818	0
3966.0	25207	1856	m	$\nu_{12}+\nu_{10a}$	1856	0
3972.0	25169	1894	vw	$\nu_{12}+\nu_{10a}$ +lattice	1895	1
3980.0	25118	1945	vw	$\nu_{9a}+\nu_{11}$ +lattice	1946	1
3990.5	25052	2011	s	$2\nu_{12}$	2010	1
3995.0	25024	2039	m	$2\nu_{12}$+lattice	2049	10
4010.5	24928	2135	w	$\nu_{12}+\nu_{18a}$	2042	7
4019.0	24875	2188	w	$\nu_{12}+\nu_{9a}$	2195	7
4034.0	24782	2281	vw	$\nu_{8a}+\nu_{4}$	2294	13
4040.5	25742	2321	m	$\nu_{8a}+\nu_{11}$	2322	1
4056.0	24648	2415	m	$2\nu_{12}+\nu_{16a}$	2421	6
4063.0	24605	2458	m	$\nu_{8a}+\nu_{10b}$	2456	2
4087.5	24458	2605	s	$\nu_{12}+\nu_{8a}$	2610	5
4109.5	24327	2736	w	$2\nu_{12}+\nu_{11}$	2727	9
4120.0	24265	2798	w	$\nu_{8a}+\nu_{9a}$	2795	3
4156.5	24052	3011	vw	ν_{2} or ν_{7a}	3008	3
4178.5	23925	3138	vw	$2\nu_{12}+\nu_{13}$	3144	6
4191.5	23851	3212	s	$2\nu_{8a}$	3210	2
4211.0	23741	3322	w	$\nu_{12}+\nu_{8a}+\nu_{11}$	3327	5
4228.0	26645	3418	w	$\nu_{12}+\nu_{8a}+\nu_{10b}(-)$	3423	5
4235.0	23606	3457	w	$\nu_{12}+\nu_{8a}+\nu_{10a}$	3461	4
4264.0	23446	3617	m	$2\nu_{12}+\nu_{8a}$	3620	3
4270.0	23413	3650	w	$2\nu_{12}+\nu_{8a}$ +lattice	3659	9
4320.0	23142	3921	w	$2\nu_{8a}+\nu_{11}$	3927	6
4340.0	23035	4028	w	$4\nu_{12}$	4020	8
4375.0	22851	4212	w	$\nu_{12}+2\nu_{8a}$	4215	3
4495.0	22241	4822	vw	$3\nu_{8a}$	4815	7

FIGURE 34

Phosphorescence from benzoic acid-d_0 in a cyclohexanecarboxylic acid host crystal at 4.2°K.

Meinel "C" spectrograph in 2nd order (10.35 Å/mm reciprocal dispersion).

Concentration (mole%)	0.03
Sample Thickness (mm)	8
Light Source	600 W Hg-Xe
Filters	8 cm H_2O + 7-54 (Corning) phosphorimeter
Slit Width (μ)	20
Kodak Film	103a-O
Exposure Time (min)	30

(Taken from Baum, 1974).

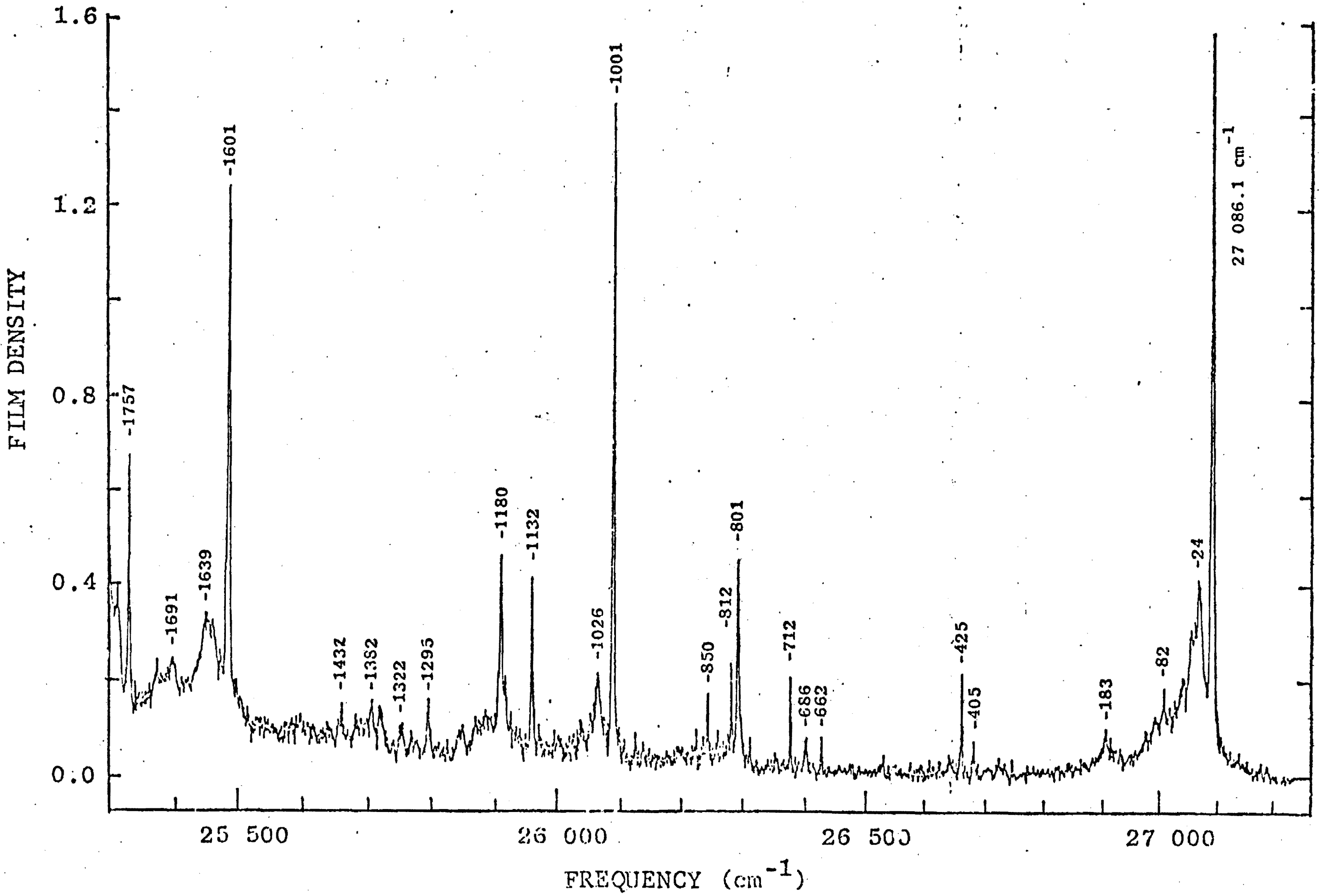
FILM DENSITY
1.6
1.2
0.8
0.4
0.0
-1757
-1691
-1639
-1601
-1432
-1382
-1322
-1295
-1180
-1132
-1026
-1001
-850
-812
-801
-712
-686
-662
-425
-405
-183
-82
-24
27 086.1 cm^{-1}
25 500
26 000
26 500
27 000
FREQUENCY (cm^{-1})

TABLE 26

PHOSPHORESCENCE SPECTRUM OF BENZOIC ACID-d0 IN CHCA

Rel. Int.[a]	Frequency (cm)[b]	Frequency Difr. (cm)	Assignment [c]	Raman,ir Freq.	Dev. [d]
vvs	27 086.1	0.0	origin		
m	27 062.1	24.1	lattice		
m	27 052.3	33.9	lattice		
w	27 037.1	49.0	lattice		
w	27 004.3	81.8	H-bond o.p. bend	88	+6
w	26 988	98	H-bond i.p. bend	98	0
vw	26 972	114	C-X torsion	120	+6
w	26 903.0	183.1	C-X wag	198	+15
vw	26 681.0	405.1	16a	408	+3
w	26 660.6	425.6	6a?		
Vvw	26 541	545	scissor	546	+1
vvw	26 527	559	scissor	557	+2
vvw	26 474	612	6b	616	+4
vw	26 423.8	662.3	i.p. fund. (ipf)	660	-2
vw	26 399.9	686.2	4	685	-1
w	26 373.7	712.5	11	711	-2
vw	26 305	781			
m	26 284.9	801.2	1	797	-4
w	26 273.8	812.4	o.p. fund. (opf)	812	0
w	26 235.9	850.3	10a	854	+4
vw	26 216.9	869.3	4+C-X wag		0
vw	26 135	951	C-H o.p. bend	948	-3
vw	26 096	990	5	989	-1
vs	26 085.4	1000.8	12	1001	0
w	26 060.1	1026.1	19a	1028	-2
			12+lattice		-1
Sh	26 050	1036	12+lattice		-1
vw	26 037	1049	12+lattice		+1
vw	26 001	1085	12+H-bond o.p. bend		+1
vw	25 966	1120	12+C-X torsion		-5
m	25 954.4	1131.8	C-X stretch	1134	+2
w	25 911.8	1174.4	15	1170	-4
m	25 906.0	1180.2	9a	1179	-1
			12+C-X wag		+4
w	25 881	1205	9a+lattice		-1
w	25 790.8	1295.3	COOH	1292	+3
vvw	25 772	1314	C-X stretch+wag		+1
vw	25 764	1322	14	1327	+5
vw	25 716	1370	9a+C-X wag		-7
w	25 704	1382	COOH?		
vw	25 675	1411	12+16a		-5
w	25 654.3	1431.8	12+6a		-5
vw	25 590.5	1495.6	18a	1494	-2
w	25 497	1589	8b	1587	-2

TABLE 26 (Cont'd)

PHOSPHORESCENCE SPECTRUM OF BENZOIC ACID-d0 IN CHCA

Rel. Int.[a]	Frequency (cm)[b]	Frequency Diff.(cm)	Assignment [c]	Raman,ir Freq.	Dev. [d]
vs	25 485.4	1600.7	8a	1601	0
			2(1)		+1
w	25 458.6	1627.6	8a+lattice		-3
w	25 446.9	1639.3	8a+lattice		-4
w	25 395	1691	12+4		0
			8a+H-bond op bend		-4
w	25 372	1714	12+11		0
			8a+C-X torsion		-1
s	25 329.6	1756.5			
w	25 312.8	1773.3			
m	25 302.2	1783.9	8a+C-X wag?		0
m	25 287.1	1799.0	12+1		+2
w	25 265.9	1820.2	12+opf		-7
w	25 243	1843	C-X stretch+11		+1
vvw	25 192	1894	9a+11		-2
vvw	25 134	1952	12+O-H o.p. bend		0
vw	25 104	1982	9a+1		-1
vvw	25 095	1991	12+5		0
m	25 084.9	2001.3	2(12)		+1
vw	25 078.0	2008.2	8a+16a		-2
w	25 060.9	2025.2	8a+6a		+2
			12+19a		+2
Sh	25 053.5	2032.6	2(12)+lattice		-2
m	25 049.1	2037.0	9a+10a		-7
vw	25 034	2052	2(12)+lattice		0
w	24 954.1	2132.0	12+C-X stretch		+1
w	24 907.2	2179.0	12+9a		+2
			2(12)+C-X wag		+6
vw	24 825	2261	8a+ipf		0
vvw	24 797	2289	8a+4		-2
vw	24 792	2294	12+CCCH		+2
w	24 772	2314	8a+11		0
			9a+C-X stretch		-2
w	24 682.3	2403.3	8a+1		-1
			2(12)+16a		+4
vw	24 672	2414	8a+opf		-1
vvw	24 654	2432	2(12)+6a		-4
vw	24 634	2452	8a+10a		-1
vvw	24 613	2473	12+18b		0
vw	24 590	2496	9a+14		+6
Sh	24 499	2587	12+8b		+3
m	24 481.3	2604.8	12+8a		-3
			12+9a+6a		+1
vw	24 456.5	2629.7	12+8a+lattice		-4

Table 26 (Cont'd)

PHOSPHORESCENCE SPECTRUM OF BENZOIC ACID-d0 IN CHCl3

Rel. Int.[a]	Frequency (cm)[b]	Frequency Diff. (cm)	Assignment [c]	Raman,ir Freq.	Dev. [d]
			8a+19a		-3
vw	24 444	2642	12+8a+lattice		-6
vw	24 354.8	2731.3	8a+C-X stretch		+2
vw	24 325	2761	12+(1757)		-4
Sh	24 314	2772	8a+15		-1
w	24 303.2	2782.9	8a+9a		-2
			12+8a+C-X wag		+1
vw	24 277	2809	2(12)+1		-6
vvw	24 219	2867	12+9a+ipf		0
vvw	24 189	2897	12+9a+11		-4
vvw	24 154	2932			
vw	24 078	3008	3(12)		-5
vw	24 052	3034	12+8a+6a		-6
vvw	23 949	3137	2(12)+C-X stretch		-3
vvw	23 917	3169	2(12)+15		+7
vw	23 899	3187	8a+8b		+3
			2(12)+9a		-5
w	23 879	3207	2(8a)		-5
vvw	23 772	3314	12+8a+11		+1
vvw	23 744	3342	8a+11+19a		-2
vw	23 728	3358	8a+(1757)		0
vvw	23 636	3450	12+8a+10a		+2
vvw	23 611	3475	2(12)+18b		-1
vvw	23 591	3495	2(12)+18a		-3
vw	23 482	3604	2(12)+8a		0
			2(8a)+16a		+3
vvw	23 357	3729	12+8a+C-X stret		+5
vw	23 300	3786	12+8a+9a		-4
vvw	23 162	3924	12+8a+14		0
vvw	23 118	3968	8a+2(9a)		-7
vvw	23 078	4008	4(12)		-4
			2(8a)+1		-5
w	22 879	4207	12+2(8a)		-4
vw	22 701	4385	2(8a)+9a		-3
			12+2(8a)+C-X wag		+1
vw	22 281	4805	3(8a)		-2

[a] - Relative intensity, qualitatively estimated from the microdensitometer tracing of photographic film. vvs = very, very strong; vs = very strong; s = strong; m = medium; w = weak; vw = very weak; vvw = very, very weak; Sh = shoulder.

[b] - Vacuum corrected values. The r.m.s. deviation is 1.5 wavenumbers.

Table 26 (Cont'd)

PHOSPHORESCENCE SPECTRUM OF BENZOIC ACID-d0 IN CHCA

[c] - The vibrational notations are the same as those described in section IV.A. i.p. fund. = in-plane fundamental; o.p. fund. = out-of-plane fundamental; C-X = ring-substituent motion. When more than one assignment is possible, the assignments are given in order of greatest probability.

[d] - For the fundamentals, the deviation is the frequency difference between the Raman (or infrared) values and the values in the emission spectrum. For the combinations and overtones, the deviation is the frequency difference between the calculated harmonic values and the observed values.

FIGURE 35

Phosphorescence Spectrum of Parafluorobenzoic Acid in Polycrystalline n-Nonane

Spex 1702 3/4 Meter Czerny Turner Monochromator

Concentration: $\sim 10^{-2}$ molar

Slit Width : 48 μ, 48 μ

Sensitivity : 1×10^{-7} amperes full scale

Time Constant: 1.0 second

Scan Rate : 20 Å/minute

Temperature : 4.2° K

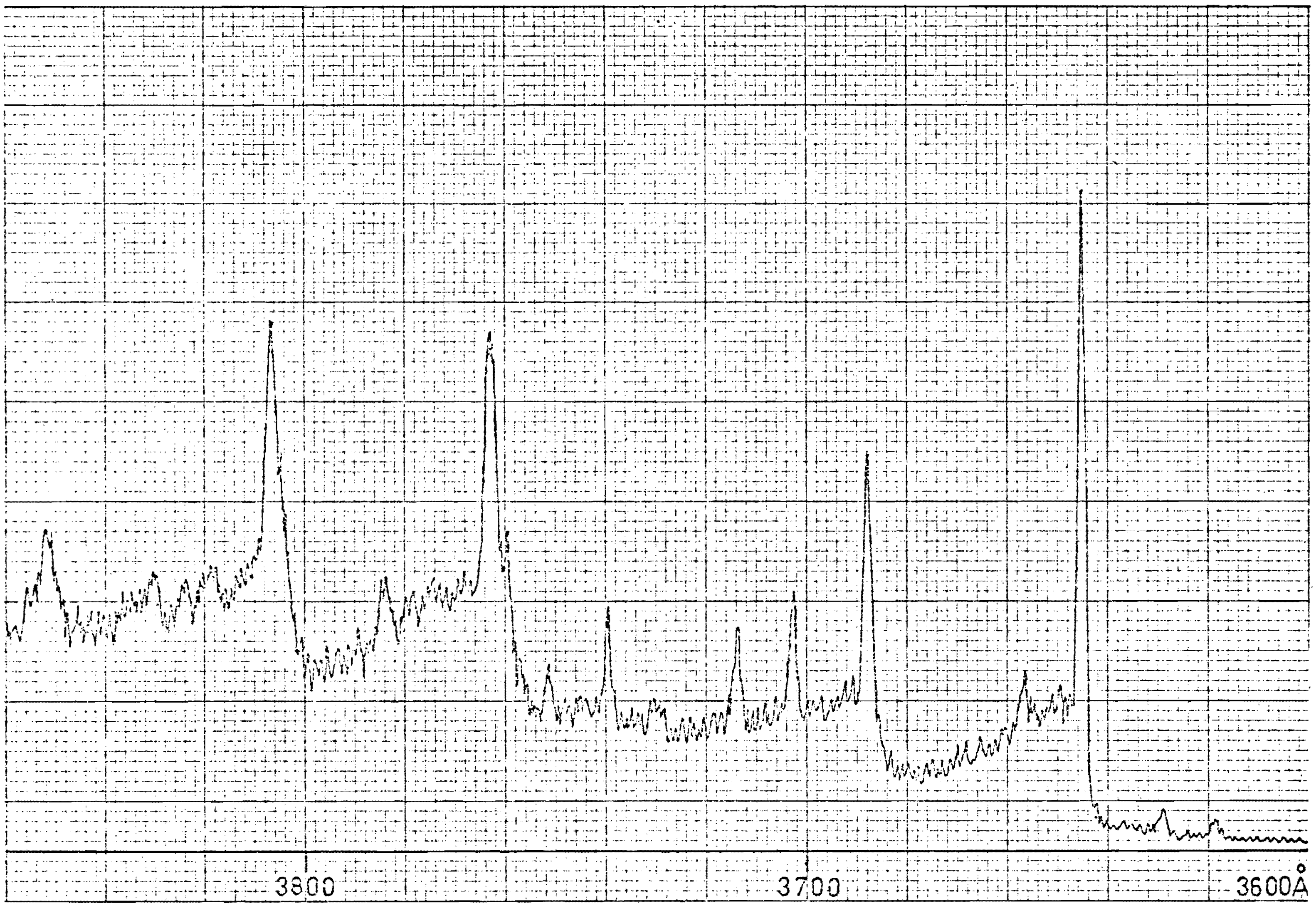
3800
3700
3600Å


4100
4000
3900 Å

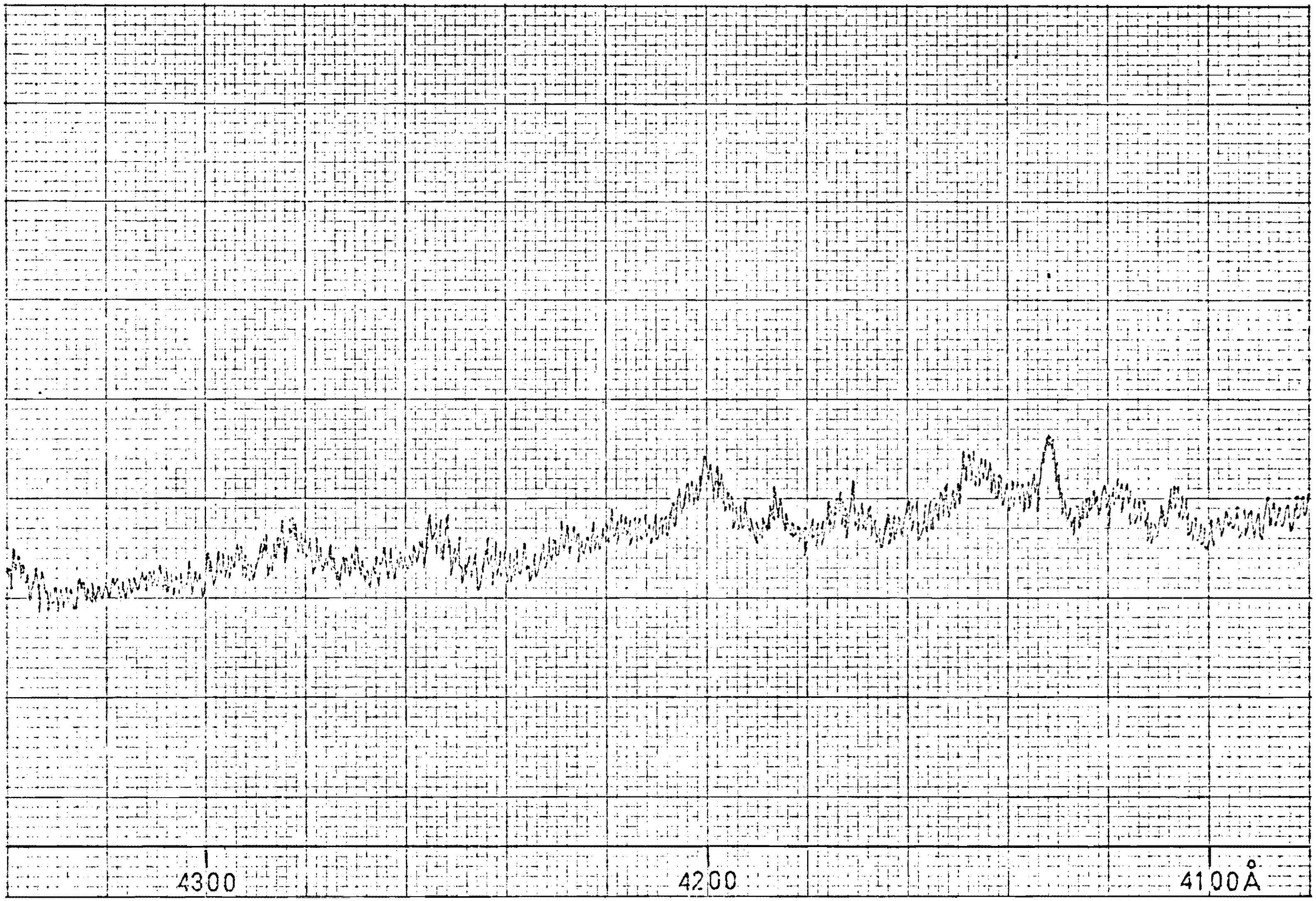
4300
4200
4100 Å

TABLE 27

This table contains the frequencies, relative intensities, and assignments of bands in the spectrum shown in Figure 35. Only bands of special interest have been assigned. These assignments have been made using the Varsanyi tables and phosphorescence frequencies. s = strong, w = weak, and vw = very weak.

λ(Å)	ν(cm^{-1})	Δν(cm^{-1})	Intensity	Assignment
3645.0	27427	0	s	
3650.0	27389	38	vw	
3656.5	27341	86	w	ν_{11}
3688.0	27107	320	s	ν_{10b}
3703.0	26997	430	m	ν_{16a}
3714.0	26918	509	m	16b
3730.0	26802	625	vw	
3740.0	26730	697	m	ν_4
3752.0	26645	782	w	ν_{10a} or ν_{17b}
3760.0	26588	839	vw	
3763.0	26567	860	s	ν_1
3784.5	26416	1011	w	
3807.0	26260	1167	s	
3819.0	26177	1250	vw	
3824.0	26143	1284	vw	
3830.0	26102	1325	vw	
3852.0	25953	1474	m	
3873.5	25809	1618	s	ν_{8a}
3886.0	25726	1701	w	
3888.0	25713	1714	w	
3910.0	25568	1859	vw	
3921.0	25497	1930	w	
3934.0	25412	2015	m	
3950.0	25309	2118	vw	
3980.0	25119	2308	w	
4004.0	24967	2460	vw	
4006.0	24956	2471	m	
4055.0	24654	2773	m	
4069.0	24569	2858	vw	
4107.0	24342	3085	vw	
4118.0	24277	3150	vw	
4132.0	24195	3232	w	
4148.0	24101	3326	vw	
4172.0	23963	3464	vw	
4186.0	23882	3545	vw	
4200.0	23802	3625	w	
4254.0	23500	3927	vw	
4283.0	23342	4085	w	
4339.0	23040	4387	vw	

FIGURE 36

Phosphorescence Spectrum of Parafluorobenzoic Acid in Polycrystalline Cyclohexane Carboxylic Acid.

Spex 1702 3/4 Meter Czerny Turner Monochromator

Concentration: ∿.7 mole percent
Slit Width : 38 μ, 38 μ
Sensitivity : 3×10^{-7} amperes full scale
Time Constant: 1.0 second
Scan Rate : 20 Å/minute
Temperature : 4.2° K

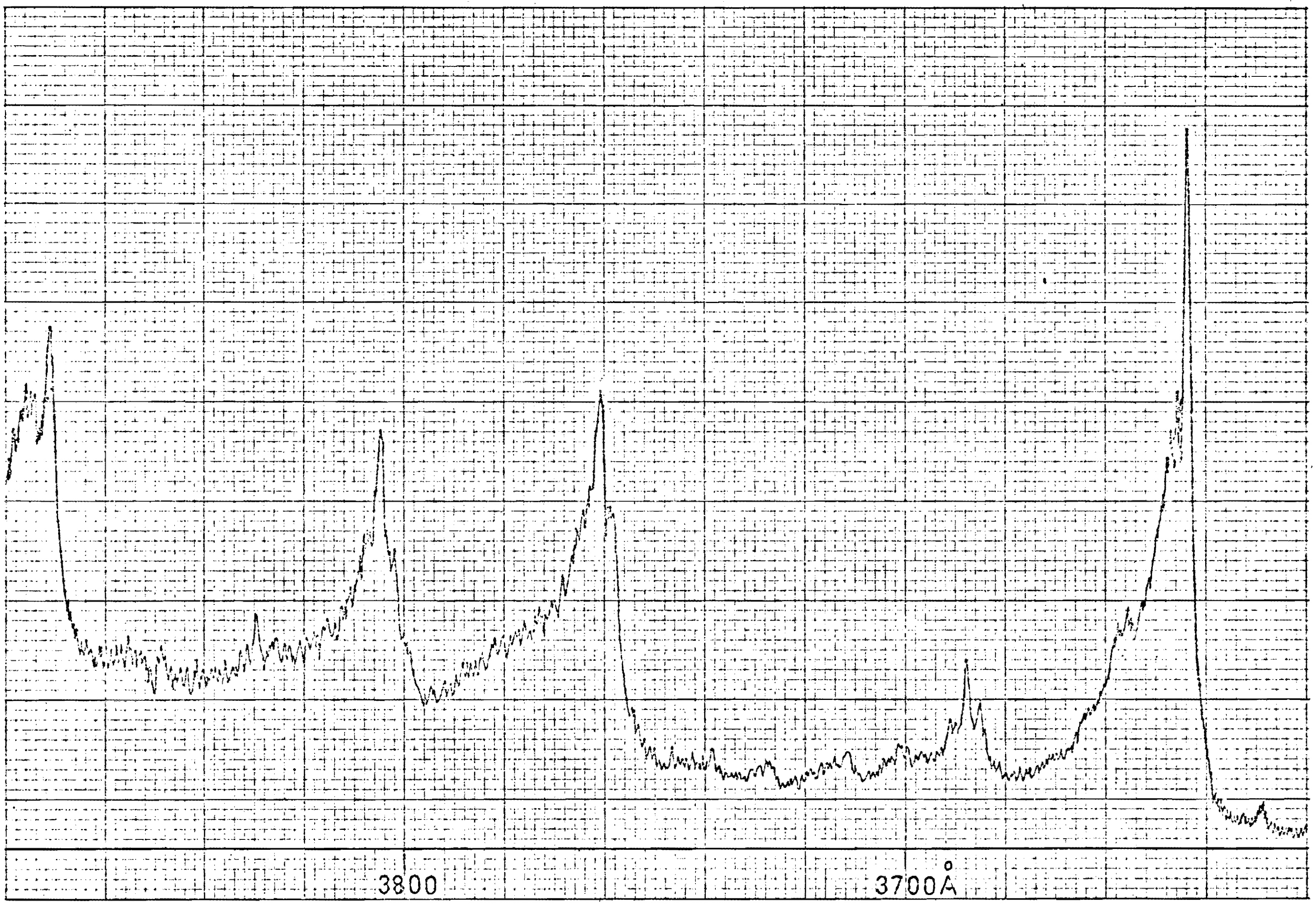
3800
3700 Å

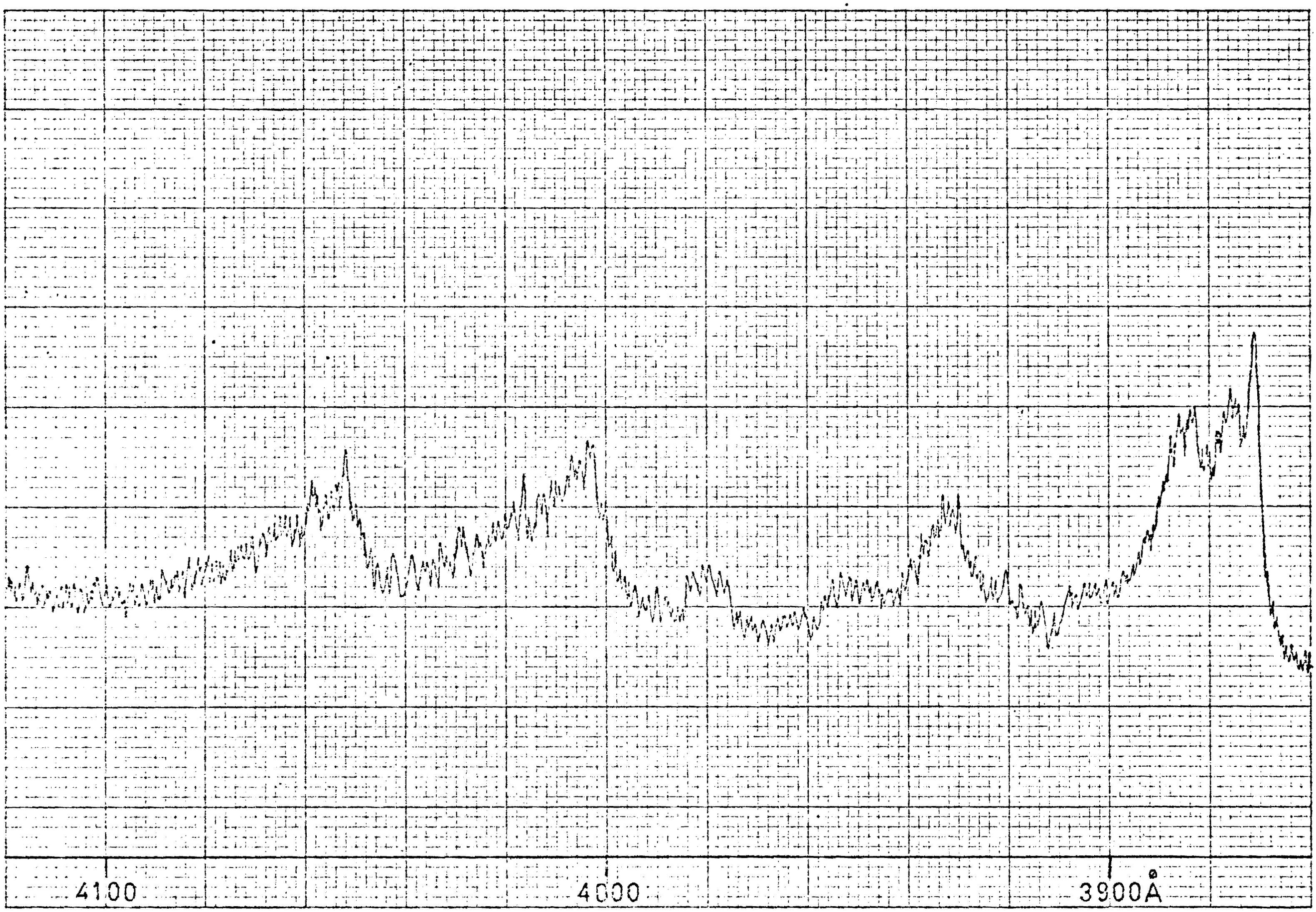
4100
4000
3900Å

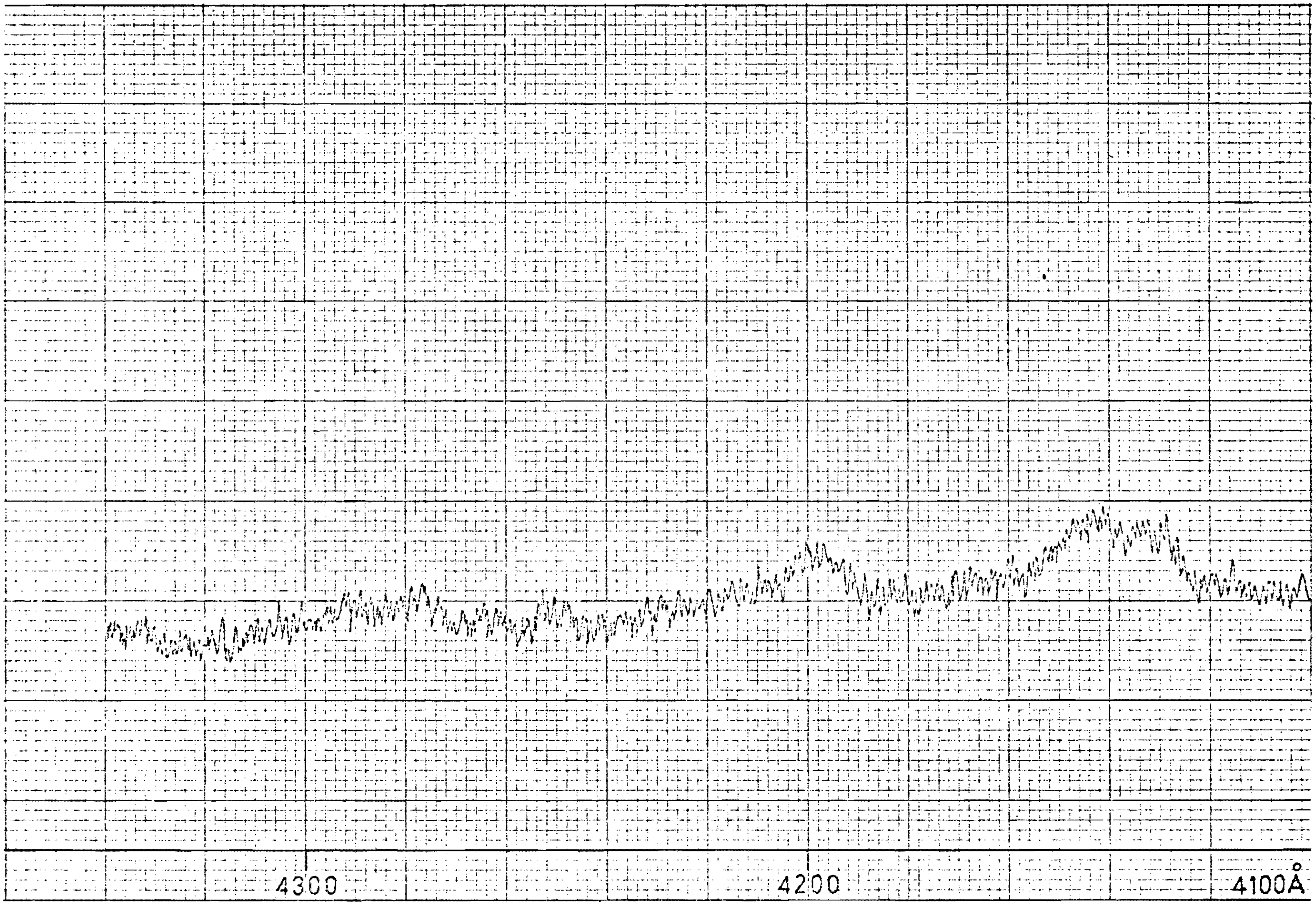
4300
4200
4100Å

TABLE 28

This table contains the frequencies, relative intensities, and assignments of bands in the spectrum shown in Figure 36. Only bands of special interest have been assigned. These assignments have been made using the Varsanyi tables and phosphorescence frequencies. s = strong, w = weak, and vw = very weak.

λ(Å)	ν(cm^{-1})	$\Delta\nu$(cm^{-1})	Intensity	Assignment
3629.5	27544	- 106		
3643.5	27438	0	s	
3645.5	27423	15	m	
3656.0	27344	94	w	ν_{11}
3685.0	27129	309	vw	
3688.0	27107	331	w	ν_{10b}
3691.0	27085	353	vw	
3701.0	27012	426	vw	ν_{16a}
3711.0	26439	499	vw	ν_{16b}
3727.0	26824	614	vw	
3738.5	26741	697	vw	ν_4
3759.0	26595	843	m	
3760.5	26585	853	s	ν_1
3802.0	26295	1143	vw	
3804.5	26277	1161	s	
3830.0	26102	1336	vw	
3871.0	25826	1612	s	ν_{8a}
3875.5	25796	1642	s	
3883.0	25743	1695	s	
3886.0	25723	1715	m	
3932.0	25425	2013	m	
3952.0	25297	2141	vw	
3980.0	25119	2319	w	
4003.0	24974	2464	m	
4052.0	25672	2566	m	
4058.5	25633	2605	w	
4132.0	24195	3243	m	
4142.0	24136	3302	m	
4198.0	23814	3624	m	

FIGURE 37

Phosphorescence Spectrum of Methyl Benzoate in Polycrystalline Benzene

Spex 1702 3/4 Meter Czerny Turner Monochromator

Concentration: $\sim 10^{-3}$ molar

Slit Width : 75 μ, 75 μ

Sensitivity : 3×10^{-7} amperes full scale

Time Constant: 0.3 seconds

Scan Rate : 20 Å/minute

Temperature : 4.2° K

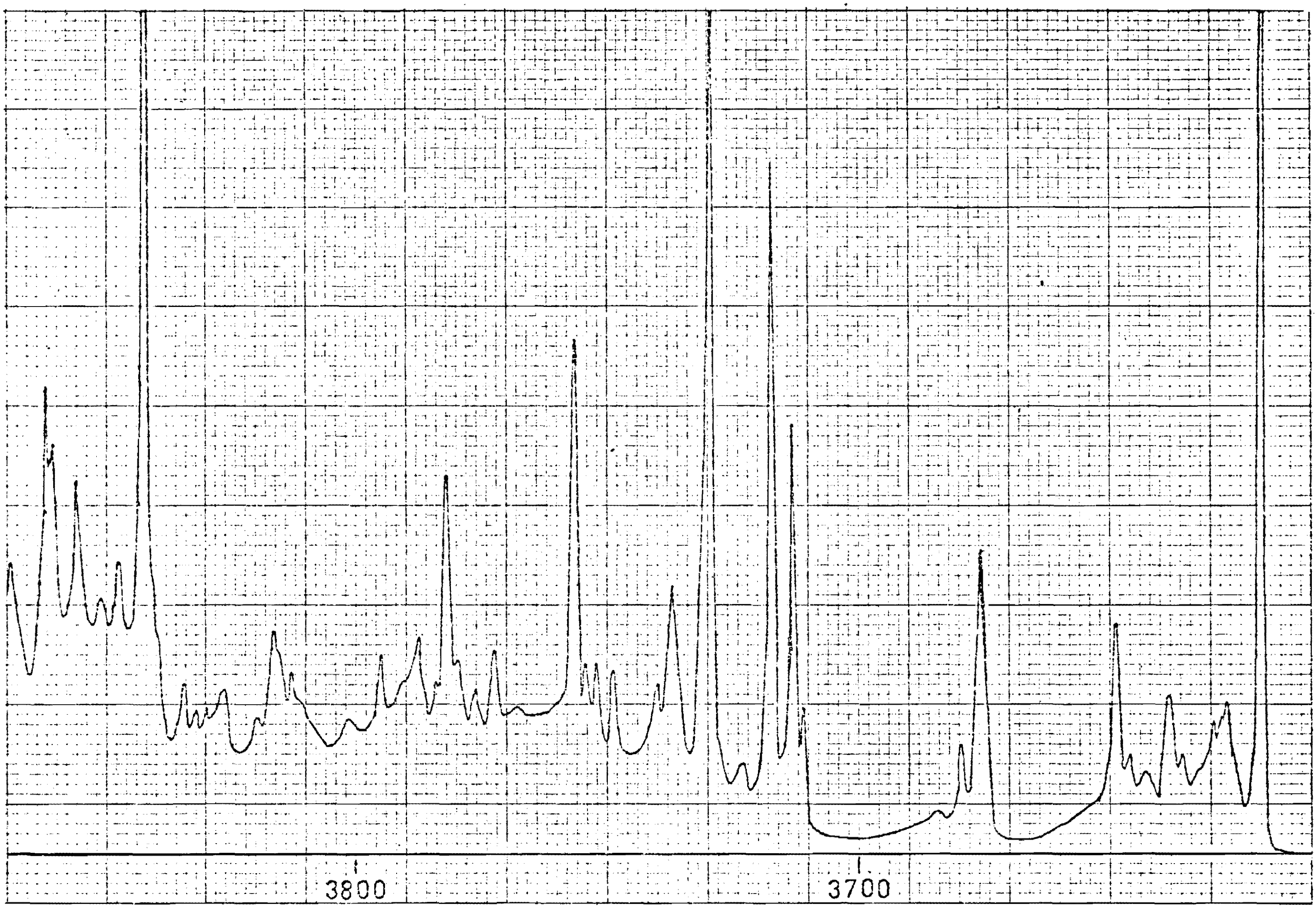
3800
3700

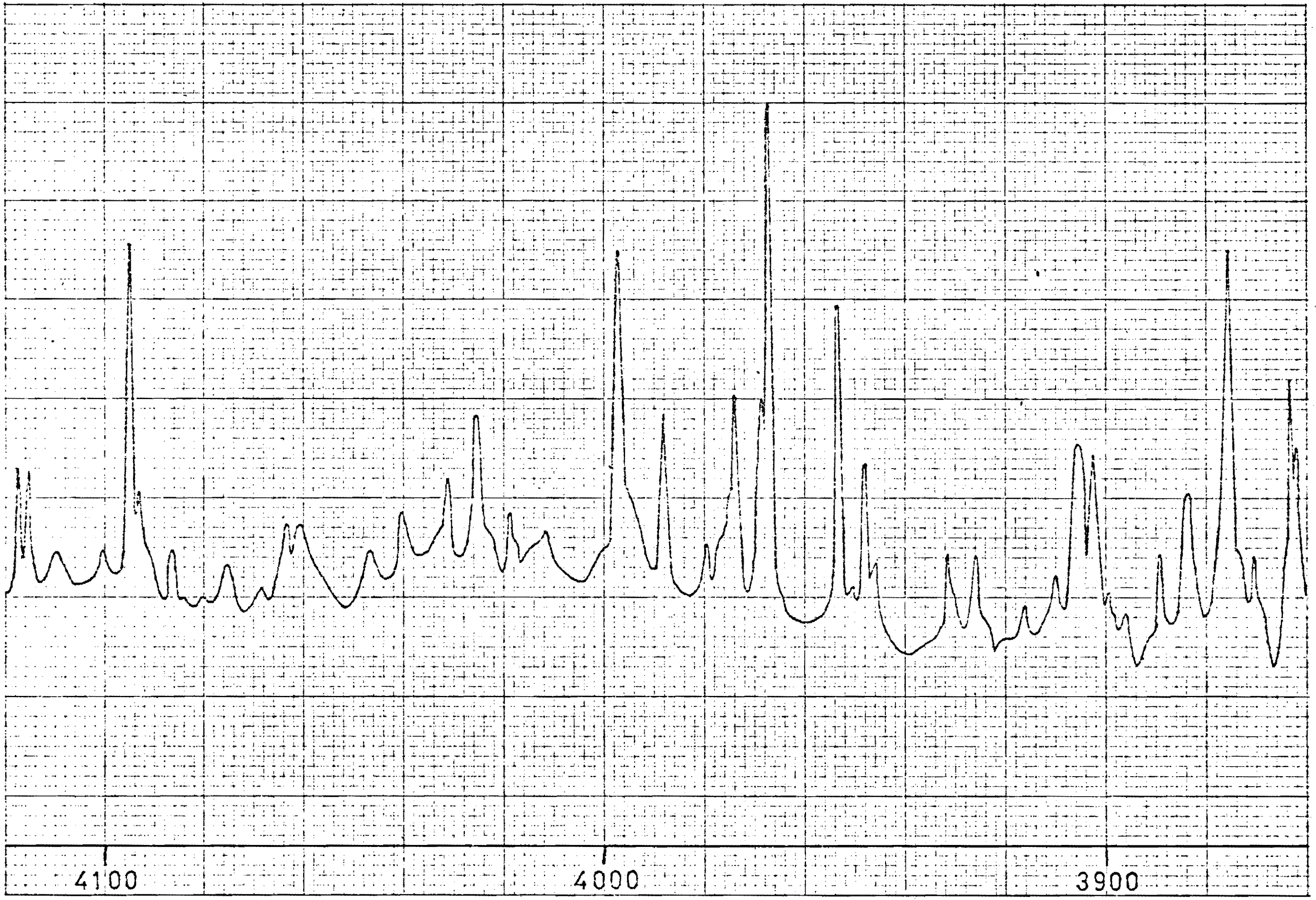
4100
4000
3900

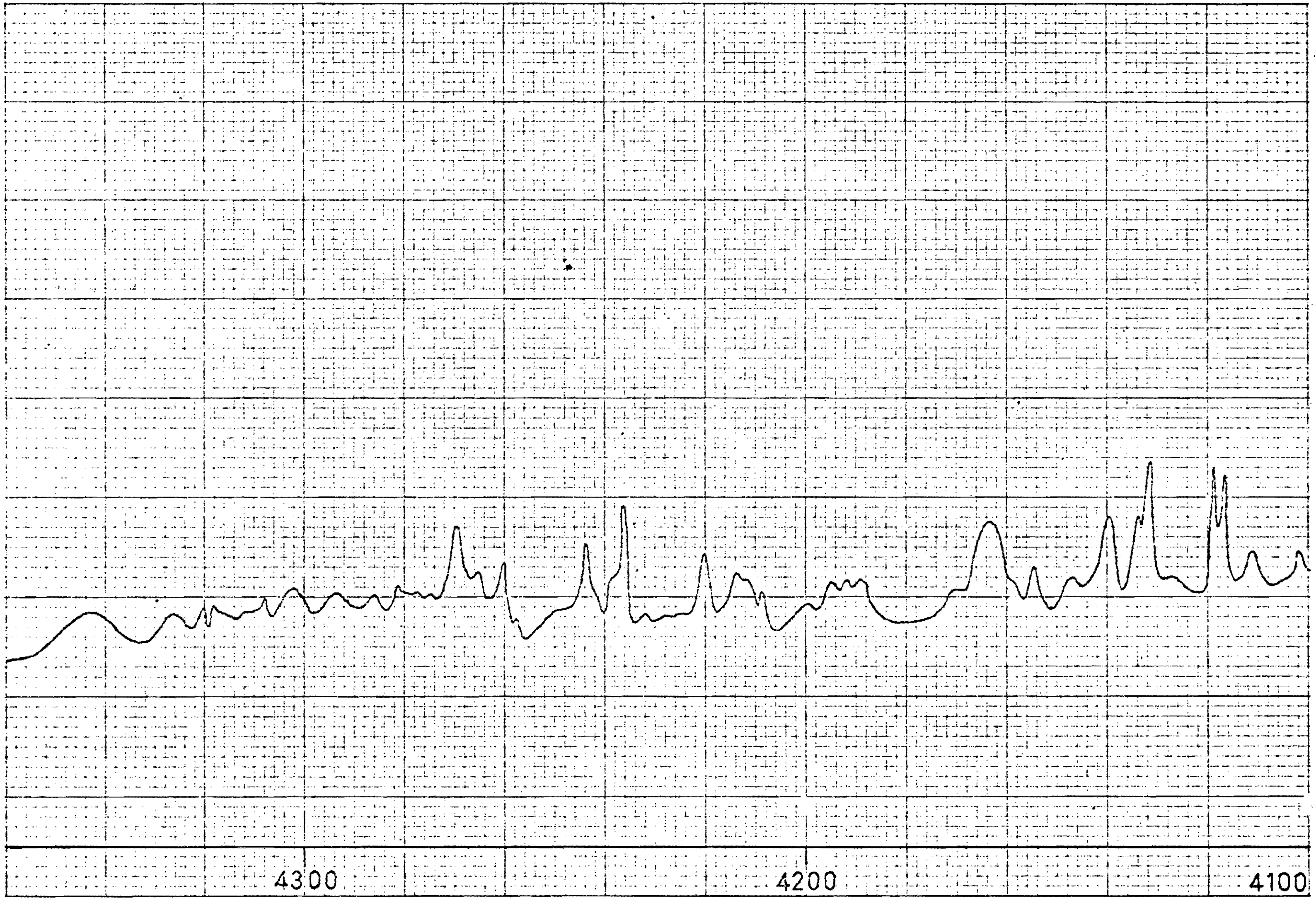
4300
4200
4100

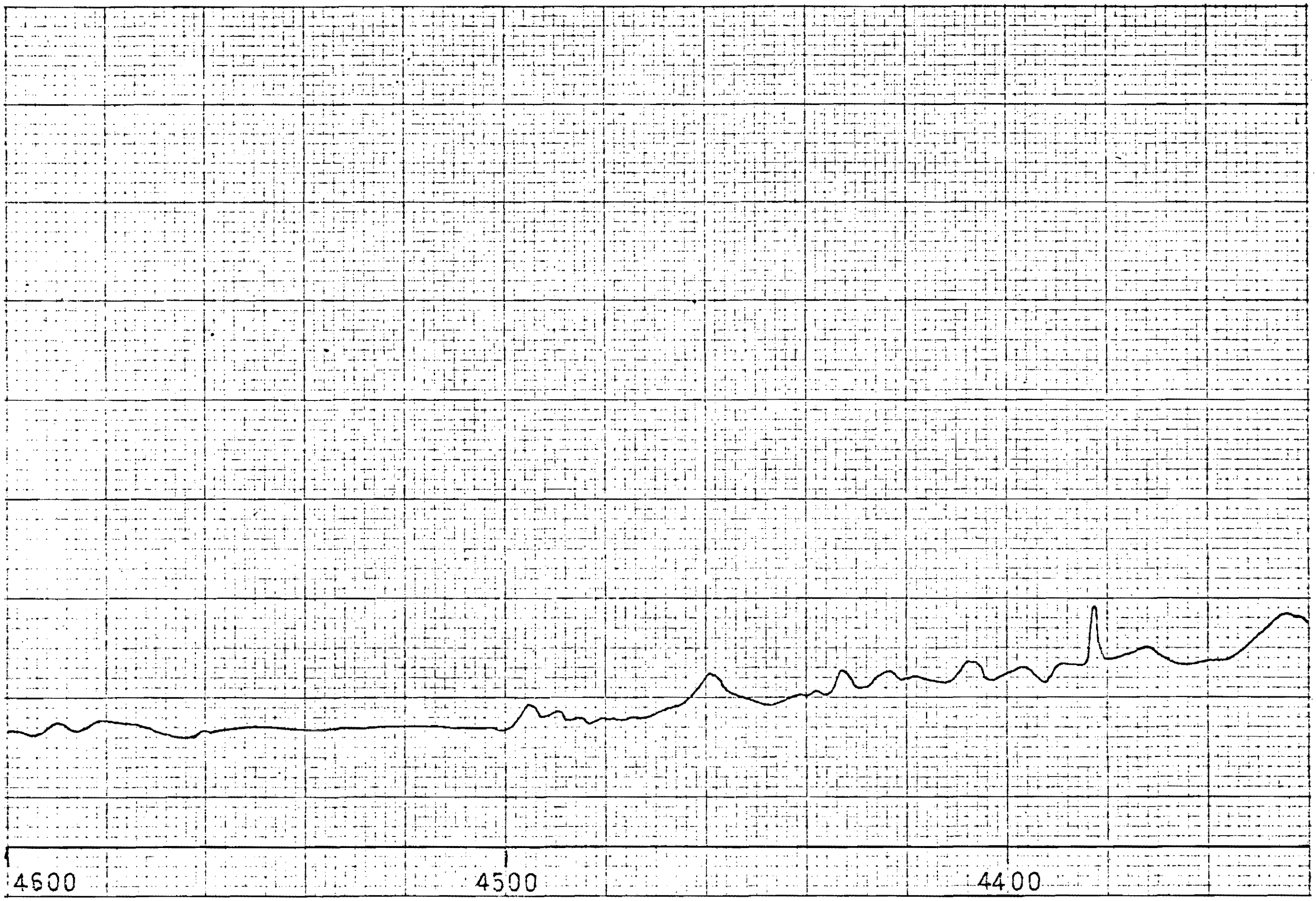
4600
4500
4400

TABLE 29

This table contains the frequencies, relative intensities, and assignments of bands in the spectrum shown in Figure 37. The assignments are based upon a consideration of the photoelectric spectra obtained in this study, as well as Baum's more accurate photographic data. Only the most probable assignments are given. For some bands, particularly combination bands, alternate assignments are possible. All Raman frequencies are rounded off to the nearest wavenumber. Actual Raman frequencies are given only for fundamentals. For combination bands sums of phosphorescence frequencies are given. s = strong, w = weak, and vw = very weak.

λ(Å)	ν(cm^{-1})	$\Delta\nu$(cm^{-1})	Intensity	Assignments	Raman Freq.(cm^{-1})	Deviation (cm^{-1})
3620.0	27616	0.0	s	Origin		
3627.0	27563	53.0	w	lattice		
3628.0	27556	60.0	vw	lattice		
3629.5	27544	72.0	vw	lattice		
639.0	27472	144	w	torsion(T)?		
3649.0	27397	219	m	$\nu_{10b}^{(+)}$	215	4
3676.0	27196	420	m	$\nu_{16a}+\nu_{6a}$	406 & ?	14 & ?
3680.0	27166	450	w	ν_{16b}	437	13
3712.0	26932	684	w	$\nu_{9b}^{(-)}$	677	7
3713.0	26925	691	s	ν_4	?	?
3718.0	26889	727	s	ν_{11}	714	13
3724.0	26845	771	vw	ν_4+lattice	780	9
3730.0	26802	814	s	$\nu_{10b}^{(-)}$	810	4
3732.0	26788	828	w	ν_1	825	3
3737.0	26752	864	m	ν_{10a}	855	9
3740.5	26727	889	vw	$\nu_{10b}^{(-)}$ + lattice	886	3
3749.0	26666	950	w	ν_{17b}	?	6
3753.0	26638	978	w	O-CH$_3$ bend	969	9
3755.0	26624	992	vw	ν_5	992	0
3757.0	26609	1007	s	ν_{12}	1005	2
3773.0	26497	1119	w	ν_{13}	1113	6
3777.0	26469	1147	vw	ν_{12}+ T	1151	4
3780.0	26448	1168	vw	ν_{15}	1161	7
3782.5	26434	1182	m	ν_{9a}	1180	2
3788.5	26388	1228	w	$\nu_{12}+\nu_{10b}^{(+)}$	1226	2
3796.0	26336	1280	w	COOCH$_3$	1280	0
3814.0	26212	1404	vw	$\nu_{9a}+\nu_{10b}^{(+)}$	1401	3
3816.0	26198	1418	vw	$\nu_{12}+\nu_{16a}$	1419	1

Table 29 (Continued)

4019.0	25875	2741	vw	$\nu_{12}+$ C=0 stretch	2750	9
4024.0	24844	2772	vw	$\nu_{8a}+\nu_{15}$	2773	1
4027.0	24825	2791	w	$\nu_{8a}+\nu_{9a}$	2782	9
4032.0	24795	2821	w	$2\nu_{12}+\nu_{10b}(-)$	2828	7
4041.5	24739	2877	w	$2\nu_{12}+\nu_{10a}$	2878	1
4047.5	24700	2916	vw	$\nu_{12}+\nu_{9a}+\nu_{11}$	2916	0
4062.0	24611	3005	w	$3\nu_{12}$	3021	16
4065.0	24593	3023	w	$\nu_{12}+\nu_{8a}+\nu_{16a}$	3032	9
4070.0	24563	3053	vw	$\nu_{12}+\nu_{8a}+$ 16b	3062	9
4076.0	24527	3089	w	$2\nu_{12}+$lattice	3093	4
4087.5	24461	3155	w	$3\nu_{12}+$ T	3165	10
4096.0	24407	3209	s	$2\nu_{8a}$	3210	1
4111.0	24318	3298	vw	$\nu_{12}+\nu_{8a}+\nu_{4}$	3303	5
4116.5	24289	3327	w	$\nu_{12}+\nu_{8a}+\nu_{11}$	3339	12
3118.5	24277	3339	w	$\nu_{8a}+$C=0 stretch	3348	9
4131.5	24200	3416	w	$\nu_{12}+\nu_{8a}+\nu_{10b}(-)$	3426	10
4133.5	24186	3430	vw	$\nu_{12}+\nu_{8a}+\nu_{1}$	3440	10
4140.0	24148	3468	w	$\nu_{12}+\nu_{8a}+\nu_{10a}$	3476	8
4147.5	24105	3512	vw	$\nu_{8a}+\nu_{9a}+\nu_{11}$	3514	2
4155.0	24061	3555	vw	$\nu_{8a}+\nu_{12}+\nu_{17b}$	3562	7
4163.5	24014	3602	w	$2\nu_{12}+\nu_{8a}$	3619	17
4171.0	23968	3648	vw	$2\nu_{8a}+\nu_{16b}$	3660	12
4220.5	23690	3926	w	$2\nu_{8a}+\nu_{11}$	3937	
4236.5	23598	4018	w	$2\nu_{8a}+\nu_{10b}(-)$	4024	6
4244.5	23556	4060	w	$2\nu_{8a}+\nu_{10a}$	4065	5
4260.5	23468	4148	w	$2\nu_{8a}+\nu_{17b}$	4160	12
4270.5	23413	4203	w	$2\nu_{8a}+\nu_{12}$	4217	14
4344.0	23014	4602	w	$3\nu_{12}+\nu_{8a}$	4626	24
4383.0	22809	4807	w	$3\nu_{8a}$	4815	8
4407.5	26282	4934	vw	$2\nu_{8a}+\nu_{12}+\nu_{11}$	4944	10
4433.0	22552	5064	vw	$2\nu_{8a}+\nu_{9a}+ + \nu_{9b}(-)$	5069	5
4460.0	22415	5201	vw	$2\nu_{12}+2\nu_{8a}$	5224	23

Table 29 (Continued)

3818.0	26184	1432	w	$\nu_{12}+\nu_{6a}$	1427	5
3827.0	26123	1493	w	$\nu_{9b}(-)+\nu_{10b}(-)$	1498	6
3830.5	26099	1517	vw	$\nu_1+\nu_4$	1519	2
3833.0	26082	1534	vw	$\nu_{13}+\nu_{6a}$	1533	1
3836.0	26061	1555	w	$\nu_1+\nu_{11}$	1555	0
3843.5	26011	1605	s	ν_{8a}	1603	2
3848.5	25977	1639	w	$\nu_1+\nu_{10b}(-)$	1642	3
3852.0	25953	1633	vw	ν_{8a}+lattice	1658	5
3857.5	25916	1700	w	$\nu_{12}+\nu_4$	1698	2
3862.0	25886	1730	w	$\nu_{12}+\nu_{11}$	1734	4
3864.0	25873	1743	m	C=0 stetch	1725	18
3870.0	25832	1784	w	$\nu_{10b}(-)$ + O-CH_3 bend	1792	8
3875.5	25796	1820	s	$\nu_{12}+\nu_{10b}(-)$	1821	1
3883.0	25746	1870	w	$\nu_{12}+\nu_{10a}$	1871	1
3889.0	25706	1910	w	$\nu_{9a}+\nu_{11}$	1909	1
3896.0	25660	1956	vw	C=0 stretch + $\nu_{10b}(+)$	1962	6
3899.5	25637	1979	vw	ν_{12}+ O-CH_3 bend	1985	6
3902.0	25621	1995	w	$\nu_{12}+\nu_5$	1997	2
3905.0	25601	2015	m	$2\nu_{12}$	2014	1
3910.0	25568	2048	vw	$\nu_{8a}+\nu_{16b}$	2055	7
3916.0	25529	2087	vw	$2\nu_{12}$+lattice	2086	1
3926.0	25464	2152	w	$2\nu_{12}$+lattice	2158	6
3932.0	25425	2191	w	$\nu_{12}+\nu_{9a}$	2189	2
3946.0	25335	2281	vw	ν_{12}+$COOCH_3$	2287	6
3948.0	25322	2294	w	$\nu_{8a}+\nu_4$	2296	2
3953.5	25290	2326	s	$\nu_{8a}+\nu_{11}$	2332	6
3967.5	25198	2418	s	$\nu_{8a}+\nu_{10b}(-)$	2416	2
3969.5	25185	2431	w	$\nu_{8a}+\nu_1$	2433	2
3974.5	25153	2463	m	$2\nu_{12}+\nu_{16b}$	2464	1
3980.0	25119	2497	vw	$\nu_{8a}+\nu_{10b}(+)$ $+\nu_{9b}(-)$	2508	11
3988.5	25065	2551	m	$\nu_{8a}+\nu_{17b}$	2555	4
3997.0	25009	2607	m	$\nu_{12}+\nu_{8a}$	2612	5
4012.5	24915	2701	vw	$2\nu_{12}+\nu_4$	2705	4

FIGURE 38

Phosphorescence Spectrum of Benzoic Acid in Polycrystalline Methyl Benzoate (Spectrum III)

Spex 1702 3/4 Meter Czerny Turner Monochromator

Concentration: 0.1 mole percent
Slit Width : 38 μ, 38 μ
Sensitivity : 3×10^{-7} amperes full scale
Time Constant: 1.0 second
Scan Rate : 20 Å/minute
Temperature : 4.2° K

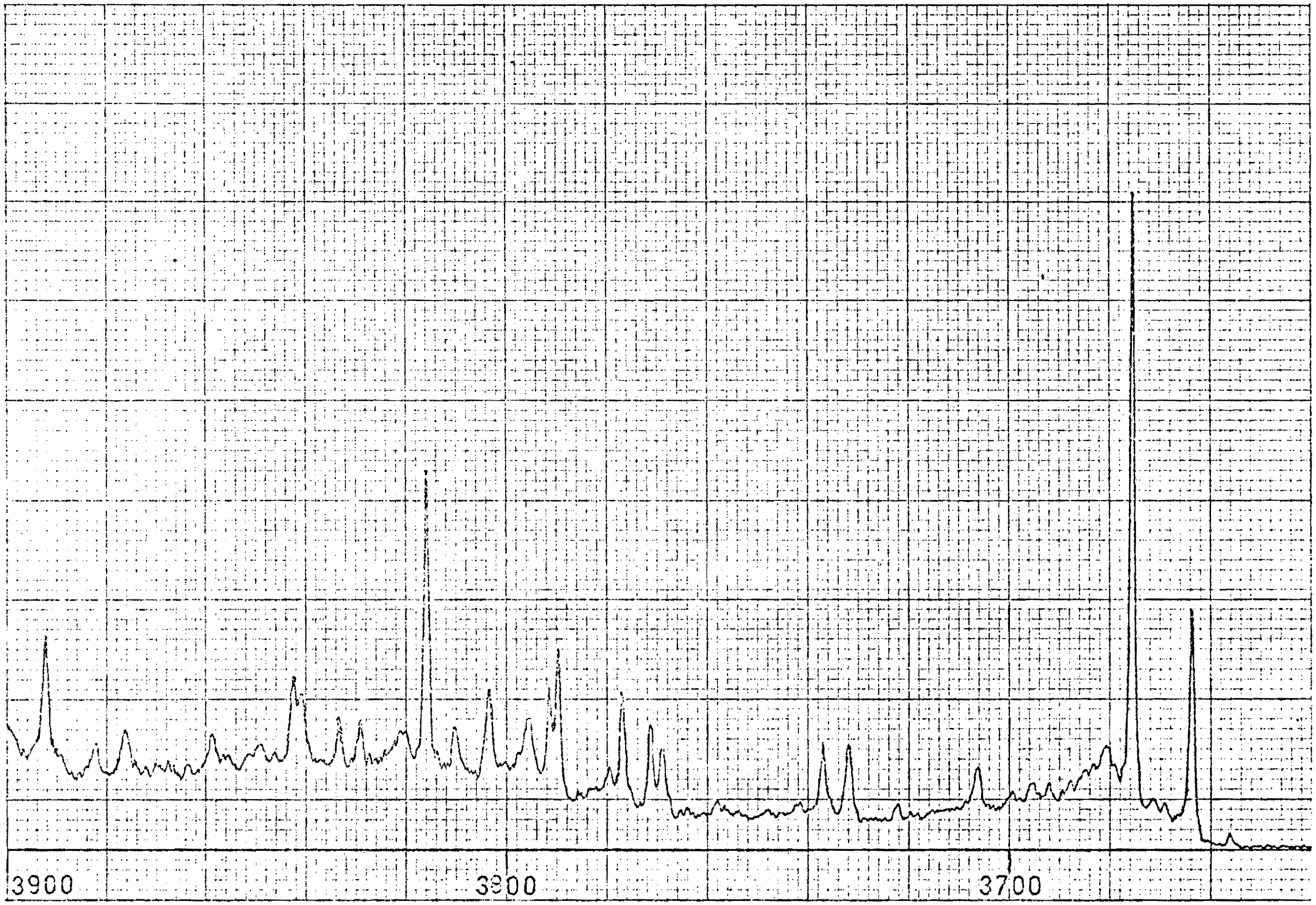
3900
3800
3700


4100
4000
3900

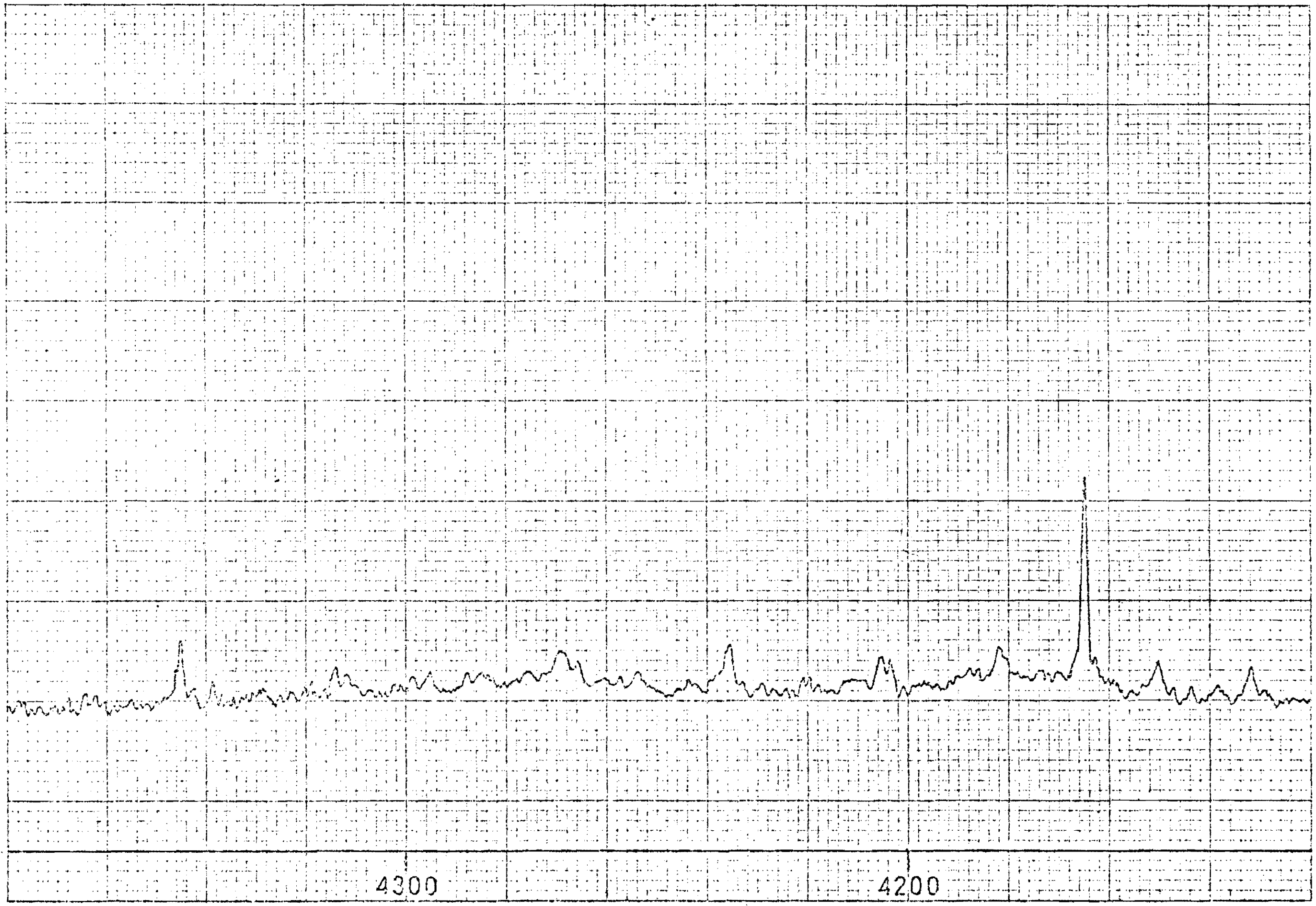
4300
4200

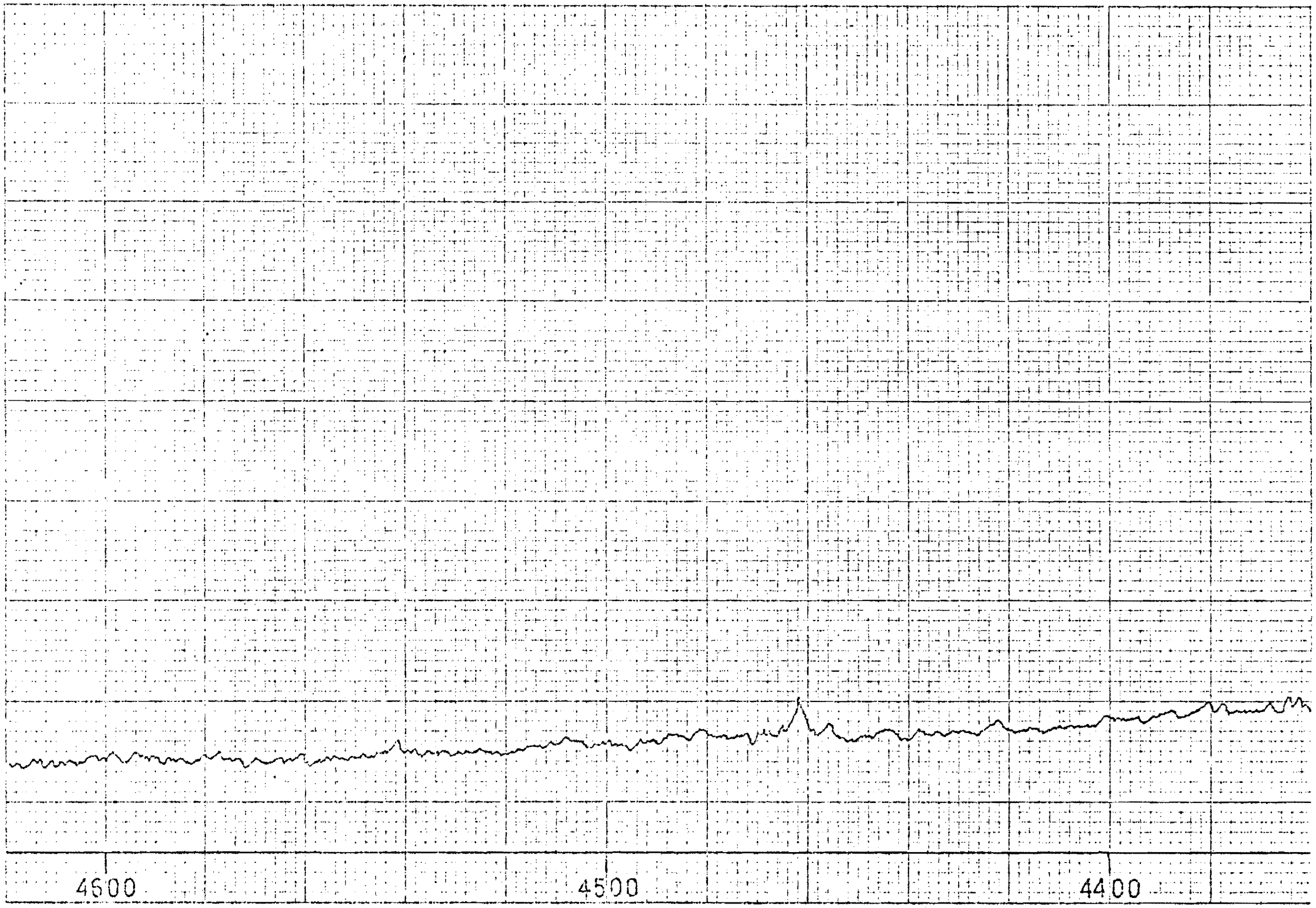
4600
4500
4400

TABLE 30

This table contains the frequencies, relative intensities, and assignments of bands shown in Figure 38. Only the most probable assignments are given. For some bands, particularly combination bands, alternate assignments are possible. All Raman frequencies are rounded off to the nearest wavenumber. Actual Raman frequencies are given only for fundamentals. For combination bands sums of phosphorescence frequencies are given. s = strong, w = weak, and vw = very weak.

λ(Å)	ν(cm^{-1})	$\Delta\nu$(cm^{-1})	Intensity	Assignment	Raman Freq.(cm^{-1})	Deviation (cm^{-1})
3663.0	27289	-86	m	O_2		
3675.0	27203	0	s	O_1		
3680.5	27163	40	vw	?		
3692.0	27078	125	vw	?		
3695.5	27052	151	vw	O_2+231		
3699.5	27023	180	vw	?		
3706.5	26972	231	vw	$\nu_{10b}(+)$	215	16
3722.0	26860	343	vw	O_2+415	329	14
3732.0	26788	415	w	ν_{16a}	406	9
3737.0	26752	451	w	ν_{16b}	437	14
3758.5	26599	604	vw	O_2+696	610	6
3769.0	26525	678	w	$\nu_{9b}(-)$	677	1
3771.0	26507	696	w	ν_4	?	?
3777.0	26469	734	w	ν_{11}	714	20
3780.0	26448	755	vw	O_2+836	750	5
3790.0	26378	825	w	$\nu_{10b}(-)$	810	15
3791.5	26367	836	w	ν_1	825	9
3795.5	26340	863	w	ν_{10a}	855	8
3803.5	26284	919	w	O_2+1005	919	0
3810.5	26236	967	vw	O-CH_3 bend	971	4
3816.0	26198	1005	m	ν_{12}	1005	0
3821.0	26164	1039	vw	ν_{18a}	1029	10
3829.0	26109	1094	vw	O_2+1175	1089	5
3833.5	26078	1125	vw	ν_{13}	1113	12
3841.0	26028	1175	w	ν_{15}	1161	14
3842.5	26017	1186	w	ν_{9a}	1180	6
3859.0	25906	1297	vw	$COOCH_3$	1280	17

Table 30 (Continued)

3876.5	25789	1414	vw	$\nu_{12}+\nu_{16a}$	1420	6
3882.0	25753	1450	vw	ν_{19b}	1455	5
3892.5	25683	1520	w	O_2+1602	1516	4
3905.0	25601	1602	s	ν_{8a}	1603	1
3912.5	25552	1651	vw	ν_{8a}+40	1642	9
3919.5	25506	1697	w	$\nu_{12}+\nu_4$	1701	4
3925.0	25471	1732	vw	$\nu_{12}+\nu_{11}$	1739	7
3939.0	25380	1823	vw	$\nu_{12}+\nu_{10b}$(-)	1830	7
3941.0	25367	1836	vw	$\nu_{12}+\nu_1$	1841	4
3945.0	25341	1862	vw	$\nu_{12}+\nu_{10a}$	1868	6
3947.5	25325	1878	vw	O_2+1967	1881	3
3954.0	25284	1919	vw	$O_2+2\nu_{12}$	1924	5
3961.5	25236	1967	vw	ν_{12}+O-CH$_3$ bend	1972	5
3968.0	25195	2008	w	$2\nu_{12}$	2010	2
3969.0	25188	2015	vw	$\nu_{8a}+\nu_{16a}$	2017	2
3974.0	25156	2047	vw	$\nu_{8a}+\nu_{16b}$	2053	6
3982.5	25103	2100	w	?		
3988.0	25068	2135	vw	$\nu_{12}+\nu_{13}$	2130	5
3994.5	25027	2176	vw	$\nu_{12}+\nu_{15}$	2180	4
3996.0	25018	2185	vw	$\nu_{12}+\nu_{9a}$	2191	6
4011.0	24924	2279	w	$\nu_{8a}+\nu_{9b}$(-)	2280	1
4013.5	24909	2294	w	$\nu_{8a}+\nu_4$	2301	7
4020.0	24869	2334	w	$\nu_{8a}+\nu_{11}$	2336	2
4023.0	24850	2353	vw	$O_2+\nu_{8a}+\nu_1$	2352	1
4034.5	24779	2424	w	$\nu_{8a}+\nu_{10b}$(-)	2427	3
4036.5	24767	2436	w	$\nu_{8a}+\nu$	2438	2
4041.0	24739	2464	vw	$\nu_{8a}+\nu_{10a}$	2464	0
4049.5	24687	2516	w	$O_2+\nu_{12}+\nu_{8a}$	2521	5
4057.5	24639	2564	vw	ν_{8a}+O-CH$_3$ bend	2569	5
4063.5	24602	2601	m	$\nu_{12}+\nu_{8a}$	2607	6
4079.0	24509	2694	vw	$\nu_{12}+\nu_{9b}$(-)	2688	6
4081.0	24497	2706	vw	$2\nu_{12}+\nu_4$	2706	0
4083.5	24482	2721	vw	$\nu_{12}+\nu_{8a}$+125	2732	11
4092.0	24431	2772	w	$\nu_{8a}+\nu_{15}$	2777	5

Table 30 (Continued)

4094.0	24419	2784	w	$\nu_{8a}+\nu_{9a}$	2788	4
4102.0	24371	2832	vw	$2\nu_{12}+\nu_{10b}^{(-)}$	2835	3
4110.0	24324	2879	vw	$2\nu_{12}+\nu_{10a}$	2873	6
4132.0	24195	3008	vw	$3\nu_{12}$	3015	7
4139.0	24154	3049	vw	$\nu_{12}+\nu_{8a}$ $+\nu_{16b}$	3058	9
4144.0	24124	3079	vw	$2\nu_{9a}+\nu_{4}$	3068	11
4150.5	24087	3116	vw	$O_2+2\nu_{8a}$	3118	2
4165.0	23999	3204	m	$2\nu_{8a}$	3204	0
4182.0	23905	3298	vw	$\nu_{12}+\nu_{8a}$ $+\nu$	3303	5
4206.0	23769	3434	vw	$\nu_{12}+\ \nu_{8a}$ ν_{1}	3443	9
4236.0	23601	3602	vw	$2\nu_{8a}$	3204	2
4269.0	23418	3785	vw	$\nu_{8a}+\nu_{12}$ $+\nu_{9a}$	3793	8
4314.0	23174	4029	vw	$4\nu_{12}$	4020	9
4345.5	23006	4197	w	$2\nu_{8a}+\nu_{12}$	4209	12
4461.5	22408	4795	vw	$3\nu_{8a}$	4806	11

FIGURE 39

Phosphorescence Spectrum of Parafluorobenzoic Acid in Polycrystalline Methyl Benzoate (Spectrum IV)

Spex 1702 3/4 Meter Czerny Turner Monochromator

Concentration: ∿1 mole percent
Slit Width : 38 μ, 38 μ
Sensitivity : 1×10^{-6} amperes full scale
Time Constant: 0.3 seconds
Scan Rate : 20 Å/minute
Temperature : 4.2° K

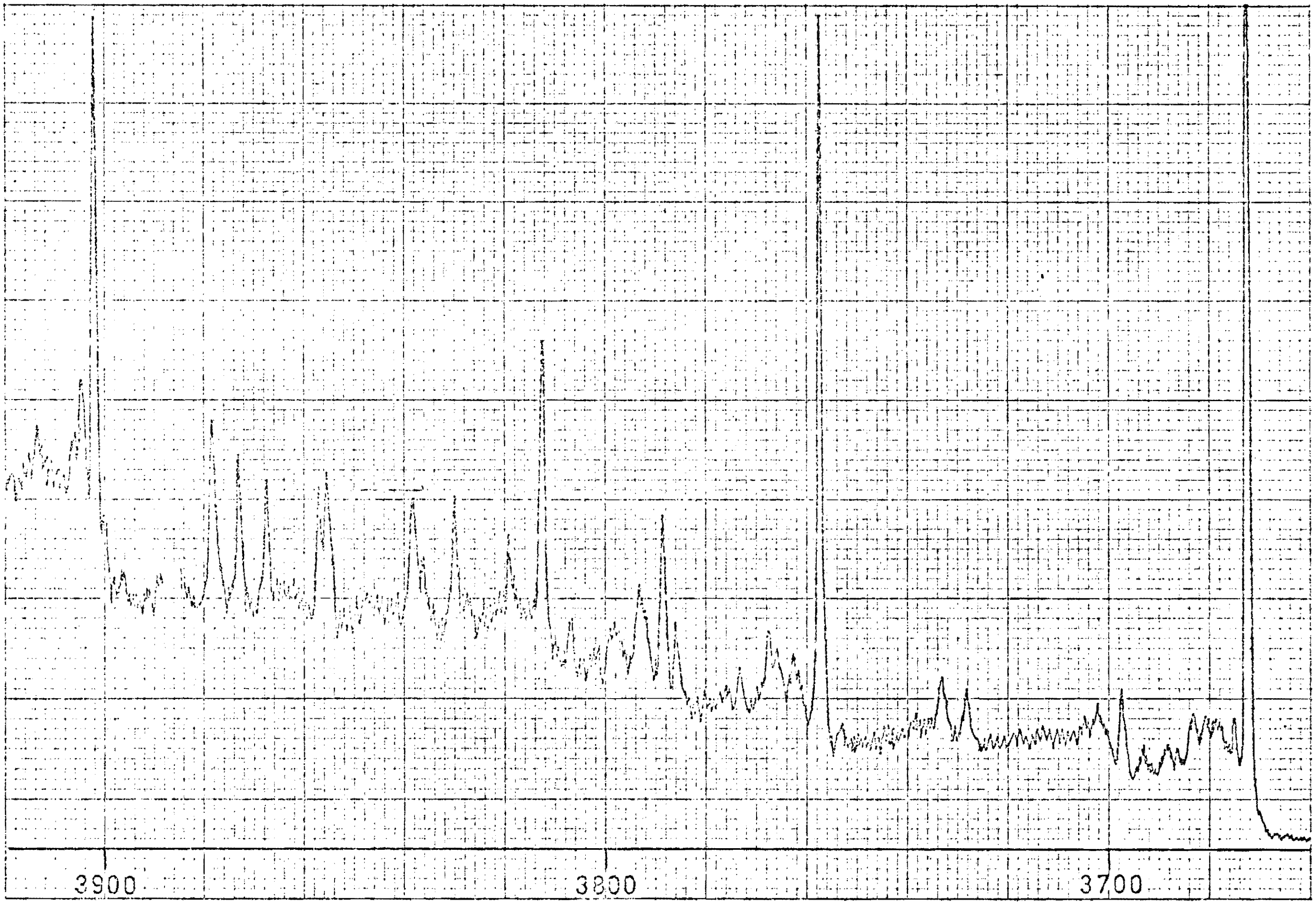
3900
3800
3700

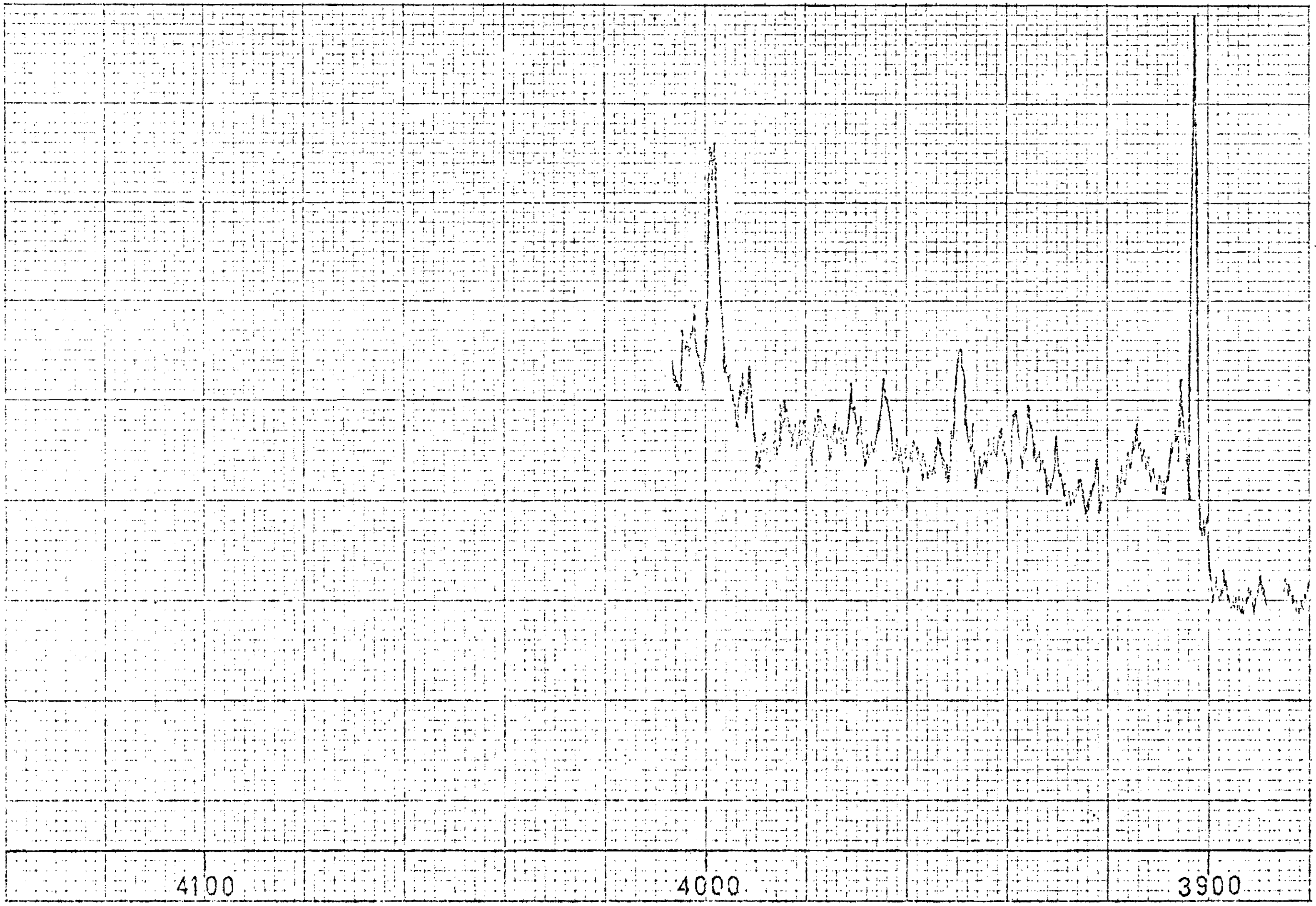
4100
4000
3900

TABLE 31

This table contains the frequencies, relative intensities, and assignment of bands shown in Figure 39. Only the most probable assignments are given. For some bands, particularly combination bands, alternate assignments are possible. All Raman frequencies are rounded off to the nearest wavenumber. Actual Raman frequencies are given only for fundamentals. For combination bands sums of phosphorescence frequencies are given. s = strong, w = weak, and vw = very weak.

λ(Å)	ν(cm^{-1})	$\Delta\nu$(cm^{-1})	Intensity	Assignment	Raman Freq(cm^{-1})	Deviation (cm^{-1})
3672.0	27225	0	s	Origin		
3675.0	27203	22	vw	lattice		
3678.0	27181	44	vw	lattice		
3681.0	27159	66	vw	lattice		
3684.0	27137	88	vw	lattice		
3688.0	27107	118	vw	?		
3693.5	27067	158	vw	?		
3697.5	27038	187	w	?		
3728.0	26816	409	w	ν_{16a}	406	3
3733.5	26777	448	w	ν_{16b}	437	11
3757.5	26606	619	s	ν_{6b}	619	0
3763.0	26567	658	w	$\nu_{6b}+44$	663	5
3768.0	26522	693	w	ν_4	?	?
3773.0	26493	732	w	ν_{11}	714	18
3786.0	26406	819	w	$\nu_{10b}(-)$	810	9
3789.0	26385	840	m	ν_1	825	15
3793.5	26353	872	w	ν_{10a}	855	17
3799.0	26315	910	vw	ν_{11} + 187	919	9
3807.5	26257	968	vw	O-CH_3 bend	971	3
3813.0	26219	1006	m	ν_{12}	1005	1
3819.5	26174	1051	w	ν_{18a}	1029	12
3830.5	26099	1126	w	ν_{13}	1113	13
3836.5	26058	1167	w	ν_{15}	1161	6
3839.0	26041	1184	w	ν_{9a}	1180	4
3856.0	25926	1299	w	$COOCH_3$	1280	19
3857.5	25916	1309	w	ν_3 or ν_{14}	1317	8
3868.0	25846	1379	w	$COOCH_3$?	1376	3
3873.0	25812	1413	w	$\nu_{12}+\nu_{16a}$	?	?
3878.5	25776	1449	w	ν_{19b}	1455	6

3886.5	25723	1502	?	ν_{19a}	1495	5
3902.5	25617	1600	s	ν_{8a}	1603	3
3905.0	25600	1625	vw	$\nu_{6b}+\nu_{12}$	1625	0
3914.0	25542	1683	vw	$\nu_{12}+\nu_{4}$	1700	17
3930.0	25438	1787	vw	$\nu_{8a}+187$	1789	2
3935.5	25403	1822	vw	$\nu_{12}+\nu_{10b}$(-)	1826	4
3938.0	25386	1839	vw	$\nu_{12}+\nu_{1}$	1847	8
3949.5	25313	1912	w	$\nu_{9a}+\nu_{11}$	1916	4
3964.5	25217	2008	w	$2\nu_{12}$	2010	2
3971.0	25175	2050	w	$\nu_{12}+18a$	2056	6
3985.0	25087	2138	vw	$\nu_{12}+\nu_{13}$	2133	5
3992.0	25043	2182	vw	$\nu_{14}+\nu_{9a}$	2191	9
3998.0	25005	2220	s	$\nu_{8a}+\nu_{6b}$	2225	5

TABLE 32

This table contains a comparison of the multiple origins observed in the phosphorescence spectra of methyl benzoate doped with benzoic acid and parafluororbenzoic acid. For spectra I and II methyl benzoate was purified by alumina and silica gel chromatography followed by vacuum distillation. For spectra III, IV, and V, zone refining was used instead of vacuum distillation. In all cases zone refined benzoic acid and parafluorobenzoic acid were used. The same sealed sample was used to obtain IV and V. s = strong, m = medium, w = weak, vw = very weak, and vvw = very very weak. See text for explanation of asterisks.

BA in MB		BA in MB		BA in MB		PFBA in MB		PFBA in MB	
I		II		III		IV		V	
3643.5	vvw								
3642.7	w							3642.5Å	w
*3648.0	s	*3650.0Å	m	3648.5Å	vvw			*3648.5	m
*3655.7	m	3657.0	w	3656.0	vw			3655.5	m
*3663.0	m	*3664.5	s	*3663.5	m			*3662.0	s
*3665.8	w			3669.0	vw			*3663.5	s
*3672.0	m			3671.5	vw	*3672.0Å			
*3682.7	m			*3675.0	s			*3694.5	m
3712.2	m								
*3733.0	s	*3734.5	m						
						3557.5	s		

D. Assignments of Excited States

Figure 40 shows the energies and assignments of benzoic acid dimer. The data for the excited singlet states was obtained by Baum (1974). He obtained the polarized absorption spectra of benzoic acid in benzene and benzoic acid single crystals. The spectrum in benzene shows highly resolved vibronic bands. However, the host absorption only allows the observation of the lowest excited singlet state of the guest. In the spectra of benzoic acid single crystals, higher states can be observed.

The polarized absorption spectrum of oriented single crystals of benzoic acid was first studied by Tanaka (1958). His data, which was obtained at room temperature using a crystal grown by sublimation, showed that the $S_o \rightarrow S_1$ transition was accurately short-axis polarized and that the $S_o \rightarrow S_2$ transition was polarized in-plane 6.5^o away from the long axis. On this basis, he assigned the lowest singlet state of L_b and the second excited singlet state to L_a + CT. The charge transfer component was included to explain the 6.5^o deviation of the transition moment.

Baum has reanalyzed Tanaka's results and has obtained his own polarized absorption spectra of oriented crystals grown between quartz plates.

FIGURE 40

This figure give the assignments and measured energies of the excited states of benzoic acid dimer. Not represented are the unobservable states having gerade symmetry and the excited triplet state observed by Porter and Windsor (see text). Oscillator strengths for transitions between these excited states and the ground state are also given (Taken from Baum, 1974.)

ENERGY LEVEL DIAGRAM FOR BENZOIC ACID DIMER

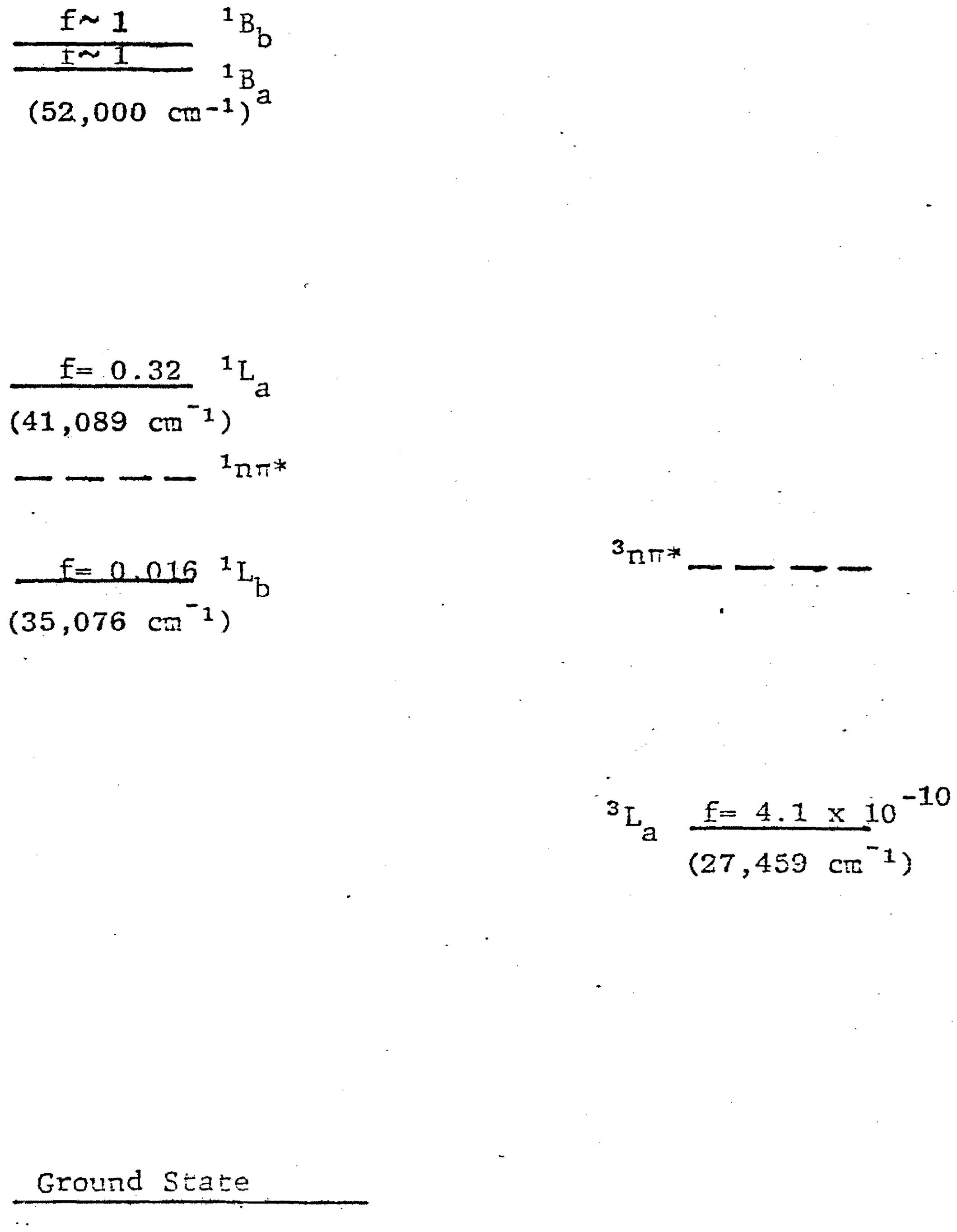

A problem with Tanaka's spectrum is that it shows a band at 2100 Å. This band is not present in solution spectra and could not be found in Baum's specta of crystals grown from zone refined benzoic acid. It is thus highly likely that Tanaka's sample contained an impurity. The only other explanation is that this band is missing in Baum's spectrum because of the strain present in the crystals grown between quartz plates. However, it is hard to imagine how strain can cause the disappearance of an electronictransition. Clearly, the presence of an impurity band would make Tanaka's polarization measurements of questionable value. However, the polarization ratios obtained by Baum are known to be somewhat inaccurate because of strain and other inhomogeneities in the crystal. And even if these technical problems could be overcome, there is still the fact that the strong third excited singlet state extends into the region of the second state. Hence, Baum concludes that polarization measurements cannot be used to determine charge transfer character. His results still require the assignment of the first excited singlet state to L_b and the second to L_a with an indeterminate amount of charge transfer character.

The third and forth singlet states are assigned to $B_{a,b}$. These states are not resolved experimentally, but calculations usually show ${}^1B_a$ to be below ${}^1B_b$ in substituted benzenes.

Because of the presence of th carbonyl group, low-lying $n\pi^*$ states are expected to be present in benzoic acid. Evidence for this is the fact that benzaldehyde and acetophenone have $^1n\pi^*$ as their lowest excited singlet states. In benzoic acid there is no evidence for $^1n\pi^*$ below ^1L_b. Indeed, there is rigorous evidence that $^1n\pi^*$ is above ^1L_b. Baum's absorption and fluorescence spectra for benzoic acid in benzene show that the fluorescense origin coincides with the absorption origin for $S_o \rightarrow L_b$. Since Kasha's rule (McGlynn _et al._, 1969) requires the fluorescent state to be the lowest excited singlet state, this is strong evidence that $^1n\pi^*$ is above ^1L_n.

Dym and Hochstrasser (1969) have presented evidence which suggests that the presence of $^1n\pi^*$ buried underneath a stronger $^1\pi\pi^*$ state will lead to a loss of vibrational resolution in the region where these states overlap. Baum's $S_o \rightarrow S_1$ absorption spectrum of benzoic acid in benzene at 4.2° K shows high resolution for at least 1900 cm^{-1} above the origin. On this basis, we suggest that $'n\pi^*$ is at least 1900 cm^{-1} above ^1L_b. We will later present evidence that $^3n\pi^*$ is nearly degenerate with ^1L_b. In aromatic aldehydes and ketones the S-T interval for $n\pi^*$ states is quite regularly close to 2000 cm^{-1}. On this basis $^1n\pi^*$ is predicted to be about 2000 cm^{-1} above ^1L_b. This is consistent with the predictions of the broadness criterion.

It should be emphasized that the concept of an $n\pi^*$ state, originally developed for formaldehyde, involves a promotion from a more-or-less localized σ lone pair oxygen orbital to an antibonding π orbital. Although this concept has recently been challenged even for formaldehyde, there is some evidence for the existence of such a localized $\sigma\pi^*$ state in benzoic acid. A recent study of the photoelectron spectra of a large number of substituted benzenes by Meeks and McGlynn (1974) shows that benzoic acid has a non-bonding frontier orbital associated with the carboxyl group that is located at -10.83 electron volts. This is evidence for the existence of a $\sigma\pi^*$ state in benzoic acid which involves a promotion from a σ orbital that is more-or-less regionalized on the carboxyl group. Because of the uncertainty introduced by configuration interaction and the unknown location of the π^* orbitals, it cannot be determined if this state will be low-lying or even if the promotion can be described as arising from a nearby lone pair oxygen orbital.

In aromatic molecules, one assumes the existence of ${}^1\sigma\pi^*$ and ${}^1\pi\sigma^*$ states. Although few direct observations are available, these states are postulated to be weak. Their importance to us stems from the possibility that they may be sources of intensity for ${}^3\pi\pi^*$ states through one-center spin-orbit coupling.

The lowest triplet state in benzoic acid is characterized by a measured lifetime of the order of seconds and a dominance (91% of total intensity, Baum, 1974) of ring vibrations in the phosphorescence spectrum. This is regarded as good evidence (McGlynn _et_ _al_. 1969) for a $^3\pi\pi^*$ assignment. By analogy with the lowest triplet state in benzene, definitely assigned as $^3B_{1u}$, we would assign the lowest triplet state in benzoic acid as ^3L_a. However, in Section E we will show that the details of the phosphorescence spectrum cannot be explained with a pure benzoid state. For the time being, we will refer to the lowest triplet state as ^3X.

Baum's absorption and excitation spectra of single crystals of benzoic acid show no absorption above ^3X until 2900 Å. In this region there are several weak broad bands that appear in the zone refined sample. The nature of these bands is unknown. Since the $S_o \rightarrow {}^3X$ spectrum is highly resolved, and since these bands do not overlap any other benzoic acid state, there is no obvious reason why they should not also be resolved if they are associated with the second triplet state. This, at least suggests that they are associated with impurities. Needless to say, the spectra of more highly purified benzoic acid should be obtained. Except for the broad bands at 2900 Å, there is no evidence for any states between ^3X and ^1L_b.

A recent study of benzoic acid luminescence by Baba and Kitamura (1972) provides evidence for a $^3n\pi^*$ state in the immediate vicinity of ^1L_b. These authors observed that the fluorescence quantum yield for benzoic acid dimer in a hydrocarbon glass at 77° K is 0.25. For what they call benzoic acid monomer, they observe no fluorescence. Baum (1974) has definitely shown by careful purification of the solvents that the "monomer" observed by these authors is a complex consisting of a benzoic acid monomer and a hydrogen-bonding impurity, most likely methyl cyclohexanol or methyl cyclohexanone. However, the model and basic conclusions put forth by these authors remains valid inspite of the impurity problem.

Baba and Kitamura explained the absence of fluoroescence in the "monomer" and the presence of fluorescence in the dimer by assuming that the $^3n\pi^*$ state expected to exist in benzoic acid was located somewhat above ^1L_b in the dimer and below ^1L_b in the "monomer". They reasoned that fluorescence would be quenched in the "monomer" because of rapid intersystem crossing from ^1L_b to the lower energy $^3n\pi^*$ state. Rapid intersystem crossing is well known to occur between $n\pi^*$ and $\pi\pi^*$ states on account of the strong spin-orbit coupling between these states (Lower and El Sayed, 1966). Because of the strong H-bonds that exist in the dimer, the energy of the $S_o \rightarrow {}^3n\pi^*$ transition in the dimer was expected to be greater than in the "monomer" making $^3n\pi^*$ above ^1L_b and thereby preventing intersystem crossing. Baum has shown that the "monomer" most likely consists of a benzoic acid monomer complexed through hydrogen bonding with a saturated impurity. Since the impurity is saturated the hydrogen bond(s) of the complex will be weak compared to the hydrogen bonds in benzoic acid dimers. Clearly, weak hydrogen bonds are just as acceptable as no hydrogen bonds in the context of the model proposed by Baba and Kitamura.

Baum's fluorescence data for benzoic acid in benzene confirms the observation of fluorescence by Baba and Kitamura. Three other studies (Tournon and El Bayoumi (1972), Parker and Hatchard (1962) and Seliskar et al. (1974) have failed to observe fluorescence in benzoic acid. Baum has also obtained the fluorescence spectrum of benzoic acid in cyclohexane carboxylic acid. In this system the emitting molecules are benzoic acid monomers complexed with host molecules. Since cyclohexane carboxylic acid is saturated, it forms weak hydrogen bonds ($K_a = 1.26 \times 10^{-5}$) like methyl cyclohexanone and methyl cyclohexanol. In confirmation of the model proposed by Baba and Kitamura, Baum observes a much weaker fluorescence in this system. The dimer fluorescence in benzene appears to be about nine times as intense. We regard the fluorescence quantum yield data obtained by Baba and Kitamura and Baum to be good evidence for the existence of a triplet state close to ^1L_b which enters into strong spin-orbit coupling with ^1L_b. Most likely this state is $^3n\pi^*$. However, benzenoid $^3\sigma\pi^*$ and $^3\pi\sigma^*$ state are also possible candidates, since the energies of these states are unknown.

The model put forth by Baba and Kitamura also implies that the absorption bands observed by Baum at 2900 Å in single crystals of benzoic acid are not associated with $^3n\pi^*$, $^3\sigma\pi^*$ or $^3\pi\sigma^*$, since intersystem crossing between L_b and these states would strongly quency fluorescence. Since appreciable fluorescence is observed, it follows that these bands are associated with impurities or else $^3\pi\pi^*$.

Triplet-triplet absorption spectra of benzoic acid in paraffin solution obtained by Porter and Windsor (1958) show a "strong" triplet state at 58,450 cm^{-1}. No other excited triplet states were observed. Baum has attempted to locate $^3n\pi^*$ using the techniques for obtaining T-T absorption spectra developed by McClure (1951). These attempts were not successful on account of interference from absorption bands associated with overtones of ground state vibrations of benzoic acid and the solvent.

E. Possible Models for the Lowest Triplet State

The presence of intense out-of-plane modes in the phosphorescence spectra of benzoic acid and methyl benzoate was first noted by Kanda, Shimada, and Takenoshita (1963). They proposed that the presence of these modes was a result of distortion by the benzene lattice. If benzoic acid were distorted, then symmetry would be lowered and the forbidden, non-totally symmetric modes of the undistorted molecule would become totally symmetric and therefore allowed.

For totally symmetric modes we expect to see even quanta vibrations, if the fundamentals are sufficiently intense. This is observed for ν_{8a} and ν_{12}. Since $\nu_{10b}{}^{(-)}$, ν_{11}, and ν_{10a} in some cases are as strong as ν_{8a} or ν_{12}, we would also expect to see even quanta of these modes if they are totally symmetric. The spectra obtained by Kanda and coworkers were not sufficiently resolved to reveal the presence of multiple quanta. However, our high resolution spectra show that even quanta of the out-of-plane modes are not active in the spectrum. On this basis, we regard it as unlikely, that distortion is the cause of the out-of-plane modes. Note that the absence of even quanta precludes distortion in either the ground or triplet states.

Another approach to the lowest triplet state of benzoic acid has been proposed by Maria and McGlynn (1970).

Their model is based upon life-time measurements of the series of acids $\emptyset-(CH_2)_n-COOH$ and some of their salts, where n = 0,1,2, and 3. These measurements show that as n is increased, the lifetime becomes more toluene-like: $\tau(n) = 2.1, 5.4,$ and 7.8 seconds for n = 0, 1, and 2, respectively. For $\emptyset-(CH_2)_n-COOPb$, $\tau(n) = 0.02, 0.01,$ 0.05 and 0.3, 0.65, and 2.4 seconds, for n = 0, 1, 2, and 3, respectively. For n = 3, the heavy atom effect is essentially absent. On this basis Maria and McGlynn concluded that the lowest triplet state of benzoic acid should be represented as a composite of the lowest triplet state of benzene and the lowest triplet state of the carboxyl group. Using the known energies for the lowest triplet states of benzene and benzoic acid, they estimated the energy of the lowest triplet state of the carboxyl group and calculated the degree of mixing of the two states:

$$^3\psi = 0.72 \ {}^3\psi_{\emptyset} + 0.68\,{}^3\psi_{COOH}.$$

It should be emphasized that $^3\psi_{\emptyset}$ is the ^3L_a state of benzene arising from a pure benzene $\pi \rightarrow \pi^*$ promotion and that $^3\psi_{COOH}$ represents a state generated by promotion of a bonding COOH π electron polarized toward the oxygen atoms to an antibonding π^* orbital polarized toward the carboxyl carbon atom. Since the excited state involves promotion of a strongly bonding electron to an antibonding orbital regionalized over the COOH group, it follows that substantial activity of totally symmetric carboxyl group modes should be observed if the description of the lowest triplet state calculated by Maria and McGlynn is correct. These authors contended that the moderate resolution of the spectrum obtained by Kanda and coworkers did not allow the conclusion that these modes were not present in the spectrum, contrary to the opinion of Kanda and coworkers. The high resolution spectra obtained in our study show that at most 9% (Baum's photographic measurement) of the phosphorescence intensity is associated with carboxyl group modes. The smallness of this intensity is incompatible with Maria and McGlynn's triplet state assuming reasonable Franck-Condon factors. However, the fact that the carboxyl group modes appear at all suggests that there is some carboxyl group character in the lowest benzoic acid triplet state, or possibly the ground state.

A problem with the study by Maria and McGlynn is that they only determined measured lifetimes, while their conceptual approach was concerned with radiative lifetimes. Two years after their study, a similar but somewhat more comprehensive study was published by Tournon and ElBayoumi (1972). These authors studied a series of benzyl derivatives of the form $\phi-(CH_2)_n-X$, where $X = CH_3$, COOH, OH, and NH_2. For X = COOH, their measurements confirmed the basic observation of Maria and McGlynn that as n increases, the lifetime approaches that of toluene: τ = 4.5, 12.0, and 17.4 seconds for n = 0, 1, and 4, respectively. τ(toluene) = 18.3 seconds. These lifetimes are radiative lifetimes calculated by taking both fluorescence and phosphorescence into account, neglecting only radiationless $S_1 \rightarrow S_o$ transitions. While their experimental results for carboxylic acids are basically the same as those of Maria and McGlynn, Tournon and ElBayonmi have offered a different interpretation. Instead of the composite molecule approach used by Maria and McGlynn, they prefer to interpret the results in terms of an intramolecular charge-transfer mechanism. The basic idea behind this approach is that the methylene groups are expected to hinder intramolecular charge transfer from the ring to the carboxyl group or in other words to make the corresponding charge transfer states very high in energy preventing appreciable mixing of these states with the lower excited states. In order to explain why the lifetime of benzoic acid is less than toluene, they assume that the charge transfer process enhances spin orbit coupling. However, no details are provided as to how this occurs. Consequently, this model must be regarded as an unproven hypothesis. None the less, it remains an interesting suggestion.

The phosphorescence spectra obtained by Maria and McGlynn and Tournon and El Bayoumi show only about five vibronic bands. In the better spectra obtained in this study as many as a hundred vibronic bands appear. This greatly increased resolution provides us with a much larger informational basis upon which to construct a model of the lowest triplet state. Before becoming involved in the details of the model which we wish to propose, let us summarize the basic questions which have to be answered:

1. Why do intense out-of-plane modes appear in the phosphorescence spectrum?
2. Why are ring out-of-plane modes so much more prominent than carboxyl group out-of-plane modes?
3. What is the basis for the environmental sensitivity of the out-of-plane modes?
4. Why do in-plane carboxyl group modes appear in the spectrum?
5. What is the basis of the environmental sensitivity of these modes?
6. Why is the lifetime of benzoic acid so much shorter than that of toluene?
7. Why does ν_{6b} appear uniquely in the phosphorescence spectrum of methyl benzoate perturbed by parafluorobenzoic acid?

We first attempt to explain the presence of the out-of-plane modes. As noted previously, the presence of only single quantum vibrations rules out distortion as a probable cause. The presence of single quantum non-totally symmetric modes in benzene and substituted benzenes is well-known. The presence of these modes has been successfully accounted for in terms of Herzberg-Teller coupling (Albrecht, 1963). In what follows we shall examine in detail the possibility that this type of coupling is involved in the mechanism responsible for the out-of-plane modes in the phosphorescence spectrum of benzoic acid. However, it is first necessary to present the basic theory of Herzberg-Teller coupling.

The solutions of Schroedinger's equation necessarily involve the coordinates of both electrons (x) and nuclei (Q). The task of finding these solutions is greatly simplified by the application of the Born-Oppenheimer approximation. This approximation allows us to write the total wavefunction as a product of an electronic wavefunction and a nuclear wavefunction (Born and Huang, 1956):

$$\Psi_n^a(x,Q) = \theta_n(x,Q)\,\chi_n^a(Q).$$

These functions satisfy the following relationships:

$$H^o\theta_n(xQ) = E_n(Q)\theta_n(x,Q) \quad \text{and}$$

$$[T(Q) + E_n(Q)]\,\chi_n^a(Q) = V_{na}\,\chi_n^a(Q) \quad ,$$

where the electronic Hamiltonian H^o consists of the kinetic energy of the electrons, electron-nuclear potential energy and nuclear-nuclear potential energy. $T(Q)$ refers to the kinetic energy of the nuclei and V_{na} is the total energy of the vibronic state.

At this level of approximation, the electronic wavefunction still depends on the nuclear coordinates as parameters. However, the dependence is not given explicitly. Clearly, it would be desirable to obtain an approximate wavefunction which depends on Q in an explicit manner. This type of approximate wavefunction was first derived by Herzberg and Teller in 1933. We present here a derivation of the Herzberg-Teller wavefunction using first-order perturbation theory. We choose as zero-order wavefunction, Born-Oppenheimer electronic wavefunctions evaluated at Q = 0, the equilibrium nuclear configuration. These functions are eigenfunctions of the electronic Hamiltonian evaluated at Q = 0:

$$H^o(0)\theta_n(x,0) = E_n(0)\theta(x,0).$$

This equation essentially describes a non-vibrating molecule. To obtain the wavefunction for a vibrating molecule, we treat the effects of vibration as a perturbation. To obtain the perturbation, we expand $H^o(Q)$ in a Taylor series, keeping only the first two terms:

$$H^{o}(Q) = H^{o}(0) + \sum_{i=1}^{3N-6} (\partial H^{o}/\partial Q_i)_o (Q_i)$$

The second term gives the perturbation for fundamental vibrations. Higher order terms represent the perturbations for overtone and combination modes. A straightforward applications of perturbation theory leads to the following wavefunction:

$$\theta_n^1(x,Q) = \theta_n^o(x,0) + \sum_{i=1}^{3n-6} \sum_{m\neq n}^{\infty} \frac{\langle \theta_m^o(x,0) \,|\, (\partial H^o/\partial Q_i)_o \,|\, \theta_n^o(x,0)\rangle \; Q_i \theta_m^o(x,0)}{E_n^o(0) - E_m^o(0)} .$$

The important thing about this wavefunction is that the dependence on Q is explicit. In the original Born-Oppenheimer electronic wavefunction the dependence on Q was not explicitly revealed. For brevity, we write:

$$Q_n^1(x,Q) = \theta_n^o(x,0) + \sum_{i=1}^{3n-6} \sum_{m\neq n}^{\infty} \lambda_{mni} \; Q_i \; \theta_m^o(x,0) .$$

The total wavefunction for the molecule can be written as:

$$\Psi_n^a(x,Q) = \theta_n^1(x,Q) \chi_n^a(Q) .$$

We can now calculate the transition moment between the ground state and one of the excited states (neglecting the spin wavefunctions):

$$M_{1a,nb} = \left\langle \theta_1^1(x,Q)\ \chi_1^a(Q) \middle| \sum_j q_j\ r_j \middle| \ \theta_n^1(x,Q)\ \chi_n^b(Q) \right\rangle .$$

Each of the electronic states in this integral consists of an infinite sum of terms.

In practice, it is, of course, not possible to consider an infinite or even a very large number of terms. Normally only a small number of terms are considered in determining a given wave function. This simplification is based on the assumption that λ is very small except for the particular terms considered. But since an infinite sum of small numbers can be large, the justification of this assumption ultimately lies in the success of the simplified wavefunction as a basis for explaining observed phenomena. In some cases, symmetry requires λ to be zero; in others a large energy denominator justifie its neglect. Since the ground state is usually well separated from the excited states in the molecules considered in this study, we approximate $\theta_1^1(x,Q)$ as $\theta_1^o(x,0)$.

Recent calculations by Ziegler and Albrecht (1974) show that this approximation is valid for benzene. We can now write the transition moment as:

$$M = \left\langle \theta_1^o(x,0)\ \chi_1^a(Q) \middle| \sum_j q_j\ r_j \middle| \left(\theta_n^o(x,0) + \sum_{i=1}^{3n-6} \sum_{m \neq n}^{\infty} \lambda_{mni} Q_i \theta_m(x,0)\right) \chi_n^b(Q) \right\rangle .$$

Since the electronic wavefunctions are orthogonal, only the components of the dipole moment operator associated with the electrons need be considered. The above expression can now be reduced as follows:

$$M = \left\langle \theta_1^o(x,0) \left| \sum_j er_j \right| \theta_n^o(x,0) \right\rangle \left\langle \chi_1^a(Q) \ \chi_n^b(Q) \right\rangle +$$

$$\sum_{l=1}^{3n-6} \sum_{m \neq n}^{\infty} \lambda_{mni} \left\langle \theta_1^o(x,0) \left| \sum_j er_j \right| \theta_m^o(x,0) \right\rangle \left\langle \chi_1^a(Q) Q_i \chi_m^b(Q) \right\rangle$$

$$\text{or} \quad M = M_{1n}^o \ S_{ab} + \sum_{i=1}^{3n-6} \sum_{m \neq n}^{\infty} \lambda_{mni} \ M_{1m}^o \ S_{abi}$$

S_{ab} is the usual Franck-Condon factor, and S_{abi} may be called a quasi Franch-Condon factor.

Let us now calculate the transition moment of an $S_1 \rightarrow S_o$ transition. At sufficiently low temperatures, the emission occurs from the lowest vibrational level of S_1. The vibrational wavefunction for this level is totally symmetric. The transition can occur to various vibrational levels of the ground state. The vibrational wavefunctions associated with these levels can be classified as either totally symmetric or non-totally symmetric. Let us consider these classes of vibrations separately. For totally symmetric ground state vibrations S_{ab} is not required to be zero by group theory. Thus vibronic transitions involving totally symmetric ground state vibrations are said to be allowed. S_{abi} is also not required by group theory to vanish. To evaluate λ_{mni}, we note that $H' = \sum_{i=1}^{3n-6} (\partial H^o/\partial Q_i)_o Q_i$ must be totally symmetric since it is part of the total Hamiltonian. This requires that Q_i and $(\partial H^o/\partial Q_i)_o$ have the same symmetry. Hence λ_{mni} will be nonzero (as far as symmetry is concerned) for totally symmetric vibrations when the electronic wavefunction $\theta_m^o(x,0)$ has the same symmetry as $\theta_n^o(x,0)$. It is thus clear that for totally symmetric vibrations, the only effect of Herzberg-Teller coupling is to add quantitative corrections to the zero-order transition moment. Since the magnitude of the zero-order transition moment is not known, it is usually not possible to determine if a given totally symmetric vibronic band in a spectrum possesses significant Herzberg-Teller intensification or not. However, in some cases, the allowed origin may be sufficiently weak that Herzberg-Teller intensification causes some vibronic bands to appear much more intensely than would be expected for normal Franck-Condon factors. In these cases, the effects of Herzberg-Teller intensification are apparent even for totally symmetric vibrations. It should also be noted that Albrecht (1960) has derived a general expression for the temperature dependence of "forbidden" transition probabilities. Since the allowed components of transition probabilities are temperature independent, a determination of the temperature dependence of vibronic intensities should allow an estimate of the magnitude of Herzberg-Teller intensification in a given vibronic band.

For non-totally symmetric vibrations, Herzberg-Teller coupling causes striking effects on the spectra. The reason for this is that S_{ab} is required to be zero for a non-totally symmetric ground state vibration. Thus, at the zero-order level, non-totally symmetric modes should not appear in the $S_1 \rightarrow S_o$ spectrum. However, S_{abi} is not required to vanish by symmetry for non-totally symmetric modes. The only group theoretical requirement is that $\theta_m^o(x,0)$ belong to the same representation as Q_i . Thus, for non-totally symmetric modes, Herzberg-Teller coupling causes "forbidden" bands to appear in the spectrum. In this sense, the spectra are qualitatively different from what is expected on the basis of zero order wave functions.

In some cases, $M_{1,m}^o$, the zero-order electronic transition moment, is zero in addition to S_{ab} being zero. In these cases the origin is forbidden and only vibronic bands appear in the spectrum. The ${}^1B_{2u}$ - ${}^1A_{1g}$ transition in benzene is such a case. In a monosubstituted benzene, such as chlorobenzene, the $S_o \rightarrow {}^1L_b$ origin is allowed, but appears weakly, and the Herzberg-Teller bands which were the only bands in the benzene spectrum, still appear prominantly (50% of total intensity) in the chlorobenzene spectrum (Bist _et al._, 1970).

Finally, it should be pointed out that the polarization of a Herzberg-Teller band that involves a non-totally symmetric mode will be different from the polarization of a vibronic band associated with a totally symmetric mode. In particular, the "forbidden" band will have the same polarization as the origin of the transition from the ground state to the state from which the intensity is borrowed. If more than one state is coupled, the polarization will be the weighted vector sum of the individual polarizations.

So far we have not considered states of different multiplicity. In order to take spin into account, it is necessary to include the spin-orbit interaction in the electronic Hamiltonian. In this case we write $H^o(o) + H_{soc}(o)$ as the Hamiltonian for a non-vibrating molecule, and we now have:

$$H'(Q) = \sum_{i=1}^{3n-6} (\partial H^o/\partial Q_i)_o \, Q_i + \sum_{i=1}^{3n-6} (\partial H_{soc}/\partial Q_i)_o Q_i$$

As for $\partial H^o/\partial Q_i)_o$ $(\partial H_{soc}/\partial Q_i)_o$ belongs to the same representation as Q_i. The second term, unlike the first, has the ability to couple states of different multiplicity. This type of coupling has been termed _spin-vibronic coupling_ by Albrecht (1963).

At this point it is appropriate to consider whether spin-vibronic coupling is responsible for the intense out-of-plane modes present in the phosphorescence spectrum of benzoic acid. The total spin-orbit coupling matrix element can be written as a sum of one-center and multi-center terms. In polycyclic aromatic molecules, the one-center terms dominate for $^3\pi\pi^*$ state (McGlynn, et al. pp. 240-241, 1969). This has also been shown to be true for aromatic carbonyl compounds (Shimada and Goodman, 1965). Using a spherically symmetric potential and hydrogen-like wave functions, it can be shown that one-center spin-orbit coupling is proportional to Z^4, where Z is the atomic number of the center. In benzoic acid, it is clear that the oxygen centers will determine a large percentage of the spin-orbit coupling. Consequently, modes involving oxygen motion are expected to be highly active if spin-vibronic coupling is a significant source of intensity for the out-of-plane modes. The phosphorescence spectrum of benzoic acid in benzene shows that the H-wag mode appears only weakly, whereas ν_{10a}, a mode that involves no carbonyl group motion, appears with moderate intensity. In other systems, ν_{10a} appears with very strong intensity. This consitutes good evidence that spin-vibronic interaction does not play a significant role in the mechanism responsible for the out-of-plane activity.

By itself , $\sum_{i=1}^{3n-6}(\partial H^o/\partial Q_i)_o Q_i$ cannot contribute to the intensity of non-totally symmetric modes in the phosphorescence spectrum because this operator cannot couple states of different multiplicity. On the other hand, it is possible to consider the perturbation

$$H' = \sum_{i=1}^{3n-6} (\partial H^o/\partial Q_i)_o Q_i + H_{soc}.$$

At the level of first-order perturbation theory, this perturbation also is incapable of contributing to the intensity of vibronic transitions involving non-totally symmetric modes. The first term does not mix singlet and triplet states and the second can at most couple a triplet state to an allowed singlet state. For such a mixed state the Franck-Condon factor would still be zero for nontotally symmetric modes. However, at the level of second-order perturbation theory, this perturbation is capable of introducing intensity associated with non-totally symmetric modes. This type of coupling has been termed <u>spin-orbit vibronic coupling</u> by Albrecht. Since second-order perturbation theory is used, the coupling scheme involves an intermediate state. This intermediate state may be either a singlet or triplet state. As a result, two classes of coupling schemes are possible:

$${}^1Z^o \longleftarrow \text{H-T} \longrightarrow {}^1Y^o \longleftarrow \text{SOC} \longrightarrow {}^3X^o \qquad \text{(A)}$$

$${}^1Z^o \longleftarrow \text{SOC} \longrightarrow {}^3Y^o \longleftarrow \text{H-T} \longrightarrow {}^3X^o \qquad \text{(B)}$$

The corrected wavefunctions associated with these coupling schemes are:

$$^3X^2 = {}^3X^o + \frac{\langle {}^1Y^o|SOC|{}^3X^o\rangle \langle {}^1Z^o|H\text{-}T|{}^1Y^o\rangle\, {}^1Z^o}{[E({}^3X^o)-E({}^1Y^o)]\ [E({}^3X^o) - E({}^1Z^o)]}$$

and $$^3X^2 = {}^3X^o + \frac{\langle {}^3Y^o|H\text{-}T|{}^3X^o\rangle \langle {}^1Z^o|SOC|{}^3Y^o\rangle\, {}^1Z^o}{[E({}^3X^o)-E({}^3Y^o)]\,[E({}^3X^o)-E({}^1Z^o)]},$$

respectively. It is clear that these coupling schemes are capable of introducing singlet character into a triplet state when a nontotally symmetric vibration is involved.

It is now necessary to determine which states of benzoic acid are acceptable candidates for $^1Z^o$, $^1Y^o$, and ^3Y. We consider states according to orbital type. McClure (1952) has shown that one-center and two-center spin-orbit coupling integrals connecting ππ* states in a planar aromatic molecule are zero because of angular momentum quenching. While the three-center integrals are non-vanishing, they are small in comparison with the strong unquenched one-center spin-orbit coupling integrals between nπ* and ππ* states or between σπ* (or πσ*) and ππ* states. Spin-orbit coupling between two nπ* states is also small on account of angular momentum quenching. Thus, in what follows we will only consider spin-orbit coupling matrix elements between states of different orbital type.

Since we are trying to construct a wavefunction that accounts for activity of out-of-plane modes, we consider only those Herzberg-Teller matrix elements which are non-vanishing for these modes. For a planar molecule, Herzberg-Teller matrix elements between states of the same orbital type vanish for out-of-plane fundamentals. On the basis of symmetry, the non-vanishing Herzberg-Teller matrix elements are between $\pi\pi^*$ and $\sigma\pi$ states. Here we intend $\sigma\pi$ to refer to benzenoid $\sigma\pi^*$ and $\pi\sigma^*$ states and carboxyl $n\pi^*$ states.

Given these constraints on spin-orbit coupling and Herzberg-Teller coupling, the only coupling schemes which are not eliminated from consideration are:

$$^1\pi\pi^* \longleftarrow (\text{H-T}) \longrightarrow {}^1\sigma\pi \longleftarrow (\text{SOC}) \longrightarrow {}^3X({}^3\pi\pi^*)$$

$$^1\pi\pi^* \longleftarrow (\text{SOC}) \longrightarrow {}^3\sigma\pi \longleftarrow (\text{H-T}) \longrightarrow {}^3X({}^3\pi\pi^*)$$

Note that $^1\sigma\pi$ states are eliminated as possible candidates for Z by the constraints on the matrix elements. An additional reason for eliminating these states is that $S_o \rightarrow {}^1\sigma\pi$ transitions are usually observed (or calculated) to be very weak. Hence these states are less favorable as intensity sources than $^1\pi\pi^*$ states, which have stronger $S_o \rightarrow {}^1\pi\pi^*$ transitions.

In order to proceed further it is necessary to consider the detailed structure of the $\pi\pi^*$ and $\sigma\pi$ states. It will be recalled that Kanda and coworkers as well as

Levshin and Rebane concluded that ^3X was a pure benzenoid $\pi\pi^*$ state, while Maria and McGlynn contended that $^3X = 0.68\ ^3\psi_{\phi} + 0.72\,^3\psi_{COOH}$. Tournon and El Bayoumi, on the other hand proposed that charge transfer states play an essential role in determining the properties of benzoic acid phosphorescence.

The conceptual framework in which the proposals of Maria and McGlynn and Tournon and El Bayoumi are cast was developed by Tanaka and Nagakura in 1954 and refined by Longuet-Higgins and Murrell in 1955. In this conceptual framework, the states of a substituted aromatic molecule are constructed from orbitals that are localized either on the aromatic ring or on the substituent group. States constructed in this manner can be divided into two classes: those which involve an excitation between different orbitals of the aromatic ring or different orbitals of the substituent group and those which involve the transfer of an electron between an aromatic orbital and a substituent orbital. The former states are referred to as locally excited (LE) states and the latter are referred to as charge transfer (CT) states.

Tanaka and Nagakura developed their theory with a one-electron Hamiltonian, which necessarily neglects electron interactions. Murrell (1962) has argued that those cases in which a large migration of charge occurs are precisely the ones for which the electron interaction terms are important. He notes that neglect of these terms leads to large qualitative disagreements between theory and experiment. For our purposes, however, these considerations are not important since we consider only qualitative arguments based on orbital types.

In what follows, we will decompose the $\pi\pi^*$ and $\sigma\pi$ states of benzoic acid into LE and CT components and examine the contributions of these components to the Herzberg-Teller and spin-orbit coupling matrix elements. Zero-order states will be represented as products of localized molecular orbitals, since our arguments will only be concerned with orbital types.

Let us first consider the Herzberg-Teller matrix element between a $\pi\pi^*$ state localized on the benzene ring and an $n\pi^*$ state localized on the carboxyl group: $\left\langle n_C\pi_C{}^* \middle| \text{H-T} \middle| \pi_R\pi_R{}^* \right\rangle$. We assume that the various orbitals are essentially identical to those in the ancestral molecules. Hence we use the subscripts "C" (carboxyl group) and "R" (benzene ring). Since the only terms in the non-relativistic electronic Hamiltonian that depend explicitly on the nuclear coordinates are the electron-nuclear potential energy terms and the nuclear-nuclear potential energy terms, it follows that the Herzberg-Teller operator is a one-electron operator. This allows us to write (assuming no reorganization):

$$\left\langle n_C\pi_C{}^* \middle| \text{H-T} \middle| \pi_R\pi_R{}^* \right\rangle = \left\langle n_C \middle| \text{H-T} \middle| \pi_R \right\rangle \left\langle \pi_C{}^* \pi_R{}^* \right\rangle .$$

Since π_C^* and π_R^* are different orbitals they are orthogonal. Hence, the integral is zero and the Herzberg-Teller matrix element vanishes. Therefore, it must be concluded that either Herzberg-Teller coupling is not responsible for the observed out-of-plane activity in the phosphorescence spectrum or else that Z, ^3X, and $^{1,3}Y$ cannot be represented as pure LE states.

To explore the latter possibility, we represent $n\pi^*$ and $\pi\pi^*$, including both LE and CT components, as follows:

$$n\pi^* = e\, n_C\pi_C^* + f\, n_C\pi_R^* + g\ \sigma_R\pi_R^* + h\ \pi_R\sigma_R^* + i\ \sigma_C\pi_C^* + j\ \pi_C\sigma_C^* + k\ \sigma_R\pi_C^*$$

$$\pi\pi^* = a\ \pi_R\pi_R^* + b\ \pi_R\pi_C^*\ c\ \pi_C\pi_R^* + d\ \pi_C\pi_C^*$$

Those terms in which both orbitals have the same subscript represent LE states; the other terms, in which the orbitals have different subscripts, are the CT states. Writing the $n\pi^*$ and $\pi\pi^*$ states in this manner is tantamount to including a limited configurational interaction among the lower configurations. It should also be pointed out that $\pi\pi^*$ states in substituted benzenes require two configurations for their representation (Goodman and Shull, 1957). It should therefore be understood that "$\pi_R\pi_R^*$" represents both configurations.

The Herzberg-Teller matrix element for these states reduces to a sum of twenty eight terms, which are shown in Table 33. Overlap considerations allow one to determine which out-of-plane modes will be favored by a given term. These modes are indicated for each non-vanishing term in Table 33. It will be noted that only two terms favor ring out-of-plane modes. These terms arise as a result of the $\sigma_R\pi_R{}^*$ and $\sigma_R\pi_C{}^*$ components of $n\pi^*$ and the $\pi_R\pi_R{}^*$ and $\pi_R\pi_C{}^*$ components of $\pi\pi^*$.

Since the final benzoic acid $n\pi^*$ state involves σ_R and $\pi_R{}^*$ orbitals it follows that both the n and π^* orbitals are delocalized over the benzoic ring. Additional support for these conclusions is found in a recent calculation by Chu and Goodman. These authors have calculated SCF INDO, n and π^* orbitals of the $^3n\pi^*$ state of benzaldehyde. The results of this calculation are shown in Figures 41 a, b, c, which show the ($2p_x$, $2p_z$) contributions to the n orbital, the s contributions to the n orbital and the $2p_y$ contributions to the π^* orbital, respectively. As indicated in these figures, both the n and π^* orbitals are delocalized over the ring. The results of the benzaldehyde calculation are thus consistent with a delocalized $n\pi^*$ concept. However, it should be noted that the representations of

TABLE 33

This table shows the terms that result when $\langle n\pi^*|H\text{-}T|\pi\pi^*\rangle$ is expanded in terms of th LE and CT components of $n\pi^*$ and $\pi\pi^*$. The vibrations favored by the various nonvanishing terms are also given. COPM = carboxyl group out-of-plane mode, ROPM = ring out-of-plane mode and X = COOH group.

ea	$\langle n_C\|H\text{-}T\|\pi_R\rangle$	$\langle \pi_C^*\pi_R^*\rangle$	= 0	
eb	$\langle n_C\|H\text{-}T\|\pi_R\rangle$	$\langle \pi_C^*\pi_C^*\rangle$		Ø-X wag and torsion
ec	$\langle n_C\|H\text{-}T\|\pi_C\rangle$	$\langle \pi_C^*\pi_R^*\rangle$	= 0	
ed	$\langle n_C\|H\text{-}T\|\pi_C\rangle$	$\langle \pi_C^*\pi_C^*\rangle$		COPM
fa	$\langle n_C\|H\text{-}T\|\pi_R\rangle$	$\langle \pi_R^*\pi_R^*\rangle$		Ø-X wag and torsion
fb	$\langle n_C\|H\text{-}T\|\pi_R\rangle$	$\langle \pi_R^*\pi_C^*\rangle$	= 0	
fc	$\langle n_C\|H\text{-}T\|\pi_C\rangle$	$\langle \pi_R^*\pi_R^*\rangle$		COPM
fd	$\langle n_C\|H\text{-}T\|\pi_C\rangle$	$\langle \pi_R^*\pi_C^*\rangle$	= 0	
ga	$\langle \sigma_R\|H\text{-}T\|\pi_R\rangle$	$\langle \pi_R^*\pi_R^*\rangle$		ROPM
gb	$\langle \sigma_R\|H\text{-}T\|\pi_R\rangle$	$\langle \pi_R^*\pi_C^*\rangle$	= 0	
gc	$\langle \sigma_R\|H\text{-}T\|\pi_C\rangle$	$\langle \pi_R^*\pi_R^*\rangle$		Ø-X wag and torsion
gd	$\langle \sigma_R\|H\text{-}T\|\pi_C\rangle$	$\langle \pi_R^*\pi_C^*\rangle$	= 0	
ha	$\langle \pi_R\|H\text{-}T\|\pi_R\rangle$	$\langle \sigma_R^*\pi_R^*\rangle$	= 0	
hb	$\langle \pi_R\|H\text{-}T\|\pi_R\rangle$	$\langle \sigma_R^*\pi_C^*\rangle$	= 0	
hc	$\langle \pi_R\|H\text{-}T\|\pi_C\rangle$	$\langle \sigma_R^*\pi_R^*\rangle$	= 0	
hd	$\langle \pi_R\|H\text{-}T\|\pi_C\rangle$	$\langle \sigma_R^*\pi_C^*\rangle$	= 0	
ia	$\langle \sigma_C\|H\text{-}T\|\pi_R\rangle$	$\langle \pi_C^*\pi_R^*\rangle$	= 0	
ib	$\langle \sigma_C\|H\text{-}T\|\pi_R\rangle$	$\langle \pi_C^*\pi_C^*\rangle$		Ø-X wag and torsion
ic	$\langle \sigma_C\|H\text{-}T\|\pi_C\rangle$	$\langle \pi_C^*\pi_R^*\rangle$	= 0	
id	$\langle \sigma_C\|H\text{-}T\|\pi_C\rangle$	$\langle \pi_C^*\pi_C^*\rangle$		COPM

Table 33 (Continued)

ja	$\langle \pi_C \vert H-T \vert \pi_R \rangle$	$\langle \sigma^*_C \pi^*_R \rangle$	$= 0$	
jb	$\langle \pi_C \vert H-T \vert \pi_R \rangle$	$\langle \sigma^*_C \pi^*_C \rangle$	$= 0$	
jc	$\langle \pi_C \vert H-T \vert \pi_C \rangle$	$\langle \sigma^*_C \; {}^*_R \rangle$	$= 0$	
jd	$\langle \pi_C \vert H-T \vert \pi_C \rangle$	$\langle \sigma^*_C \pi^*_C \rangle$	$= 0$	
ka	$\langle \sigma_R \vert H-T \vert \pi_R \rangle$	$\langle \pi^*_C \pi^*_R \rangle$	$= 0$	
kb	$\langle \sigma_R \vert H-T \vert \pi_R \rangle$	$\langle \pi^*_C \pi^*_C \rangle$		ROPM
kc	$\langle \sigma_R \vert H-T \vert \pi_C \rangle$	$\langle \pi^*_C \pi^*_R \rangle$	$= 0$	
kd	$\langle \sigma_R \vert H-T \vert \pi_C \rangle$	$\langle \pi^*_C \pi^*_C \rangle$		Ø-X wag and torsion

FIGURE 41

(a) $(2p_x, 2p_z)$ contributions to SCF n orbital from ground state

(b) s contributions to SCF n orbital from ground state

(c) $2p_y$ contributions to SCF π^* orbital from $^3n\pi^*$ state

(Taken from Chu and Goodman, 1975)

FIGURE 41

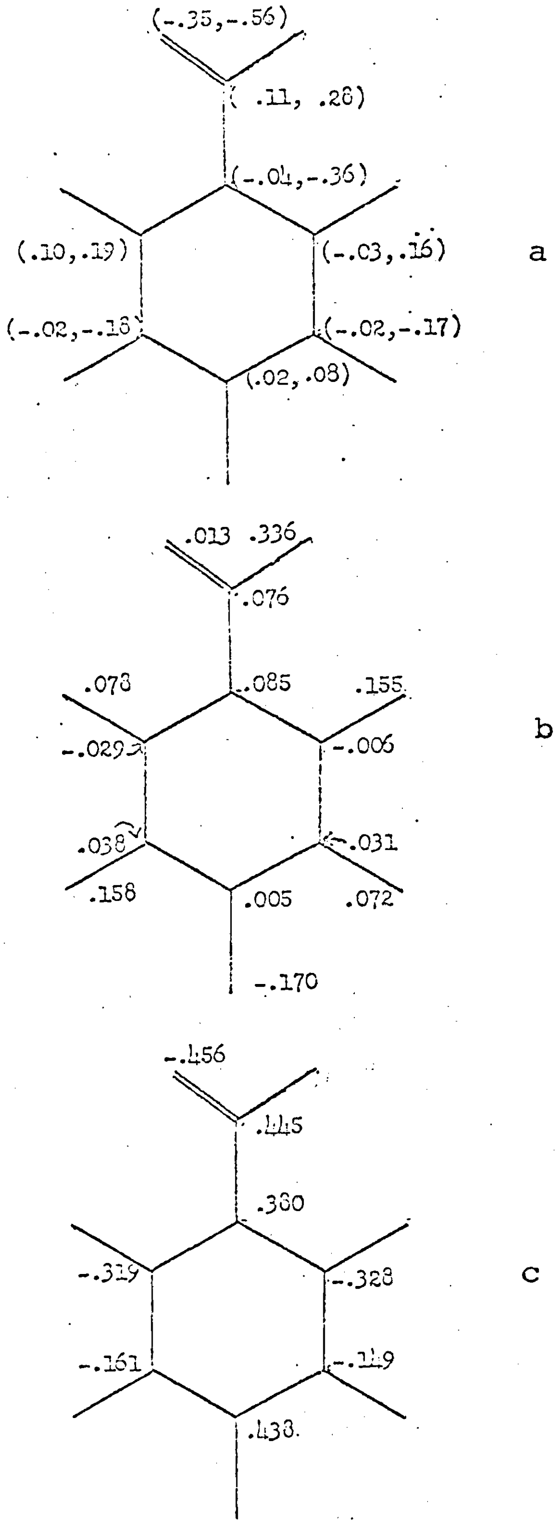
(-.35,-.56)
(.11, .28)
(-.04,-.36)
(.10,.19)
(-.03,.16)
(-.02,-.18)
(-.02,-.17)
(.02,.08)
a
.013
.336
.076
.078
.085
.155
-.029
-.006
.038
.031
.158
.005
.072
-.170
b
-.456
.445
.380
-.319
-.328
-.161
-.149
.438
c

$n\pi^*$ and $\pi\pi^*$ states in terms of LE and CT components, in a sense go beyond the SCF single configuration descriptions of these states because of the inclusion of some correlatory terms. It is interesting to note that the $S_o \rightarrow {}^1n\pi^*$ transition in benzaldehyde shows the same type of Herzberg-Teller activity that characterize the $T_1 \rightarrow S_o$ transition in benzoic acid. In both cases, ring out-of-plane modes predominate. Most remarkably, ν_{11} is the most active mode in both cases, despite the differences in orbital descriptions of the excited states in the two molecules. It should be acknowledged that the results of the calculation by Chu and Goodman have inspired the qualitative analysis presented here. To proceed further it is necessary to consider the environmental sensitivity of the out-of-plane modes in benzoic acid. However, before doing so, it will be advantageous to discuss the carboxyl group in-plane modes that are active in the benzoic acid phosphorescence spectra.

As discussed previously, Maria and McGlynn calculated that the lowest triplet state in benzoic acid consisted of a 1:1 mixture ${}^3\psi_{\emptyset}$ and ${}^3\psi_{COOH}$. The observed intensity of carboxyl group modes (9%) is small for such a large amount of carboxyl group character, assuming reasonable Franck-Condon factors. However, in view of the severe approximations made in their calculations, it is not surprising that their predictions are quantitatively in error. We assume that the weak presence of the carboxyl group modes indicates the presence of at least a small percentage of carboxyl group character in the benzoic acid triplet state. The most interesting aspect of the carboxyl group modes is their environmental dependence. In benzene matrix some modes are quite strong. For example, the C=0 stretching mode (Raman active version) is almost as intense as ν_{8a} in this matrix. In the mixed isotopic crystal, this mode is much weaker. The same is true of nonane matrix. We propose that this variability is the result of different degrees of non-planarity of the carboxyl group relative to the plane of the benzene rings. X-ray data shows that the carboxyl group determines a plane that makes an angle of about 2° with the plane of the rings. Jeffrey and Sax (1963) have suggested that while the planar configuration is probably the most stable for the free molecule, steric packing requirements cause a deviation from planarity in the crystal. In this connection, it must be remembered that the x-ray data were obtained at room temperature. At 4.2° K, the unit cell will be smaller, most likely making the deviation from planarity even greater. We therefore propose that the relatively greater intensity of the carboxyl group modes in benzene is a result of a smaller deviation from planarity. Tilting the carboxyl group reduces conjugation between the $2p\pi$ orbitals of the ring atoms and those of the carboxyl group. This causes the coefficient of the ${}^3\pi_C\pi_C{}^*$ component of ${}^3X$ to become smaller, making the carboxyl group modes weaker. This argument is concerned only with the electronic transition moment. Franck-Condon factors must also be considered. In general we expect an increase in non-planarity to lead to a less rigid molecule. In a less rigid molecule we expect Franck-Condon factors to be larger. Since the observed intensities are decreased rather than increased in the more non-planar molecule, we conclude that the change in the electronic transition moment overrides changes in Franck-Condon factors.

We now return to the out-of-plane modes. Let us first consider what effects the non-planarity of the carboxyl group is expected to have on the activity of these modes. Before we concluded that if $\pi\pi^*$ were written as $a\ \pi_R\pi_R{}^* + b\ \pi_R\pi_C{}^* + c\ \pi_C\pi_R{}^* + d\ \pi_C\pi_C{}^*$, only a and b were important for Herzberg-Teller coupling involving out-of-plane ring modes. As argued above, tilting the carboxyl group should reduce coefficient d. Coefficient b should also be reduced, but to a lesser extent than d because $\pi_C\pi_C{}^*$ has both orbitals on the carboxyl group while $\pi_R\pi_C{}^*$ has only one.

Additional distinction can be made for the two types of benzenoid states, the a- and b-type states (Platt notation). The b-type states are nodal at the 1 and 4 positions, while the a-type states are non-nodal at these positions. In order for a $\pi_R\pi_C{}^*$ charge transfer state to mix with a b-type LE state it must have the same nodal properties as this LE state. The same is true for an a-type state (Murrell, 1966). Since the b-type states are nodal at the substituent position, it is reasonable to assume that the CT components of these states will be less affected by tilting of the carboxyl group than the a-type states. In other words, tilting will reduce the CT character of a-type states more effectively than for b-type states. This assumption is supported by a calculation on aniline carried out by Khalil, Meeks, and McGlynn (manuscript in preparation). These authors find that tilting the substituent group causes a greater frequency shift and greater loss of intensity in ^1L_a than in ^1L_b.

In order to determine experimentally, the effect of a non-planar carboxyl group, we compare the spectra of benzoic acid in benzene and benzoic acid d_o in d_5. In the benzene matrix, ν_{16a} has about the same intensity as ν_{16b}. ν_{10a} is of medium intensity and ν_{11} is the strongest out-of-plane mode. ν_4 has about 40% of the intensity of ν_{11}. In the mixed isotopic crystal, ν_{10a}

is the strongest out-of-plane mode. ν_{16a} is much stronger than ν_{16b} and ν_{11} and ν_4 are both reduced by 50% relative to ν_{12}. It thus appears that the more planar molecule that exists in the benzene matrix is correlated with a dominance of out-of-plane modes that have amplitude at the 1 and 4 positions of the ring, while in the less planar molecule that exists in the mixed isotopic crystal, modes which have no amplitude at the 1 and 4 positions are dominant. This behavior is explained by assuming that the Herzberg-Teller coupling is occurring between nπ* and a- and b-type singlet states (^1L_b, ^1B_b, ^1L_a, ^1B_a), with the coupling between ^1X_a and $^1n\pi^*$ occurring through modes that have amplitude at the 1 and 4 positions and the coupling between ^1X_b and $^1n\pi^*$ occurring through modes that have no amplitude at these positions. Since tilting the carboxyl group would reduce the charge transfer character in the a-type states more than in the b-type states, it is understandable that ν_{16b}, ν_{11} and ν_4 are reduced relative to ν_{10a} and ν_{16a} in the mixed isotopic crystal. If we assume C_{2v} symmyetry for benzoic acid monomer, this argument can be made more systematic. ^1X_a, ^1X_b and $^1n\pi^*$ belong to the A_1, B_1 and B_2 representations, respectively. ν_{10a}, ν_{16a} belong to the a_2 representation and ν_4, ν_{11}, and ν_{16b} to the b_2 representation. Since $A_1 \cdot a_2 = A_2 \neq B_2$, a_2 vibrations cannot couple 'nπ* with ^1X_a.

But $B_1 \cdot a_2 = B_2$, so these vibrations can couple $^1n\pi^*$ with ^1X_b. $B_1 \cdot b_2 = A_2 \neq B_2$ so b_2 vibrations cannot couple $^1n\pi^*$ with ^1X_b. However, $A_1 \cdot b_2 = B_2$. Thus b_2 vibrations can couple ^1X_a and $^1n\pi^*$. The important point here is that tilting the carboxyl group affects a_2 and b_2 modes differently.

In this analysis, we have not considered quasi Franck-Condon factors. Using harmonic wavefunctions, quasi Franck-Condon factors can be shown to be proportional to $\sqrt{\nu}$, where ν is the frequency of vibration. Since the observed out-of-plane frequencies in benzene host differ from those in the mixed isotopic crystal by less than 0.2%, it follows that a neglect of these factors is justified.

As noted previously, out-of-plane ring modes can acquire Herzberg-Teller activity as a result of

$$ga\langle \sigma_R\pi_R^* | H\text{-}T | \pi_R\pi_R^* \rangle \quad \text{and} \quad kb\langle \sigma_R\pi_C^* | H\text{-}T | \pi_R\pi_C^* \rangle.$$

It might be argued that the former matrix element is mainly responsible for the observed activity. One could argue further that tilting of the carboxyl group would also reduce the percentage of the $\sigma_R\pi_R^*$ component of the $n\pi^*$ state. However, since this component couples with $\pi_R\pi_R^*$ and not with $\pi_R\pi_C^*$, it follows that tilting should not lead to a preferential reduction of b_2 modes over a_2 modes. Both types should be reduced equally. Since we in fact observe a preferential reduction, it follows that the charge transfer components of the $n\pi^*$ and $\pi\pi^*$ states (namely, $\sigma_R\pi_C^*$ and $\pi_R\pi_C^*$) play a significant role in the Herzberg-Teller coupling between these states.

In benzoic acid, $^1n\pi^*$ cannot be observed. However, in benzaldehyde $^1n\pi^*$ is the lowest singlet state. As noted previously the $S_o \rightarrow {}^1n\pi^*$ spectrum shows out-of-plane activity. Multiple quanta of these modes are not active and ring modes predominate over aldehyde modes. ν_{11} has the greatest intensity. Vapor spectra obtained by Hollas _et_ _al_., (1968) and Smolarek _et_ _al_., (1972) together with polarized $S_o \rightarrow S_1$ excitation spectra (photoselection method) obtained by Shimada and Goodman (1965) imply that ν_{11} is predominantly long-axis polarized, indicating that ν_{11} couples $^1n\pi^*$ to ^1L_a or ^1B_a. These observations are fully consistent with the model we have constructed to explain the presence of out-of-plane ring modes in the $T_1 \rightarrow S_o$ spectrum of benzoic acid. Attempts by Baum to obtain the polarized phosphorescence spectra of benzoic acid in benzene were beset with experimental difficulties. However, his data shows that ν_4 is parallel to ν_{11}, as required by our model.

So far we have not considered Herzberg-Teller coupling in the triplet manifold. Assuming that the $^3\pi_R\pi_R^*$ component of the lowest triplet state is ^3L_a, C_{2v}

symmetry only allows b_2 vibrations to couple ^3L_a with $^3n\pi^*$. It thus appears that the spin-orbit vibronic coupling scheme which has the Herzberg-Teller coupling in the singlet manifold is primarily responsible for the activity of a_2 out-of-plane modes. The activity of b_2 vibrations can, of course, be due to both coupling schemes. This argument only applies to mixed dimers in which the excitation is localized on a benzoic acid monomer. For benzoic acid in benzene and n-nonane, we have homogeneous dimers. If C_{2v} symmetry is appropriate for the monomer, then D_{2h} symmetry will be appropriate for the dimer. Figures 42 and 43 give the representations of ^1X_a , ^1X_b , $^1n\pi^*$, $^3n\pi^*$, and ^3L_a in the C_{2v} and D_{2h} point groups, respectively,as well as the possible coupling routes for the various representations of out-of-plane vibrations. For C_{2v} , the important conclusions yielded by this diagram are that a_2 vibrations couple only to the R_z (long-axis) magnetic sublevel, while b_1 vibrations couple to the R_x (short axis) and R_y (perpendicular axis) sublevels. A similar relationship occurs for D_{2h} symmetry: b_{1g} and b_{1u} vibrations couple to only one magnetic sublevel, while b_{2g} vibrations couple to two sublevels.

Vibronic bands associated with modes that couple to only one magnetic sublevel should exhibit an accurately exponential decay of phosphorescence intensity following

FIGURE 42

This figure shows the possible spin-orbit vibronic coupling routes for a_2 and b_2 out-of-plane vibrations, assuming C_{2v} symmetry for benzoic acid monomer. "$\sigma\pi$" denotes a general B_2 state and may be either $n\pi^*$, $\sigma\pi^*$ or $\pi\sigma^*$. The sequence of energy levels has been arranged for convenience.

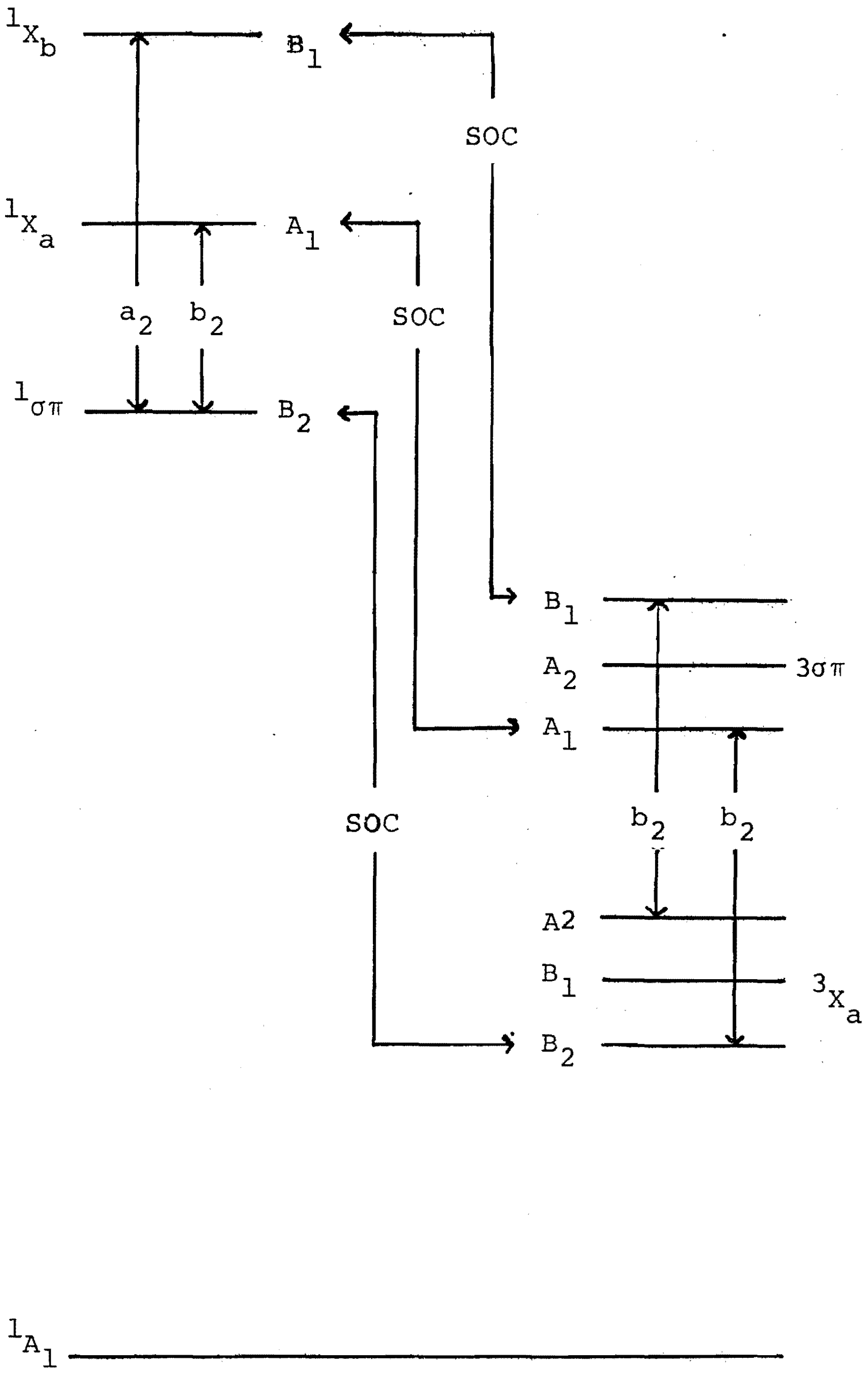

^1X_b
B_1
SOC
^1X_a
A_1
a_2
b_2
SOC
$^1\sigma\pi$
B_2
B_1
A_2
$3\sigma\pi$
A_1
SOC
b_2
b_2
A2
B_1
^3X_a
B_2
$^1A_1$

FIGURE 43

This figure shows the possible spin-orbit vibronic coupling routes for b_{1g} , b_{2g} , and b_{1u} out-of-plane vibrations, assuming D_{2h} symmetry for benzoic acid dimer. "σπ" devotes a general B_{3u} or B_{2g} state and may be either nπ", σπ* , or πσ*. The sequence of energy levels has been arranged for convenience.

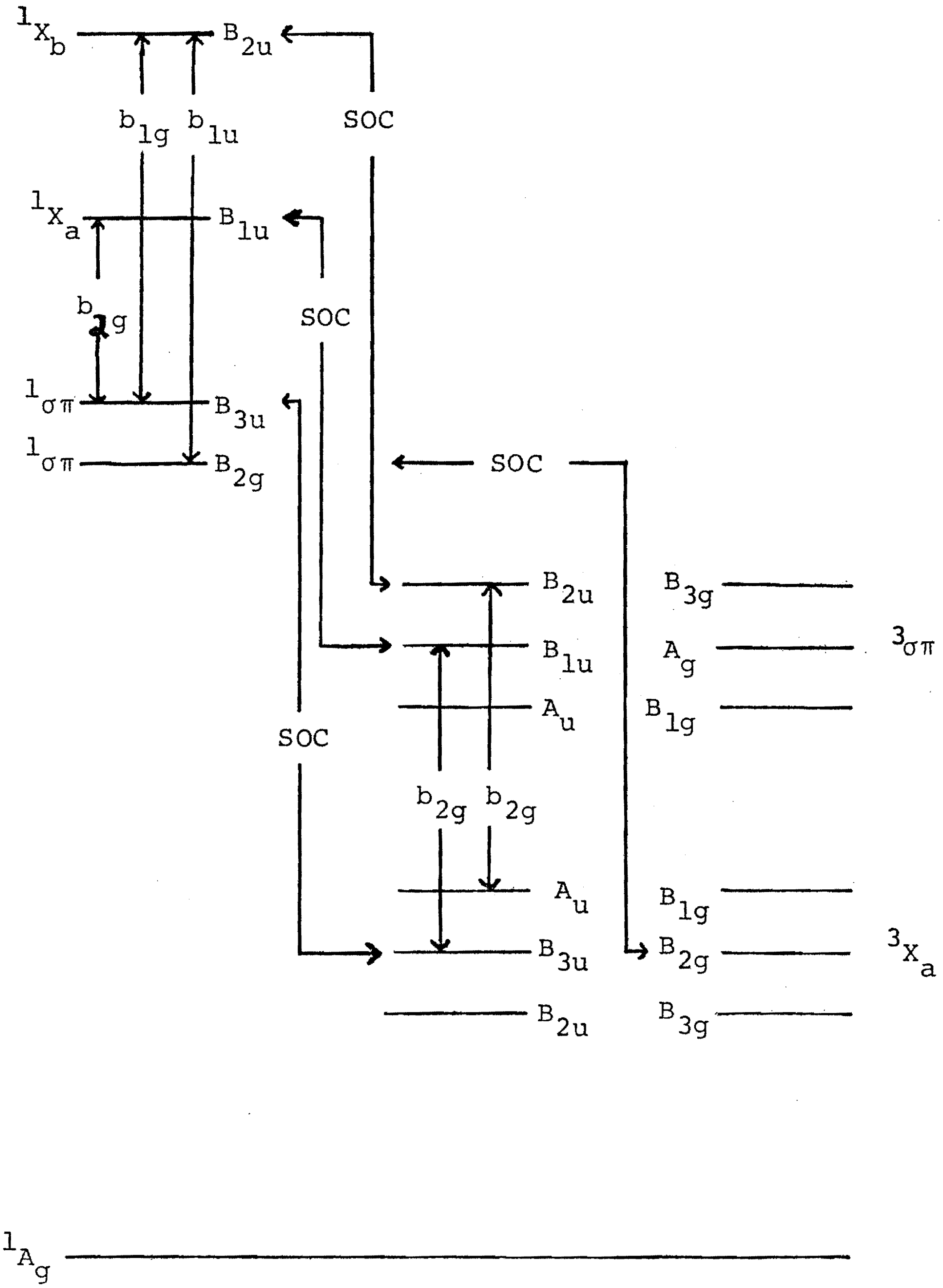

^1X_b
B_{2u}
b_{1g}
b_{1u}
SOC
^1X_a
B_{1u}
b_{2g}
SOC
$^1\sigma\pi$
B_{3u}
$^1\sigma\pi$
B_{2g}
SOC
B_{2u}
B_{3g}
B_{1u}
A_g
$^3\sigma\pi$
A_u
B_{1g}
SOC
b_{2g}
b_{2g}
A_u
B_{1g}
B_{3u}
B_{2g}
^3X_a
B_{2u}
B_{3g}
^1A_g

a short pulse of exciting light, provided that the temperature of the sample is sufficiently low to make the spin-lattice relaxation time much longer than the phosphorescence lifetime. For modes that couple to two sublevels, we expect to observe a non-exponential decay, provided that the lifetimes of the sublevels are sufficiently different in magnitude. Baum (1974) has found that the decay of the total phosphorescence emission at 1.4° K shows a marked deviation from exponentiality. This implies that 1.4° K is sufficiently cold to make the spin-lattice relaxation time appreciably greater than the phosphorescence life time. It also implies that the lifetimes of the sublevels are sufficiently different to be observed. Unfortunately, lifetime measurements of individual vibronic bands were not obtained.

The spin-orbit vibronic coupling schemes depicted in Figure 42 and 43 allow one to make predictions about the polarization of the various kinds of vibronic bands in the phosphorescence spectrum. First of all, the origin of the phosphorescence spectrum derives its intensity through first order spin-orbit coupling to $^1n\pi^*$, $^1\sigma\pi^*$ and $\pi\sigma^*$ states. $S_o \rightarrow {}^1\sigma\pi$ transitions are polarized out-of-plane. Consequently, the phosphorescence origin should be out-of-plane polarized. Vibronic bands involving totally symmetric modes should also be out-of-plane polarized, provided these bands are not intensified by a spin-orbit vibronic coupling scheme that involves a $^1\pi\pi^*$ state as the final state. For C_{2v} symmetry, vibronic bands corresponding to out-of-plane modes belonging to the a_2 representation should have the same polarization as the $S_o \rightarrow {}^1X_b$ transition. ^1X_b can be either ^1L_b or ^1B_b, or both. Baum's data shows that the $S_o \rightarrow {}^1L_b$ transition is short axis polarized, as expected on the basis of C_{2v} symmetry. ^1B_b and ^1B_a cannot be resolved in Baum's spectra, but on the basis of C_{2v} symmetry, ^1B_b should also be short axis polarized. Vibronic bands corresponding to b_2 out-of-plane modes should have a polarization that is a weighted average of the polarization of the $S_o \rightarrow {}^1X_a$ and $S_o \rightarrow {}^1X_b$ transitions. ^1X_a can be either ^1L_a or ^1B_a , or both. C_{2v} symmetry requires these transitions to be long axis polarized. Baum's data for ^1L_a is consistent with long axis polarization but a definite conclusion is not possible because ^1B_a and ^1B_b overlap ^1L_a. For D_{2h} symmetry, Figure 43 shows that the same conclusions hold in all cases. Note that the a_2 representation correlates with the b_{1g} and b_{1u} representations and the b_2 representation correlates with the b_{2g} representation.

As noted previously, Baum's attempts to obtain the polarized phosphorescence spectrum of benzoic acid doped into single crystals of benzene were unsuccessful on account of experimental problems. We have obtained the polarized phosphorescence and $S_o \rightarrow S_1$ excitation spectra of benzoic acid and parafluorobenzoic acid in EPA and 2-methyl-tetrahydrofuran glasses at 77^o K using the photoselection method. Since the photoselection method had previously proven successful with azines and polyacenes (Krishna and Goodman, 1961 and 1962) it was our hope that it would prove successful with benzoic acid. This hope has not materialized. Our data show that the origin in the benzoic acid phosphorescence spectrum has a polarization of + 0.1 when ${}^1L_b$ is excited. This polarization corresponds to a transition moment that is more than 2/3 in-plane (Albrecht 1961). The origin in the parafluorobenzoic acid spectrum taken under similar conditions has a polarization of 0.0. This corresponds to a transition moment that is 2/3 in-plane. In-plane components this large are contrary to our expectation that the origin should be predominantly out-of-plane polarized. Because benzoic acid has low frequency out-of-plane modes, it is difficult to interpret low resolution polarization spectra since these modes are not resolved. This raises the possibility that the observed in-plane polarization of the broad "origin" band is the vector sum of the out-of-plane polarization of the origin band and the in-plane polarization of unresolved vibronic bands corresponding to low frequency out-of-plane modes. Another possibility is that the transition moment of the origin actually contains a large in-plane component. It is interesting to consider possible explanation for in-plane polarization.

As noted previously, the carboxyl group deviates from the plane of the benzene rings. A deviation from planarity raises the possibility of a breakdown of σ-π separability. An appealing idea is that the field of the benzene ring breaks the σ-π separability in the carboxyl group. In this case we can write

$$^1n_C\pi_C^*(\text{tilted}) = a\ ^1n_C\pi_C(\text{untilted}) + b\ ^1\pi_C\pi_C^*.$$

For small angles, a would be much greater than b. This would still allow strong spin-orbit coupling between $^1n_C\pi_C^*$(tilted) and $^3\pi_C\pi_C^*$. On the other hand the $S_o \rightarrow {}^1n_C\pi_C^*$(tilted) transition would likely have a large in-plane component because the $^1\pi_C\pi_C^*$ component should be much more allowed than the $^1n_C\pi_C^*$(untilted) component. We regard a σ-π breakdown in the carboxyl group as much more likely than a σ-π breakdown in the benzene ring since the latter structure is much more rigid than the carboxyl group. As far as we are able to determine a small breakdown of σ-π separability in the carboxyl group would not alter our previous conclusions, except those concerning expected polarizations. Clearly, high resolution polarized emission spectra are needed to clarify further the nature of the electronic states in benzoic acid.

Having established the possible role of CT states in the spin-orbit vibronic coupling schemes that we propose to be responsible for the activity of the out-of-plane modes, it is now fruitful to examine the influence of hydrogen bonding on the activity of these modes.

The second-order correction to ${}^3X^o$ introduced by the spin-orbit vibronic coupling schemes that we have proposed to account for out-of-plane activity is given by the following expression:

$$
\begin{aligned}
{}^3X^2 = {}^3X^o &+ \frac{\langle {}^1\pi\pi^* | \mathrm{SOC} | {}^3n\pi^* \rangle}{E({}^3X^o) - E({}^1\pi\pi^*)} \cdot \frac{\langle {}^3n\pi^* | \mathrm{H\text{-}T} | {}^3X^o \rangle \, {}^1\pi\pi^*}{E({}^3X^o) - E({}^3n\pi^*)} \\
&+ \frac{\langle {}^1\pi\pi^* | \mathrm{H\text{-}T} | {}^1n\pi^* \rangle}{E({}^3X^o) - E({}^1\pi\pi^*)} \cdot \frac{\langle {}^1n\pi^* | \mathrm{SOC} | {}^3X^o \rangle \, {}^1\pi\pi^*}{E({}^3X^o) - E({}^1n\pi^*)}
\end{aligned}
$$

In order to evaluate the effect of a change in H-bond strength on the activity of an out-of-plane mode, it is necessary to consider the effects of a change in H-bond strength on the energy denominators and matrix elements in the above expression.

Since the energy denominators in this expression are 8000 cm^{-1} or greater in benzoic acid dimer, it follows that large percentage changes in the energy denominators will not result from changes in H-bond strength (Brealey and Kasha, 1955). Thus, changes in energy denominators cannot account for the large (factor of 7) changes in out-of-plane activity which we observe.

Previously we noted that quasi Franck-Condon factors were proportional to $\sqrt{\nu}$ assuming harmonic wavefunctions, where ν is the frequency of vibration. Since the out-of-plane frequencies differ by less than 0.2% in the various matrices considered in this study, it follows that quasi Franck-Condon factors should be nearly equal in these matrices. Consequently, differences in quasi Franck-Condon factors cannot account for the observed differences in out-of-plane activity.

In order to determine the effect of a change in H-bond strength on the product of Herzberg-Teller and spin-orbit coupling matrix elements, we decompose the states into LE and CT components and determine which terms can be neglected.

Previously we showed that the terms important for Herzberg-Teller coupling between an $n\pi^*$ and $\pi\pi^*$ state involving an out-of-plane ring mode are:

$$ga \left\langle \sigma_R \pi_R{}^* \middle| H\text{-}T \middle| \pi_R \pi_R{}^* \right\rangle$$

$$kb \left\langle \sigma_R \pi_C{}^* \middle| H\text{-}T \middle| \pi_R \pi_C{}^* \right\rangle$$

To determine the terms important for spin-orbit coupling between an $n\pi^*$ and a $\pi\pi^*$ state, we decompose these states into LE and CT components as before and evaluate the matrix element. This leads to a sum of twenty eight terms, which are shown in Table 34. Eighteen of these terms are zero because of orbital orthogonality. Overlap considerations disfavor an additional five, which we set equal to zero, and indicate by asterisks.

The remaining ~~six~~ five terms are:

$$\text{de} \ \langle \pi_C \pi_C^* | \text{SOC} | n_C \pi_C^* \rangle$$

$$\text{cf} \ \langle \pi_C \pi_C^* | \text{SOC} | n_C \pi_R^* \rangle$$

$$\text{ag} \ \langle \pi_R \pi_R^* | \text{SOC} | \sigma_R \pi_R^* \rangle$$

$$\text{di} \ \langle \pi_C \pi_R^* | \text{SOC} | \sigma_C \pi_C^* \rangle$$

$$\text{bk} \ \langle \pi_R \pi_C^* | \text{SOC} | \sigma_R \pi_C^* \rangle$$

At this point, it is necessary to consider the effects of hydrogen bonding on the LE, CT compositions of $n\pi^*$ and $\pi\pi^*$ states. For $\pi\pi^*$ states, we rely on Baum's semiempirical calculations. He has used three types of calculations (INDO, CNDO/S-CI, and Pariser-Parr-Pople) to calculate the wavefunctions for the lower lying $\pi\pi^*$ states of benzoic acid. We wish to point out the need for caution concerning conclusions based on these calculations, since benzoic acid is a complicated molecule for the present state of valence theory. Recent detailed calculations on as small a molecule as formaldehyde (Ozkan, Chu, and Goodman, 1975) amply illustrate the pitfalls of approximate

TABLE 34

This table shows the terms that result when $\langle \pi\pi^* | \mathrm{SOC} | n\pi^* \rangle$ is expanded in terms of the LE and CT components of $\pi\pi^*$ and $n\pi^*$. Terms denoted by an asterisk are disfavored by overlap considerations and are set equal to zero on this basis.

ae	$\langle \pi_R \pi_R^* \| \mathrm{SOC} \| n_C \pi_C^* \rangle$	=	0	
be	$\langle \pi_R \pi_C^* \| \mathrm{SOC} \| n_C \pi_C^* \rangle$	=	0	*
ce	$\langle \pi_C \pi_R^* \| \mathrm{SOC} \| n_C \pi_C^* \rangle$	=	0	
de	$\langle \pi_C \pi_C^* \| \mathrm{SOC} \| n_C \pi_C^* \rangle$			
af	$\langle \pi_R \pi_R^* \| \mathrm{SOC} \| n_C \pi_R^* \rangle$	=	0	*
bf	$\langle \pi_R \pi_C^* \| \mathrm{SOC} \| n_C \pi_R^* \rangle$	=	0	
cf	$\langle \pi_C \pi_R^* \| \mathrm{SOC} \| n_C \pi_R^* \rangle$			
df	$\langle \pi_C \pi_C^* \| \mathrm{SOC} \| n_C \pi_R^* \rangle$	=	0	
ag	$\langle \pi_R \pi_R^* \| \mathrm{SOC} \| \sigma_R \pi_R^* \rangle$			
bg	$\langle \pi_R \pi_C^* \| \mathrm{SOC} \| \sigma_R \pi_R^* \rangle$	=	0	
cg	$\langle \pi_C \pi_R^* \| \mathrm{SOC} \| \sigma_R \pi_R^* \rangle$	=	0	*
dg	$\langle \pi_C \pi_C^* \| \mathrm{SOC} \| \sigma_R \pi_R^* \rangle$	=	0	
ah	$\langle \pi_R \pi_R^* \| \mathrm{SOC} \| \pi_R \sigma_R^* \rangle$	=	0	
bh	$\langle \pi_R \pi_C^* \| \mathrm{SOC} \| \pi_R \sigma_R^* \rangle$	=	0	
ch	$\langle \pi_C \pi_R^* \| \mathrm{SOC} \| \pi_R \sigma_R^* \rangle$	=	0	
dh	$\langle \pi_C \pi_C^* \| \mathrm{SOC} \| \pi_R \sigma_R^* \rangle$	=	0	

Table 34 (Continued)

ai $\langle \pi_R \pi_R^* | \mathrm{SOC} | \sigma_C \pi_C^* \rangle = 0$

bi $\langle \pi_R \pi_C^* | \mathrm{SOC} | \sigma_C \pi_C^* \rangle = 0$ *

ci $\langle \pi_C \pi_R^* | \mathrm{SOC} | \sigma_C \pi_C^* \rangle = 0$

di $\langle \pi_C \pi_C^* | \mathrm{SOC} | \sigma_C \pi_C^* \rangle$

aj $\langle \pi_R \pi_R^* | \mathrm{SOC} | \pi_C \sigma_C^* \rangle = 0$

bj $\langle \pi_R \pi_C^* | \mathrm{SOC} | \pi_C \sigma_C^* \rangle = 0$

cj $\langle \pi_C \pi_R^* | \mathrm{SOC} | \pi_C \sigma_C^* \rangle = 0$

dj $\langle \pi_C \pi_C^* | \mathrm{SOC} | \pi_C \sigma_C^* \rangle = 0$

ak $\langle \pi_R \pi_R^* | \mathrm{SOC} | \sigma_R \pi_C^* \rangle = 0$

bk $\langle \pi_R \pi_C^* | \mathrm{SOC} | \sigma_R \pi_C^* \rangle$

ck $\langle \pi_C \pi_R^* | \mathrm{SOC} | \sigma_R \pi_C^* \rangle = 0$

dk $\langle \pi_C \pi_C^* | \mathrm{SOC} | \sigma_R \pi_C^* \rangle = 0$ *

quantum mechanical calculations. However, it should be emphasized that we have used only the qualitative trends predicted by Baum's calculations. None of our conclusions depend on the specific quantative results of his calculations.

The CNDO/S-CI and PPP calculations show that L_b, ${}^{1,3}L_a$, ${}^1B_b$, and ${}^1B_a$ are basically benzenoid in character but do possess small amounts of charge transfer character. The results of these calculations for benzoic acid monomer are shown in Table 35. The calculated effects of hydrogen bonding upon ${}^1L_b$ and ${}^1L_a$ (other states not calculated) are given in Table 36. This table reveals three important results: (1) A hydrogen bond to the carbonyl oxygen atom is calculated to increase the net ring to carboxyl group charge transfer character in ${}^1L_b$ and ${}^1L_a$, while a hydrogen bond to the hydroxyl hydrogen atom is calculated to decrease the net ring to carboxyl group charge transfer character in these states; (2) If the H-bonds are equally strong, the bond to the carbonyl oxygen atom is predicted to have the dominant effect; (3) The a-type and b-type states do not contain greatly different amounts of charge transfer character. In what follows we will assume that these conclusions also hold for ${}^1B_a$ and ${}^3L_a$.

Since Baum's calculations predict that the LE, CT compositions of $\pi\pi^*$ states will be sensitive to hydrogen bonding, it follows that the activity of the out-of-plane

TABLE 35. Singlet states of benzoic acid (monomer). (Taken from Baum, 1974)

	Wavelength (mu)			Oscillator Strength			Polarization[b]		State[c]	Charge-Transfer[d]	
	obs[a]	CNDO	PPP	obs[a]	CNDO	PPP	obs	CNDO		CNDO	PPP
C-Band	278	270	265	0.014	0.003	0.011	Y	Y	^1L_b	0.05	0.20
B-Band	230	220	227	0.19	0.12	0.21	Z	Z	^1L_a	0.06	0.26
A-Band	196	193	198	0.4	0.41	0.54	--	Z	^1B_a	0.02	--
	193	191	193	0.5	0.51	0.90	--	Y	^1B_b	0.00	--

---

[a] See text in Appendix. [b] Y = short-axis; Z = long-axis of molecule. [c] Platt notation; assigned on the basis of the polarization and CI composition. [d] The fractional transfer of an electron from the aromatic ring to the carboxyl group is predicted to be 0.10 in the ground state by CNDO (0.04 by PPP). The additional transfer to the substituent with excitation is listed under charge-transfer.

Table 36

Calculated changes in electron density upon excitation of benzoic acid.

	Monomer		Proton Donor		Proton Acceptor		Proton Donor and Acceptor	
Atom	^1L_b	^1L_a	^1L_b	^1L_a	^1L_b	^1L_a	^1L_b	^1L_a
C(OOH)	+.151	+.194	+.120	+.148	+.259	+.333	+.208	+.274
= O	+.042	+.055	+.025	+.034	+.047	+.062	+.039	+.049
O(H)	+.007	+.009	+.016	+.013	+.013	+.018	+.021	+.025

(Taken from Baum, 1974)

modes should also be sensitive to hydrogen bonding since, as we have shown, CT components play an important role in the mechanism responsible for these modes.

Unfortunately, the influence of hydrogen bonding on $n\pi^*$ states in benzoic acid has not been calculated. Hence, we must rely on physical intuition. Since, from the classical point of view, the non-bonding electrons participate in the hydrogen bond to the carbonyl oxygen atom, we think it reasonable to assume that a hydrogen bond to this atom will reduce the delocalization of an $n\pi^*$ state over the benzene ring. On the other hand, the additional electronic charge associated with the hydrogen bond to the hydroxyl hydrogen atom should repel the non-bonding electrons, increasing the delocalization over the benzene ring. Since an $n\pi^*$ state has its greatest density in the region of the carbonyl oxygen atom, a hydrogen bond to this atom should have a greater effect than a hydrogen bond to the hydroxyl hydrogen atom of equal strength. It thus follows that the LE, CT composition of $n\pi^*$ states are also affected by hydrogen bonding. Since $n\pi^*$ states are the intermediate states in the two spin-orbit vibronic coupling schemes which we have proposed to account for the out-of-plane activity, it may be concluded that out-of-plane intensity should also be sensitive to hydrogen bond effects on $n\pi^*$ states.

It will be recalled that $n\pi^*$ and $\pi\pi^*$ are written as

$$n\pi^* = e\ n_C\pi_C^* + f\ n_C\pi_R^* + g\ \sigma_R\pi_R^* + h\ \pi_R\sigma_R^* + i\ \sigma_C\pi_C^* + j\ \pi_C\sigma_C^* + k\ \sigma_R\pi_C^*$$

$$\pi\pi^* = a\ \pi_R\pi_R^* + b\ \pi_R\pi_C^* + c\ \pi_C\pi_R^* + d\ \pi_C\pi_C^*$$

A reduction in the delocalization of $n\pi^*$ over the benzene ring requires, in general, an increase in e, i, and j and a decrease in f, g, h, and k. However, since our intuitive considerations only require a net decrease in the delocalization, it is not necessary that e, i, and j all increase or that f, g, h, and k all decrease. Since we do not have detailed information about the wavefunction, more definite predictions cannot be made. An increase in the ring to carboxyl group CT character in the $\pi\pi^*$ state requires an increase in coefficient b. Definite statements about whether a, c, and d increase or decrease are not possible on the basis of available information.

In spite of the uncertainties, it is clear that an increase (or decrease) in H-bond strength should cause some coefficients to increase and some to decrease. This creates the possibility that there exists an optimum hydrogen bond strength which maximizes the product of the spin-orbit coupling and Herzberg-Teller coupling matrix elements. We include this consideration in order to offer a possible rationalization of the observed environmental dependence of the out-of-plane modes. This enivronmental dependence suggests that there is an optimum H-bond strength which maximizes the out-of-plane activity.

We now consider the observed environmental effects on out-of-plane activity. In this section we attempt to show that differences in H-bond strength are the major cause of the difference in out-of-plane activity observed in the various matrices. We also attempt to show that the data are consistent with the existence of an optimum H-bond strength that maximizes the out-of-plane intensity.

Previously, we proposed that differences in the relative intensities of a_2 and b_2 out-of-plane modes were dependent on the degree of non-planarity of the carboxyl group. Clearly, in attempting to determine the effects of different H-bond environments on out-of-plane activity, it is necessary to distinguish between these effects and effects resulting from non-planarity.

Fortunately, this distinction can be made on a qualitative basis by monitoring the relative intensities of in-plane modes involving carboxyl group motion.

As discussed in Section III, the phosphorescence spectra of benzoic acid d_o in n-nonane and benzoic acid d_o in d_5 are similar with regard to activity of in-plane carboxyl group modes and the a_2 versus b_2 pattern of out-of-plane intensities. The only difference between the spectra is that out-of-plane activity in nonane host is slightly less than in the mixed isotopic crystal. Both of these systems correspond to what may be called the "more non-planar" case in which the C=0 stretching mode appears weakly and other modes involving carboxyl group motion such as ν_1 and ν_{6a} are missing. This case is distinguished from what we will call the "less non-planar" case, exemplified by benzoic acid in benzene, in which the C=0 stretching mode is strong and ν_1 and ν_{6a} appear with weak-to-medium intensity.

The close similarity of the mixed isotopic crystal and nonane host spectra allow several important conclusions. As discussed in Section III benzoic acid exists as a dimer in n-nonane and emits as a monomer in the mixed isotpic crystal. From this, it follows that dimerization has no effect on the activity of the out-of-plane modes. We can also conclude that the polarity of the host and aromatic versus aliphatic properties of the host have no significant effect on out-of-plane activity.

A comparison of the phosphorescence spectra of benzoic acid d_o in d_5 and parafluorobenzoic acid in benzoic acid d_o shows that the spectra are identical except that the out-of-plane activity is reduced by about 40% in the latter system. As discussed in section III the emitting species in the latter system is very likely a benzoic acid monomer perturbed by a parafluorobenzoic acid molecule. Thus in both systems the emission comes from the benzoic acid d_o part of a mixed dimer. The environment of a d_o - d_5 complex in the mixed isotopic crystal largely consists of d_5 - d_5 dimers. The environment of a BA-PFBA complex largely consists of d_o - d_o dimers. Thus, the environments of the two complexes should be very similar. The complexes should also be similar with regard to non-planarity of the carboxyl group, since their spectra show that both belong to the "more non-planar" case. On the other hand, the complexes differ with regard to H-bond strength. The H-bonds in the BA-PFBA complex should be stronger than those in the d_o - d_5 complex, since the K_a of parafluorobenzoic acid is 7.2×10^{-5} and that for benzoic acid is 6.3×10^{-5}. Consequently, we are inclined to attribute the weaker out-of-plane activity associated with the BA-PFBA complexes to the stronger H-bonds. In making this attribution, we are assuming that the observed difference in activity is not due to radiationless processes. Finally, it should be pointed out that another way in which the complexes differ is that the dipole moment of parafluorobenzoic acid is somewhat larger than the dipole moment of benzoic acid d_5. However, at least in the context of our model, which involves spin-orbit vibronic coupling as the mechanism responsible for out-of-plane modes, there is no apparent way in which the different dipole moment could have an effect on out-of-plane activity.

The most striking environmental dependence of the out-of-plane modes is revealed in the phosphorescence spectrum of benzoic acid d_o in cyclohexane carboxylic acid (Baum, 1974). In this spectrum the intensity of the out-of-plane modes relative to the totally symmetric system is about a factor of five smaller than for benzoic acid in benzene. We compare this system with benzoic acid in benzene since both systems belong to the "less non-planar" case, which shows a strong C=0 stretching mode, and weak to medium intensity for ν_1 and ν_{6a}. Since both systems belong to the "less non-planar" case, and moreover, since the relative intensities of the carboxyl group modes are quite similar, we conclude that non-planarity effects cannot account for the large reduction in out-of-plane activity. Further, since monomer-dimer and solvent polarity effects have been eliminated as significant perturbations of out-of-plane activity, we attribute the weaker out-of-plane activity to the weaker H-bonds that exist in the BA-CHCA complexes. The K_a of cyclohexane carboxylic acid is 1.26×10^{-5}. As before, we assume that radiationless processes do not play an important role.

The fact that both stronger H-bonds (BA-PFBA) and weaker H-bonds (BA-CHCA) apparently lead to a smaller out-of-plane activity, compared to that observed for $d_o - d_5$, suggests that there exists an optimum H-bond strength which maximizes out-of-plane activity. It also follows that the H-bond strength in the $d_o - d_5$ complex is closer to this optimum value than the strengths of the H-bonds in the other two systems. As we previously argued, the existence of such an optimum H-bond strength can be rationalized in terms of the expected effects of H-bonding on the LE, CT compositions of $n\pi^*$ and $\pi\pi^*$ states.

As noted in Section IIIC, the phosphorescence spectrum of paraflorobenzoic acid in n-nonane shows a much smaller percentage of out-of-plane activity than observed for benzoic acid in n-nonane. We are unable to explain this reduced activity. However, good evidence that the mechanism responsible for out-of-plane activity in parafluorobenzoic acid is the same as that in benzoic acid can be found in the phosphorescence spectrum of parafluorobenzoic acid in cyclohexane carboxylic acid. In this spectrum, the out-of-plane activity, is much less than that observed with nonane host. Thus, the environmental sensitivity of out-of-plane modes in parafluorobenzoic acid parallels that observed for benzoic acid. As before, we attribute the reduced out-of-plane activity in cyclohexane carboxylic acid host to the weaker H-bonds in the PFBA-CHCA complex.

The phosphorescence spectrum of methyl benzoate in benzene shows out-of-plane activity which is comparable in magnitude to that observed for benzoic acid in benzene. This fact is somewhat puzzling in view of the fact that weak H-bonds (BA-CHCA) lead to weak out-of-plane activity in benzoic acid. There is, of course, the fact that the hydroxyl hydrogen in benzoic acid is replaced by a methyl group in methyl benzoate. We are inclined to rationalize the intense out-of-plane activity in methyl benzoate by assuming that the reduced CT character in the $\pi\pi^*$ states that should result from the absence of a hydrogen bond to the carbonyl oxygen atom is compensated by an increased delocalization of $n\pi^*$ states over the ring as a result of the presence of the methyl group. According to our intuition, the methyl group should repel the non-bonding electrons more than a hydroxyl hydrogen atom because it contains more electrons spread over a larger region of space. Good evidence that the $^1\pi\pi^*$ states in methyl benzoate have less CT character than those in benzoic acid can be found in the absence of Herzberg-Teller activity in the $S_o \rightarrow {}^1L_b$ transition of methyl benzoate. The corresponding transition in benzoic acid shows appreciable Herzberg-Teller activity. This will be discussed in detail in connection with the phosphorescence spectrum of methyl benzoate perturbed by parafluorobenzoic acid. An indication that the mechanism responsible for out-of-plane activity in methyl benzoate is fundamentally the same as that in benzoic acid can be found in the environmental dependence of this activity. As will be shown in what follows, out-of-plane activity in methyl benzoate shows a strong sensitivity to hydrogen bonding.

The system consisting of benzoic acid in methyl benzoate shows multiple sites which are differently populated in the several spectra obtained in this study (see Table 32 in Section IIIC). In this analysis, we consider only spectrum III, which shows two principal sites. The spectra associated with these sites are identical. Since these sites are not present in the spectrum of pure (zone refined) methyl benzoate, we assume that they are associated with the benzoic acid guest molecules. However, it is not known for certain whether the emission comes from guest molecules or from guest induced defects. A comparison of this spectrum with the spectrum of parafluorobenzoic acid in methyl benzoate (IV) shows that these spectra have similar vibrational frequencies and intensities. Since the latter emission is definitely associated with guest induced defects, it is likely that spectrum III also derives from guest-induced defects. We assume that the guest-induced defect consists of a methyl benzoate molecule hydrogen bonded to a benzoic acid molecule and that the excited state from which emission occurs is localized on the methyl benzoate molecule.

An important feature of the phosphorescence emission of benzoic acid in methyl benzoate is the relatively weak out-of-plane activity (<20% of origin intensity). According to our model, the H-bond to the carbonyl oxygen atom should reduce the delocalization of the $n\pi^*$ states over the ring.

Apparently, the increase in CT character in the $\pi\pi^*$ states that should result from this H-bond does not compensate for the reduced delocalization of the $n\pi^*$ states.

For parafluorobenzoic acid in methyl benzoate we consider only spectrum IV which shows a single origin, Spectrum V shows multiple origins and little vibrational structure. The prominent bands in the phosphorescence spectrum of parafluorobenzoic acid in methyl benzoate correspond to methyl benzoate frequencies. This conclusion is firm because the frequencies of the fluorinated molecule are distinctly different from those of methyl benzoate. We therefore assume that the phosphorescence emission comes from guest-induced defects which consist of methyl benzoate moleculeshydrogen bonded to parafluorobenzoic acid molecules. This spectrum also shows weak out-of-plane modes which we rationalize in the same manner as for the phosphorescence spectrum of benzoic acid in methyl benzoate.

The interpretation of the environmental dependence of the out-of-plane modes presented here for methyl benzoate and previously for benzoic acid is necessarily speculative and cannot be proven by the available data. We have included this interpretation because it is consistent with the data and because it is a natural extension of the localized molecular orbital approach.

As noted previously, the phosphorescence spectrum of parafluorobenzoic acid in methyl benzoate (IV) closely resembles the spectrum of benzoic acid in methyl benzoate (III). There is, however, a striking difference with regard to one feature. In the former spectrum, a band corresponding to ν_{6b} appears with intensity comparable to that of the origin, while in the latter spectrum, a band corresponding to ν_{6b} cannot be detected. It should be noted, however, that other spectra (I and II) for benzoic acid in methyl benzoate do show the intense ν_{6b} band (see Table 32 in Section III C. Unlike spectra I and II, spectrum IV shows only one origin and exhibits good vibrational resolution. Consequently, we only consider spectrum IV in our analysis of the ν_{6b} band.

As discussed in Section III, the band corresponding to ν_{6b} in spectrum IV is definitely a vibronic band. The data shows that this band cannot correspond to an impurity origin or the origin of a site. It is also firmly established that two quanta of ν_{6b} are too weak to be detected.

Before attempting to account for the activity of ν_{6b} in the phosphorescence spectrum, it will be helpful to consider the activity of ν_{6b} in the $S_o \rightarrow S_1$ absorption spectra of benzene, benzoic acid, methyl benzoate, and other monosubstituted benzenes.

The vibration ν_{6b} appears as a prominant band in the $S_o \rightarrow {}^1B_{1u}$ absorption spectrum of benzene. In fact, ν_{6b} accounts for 95% of the "forbidden" activity in the benzene spectrum (Callomon, <u>et al</u>., 1966). In phenol, where the $S_o \rightarrow {}^1L_b$ transition is allowed, ν_{6b} accounts for 40% of the forbidden activity (Bist et al., 1966). ν_{6b} is also a prominent Herzberg-Teller mode in the $S_o \rightarrow L_b$ spectra of other monosubstituted benzenes.

In his high resolution study of the singlet states of benzoic acid, Baum has obtained the $S_o \rightarrow L_b$ spectra of benzoic acid in benzene, benzoic acid in cyclohexane carboxylic acid, and methyl benzoate in benzene. All of these spectra were obtained at 4.2° K using oriented single crystals. The spectrum of benzoic acid in benzene was obtained with polarized and unpolarized light. The other spectra were obtained only with unpolarized light.

Considering only those spectra obtained with unpolarized light, his data show that the intensity of ν_{6b} is 70% of the origin intensity in benzene host and 7% in cyclohexane carboxylic acid host. In the methyl benzoate spectrum ν_{6b} cannot be detected. The signal/noise ratio in this spectrum is such that the intensity of ν_{6b} must be less than 6% of the origin intensity. It should be pointed out that the reduced intensity of ν_{6b} in cyclohexane carbocylic acid host in principle may be due to orientation factors. However, since unpolarized light was used, it is unlikely that all or even most of this reduction in intensity is due to orientation factors. Unfortunately, the structure of the cyclohexane carboxylic acid unit cell is not known.

Baum's spectrum for benzoic acid obtained with polarized light shows that the ν_{6b} band is polarized parallel to the long-axis of benzoic acid and that the totally symmetric system is polarized perpendicular to the long-axis. The nature of the benzene unit cell prevents a distinction between the out-of-plane and short axis polarization. These polarization results are exactly as expected for a monosubstituted benzene obeying C_{2v} symmetry. In such a molecule the $S_o \rightarrow {}^1L_b({}^1B_1)$ transition is short-axis polarized. ν_{6b} belongs to the b_1 representation, allowing Herzberg-Teller coupling between ${}^1L_b$ and ${}^1A_1$. Since $S_o \rightarrow {}^1A_1$ transitions are long axis polarized, the vibronic band corresponding to ν_{6b} must be long-axis polarized, which is what Baum observes. The lower lying ${}^1A_1$ states in benzoic acid are ${}^1L_a$ and ${}^1B_a$.

It thus appears that ν_{6b} is active in the $S_o \rightarrow {}^1L_b$ spectrum of benzoic acid as a result of Herzberg-Teller coupling between ${}^1L_b$ and ${}^1X_a$. Baum's data also shows that this Herberg-Teller activity is environment sensitive.

Previously we developed a conceptual framework in which the out-of-plane activity in the phosphorescence spectra of benzoic acid could be accounted for in terms of spin-orbit vibronic coupling involving $n\pi^*$ and $\pi\pi^*$

states that consist of a mixture of LE and CT states. Pure LE states were shown to be incompatible with the data. It was further shown that the environmental sensivitity of the out-of-plane activity could be explained by assuming that H-bond strength plays a role in determining the LE, CT composition of the $n\pi^*$ and $\pi\pi^*$ states. In what follows we will use this same conceptual framework to explain the behavior of ν_{6b} in Baum's singlet spectra and to explain the appearance of ν_{6b} in our phosphorescence spectrum of methyl benzoate perturbed by parafluorobenzoic acid.

We first consider Herzberg-Teller coupling in the singlet manifold. As before, we decompose ${}^1\pi\pi^*$ states into LE and CT components:

$$ {}^1L_b = \alpha\, {}^1(\pi_R\pi_R)_b + \beta\, {}^1(\pi_R\pi_C{}^*)_b + \gamma\, {}^1(\pi_C\pi_R{}^*)_b + \delta\, {}^1(\pi_C\pi_C{}^*)_b $$

$$ {}^1X_a = a\, {}^1(\pi_R\pi_R{}^*)_a + b\, {}^1(\pi_R\pi_C)_a + c\, {}^1(\pi_C\pi_R{}^*)_a + d\, {}^1(\pi_C\pi_C{}^*)_a $$

The Herzberg-Teller matrix element between these states reduces to a sum of 16 terms, which are given in Table 37. Eight of these terms are zero because of orbital orthogonality. Taking into account the fact that ν_{6b} is a pure ring mode, six others are disfavored by overlap considerations. These terms are indicated by asterisks. The remaining two terms are:

TABLE 37

This table shows the terms that result when $\langle {}^1L_b | H-T | {}^1X_a \rangle$ is expanded in terms of the LE and CT components of ${}^1L_b$ and ${}^1X_a$. Terms denoted by an asterisk are disfavored by overlap considerations for mode ν_{6b}, a pure ring mode. "a" and "b" subscripts are omitted for simplicity.

αa	$\langle \pi_R \vert H-T \vert \pi_R \rangle$	$\langle \overset{*}{\pi}_R \overset{*}{\pi}_R \rangle$		
αb	$\langle \pi_R \vert H-T \vert \pi_R \rangle$	$\langle \overset{*}{\pi}_R \overset{*}{\pi}_C \rangle$	= 0	
αc	$\langle \pi_R \vert H-T \vert \pi_C \rangle$	$\langle \overset{*}{\pi}_R \overset{*}{\pi}_R \rangle$	= 0	*
αd	$\langle \pi_R \vert H-T \vert \pi_C \rangle$	$\langle \overset{*}{\pi}_R \overset{*}{\pi}_C \rangle$	= 0	
βa	$\langle \pi_R \vert H-T \vert \pi_R \rangle$	$\langle \overset{*}{\pi}_C \overset{*}{\pi}_R \rangle$	= 0	
βb	$\langle \pi_R \vert H-T \vert \pi_R \rangle$	$\langle \overset{*}{\pi}_C \overset{*}{\pi}_C \rangle$		
βc	$\langle \pi_R \vert H-T \vert \pi_C \rangle$	$\langle \overset{*}{\pi}_C \overset{*}{\pi}_R \rangle$	= 0	
βd	$\langle \pi_R \vert H-T \vert \pi_C \rangle$	$\langle \overset{*}{\pi}_C \overset{*}{\pi}_C \rangle$	= 0	*
γa	$\langle \pi_C \vert H-T \vert \pi_R \rangle$	$\langle \overset{*}{\pi}_R \overset{*}{\pi}_R \rangle$	= 0	*
γb	$\langle \pi_C \vert H-T \vert \pi_R \rangle$	$\langle \overset{*}{\pi}_R \overset{*}{\pi}_C \rangle$	= 0	
γc	$\langle \pi_C \vert H-T \vert \pi_C \rangle$	$\langle \overset{*}{\pi}_R \overset{*}{\pi}_R \rangle$	= 0	*
γd	$\langle \pi_C \vert H-T \vert \pi_C \rangle$	$\langle \overset{*}{\pi}_R \overset{*}{\pi}_C \rangle$	= 0	
δa	$\langle \pi_C \vert H-T \vert \pi_R \rangle$	$\langle \overset{*}{\pi}_C \overset{*}{\pi}_R \rangle$	= 0	
δb	$\langle \pi_C \vert H-T \vert \pi_R \rangle$	$\langle \overset{*}{\pi}_C \overset{*}{\pi}_C \rangle$	= 0	*
δc	$\langle \pi_C \vert H-T \vert \pi_C \rangle$	$\langle \overset{*}{\pi}_C \overset{*}{\pi}_R \rangle$	= 0	
δd	$\langle \pi_C \vert H-T \vert \pi_C \rangle$	$\langle \overset{*}{\pi}_C \overset{*}{\pi}_C \rangle$	= 0	*

$$\alpha a \left\langle {}^1(\pi_R\pi_R{}^*)_b \middle| H\text{-}T \middle| {}^1(\pi_R\pi_R{}^*)_a \right\rangle$$

$$\beta b \left\langle {}^1(\pi_R\pi_C{}^*)_b \middle| H\text{-}T \middle| {}^1(\pi_R\pi_C{}^*)_a \right\rangle$$

Baum's calculations predict that an increase in H-bond strength will increase both β (${}^1L_b$) and b if ${}^1X_a = {}^1L_a$. As noted previously we assume that b will also increase if ${}^1X_a = {}^1B_a$. If c, d, γ, and δ do not change, then a and α will decrease because of normalization requirements. However, Baum's calculations also predict that a and α are close to 1, so we do not expect large percentage changes in these coefficients in either direction in view of the predicted changes in CT character that occur upon H-bond formation (see Table 36). Thus we have the clear prediction that any change in the Herzberg-Teller activity of ν_{6b} due to a change in H-bond strength will mainly be the result of a change in the percentage of $\pi_R\pi_C{}^*$ character in ${}^1L_b$, ${}^1L_a$, and possibly ${}^1B_a$. Since Baum's data shows that ν_{6b} activity decrease by an order of magnitude when the H-bonds are weakened, it follows that the observed Herzberg-Teller activity of ν_{6b} in the $S_o \rightarrow {}^1L_b$ spectrum of benzoic acid is due primarily to the presence of $\pi_R\pi_C{}^*$ character in ${}^1L_b$, ${}^1L_a$ and possibly ${}^1B_a$.

Since ν_{6b} cannot be observed in the $S_o \rightarrow {}^1L_b$ spectrum of methyl benzoate, the above conclusion suggests that the $\pi_R\pi_C{}^*$ character in the ${}^1L_b$, ${}^1L_a$ and ${}^1B_a$ states of methyl benzoate is much smaller than in benzoic acid.

At this point, it is appropriate to return to a consideration of the activity of ν_{6b} in phosphorescence spectrum of methyl benzoate perturbed by parafluorobenzoic acid. In section III it was pointed out that no bands corresponding to the fluorinated molecule appear in this spectrum. On this basis we assume that the excited triplet state from which phosphorescence occurs is localized on a methyl benzoate molecule perturbed by a parafluorobenzoic acid molecule. We also assume C_{2v} symmetry for the perturbed methyl benzoate molecule.

As for the out-of-plane modes, we attempt to account for ν_{6b} activity in terms of a spin-orbit vibronic coupling scheme. Given the C_{2v} group-theoretical constraints on Herzberg-Teller coupling for ν_{6b} and neglecting spin-orbit coupling matrix elements between states of the same orbital type, there is only one spin-orbit vibronic coupling scheme in which ν_{6b} can play a role:

$$^{1}\sigma\pi \leftarrow \text{SOC} \rightarrow {}^{3}X_b(B_1) \leftarrow \text{H-T} \rightarrow {}^{3}X_a(A_1)$$

Here $^{1}\sigma\pi$ represents either benzenoid $^{1}\sigma\pi^*$ or $^{1}\pi\sigma^*$ states or else a carboxyl $^{1}n\pi^*$ state. As for benzoic acid we assign the $^{3}\pi_R\pi_R^*$ component of $^{3}X_a$ to $^{3}L_a$. The indicated representations of the states refer only to the spatial parts of the wavefunctions.

Since ν_{6b} is uniquely prominent as an in-plane Herzberg-Teller mode in the $S_o \rightarrow {}^1L_b$ spectra of a number of monosubstituted benzenes, we consider it likely that the intense activity of ν_{6b} in the $T_1 \rightarrow S_o$ spectrum of the MB-PFBA complexe indicates that the triplet π orbitals involved in Herzberg-Teller coupling through ν_{6b} have the same modal properties as the corresponding singlet orbitals which lead to ν_{6b} activity. These π orbitals may be associated with the $\pi_R\pi_R{}^*$ or $\pi_R\pi_C{}^*$ components of ${}^3X_a$ and ${}^3X_b$. Hence we use the Platt notation "a" and "b" subscripts of the expected model properties of these orbitals; i.e., b-type orbitals are modal at the 1 and 4 positions. While we tend to regard ${}^3X_a$ as basically ${}^3L_a$, it should not be inferred that ${}^3X_b$ is basically ${}^3L_b$. As will become apparent, it would not be inconsistent with the data if ${}^3X_b$ were basically ${}^3\pi_C\pi_C{}^*$.

An attempt to account for the activity of ν_{6b} with this spin-orbit vibronic coupling mechanism is confronted with a serious problem. Because spin-orbit vibronic coupling is a second order effect, we expect this mechanism to introduce much less intensity than direct first order spin-orbit between ${}^3X_a$ and ${}^1\sigma\pi$, the same final state. It should be noted that the spin-orbit coupling energy denominators are the same in both cases. Contrary to this expectation we observe ν_{6b} to be as intense as the origin. In what follows we attempt to rationalize this anomaly by considering the possible LE, CT compositions of ${}^1\sigma\pi$, ${}^3X_b$, and ${}^3X_a$. An additional constraint on the composition of these states derives from the very weak activity of out-of-plane ring modes that accompanies intense ν_{6b} activity.

We now decompose ${}^1\sigma\pi$ and ${}^3X_b$ into LE and CT components and consider the contributions of the various components to the spin-orbit coupling matrix element between these states. We write ${}^1\sigma\pi$ and ${}^3X_b$ as follows:

$$\begin{aligned} {}^1\sigma\pi = {} & e\ {}^1n_C\pi_C{}^* + f\ {}^1n_C\pi_R{}^* + g\ {}^1\sigma_R\pi_R + h\ {}^1\pi_R\sigma_R{}^* \\ & + i\ {}^1\sigma_C\pi_C{}^* + j\ {}^1\pi_C\sigma_C{}^* + k\ {}^1\sigma_R\pi_C{}^* \end{aligned}$$

$${}^3X_b = \alpha\ {}^3\pi_R\pi_R{}^* + \beta\ {}^3\pi_R\pi_C{}^* + \gamma\ {}^3\pi_C\pi_R{}^* + \delta\ \pi_C\pi_C{}^*$$

The spin-orbit coupling matrix element between these states consist of a sum of twenty eight terms which are shown in Table 38. Eighteen of these terms vanish because of orbital orthogonality. Among the other ten, overlap considerations disflavor five additional terms, which we set equal to zero. These terms are indicated by asterisks. The five remaining terms are:

TABLE 38

This table shows the terms that result when $\langle {}^3X_b | \mathrm{SOC} | {}^1\sigma\pi \rangle$ is expanded in terms of the LE and CT components of ${}^3X_b$ and ${}^1\sigma\pi$. Terms denoted by an asterisk are disfavored by overlap considerations and are set equal to zero on this basis. "b" subscripts are omitted for simplicity.

αe	$\langle {}^3\pi_R\pi_R^* \vert \mathrm{SOC} \vert {}^1n_C\pi_C^* \rangle$	$= 0$	
βe	$\langle {}^3\pi_R\pi_C^* \vert \mathrm{SOC} \vert {}^1n_C\pi_C^* \rangle$	$= 0$	*
γe	$\langle {}^3\pi_C\pi_R^* \vert \mathrm{SOC} \vert {}^1n_C\pi_C^* \rangle$	$= 0$	
δe	$\langle {}^3\pi_C\pi_C^* \vert \mathrm{SOC} \vert {}^1n_C\pi_C^* \rangle$		
αf	$\langle {}^3\pi_R\pi_R^* \vert \mathrm{SOC} \vert {}^1n_C\pi_R^* \rangle$	$= 0$	*
βf	$\langle {}^3\pi_R\pi_C^* \vert \mathrm{SOC} \vert {}^1n_C\pi_R^* \rangle$	$= 0$	
γf	$\langle {}^3\pi_C\pi_R^* \vert \mathrm{SOC} \vert {}^1n_C\pi_R^* \rangle$		
δf	$\langle {}^3\pi_C\pi_C^* \vert \mathrm{SOC} \vert {}^1n_C\pi_R^* \rangle$	$= 0$	
αg	$\langle {}^3\pi_R\pi_R^* \vert \mathrm{SOC} \vert {}^1\sigma_R\pi_R^* \rangle$		
βg	$\langle {}^3\pi_R\pi_C^* \vert \mathrm{SOC} \vert {}^1\sigma_R\pi_R^* \rangle$	$= 0$	
γg	$\langle {}^3\pi_C\pi_R^* \vert \mathrm{SOC} \vert {}^1\sigma_R\pi_R^* \rangle$	$= 0$	*
δg	$\langle {}^3\pi_C\pi_C^* \vert \mathrm{SOC} \vert {}^1\sigma_R\pi_R^* \rangle$	$= 0$	
αh	$\langle {}^3\pi_R\pi_R^* \vert \mathrm{SOC} \vert {}^1\pi_R\sigma_R^* \rangle$	$= 0$	
βh	$\langle {}^3\pi_R\pi_C^* \vert \mathrm{SOC} \vert {}^1\pi_R\sigma_R^* \rangle$	$= 0$	

Table 38 (Continued)

γh $\left\langle {}^3\pi_C\pi_R^* \middle| \mathrm{SOC} \middle| {}^1\pi_R\sigma_R^* \right\rangle = 0$

δh $\left\langle {}^3\pi_C\pi_C^* \middle| \mathrm{SOC} \middle| {}^1\pi_R\sigma_R^* \right\rangle = 0$

αi $\left\langle {}^3\pi_R\pi_C^* \middle| \mathrm{SOC} \middle| {}^1\sigma_C\pi_C^* \right\rangle = 0$

βi $\left\langle {}^3\pi_R\pi_C^* \middle| \mathrm{SOC} \middle| {}^1\sigma_C\pi_C^* \right\rangle = 0$ *

γi $\left\langle {}^3\pi_C\pi_R^* \middle| \mathrm{SOC} \middle| {}^1\sigma_C\pi_C^* \right\rangle = 0$

δi $\left\langle {}^3\pi_C\pi_C^* \middle| \mathrm{SOC} \middle| {}^1\sigma_C\pi_C^* \right\rangle$

αj $\left\langle {}^3\pi_R\pi_R^* \middle| \mathrm{SOC} \middle| {}^1\pi_C\sigma_C^* \right\rangle = 0$

βj $\left\langle {}^3\pi_R\pi_C^* \middle| \mathrm{SOC} \middle| {}^1\pi_C\sigma_C^* \right\rangle = 0$

γj $\left\langle {}^3\pi_C\pi_R^* \middle| \mathrm{SOC} \middle| {}^1\pi_C\sigma_C^* \right\rangle = 0$

δj $\left\langle {}^3\pi_C\pi_C^* \middle| \mathrm{SOC} \middle| {}^1\pi_C\sigma_C^* \right\rangle = 0$

αk $\left\langle {}^3\pi_R\pi_R^* \middle| \mathrm{SOC} \middle| {}^1\sigma_R\pi_C^* \right\rangle = 0$

βk $\left\langle {}^3\pi_R\pi_C^* \middle| \mathrm{SOC} \middle| {}^1\sigma_R\pi_C^* \right\rangle$

γk $\left\langle {}^3\pi_C\pi_R^* \middle| \mathrm{SOC} \middle| {}^1\sigma_R\pi_C^* \right\rangle = 0$

δk $\left\langle {}^3\pi_C\pi_C^* \middle| \mathrm{SOC} \middle| {}^1\sigma_R\pi_C^* \right\rangle = 0$ *

$$\delta e \quad \left\langle {}^3(\pi_C\pi_C{}^*)\,|\mathrm{SOC}|\,{}^1n_C\pi_C{}^*\right\rangle$$

$$\gamma f \quad \left\langle {}^3(\pi_C\pi_R{}^*)\,|\mathrm{SOC}|\,{}^1n_C\pi_R{}^*\right\rangle$$

$$\alpha g \quad \left\langle {}^3(\pi_R\pi_R{}^*)\,|\mathrm{SOC}|\,{}^1\sigma_R\pi_R{}^*\right\rangle$$

$$\delta i \quad \left\langle {}^3(\pi_C\pi_C{}^*)_b\,|\mathrm{SOC}|\,{}^1\sigma_C\pi_C{}^*\right\rangle$$

$$\beta k \quad \left\langle {}^3(\pi_R\pi_C{}^*)_b\,|\mathrm{SOC}|\,{}^1\sigma_R\pi_C{}^*\right\rangle$$

Since the data requires the spin-orbit coupling matrix element between ${}^1\sigma\pi$ and ${}^3X_a$ to be much smaller than the matrix element between ${}^1\sigma\pi$ and ${}^3X_b$, it is also necessary to consider the former matrix element. We write ${}^3X_a$ as follows:

$${}^3X_a = a\ {}^3(\pi_R\pi_R{}^*)_a + b\ {}^3(\pi_R\pi_C{}^*)_a + c\ {}^3(\pi_C\pi_R{}^*)_a + d\ {}^3(\pi_C\pi_C{}^*)_a$$

By exactly the same argument as before, we find that the important terms for the spin-orbit coupling matrix element between ${}^1\sigma\pi$ and ${}^3X_a$ are:

$$de \quad \left\langle {}^3(\pi_C\pi_C{}^*)_a\,|\mathrm{SOC}|\,{}^1n_C\pi_C{}^*\right\rangle$$

$$cf \quad \left\langle {}^3(\pi_C\pi_R{}^*)_a\,|\mathrm{SOC}|\,{}^1n_C\pi_R\right\rangle$$

$$ag \quad \left\langle {}^3(\pi_R\pi_R{}^*)_a\,|\mathrm{SOC}|\,{}^1\sigma_R\pi_R{}^*\right\rangle$$

$$di \quad \left\langle {}^3(\pi_C\pi_C{}^*)_a\,|\mathrm{SOC}|\,{}^1\sigma_C\pi_C{}^*\right\rangle$$

$$bk \quad \left\langle {}^3(\pi_R\pi_C{}^*)_a\,|\mathrm{SOC}|\,{}^1\sigma_R\pi_C{}^*\right\rangle$$

In each matrix element two terms depend on the $\pi_C\pi_C{}^*$ component. Neglecting for the moment, the other ^{3} terms in each matrix element, it is clear that one matrix element will be much larger than the other if it contains much more $\pi_C\pi_C^*$ character. In particular, if $\delta >> d$, then $\langle {}^1\sigma\pi | SOC | {}^3X_b \rangle >> \langle {}^1\sigma\pi | SOC | {}^3X_a \rangle$. Thus, if the terms in each matrix element involving $\pi_R\pi_C^*$, $\pi_R\pi_R^*$ and $\pi_C\pi_R^*$ components can be neglected, the intense activity of ν_{6b} can be rationalized in terms of the amount of $\pi_C\pi_C^*$ character in ${}^3X_a$ and ${}^3X_b$.

Unfortunately, the data is insufficient to prove that the $\pi_R\pi_C^*$, $\pi_R\pi_R^*$ and $\pi_C\pi_R^*$ components of ${}^3X_{a,b}$ do not play a significant role in the spin-orbit coupling matrix elements between ${}^1\sigma\pi$ and ${}^3X_{a,b}$. However, in what follows we will propose LE, CT compositions of ${}^1\sigma\pi$, ${}^3X_b$. and ${}^3X_a$ that lead to the conclusion that these terms are unimportant. Because of insufficient data, the most that we are able to do is show that the proposed compositions of states are consistent with the spectra and with our proposed geometry for the MB-PFBA complex that is associated with intense ν_{6b} activity.

We first propose that ${}^1\sigma\pi$ is regionalized on the carboxyl group. That is, the coefficient f, g, h, and k are assumed to be negligible. An immediate consequence of this is that only terms involving the $\pi_C\pi_C^*$ components of ${}^3X_a$ and ${}^3X_b$ are important for spin-orbit coupling. In line with our previous considerations, it is assumed that ${}^3X_b$ has much more $\pi_C\pi_C^*$ character than ${}^3X_a$.

We next propose that ${}^3X_a$ and ${}^3X_b$ possess appreciable $\pi_R\pi_C^*$ character. The motivation for this assumption derives from our previous conclusions that ν_{6b} activity in the singlet manifold results primarily from $\pi_R\pi_C{}^*$ character. This assumption is fully compatible with the weak out-of-plane activity that accompanies intense ν_{6b} activity, because $^1\sigma\pi$ is regionalized. Previously we showed that Herzberg-Telling coupling between a $\sigma\pi$ stae and a $\pi\pi^*$ state involving ring out-of-plane modes required either $\sigma_R\pi_R{}^*$ or $\sigma_R\pi_C{}^*$ components. A regionalized $\sigma\pi$ states does not possess these components.

It thus appears that a regionalized $^1\sigma\pi$ state and $^3\pi\pi^*$ states having appreciable $\pi_R\pi_C{}^*$ character and appropriate amounts of $\pi_C\pi_C{}^*$ character are fully compatible with the data. In view of our previous arguments concerning the effects of hydrogen bonding on the LE, CT composition of $n\pi^*$ and $\pi\pi^*$ states, it is clear that a regionalized $\sigma\pi$ state and large $\pi_R\pi_C{}^*$ character in ^3X_a and ^3X_b are jointly compatible with a strong hydrogen bond to the methyl benzoate carbonyl oxygen atom. We therefore propose that the geometry of the complex associated with intense ν_{6b} activity leads to the formation of a strong hydrogen bond between the methyl benzoate and paraflorobenzoic acid molecules.

At this point it is appropriate to consider which configurations of the MB-PFBA complex allow the formation of strong hydrogen bonds. An inspection of the possible orientations of the two molecules shows that there are two configurations, one being the mirror image of the other which should favor the formation of unusually strong hydrogen bonds. If the plane of the parafluorobenzoic acid ring is perpendicular to the plane of the methyl benzoate ring, it is possible for the n orbital on themethyl benzoate carbonyl oxygen atom to conjugate with the 2pπ orbital on the hydroxyl oxygen atom of parafluorobenzoic acid. This should lead to a bond much stronger than the H-bonds in benzoic acid dimers.

It must be emphasized that we have not shown that the data requires the proposed compositions of $\sigma\pi$ and $\pi\pi^*$ states. Rather all that has been shown is that the data, the proposed compositions of states and the proposed geometry are mutually consistent.

In conclusion we wish to summarize our answers to the questions raised at the beginning of this section:

1. We have proposed that the intense out-of-plane activity in the phosphorescence spectra of benzoic acid arises as a result of a second-order spin-orbit vibronic coupling mechanism which couples ^3X to a $^1\pi\pi^*$ final state via an $n\pi^*$ intermediate state. Since $S_o \rightarrow {}^1\pi\pi^*$ transitions are 10^2 to 10^4 times as intense as $S_o \rightarrow {}^1n\pi^*$ (and presumably $^1\sigma\pi^*$ and $^1\pi\sigma^*$) transitions, it is understandable that the second-order mechanism can introduce intensity comparable to that introduced by first order spin-orbit coupling between ^3X and $^1n\pi^*$ (or $^1\sigma\pi^*$ or $^1\pi\sigma^*$), which is believed to be the main source of intensity for the

origin and totally symmetric vibronic bands.

2. The dominance of ring out-of-plane modes over carboxyl group out-of-plane modes has been rationalized in terms of the valence (i.e. LE, CT) compositions of ^3X, the intermediate $n\pi^*$ state, and the final $^1\pi\pi^*$ state.

3. The environmental dependence of the out-of-plane activity has been rationalized in terms of changes in the LE, CT compositions of the relevant states, that arise as a result of changes in H-bond strength and non-planarity of the carboxyl group.

4. In agreement with Maria and McGlynn, we have concluded that the presence of in-plane carboxyl group modes is associated with the presence of $^3\pi_C\pi_C^*$ character in ^3X.

5. The environmental dependence of the in-plane carboxyl group modes has been attributed to a non-planarity of the carboxyl group, the degree of non-planarity being different in different environments. Tilting the carboxyl group is expected to alter the amount of $^3\pi_C\pi_C^*$ character in ^3X.

6. The shorter radiative lifetime of benzoic acid compared to that of toluene is most likely the result of first-order spin-orbit coupling between ^3X and $^1n\pi^*$ and second-order spin-orbit vibronic coupling between ^3X and $^1\pi\pi^*$. These intensity sources are not present in toluene. Heavy atom effects associated with the oxygen

atoms may also play a role.

7. The intense activity of ν_{6b} associated with some configurations of the MB-PFBA complex has been rationalized in terms of a second-order spin-orbit vibronic coupling scheme involving a $\pi\pi^*$ intermediate state and a $^1n\pi^*$ final state. The ability of the second-order mechanism to compete with first-order spin-orbit coupling between ^3X_a and the same final state has been rationalized by assuming that the intermediate state has much more $^3\pi_C\pi_C{}^*$ character than ^3X_a the emitting state. We have proposed LE, CT compositions of ^3X_a , the intermediate state and the final state which are consistent with the data and the presence of a strong H-bond in the MB-PFBA complex. We have also proposed a geometry of the complex which is consistent with a strong H-bond.

Although some of the conclusions reached in this analysis of the lowest triplet state of benzoic acid depend upon unproven valence and geometric assumptions we consider that it has been demonstrated that the conceptual framework developed in this analysis gives considerable physical insight into the electronic structure of benzoic acid. This conceptual framework should be a useful starting point for future studies of benzoic acid and other aromatic carbonyl compounds.

F. Recommendations for Future Studies

One of the more important experimental goals of a future study of benzoic acid should be a determination of the polarization properties of the phosphorescence and fluorescence emission. This data together with the polarized absorption spectra already available would allow an identification of the intensity sources of both the totally symmetric and non-totally symmetric vibronic bands in the phosphorescence spectrum and would thereby provide a consistency check on the spin-orbit coupling and spin-orbit vibronic coupling schemes proposed in this study.

Another important goal should be a measurement of the phosphorescence lifetime of each vibronic band in the phosphorescence spectrum at 1.4° K or lower. As we have pointed out, the spin-orbit vibronic coupling scheme proposed to account for out-of-plane ring modes allows the prediction that a_2 modes will couple to only one magnetic sublevel of the lowest triplet state and that b_2 modes will couple to two sublevels. A failure to observe the expected exponential (a_2) or non-exponential (b_2) decay would indicate either that the proposed mechanism is incorrect or else that the symmetry is lower than C_{2v}. These considerations also apply to the spin-orbit vibronic coupling mechanism proposed to account for the activity of ν_{6b} in the phosphorescence spectrum of methyl benzoate perturbed by parafluorobenzoic acid.

As discussed in Section III D, Baum's efforts to locate $^3n\pi^*$ using the triplet-triplet absorption method developed by McClure was unsuccessful on account of interference from overtones of ground state vibrations. To bypass this difficulty we propose the following excitation experiment. First the triplet state is populated by a strong flash photolysis type lamp. Because of the long lifetime of benzoic acid at 4.2° K, a substantial concentration of excited states should be produced. Using monochromatic light of the appropriate wavelength, molecules are taken from the lowest triplet state to $^3n\pi^*$. Most molecules will return to the lowest triplet state on account of rapid internal conversion. But since $^3n\pi^*$ is only slightly higher in energy than ^1L_b , the spin-orbit coupling between $^3n\pi^*$ and ^1L_b is expected to be substantial. This creates the possibility of sufficient intersystem crossing from $^3n\pi^*$ to ^1L_b to yield detectable delayed fluorescence, which would be well separated in wavelength from the phosphorescence emission and which could be measured after the flash lamp is completely extinguished. By monitoring fluorescence it should be possible to determine the $T_1 \rightarrow {}^3n\pi^*$ absorption spectrum. In this procedure absorption by overtones of ground state vibrations would only attenuate the light and would not lead to any delayed fluorescence. Thus interference from ground state vibrations would be largely eliminated. Presumably polarized spectra could also be obtained with this technique. It should be pointed out that benzoic acid dimer, rather than complexed monomer should be used in this experiment, since in the dimer the presence of both gerade and ungerade $^3\pi\pi^*$ and $^3n\pi^*$ states leads to electric dipole allowed transitions between these states. In the monomer only ungerade excited states are present and the transition is electric dipole forbidden.

In addition to these experimental goals, two types of theoretical studies are definitely needed: (1) A valence calculation on the vertical excited states such that the several lowest singlet and triplet states are treated at the same level of approximation (e.g. SCF) and with subsequent decomposition into LE and CT components, and (2) A study of the lowest triplet state potential surface problem for selected carboxyl group modes.

REFERENCES

Albrecht, A. C., J. Chem. Phys., 33, 156 (1960).

Albrecht, A. C., J. Mol. Spec, 6, 84 (1961).

Albrecht, A. C., J. Chem. Phys,, 38, 354 (1963).

Baba, H. and Kitamura, M., J. Mol. Spectrosc., 41, 302 (1972).

Bailey, C. R., Gordon, R. R., Hale, J. B., Herzfeld, N., Ingold, C. K. and Poole, H. G., J. Chem. Soc. 299 (1946).

Baum, J. C., Ph. D. Thesis, Princeton, Univ., Princeton, N. J., 1974.

Bist, H. D., Brand, J.C.D., and Williams, D.R., J. Mol. Spectrosc., 21, 76 (1966).

Bist, H. D., Sarin, V. N., Ojha, A., and Jain, Y.S., Appl. Spectrosc., 24, 292 (1970).

Blinc, R. and Hadzi, E. in "Hydrogen Bonding", D. Hadzi, ed., Pergamon Press, Ltd. London, 1959, p. 147.

Born, H. and Huang, K., "Dynamical Theory of Crystal Lattices," Clarendon Press, Oxford, Eng. (1956).

Bratoz, S., Hadzi, D., and Sheppard, N., Spectrochim. Acta, 8, 249 (1956).

Brealey, G.J. and Kasha, M., J. Amer. Chem. Soc., 77, 4462 (1955).

Brodersen, S. and Langseth, A., Mat. fys. Skr. Kong. Dansk. Vid. selsk., 1, 1 (1956).

Brooks, C.J.W., Eglinton, G., and Morman, J.F., J. Chem. Soc., 106 (1961).

Buswell, A. M., Rhodebush, W. H., and Roy, M. F., J. Amer. Chem. Soc., 60, 2239 (1938).

Callomon, J.H., Dunn, T.M. and Mills, J.M., Phil. Trans. Roy. Soc. (London), 259A, 499 (1966).

Chu, S.Y. and Goodman, L., manuscript in preparation.

Cleveland, F. F., J. Chem. Phys., 13, 101 (1945).

Cojan, J. and Renaux, A., Acad. Sci. (Paris) Compt. Rend. Series C, 247, 1111 (1958).

Colombo, L. and Furic, K., *Spectrochim. Acta.*, *27A*, 1773 (1971).

Cotton, F. A., "Chemical Applications of Group Theory", Wiley-Interscience, New York, 1971.

Craig, D. P. and Walmsley, S.H., "Excitons in Molecular Crystals", W. A. Benjamin, Inc., New York, 1968.

Davies, M. M. and Sutherland, G.B.B.M., *J. Chem. Phys.*, *6*, 755, 767 (1938).

Davydov, A.S., "Theory of Molecular Excitons," McGraw Hill Inc., New York, N.Y., 1962.

Delorme, P., *J. Ch. Phys.*, *61*, 97 (1964).

Duben, A., Goodman, L., and Koyanagi, M., in "Excited States," Vol. I, E. C. Lim, Ed., Academic Press, Inc., New York, New York, 1974, p. 295.

Duinker, J. C. and Mills, I. M., *Spectrochim. Acta*, *24A*, 417 (1968).

Dym, S. and Hochstrasser, R. M., *J. Chem. Phys.*, *51*, 2458 (1969).

Genzel, L., Happ, H., and Weber, R., *Z. Phys.*, *154,* 1 (1959). also, Genzel, L., *Z. Phys.*, *144*, 311 (1956).

Gonzalez-Sanchez, F., *Spectrochim. Acta*. *12*, 17 (1958).

Goodman, L. and Koyanagi, M., *Mol. Photochem.*, *4*, 369 (1972).

Goodman, L. and Shull, H., *J. Chem. Phys.*, *27*, 1388 (1957).

Haaland, D. M. and Nieman, G. C., *J. Chem. Phys.*, *59*, 4435 (1973).

Hadzi, D. and Sheppard, N., *Proc. Roy. Soc., Ser. A*, *216*, 247 (1953).

Hadzi, D. and Pintar, M., *Spectrochim. Acta*, *12*, 162 (1958).

Hayashi, S. and Kimura, N., Bull. *Inst. Chem. Res., Kyoto Univ.*, *44,* 335 (1966).

Hayashi, S. and Umemura, J., *J. Chem. Phys.*, *60*, 2630 (1974).

Herzberg, G., "Molecular Spectra and Molecular Structure. II, Infrared and Raman Spectra of Polyatomic Molecules", Van Nostrand Reinhold Co., New York, N.Y., 1947.

Herzberg, G. and Teller, E., Z. Phys. Chem. (Leipz.), 21, 410 (1933).

Hochstrasser, R.M., "Molecular Aspects of Symmetry", W. A. Benjamin, Inc., New York, 1966.

Hollas, J. M., Gregorak, E. and Goodman, L., J. Chem. Phys. 49, 1745 (1968).

Hussey, A.S., J. Amer. Chem. Soc., 73, 1364 (1951).

Jeffrey, G. A. and Sax, M., Acta. Cryst. 16, 430 (1963).

Kakiuti, Y., Matumura, R., Eguti, H., and Suzuki, R., Nippon Kagaku Zasshi, 82, 830 (1961).

Kanda, Y., Shimada, R., and Takenoshita, Y., Spectrochim. Acta, 19, 1249 (1963).

Khalil, O.S., Meeks, J. L., and McGlynn, S.P., manuscript in preparation.

Kohlrausch, K.W.F., Ramanspektren, S. 381 (1953). Also Landolt-Bornstein Tabellen, Zahlenwerte und Funktionen, I Band 2 Teil, S. 535.

Krishna, V. G. and Goodman, L., Nature, 191, 800 (1961).

Krishna, V. G. and Goodman, L., J. Chem. Phys., 37, 912 (1962).

Latimer, W. M. and Rodebush, W. H., J. Amer. Chem. Soc. 42, 1432 (1920).

Levshin, V. L. and Rebane, V. N., Opt. Spektrosk. Aka. Nauk SSSR, Otd. Fiz-Mat. Nauk, Sb. Statei, 1, 84 (1963)

Lewis, G. N. and Kasha, M., J. Amer. Chem. Soc., 66, 2100 (1944).

Lin, C. T., Gwaiz, A. A. and M. A. El Sayed, J. Amer. Chem. Soc., 94, 8234 (1972).

Longuet-Higgins, H.C. and Murrell, J.N., Proc. Phys. Soc., A68, 601 (1955).

Lower, S. K. and El Sayed, M. A., Chem. Rev., 66, 199 (1966).

Maier, W. and Schifferdecker, Spectrochim. Acta., 18, 709 (1962).

McClure, D.S., J. Chem. Phys., 17, 905 (1949).

McClure, D. S., J. Chem. Phys., 19, 670 (1951).

McClure, D. S., J. Chem Phys., 20, 682 (1952).

McGlynn, S. P., Azumi, T., and Kinoshita, M., "Molecular Spectroscopy of the Triplet State," Prentice-Hall, Inc., Englewood Cliffs, N.J., 1969.

McWhinnie, W. R. and Poller, R. C., Spectrochim. Acta., 22, 501 (1966).

Meeks, J. and McGlynn, S.P., unpublished results (1974).

Meshitsuka, S., Takahashi, H., Higasi, K., and Schrader, B., Bull. Chem. Soc. Jap., 45, 1664 (1972).

Miyazawa, T., J. Mol. Spectrosc., 4, 168 (1960).

Murray, F. E. and Sundaram, S., Canadian Journal of Chemistry 39, 1625 (1961).

Murrell, J.N., Tetrahedron, 19, 277 (1963).

Murty, G.V.L.N. and Seshadri, T. R., Proc. Indian Acad. Sci. A, 19, 17 (1944).

Nagakura, S. and Tanaka, J., J. Chem. Phys., 22, 236 (1954).

Nurmakhametov, R.N., Belaits, I.L., and Shigorin, D.N., Russ. J. Phys. Chem., 41, 1032 (1967).

Odinokov, S.E., Maximov, O.B., and Dzizenko, A.K., Spectrochimica Acta, 25A, 131 (1969).

Ozkan, I., Chu, S.Y. and Goodman, L., submitted to J. Chem. Phys.

Parker, C. A. and Hatchard, C. G., Analyst, 87, 664 (1962).

Pauling, L. and Brockway, L.O., Proc. Nat. Acad. Sci. U.S., 20, 336 (1934).

Pfann, W. G., "Zone Melting", John Wiley & Sons, Inc., New York, 1959.

Pinchas, S., Samuel, D. and Weiss, Proday, M., J. Chem. Soc. 2382 (1961).

Pinchas, S., J. Phys. Chem., 69, 2256 (1965).

Porter, G. and Windsor, M. W., Proc. Roy. Soc. (London), A245, 238 (1958).

Pyatnitskii, B. A., Dokl. Akad. Nauk SSSR, 57, 771 (1941).

Pyatnitskii, B.A., Dokl. Akad. Nauk SSSR, 62, 59 (1948).

Pyatnitskii, B. A., Dokl. Adad. Nauk SSSR, 68, 281 (1949).

Schildknecht, H., "Zone Melting", Academic Press, New York, 1966.

Seliskar, C. J., Khalil, O.S., and McGlynn, S.P. in "Excited States," Vol. 1. E. C. Lim, Ed., Academic Press, Inc., New York, N.Y., 1974.

Shimeda, R., and Goodman, L., J. Chem. Phys., 43, 2027 (1965).

Shpolskii, E.V., Sov. Phys. Usp., 6, 411 (1963) and references therein.

Sim, G. A., Robertson, J.M., and Goodwin, T. H., Acta Cryst., 8, 157 (1955).

Smolarek, J., Zwarich, R., and Goodman, L., J. Mol. Spec., 43, 416 (1972).

Stanevich, A. E., Opt. Spektrosk. 16, 446 (1964). (Opt. Spectry., 16, 243 (1964).)

Statz, G. and Lippert, E., Ber. Bunsenges, Phys. Chem., 71, 673 (1967).

Suzuki, M., Yokoyama, T., and Ito., M., Spectrochim. Acta, 24A, 1091 (1968).

Tanaka, J., Nippon Kagaku Zasshi, 79, 1379 (1958).

Teplyakov, P. A. and Grosul, V. P., Ukr. Fiz. Zh. 6, 816 (1961).

Tournon, J. and El-Bayoumi, M. A., J. Chem. Phys., 56, 5128 (1972).

Varsanyi, G., "Vibratinal Spectra of Benzene Derivatives," Academic Press, New York, 1969.

von Kowalski, J., Physik, Z., 12, 956 (1911).

Wall, F. T. and Clausen, W. F., J. Amer. Chem., 61, 2812 (1939).

Whiffen, D.H., J. Chem. Soc., 1350 (1956).

Wood, J.L., J. Mol. Structure, 13, 141 (1972).

Wyncke, B., Hadni, A., Wendling, H., Gerbaux, X., Strimer, P., and Morlot, G., J. Phys. (Paris), 29, 851 (1968).

Ziegler, L. and Albrecht, A. C., J. Chem. Phys., 60, 3558 (1974).